Trends in Augmentation of Human Performance 2

Panagiotis Artemiadis *Editor*

Neuro-robotics

From brain machine interfaces to rehabilitation robotics

Springer

Neuro-Robotics

Trends in Augmentation of Human Performance

Series Ed.: Cutsuridis, Vassilis

Human performance enhancement refers to the augmentation of human skills, attributes and competencies through the use of technology, medicine and therapy designed to replace or increase human performance capability. In the turn of the second decade of the 21st century the convergence of the neurosciences including neuroimaging, genetics and cognitive science, neurotechnology and informatics is creating powerful tools that have the potential to significantly enhance human performance.

Three broad domains of human performance enhancement will be covered by the book series: (1) Enhancement of human performance to restore normal human capability from the disabled or dysfunctional, (2) enhancement of human performance to superhuman levels, and (3) Ethical consequences of the first two domains.

Examples of the first domain will include but not limited to restoration of sight, hearing, memory, mobility, reversing aging effects, prosthesis of limbs, brain-machine interface and genetic manipulation. Examples of the second domain will include, but not limited to enhanced memory, augmentation of vision, hearing, strength, mobility, brain-machine and machine-brain interfaces.

This series will publish works of the highest quality that advance the understanding and practical application of human performance enhancement. Research monographs, introductory and advanced level textbooks, volume editions and proceedings will be considered. Please contact the editors with your book ideas.

Finally, an advisory board of distinguished scientists from the fields on neurotechnology, neurosciences, cybernetics, cognitive sciences, psychophysics, psychiatry, genetics, neuropharmacology, neuroimaging and ethics will assist the book series editor with the selection of future book proposals. The advisory board members will also serve as reviewers of future book proposals.

For further volumes:
http://www.springer.com/series/10849

Panagiotis Artemiadis
Editor

Neuro-Robotics

From Brain Machine Interfaces to Rehabilitation Robotics

Springer

Editor
Panagiotis Artemiadis
School for Engineering of Matter,
Transport, and Energy
Arizona State University
Tempe, AZ, USA

ISSN 2213-1310 ISSN 2213-1329 (electronic)
ISBN 978-94-017-8931-8 ISBN 978-94-017-8932-5 (eBook)
DOI 10.1007/978-94-017-8932-5
Springer Dordrecht Heidelberg New York London

Library of Congress Control Number: 2014943919

Printed on acid-free paper

Springer is part of Springer Science+Business Media (www.springer.com)

Preface

Neuro-Robotics is definitely one of the most multidisciplinary fields of the last decades, combining information and knowledge from neuroscience, engineering and computer science. It is the science and technology of embodied autonomous neural systems, as defined by Dr. Frederic Kaplan (EPFL, Switzerland). Those neural systems include bio-inspired algorithms, models, as well as actual biological systems. The neural systems-machine interaction ranges from physical interaction to computational control interfaces. This interaction is usually bi-directional, affecting both the machines and the neural systems that drive them. Through the framework of neuro-robotics, artificial intelligence and brain plasticity appear in parallel, evolve together, and finally result in the human-machine embodiment.

This book provides a snapshot of the current state-of-the-art research projects around the world, conducted by pioneers in the field. It focuses on the results from the strategic alliance between Neuroscience and Robotics that help the scientific community to better understand the brain as well as design robotic devices and algorithms for interfacing humans and robots (conceptually and physically). The central aim of the book is to collect high-impact works and be an informational resource for anyone interested in working on models and hardware that promote the fusion of neuroscience and robotics, in order to help the mobility impaired, as well as augment human capabilities.

The book is divided into three parts: (1) neuro-robotics: the new frontier, (2) human-machine interfaces for performance augmentation and (3) rehabilitation robotics. In the first part, state-of-the art approaches on human-machine neural control interfaces are presented, focusing on both teleoperated systems and prosthetic devices. In the second part, architectures and devices that augment human performance and capabilities are discussed. These architectures are analyzed from both the machine and the human perspective, and ways to relate those two entities are analyzed. In the third part, state-of-the-art approaches on rehabilitation robotics are presented. Research and clinical data are presented to validate and quantify the efficacy of robot-assisted method for providing therapy to the mobility impaired.

This book will be of great interest and value to roboticists, neuroscientists, clinicians and physiotherapists, and others interested in developing models, algorithms and hardware interfacing with humans. Graduate level students and trainees in all of these fields will find this book a significant source of information.

Finally, I would like to thank all contributing authors who made this book possible. I would like to thank the members of the Springer editorial and production team for their help and support. This work is dedicated to my wife Spyridoula, and daughter Natalia.

Tempe, AZ, USA Panagiotis Artemiadis

Contents

Part I
Neuro-Robotics: The New Frontier

Chapter 1
A Learning Scheme for EMG Based Interfaces: On Task Specificity in Motion Decoding Domain

Minas Liarokapis, Kostas J. Kyriakopoulos, and Panagiotis Artemiadis

Abstract A complete learning scheme for EMG based interfaces is used to discriminate between different reach to grasp movements in 3D space. The proposed scheme is able to decode human kinematics, using the myoelectric activity captured from human upper arm and forearm muscles. Three different task features can be distinguished: subspace to move towards, object to be grasped and task to be executed (with the grasped object). The discrimination between the different reach to grasp movements is accomplished with a random forest classifier. The classification decision triggers task-specific motion decoding models that outperform "general" models, providing better estimation accuracy. The proposed learning scheme takes advantage of both a classifier and a regressor, that cooperate advantageously in order to split the space, confronting with task specificity, the nonlinear relationship between the EMG signals and the motion to be estimated. The proposed scheme can be used for a series of EMG-based interfaces, ranging from EMG based teleoperation of robot arm hand systems to muscle computer interfaces and EMG controlled neuroprosthetic devices.

Keywords ElectroMyoGraphy (EMG) • EMG based interfaces • Learning scheme • Task specificity

M. Liarokapis (✉) • K.J. Kyriakopoulos
National Technical University of Athens, Athina, Greece
e-mail: mliaro@mail.ntua.gr; kkyria@mail.ntua.gr

P. Artemiadis
School for Engineering of Matter, Transport, and Energy, Arizona State University, Tempe, AZ 85287, USA
e-mail: panagiotis.artemiadis@asu.edu

P. Artemiadis (ed.), *Neuro-Robotics: From Brain Machine Interfaces to Rehabilitation Robotics*, Trends in Augmentation of Human Performance 2,
DOI 10.1007/978-94-017-8932-5_1,

1.1 Introduction

Electromyography was first used, for the control of advanced prosthetic devices, 30 years ago [1]. Over the last decades, the field of EMG based interfaces has received increased attention, as many applications of mainly surface electromyography (sEMG), have been proposed. Some of those applications are; EMG based teleoperation [2, 3] in remote or dangerous environments, EMG based control of advanced prosthetic limbs [4] that help patients regain lost dexterity, EMG controlled exoskeletons [5] for rehabilitation purposes and muscle computer interfaces as an alternative means for human computer interaction [6] and [7]. Although EMG based interfaces are very promising and may have a vital role in human robot/computer interaction applications for the years to come, some of their disadvantages that have been identified and discussed in many studies in the past are; the high-dimensionality and complexity of the human musculo-skeletal system and the non-linear relationship between the human myoelectric activity and the motion or force to be estimated.

Principal components analysis (PCA) has been used by several studies in the past, for the investigation of human hand kinematic and/or muscle synergies. In [8] optical markers were mounted on 23 different points on the human hand and kinematics were captured during an unconstrained haptic exploration task. PCA was applied in order to conclude to a set of hand postures, representative of most naturalistic postures that appear during object manipulation. The studies conducted by Santello et al. [9] and Todorov et al. [10] identified – capturing the human hand kinematics with datagloves – a limited number of postural synergies "representing" most of the variance, for a wide variety of object grasps. In [11] a similar study was conducted, using a camera-based motion capture system. Regarding muscle synergies, glove measurements combined with EMG activity were acquired in [12], from subjects using the American Sign Language (ASL) manual alphabet, revealing temporal synergies across different muscles, during different hand movements. Muscle synergies ability to formulate a predictive framework, capable to associate muscular co-activation patterns derived from EMGs with new static hand postures, was investigated in [13].

As we have already mentioned one of the main difficulties that researchers face in the field of EMG based interfaces, is the highly nonlinear relationship between the human myoelectric activity and human kinematics, as described in [14]. This difficulty forced the majority of researchers to avoid to decode a continuous representation of human kinematics, choosing to focus on a discrete approach, such as the directional control of a robotic wrist [15] or the control of multifingered robot hands to a series of discrete postures [16, 17] and [18–21]. For doing so, machine learning techniques and more specifically classification methods were used. In [16] and [17] classifiers were used to discriminate based on the human myoelectric activity, between independent human hand's digit movements or different hand postures. Castellini et al. [22] used forearm surface EMGs for the feed-forward control of a hand prosthesis, discriminating between three different grip types (power grasp, index precision grip and middle-ring-pinky precision grip), in real-time. Brochier et al. [23] used the myoelectric activity of two adult macaque monkeys, to discriminate muscular co-activation patterns associated with different grasping postures. The latter study was conducted for grasping tasks involving 12 objects of different shapes. Although the discrete EMG based control approach, has been used in many studies and has led to many interesting applications, the use of finite postures may cause severe problems such as the lack of motion smoothness. In fact for most EMG based interfaces (such as the EMG based teleoperation studies), the execution of everyday life tasks that require decoding of complete trajectories, is of paramount importance. Thus, a specification for any proposed methodology, should be to address the issues of continuous and smooth control.

Regarding the continuous EMG based control approach, various techniques have been used to provide estimates of human kinematics based on human myoelectric activity. Some of them are; the Hill-based musculoskeletal model, the state-space model, artificial neural network based models, support vector regression based models and random forests based models. The Hill-based musculoskeletal model [24] is the most commonly used model, for continuous EMG based control of robotic devices, using human motion decoded from EMG signals. Some applications of the Hill-based model can be found in [14] and [25–28]. However the aforementioned Hill model based studies, typically focus on few degrees of freedom (DoFs), because Hill model equations are non-linear and there is a large number of unknown parameters per muscle. State-space models were used by Artemiadis et al. in [2, 29] and [30]. In [29], a state-space model was used to estimate human arm kinematics from the myoelectric activity os muscles of the upper-arm and the forearm, while emphasis was given to the non-stationarity of the EMG signals and the evolution of signal quality over time (i.e., due to muscle fatigue, sweat etc.). In [2] and [30] authors proposed a methodology that "maps" muscular activations to human arm motion, using a state space model and the low dimensional embeddings of the myoelectric activity (input) and kinematics (output). Artificial neural networks (ANN) were used in [31] to estimate the continuous motion of the human fingers, using the myoelectric activity of forearm muscles (only one degree of freedom per finger was decoded), in [32] to control using EMG signals a robot arm with one degree of freedom and in [33] to decode from EMG signals human arm motion, restricting the analyzed movements to single-joint isometric motions.

All the aforementioned studies, addressed the issue of EMG based continuous human motion estimation, but none of them focused on the full human arm-hand system coordination. A Support Vector Machines (SVM) based regressor was used in [3] to decode full arm hand system kinematics. However, only the position and orientation of the human end-effector (wrist) and one DoF for the human grasp, were decoded. Such a choice limits method's applicability to everyday life scenarios, where independent finger motions are of paramount importance. Finally the latter method requires smooth and slow movements from the user.

In [34, 35] and [36], we proposed a learning scheme that combines a classifier with a regressor to perform task-specific EMG-based human motion estimation for reach to grasp movements. Principal Component Analysis (PCA) was applied to extract the low dimensional manifolds of the EMG activity and human motion. These low dimensional spaces, were used to train different task-specific models, formulating a regression problem. The scheme was used to discriminate first the task to be executed and trigger then a task-specific EMG based motion decoding model, which achieves better estimation results than "general" models. The estimated output was back projected in the high dimensional space (27 DoFs) to provide an accurate estimate of the full human arm-hand system motion. A similar methodology was recently proposed in [37], where classification techniques were used in order to discriminate between reach to grasp movements towards objects of different sizes and weights. Recently, we extended the learning scheme proposed in [36], in order to discriminate also the "task to be executed", as well as to perform efficient features selection with random forests [38]. The final scheme discriminates three different task features: position to move towards, object to be grasped and task to be executed (with the object). The scheme consists once again of a classifier combined with a regressor. The classifier uses sEMG to discriminate between different reach to grasp tasks, in the m-dimensional space (where m is the number of EMG channels) of myoelectric activations, while the regressor is used to train models for every possible task. Then based on the classification decision, an appropriate EMG-based task-specific motion decoding model, can be triggered. The regression problem is once again formulated using the low-d spaces of the human EMG signals (input) and the human motion (output). It must be noted that for these last five studies the classification accuracy constantly increases – as the reach to grasp movement evolves – providing always an early decision (at the beginning of reach to grasp movement) of the task to be executed.

In this chapter we formulate a complete learning scheme for EMG based interfaces, that takes advantage of a classifier which is combined with a regressor. The classifier and the regressor cooperate advantageously in order to split the task space and provide better estimation accuracy, with task specific models. The whole scheme is based on the random forests methodology for classification and regression. EMG signals are used to discriminate different reach to grasp movements in 3D space. Task specificity is introduced in three different levels, suggesting that the myoelectric activity differentiates; between reach to grasp movements towards different subspaces, between reach to grasp movements towards different objects, as well as between reach to grasp movements towards a specific object placed at a specific position, but with the intention to perform different tasks while the object is grasped. The classifier uses the human myoelectric activity, to discriminate between those different reach to grasp movements in the m-dimensional space of the EMG signals (m is the number of channels). The regressor is first used to train task-specific models for all possible tasks, so as for a task-specific model to be triggered, based on the classification decision. Classification decision is taken at a frequency of 1 kHz, enabling our scheme to identify the task in real time. The proposed scheme can provide continuous estimates of the full human arm hand system kinematics (27 DoFs modeled, 7 for the human arm and 20 for the human hand). Those estimates can be used by a series of EMG based interfaces.

The rest of the chapter is organized as follows: Sect. 1.2 analyzes the apparatus and the experiments conducted, Sect. 1.3 focuses on the different methods used to formulate the proposed EMG-based learning scheme, results for EMG based classification and task specific EMG based motion estimation are presented in Sect. 1.4, while Sect. 1.5 concludes the chapter.

1.2 Apparatus and Experiments

1.2.1 Experimental Protocol

Two different types of experiments were conducted for the formulation of the proposed learning scheme. All experiments were performed by five (4 male, 1 female) healthy subjects 21, 24, 27, 28 and 40 years old. The subjects gave informed consent of the experimental procedure and the experiments were approved by the Institutional Review Board of the National Technical University of Athens. Experiments were performed by all subjects, using their dominant hand (right hand for all subjects involved).

During experiments the subjects were instructed to perform different reach to grasp movements in 3D space, to reach and grasp different objects placed at different positions, in order to execute different tasks with the grasped objects. The object positions were marked on different shelves of a bookcase, as depicted in Fig. 1.1.

The first type of experiments, involved reach to grasp movements towards different positions (five different positions depicted in Fig. 1.1) and different objects (a mug, a rectangular shaped object and a marker) and was used for EMG-based "subspace discrimination" and "object discrimination". The second type of experiments, involved reach to grasp movements towards specific positions and objects, in order to execute two different tasks (two classes), with the same object. A tall glass, a wine glass, a mug and a mug plate were used for the second type of task discrimination experiments. The first experiments were used for the initial formulation of the learning framework proposed in [34] and were once again used in [38] together with the second type of experiments, to discriminate between different tasks and compute feature variables importance for different positions, objects and tasks.

The tasks executed for the second type of experiments appear in Fig. 1.2. During the experiments, each subject conducted several trials, for each position, object and task combination. In order to ensure data quality and avoid fatigue, adequate resting time of 1 min, was used between consecutive trials.

1.2.2 Motion Data Acquisition

In order to capture efficiently human kinematics – using appropriate motion capture systems – the kinematic models of the human arm and the human hand must

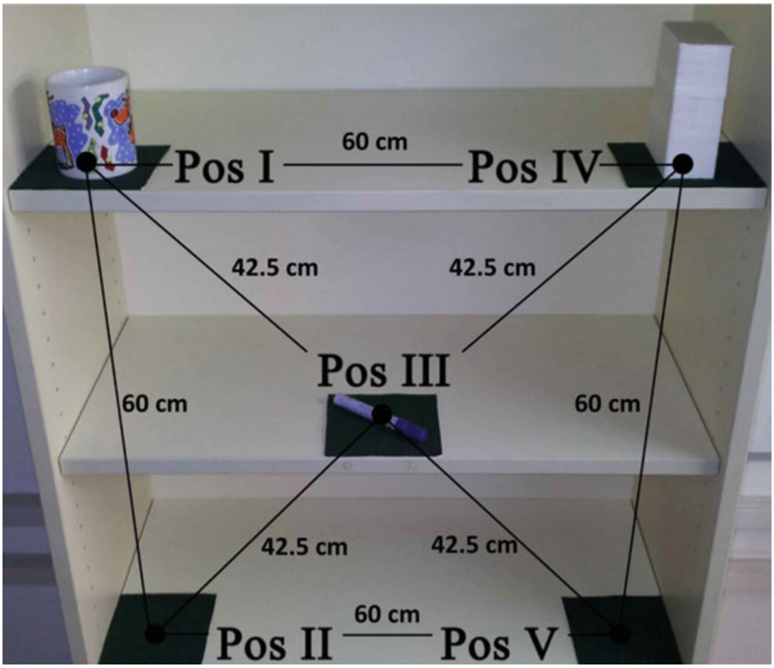

Fig. 1.1 A bookcase containing three different objects (a marker, a rectangular-shaped object and a mug), placed at five different positions, at three different shelves, is depicted. A superimposed diagram presents the distances between the different object positions. These five positions were used for both types of experiments

Fig. 1.2 Tasks executed for the second type of experiments. The tall glass tasks were: task 1, side grasp (to drink from it) and task 2, front grasp (to transpose it). The wine glass tasks were: task 1, side grasp (to drink from it) and task 2, stem grasp (to drink from it). The mug tasks were: task 1, handle grasp (to drink from it) and task 2, top grasp (to transpose it). Finally the mug plate tasks were: task 1, side grasp (to lift and hold it) and task 2, top grasp (to transpose it)

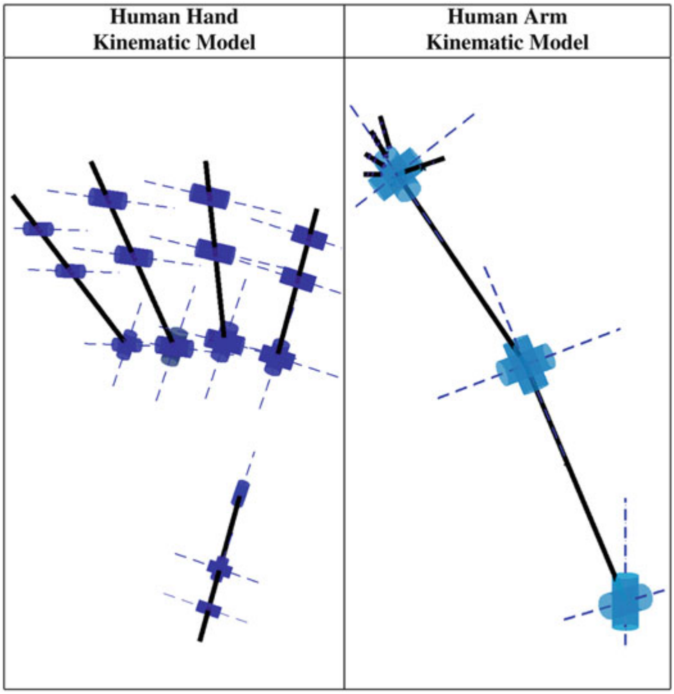

Fig. 1.3 Kinematic models depicting the degrees of freedom (DoFs) of the human arm and hand

be described. The kinematic model of the human arm, that we use in this study, consists of three rotational degrees of freedom (DoFs) to model shoulder joint, one rotational DoF for elbow joint, one rotational DoF for pronation-supination and two rotational DoFs for wrist flexion/extension and abduction/adduction. The kinematic model of the human hand consists of 20 rotational DoFs, 4 for each one of the 5 fingers. Regarding fingers we used for the four kinematically identical fingers (index, middle, ring and pinky) three rotational DoFs to model flexion-extension of the different joints and one rotational DoF for abduction-adduction. Human thumb is modeled, using two rotational DoFs for flexion-extension, one rotational DoF for abduction-adduction and one rotational DoF to describe palm's mobility that allows thumb to oppose to other fingers. The kinematic models of the human arm and hand are presented in Fig. 1.3.

In order to capture the human arm hand system motion in 3D space, extracting the corresponding joint angles (27 modeled DoFs), we used a dataglove for the human hand and a magnetic position tracking system for the human arm. The Isotrak II® (Polhemus Inc.) magnetic motion capture system used, is equipped with two position tracking sensors and a reference system. The two sensors of Isotrak II, were placed on the elbow and the wrist respectively, while the reference system was placed on the user's shoulder. Having captured the positions of the human shoulder, elbow and wrist, the inverse kinematics of the human arm can

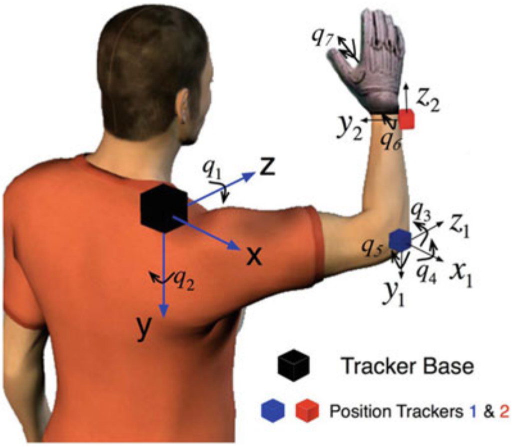

Fig. 1.4 Two position tracking sensors of Isotrak II are used to capture user's shoulder, elbow and wrist position in 3D space, while a dataglove is used to capture the wrist and fingers joint angles. The position tracker reference system is placed on the shoulder. The human arm joint values can be computed through the human arm's inverse kinematics. q_1 and q_2 jointly correspond to shoulder flexion-extension and adduction-abduction, q_3 to shoulder internal-external rotation, q_4 to elbow flexion-extension, q_5 to pronation-supination and q_6 and q_7 jointly correspond to wrist flexion-extension and adduction-abduction

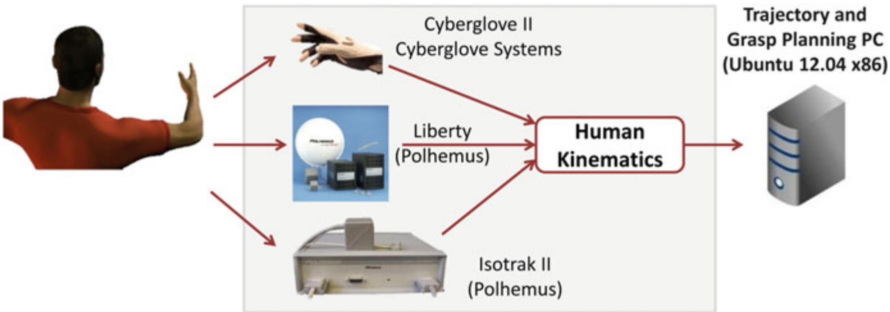

Fig. 1.5 Different motion capture systems, used to capture human arm hand system motion, are depicted

be computed, following the directions provided in [39]. Alternatively for human robot interaction applications, a human to robot motion mapping procedure like the one proposed in [40], can be used. Regarding the human hand, the Cyberglove II® (Cyberglove Systems), is used to measure the 2 DoFs of the wrist (flexion-extension and abduction-adduction) and the 20 DoFs of the human fingers. The experimental setup that was used to track human arm hand system kinematics, is depicted in Fig. 1.4 and the different motion capture systems are depicted in Fig. 1.5.

1.2.3 Electrode Positioning and EMG Data Acquisition

In total, we recorded the myoelectric activity of 16 muscles, of the upper arm (8 muscles) and the forearm (8 flexor and extensor muscles). More specifically the chosen muscles are: flexor pollicis longus, flexor digitorum superficialis, flexor carpi ulnaris, flexor carpi radialis, extensor pollicis longus, extensor indicis, extensor carpi ulnaris, extensor carpi radialis, deltoid anterior, deltoid posterior, deltoid middle, trapezius, teres major, brachioradialis, biceps brachii and triceps brachii. The selection of the muscles and the placement of the surface electromyography electrodes, was based on the related literature [16, 41]. In order to achieve easy, portable and fast to use training schemes several researchers have chosen to place the EMG electrodes, in specific regions but in random (not precise) positions [3]. We believe that the next generation of epidermal electronics [42] will make the electrode positioning faster and easier, thus we choose to take advantage of the higher signal to noise ratio, that accurate electrode positioning offers.

EMG signals were acquired and conditioned using an EMG system (Bagnoli-16®, Delsys Inc.), equipped with single differential surface EMG electrodes (DE-2.1®, Delsys Inc.). A signal acquisition board (NI-DAQ 6036E®, National Instruments), was used for signal digitization and data acquisition.

1.2.4 EMG and Motion Data Processing

Regarding data processing, EMG signals were band-pass filtered (20–450 Hz), sampled at 1 kHz, full-wave rectified and low-pass filtered (Butterworth, fourth order, 8 Hz), while for the position measurements, which were provided by the position tracking system at the frequency of 30 Hz, an antialiasing finite-impulse-response filter (low pass, order: 24, cutoff frequency: 100 Hz), was used to resample them at a frequency of 1 kHz (same as the sampling frequency of the EMG signals).

1.2.5 Muscular Co-activation Patterns Extraction

After data collection, all EMG recordings, were pre-processed and epochs of data were created. Those epochs included the different reach-to-grasp movements captured during the experiments. Then, all data were resampled at 100 Hz, where each sample at the new frequency (100 Hz) was calculated as the mean value of ten (10) samples of the original frequency (1 kHz). Based on the profiles of the rectified EMG signals at the new frequency, the onset of muscular activations was defined comparing the amplitude of each muscle's myoelectric activation to it's relaxed state. Finally, epochs including only muscular activations captured during the actual

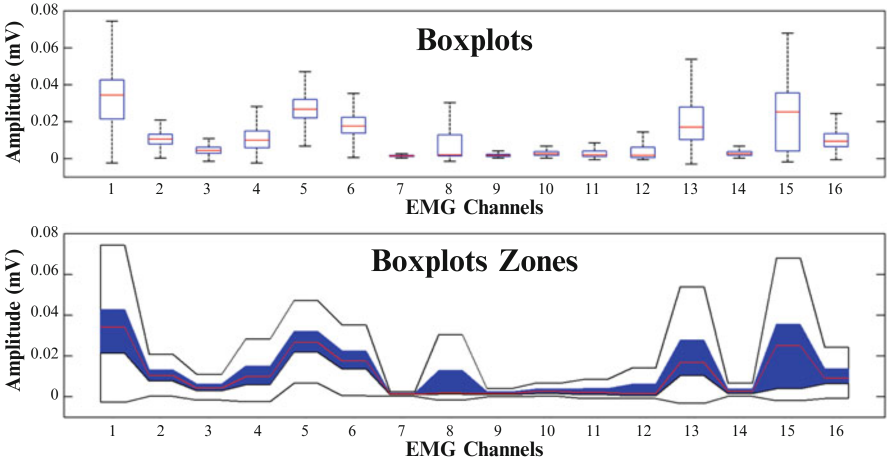

Fig. 1.6 Comparison of a Boxplot and a "Boxplot Zone" visualization of muscular co-activation patterns across sixteen (16) muscles of the upper arm and the forearm for one subject (Subject 1), performing reach to grasp movements towards a mug placed at position I

tasks were created, and were used to formulate synergistic profiles, using a novel statistical representation technique, that we introduced and which we call "Boxplot Zones".

A boxplot (alt. box-and-whisker plot) is a method to graphically depict groups of numerical data, through the following five-number summaries: smallest observation (sample minimum), lower quartile (Q1), median (Q2), upper quartile (Q3), and largest observation (sample maximum). Boxplot zones were first defined in [34] to visualize muscular co-activation patterns and are an equivalent of boxplots, while more visually informative representation, suitable for the representation of synergistic profiles. Boxplot zones consist of three different layers. The first layer includes the median line, connecting the medians of all boxplots. The second layer includes the box zone (blue zone), connecting the boxes that contain all the values between the lower and the upper quartile, while the third layer includes the whisker zone (white zone), connecting the whiskers that mark the largest and the smallest observation. A direct comparison of a boxplot and a boxplot zone visualization, can be found in Fig. 1.6.

In Fig. 1.7 we present a "boxplot zones" based visualization of muscular co-activation patterns of sixteen (16) muscles (of the upper arm and the forearm), for one subject (Subject 1) executing reach to grasp movements, towards five (5) different positions in 3D space, to grasp three (3) different objects. The muscular co-activation patterns presented in Fig. 1.7 in terms of synergistic profiles formulated with boxplot zones, depict a significant differentiation between the different reach-to-grasp movements, although the same joints of the arm hand system (human upper arm joints and human hand finger joints) are involved, but for a different task. More precisely, if we examine the synergistic profiles (muscular co-activation patterns)

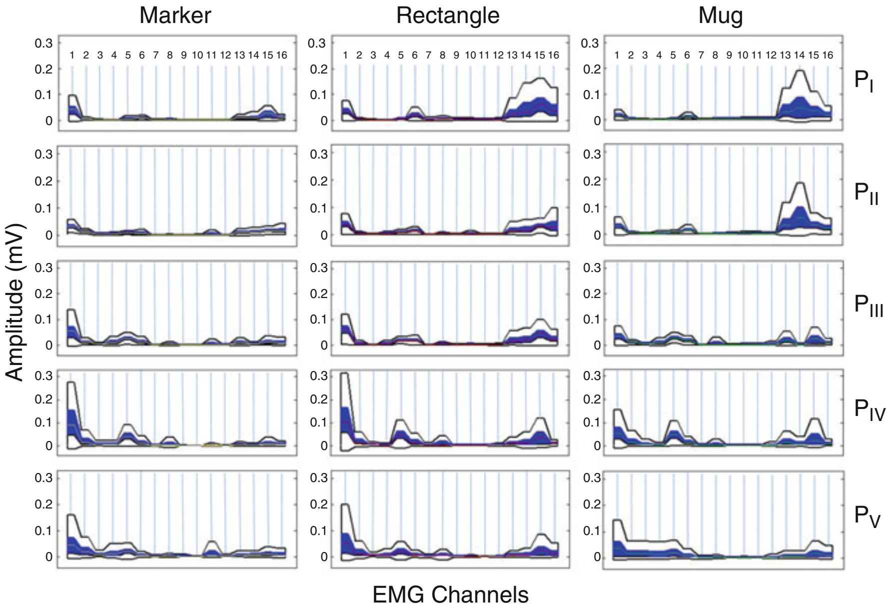

Fig. 1.7 "Boxplot Zones" visualization of muscular co-activation patterns of sixteen (16) muscles (of the upper arm and the forearm), for one subject (Subject 1) performing reach to grasp movements towards, five different positions (P_I, P_{II}, P_{III}, P_{IV} and P_V) in 3D space, to grasp three different objects (a marker, a rectangle and a mug). The sixteen (16) muscles are reported in the following order (1–16): deltoid anterior, deltoid middle, deltoid posterior, teres major, trapezius, biceps brachi, brachioradialis, triceps brachii, flexor pollicis longus, flexor digitorum superficialis, flexor carpi ulnaris, flexor carpi radialis, extensor pollicis longus, extensor indicis, extensor carpi ulnaris and extensor carpi radialis

across different subspaces (different positions), we notice that the activity of the muscles of the upper-arm (EMG channels 1–8) reflects most of the differentiation. In contrast, if we examine the muscular co-activation patterns across different objects, placed in the same subspace (a specific position), the activity of the muscles of the forearm (EMG channels 9–16) reflects most of the differentiation.

In Fig. 1.8 we present a "boxplot-zones" based visualization of muscular co-activation patterns differentiation, for 16 muscles of the human upper-arm and fore-arm, for 3 different subjects performing different reach to grasp movements, towards five (5) different positions in 3D space, to grasp a specific object (rectangular-shaped object).

As we have already noted there is a significant differentiation between muscular co-activation patterns associated with different reach to grasp movements. Statistical significance of muscular co-activation patterns differentiation, can be assessed using appropriate statistical tests. More precisely the Lilliefors test (adaptation of the Kolmogorov-Smirnov test) was used to test the null hypothesis that the EMG data – containing the myoelectric activations – come from a normal distribution. The test rejects the null hypothesis at the 5 % significance level ($p = 0.05$), so the

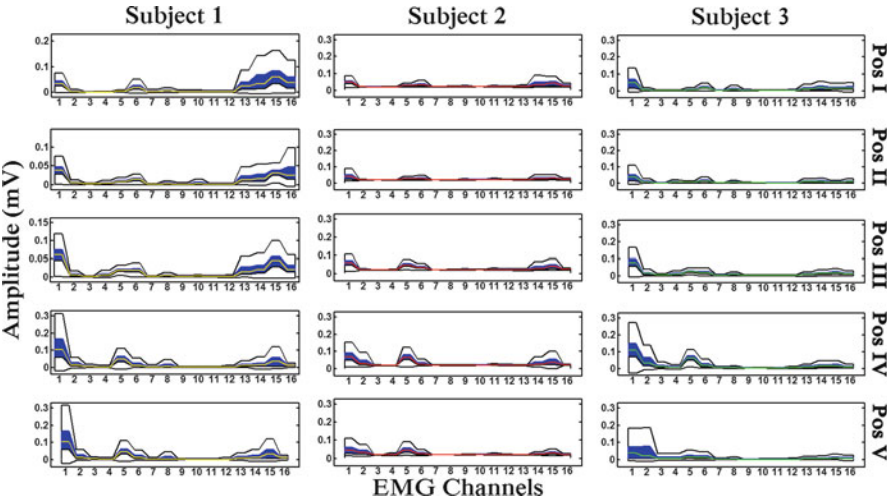

Fig. 1.8 "Boxplot Zones" visualization of different muscular co-activation patterns of sixteen (16) muscles of the upper arm and the forearm, for three (3) different subjects performing reach to grasp movements towards, the aforementioned five (5) positions in 3D space, to grasp a specific object (a rectangle)

data are not normally distributed. Thus, we use non parametric tests such as, the Kruskal-Wallis and the Wilcoxon rank sum test, in order to assess the significance of muscular co-activation patterns differentiation, for different strategies.

The Kruskal-Wallis compares the medians of the myoelectric activity of the selected muscles, for different muscular co-activation patterns, and returns the p value for the null hypothesis that all samples are drawn, from the same population (or from different populations with the same distribution). The Wilcoxon rank sum test, performs a two-sided rank sum test of the null hypothesis that data of myoelectric activations with different muscular co-activation patterns, are independent samples from identical continuous distributions, with equal medians.

More details regarding the statistical procedures used, the reader can find in [43]. All tests were performed to check the differentiation of muscular co-activation patterns for the following three cases:

- For the same reach to grasp movement, between different subjects.
- For reach to grasp movements towards five different positions in 3D space.
- For reach to grasp movements towards three different objects, placed at a specific position in 3D space.

For all sets, confidence levels were set at 95 %. All tests null hypotheses for all three cases were rejected, proving that muscular co-activation patterns differentiate, between different subjects and between different tasks. In Fig. 1.9, we present the means and the confidence intervals of EMG activity across eight muscles of the upper arm and eight muscles of the forearm, for a subject performing reach to grasp movements, towards three (3) different objects. In Fig. 1.10, we present the means

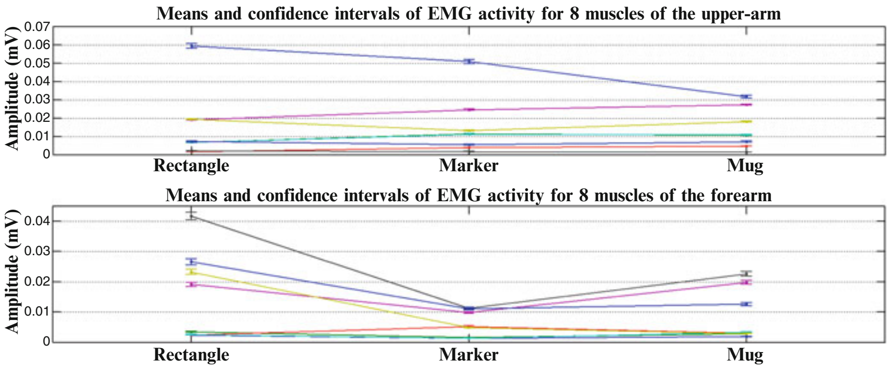

Fig. 1.9 Means and confidence intervals of EMG activity across eight (8) muscles of the upper arm and eight (8) flexor and extensor muscles of the forearm, for one subject (Subject 1) performing reach to grasp movements, towards three (3) different objects, placed at a specific position (Pos 3) in 3D space

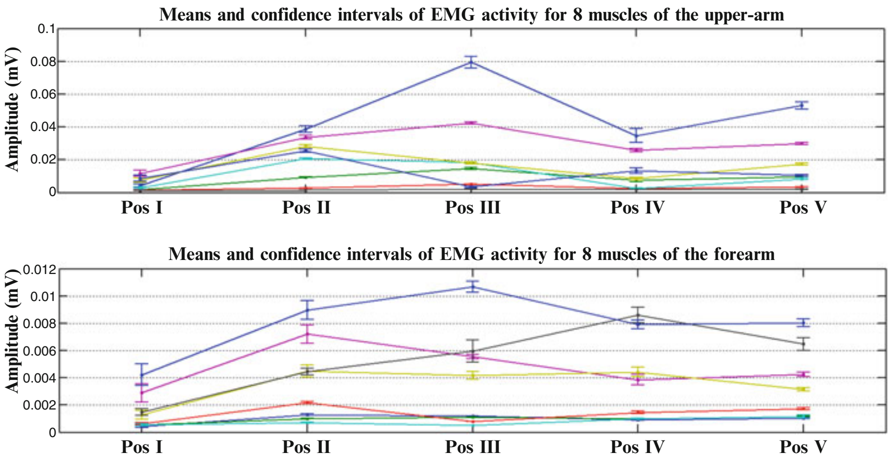

Fig. 1.10 Means and confidence intervals of EMG activity across eight (8) muscles of the upper arm and eight (8) flexor and extensor muscles of the forearm, for one subject (Subject 1) performing reach to grasp movements, towards a marker, placed at five (5) different positions in 3D space

and the confidence intervals of EMG activity across eight muscles of the upper arm and eight muscles of the forearm for a subject performing reach to grasp movements, towards a marker, placed at five (5) different positions in 3D space.

Therefore, we conclude that the muscular co-activation patterns vary significantly not only between different subjects, but also between different reach-to-grasp movements of the same subject (towards different subspaces or different objects placed at specific position), and therefore should be considered and analyzed as subject-specific and task-specific characteristics.

1.3 Methods

In this section we present some typical specifications for EMG based interfaces and we describe the problem formulation and the methods used for discrimination of different muscular co-activation patterns, associated with different reach to grasp movements (classification) and EMG based motion estimation (regression).

1.3.1 Classification and Regression Modules

Some specifications that every EMG-based learning scheme should have, are:

- To be able to “decide” on user’s intention (classification part).
- To decode a continuous representation of human motion (regression part).
- To allow its application at a robot control scheme, in real time.
- To be easy and fast to be trained for different users (as musculoskeletal characteristics may vary significantly across subjects).
- To be able to handle multidimensional spaces and large databases of myoelectric and motion data.

In this chapter we present an EMG-based learning scheme, using the Random Forests (RF) technique – which meets the aforementioned specifications – for both classification and regression. Thus, the classifier and the regressor cooperate advantageously, in order to split the task space and confront the non-linear relationship between the EMG signals the motion to be estimated, with task specific models that provide better estimation accuracy than the “general” models (built for all tasks).

In Fig. 1.11 we present a block diagram of a typical random forests based classification procedure. Random forests are used for a multiclass classification problem, where we need to discriminate between reach to grasp movements, towards different positions, different objects (to be grasped) and different tasks (to be executed with the object) in 3D space, using human myoelectric activity (EMG).

In Fig. 1.12 we present the block diagram for a typical random forests based regression procedure. The task specific models trained are used to estimate for new EMG data (not previously seen during training) “new” human arm hand system kinematics.

A complete block diagram of the EMG-based learning scheme proposed, is depicted in Fig. 1.13. Two main modules appear, the classification module and the task specific model selection module. Classification module provides decision for subspace to move towards, object to be grasped and task to be executed (with the object). Task specific model selection module, examines classification decisions and triggers a subspace, object and task specific motion decoding model.

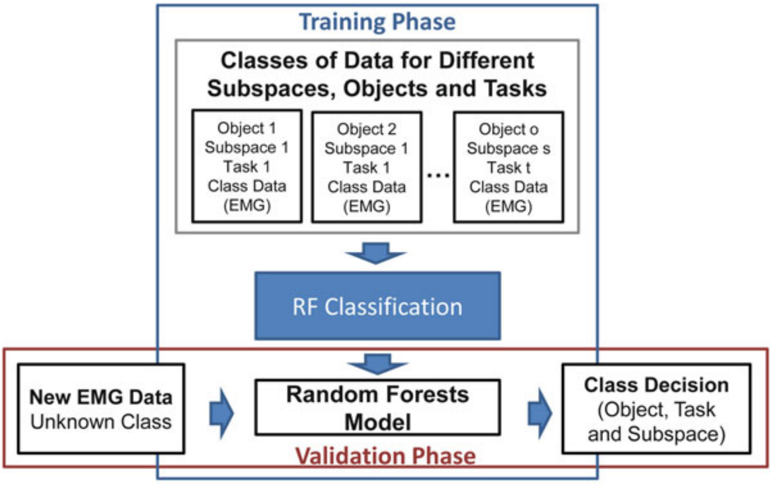

Fig. 1.11 Block diagram of the classification procedure

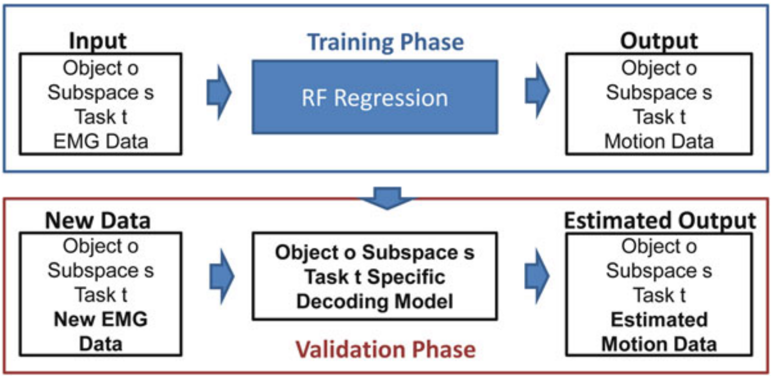

Fig. 1.12 Block diagram of the regression procedure

1.3.2 Multiclass Classification in the m-Dimensional Space of Myoelectric Activations (m-Number of EMG Channels)

As we have already noted, synergistic profiles depicted in terms of "boxplot zones" in Fig. 1.7 denote that there is a significant differentiation of muscular co-activation patterns for reach to grasp movements towards different positions and different objects placed at the same position. In order to be able to take advantage of this differentiation, we choose to discriminate the different reach to grasp movements

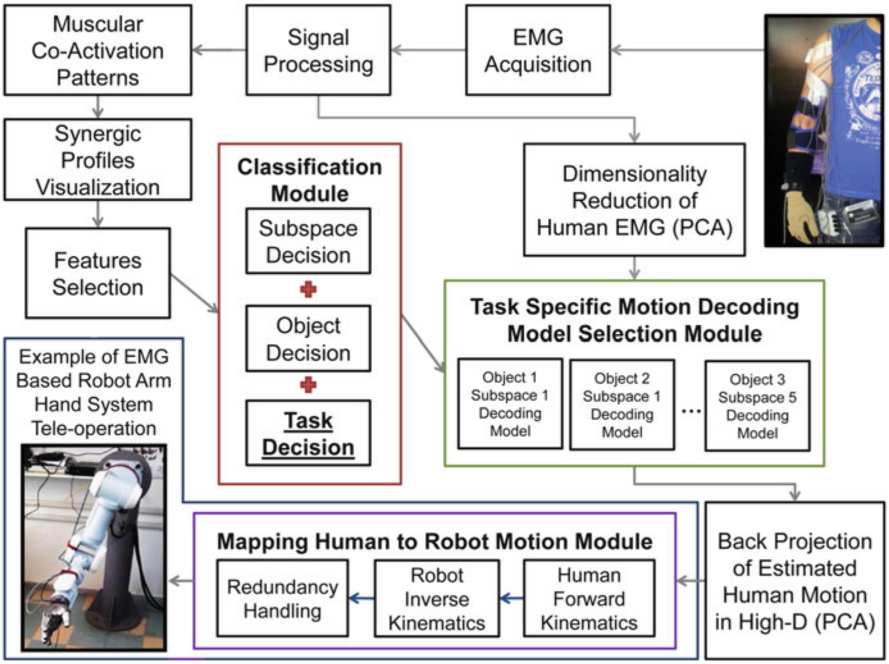

Fig. 1.13 A block diagram of the proposed EMG-based learning scheme is presented. Two main modules, formulate the "backbone" of the learning scheme, the classification module and the task specific model selection module. Classification module (based on the classifier) provides decision for subspace to move towards, object to be grasped and task to be executed with the object. Task specific model selection module (based on the regressor) examines classification decisions and triggers a subspace, object and task specific motion decoding model (from all possible models trained). The task specific motion decoding model efficiently estimates the full human arm hand system motion (27 joint values), using human myoelectric activity (EMG signals). Finally an EMG-based interface can take advantage of the proposed scheme and the estimated human motion. For example a human to robot motion mapping procedure may take as input the estimated human arm hand system motion, to generate equivalent robot motion, as described in [40]. A possible application of the proposed learning scheme, is the EMG-based teleoperation of a robot arm hand system

in the m-dimensional space of the myoelectric activations (where m is the number of EMG channels), using the EMG signals to "decide" on the task to be performed (human intention decoding).

In Fig. 1.14 we present a typical classification problem of discriminating based on the myoelectric activity of 16 muscles of the human arm hand system, two different strategies for reaching and grasping a specific object placed in two different positions. Reaching, grasping and return phases are depicted. The top subplot presents the distance between the two classes in the 16-dimensional space (16 EMG channels are used). Such a distance, give us a measure of classes separability (i.e., how easily these classes can be discriminated). The bottom subplot, presents the evolution of classification decision over time. The accumulation of misclassified

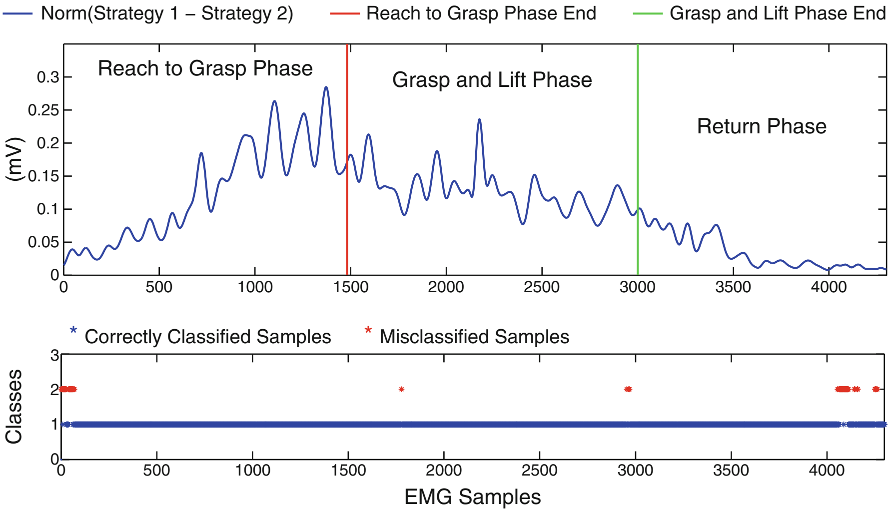

Fig. 1.14 Comparison of two reach to grasp movements towards a marker placed at position I (Strategy I) and a marker placed at position II (Strategy II). First subplot presents the distance of the two strategies in the m-dimensional space (where m = 16 the number of the EMG channels). The second subplot focuses on the evolution of classification decision per sample, over time

samples is reasonable for those time periods, when the distance between the two classes is small (i.e. begin and end of experiments, when human end-effector (wrist), is close to its starting position).

In Fig. 1.15 we present the classification problem of discriminating two different reach to grasp movements, towards a specific object placed at a specific position, but in order to execute two different tasks (with the object). Once again, top subplot presents the distance between the two classes in the 15-dimensional space (15 EMG channels are used), as well as the reaching, grasping and return phases. Bottom subplot presents once again the evolution of the classification decision and there is a similar with Fig. 1.14, accumulation of misclassified samples for the time periods, that the distance between the two tasks is small (i.e. begin and end of the experiment).

1.3.2.1 Random Forests Classifier

The Random Forests technique proposed by Tin Kam Ho of Bell Labs [44] and Leo Breiman [45], can be used for classification creating an ensemble classifier that consists of many decision trees. The Random Forests classifier's output, is the class that is the mode of the individual trees class's output. Thus, the classifier consists of a collection of tree structured classifiers $\{h(\mathbf{x}, \Theta_N), N = 1, \ldots\}$ where $\{\Theta_N\}$ are independent identically distributed random vectors. Each decision tree of the random forest, casts a vote for the most popular class at input $\mathbf{x}$.

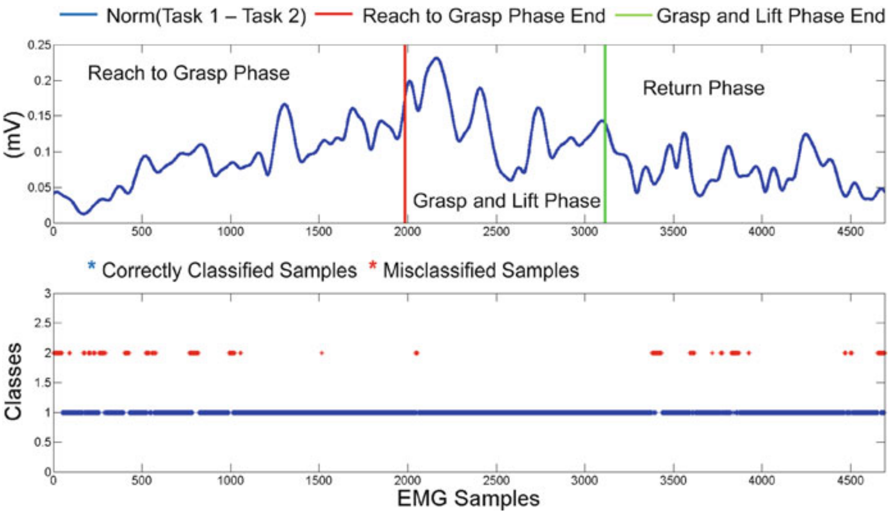

Fig. 1.15 Comparison of two reach to grasp movements, towards Position I to grasp a tall glass with two different grasps (side grasp and front grasp), to execute two different tasks. First subplot presents the distance of the two tasks in the m-dimensional space (where $m = 15$ the number of the EMG channels). The second subplot focuses on the evolution of classification decision per sample, over time

The classification procedure for N trees grown is presented in Fig. 1.16. Some advantages of the random forests technique for classification are:

- Runs efficiently and fast on large databases.
- Provides high accuracy.
- Does not overfit.
- Provides feature variables importance.
- Can handle thousands of input variables without variable deletion.
- Can handle multiclass classification problems.
- Can be used efficiently in multidimensional spaces.

1.4 Features Selection with Random Forests

In the aforementioned classification examples we used the random forests technique to discriminate, between different reach to grasp movements in the m-dimensional space of the myoelectric activations, using multiple EMG channels (m is 15 or 16). Its quite typical for EMG based interfaces, a limited number of EMG channels to be available (e.g., due to cost or complexity limitations), or EMG electrodes positioning to be not precise (some EMG channels may be more noisy). Thus, a fundamental question is: “Is it possible to select which EMG channels are the

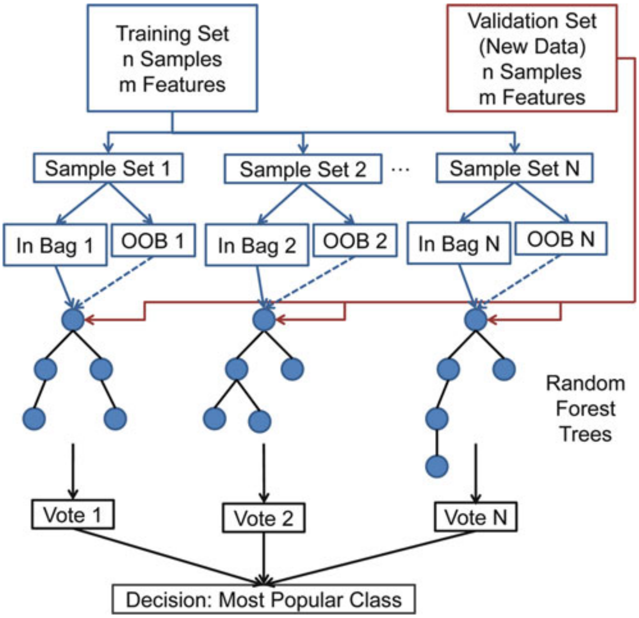

Fig. 1.16 Random forests based classification procedure for N trees grown. OOB stands for out-of-bag samples

most important? How this features selection can be accomplished?". With Random Forests we can perform efficient features selection, using their ability to compute the importance score of each feature variable and consequently access the relative importance for all feature variables (e.g., EMG channels).

More precisely random forests use for the construction of each tree, a different bootstrap sample set from the original data. One-third of the samples are left out of the bootstrap sample set (out-of-bag samples) and are not used in the construction of the Nth tree. Feature variables importance, is computed as follows; in every grown tree in the forest, we put down the out-of-bag samples and count the number of votes cast for the correct class. Then the values of a variable m are randomly permuted in the out-of-bag samples and these samples are put down the tree. Subtracting the number of votes casted for the correct class in the m-variable permuted out-of-bag data from the previously computed number of votes for the correct class in the untouched out-of-bag data, we get the importance score of a feature variable m for each tree. The raw importance score for each feature variable m is the average importance score for all trees of the random forest. The random forests feature variable importance calculation procedure, is depicted in Fig. 1.17.

In case that we want to reduce the number of EMG channels used (in this study we have already used 15 and 16 EMG channels), random forests can be initially run with all the variables (EMG channels) and then run once again with the most important variables selected during the first run. For example, we can use the

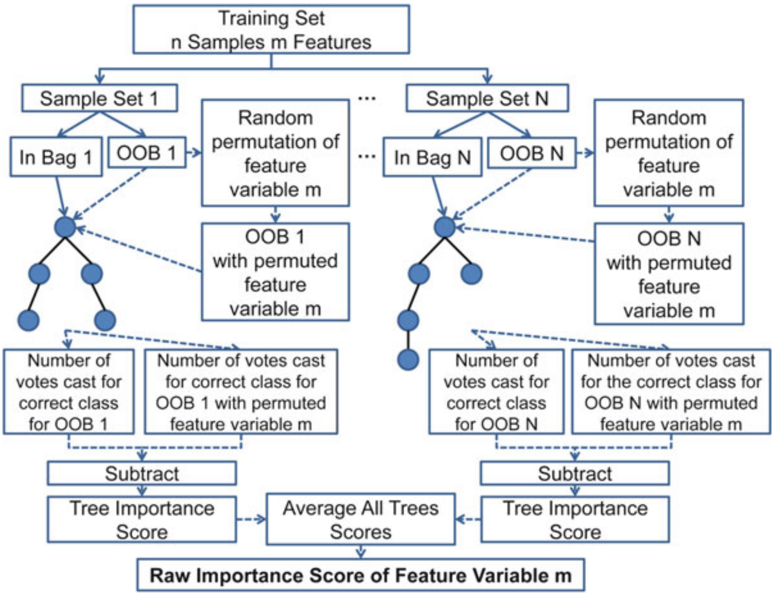

Fig. 1.17 Diagram of the random forests feature variable importance calculation procedure. OOB stands for out-of-bag samples

random forests classifier with all 15 EMG channels, compute the feature variables importance and re-solve the classification problem, using the most "important" EMG channels. Before doing so, we present the feature variables importance for the problems of discriminating from EMG signals, reach to grasp movements towards, different subspaces, different objects and different tasks.

In Fig. 1.18 we present the importance plots of different feature variables (EMG channels), for two different cases, subspace discrimination and object discrimination. We can notice that for subspace discrimination, the feature variables corresponding to upper-arm muscles (first 8 EMG channels) appear to have increased importance, while for object discrimination the feature variables corresponding to the forearm muscles (last 8 EMG channels), accumulate most of the importance.

This latter evidence can also be verified by the fact that for reach to grasp movements towards different subspaces, the muscular co-activation patterns of the upper-arm muscles accumulate most of the differentiation, while for reach to grasp movements towards different objects, the muscular co-activation patterns of the forearm muscles (responsible for grasping), accumulate most of the differentiation. More details can be found in [34].

In Fig. 1.19 we present the importance plots for different feature variables (EMG channels), for task discrimination. Four different barplots are depicted, that contain the importance scores per variable for different objects placed in position I. We can notice that the feature variables corresponding to the forearm muscles (last 8 EMG channels) appear to have once again increased importance

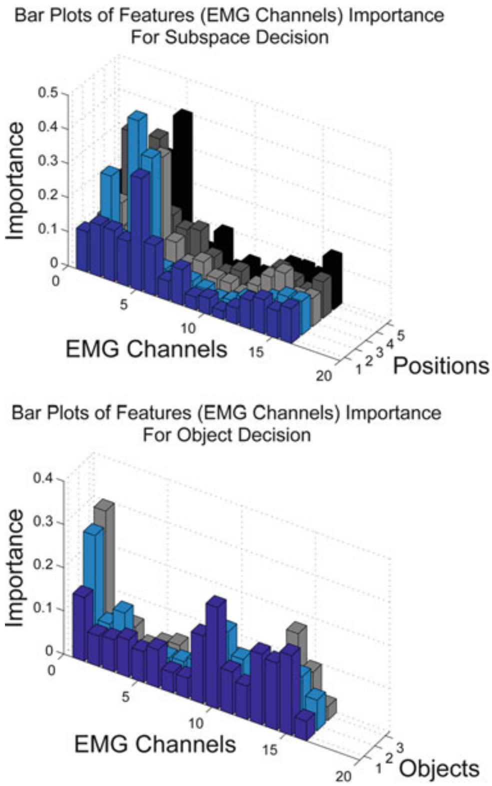

Fig. 1.18 Importance plots of feature variables (EMG channels) – expressed as mean decrease in accuracy – for Subject I, for subspace and object discrimination respectively. For subspace discrimination data involving all objects are used, while for object discrimination, a specific position is used (Pos I). Positions 1–5 correspond to positions Pos I to Pos V. Objects 1, 2 and 3 correspond to mug, marker and rectangle respectively

(similarly to object discrimination), since the forearm muscles are responsible for hand preshaping, in order to grasp and/or manipulate objects.

1.4.1 Task Specific Motion Decoding Models

1.4.1.1 Task Specific EMG Based Motion Decoding Models Based on Random Forests Regression

The Random Forests technique can also be used for regression, growing trees depending on a random vector Θ such that the tree predictor $h(\mathbf{x}, \Theta)$ takes on numerical values (not class labels used for classification). The random forest predictor, is formed similarly to the classification case, as appeared in Fig. 1.16, by taking instead of the most popular class, the average over the N trees of the forest $\{h(\mathbf{x}, \Theta_N)\}$.

Some advantages of the random forests regression are the following:

- Are easily implemented and trained.
- Are very fast in terms of time spent for training and prediction.

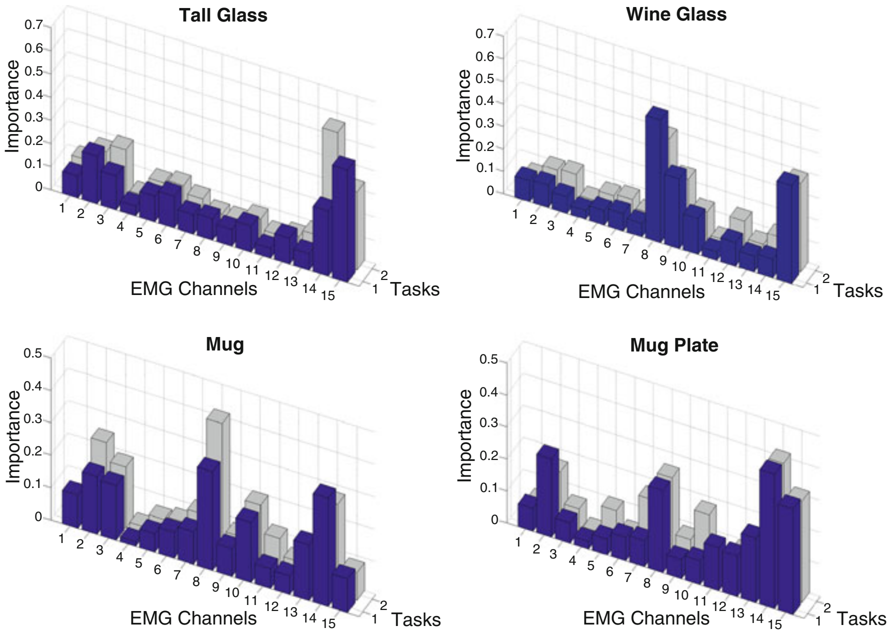

Fig. 1.19 Importance plots of feature variables (EMG channels) for task discrimination. Reach to grasp movements towards all objects placed in Position I were performed, so as to execute two different tasks per object. A list of the tasks executed can be found in Fig. 1.2

- Can be parallelized.
- Can handle thousands of input variables and run efficiently on large databases (similarly to classification).
- Are resistant to outliers.
- Have very good generalization properties.
- Can output more information than just class labels (e.g., sample proximities, visualization of output decision trees etc.).

1.4.1.2 Dimensionality Reduction

In order to formulate the regression problem used in this study, we need the low-dimensional spaces of the myoelectric activations and the human motion. Thus, in order to represent our data in low-d spaces, we used the Principal Components Analysis (PCA), dimensionality reduction method. For the EMG signals recorded, a 4-D space suffices, representing most of the original high-dimensional data variance (more than 92 %). Regarding the human arm hand system kinematics, a 4-D space once again suffices to describe adequately the 27-DoF motion of the human arm hand system, representing most (94 %) of the original data variance. We chose to use the PCA as a dimensionality reduction technique – in order to take advantage of the underlying covariance of our data – representing also the same variability in a low-d space, without losing important information of the original data. More details regarding the employment of PCA in EMG based interfaces, can be found in [2].

1.5 Results

1.5.1 Classifiers Comparison

In order to validate our hypothesis that random forests based classification is an ideal method for EMG based interfaces, we have applied a wide variety of classification techniques in our dataset, comparing them with random forests, in terms of classification accuracy and time required for training.

More precisely, we performed Support Vector Machines (SVM) based classification (with a Radial Basis Function (RBF) kernel), we constructed a single hidden-layer Neural Network (NN) with ten hidden units (trained with the Levenberg-Marquardt backpropagation algorithm) and we used the k nearest neighbors (kNN) classifier, for the simplest case where $k = 3$. Finally random forests were grown with ten trees for speed. Random Forests outperformed the classification performance of all other classifiers and performed quite well in terms of speed of execution. More details regarding the comparison of classification results, can be found in [34].

The classification success rate (classification accuracy) is defined, as the percentage of EMG data points classified to the correct reach to grasp movement. It must be noted that the classification is done for every acquired EMG data point, thus the proposed learning scheme is able to decide in real-time the reach to grasp movement to be performed (for a specific task), and even switch to different tasks online. All classification results presented in this section, are the average values over the five rounds, of the five-fold cross-validation method applied.

The training dataset that was used to compare classifiers in terms of speed of execution, involved Subject 1 data of reach to grasp movements towards different objects, placed at Position I (Class I) and Position II (Class II). Results are reported in Table 1.1. All benchmarks were performed using MATLAB (Mathworks) in a standard PC with Intel(R) Core(TM) I5 CPU 611 @3.33 GHz and 4 GB RAM (DDR3) memory.

The training dataset that was used to compare classifiers in terms of classification accuracy, involved Subject 1 data of reach to grasp movements towards two objects (two classes), placed across three different positions in 3D space. Results are reported in Table 1.2.

Table 1.1 Comparison of classifiers in terms of time required for training

Classifiers	Samples	Training time (s)
	2 classes of 1,500	0.011
LDA	2 classes of 15,000	0.058
	2 classes of 1,500	0.005
QDA	2 classes of 15,000	0.051
	2 classes of 1,500	0.014
kNN	2 classes of 15,000	1.65
	2 classes of 1,500	1.06
ANN	2 classes of 15,000	16.05
	2 classes of 1,500	0.34
SVM	2 classes of 15,000	7.09
	2 classes of 1,500	0.06
Random forests	2 classes of 15,000	0.87

Table 1.2 Comparison of classifiers for discriminating two different reach to grasp movements, towards two objects placed across three different positions in 3D space, for Subject 1

Classifiers	Positions	Mug (%)	Rectangle (%)
	Pos I	96.75	83.36
LDA	Pos III	96.50	90.40
	Pos V	91.44	95.00
	Pos I	95.34	80.52
QDA	Pos III	97.30	91.45
	Pos V	92.30	95.60
	Pos I	96.33	81.63
kNN	Pos III	98.20	94.50
	Pos V	96.50	98.68
	Pos I	94.67	84.63
ANN	Pos III	98.50	94.76
	Pos V	94.52	98.87
	Pos I	97.46	87.42
SVM	Pos III	98.81	94.50
	Pos V	98.00	96.50
	Pos I	99.67	89.02
Random forests	Pos III	100	96.50
	Pos V	98.87	99.00

1.5.2 Comparison of Different Decoding Methods

In order to validate our hypothesis that random forests based regression is an ideal method for EMG based interfaces, we have applied also a wide variety of regression techniques in our data, comparing them with random forests, in terms of estimation accuracy and time spent for training. More specifically we performed Multiple Linear Regression (MLR), we created a State-Space model as described in [2], we performed SVM regression (with a RBF kernel) and we constructed a single hidden layer Neural Network with ten hidden units (trained with the Levenberg-Marquardt backpropagation algorithm). Finally random forests were used as a regression technique, growing ten (10) decision trees, to increase speed of execution and computational efficiency.

Table 1.3 Time spend for the training procedure across different methods for a specific dataset (10,000 samples) that serves as a benchmark (average values)

Method	Time (s)
MLR	0.0054
State space	8.65
ANN	28.83
SVM	27.72
Random forests	5.89

Table 1.4 Comparison of different methods and estimation results, for specific position (Pos III) and specific object (Marker), for Subject 1. Average values for different validation set splittings

Method	Arm joints similarity (%)	Hand joints similarity (%)
MLR	81.60	84.31
State space	82.74	85.10
ANN	85.10	86.92
SVM	86.01	88.90
Random forests	86.93	90.42

The formulated regression problem, was to map the low-d space (4 dimensions) of the myoelectric activity (EMG signals), to the low-d space (4 dimensions) of the human motion. The low-d spaces of human myoelectric activations and human motion were extracted using the PCA method. Then the estimated low-d human motion was back-projected to the high-d space providing an estimate of the full human arm hand system kinematics (27 DoFs). As far as the estimation accuracy is concerned, we compared the methods for different datasets, estimating human motion for reach to grasp movements, towards different positions, as well as different objects placed at the same position.

Regarding training time, we chose to compare the different techniques in terms of time required for training, applying the various methods to a separate dataset, that serves as a benchmark. In Table 1.3, we can notice that random forests outperform most other techniques, in terms of speed of execution.

In Table 1.4 we can notice that random forests outperform also the other regression techniques, such as the Support Vector Machines (SVM) and the Artificial Neural Networks (ANN), in terms of estimation accuracy. In order to compare the different regressors a standard PC with an Intel(R) Core(TM) I5 CPU 611 @3.33 GHz, equipped with a 4 GB RAM (DDR3) memory, was once again used. The benchmark was performed using MATLAB (Mathworks). More information regarding the regression techniques comparison results, can be found in [35].

1.5.3 Classification Results

In Table 1.5, we present the classification results across different reach to grasp movements, for a specific position and three different objects (three classes) for all subjects, using the random forest method.

Table 1.5 Classification accuracy across different reach to grasp movements towards a specific position and three different objects (three classes), for all subjects (using random forests)

	Objects (Classes)		
Positions	Mug (%)	Marker (%)	Rectangle (%)
Pos I	87.82 (±4.52)	91.15 (±5.31)	88.82 (±4.63)
Pos II	84.24 (±5.99)	90.40 (±4.52)	91.81 (±5.41)
Pos III	84.78 (±5.78)	86.72 (±5.16)	85.39 (±4.95)
Pos IV	83.24 (±6.14)	84.17 (±6.21)	86.93 (±4.83)
Pos V	86.55 (±4.39)	89.32 (±3.81)	90.74 (±3.78)

Table 1.6 Classification accuracy across different reach to grasp movements, for a specific object and five different object positions (five classes), for all subjects (using random forests)

Positions	Objects		
(Classes)	Mug (%)	Marker (%)	Rectangle (%)
Pos I	86.01 (±4.16)	89.83 (±4.01)	87.01 (±6.57)
Pos II	83.76 (±6.24)	87.95 (±4.78)	88.43 (±5.51)
Pos III	89.74 (±3.41)	87.23 (±4.92)	90.30 (±4.01)
Pos IV	91.23 (±2.39)	90.05 (±4.86)	90.51 (±3.92)
Pos V	91.80 (±3.45)	92.34 (±2.69)	90.90 (±3.01)

Table 1.7 Classification accuracy across different reach to grasp movements towards different positions, for all objects and subjects (using random forests)

Positions				
Pos I (%)	Pos II (%)	Pos III (%)	Pos IV (%)	Pos V (%)
88.51	86.29	87.91	89.20	91.02

In Table 1.6 we present the classification accuracy across different reach to grasp movements, for a specific object and five different object positions (five classes), for all subjects, using the random forest method.

In Table 1.7 we present the classification accuracy of random forest models, across reach to grasp movements towards five different positions (five classes), for all objects and subjects, using the random forest method.

In Table 1.8, we present the classification results achieved, using 15 EMG channels to discriminate between reach to grasp movements, towards specific position and object combinations (for all objects and positions), to execute two different tasks per object (two classes). As it can noticed, classification accuracy is consistently high across different positions, different objects and different tasks. The latter evidence proves the efficiency of the proposed scheme for various reach to grasp movements and tasks.

In Table 1.8, we reported some interesting classification results for task discrimination, using a lot of EMG channels (15 EMG channels) which typically may not be available, due to hardware, cost or other limitations. Thus in this work we use the random forests technique to compute the feature variables (EMG channels)

Table 1.8 Classification accuracy across different reach to grasp movements, towards different positions and objects, to execute two different tasks (two classes). Random forests classifier was used for 15 EMG channels, of Subject 1 data

Tall glass		
Tasks	Side grasp (%)	Front grasp (%)
Pos I	76.31 (±7.41)	78.87 (±4.72)
Pos II	89.77 (±5.43)	87.88 (±9.42)
Pos III	84.86 (±8.27)	85.75 (±2.38)
Pos IV	89.69 (±5.61)	86.82 (±8.06)
Pos V	87.56 (±8.20)	90.36 (±4.77)
Wine glass		
Tasks	Side grasp (%)	Stem grasp (%)
Pos I	84.14 (±4.15)	85.20 (±4.59)
Pos II	71.23 (±5.19)	79.72 (±9.31)
Pos III	66.64 (±8.15)	77.71 (±11.47)
Pos IV	87.98 (±5.21)	89.02 (±5.81)
Pos V	66.44 (±8.66)	64.28 (±7.62)
Mug		
Tasks	Handle grasp (%)	Top grasp (%)
Pos I	89.33 (±6.66)	90.74 (±6.78)
Pos II	79.77 (±6.74)	82.31 (±7.02)
Pos III	75.98 (±9.63)	83.52 (±7.03)
Pos IV	84.91 (±3.83)	86.99 (±5.20)
Pos V	77.83 (±5.79)	77.36 (±3.95)
Mug plate		
Tasks	Side-pinch grasp (%)	Top grasp (%)
Pos I	84.98 (±2.52)	81.76 (±4.99)
Pos II	89.58 (±6.11)	92.76 (±4.27)
Pos III	86.73 (±7.57)	95.58 (±1.92)
Pos IV	87.16 (±6.59)	85.64 (±9.86)
Pos V	91.62 (±3.08)	90.78 (±2.98)

importance for each position and object combination and resolve the classification problems for task discrimination, using the six most important EMG channels.

Results for task discrimination, using the most important EMG channels, are reported in Table 1.9. We can notice that even for the reduced number of feature variables (EMG channels), classification accuracy remains consistently high and the results are equal or better than the initial results (with the 15 EMG channels).

In the aforementioned results, is evident that the classification accuracy and the overall ability of our scheme to discriminate different reach to grasp movements, towards different tasks (executed with the same object), depends on:

- The “distance” (in the configuration space) between the final postures of the full human arm hand system, that correspond to different tasks.

For example the two tasks of the tall glass, mug and mug plate result to completely different human wrist angles (wrist motion strongly affects forearm muscles). Thus, for these tasks better classification results can be achieved, in contrast to the wine

Table 1.9 Classification accuracy across different reach to grasp movements, towards different positions and objects, to execute two different tasks (two classes), for Subject 1. Random forests were used with the six most important EMG channels selected using the features selection method

Tall glass		
Tasks	Side grasp (%)	Front grasp (%)
Pos I	81.43 (±2.64)	79.91 (±7.69)
Pos II	89.79 (±7.35)	90.79 (±7.97)
Pos III	82.84 (±9.12)	88.76 (±3.34)
Pos IV	89.82 (±5.89)	87.71 (±7.97)
Pos V	84.66 (±9.98)	92.85 (±4.14)
Wine glass		
Tasks	Side grasp (%)	Stem grasp (%)
Pos I	86.77 (±3.72)	84.30 (±3.77)
Pos II	74.50 (±9.81)	81.20 (±9.64)
Pos III	72.62 (±8.66)	79.39 (±13.56)
Pos IV	86.90 (±8.40)	87.61 (±5.95)
Pos V	63.41 (±6.88)	64.24 (±9.72)
Mug		
Tasks	Handle grasp (%)	Top grasp (%)
Pos I	87.17 (±4.67)	87.85 (±4.59)
Pos II	80.10 (±7.36)	83.72 (±5.87)
Pos III	77.90 (±5.40)	81.43 (±6.98)
Pos IV	85.35 (±4.14)	84.98 (±6.07)
Pos V	81.06 (±8.29)	78.95 (±9.57)
Mug plate		
Tasks	Side-pinch grasp (%)	Top grasp (%)
Pos I	84.34 (±5.57)	83.60 (±3.44)
Pos II	90.74 (±4.59)	94.01 (±3.49)
Pos III	85.55 (±12.07)	95.61 (±2.89)
Pos IV	86.74 (±10.18)	83.79 (±7.27)
Pos V	91.00 (±2.23)	92.28 (±3.03)

glass tasks that involve mainly finger motions and variations of the aperture (less differentiation of muscular co-activation patterns).

- The position of the object to be grasped, as different positions result to different classification accuracies for the same object and tasks.

For example for positions I and IV the classifier achieves better classification accuracy for wine glass and mug, while positions II and V achieves better results for tall glass and mug plate.

1.5.3.1 Majority Vote Criterion

Given the fact that the classification decision in our scheme is taken at a frequency of 1 kHz, we can use a sliding window of width N, in order for all the N samples to be used for the classification decision. Inside this window, we can use the Majority

Table 1.10 Classification accuracy across different reach to grasp movements of Subject 1, towards a specific object (Marker) and varying object position, using random forests and random forests with MVC (in a sliding window of N = 50 samples)

	Subject1				
Object rectangle	Pos I (%)	Pos II (%)	Pos III (%)	Pos IV (%)	Pos V (%)
Random forests	87.03	91.61	90.51	86.25	92.61
RF with MVC	100	100	100	100	100

Table 1.11 Estimation results for a specific object (a marker) across all five object positions, for Subject 1, using a random forests model

Position	Arm similarity (%)	Hand similarity (%)
Pos I	83.78 ±4.01	83.43 ±13.77
Pos II	88.80 ±3.98	86.60 ±15.02
Pos III	86.93 ±3.95	90.42 ±10.47
Pos IV	89.47 ±6.25	83.73 ±16.12
Pos V	91.53 ±6.57	89.04 ±10.09
All	80.19 ±7.32	81.15 ±16.24

Vote Criterion (MVC), which classifies all the samples of a set of N samples, in the class that was the most common between them (the class gathering the most votes). The use of the majority vote criterion, can improve the classification results acquired with the proposed methods.

More details regarding the sliding window and the MVC can be found in [34] and [46]. In Table 1.10, we present improved classification results using the majority vote criterion in a sliding window of $N = 50$ samples, for Subject 1 performing reach to grasp movements, towards a specific object (marker) and varying object position.

1.5.4 Task Specific Motion Decoding Results

In this section we present the EMG-based motion estimation results, for reach to grasp movements towards three different objects, placed at five different positions in 3D space. Highly accurate estimation results are achieved using task-specific random forest models, triggered from our scheme, taking into account the classification decision on the "task" to be executed.

More specifically in Table 1.11 we present estimation results for five subspace specific models, trained with Subject 1 data, to decode human motion during reach to grasp movements, towards five different positions to grasp a specific object (marker). In Table 1.12 we present estimation results for three object specific models, trained with Subject 1 data, to decode human motion during reach to grasp movements, towards a specific position (Pos I), to grasp three different objects (a marker, a rectangle and a mug).

Table 1.12 Estimation results for a specific position (Pos III) and all three different objects, for Subject 1, using a random forests model

Object	Arm similarity (%)	Hand similarity (%)
Marker	86.93 ±3.95	90.42 ±10.47
Rectangle	87.76 ±4.13	82.33 ±12.31
Mug	89.62 ±5.13	83.52 ±13.57
All	83.26 ±7.2	80.47 ±11.72

Table 1.13 Estimation results for specific position (Pos III) and specific object (a rectangle), for all subjects using a random forests model

Subject	Arm similarity (%)	Hand similarity (%)
Subject 1	87.76 ±4.13	82.33 ±10.47
Subject 2	85.91 ±6.21	81.59 ±11.78
Subject 3	89.44 ±4.30	84.93 ±14.93
Subject 4	87.32 ±5.34	85.28 ±10.16
Subject 5	82.11 ±7.79	80.54 ±16.32

In Tables 1.11 and 1.12 we can notice, that the models trained for each position or object separately, outperformed the "general" models built for all positions (for a marker) and all objects (placed at specific position, Pos III). With the term "general" models we mean those models trained for all positions in 3D space or all objects placed at a specific position (training of "general" models requires a training set that contains data for all classes of a specific problem).

Finally in Table 1.13 its evident, that the estimation results were usually better for the human arm (better estimation accuracy for human arm motion was achieved) than for the case of the human hand (human fingers motion). Such a finding, supports the applicability of our method, since precisely estimating the position of the human arm hand system end-effector (wrist), is far more important than fingers placement.

Similarity between the estimated and the captured human motion is defined as:

$$S = 100(1 - RMS(q_c - q_e)/RMS(q_c))\% \tag{1.1}$$

where RMS is:

$$RMS(q_c - q_e) = \sqrt{\frac{\sum_{i=1}^{n}(q_c - q_e)^2}{n}} \tag{1.2}$$

where q_c are the captured joint values, q_e the estimated joint values and n the number of samples. In Fig. 1.20 we compare the estimated from the task-specific model, user's wrist position, with the user's wrist position captured using the Isotrak II motion capture system, during the experiments. The data used are part of a validation set, not previously seen during training.

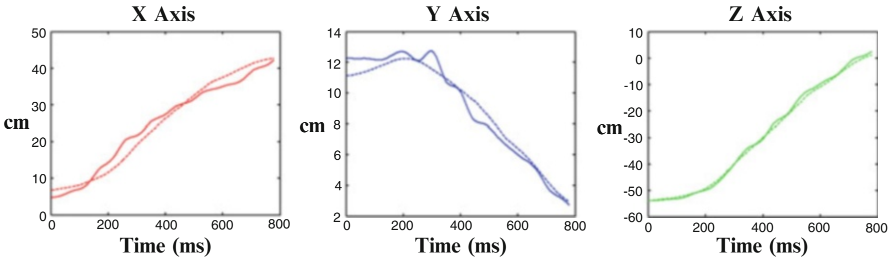

Fig. 1.20 EMG-based human end-effector (wrist) position estimation (using a task-specific motion decoding model). *Straight lines* represent the captured values (during the experiments), while the *dashed lines* represent the estimated values

1.6 Conclusions

A complete learning scheme for EMG based interfaces, has been proposed. A regressor and a classifier cooperate advantageously in order to split the task space, and achieve better motion decoding for reach to grasp movements, using task specific models. Thus, the proposed scheme is formulated so as to first discriminate between different reach to grasp movements, providing an appropriate classification decision and then trigger a task-specific EMG based motion decoding model, that achieves better motion estimation, than the "general" models. Principal Component Analysis (PCA) is used to represent in low dimensional manifolds the human myoelectric activity and the human motion. The regression problem is then formulated using these low-dimensional embeddings. The estimated output (human motion) can be back projected in the high dimensional space (27 DoFs), in order to provide an accurate estimate of the full human arm-hand system motion. The proposed scheme can be used by a series of EMG-based interfaces and for applications that range from human computer interaction and human robot interaction, to rehabilitation robotics and prosthetics. Regarding future research directions, we plan to apply the proposed scheme for the EMG based teleoperation of the robot arm-hand system Mitsubishi PA10 DLR/HIT II, taking into account the non-stationary characteristics of the EMG signals.

References

1. Graupe D, Salahi J, Kohn KH (1982) Multifunctional prosthesis and orthosis control via microcomputer identification of temporal pattern differences in single-site myoelectric signals. J Biomed Eng 4(1):17–22
2. Artemiadis PK, Kyriakopoulos KJ (2010) EMG-based control of a robot arm using low-dimensional embeddings. IEEE Trans Robot 26(2):393–398
3. Vogel J, Castellini C, van der Smagt PP (2011) EMG-based teleoperation and manipulation with the DLR LWR-III. In: IEEE/RSJ international conference on intelligent robots and systems (IROS), San Francisco, pp 672–678

4. Cipriani C, Zaccone F, Micera S, Carrozza MC (2008) On the shared control of an EMG-controlled prosthetic hand: analysis of user prosthesis interaction. IEEE Trans Robot 24(1):170–184
5. Lucas L, DiCicco M, Matsuoka Y (2004) An EMG-controlled hand exoskeleton for natural pinching. J Robot Mech 16(5):482–488
6. Costanza E, Inverso SA, Allen R, Maes P (2007) Intimate interfaces in action: assessing the usability and subtlety of EMG-based motionless gestures. In: Proceedings of the SIGCHI conference on human factors in computing systems, ser. CHI '07, San Jose. ACM, New York, pp 819–828
7. Saponas TS, Tan DS, Morris D, Balakrishnan R (2008) Demonstrating the feasibility of using forearm electromyography for muscle-computer interfaces. In: Proceedings of the twenty-sixth annual SIGCHI conference on human factors in computing systems, ser. CHI '08, Florence. ACM, New York, pp 515–524
8. Thakur PH, Bastian AJ, Hsiao SS (2008) Multidigit movement synergies of the human hand in an unconstrained haptic exploration task. J Neurosci 28(6):1271–1281
9. Santello M, Flanders M, Soechting JF (1998) Postural hand synergies for tool use. J Neurosci 18(23):10105–10115
10. Todorov E, Ghahramani Z (2004) Analysis of the synergies underlying complex hand manipulation. In: Proceedings of the 26th annual international conference of the IEEE engineering in medicine and biology society, EMBS '04, San Francisco, Sept 2004, vol 2, pp 4637–4640
11. Mason CR, Gomez JE, Ebner TJ (2001) Hand synergies during reach-to-grasp. AIP J Neurophys 86(6):2896–2910
12. Klein Breteler MD, Simura KJ, Flanders M (2007) Timing of muscle activation in a hand movement sequence. Oxf J Cereb Cortex 17:803–815
13. Ajiboye AB, Weir RF (2009) Muscle synergies as a predictive framework for the EMG patterns of new hand postures. J Neural Eng 6(3):036004
14. Zajac FE (1986) Muscle and tendon: properties, models, scaling and application to biomechanics and motor control. In: Bourne JR (ed) CRC critical reviews in biomedical engineering, vol 19, no 2. CRC, Boca Raton, pp 210–222
15. Fukuda O, Tsuji T, Kaneko M, Otsuka A (2003) A human-assisting manipulator teleoperated by EMG signals and arm motions. IEEE Trans Robot Autom 19(2):210–222
16. Maier S, van der Smagt P (2008) Surface EMG suffices to classify the motion of each finger independently. In: Proceedings of the international conference on motion and vibration control (MOVIC), Munich
17. Bitzer S, van der Smagt P (2006) Learning EMG control of a robotic hand: towards active prostheses. In: Proceedings 2006 IEEE international conference on robotics and automation (ICRA), Orlando, May 2006, pp 2819–2823
18. Zhao J, Xie Z, Jiang L, Cai H, Liu H, Hirzinger G (2005) Levenberg-marquardt based neural network control for a five-fingered prosthetic hand. In: Proceedings of the 2005 IEEE international conference on robotics and automation, ICRA, Barcelona, Apr 2005, pp 4482–4487
19. Zecca M, Micera S, Carrozza MC, Dario P (2002) Control of multifunctional prosthetic hands by processing the electromyographic signal. Crit Rev Biomed Eng 30(4–6):459–485
20. Nishikawa D, Yu W, Yokoi H, Kakazu Y (1999) EMG prosthetic hand controller using real-time learning method. In: IEEE SMC '99 conference proceedings: 1999 IEEE international conference on systems, man, and cybernetics, Tokyo, vol 1, pp 153–158
21. Takahashi K, Nakauke T, Hashimoto M (2007) Remarks on hands-free manipulation using bio-potential signals. In: IEEE international conference on systems, man and cybernetics, Montreal, Oct 2007, pp 2965–2970
22. Castellini C, Fiorilla AE, Sandini G (2009) Multi-subject/daily-life activity EMG-based control of mechanical hands. J Neuroeng Rehabil 6:1–11
23. Brochier T, Spinks RL, Umilta MA, Lemon RN (2004) Patterns of muscle activity underlying object-specific grasp by the macaque monkey. J Neurophysiol 92(3):1770–1782

24. Hill A (1938) The heat of shortening and the dynamic constants of muscle. Proc R Soc Lond Ser B 126(843):136–195
25. Cavallaro E, Rosen J, Perry J, Burns S, Hannaford B (2005) Hill-based model as a myoprocessor for a neural controlled powered exoskeleton arm – parameters optimization. In: Proceedings of the 2005 IEEE international conference on robotics and automation, ICRA, Barcelona, Apr 2005, pp 4525–4530
26. Artemiadis P, Kyriakopoulos K (2005) Teleoperation of a robot manipulator using EMG signals and a position tracker. In: IEEE/RSJ international conference on intelligent robots and systems (IROS), Edmonton, Aug 2005, pp 1003–1008
27. Potvin J, Norman R, McGill S (1996) Mechanically corrected EMG for the continuous estimation of erector spinae muscle loading during repetitive lifting. Eur J Appl Physiol Occup Physiol 74:119–132
28. Lloyd DG, Besier TF (2003) An emg-driven musculosceletal model to estimate muscle forces and knee joint movements in vivo. J Biomech 36:765–776
29. Artemiadis P, Kyriakopoulos K (2011) A switching regime model for the EMG-based control of a robot arm. IEEE Trans Syst Man Cybern B Cybern 41(1):53–63
30. Artemiadis P, Kyriakopoulos K (2007) EMG-based teleoperation of a robot arm using low-dimensional representation. In: IEEE/RSJ international conference on intelligent robots and systems, IROS 2007, San Diego, 29 Oct 2007–2 Nov 2007, pp 489–495
31. Smith RJ, Tenore F, Huberdeau D, Etienne-Cummings R, Thakor NV (2008) Continuous decoding of finger position from surface EMG signals for the control of powered prostheses. In: 30th annual international conference of the IEEE engineering in medicine and biology society, EMBS, Vancouver, Aug 2008, pp 197–200
32. Ryu W, Han B, Kim J (2008) Continuous position control of 1 dof manipulator using EMG signals. In: Third international conference on convergence and hybrid information technology, ICCIT '08, Busan, vol 1, Nov 2008, pp 870–874
33. Koike Y, Kawato M (1995) Estimation of dynamic joint torques and trajectory formation from surface electromyography signals using a neural network model. Biol Cybern 73:291–300
34. Liarokapis MV, Artemiadis PK, Katsiaris PT, Kyriakopoulos KJ, Manolakos ES (2012) Learning human reach-to-grasp strategies: towards EMG-based control of robotic arm-hand systems. In: IEEE international conference on robotics and automation (ICRA), St. Paul, May 2012, pp 2287–2292
35. Liarokapis MV, Artemiadis PK, Katsiaris PT, Kyriakopoulos KJ (2012) Learning task-specific models for reach to grasp movements: towards EMG-based teleoperation of robotic arm-hand systems. In: 4th IEEE RAS EMBS international conference on biomedical robotics and biomechatronics (BioRob), Rome, June 2012, pp 1287–1292
36. Liarokapis MV, Artemiadis PK, Kyriakopoulos KJ, Manolakos ES (2013) A learning scheme for reach to grasp movements: on EMG-based interfaces using task specific motion decoding models. IEEE J Biomed Health Inform 17(5):915–921
37. Fligge N, Urbanek H, van der Smagt P (2012) Relation between object properties and emg during reaching to grasp. J Electromyogr Kinesiol 23(2):402–410
38. Liarokapis MV, Artemiadis PK, Kyriakopoulos KJ (2013) Task discrimination from myoelectric activity: a learning scheme for EMG-based interfaces. In: IEEE international conference on rehabilitation robotics (ICORR), Seattle, June 2013, pp 1–6
39. Artemiadis PK, Katsiaris PT, Kyriakopoulos KJ (2010) A biomimetic approach to inverse kinematics for a redundant robot arm. Auton Robots 29(3–4):293–308
40. Liarokapis MV, Artemiadis PK, Kyriakopoulos KJ (2012) Functional anthropomorphism for human to robot motion mapping. In: 21st IEEE international symposium on robot and human interactive communication (RO-MAN), Paris, Sept 2012, pp 31–36
41. Cram JR, Kasman GS, Holtz J (1998) Introduction to surface electromyography. Gaithersburg, Md., Aspen Publishers.
42. Dae Hyong K et al (2011) Epidermal electronics. Science 333:838–843
43. Sheskin DJ (2007) Handbook of parametric and nonparametric statistical procedures, 4th edn. Chapman & Hall/CRC, Boca Raton

44. Ho TK (1995) Random decision forests. In: Proceedings of the third international conference on document analysis and recognition, Montréal, Aug 1995, vol 1, pp 278–282
45. Breiman L (2001) Random forests. Mach Learn 45(1):5–32
46. Theodoridis S, Koutroumbas K (2009) Pattern recognition, 4th edn. Academic/Elsevier Science, Amsterdam/London

Chapter 2
State of the Art and Perspectives of Ultrasound Imaging as a Human-Machine Interface

Claudio Castellini

Abstract Medical ultrasound imaging is a diagnostic tool based upon ultrasound wave production, propagation and processing, in use since the 1950s in the hospitals all over the world. The technique is totally safe, relatively cheap, easy to use and provides live images of the interiors of the human body at both high spatial and temporal resolutions. In this chapter we examine its use as a novel human-machine interface. Recent research indicates that it actually represents an effective, realistic tool for intention gathering, at least for the hand amputees. Given the current state of the art, medical ultrasound imaging can be used to control an upper-limb prosthesis to a high degree of precision; moreover, the related calibration procedure can be made extremely short and simple, with the aim of building an ultrasound-based online control system. We propose and discuss its pros and cons as an interface for the disabled, we elaborate on its potentialities as a tool for intention gathering, and we show that it has great potential in the short- and mid-term.

Keywords Ultrasound imaging • Human-machine interfaces • Rehabilitation robotics

2.1 Introduction

Medical ultrasound imaging (from now on, US imaging) has nowadays become a standard diagnostic tool in hospitals. It is used to visualise essentially all human body structures and sports an enormous wealth of information, to the point that a trained specialist can diagnose a wide range of conditions just by looking at the live images it gathers. US imaging is also widely employed as a pre-operating tool along

C. Castellini, Ph.D. (✉)
Robotics and Mechatronics Center, German Aerospace Center, Oberpfaffenhofen, Germany
e-mail: claudio.castellini@dlr.de

P. Artemiadis (ed.), *Neuro-Robotics: From Brain Machine Interfaces to Rehabilitation Robotics*, Trends in Augmentation of Human Performance 2,
DOI 10.1007/978-94-017-8932-5_2,

with other kinds of medical imaging such as, e.g., magnetic resonance and positron emission tomography; and during invasive procedures (interventional ultrasonography) to guide the insertion of operating tools into the body. (A comprehensive reference about US imaging, its foundations and physics, and even its therapeutic uses, can be found in [12].)

With respect to the above-mentioned imaging techniques however, it has at least three definite advantages: firstly, it does not entail direct radiation, nor any radioactive contrast means to be injected in the patient's body; this means that its level of safety is much higher – it is actually considered harmless [46]. Secondly, it enforces high imaging resolution, both spatial and temporal. Thirdly, the equipment to perform US imaging is, at least if compared to other techniques, extremely cheap and lightweight. US imaging machines are nowadays to be found in any hospital of any medium- to large-sized city; their buying and maintenance costs are low; and recently, hand-held US imaging machines have appeared on the market, as large and heavy as a smartphone, their cost hovering around a few thousand dollars.

From the point of view of rehabilitation robotics, what we are looking at is indeed a novel human-machine interface (HMI). The ideal HMI for this field must be cheap, lightweight, safe and rich in information; and so far, the only successful method is surface electromyography (sEMG from now on), with its applications to self-powered hand prosthetic control. Yet, sEMG is far from meeting all the above-mentioned requirements: according to recent surveys [2, 36, 37], one quarter to one third of hand amputees reject prostheses controlled via sEMG, due to low reliability, weight, trouble with maintenance, low dexterity, and poor visual appearance. In fact, the sEMG signal can change due to several unpredictable factors – sweat, muscle fatigue, electrode displacement, etc. [7] – and is therefore far from being reliable.

We claim, and we will illustrate in the following, that medical ultrasound imaging has the potential to become an alternative, or additional, HMI for rehabilitation robotics. In this chapter we will first outline the historical development of medical ultrasound imaging as a diagnostic tool, which is rooted in the pioneeristic work of Karl Dussik in the 1940s. We will then sketch the basic functioning principles of the technique, and shorty report upon the current uses of pattern-matching technique in advanced ultrasound image processing, especially as far as prosthetics is concerned.

We will then move on to examine recent research leading to the idea of US imaging as a fully-fledged HMI for the disabled. In particular, the chapter revolves around the only two research efforts on this topic found so far in the community. Results therein indicate that (forearm) ultrasonography can detect the kinematic/dynamic configuration of the wrist and fingers with a high degree of finesse. The generality of the approaches presented lets us claim that similar results could be obtained in many other applications (e.g., lower-limb prosthetics).

2.2 Background

2.2.1 Historical Remark

The first achievements in the direction of medical ultrasound imaging lie within the analytical theory of wave propagation as laid out in the works of Euler, D'Alembert and Lagrange in the eighteenth century. This theory contains the basis to interpret the reflection of a wave which has been intentionally emitted and propagates through a heterogeneous medium. Namely, it appeared from the propagation equations that each time a differential in the medium density and/or resistance to contraction was found, part of the energy of the wave would be reflected back – an echo would be produced.

Of equally high interest is the discovery of the piezoelectric effect in 1880 by Pierre and Jacques Curie. Piezoelectric materials, it was discovered, would react to the application of a voltage differential by contracting; if immersed in a suitable medium, they would propagate a mechanical wave through it. The piezoelectric effect worked the other way around, too: when pressure was applied to a piezoelectric material, a voltage differential at the surface of the material would arise. These materials could then be used as transducers: acting both as emitters of mechanical waves, and as receivers. These two strands of research came together, according to Cobbold [12], around 1916 with the work of Paul Langevin, Robert W. Wood and Alfred L. Loomis [21]. Research in this field was fueled, as it often happens, by a military application, namely the detection of submarines, which would later lead to the invention of the sonar; at the same time, the effects of ultrasound waves on biological tissue had been reported of by the above-mentioned authors. It was then clear that the emission/reflection of ultrasonic waves could in principle be used to inspect the internal structure of living beings.

The history of ultrasound as a medical device stems from these findings and officially begins, at least according to Kane et al. [31], in 1942, when Karl Dussik [17] attempted a full-breadth ultrasonic scan of the cranium of a brain tumour patient. In that paper, along with a theoretical treatment of the subject, fundamental considerations are made about the possibility of visualising several tissues at the same time, exploiting the above-mentioned principle of wave reflection at the interfaces. Figure 2.1 shows the apparatus Dussik built and used at that time.

In 1948, the first Congress of Ultrasound in Medicine was held in Erlangen, Germany; in 1955 the terms *A-mode* and *B-mode* ultrasound scanning (in turn, amplitude- and brightness-modes) were used for the first time, namely by John J. Wild at Cambridge. Lastly, in 1958 Ian Donald started using ultrasonic scanning as an aid to medical diagnoses in the case of an abdominal tumour; his pioneeristic result were published in *Lancet* [15]. Two years later, he developed the first two-dimensional ultrasonic scanner, and this is probably the point where modern ultrasound imaging is born.

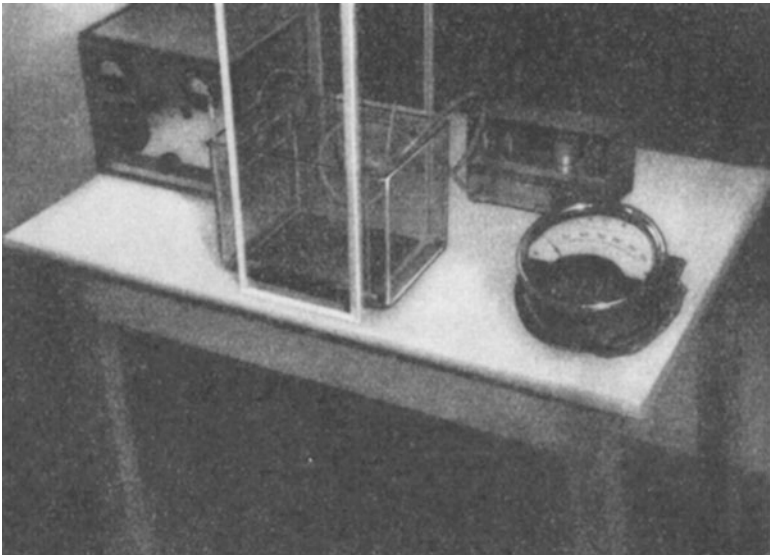

Fig. 2.1 Karl Dussik's apparatus to generate ultrasonic waves, built in 1942 (Reproduced from [17])

Musculoskeletal ultrasonography, that is, ultrasound scanning of bones, muscles and tendons, starts in 1958 again thanks to Dussik [18] who measured the acoustic attenuation of articular and periarticular tissues. To obtain a US image of a musculoskeletal structure though, one must wait until McDonald and Leopold's 1972 paper [34]; in which it is stated that two musculoskeletal conditions (namely, Baker's cysts and peripheral oedema) produce two different ultrasound patterns, which can be distinguished both from each other and from a healthy condition.

This is likely to be one of the first general diagnostic statements of a musculoskeletal condition based upon ultrasound imaging.

Although the basic principle has not changed, the performances of today's ultrasound machines are excellent under all points of view. Thanks to the blazing advancements in both piezoelectric technology, microelectronics and computer processing power, modern ultrasound machines can obtain full-resolution B-mode ultrasonic scans, that is, grey-valued images, of essentially any body structure. Current machines [28] reach temporal resolutions of up to 100 frames per second, spatial resolutions of 0.3–1 mm in the direction parallel to the transducer (the device leaning against the subject's skin), can visualise up to 15×15 cm of tissue, and can be made so small that they are not bigger than a smartphone; there are examples of commercial hand-held ultrasound machines weighing 390 g with a 3.5″ display.

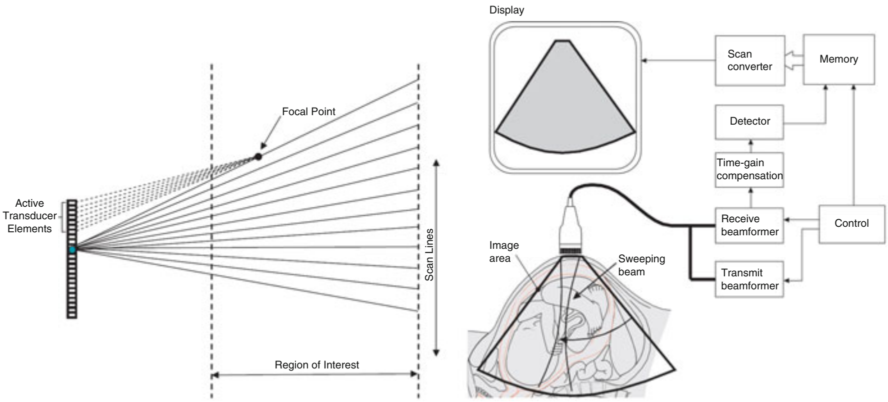

Fig. 2.2 (*Left*) A graphical representation of how ultrasound imaging works (Reproduced from [1]); (*right*) a scheme of the typical linear B-mode ultrasonographic device (Reproduced from [28])

2.2.2 Technological Principles of Ultrasound Imaging

A full mathematical treatment of (medical) ultrasound imaging can be found, e.g., in [12, 28]; what follows is an informal description of the physics and technology underlying medical imaging. For a more technical description of how a medical ultrasonography device works, see, e.g., [1].

With the term *ultrasound* it is commonly meant sound waves of frequency over 20 kHz. The propagation speed v of a sound (mechanical) wave in a physical medium depends on the mechanical characteristics of the medium itself according to the relation $v = \sqrt{\frac{B}{\rho}}$, where B is the medium's adiabatic bulk modulus and ρ is the medium's density. (The adiabatic bulk modulus measures the resistance of a substance to uniform compression.) Therefore, wherever a gradient in the medium's density or stiffness is found, v will change and so will the energy associated to the wave. The differential in energy can in general result in wave absorption, transmission and reflection; in a real situation, all three phenomena will occur to different degrees, and the phenomenon will be particularly evident each time the wave hits the boundary between two different mediums.

As a result of that, any device able to measure the reflection of a definite wave after it has travelled back and forth in a region of interest will be able to determine what boundaries the wave itself has been travelling through before being attenuated beyond recognition. In the case of ultrasound waves, this principle lies beneath the ability of some animal species such as, e.g., bats to navigate flight and to locate food sources.

In the case of ultrasound imaging (see Fig. 2.2, left panel), an array of piezoelectric transducers is used to focus a multiplexed, synchronised set of ultrasound waves (beam) over a line lying at few centimeters' distance from the array. Each element of the array can, in turn, be used to convert the echo(es) of the emitted wave into a voltage. By accurately timing the echoes, one can determine the nature of the medium through which the wave has propagated; in particular, the echoes form the profile of the boundaries encountered along a straight line stretching away from the transducers. This information can be plotted, forming the so-called A-mode ultrasonography.

By employing a multiplexing device (beamformer), all transducers in the array can be synchronised to gather closely spaced profiles. The net result is a two-dimensional representation of the section of the medium lying ahead of the array, or a so-called B-mode ultrasonography. (The array is often called the *probe* of the ultrasound machine, or, with a slight abuse of language, *the transducer*.) The intensity in the profiles, and therefore in their 2D juxtaposition (image) denotes rapid spatial variations in B and/or ρ, therefore indicating abrupt changes of medium – interfaces. Figure 2.2 (right panel) shows a scheme of the typical B-mode ultrasonographic device: the ultrasound beam generated by the transmit beamformer sweeps the tissues of interest, generating reflections at each point in space where an interface between two tissues is found. Corresponding reflections are captured by the transducers and converted to a grey-valued image by a receive beamformer coupled with a time-delay compensation device. As a result, "ridges" in the image denote tissue interfaces.

The frequency selected for the ultrasound waves must be tuned, within a reasonable range, according to the tissue under examination and the required focus depth and depth of field; typically, wave frequencies are between 2 and 18 MHz.

2.2.3 *Ultrasound Imaging in Rehabilitation Robotics*

In rehabilitation robotics, a complex robotic artifact must be somehow interfaced with a disabled human subject. Depending on the task the subject requires and on which functionalities the robotic artifact provides, the rehabilitation engineer must figure out how to let the subject control the artifact to the best possible extent – the main issues here are those of reliability, dexterity and practical usability. An HMI lies therefore at the core of such a man-machine integration, and must be targeted on the patient's needs and abilities.

In particular, one must figure out, first of all, what kind of signals best suit the target application. The signals must be recognisable into stable and repeatable patterns, and must be produced by the subject with a reasonable effort, both physical and cognitive. Such patterns must then be converted into (feed-forward) control signals, i.e., motion or force commands for the robotic artifact. One early example of such a successful HMI is sEMG, initially developed as a diagnostic tool for assessing peripheral neural disorders and muscular conditions; from the 1960s on then, it was applied to control single-degree-of-freedom hand prosthesis, and its use has then progressed towards lower- and upper-limb self-powered prostheses [37]. More or less at the same time, advanced pattern recognition techniques started being used to convert the sEMG signal patterns into control signals, whenever the dexterity of the prosthesis called for a finer detection of the subject's intentions [14, 19, 35].

The wealth of information delivered by medical ultrasound imaging, therefore, calls for the exploration of its use as a novel HMI in this field. The idea of applying machine learning techniques to ultrasound images in general is not new. Recent examples include, e.g., the recognition of skin cancer [30], tumor segmentation [50] and anatomical landmarks detection in the foetus [39]. But, as far rehabilitation robotics is concerned, the literature is scarce. To the best of our knowledge, at the time of writing the only application is that of 3D ultrasound imaging to the visualisation of residual lower limbs and to assess the ergonomy of lower-limb prostheses [16, 38].

2.3 Sonomyography

The first real use of US imaging as an HMI appears in 2006 and is due to Yong-Ping Zheng et al. [51]. The associated technique is called *sonomyography*. The authors focus on the large extensor muscle of the forearm, *M. Extensor Carpi Radialis*, and perform a wrist flexion/extension experiment on six intact subjects and three trans-radial amputees. In the study, two rectangular blocks are used to track the upper and lower boundaries of the muscle; tracking is enforced using a custom tracking algorithm based upon 2D cross-correlation between subsequent frames. The estimated muscle thickness is the distance between the centres of the two blocks. See Fig. 2.3.

The wrist flexion angle is determined using a motion tracking system and four markers placed on the subject's wrist and dorsum of the hand; in the case of the amputees, the subjects were asked to imagine flexing and extending the imaginary wrist while listening to an auditory cue (metronome). The correlation coefficient

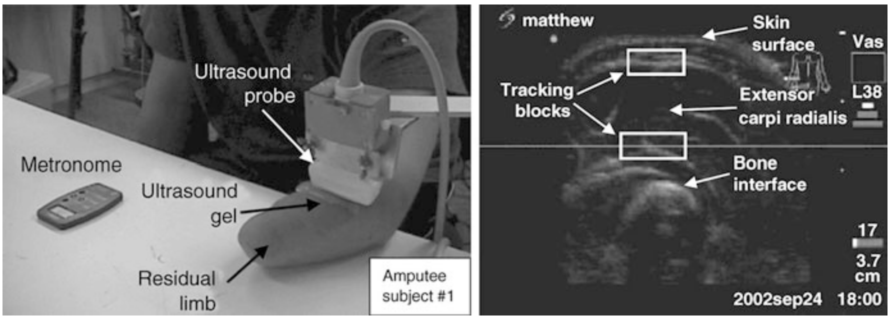

Fig. 2.3 Determining the wrist flexion angle via ultrasound imaging. (*Left*) The setup; (*right*) a typical US image (Reproduced from [51])

between the estimated muscle width and the wrist flexion angle is evaluated, showing high correlation in the cases of the intact subjects (linear regression average R^2 coefficient 0.875). A qualitative analysis of the results for the amputees is promising.

Extensive work on the same topic follows in a series of studies. In [26] high correlation is shown among wrist angle, sonomyography and the root-mean-square of the sEMG signal, which is well-known to be quasi-linearly related to the force exerted by a muscle [14]. The proposed approach is therefore validated by comparison with a standard technique and with the ground truth. In [42] a new algorithm is presented which further improves the previous results; lastly, in [23] a successful discrete tracking task controlled by sonomyography is presented. The subject pool is this time sensibly larger (16 intact subjects). As a follow-up, the feasibility of using sonomoygraphy to control a hand prosthesis has been demonstrated [10, 11, 42], but still limited to wrist flexion and extension. Attempts have been made to improve the estimation of wrist angle from sonomyography using support vector machine and artificial neural network models [24, 47].

More recently, sonomyography has been successfully extended to elbow flexion/extension, wrist rotation, knee flexion/extension and ankle rotation [52]. Lastly, and this is probably the most interesting result so far [24], the approach is extended to A-mode ultrasonography: a wearable, single ultrasound transducer is used to determine the wrist flexion angle via a support vector machine [3, 13]. A-mode ultrasonography is enforced by means of commercially available single ultrasound transducers applied on the subject's skin, much like sEMG electrodes. This opens up the possibility of miniaturising the sonomyography hardware and make it wearable. The issue of signal generation and conditioning is still open, though.

In the above-mentioned corpus of research, the authors have never considered more than one feature at the same time. This restricted focus is probably motivated by the diversity and complexity of the changes in US images as joint positions change: the single identified feature is related to a precise anatomical change, a relation which would be quite hard to assess in the general case. It is likely that a more general treatment in that case would require a detailed model of the kinematics of the human forearm, *plus* a detailed model of the changes in the projected US image as the hand joints move – a task which seems overtly complex. The only attempt so far at modelling finger positions appears in [43, 44], where significant differences among optical flow computations for finger flexion movements are reported and classified.

2.4 Ultrasound Imaging as a Realistic HMI

The only other attempt at establishing US imaging as an HMI, as far as we know, is that carried on in our own group. In particular, with respect to sonomyography, this approach does not rely on anatomical features of the forearm (as visualised in

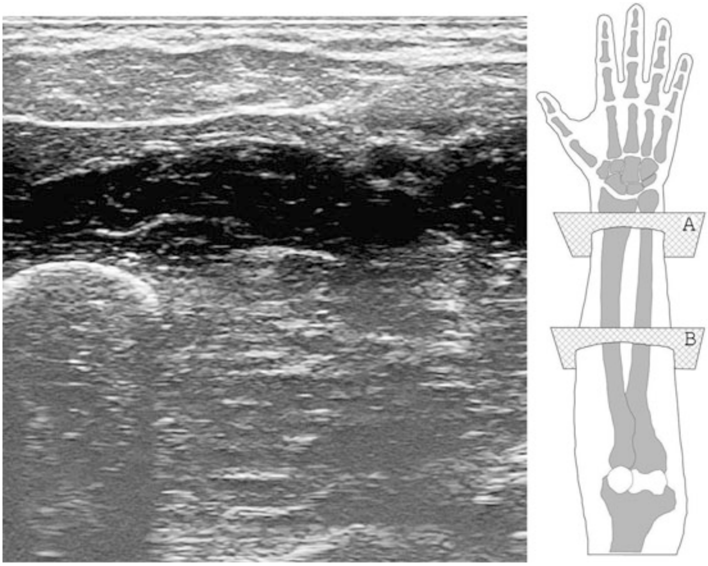

Fig. 2.4 (*Left*) A typical ultrasound image obtained during the qualitative analysis carried on in [5]. The ulna is clearly visible in the bottom-left corner, while the flexor muscles and tendons are seen in the upper part. (*Right*) A graphical representation of the human forearm and hand (right forearm; dorsal side up). The transducer is placed onto the ventral side; planes *A* and *B* correspond to the sections of the forearm targeted by the analysis

the ultrasonic images), but rather considers the images as a global representation of the activity going on in the musculoskeletal structure, as a human subject performs movement or force patterns with the hand. (This approach cannot therefore be consistently called "sonomyography", as the targeted structures are not restricted to muscles, but rather all organs are considered, i.e., veins and arteries, bones, nerves, connective and fat tissue, etc.)

2.4.1 Ultrasound Images of the Forearm

In [5, 49] the first qualitative/quantitative analysis of the ultrasonographic images of the human forearm, with respect to the finger movements, was carried out. Extensive qualitative trials were performed, i.e., live ultrasound images of sections of the human forearm were considered, while the subject would turn the wrist and/or flex the fingers, both singularly and jointly. An example is visible in Fig. 2.4.

One first result was that clearly, subsequent images related to each other in non-trivial ways. Human motion is in general enacted by contracting the muscles. When a muscle contracts, its length reduces but its mass must obviously remain constant; as a consequence, the muscle swells, mainly in the region where most muscle fibers are concentrated. This region, colloquially referred to as the muscle belly, expands in the directions orthogonal to the muscle axis; at the same time, the other organs in the forearm must accordingly shift around – this includes the bones, nerves, tendons and connective/fat tissue.

In the experiment, the ultrasound probe was held orthogonal to the forearm main axis, visually resulting in a complex set of motions: muscle sections (elliptical structures in the images) would shrink and expand; sometimes the muscle-muscle and muscle-tendon boundaries would disappear and reappear; and meanwhile, all other structures around would move in essentially unpredictable ways. It was clear that the deformations seen in the images could not easily be described in terms of simple primitives, such as, e.g., rotations, translations and contractions/expansions. Only very few simple features could have been explicitly targeted using anatomical knowledge, as it had been done in sonomyography; but as well, anatomy varies across subjects, which would have hampered the general applicability of the approach.

At the same time, it was apparent that whatever force the subject exerted (the three degrees of freedom of the wrist, the motion of single fingers down to the distal joints, etc.) was related point-to-point to the images. Muscular forces relate to torques at the joints, which in turn relate to measurable forces at the end effectors, for example at the fingertips. In the visual inspection there was no hysteresis effect, and each single dynamic configuration of the musculoskeletal structures under the skin would clearly correspond to a different image. This was the case both when the fingers would freely move and when they would apply force against a rigid surface or an object to be grasped. (Actually, that hinted at the fact that free movement actually represents the application of small forces, that is, those needed to counter the intrinsic impedance of the musculoskeletal structures.)

One direct consequence of this is that wrist and finger positions and forces could clearly be directly related *point by point* to each single image. This hinted at the possibility of using *spatial features* of the ultrasound images to predict the hand kinematic configuration (rather than, e.g., the optical flow or other features involving the time derivative of the images). This would have the advantage of being independent of the speed with which forces were applied.

Another very interesting characteristic of the forearm US images was that changes related to the hand/forearm kinematic configuration were almost totally local; e.g., it was tested that when the subject flexed the little finger, deformations would happen almost only in a certain region of the images; the region is loosely determined by the underlying anatomy. If, e.g., the US transducer was placed on the ventral side of the wrist, orthogonal to the axis of the forearm, then the action would be limited almost exclusively to the tendon leading out of the large flexor muscle (*M. Flexor Digitorum Superficialis*) controlling the little finger. The tendon pulls backwards and forwards parallel to the forearm axis, and appears as an elliptic structure growing and shrinking in a corner of the images. This further suggested the use of *local* spatial features of the images.

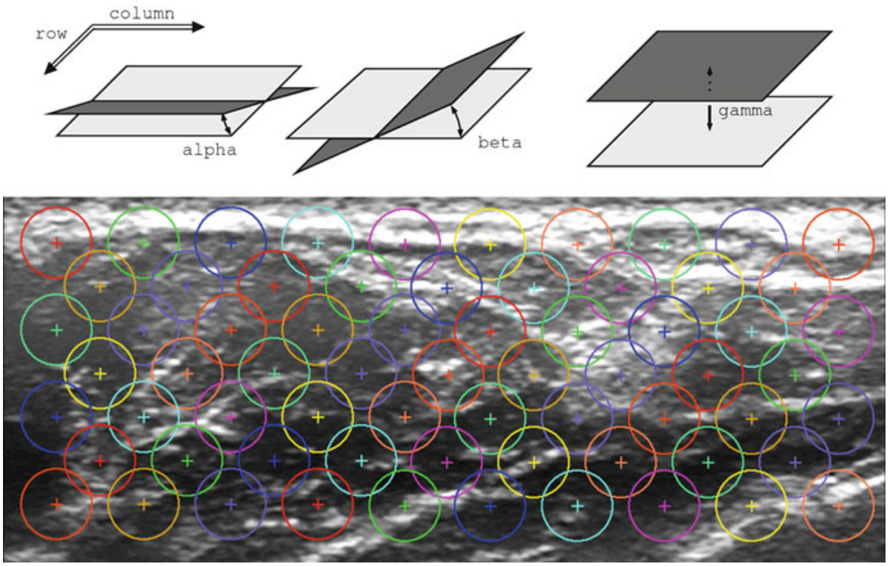

Fig. 2.5 (*Above*) A graphical representation of the meaning of the spatial features $\alpha_i, \beta_i, \gamma_i$; (*below*) the grid of interest points, as laid out on a typical US image (Reproduced from [49])

2.4.2 Relating US Images and Finger Angles/Forces

In the above-mentioned paper and in the subsequent [8], it was established that linear local spatial first-order approximations of the grey levels are *linearly related* to the angles at the metacarpophalangeal joints of the hand, leading to an effective prediction of the finger positions. More in detail, a uniform grid of N interest points, $p_i = (x_i, y_i), i = 1, \ldots, N$, was considered; a circular region of interest (ROI) of radius $r > 0$, centered around each interest point, would then be determined:

$$\mathrm{ROI}_i = \{(x, y) : (x - x_i)^2 + (y - y_i)^2 \leq r^2\}$$

Lastly, for each ROI, a local spatial first-order approximation of the grey values of its pixels $G(x, y)$ was evaluated:

$$G(x, y) \approx \alpha_i(x_i - x) + \beta_i(y_i - y) + \gamma_i$$

for all $(x, y) \in \mathrm{ROI}_i$. Intuitively, α_i denotes the mean image gradient along the x direction (rows of the image), β_i is the same value along the y (columns) direction, and γ_i is an offset. Figure 2.5 shows the grid of points and graphically illustrates the meaning of these features.

The above remark about the locality of the image changes is reflected in the changes in the feature values: Fig. 2.6 shows a correlation diagram, obtained by

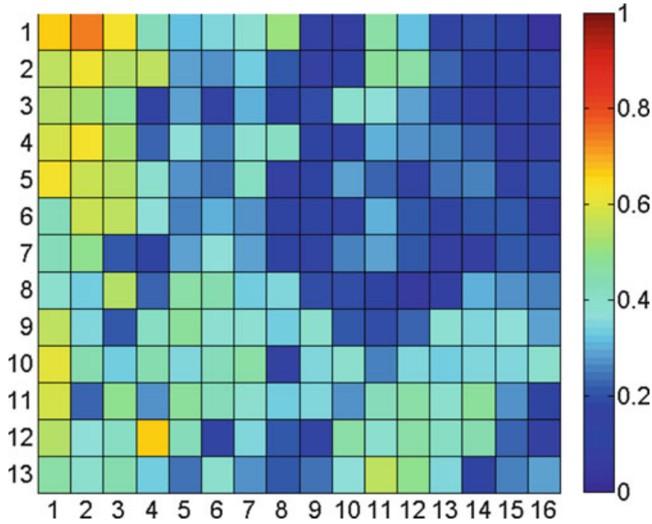

Fig. 2.6 Correlation diagram of the movement of the little finger. Each entry in the matrix denotes, for each region of interest i, the Pearson correlation coefficient between $\frac{\alpha_i+\beta_i+\gamma_i}{3}$ and the dataglove sensor values obtained while moving the little finger

considering the Pearson correlation coefficient between the average of $\alpha_i, \beta_i, \gamma_i$ and values of the sensor of the little finger of a dataglove (experiment reported in [8]). As is apparent from the figure, the movement of the little finger is strongly correlated to the feature values in the upper-left corner of the images.

Consider now the metacarpophalangeal angles of a finger, θ^{MCP}; if the above-mentioned features are considered, then

$$\theta^{MCP} = \mathbf{w}^T \mathbf{v}$$

where $\mathbf{v}$ is the vector of spatial features, and $\mathbf{w}^T$ is a vector of coefficients that can easily be estimated using, e.g., least-squares regression [4]. In general, given n (sample,target) pairs $\{\mathbf{x}_i, y_i\}_{i=1}^n$, the optimal $\mathbf{w}$ is

$$\mathbf{w} = (X^T X)^{-1} X^T \mathbf{y} \tag{2.1}$$

where the matrix and vector $X, \mathbf{y}$ are formed by juxtaposing all samples and target values. This is the exact solution to the problem, and it involves inverting the $d \times d$ matrix $X^T X$, where d is the dimension of $\mathbf{v}$. The task is therefore dominated by d rather than by the number of samples used to estimate the relationship, n, which is usually much larger than d.

The claim of linearity was validated in [5, 8] by collecting data from 10 intact subjects and having them freely move the fingers while recording the US images of the wrist, and the finger angles using a dataglove. A rough 3D hand model on a

Fig. 2.7 The experimental setup used in [5, 8] to record US images and metacarpophalangeal angles. A 3D hand model would teach the subject the motion to imitate; the ultrasound probe was held against the subject's wrist using a vise; and a dataglove was used to collect the MCP joint angles

computer screen would show the subject the visual stimulus, inducing by imitation a certain motion of a finger. (Figure 2.7 shows the setup used therein.)

The regression error, evaluated as the root-mean-square error normalised over the dataglove sensor range, was found to be as little as 1–2 %. The accuracy analysis was extended in [49] (see Fig. 2.8) to the case in which fewer ROIs were selected, or in the case the radius of the ROIs, r, changed. It was discovered that the error was not very sensitive across a large range of radius values of the ROIs, but rather sensitive to the spacing of the grid.

In [6, 45], the analysis was extended to finger forces, thanks to the use of a force sensor. The same features were extracted from the ultrasound images, and the same technique was applied to obtain a regression map between forces $\mathbf{f}$ and spatial features, obtaining for each finger force $\mathbf{f}^{FINGER}$ a relationship

$$\mathbf{f}^{FINGER} = \mathbf{w}^T \mathbf{v}.$$

where $\mathbf{w}$ was found by a regularised variant of the least-squares regression method called *ridge regression*. With respect to Eq. 2.1, in this case

$$\mathbf{w} = (X^T X + \lambda I_d)^{-1} X^T \mathbf{y} \tag{2.2}$$

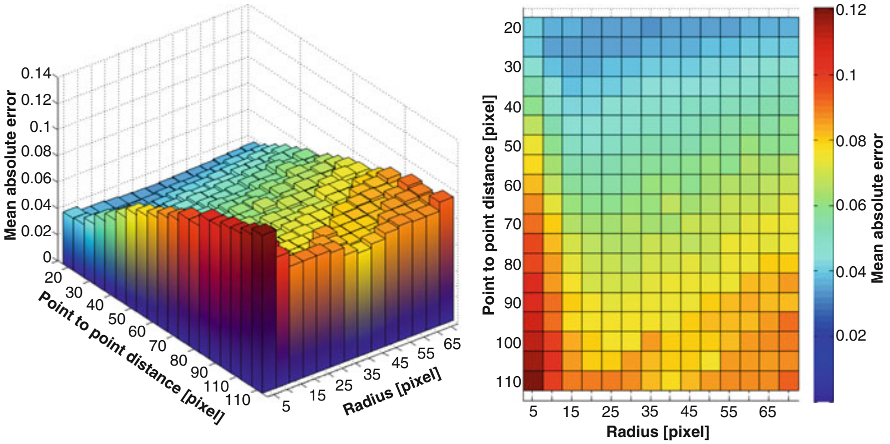

Fig. 2.8 Error analysis as the number of features considered changes, namely as the inter-ROI distance and ROI radius is varied

where I_d is the identical matrix of dimension $d \times d$ and $\lambda > 0$ is the regularisation coefficient, which was consistently set at the standard value of 1. (It was verified that altering λ would not change the results.)

In an experiment involving 10 intact subjects, it was assessed that the approximation obtained using Eq. 2.2 could predict all finger forces with a maximal error of about 2 % of the sensor signal range.

2.4.3 A Realistic Implementation

The feasibility of the approach was further verified in [6, 45], by setting up a realistic experimental scenario for this novel HMI. A minimal set of requirements was assessed for this technique to be applied to hand amputees; namely, (1) that the training (calibration) phase be short; (2) that it entail simple imitation tasks; (3) that it need no sensors; and lastly, (4) that the system be able to acquire new knowledge when required. These requirements are in general motivated by the bad condition of an amputee's stump, which quickly elicits fatigue and stress; moreover, amputees obviously the lack sensory feedback from the missing limb, which makes it hard (if not impossible) for the amputee to apply graded forces. Lastly, there is in principle no way of gathering ground truth, since no force sensors and/or datagloves can be used. The fourth requirement is motivated by the necessity of retraining previous patterns in case the signal changes due to, e.g., movement of the ultrasound transducer, or in order to improve the current prediction in case the subject is unsatisfied with it. Notice, anyway, that the vast majority of amputees have phantom feelings that *do not* correspond to the intended force/movement patterns;

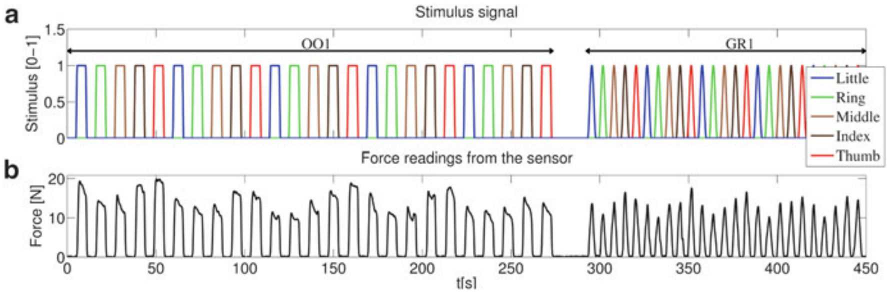

Fig. 2.9 (**a**) Part of the stimulus administered to the subjects in the experiment of [6, 45]. In an "on-off" phase (OO1), only rest and maximum force were induced for each finger; in the graded phase (GR1) the subjects had to exert force following a squared sinusoidal pattern. (**b**) Typical forces, as actually measured by a force sensor during the experiment

therefore a further effort is required to ignore the feeling and this further motivates the requirement for a simple calibration task.

The realistic scenario set up in the above-mentioned papers consisted of a psychophysical task which only entailed resting and pressing with maximum force on a table, following a simple visual stimulus, the so-called "on-off" training. (A force sensor was actually used just to compare the results with the actual ground truth.) The regression machines so obtained were then tested on data obtained while following a fully-fledged sinusoidal pattern of finger forces, and observing whether training on the visual stimulus only would entail a remarkable loss in performance.

The stimuli were organised in two identical sessions, and each session was likewise divided in two parts, according to the kind of stimulus administered: an *on-off* phase (OO) and a *graded* phase (GR). The complete structure of the stimulus for one of the sessions is displayed in Fig. 2.9.

The results showed that this was not the case: on-off training could be employed to predict graded forces, and training on a visual stimulus produced errors (around 10 %) of the same order of magnitude of those obtained using the sensors force values. See Fig. 2.10.

2.4.4 Incremental Learning

Lastly, the fourth requirement of Sect. 2.4.3 was enforced by exploiting the linearity of the relationships found. Ridge regression was here implemented in its incremental variant (incremental or recursive ridge regression in the signal processing community, see [41]), in which the regression vector(s) **w** can be updated as soon as a new (sample,target) pair is available, and no complex computational operation is required. As a result, the system was demonstrated to work seamlessly at 30 Hz and could acquire new knowledge whenever required, de facto blurring the

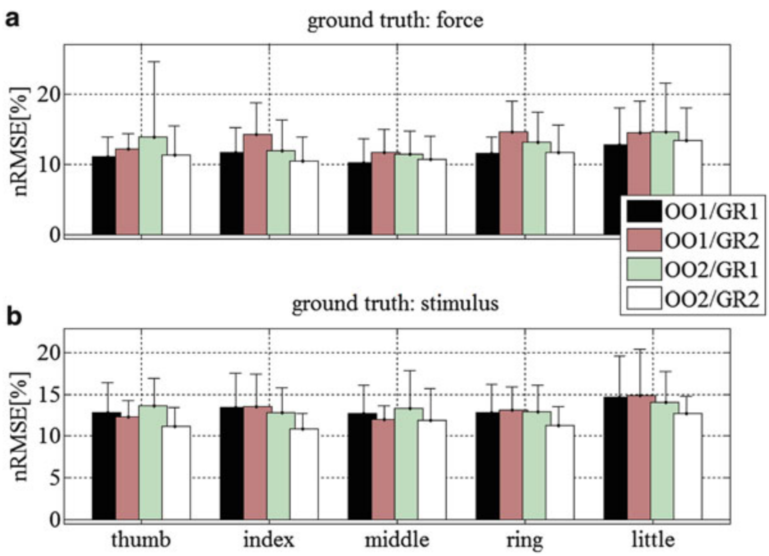

Fig. 2.10 Normalised root-mean-square error when training on an on-off dataset and testing on graded forces. The legend denotes the training/testing datasets, e.g., OO1/GR2 means that least-squares regression was evaluated with data gathered during the first on-off phase and the prediction error was evaluated on data gathered during the second graded phase. (*Top panel*) With the force as ground truth; (*bottom panel*) with the stimulus as ground truth. Each bar and stem represents the mean nRMSE and one standard deviation obtained over 10 intact subjects

distinction between the training and the prediction phase, typical of more complex machine learning methods. Such a system is strictly bound in space and is therefore independent of the time spent while adapting to the subject.

Consider Eq. 2.2 again, and define for simplicity $\mathbf{w} = A\mathbf{b}$ where $A \triangleq (X^T X + \lambda I_d)^{-1}$ and $\mathbf{b} \triangleq X^T \mathbf{y}$. As a new (sample,target) pair $(\mathbf{x}', y')$ is acquired, the updated regression vector $\mathbf{w}'$ can be obtained by juxtaposing the new sample to X and $\mathbf{y}$

$$X' = \begin{bmatrix} X \\ \mathbf{x}' \end{bmatrix} \quad \text{and} \quad \mathbf{y}' = \begin{bmatrix} \mathbf{y} \\ y' \end{bmatrix}$$

and then calculating A' and $\mathbf{b}'$. The interesting part is that there is no need to compute the inverse of $(X^T X + \lambda I_d)$ at each such update, as it happened in Eq. 2.2, since A can be directly updated using a rank-1 update, e.g., by using the Sherman-Morrison formula [25]:

$$A' = A - \frac{A\mathbf{x}'\mathbf{x}'^T A}{1 + \mathbf{x}'^T A\mathbf{x}'} \quad \text{and} \quad \mathbf{b}' = \mathbf{b} + \mathbf{x}' y'$$

As expected, adding a new sample will not increase the size of A, which always remains of size $d \times d$ – the system is strictly bound in space, irrespective of how

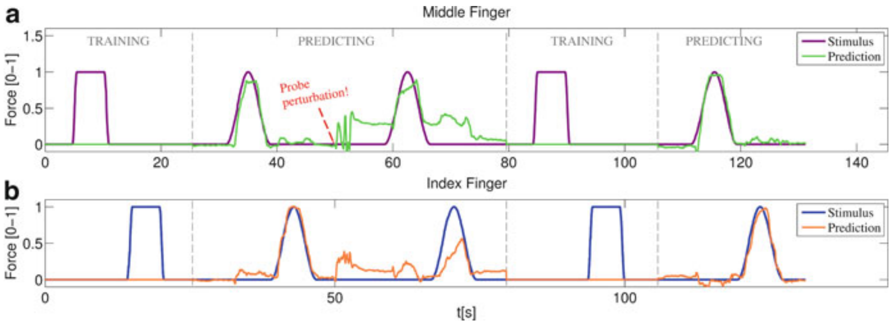

Fig. 2.11 Incremental training/testing in the experiment of [45]. After a perturbation in the position of the US probe reduces the quality of the prediction, new knowledge is acquired by the system. The prediction quickly recovers the accuracy obtained with the initial training. (**a**) Stimulus and prediction values for the middle finger; (**b**) stimulus and prediction values for the index finger

many updates are done. The time complexity of a rank-1 update is O(d^2), again independent of the total number of samples acquired so far, n. The net result is that the linear model can be updated each time new knowledge is available or is required, as neither the time- nor the space complexity grow as new samples are acquired. The system can switch back and forth from training to prediction and can then improve over time, as soon as the subject claims that the prediction is no longer accurate, or external events (e.g., a sudden movement of the ultrasound probe) happen.

Both a simulated online environment and a real implementation of the system were presented in [45]; Fig. 2.11 shows the temporal behaviour of the accuracy of the prediction, in the presence of an external disturbance and the subsequent acquisition of new knowledge to take that into account. The average timings reported therein for updating the linear model and predicting new values are, in turn, of 16.5 and 3.7 ms.

2.5 Discussion

2.5.1 Ultrasound Imaging as a Human Machine Interface

The extensive experiments conducted in the works summed up in this chapter indicate that medical ultrasound imaging has the potentiality to become a fully-fledged HMI for the disabled, at least as far as hand amputees are concerned.

Sonomyography (Sect. 2.3) is being studied since 2006, and has been employed to control a one-degree-of-freedom wrist prosthesis; its prediction of the wrist angle during extension shows a high correlation coefficient with the ground truth;

experiments with amputees are reported as promising. An interesting issue explored in this research is that of employing 1-dimensional (A-mode) ultrasonography, by means of single ultrasound transducers placed on the subject's forearm. These transducers are as large as standard sEMG electrodes and could potentially be embedded in an instrumented silicon liner or prosthetic socket, much as it happens with that kind of electrodes. Sonomyography represents then a very promising ongoing attempt at employing medical ultrasonography as an HMI, albeit so far restricted to large musculoskeletal structures. It may take some time to fully demonstrate the potential of sonomyography, given the fact that conventional medical US equipments are not designed for this purpose. For practical HMI applications using sonomyography, a number of challenges should be overcome, including probe miniaturization, probe attachment on skin, complexity of data collection system, signal processing for extracting meaningful data, multiple channel operation, and cost of system. Considering that US can provide not only signal but also cross-sectional image of muscle, more information can be extracted for the purpose of HMI. For this point, the above reviewed studies of sonomography are just the beginning of the field, in both method development and application.

Furthermore, in Sect. 2.4, it is shown that a surprisingly simple system, based upon linear regression, can be used to predict the angles at the metacarpophalangeal hand joints, and the forces at the fingertips of a human intact subject. The precision is of the order of magnitude of 2 % of the signal ranges when a dataglove or a force sensor are used; it reaches 10–15 % of the range when a visual stimulus is used. Furthermore, it is shown that a simple on-off task is enough to predict graded forces, and that no sensors are required to complete the calibration phase. This goes in the direction of providing a realistic scenario for the usage of such a device by amputees. Lastly, by exploiting the linearity of the relationship, an incremental system has been demonstrated, able to seamlessly run at 30 Hz and switch between training and prediction, paving the way to add new knowledge whenever required by the subject.

2.5.2 Advantages, Disadvantages, Perspectives

HMIs for the disabled are currently an extremely hot topic in both neuroscience, signal processing, machine learning and – of course – rehabilitation robotics. As is said in the introduction to this chapter, the only widely and practically used HMI for hand amputees is, currently, sEMG, which is however still far from representing the ideal solution to the problem of hand prosthesis feed-forward control. This is true to the point that many attempts at finding novel HMIs to replace or complement it have been carried out. Even if we limit ourselves to non-invasive HMIs, and to those HMIs which only interface to the peripheral nervous system (i.e., we do not consider brain-machine interfaces, computer vision, gaze tracking, etc.), we are faced with a plethora of different methods used to gather the intention of a patient from the forearm. These include, e.g., mechanomyography [27], magnetomyography [32] and pressure-based myography [48]. A thorough comparison among these techniques is still lacking, although their integration (fusion) is explicitly being called for:

> Given the difficulty of robust control solely by using EMG, the use of other sensor modalities seems necessary for the control of complex devices. The rich multimodal input would not only allow for the improved control but could also lead to the development of intelligent controllers that are able to operate somewhat autonomously, thereby taking over some of the burden from the user. [...] inertial measurement units can measure the orientation and movement of the prosthesis and from this, the intention of the user and the phase of the reaching movement could be predicted, complementing the information obtained via a myoelectric interface. [...] The next steps in this direction should be the implementation of sensor-fusion approaches, in which inertial, myoelectric, and possibly other information sources (e.g., artificial vision) are integrated. [29]

The technique presented in this chapter is still too young to be fully compared with these alternative systems (although Zheng et al. already have provided some evidence of its competitiveness with respect to sEMG, see [22, 23, 26]). Nevertheless we think that medical ultrasound imaging will become one such source of information in the medium term. This claim is supported by its simplicity of use (from the point of view of computation) and by the precision it can achieve while predicting positions *and* forces associated with muscular activity. The main advantage of US imaging lies in its high spatial *and* temporal resolution, which enables the detection of tiny changes in the musculoskeletal structure. Actually, the prediction of finger positions is tantamount to the prediction of the small forces involved in free movement, which sEMG can probably hardly detect.

Of course, the development of US imaging as an HMI is in its early stages and a number of disadvantages must still be taken into account. Firstly, the fact that the B-mode ultrasonography is not yet embeddable in a prosthetic socket, although it has recently become portable (see the Background section). As far as A-mode ultrasound is concerned, such embedding of single ultrasonic transducers presents the non-trivial technological issue of the miniaturisation of the electronics required to form the ultrasonic beam. Secondly, although ultrasonic scanning has been declared harmless (see the Introduction), the *medium-term* effects of it on human tissue are still unknown. Continually injecting ultrasonic waves in the stump of an amputee for, e.g., 6–12 h might be detrimental and induce biological damage.

Therefore, there is probably still some time before US imaging will be embedded in a hand prosthesis. Meanwhile however, there is a further interesting possibility. The feasibility of US imaging as a means to predict finger *positions* opens up the scenario of relieving several forms of neuropathic pain. The approach is probably not limited to amputees, but also to a wide range of muscle/nerve injury patients; actually, in all cases in which the motor commands do not result any longer in coherent sensorial feedback pattern.

More in detail: with the term *imaginary limb* we mean here the *intended* configuration of the hand; i.e., what the patient wants the hand to do. This is in contrast to the so-called phantom limb, that is the residual sensorial image of the missing limb. It is well known that the two limbs very seldom coincide, due to the peripheral and central nervous system reorganisation that regularly happens after an amputation; the phantom limb is usually felt as cramped in an unusual or impossible position. This discrepancy in the sensori-motor feedback loop is thought to be at the basis of, e.g., phantom-limb pain; this is a current opinion in neuroscience and stems from Flor et al.'s [20] and and Ramachandran et al.'s [40] seminal works. Complex regional pain syndrome [33] is thought to be another manifestation of this problem.

Medical ultrasound imaging could then be used to *visualise the imaginary limb* and showing it to the patient in real time. One could think of this as a psychophysical treatment, akin and much superior to mirror therapy [9], in which a good visual illusion of the missing hand would alleviate the pain, when administered regularly over time.

Acknowledgements We gratefully acknowledge Dr. Yong-Ping Zheng of the Interdisciplinary Division of Biomedical Engineering, Hong Kong Polytechnic University, Hong Kong, China, for thoroughly reviewing the section about sonomyography.

We also acknowledge all colleagues involved in this topic, first and foremost David Sierra González, then Dr. Georg Passig, Emanuel Zarka, Thilo Wüsthoff, Santiago Pérez Chávez, Markus Nowak and Prof. Patrick van der Smagt.

References

1. Ali M, Magee D, Dasgupta U (2008) Signal processing overview of ultrasound systems for medical imaging. White paper, Texas Instruments, Inc.
2. Atkins DJ (1996) Epidemiologic overview of individuals with upper-limb loss and their reported research priorities. J Prosthet Orthot 8(1):2–11
3. Boser BE, Guyon IM, Vapnik VN (1992) A training algorithm for optimal margin classifiers. In: Haussler D (ed) Proceedings of the 5th annual ACM workshop on computational learning theory, Pittsburgh. ACM, pp 144–152
4. Bretscher O (2008) Linear algebra with applications, 4th edn. Pearson, London
5. Castellini C, Passig G (2011) Ultrasound image features of the wrist are linearly related to finger positions. In: Proceedings of IROS – international conference on intelligent robots and systems, San Francisco, pp 2108–2114
6. Castellini C, Sierra González D (2013) Ultrasound imaging as a human-machine interface in a realistic scenario. In: Proceedings of IROS – international conference on intelligent robots and systems, Tokyo
7. Castellini C, van der Smagt P (2009) Surface EMG in advanced hand prosthetics. Biol Cybern 100(1):35–47
8. Castellini C, Passig G, Zarka E (2012) Using ultrasound images of the forearm to predict finger positions. IEEE Trans Neural Syst Rehabil Eng 20(6):788–797
9. Chan BL, Witt R, Charrow AP, Magee A, Howard R, Pasquina PF, Heilman KM, Tsao JW (2007) Mirror therapy for phantom limb pain. N Engl J Med 357(21):2206–2207
10. Chen X, Zheng YP, Guo JY, Shi J (2010) Sonomyography (SMG) control for powered prosthetic hand: a study with normal subjects. Ultrasound Med Biol 36(7):1076–1088
11. Chen X, Chen S, Dan G (2011) Control of powered prosthetic hand using multidimensional ultrasound signals: a pilot study. In: Proceedings of the 6th international conference on universal access in human-computer interaction: applications and services – volume Part IV, UAHCI'11, Orlando. Springer, pp 322–327
12. Cobbold RSC (2007) Foundations of biomedical ultrasound. Biomedical engineering. Oxford University Press, Oxford/New York

13. Cristianini N, Shawe-Taylor J (2000) An introduction to support vector machines (and other Kernel-based learning methods). Cambridge University Press, UK. http://www.amazon.com/Kernel-Methods-Pattern-Analysis-Shawe-Taylor/dp/0521813972
14. De Luca CJ (1997) The use of surface electromyography in biomechanics. J Appl Biomech 13(2):135–163
15. Donald I, MacVicar J, Brown TG (1958) Investigation of abdominal masses by pulsed ultrasound. Lancet 271(7032):1188–1195
16. Douglas T, Solomonidis S, Sandham W, Spence W (2002) Ultrasound imaging in lower limb prosthetics. IEEE Trans Neural Syst Rehabil Eng 10(1):11–21
17. Dussik KT (1942) Über die möglichkeit, hochfrequente mechanische schwingungen als diagnostisches hilfsmittel zu verwerten (On the possibility of using ultrasound waves as a diagnostic aid). Zeitschrift für die gesamte Neurologie und Psychiatrie 174(1):153–168
18. Dussik KT, Fritsch DJ, Kyriazidou M, Sear RS (1958) Measurements of articular tissues with ultrasound. Am J Phys Med 37:160–165
19. Finley FR, Wirta RW (1967) Myocoder studies of multiple myopotential response. Arch Phys Med Rehabil 48(11):598–601
20. Flor H, Elbert T, Knecht S, Wienbruch C, Pantev C, Birbaumers N, Larbig W, Taub E (1995) Phantom-limb pain as a perceptual correlate of cortical reorganization following arm amputation. Nature 375(6531):482–484
21. Graff KF (1981) A history of ultrasonics. In: Mason WP, Thurston RN (eds) Physical acoustics, vol 15. Academic, New York, pp 1–99
22. Guo JY, Zheng YP, Huang QH, Chen X, He JF, Chan HLW (2009) Performances of one-dimensional sonomyography and surface electromyography in tracking guided patterns of wrist extension. Ultrasound Med Biol 35(6):894–902
23. Guo JY, Zheng YP, Kenney LPJ, Bowen A, Howard D, Canderle JJ (2011) A comparative evalaution of sonomyography, electromyography, force, and wrist angle in a discrete tracking task. Ultrasound Med Biol 37(6):884–891
24. Guo JY, Zheng YP, Xie HB, Koo TK (2013) Towards the application of one-dimensional sonomyography for powered upper-limb prosthetic control using machine learning models. Prosthet Orthot Int 37(1):43–49
25. Hager W (1989) Updating the inverse of a matrix. SIAM Rev 31(2):221–239
26. Huang Q, Zheng Y, Chen X, He J, Shi J (2007) A system for the synchronized recording of sonomyography, electromyography and joint angle. Open Biomed Eng J 1:77–84
27. Islam MA, Sundaraj K, Ahmad RB, Ahamed NU (2013) Mechanomyogram for muscle function assessment: a review. PLoS ONE 8(3):e58902
28. Jensen JA (2002) Ultrasound imaging and its modeling. In: Fink M, Kuperman W, Montagner J, Tourin A (eds) Imaging of complex media with acoustic and seismic waves. Topics in applied physics, vol 84. Springer, Berlin, pp 135–166
29. Jiang N, Dosen S, Muller K, Farina D (2012) Myoelectric control of artificial limbs – is there a need to change focus? IEEE Signal Process Mag 29(5):152–150
30. Jørgensen TM, Tycho A, Mogensen M, Bjerring P, Jemec GB (2008) Machine-learning classification of non-melanoma skin cancers from image features obtained by optical coherence tomography. Skin Res Technol 14(3):364–369
31. Kane D, Grassi W, Sturrock R, Balint PV (2004) A brief history of musculoskeletal ultrasound: “from bats and ships to babies and hips”. Rheumatology 43(7):931–933
32. Mackert BM (2004) Magnetoneurography: theory and application to peripheral nerve disorders. Clin Neurophysiol 115(12):2667–2676
33. Maihöfner C, Baron R, DeCol R, Binder A, Birklein F, Deuschl G, Handwerker HO, Schattschneider J (2007) The motor system shows adaptive changes in complex regional pain syndrome. Brain 130(10):2671–2687
34. McDonald DG, Leopold GR (1972) Ultrasound B-scanning in the differentiation of baker’s cyst and thrombophlebitis. Br J Radiol 45:729–732

35. Merletti R, Botter A, Troiano A, Merlo E, Minetto M (2009) Technology and instrumentation for detection and conditioning of the surface electromyographic signal: state of the art. Clin Biomech 24:122–134
36. Micera S, Carpaneto J, Raspopovic S (2010) Control of hand prostheses using peripheral information. IEEE Rev Biomed Eng 3:48–68
37. Peerdeman B, Boere D, Witteveen H, in 't Veld RH, Hermens H, Stramigioli S, Rietman H, Veltink P, Misra S (2011) Myoelectric forearm prostheses: state of the art from a user-centered perspective. J Rehabil Res Dev 48(6):719–738
38. Ping H, Xue K, Murka P (1997) 3-D imaging of residual limbs using ultrasound. J Rehabil Res Dev 34(3):269–278
39. Rahmatullah B, Papageorghiou A, Noble J (2012) Image analysis using machine learning: anatomical landmarks detection in fetal ultrasound images. In: IEEE 36th annual computer software and applications conference (COMPSAC), 2012, Izmir, pp 354–355
40. Ramachandran VS, Rogers-Ramachandran D, Cobb S (1995) Touching the phantom limb. Nature 377(6549):489–490
41. Sayed AH (2008) Adaptive filters. Wiley/IEEE, Hoboken
42. Shi J, Chang Q, Zheng YP (2010) Feasibility of controlling prosthetic hand using sonomyography signal in real time: preliminary study. J Rehabil Res Dev 47(2):87–98
43. Shi J, Hu S, Liu Z, Guo J, Zhou Y, Zheng Y (2010) Recognition of finger flexion from ultrasound image with optical flow: a preliminary study. In: Proceedings of the international conference on biomedical engineering and computer science (EMBC), Wuhan, pp 1–4
44. Shi J, Guo J, Hu S, Zheng Y (2012) Recognition of finger flexion motion from ultrasound image: a feasibility study. Ultrasound Med Biol 38(10):1695–1704
45. Sierra González D, Castellini C (2013) A realistic implementation of ultrasound imaging as a human-machine interface for upper-limb amputees. Front Neurorobot 7:17
46. World Health Organisation (1998) Training in diagnostic ultrasound: essentials, principles and standards: report of a WHO study group. WHO technical report series, nr. 875, World Health Organisation
47. Xie H, Zheng Y, Guo J, Chen X, Shi J (2009) Estimation of wrist angle from sonomyography using support vector machine and artificial neural network models. Med Eng Phys 31(3): 384–391
48. Yungher DA, Wininger MT, Barr J, Craelius W, Threlkeld AJ (2011) Surface muscle pressure as a measure of active and passive behavior of muscles during gait. Med Eng Phys 33(4): 464–471
49. Zarka ER (2011) Prediction of finger movements using ultrasound images. Master thesis, DLR – German Aerospace Center, Germany and University of Applied Sciences Technikum Wien, Austria
50. Zhang J, Ma K, Er M, Chong V (2004) Tumor segmentation from magnetic resonance imaging by learning via one-class support vector machine. In: International workshop on advanced image technology (IWAIT '04), Singapore, pp 207–211
51. Zheng Y, Chan M, Shi J, Chen X, Huang Q (2006) Sonomyography: monitoring morphological changes of forearm muscles in actions with the feasibility for the control of powered prosthesis. Med Eng Phys 28:405–415
52. Zhou G, Zheng YP (2012) Human motion analysis with ultrasound and sonomyography. In: Proceedings of the international conference on biomedical engineering and computer science (EMBC), San Diego, pp 6479–6482

Chapter 3
Considering Limb Impedance in the Design and Control of Prosthetic Devices

Eric Perreault, Levi Hargrove, Daniel Ludvig, Hyunglae Lee, and Jon Sensinger

Abstract The mechanical properties of our limbs and how those properties are regulated by the nervous system endow us with the ability to interact with our environment in numerous predictable and effective ways. While there have been many recent advances in the design and control of prosthetic limbs, none yet have the capacity to regulate their mechanical impedance over the range achievable by

E. Perreault (✉)
Department of Biomedical Engineering, Northwestern University, Evanston, IL, USA

Department of Physical Medicine and Rehabilitation, Northwestern University, Chicago, IL, USA

Sensory Motor Performance Program, Rehabilitation Institute of Chicago, Chicago, IL, USA
e-mail: e-perreault@northwestern.edu

L. Hargrove
Department of Biomedical Engineering, Northwestern University, Evanston, IL, USA

Department of Physical Medicine and Rehabilitation, Northwestern University, Chicago, IL, USA

Center for Bionic Medicine, Rehabilitation Institute of Chicago, Chicago, IL, USA

D. Ludvig
Department of Physical Medicine and Rehabilitation, Northwestern University, Chicago, IL, USA

Sensory Motor Performance Program, Rehabilitation Institute of Chicago, Chicago, IL, USA

H. Lee
Department of Biomedical Engineering, Northwestern University, Evanston, IL, USA

Sensory Motor Performance Program, Rehabilitation Institute of Chicago, Chicago, IL, USA

J. Sensinger
Institute of Biomedical Engineering, University of New Brunswick, Fredericton, NB, Canada

Department of Electrical and Computer Engineering, University of New Brunswick, Fredericton, NB, Canada

Department of Physical Medicine and Rehabilitation, Northwestern University, Chicago, IL, USA

P. Artemiadis (ed.), *Neuro-Robotics: From Brain Machine Interfaces to Rehabilitation Robotics*, Trends in Augmentation of Human Performance 2,
DOI 10.1007/978-94-017-8932-5_3, © Springer Science+Business Media Dordrecht 2014

human limbs, or to replicate the functions that neuromuscular impedance control makes possible. The premise of this chapter is that designing prosthetic limbs capable of replicating the essential functions endowed by impedance control would lead to more natural and capable devices. The chapter summarizes current understanding of how human limb impedance is regulated, and attempts at replicating the functions afforded by impedance control in prosthetic limbs. It also highlights challenges and possible solutions in each of these areas.

Keywords Prosthetic • Impedance • Stiffness • Muscle • Design

3.1 Introduction

The mechanical properties of our limbs strongly influence our ability to interact with the physical environment. These mechanical properties can be quantified by the impedance of the limb, which describes the forces and torques generated in response to externally imposed displacement perturbations. The relatively small impedance that accompanies low levels of muscle activation facilitates stable contact with rigid surfaces, whereas the increased impedance associated with higher levels of muscle activity allows the limb to remain stable even in the presence of large destabilizing loads, such as those encountered during the use of many tools. The impedance of the limb also influences proprioception, determining how forces encountered at the hand or foot are transmitted to the trunk. The central nervous system adapts the impedance of our limbs in a task-dependent manner using a diversity of voluntary and involuntary motor pathways. This task-dependent regulation of impedance endows us with the ability to interact with our environment in many wonderful ways that cannot yet be replicated by prosthetic devices.

To date, few prosthetic devices incorporated explicit impedance control. Furthermore, none have had the capacity to regulate impedance over the range that can be achieved by the human limbs or, more importantly, to replicate the functions that neuromuscular impedance control makes possible. The underlying premise of this chapter is that designing prosthetic limbs capable of replicating the essential functions endowed by impedance control would lead to more natural and capable devices. However, there are many challenges associated with designing and building prostheses with this ability. These include: understanding how the impedance of intact limbs is modulated in a task-dependent manner and which components of this modulation are critical to performance, determining how limb impedance can be estimated during the functional tasks most relevant to prosthetic users, and designing prosthetic limbs that can replicate the essential task-dependent behaviors of our intact limbs. Our chapter addresses the current state-of-the-art in each of these areas.

3.2 Mechanisms Contributing to the Regulation of Human Limb Impedance

3.2.1 Musculoskeletal

There are many physiological mechanisms that can contribute to the impedance of a limb, and the net impedance results from the integrated actions of the neural and biomechanical systems. Though it is difficult to completely isolate the contributions from each system, we will start by examining how the properties of the musculoskeletal system contribute to limb impedance, acknowledging that many of those properties can be altered by changes in neural activation.

At a fixed posture, impedance can be tuned via changes muscle activation. An important muscle property that contributes to limb impedance is stiffness, the length-dependent or static component of impedance. For small rapid perturbations, the initial forces generated by a muscle can be described in terms of its short-range stiffness [92]. Numerous studies have suggested that short-range stiffness is a major contributor to the stiffness of an intact joint [18, 25, 56, 60, 74]. The short-range stiffness of a muscle depends on the number of active cross-bridges acting in series with the passive structures of the muscle, including the tendon and aponeurosis [75]. Because the cross-bridge and tendon elements act in series, the one with the lowest stiffness dominates the net stiffness of the entire muscle-tendon unit. Cross-bridge stiffness scales linearly with force, causing this to be the dominant factor at low levels of muscle activation. Tendon stiffness remains nearly constant, particularly at the higher levels of force for which it becomes most significant. Together, these components result in a muscle-tendon stiffness that increases monotonically with muscle force (Fig. 3.1a). The maximum stiffness that can be obtained is determined by the architectural properties of the muscle, and the passive structures to which it is connected [29, 30].

The impedance of a joint is determined by the inertial properties of the segments distal to that joint, and the viscoelastic properties of the passive tissues and the muscles acting across that joint. At a given joint angle, this impedance can be modulated through changes in muscle activation. The stiffness contributed by each muscle is scaled by the square of the muscle moment arm. There is also a kinematic stiffness proportional to the muscle force and the change in moment arm with joint angle [48]. Both of these factors emphasize the importance of geometry in determining limb stiffness [54, 53]. Due to the redundancies in the neuromuscular system, the stiffness of a joint can be modulated independently from the position and torque about that joint by selecting the muscles to be used for a given task and the relative activation of those muscles (Fig. 3.1b; [58]). These principles were a motivating factor in the development and use of impedance control in the field of robotics, and the recent application of these techniques to prosthetic control [1, 2].

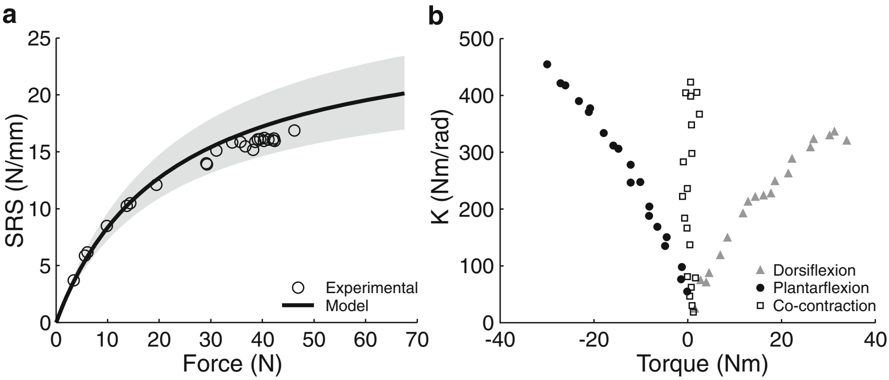

Fig. 3.1 Intrinsic stiffness of muscles and joints. (**a**) Short-range stiffness (SRS) for the plantaris muscle of the feline cat limb. *Circles* show experimental data from a single animal. *Solid line* shows short-range stiffness estimated from only the architectural parameters of the muscle. Similarity between experimental and modeled results illustrates how muscle short-range stiffness depends largely on muscle architecture (Adapted from [29]). (**b**) Stiffness for the human ankle joint during isometric dorsiflexion (*triangles*), plantarflexion (*circles*) and co-contraction with nearly zero net torque (*squares*). Figure illustrates how selective muscle co-contraction can be used to regulate joint stiffness independent from joint torque (Adapted with author permission from [58])

Although assessments of muscle and joint impedance have contributed much to our understanding of the physiological mechanisms underlying stiffness regulation, few tasks are completed using individual muscles or joints. Rather, it is the coordinated activities of multiple muscles and joints that allow us to perform the vast repertoire of tasks we complete each day. For this reason, there has been much research into the regulation of multijoint impedance [19, 32, 39, 43, 77, 85], which is typically quantified by the endpoint impedance of a limb. Endpoint impedance describes the mechanical properties of a limb at the point of contact with the environment. As such, it is particularly relevant to understanding how we interact with our physical world and also for designing prosthetic devices the aid that ability. For most joints and limbs, impedance can be characterized well by a system having inertial, viscous and elastic (stiffness) properties [44, 58, 83]. To date that vast majority of studies considering endpoint impedance have focused on the arm, and many have only considered the stiffness component of impedance, thought to be most relevant for postural control (Fig. 3.2).

Hogan first proposed that the nervous system may explicitly control stiffness and that the redundancy of the human motor system may allow stiffness to be regulated independently from movements or forces required to complete a given task [49]. For a multi-joint system such as the human arm, impedance can be regulated not only by changes in volitional muscle activation described above, but also by changes in limb posture [38, 77]. Indeed, when subjects are free to choose between changes in muscle activation or changes in posture, they first choose to select postures that match the mechanical properties of the limb to the

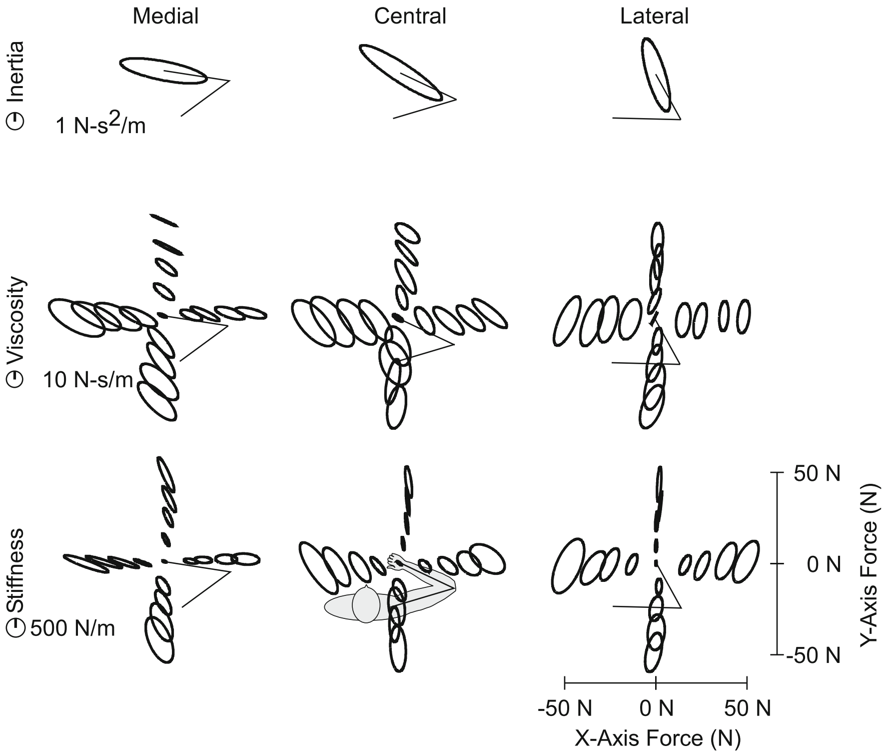

Fig. 3.2 Endpoint impedance of the human arm for different postures and endpoint forces. Three postures were tested, as indicated by the stick figure of the arm. Impedance was estimated for 17 different voluntary loads at each posture. The inertial, viscous and stiffness components of impedance are represented by an ellipse; the size of the ellipse represents the magnitude of the impedance component, and the orientation illustrates the direction in which each component most resists external perturbations of posture. Each ellipse is centered about a location corresponding to the average force exerted by the subject, except for the inertial ellipses which only changes with posture. These results indicate how both posture and muscle activation (i.e. voluntary force generation) influence the viscous and elastic components of endpoint impedance (Figure adapted from [83])

task being performed [118]. This approach likely reduces the effort required to complete the task, and may also increase performance through the reduction of motor noise associated with increased contraction [102]. The coupling between joints can be regulated by activating multi-joint muscles, which have an important role in transferring loads throughout the limb [130]. Selective activation of multi-joint muscles also provides a method for manipulating the spatial characteristics of endpoint stiffness (e.g. the direction of maximal stiffness and the relative stiffness in different directions), and maintaining stability [39, 44, 49, 72]. These important coupling issues have been considered for some time in the design of passive lower limb prostheses, but not upper limb prostheses. The advent of powered devices provides an opportunity to reconsider the potential benefits of inter-joint coupling and whether or not it might be beneficial to the use of upper limb prostheses.

3.2.2 Neural Feedback

There are numerous feedback mechanisms that can alter muscle activation and therefore change how the neuromuscular system responds to external perturbations of posture. These mechanisms thus influence the apparent mechanical properties of a muscle, joint or limb. Importantly, the behavior of many feedback mechanisms changes in a task-dependent manner [76, 90, 110], potentially providing insight to how the behavior of prosthetic devices might also be controlled to improve human performance in a wide range of tasks.

Rapid feedback mechanisms that occur prior to the onset of volitional activity are often described as reflexes or rapid motor responses. Those elicited by displacements of a muscle or limb are coined stretch reflexes. Houk was among the first to propose that spinally mediated stretch reflexes serve to regulate muscle stiffness [52]. Nichols and Houk [79] demonstrated this role in the cat soleus muscle, showing that stretch reflexes can compensate for nonlinearities, such as yielding, keeping stiffness relatively constant during stretch and release. Hoffer and Andreassen [47] extended these results throughout the physiological range of length and tension. They demonstrated that reflexes contribute to the stiffness of the muscle throughout this range and that they serve to keep stiffness nearly constant for muscle forces above approximately 25 % of maximum. Spinal stretch reflexes are similarly active for intact joints and limbs, and it has been suggested that they can contribute as much as 30–50 % of the net torque generated in response to postural perturbations [6, 21, 59, 84, 113]. The precise estimates depend on the joint being studied, as well as the techniques used to estimate reflex contributions to the net stiffness of a limb.

Reflex contributions to the mechanical properties of a limb can be varied in a task-dependent manner. Ludvig et al. [70] demonstrated that spinal reflex contributions to joint stiffness can be controlled independently from the intrinsic (e.g. short-range stiffness) contributions that vary with changes in steady state muscle activity. Longer latency stretch-evoked reflexes, including those mediated by supraspinal structures [22, 37, 81, 86], display even more task-dependence. One role particularly relevant to the regulation of impedance is that the sensitivity of longer latency stretch reflexes has been shown to increase to compensate for changes in the mechanical properties of the environment with which a limb is interacting. Specifically, reflex sensitivity increases during interactions with compliant environments relative to that observed during interactions with more rigid environments [4, 33, 34]. These results suggest that longer-latency stretch reflexes may serve to increase joint stiffness and stability during tasks in which that stability is not provided by the environment.

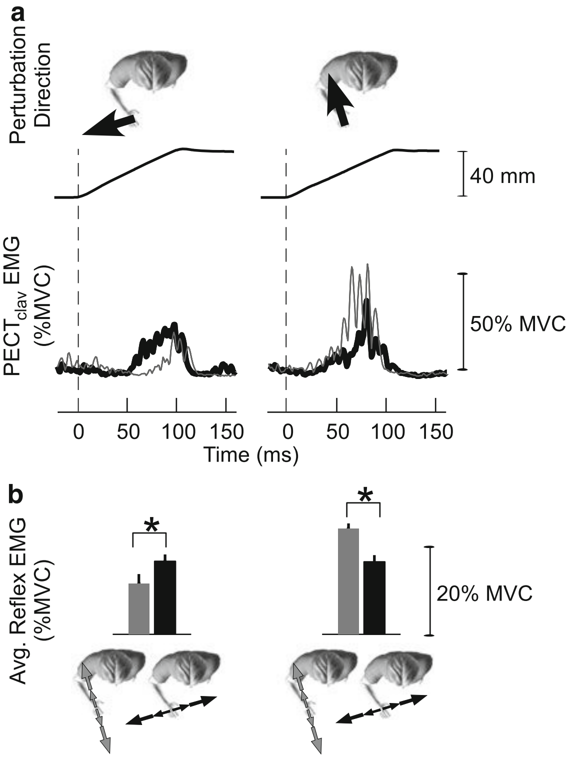

Fig. 3.3 Long-latency reflex adaptation in the human arm. Electromyogram (EMG) responses are from the clavicular head of the pectoralis muscle (PECT$_{clav}$) in response to ramp displacements applied to the hand. Displacements perturbations were applied as subjects interacted with unstable loads oriented along the hand-shoulder axis (*gray lines* and *bars*) or orthogonal to that direction (*black lines* and *bars*). Background muscle activation was constant for both loads. Results from one subject are shown in (**a**); group results from 5 subjects are in (**b**). Stretch reflex responses elicited by identical perturbations depended on the orientation of the unstable load illustrating how these feedback responses can compensate for changes in the mechanical properties with which a subjects interacts. Further details can be found in [63, 62]

Stretch-evoked reflexes are also important for coordinating mechanical coupling throughout the limb. Many tasks, such as tool use, compromise arm stability along specific directions relative to the tool [93]. Stretch reflexes tuned to those directions could present an efficient mechanism for regulating arm impedance in a task appropriate manner. To be effective, such tuning would need to coordinate the activity of muscles throughout the limb so as to match the mechanical properties of the limb to those of the environment. Evidence for such adaptation and coordination was recently provided by examining how stretch reflexes throughout the arm adapt to environments that compromise limb stability along specific directions (Fig. 3.3; [62, 63]). A related role of long-latency reflexes is to compensate for the coupling torques between joints that arise during multi-joint movements [64].

Together, these findings highlight how the nervous system uses feedback to regulate limb mechanics and to adjust those mechanics in a task-relevant manner. These behaviors have already motivated some prosthetic designs [35] and may provide insight to how more complex behaviors, requiring the coordinated activity of multiple joints, may ultimately be implemented in a robotic device.

3.3 Estimating Impedance Relevant to Prosthetic Use

Whereas much has been learned about the regulation of human limb impedance, most studies have been performed under conditions relevant to only a limited repertoire of functions. These include tasks performed at a single posture and at fixed levels of muscle activation. These conditions allow for precise estimates of the limb mechanics, but it can be difficult to extend them to more dynamic conditions. Some elegant work toward this goal has been completed during upper limb movements [8, 19, 42], and for rapidly varying changes in muscle activation [71], though each of these studies still involved constraints not present during most natural tasks.

One of the most striking omissions in the literature is a lack of information regarding whole leg impedance during locomotion. This omission is due largely to the challenges associated estimating leg during all phases of the gait cycle. Experimental estimates of limb impedance require controlled perturbations to be applied to the limb, and the relevant forces and displacements to be measured [58]. These tasks are very difficult to achieve during gait, especially without disrupting natural gait patterns. Numerous studies have characterized the torque-angle curves during various locomotor tasks, but these cannot be used to estimate impedance [96]. Hence, the full information required to replicate the impedance of an intact leg in a prosthetic device is not yet available.

Two recent studies have made strides toward this goal by partially quantified leg impedance during locomotion. Each focused on the ankle. Rouse et al. [97] used a robotic platform to perturb the ankle during the stance phase, while Lee and Hogan [69] used a robotic exoskeleton to perturb the ankle during swing. Together, these studies provide the first glimpses into how ankle impedance is modulated throughout the locomotor cycle (Fig. 3.4). An interesting finding of each is that the estimated stiffness is low relative to that estimated when similar torques are produced during isometric conditions (for comparison see [55]). Furthermore, Rouse demonstrated that the estimates ankle stiffness was not significantly different than the slope of the torque-angle curve for this joint, which would not be expected a priori [96]. This empirical finding suggests that ankle stiffness during a large portion of stance phase can be approximated by a nonlinear spring, as described in more detail below. While the results shown in Fig. 3.4 were restricted to ankle motion in the sagittal plane, Lee et al. [67, 68] have also reported passive and active measures of ankle impedance in multiple degrees of freedom, including plantarflexion-dorsiflexion and inversion-eversion, which could ultimately be useful for generating more naturally compliant ankle motions in a prosthetic device.

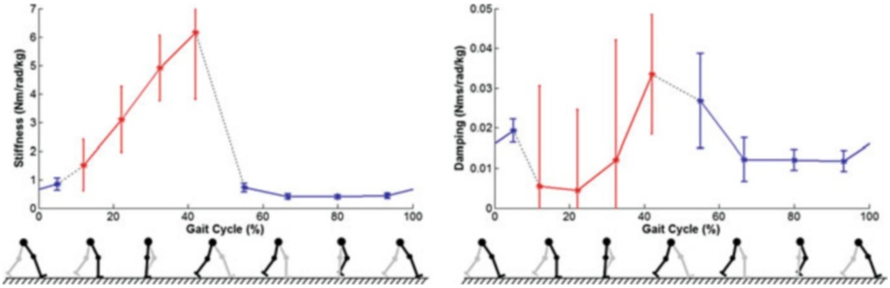

Fig. 3.4 Stiffness and damping properties of the human ankle during locomotion. The stance phase accounts for approximately 60 % of the gait cycle, beginning with heel-strike and ending with toe-off of the same foot, and the swing phase accounts for the remaining 40 % of the gait cycle. Ankle stiffness (*left*) and damping (*right*) values were normalized by bodyweight. *Asterisks* and *error bars* denote the mean and standard deviation, respectively. *Red* and *blue* colors denote results from Rouse et al. ([98]) and Lee and Hogan ([69]), respectively. No results were available for the regions indicated by the *dashed gray lines*. Note that the ankle stiffness showed an increasing trend throughout the stance phase until the contralateral leg hits the ground, and remained relatively constant during the swing phase. The damping also showed the similar trend as the stiffness, except for possible the drop in the early gait cycle

Due to the experimental challenges associated with estimating the impedance of the whole leg during locomotion [61], a number of alternative methods have been proposed. Pfeiffer et al. [87] developed an indirect method based on scalable models of muscle stiffness [29, 53]. This approach requires knowledge of only muscle activity, which is relatively easy to obtain, rather than the ability to perturb the limb throughout all phases of the locomotor cycle. This technique has been validated for the isometric conditions during which leg impedance can readily be measured experimentally, but stiffness estimates obtained during isometric conditions appear to be larger than those during dynamic conditions even for matched torque levels [69, 98]. Nevertheless, this modeling approach could be useful for providing an upper bound on the stiffness of the entire limb.

A very different strategy was recently developed by Aghasadeghi et al. [3], who used a parameter estimation algorithm to learn the impedance parameters of an equivalent leg controller that can replicate an observed locomotor trajectory. It is important to note that the goal of this work was to develop a controller that could replicate the kinematics of unimpaired gait (Fig. 3.5) without regard for how well these parameters matched the true impedance of the underlying system. The initial results of using this approach for prosthetic control are described below. They are promising, suggesting that it may not be necessary to precisely determine the mechanical properties of the intact limb as long as an equivalent controller can be obtained. To maintain perceptual and kinematic symmetry, however, it is likely that any equivalent controller will need to have mechanical properties reasonably similar to the intact limb. The exact degree of similarity remains to be determined.

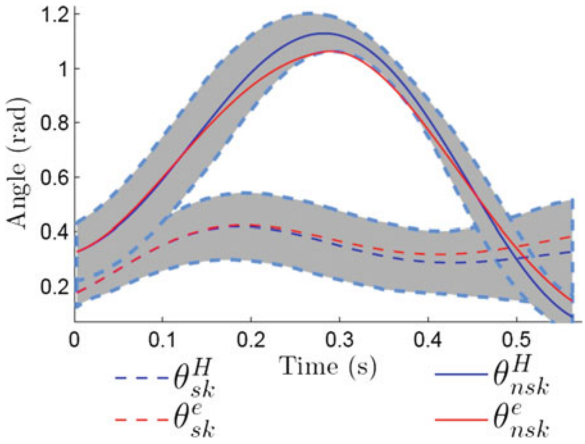

Fig. 3.5 Measured and modeled kinematics of the knee during the swing (θ_{nsk}) and stance (θ_{sk}) phases of locomotion. Superscript H corresponds to measured angles from a healthy subject walking at a self-selected pace. Superscript e corresponds to the angles obtained when simulating an equivalent impedance controller at the knee (Figure adapted from [3])

3.4 Mechanics of Traditional Prosthetic Limbs

The previous section discussed some of the physiological mechanisms contributing to the mechanical properties of human limbs, how those properties can be estimated, and how they are varied across tasks. While many of these issues remain active research areas, the importance of limb mechanics and the need to replicate some of their essential features in the design of prostheses has been appreciated for some time. This section provides an overview of some traditional approaches towards achieving this goal.

One critical feature influencing the performance of a prosthetic device is the mechanical interface that it presents between the user and the environment. This interface is affected by how the prosthesis is attached to the user, and by the mechanical design and control of the device itself. The net impedance of the prosthesis-user system is the serial connection of these two components. If there is a large discrepancy between the impedance of each component, the net impedance can be dominated by a single component. Although both the interface with the user and the design of the device are critical, few studies have considered each of these components in detail, even when the main objective has been to develop a system that presents an appropriate impedance to the environment. Therefore, a brief history of prosthetic design may be instructive for understanding how mechanical considerations have enhanced or limited prosthetic performance.

3.4.1 Mechanical Interfaces Between the User and Prosthesis

Almost all prostheses are attached via a socket covering the residual limb; much like a shoe covers a foot. These sockets are custom-made for each patient, usually by a certified clinician. A socket is normally placed over a substantial amount of soft tissue that surrounds a bone, except in the case of joint disarticulations. This soft tissue interface results in significant compliance that can limit the impedance between the user and the environment [132]. For a transhumeral prostheses, the rotational stiffness of this interface ranges from 40 to 120 Nm/rad [107]. Thus, it is not possible to create a trans-humeral prosthesis with a stiffness greater than this value when using a traditional socket. There are two promising alternatives to the socket interface. The first is osseointegration [15–17, 120], in which a steel connector is implanted into the residual bone. This connector protrudes from the bone through the skin, and is attached directly to the prosthesis providing a rigid interface from the prosthesis to the user. Invented in the 1990s, there are still concerns regarding deep infection of the bone [13], although progress continues to be made both in the implant design and in care of the insertion point. A more conservative interface is the SISA implant [100], a T-shaped device embedded in the distal end of the residual limb to replicate the function of the condyles present after a disarticulation. A less aggressive historical variant is the Marquardt osteotomy [80], in which the bone is broken and reset at 45° angle, or for lower-limb, the Ertl osseoperiosteal tibiofibular synostosis [57], in which a bone-bridge fuses the tibia and fibula together. With any of these approaches, the prosthesis can use these 'condyles' to achieve a more rigid connection, although one that is still substantially more compliant than the intact skeletal system.

3.4.2 Mechanical Design and Control of Prostheses

3.4.2.1 Upper Limb Prostheses

The mechanical designs for upper limb prostheses can be segregated in to four broad categories: (a) passive cosmetic devices, (b) activity-specific devices (e.g. a swimming paddle or screw-driver attachment), (c) body-powered devices, and (d) externally powered devices, of which the majority are myoelectric prostheses [126]. Here we will focus on the latter two categories for which general considerations of impedance control are most relevant.

In North America the majority of users prefer body-powered devices, due to the greater function they currently provide [114], their light weight and rugged design [41], and the simple manual control and associated proprioceptive feedback via extended physiological proprioception [112]. Though in common use, body-powered devices are often overlooked by researchers who tend to favor robotic prostheses, even though the performance of commercially available body powered devices has been estimated to exceed that of robotic devices by approximately 200 % [114]. Control of body-powered prostheses is commonly achieved through a Bowden cable that couples motion of an intact joint to movement of the terminal device. For example, using movements of the shoulders to control the grasp of a prosthetic arm. This direct coupling to the motions of the user allows for more accurate control of position and force [125], and more intuitive sensory feedback to the user [112] than can presently be obtained with myoelectric prostheses [74, 131]. Although there are many benefits, there are also limitations associated with body-powered devices. Most are associated with the limited motion of the intact joint used to control the device, especially since sufficient slack must be left in the cable to ensure that the prosthesis is not unintentionally activated when the intact joint is moved for purposes other than prosthetic control. For transhumeral prostheses, in which enough cable excursion must be available to operate both the terminal device (50 mm of excursion required) and the elbow (an additional 63 mm of excursion required), cable excursion is even a more limited resource [31, 40]. This limited excursion also restricts the options for implementing biomimetic impedance levels in a body-powered device because a compliant mechanism requires more cable excursion to achieve the same endpoint position than a rigid mechanism. This tradeoff has been seen most clearly by several groups designing body-powered continuously-variable transmissions (CVTs) [108, 123]. These devices operate similar to Robogrip™ pliers, in that they move quickly until an object is grasped. Further displacement shifts the gear ratio, such that user forces result in higher endpoint forces. However, the excursion necessary to shift the gear ratio is often an expense prosthetic users are not willing to pay [123].

Myoelectric devices are becoming more common in North America, and many people alternate between body-powered and myoelectric prehensors, since almost all end-effectors are interchangeable. In Europe, the majority of upper limb prosthetic users with an active prehensor prefer myoelectric devices to body-powered devices [66]. This increasing use of myoelectric devices creates opportunities with respect to impedance control.

There are two important factors influencing the impedance that can be rendered by a myoelectric prosthesis. The first is the gear ratio between each actuator and the motion of the corresponding degrees-of-freedom. The intact musculoskeletal system employs strong actuators (muscles) with a limited range of excursions and speeds. Muscle actions are transmitted to appropriately scaled endpoint motions using bones as lever arms to amplify motions and scale down forces. In contrast to muscles, electric motors are generally weaker than required, thereby limiting size and weight, but have high speeds and an unlimited range of excursions. We accordingly use substantial transmissions to increase the force and decrease the speed into a functionally relevant range. These transmissions are often substantial (e.g., 600:1–1,500:1), and have two important effects. First, these high gear ratios improve the ability of the prosthesis to render positions, but drastically reduce the ability to render forces since the influence of the gear ratio has an opposite effect on these two quantities. Second, transmissions create amplify the motor impedance by the square of the gear ratio [26], making it difficult to obtain biomimetic impedance values. Of particular importance is the inertia of the rotor. Although some have advocated impedance-rendering control strategies [5, 45], the inertia of the rotor, amplified by the square of the gear ratio, tends to dominate the net impedance above moderate frequencies (e.g., 10 Hz) [107, 133].

The second factor limiting the impedance of myoelectric devices is that end-users often need to hold an object for extended periods of time. Weight is of paramount importance in prosthesis design [9–11], and even 50 g can result in the rejection of a device. Because electric motor-transmissions are inherently inefficient, particularly at stall-torque (0 % efficiency), current myoelectric prostheses use non-backdrivable 2-way clutches [28] to conserve power during periods in which it is necessary to forcefully grasp an object or maintain an arm against gravity for extended periods. It is possible but non-trivial to render impedances in light of these clutches [106].

3.4.2.2 Lower Limb Prostheses

For the reasons described above, both body-powered and myoelectric upper limb prosthesis have avoided compliance in their mechanisms. In contrast, impedance has been more widely considered in the design of lower limb prostheses, which are repeatedly used as a mechanical interface between the user and the ground. Many elegant mechanical designs have emerged over the last 500 years, with perhaps the most notable being the Anglesey leg, which used compliant cat-gut tendons to couple ankle and knee joints [14] as do the gastrocnemius muscles in an intact limb. A more recent incarnation of this leg is the hydraulically coupled Hydracadence 2 [99], which also couples the ankle and knee joints.

Prosthetic feet and ankles are a common place to incorporate mechanical compliance. Prosthetic feet serve four purposes: they absorb impact energy at the heel during initial contact; they store energy during mid-stance; they release energy during toe-off, and they provide stability during standing. SACH (solid ankle, cushioned heel) feet became popular in the 1950s due to the energy-absorbing properties of their cushioned heel, which serves as a damper. More recently dynamic feet with flexible carbon plates have become very popular; these can store up to 90 % of the energy placed into them during stance. Multi-axis feet add moderate compliance in other directions, including for torsional and side-to-side motions [57].

The mechanical properties of prosthetic knees have traditionally been designed to be dissipative, since the knee does not generate positive net power during level-ground walking [128]. Although simple friction joints work well at a single cadence, pneumatically or hydraulically regulated knees function better over a wide range of cadences, since the viscosity of their dissipative elements can be tuned appropriately [101]. More recent knees use microcontrollers to fine-tune dissipation over a range of speeds and activities [65]. Lower-limb prostheses that actively generate power have recently received renewed attention in light of improved actuator capabilities (e.g. [35, 46, 117]). Many of these legs actively exploit tunable impedance characteristics [82], some of which are highlighted below.

In summary, many prosthetic feet have substantial compliance, typically designed as an energy-storing element. In contrast, the majority of prosthetic knees have notable damping, either static or variable in nature.

3.5 Innovations in the Mechanical Design and Control of Prostheses

3.5.1 Mechanical Design

Continuously variable transmissions, which have not worked well for body-powered prostheses due to the excursion issues described above, have improved the performance of myoelectric prosthesis, where excursion is not a concern. For example, the Otto Bock Dynamic arm uses an elegant transmission in the elbow joint that couples with a cable, such that the arm reverts to zero impedance at full extension [91]. Zero impedance during full extension is important to facilitate a natural free-swing during walking, both to minimize energy consumption by the user and to facilitate a cosmetic appearance.

Series elastic actuators [88, 89] are a promising technology for regulating the impedance of a prosthetic device. The intentional introduction of compliance within an otherwise rigid electromechanical actuator has conventionally been avoided, because it reduces high-frequency performance and high-magnitude force generation; it also has the potential to introduce substantial dynamics between the sensors and actuators, which can limit the gains of a feedback controller. Nevertheless, for many applications these disadvantages are outweighed by the many advantages. These include: improved force rendering, improved force sensing fidelity [109], larger stable feedback gains when the sensors and actuators are collocated [127], and improved power densities that can be obtained by storing energy in the elastic transmission as is done in biological tendons [94]. This property of a series elastic actuator is often described as a catapult effect [5, 82]. Finally, series elastic actuators limit the maximum impedance at high frequencies [88, 89], which can be used to purposefully limit force levels, as an elastic transmission will reduce environmental contact forces transmitted through the actuator [5, 133]. For actuators with low endpoint inertia and viscosity, an elastic transmission also would limit the magnitude of the forces exerted on the environment. For these reasons, series elastic actuators are well suited to applications involving robot-human interaction. Accordingly, they been researched for application in rehabilitation devices including prosthetic ankles and elbows [7, 46, 105], rehabilitation robots for stroke therapy [115, 124], and other devices [119]. Active modulation of the impedance of these devices has been investigated for upper limb prostheses [12, 23, 36, 105], but has not yet been clinically implemented.

It should be noted that conventional designs have placed the compliant element in series between the actuator and end-effector, but it has recently been demonstrated that the compliant element may be placed between the transmission ground and the prosthesis housing [104]. Doing so adds the inertia of the transmission ground, but allows the instrumentation of the compliance to avoid continuous rotation and the associated difficulties instrumenting wires to a continuously rotating object.

Variable-impedance actuators have received increasing interest in the last decade, especially within the field of robotics [119]. There are a number of approaches to vary the impedance, and also a number of difficulties, including minimizing energy consumption, frequency of the impedance adjustment, and avoiding saturation of the compliance by stiction or backlash of the impedance-adjusting mechanism. Due to the proliferation of designs, there have been recent efforts to define a taxonomy of approaches [121] and to identify those that are best suited to specific applications [20]. To date, however, no clear case has been made for using these devices as part of a prosthesis. Although mechanical arguments certainly can be made, current variable impedance actuators are heavy, and even small increases in weight ($\sim$50 g) can lead to the rejection of a prosthesis. Hence, any device that increases the net weight of a prosthesis is likely to fail as a product [103]. Although variable-impedance actuators have been shown to reduce weight relative to an actuator without compliance, they have not yet been shown to reduce weight relative to series elastic actuators. However, since the variable impedance actuator field is very active and relatively new, there remains the possibility that solutions with reduced weight and ample impedance control may still be found.

3.5.2 Active Control of Impedance

So far, we have largely considered devices that rely on clever mechanical designs to impart desired mechanical properties to an actuator or prosthesis. An alternative approach is to use feedback control to regulate a desired impedance explicitly. In addition to rendering the desired mechanical properties, it is also critical to ensure that the actively controlled impedance remains stable during interactions with the environment. Below we briefly summarize three methods for achieving these goals. Further details can be found in [50].

Under ideal conditions where the intrinsic mechanical impedance of the system to be controlled is low (e.g., low friction and low inertia), a simple position-based feedback controller (e.g. a proportional-derivative controller) can be used to regulate impedance. Here, impedance is set simply by the feedback gains; the proportional term regulates stiffness and the derivative term damping. This controller enables independent regulation of motion and impedance through a selection of these gains and the desired motion One important feature of this impedance controller is that it exhibits passive behavior, which guarantees stability when in contact with any other passive environment [27].

It often is nontrivial to design a robot or prosthesis with low intrinsic mechanical impedance. Furthermore, feedback delays or unmodeled dynamics between the sensors and actuators can compromise stability by creating nonpassive behavior. One approach for dealing with these issues is to incorporate force feedback as well as motion feedback. Increasing the force feedback gain decreases the apparent impedance of the system. While this approach can work for modest feedback gains, attempts to reduce the apparent system inertia too much below the actual inertia will lead to instability. Substantial improvements can be obtained using natural admittance control though stability cannot be guaranteed [78]. For these reasons, most prosthetic devices incorporating impedance control have relied on simple feedback that ensures stability at the expense of rendering performance.

3.5.3 Impedance Control for the Upper Limb

Hogan [51] first proposed impedance control of upper limb prostheses, and assessed its performance [1, 2]. This prosthesis allowed the user to modulate the stiffness of the elbow, but only over a small range (0.5–7 Nm/rad), and only in a constrained environment. The user was able to modulate stiffness by co-contracting their muscles; the damping coefficient was fixed at 0.5, and inertia was fixed at 0.05 kg m^2. Co-contraction modulation was observed when impedance control was used, but not when velocity control was used. It was also observed that impedance control smoothed velocity transitions, although no kinematic differences existed between the two controllers. No difference between impedance control and velocity control was observed when cutting meat, donning a sock, or rolling dough, although several experiment characteristics such as confounding motion paradigm and impedance paradigm, along with the small range of adjustable impedance, may have biased results [105].

English and Russel [36] designed a variable impedance actuator for application as a prosthesis in the late 1990s. Their design required quadratic springs, however, which were too difficult to fabricate at the time to allow for clinical investigation. More recent variable impedance actuator implementations have allowed the use of conventional spring, thus avoiding this problem [119].

Although series elastic actuators have a fixed impedance, they render highly accurate forces, and can thus be used to render a virtual impedance below their physical impedance [95, 105]. Sensinger and Weir [105] used a custom torsional spring that passed through the interior of a motor and harmonic drive to achieve a compact series elastic actuator (Fig. 3.6). This actuator was packaged in a housing the same size as a commercial prosthetic elbow, and tested by a variety of able-bodied persons and persons with a transhumeral amputation or shoulder disarticulation. The spring was instrumented with strain gauges to measure torque, and impedance was regulated over a range of [stiffness = 2–102 Nm/rad, viscosity = 0–10 Nm/(rad/s)]. The velocity of the prosthetic elbow was set to be proportional to the amplitude of the user's EMG signals – a control strategy commonly used in the clinic since integration of the noisy EMG signal results in a better controlled position response than using a rate-limiter or low-pass filter could achieve [24, 105, 125]. Users modulated impedance levels by the co-contraction of their agonist and antagonist muscles. Although this is a biomimetic approach, EMG signals are very noisy [24], and it was difficult for subjects to simultaneously regulate the motion of the device and the impedance of the arm.

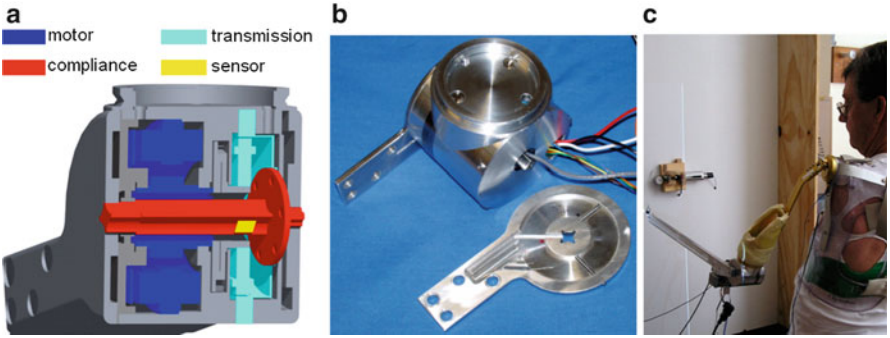

Fig. 3.6 Use of a series-elastic actuator to render impedance control in a prosthetic elbow. (**a**) The spring is passed through the center of the motor and transmission to achieve a compact design. (**b**) Physical mechanism. (**c**) Subject controlling the device using impedance control

More recently Christenson [23] and Blank et al. [12] used alternative strategies to modulate discrete levels of impedance independently of myoelectric control signals. These approaches offer much promise, particularly at distal joints such as the wrist and fingers where the socket-residual-limb interface does not saturate impedance.

3.5.4 Impedance Control for the Lower Limb

Microprocessor-controlled, mechanically active prosthetic legs have recently become commercially available, and several additional prototypes are in various stages of development ([35]; Ossur knee; [116]). These devices typically use a hierarchical control strategy. The higher level is comprised of a finite state machine which often subdivides locomotion into different activities (e.g. walking, stair-climbing) and also subdivides the gait into discrete phases (e.g. stance phase, swing phase) [122]. The current state of the device then provides control information to lower-level controllers to ensure that the actuator behaves properly (Fig. 3.7).

Early commercially available devices were programmed to follow a state-dependent position trajectory (e.g. Ossur knee). A subtle yet significant issue with position-based control is that suitable motion tracking requires a high-output impedance, which forces the amputee to react to the limb rather than interact with it [116]. Furthermore, high-output impedance may also present safety issues if the device inadvertently comes into contact with the environment. For example, if a user did not clear a curb when walking across the street, then the contact between the stiff prosthesis and the ground make knock the user off-balance or even injure the residual limb.

Fig. 3.7 Individual ambulating with a powered knee-ankle prosthesis that incorporates active impedance control

A more attractive low-level control solution is to use impedance control in some or all of the states [7, 116]. This allows the user to interact with the device rather than ride on top of the device. Sup et al. performed a regression analysis on gait data to determine impedance values (stiffness and damping and equilibrium terms) that would result in joint torques similar to those produced by healthy control subjects [129]. It should be noted that the estimated parameters are not necessarily physiological estimates of the users' true impedances as the regression solution is non-unique and needs to be constrained. Fine-tuning of impedance parameters for lower-limb prostheses (or biped simulations) is traditionally done experimentally, requiring hours of manual tuning of these parameters for every controller within each phase and for every human subject.

Improving the initial estimation of impedance parameters may significantly reduce the time required to configure the control system. Aghasadeghi et al. [3] recently described a biped simulation for which a prosthetic leg was controlled with an impedance controller and the remaining system was controlled with a human-inspired controller. The simulation allows characteristics of the prosthesis, such as its mass, inertia, intrinsic damping, etc. to be specified and optimizes to find impedance parameters that result in near-normal locomotion. This is in contrast to the regression reported by Sup, which considered only the kinematics of the knee and ankle and did not consider interactions with the remainder of the body. As a result, the human-inspired controlled proposed by Aghasadeghi allows the evolution of the gait to be investigated over multiple strides so that compensations required by the intact limb may be evaluated. When testing with control subjects walking using a bypass prosthesis, qualitative feedback indicated that the parameters resulting from the optimization compared favorably with hand-tuned impedance parameters, but with a greatly reduced demand on clinician time.

When considering the ankle, the relationship between the prosthetic ankle position and the torque generated during walking has been used to guide the development of both passive and active ankles [7]. The slope of the torque-angle relationship, known as the quasi-stiffness, specified the stiffness of a mechanical spring required to provide normal joint torque. Rouse et al. ([98] see Fig. 3.4 and associated text) recently showed that the quasi-stiffness was nearly equivalent to the actual stiffness of the ankle-foot in healthy control subjects during a substantial portion of the locomotor stance phase. This relationship could be parameterized by:

$$k_{ankle} = W * (13.6 * \theta_{ankle} + 1.6)$$

where k represented joint angular stiffness in Nm/rad, and W represented the subject's body weight in kg. When programmed into a mechanically active prosthetic leg, this position-dependent stiffness allowed amputees to walk comfortably over level ground and on slopes [111]. These promising preliminary results suggest that appropriate estimates of joint impedances, both knee and ankle, across a broad range of activities may be incorporated into the control framework of lower limb prosthetic devices.

3.6 Summary

Prosthetic designers have long appreciated the importance of limb mechanics. Advances in the actuator technology, miniaturization and control over the past 30 years have created the possibility that prosthetic devices may soon be able to replicate the task-dependent control of limb impedance present in an intact limb. Understanding which features of this task-dependent regulation are critical for restoring motor function remains an active research area, and one that may help guide the design and control of the next generation of prostheses.

References

1. Abul-Haj CJ, Hogan N (1990) Functional assessment of control-systems for cybernetic elbow prostheses – Part I: description of the technique. IEEE Trans Biomed Eng 37:1025–1036
2. Abul-Haj CJ, Hogan N (1990) Functional assessment of control systems for cybernetic elbow prostheses–Part II: application of the technique. IEEE Trans Biomed Eng 37:1037–1047. doi:10.1109/TBME.1990.1438510

3. Aghasadeghi N, Zhao H, Hargrove LJ, et al (2013) Learning impedance controller parameters for lower-limb prostheses. In: IEEE/RSJ International conference on intelligent robots and systems (IROS), Tokyo, pp 1–7
4. Akazawa K, Milner TE, Stein RB (1983) Modulation of reflex EMG and stiffness in response to stretch of human finger muscle. J Neurophysiol 49:16–27
5. Albu-Schaffer A, Eiberger O, Grebenstein M et al (2008) Soft robotics – From torque feedback-controlled lightweight robots to intrinsically compliant systems. IEEE Robot Autom Mag 15:20–30. doi:10.1109/Mra.2008.927979
6. Allum JHJ, Mauritz K-H, Vogele H (1982) The mechanical effectiveness of short latency reflexes in human triceps surae muscles revealed by ischaemia and vibration. Exp Brain Res 48:153–156
7. Au SK, Weber J, Herr H (2009) Powered ankle–foot prosthesis improves walking metabolic economy. IEEE Trans Robot 25:51–66. doi:10.1109/TRO.2008.2008747
8. Bennett DJ, Hollerbach JM, Xu Y, Hunter IW (1992) Time-varying stiffness of human elbow joint during cyclic voluntary movement. Exp Brain Res 88:433–442
9. Biddiss E, Beaton D, Chau T (2007) Consumer design priorities for upper limb prosthetics. Disabil Rehabil Assist Technol 2:346–357. doi:10.1080/17483100701714733
10. Biddiss E, Chau T (2007) Upper-limb prosthetics: critical factors in device abandonment. Am J Phys Med Rehabil Assoc Acad Phys 86:977–987. doi:10.1097/PHM.0b013e3181587f6c
11. Biddiss EA, Chau TT (2007) Upper limb prosthesis use and abandonment: a survey of the last 25 years. Prosthet Orthot Int 31:236–257. doi:10.1080/03093640600994581
12. Blank A, Okamura AM, Whitcomb LL (2011) Task-dependent impedance improves user performance with a virtual prosthetic arm. IEEE International Conference on Robotics and Automation (ICRA), Shanghai, pp 2235–2242
13. Bloebaum R (2006) International symposium on osseointegration. Chicago, IL
14. Bowker JH, Pritham CH (2004) The history of amputation surgery and prosthetics. In: Smith DG, Michael JW, Bowker JH (eds) Atlas of amputations and limb deficiencies, 3rd edn. American Academy of Orthopaedic Surgeons, Rosemont, pp 3–19
15. Branemark PI (1983) Osseointegration and its experimental background. J Prosthet Dent 50:399–410
16. Branemark PI, Rydevik BL, Myers RR (2001) Osseointegration in skeleta reconstruction and rehabilitation: a review. J Rehabil Res Dev 38:175–191
17. Branemark PI, Rydevik BL, Skalak R (1997) Osseointegration in the skeletal reconstruction and joint replacement. Quintessence Publishing Co, Chicago
18. Bunderson NE, Burkholder TJ, Ting LH (2008) Reduction of neuromuscular redundancy for postural force generation using an intrinsic stability criterion. J Biomech 41:1537–1544. doi:10.1016/j.jbiomech.2008.02.004
19. Burdet E, Osu R, Franklin DW et al (2001) The central nervous system stabilizes unstable dynamics by learning optimal impedance. Nature 414:446–449
20. Carloni R, Visser LC, Member S et al (2012) Variable stiffness actuators: a port-based power-flow analysis. IEEE Trans Robot 28:1–11
21. Carter RR, Crago PE, Keith MW (1990) Stiffness regulation by reflex action in the normal human hand. J Neurophysiol 64:105–118
22. Cheney PD, Fetz EE (1984) Corticomotoneuronal cells contribute to long-latency stretch reflexes in the rhesus monkey. J Physiol Lond 349:249–272
23. Christenson J (2010) Design and analysis of a series elastic actuator for use as a prosthetic wrist with accompanying control strategies. MS thesis, Northwestern University
24. Clancy EA, Bouchard S, Rancourt D (2001) Estimation and application of EMG amplitude during dynamic contractions. IEEE Eng Med Biol Mag 20:47–54
25. Colebatch JG, McCloskey DI (1987) Maintenance of constant arm position or force: reflex and volitional components in man. J Physiol Lond 386:247–261
26. Colgate JE (1993) Robust impedance shaping telemanipulation. IEEE Trans Robot Autom 9:374–384

27. Colgate JE, Hogan N (1988) Robust control of dynamically interacting systems. Int J Control 48:65–88
28. Controzzi M, Cipriani C, Carrozza MC (2010) Miniaturized non-back-drivable mechanism for robotic applications. Mech Mach Theory 45:1395–1406. doi:10.1016/j.mechmachtheory.2010.05.008
29. Cui L, Perreault EJ, Maas H, Sandercock TG (2008) Modeling short-range stiffness of feline lower hindlimb muscles. J Biomech 41:1945–1952. doi:10.1016/j.jbiomech.2008.03.024
30. Cui L, Perreault EJ, Sandercock TG (2007) Motor unit composition has little effect on the short-range stiffness of feline medial gastrocnemius muscle. J Appl Physiol 103:796–802. doi:10.1152/japplphysiol.01451.2006
31. Cupo ME, Sheredos S (1998) Clinical evaluation of a new, above-elbow, body-powered prosthetic arm: a final report. J Rehabil Res Dev 35:431–446
32. Darainy M, Towhidkhah F, Ostry DJ (2007) Control of hand impedance under static conditions and during reaching movement. J Neurophysiol 97:2676–2685. doi:10.1152/jn.01081.2006
33. Dietz V, Discher M, Trippel M (1994) Task-dependent modulation of short- and long-latency electromyographic responses in upper limb muscles. Electroencephalogr Clin Neurophysiol 93:49–56
34. Doemges F, Rack PMH (1992) Changes in the stretch reflex of the human first dorsal interosseous muscle during different tasks. J Physiol Lond 447:563–573
35. Eilenberg MF, Geyer H, Herr H (2010) Control of a powered ankle-foot prosthesis based on a neuromuscular model. IEEE Trans Neural Syst Rehabil Eng 18:164–173. doi:10.1109/TNSRE.2009.2039620
36. English CE, Russell D (1999) Mechanics and stiffness limitations of a variable stiffness actuator for use in prosthetic limbs. Mech Mach Theory 34:7–25
37. Evarts EV (1973) Motor cortex reflexes associated with learned movement. Science 179: 501–503
38. Flash T, Mussa-Ivaldi FA (1990) Human arm stiffness characteristics during the maintenance of posture. Exp Brain Res 82:315–326
39. Franklin DW, Liaw G, Milner TE et al (2007) Endpoint stiffness of the arm is directionally tuned to instability in the environment. J Neurosci 27:7705–7716
40. Fryer CM, Michael JW (2004) Harnessing and controls for body-powered devices. In: Smith DG, Michael JW, Bowker JH (eds) Atlas of amputations and limb deficiencies, 3rd edn. American Academy of Orthopaedic Surgeons, Rosemont, pp 131–143
41. Fryer CM, Stark GE, Michael JW (2004) Body-powered components. In: Smith DG, Michael JW, Bowker JH (eds) Atlas of amputations and limb deficiencies, 3rd edn. American Academy of Orthopaedic Surgeons, Rosemont, pp 131–143
42. Gomi H, Kawato M (1996) Equilibrium-point control hypothesis examined by measured arm stiffness during multijoint movement [see comments]. Science 272:117–120
43. Gomi H, Konno T (1998) Real time estimation of time-varying human multijoint arm viscoelasticity during movements. Proc Int Conf IEEE/EMBS 20:2341–2342
44. Gomi H, Osu R (1998) Task-dependent viscoelasticity of human multijoint arm and its spatial characteristics for interaction with environments. J Neurosci 18:8965–8978
45. Hirzinger G, Sporer N, Albu-Schaffer A, et al (2002) DLR's torque-controlled light weight robot III – Are we reaching the technological limits now? International conference on robotics and automation, pp 1710–1716
46. Hitt JK, Sugar TG, Holgate M, Bellman R (2010) An active foot-ankle prosthesis with biomechanical energy regeneration. J Med Devices Trans ASME 4:011003. doi:10.1115/1.4001139
47. Hoffer JA, Andreassen S (1981) Regulation of soleus muscle stiffness in premammillary cats: intrinsic and reflex components. J Neurophysiol 45:267–285
48. Hogan N (1990) Mechanical impedance of single-and multi-articular systems. In: Winters JM, Woo SLY (eds) Multiple muscle systems. Springer, New York
49. Hogan N (1985) The mechanics of multi-joint posture and movement control. Biol Cybern 52:315–331

50. Hogan N, Buerger S (2005) Impedance and interaction control. In: Kurfess T (ed) Robotics and automation handbook. CRC Press, New York
51. Hogan N (1982) Prostheses should have adaptively controllable impedance. Proceedings of IFAC symposium, Columbus, OH, pp 155–162
52. Houk JC (1972) The phylogeny of muscular control configurations. In: Houk JC (ed) Biocybernetics IV. Fischer, Jena, pp 125–144
53. Hu X, Murray WM, Perreault EJ (2011) Muscle short-range stiffness can be used to estimate the endpoint stiffness of the human arm. J Neurophysiol 105:1633–1641. doi:10.1152/jn.00537.2010
54. Hu X, Murray WM, Perreault EJ (2012) Biomechanical constraints on the feedforward regulation of endpoint stiffness. J Neurophysiol. doi:10.1152/jn.00330.2012
55. Hunter IW, Kearney RE (1982) Dynamics of human ankle stiffness: variation with mean ankle torque. J Biomech 15:747–752
56. Joyce GC, Rack PMH, Ross HF (1974) The forces generated at the human elbow joint in response to imposed sinusoidal movements of the forearm. J Physiol 240:351–374
57. Kapp S, Fergason JR (2004) Transtibial amputation: prosthetic management. In: Smith DG, Michael JW, Bowker JH (eds) Atlas of amputation and limb deficiencies, 3rd edn. American Academy of Orthopaedic Surgeons, Rosemont, pp 503–515
58. Kearney RE, Hunter IW (1990) System identification of human joint dynamics. CRC Crit Rev Biomed Eng 18:55–87
59. Kearney RE, Stein RB, Parameswaran L (1997) Identification of intrinsic and reflex contributions to human ankle stiffness dynamics. IEEE Trans Biomed Eng 44:493–504
60. Kirsch RF, Boskov D, Rymer WZ (1994) Muscle stiffness during transient and continuous movements of cat muscle: perturbation characteristics and physiological relevance. IEEE Trans Biomed Eng 41:758–770
61. Koopman B, Van Asseldonk EHF, Van der Kooij H (2010) In vivo measurement of human knee and hip dynamics using MIMO system identification. IEEE EMBC conference, Buenos Aires, pp 3426–3429
62. Krutky MA, Ravichandran VJ, Trumbower RD, Perreault EJ (2010) Interactions between limb and environmental mechanics influence stretch reflex sensitivity in the human arm. J Neurophysiol 103:429–440. doi:10.1152/jn.00679.2009
63. Krutky MA, Trumbower RD, Perreault EJ (2012) Influence of environmental stability on the regulation of endpoint impedance during the maintenance of arm posture (in revision)
64. Kurtzer IL, Pruszynski JA, Scott SH (2008) Long-latency reflexes of the human arm reflect an internal model of limb dynamics. Curr Biol 18:449–453. doi:10.1016/j.cub.2008.02.053
65. Lake C, Miguelez JM (2003) Comparative analysis of microprocessors in upper limb prosthetics. J Prosthet Orthot 15:48–63. doi:10.1097/00008526-200304000-00004
66. LeBlanc M (1988) Use of prosthetic prehensors. Prosthet Orthot Int 12:152–154
67. Lee H, Ho P, Rastgaar MA et al (2014) Multivariable static ankle mechanical impedance with active muscles. IEEE TNSRE 22(1):44–52. doi:10.1109/TNSRE.2013.2262689
68. Lee H, Ho P, Rastgaar MA et al (2011) Multivariable static ankle mechanical impedance with relaxed muscles. J Biomech 44:1901–1908. doi:10.1016/j.jbiomech.2011.04.028
69. Lee H, Hogan N (2013) Investigation of human ankle mechanical impedance during locomotion using a wearable ankle robot. In: IEEE international conference on robotics and automation (ICRA), pp 2636–2641
70. Ludvig D, Cathers I, Kearney RE (2007) Voluntary modulation of human stretch reflexes. Exp Brain Res 183:201–213. doi:10.1007/s00221-007-1030-0
71. MacNeil JB, Kearney RE, Hunter IW (1992) Identification of time-varying biological systems from ensemble data. IEEE Trans Biomed Eng 39:1213–1225. doi:10.1109/10.184697
72. McIntyre J, Mussa-Ivaldi FA, Bizzi E (1996) The control of stable arm postures in the multijoint arm. Exp Brain Res 110:248–264
73. Micera S, Carpaneto J, Raspopovic S (2010) Control of hand prostheses using peripheral information. IEEE Rev Biomed Eng 3:48–68

74. Misiaszek JE (2006) Control of frontal plane motion of the hindlimbs in the unrestrained walking cat. J Neurophysiol 96:1816–1828. doi:10.1152/jn.00370.2006
75. Morgan DL (1977) Separation of active and passive components of short-range stiffness of muscle. Am J Physiol 232:C45–C49
76. Mugge W, Schuurmans J, Schouten AC, Van Der Helm FCT (2009) Sensory weighting of force and position feedback in human motor control tasks. J Neurosci 29:5476–5482. doi:10.1523/JNEUROSCI.0116-09.2009
77. Mussa-Ivaldi FA, Hogan N, Bizzi E (1985) Neural, mechanical, and geometric factors subserving arm posture in humans. J Neurosci 5:2732–2743
78. Newman WS (1992) Stability and performance limits of interactions controllers. J Dyn Syst 114:563–570
79. Nichols TR, Houk JC (1976) Improvement in linearity and regulation of stiffness that results from actions of stretch reflex. J Neurophysiol 39:119–142
80. Owens P, Ouellette EA (2004) Elbow disarticulation and transhumeral amputation: surgical management. In: Smith DG, Michael JW, Bowker JH (eds) Atlas of amputations and limb deficiencies, 3rd edn. American Academy of Orthopaedic Surgeons, Rosemont, pp 239–241
81. Palmer E, Ashby P (1992) Evidence that a long latency stretch reflex in humans is transcortical. J Physiol Lond 449:429–440
82. Paluska D, Herr H (2006) The effect of series elasticity on actuator power and work output: implications for robotic and prosthetic joint design. Robot Auton Syst 54:667–673
83. Perreault E, Kirsch R, Crago P (2004) Multijoint dynamics and postural stability of the human arm. Exp Brain Res 157:507–517. doi:10.1007/s00221-004-1864-7
84. Perreault EJ, Crago PE, Kirsch RF (2000) Estimation of intrinsic and reflex contributions to muscle dynamics: a modeling study. IEEE Trans Biomed Eng 47:1413–1421
85. Perreault EJ, Kirsch RF, Crago PE (2002) Voluntary control of static endpoint stiffness during force regulation tasks. J Neurophysiol 87:2808–2816. doi:10.1152/jn.00590.2001
86. Petersen N, Christensen LO, Morita H et al (1998) Evidence that a transcortical pathway contributes to stretch reflexes in the tibialis anterior muscle in man. J Physiol Lond 512(Pt 1):267–276
87. Pfeifer S, Vallery H, Hardegger M et al (2012) Model-based estimation of knee stiffness. IEEE Trans Biomed Eng 59:2604–2612. doi:10.1109/TBME.2012.2207895
88. Pratt GA, Williamson MM (1995) Series elastic actuators. IEEE/RSJ International conference on intelligent robots and systems, Pittsburgh, PA, pp 399–406
89. Pratt GA, Williamson MM, Dillworth P et al (1995) Stiffness isn't everything. Fourth international symposium on experimental robotics, Stanford, CA, pp 253–262
90. Pruszynski JA, Kurtzer I, Scott SH (2008) Rapid motor responses are appropriately tuned to the metrics of a visuospatial task. J Neurophysiol 100:224–238. doi:10.1152/jn.90262.2008
91. Puchhammer G (2006) Future actuating technologies for upper-extremity prosthetic devices. In: 10th International conference on new actuators, Bremen, Germany, pp 301–307
92. Rack PMH, Westbury DR (1974) The short range stiffness of active mammalian muscle and its effect on mechanical properties. J Physiol 240:331–350
93. Rancourt D, Hogan N (2009) The biomechanics of force production. Adv Exp Med Biol 629:645–661. doi:10.1007/978-0-387-77064-2_35
94. Roberts TJ, Marsh RL, Weyand PG, Taylor CR (1997) Muscular force in running turkeys: the economy of minimizing work. Science 275:1113–1115
95. Robinson DW, Pratt JE, Paluska DJ, Pratt GA (1999) Series elastic actuator development for a biomimetic walking robot. IEEE/ASME International conference on advanced intelligent mechanisms, Atlanta, GA, pp 561–568
96. Rouse EJ, Gregg RD, Hargrove LJ, Sensinger JW (2013) The difference between stiffness and quasi-stiffness in the context of biomechanical modeling. IEEE Trans Biomed Eng 60: 562–568. doi:10.1109/TBME.2012.2230261
97. Rouse EJ, Hargrove LJ, Perreault EJ et al (2013) Development of a mechatronic platform and validation of methods for estimating ankle stiffness during the stance phase of walking. J Biomech Eng 135:81009. doi:10.1115/1.4024286

98. Rouse E, Hargrove L, Perreault E, Kuiken T (2014) Estimation of human ankle impedance during the stance phase of walking. IEEE Trans Neural Syst Rehabil Eng. doi:10.1109/TNSRE.2014.2307256
99. Sapin E, Goujon H, de Almeida F et al (2006) Functional gait analysis of transfemoral amputees using Hydracadence® knee joints compared with other single axis prosthetic knees with hydraulic swing. International symposium of the analysis of 3D human movement, Valenciennes, France
100. Schonhow T, Kristensen T, Siversten S, Wits E (2005) New technology for the suspension of trans-humeral prostheses – SISA (Subfascial Implant supported attachment). Myoelectric controls symposium, pp 88–92
101. Schuch CM, Pritham CH (2004) Transfemoral amputation: prosthetic management. In: Smith DG, Michael JW, Bowker JH (eds) Atlas of amputations and limb deficiencies, 3rd edn. American Academy of Orthopaedic Surgeons, Rosemont, pp 541–555
102. Selen LPJ, Franklin DW, Wolpert DM (2009) Impedance control reduces instability that arises from motor noise. J Neurosci 29:12606–12616. doi:10.1523/JNEUROSCI.2826-09.2009
103. Sensinger JW (2010) Selecting motors for robots using biomimetic trajectories: optimum benchmarks, windings, and other considerations. IEEE conference on robotics and automation, Anchorage, AK, pp 4175–4181
104. Sensinger JW, Burkart LE, Pratt GA, Weir R (2013) Effect of compliance location in series elastic actuators. Robotica 31:1313–1318
105. Sensinger JW, Weir REF (2008) User-modulated impedance control of a prosthetic elbow in unconstrained, perturbed motion. IEEE Trans Biomed Eng 55:1043–1055. doi:10.1109/Tbme.2007.905385
106. Sensinger JW, Weir RF (2005) Design and analysis of a non-backdrivable series elastic actuator. Rehabilitation Robotics
107. Sensinger JW, Weir RFF (2008) Modeling and preliminary testing socket-residual limb interface stiffness of above-elbow prostheses. IEEE Trans Neural Syst Rehabil Eng 16: 184–190. doi:10.1109/Tnsr.E.2008.918388
108. Sensinger JW, Weir RFF (2007) Inherently compensating body powered elbow. Vancouver
109. Sensinger JW, Weir RFF (2006) Improvements to series elastic actuators. IEEE/ASME International conference on mechatronic and embedded systems and applications, Beijing, pp 160–166
110. Shemmell J, Krutky MA, Perreault EJ (2010) Stretch sensitive reflexes as an adaptive mechanism for maintaining limb stability. Clin Neurophysiol 121:1680–1689. doi:10.1016/j.clinph.2010.02.166
111. Simon AM, Fey N, Finucane S, et al (2013) Strategies to reduce the configuration time of a powered knee and ankle prosthesis across patients and multiple ambulation modes. IEEE International conference on rehabilitation robotics (ICORR), Seattle
112. Simpson D (1974) The choice of control system for the multimovement prosthesis: extended physiological proprioception (e.p.p.). In: Herbert P (ed) The control of upper extremity prostheses and orthoses. Thomas Books, Springfield, pp 146–150
113. Sinkjaer T, Toft E, Andreassen S, Hornemann BC (1988) Muscle stiffness in human ankle dorsiflexors: intrinsic and reflex components. J Neurophysiol 60:1110–1121
114. Stein RB, Walley M (1983) Functional comparison of upper extremity amputees using myoelectric and conventional prostheses. Arch Phys Med Rehabil 64:243–248
115. Sulzer J, Peshkin M, Patton J (2008) Pulling your strings: cable moment arm manipulation as a method of joint actuation. IEEE Robot Autom Mag 15:70–78
116. Sup F, Bohara A, Goldfarb M (2008) Design and control of a powered transfemoral prosthesis. Int J Robot Res 27:263–273
117. Sup F, Varol HA, Mitchell J et al (2009) Preliminary evaluations of a self-contained anthropomorphic transfemoral prosthesis. IEEE ASME Trans Mechatron 14:667–676. doi:10.1109/TMECH.2009.2032688

118. Trumbower RD, Krutky MA, Yang B-S, Perreault EJ (2009) Use of self-selected postures to regulate multi-joint stiffness during unconstrained tasks. PLoS One 4:e5411. doi:10.1371/journal.pone.0005411.t001
119. Van Ham R, Sugar TG, Vanderborght B et al (2009) Compliant actuator designs review of actuators with passive adjustable compliance/controllable stiffness for robotic applications. IEEE Robot Autom Mag 16:81–94. doi:10.1109/Mra.2009.933629
120. van Steenberghe D, Quirynen M, Svensson B, Branemark PI (2003) Clinical examples of what can be achieved with osseointegration in anatomically severely compromised patients. Periodontology 2000 33:90–104
121. Vanderborght B, Van Ham R, Lefeber D et al (2009) Comparison of mechanical design and energy consumption of adaptable, passive-compliant actuators. Int J Robot Res 28:90–103. doi:10.1177/0278364908095333
122. Varol HA, Sup F, Goldfarb M (2010) Multiclass real-time intent recognition of a powered lower limb prosthesis. IEEE Trans Biomed Eng 57:542–551. doi:10.1109/TBME.2009.2034734
123. Veatch BD (2004) A combination VO/VC terminal device with variable mechanical advantage. American Academy of Orthotics and Prosthetics
124. Veneman JF, Kruidhof R, Hekman EEG et al (2007) Design and evaluation of the LOPES exoskeleton robot for interactive gait rehabilitation. IEEE Trans Neural Syst Rehabil Eng 15:379–386
125. Vodovnik L, Rebersek S (1974) Information-content of myo-control signals for orthotic and prosthetic systems. Arch Phys Med Rehabil 55:52–56
126. Weir RFF, Sensinger JW (2009) Design of artificial arms and hands for prosthetic applications. In: Kutz M (ed) 2nd ed. McGraw-Hill, New York, pp 537–598
127. Whitney DE (1977) Force feedback control of manipulator fine motions. J Dyn Syst Meas Control 99:91–97
128. Winter DA (1983) Energy generation and absorption at the ankle and knee during fast, natural, and slow cadences. Clin Orthop Relat Res 197:147–154
129. Winter DA (1990) Biomechanics and motor control of movement, 2nd edn. Wiley, Toronto
130. Zajac FE, Neptune RR, Kautz SA (2002) Biomechanics and muscle coordination of human walking. Part I: introduction to concepts, power transfer, dynamics and simulations. Gait Posture 16:215–232
131. Zecca M, Micera S, Carrozza MC, Dario P (2002) Control of multifunctional prosthetic hands by processing the electromyographic signal. Crit Rev Biomed Eng 40:459–485
132. Zheng Y, Mak AFT, Leung AKL (2001) State-of-the-art methods for geometric and biomechanical assessments of residual limbs: a review. J Rehabil Res Dev 38:487–504
133. Zinn M, Khatib O, Roth B, Salisbury JK (2004) Playing it Safe. IEEE Robot Autom Mag 11:12–21

Chapter 4
Multi-axis Capability for Powered Ankle-Foot Prostheses

Evandro M. Ficanha, Mohammad Rastgaar, and Kenton R. Kaufman

Abstract The ankle joint of lower extremity powered prostheses are generally designed to be capable of controlling a single degree of freedom (DOF) in the sagittal plane, allowing a focus on improved mobility in straight walking. However, the single DOF ankle movements are rare in normal lower limb actions such as walking on a straight path or turning when the ankle movements in both sagittal and frontal planes are significant. Therefore, the effectiveness of next-generation lower extremity prostheses may be significantly enhanced by improved understanding of the ankle dynamics in both sagittal and frontal planes during different maneuvers and by implementing strategies to account for these intricacies in prosthesis design.

In this chapter, the concept of a multi-axis powered ankle-foot prosthesis is introduced. The feasibility of this concept, to the extent allowed, by a proof of concept prototype is shown. Further, the design kinematics and its mechanical impedance in non-load bearing conditions are evaluated and discussed. It is shown that the proposed cable-driven mechanism for the multi-axis powered ankle-foot prosthesis is capable of closely mimicking the ankle movements in both sagittal and frontal planes during step turn and walking on straight path.

Keywords Multi-axis ankle-foot prosthesis • Powered lower extremity prosthesis • Human ankle impedance • Cable-driven prosthesis

---

E.M. Ficanha • M. Rastgaar (✉)
Department of Mechanical Engineering-Engineering Mechanics, Michigan Technological University, Houghton, MI 49931, USA
e-mail: Rastgaar@mtu.edu

K.R. Kaufman
Motion Analysis Laboratory, Department of Orthopedic Surgery, Mayo Clinic and Mayo Foundation, Rochester, MN 55905, USA

P. Artemiadis (ed.), *Neuro-Robotics: From Brain Machine Interfaces to Rehabilitation Robotics*, Trends in Augmentation of Human Performance 2,
DOI 10.1007/978-94-017-8932-5_4,

4.1 Introduction

Recent advances in powered prostheses promise to significantly improve the quality of life and well-being for individuals with impaired mobility. A majority of people without disabilities, 61.4 % to be exact, report their health to be excellent. In sharp contrast, only 28.4 % of people with disabilities report the same. Moreover, people with disabilities are at a greater risk for secondary conditions (e.g., injury, obesity, and hypertension) that can further impact well-being and diminish overall quality of life [1]. A better understanding of the complexities surrounding lower limb prostheses, which are needed for walking and daily activity will lead to increased health and well-being for the 1.7 million limb amputees in the US, the majority of whom have lower extremity amputations [2, 3]. The ankle joint of lower extremity powered prostheses currently commercially available is capable of controlling only one degree of freedom (DOF) in the sagittal plane, allowing a focus on improved mobility in straight walking. Turning, however, plays a major role in daily living activities and requires ankle torque in both sagittal and frontal planes. Therefore, the effectiveness of next-generation lower extremity prostheses may be significantly enhanced by improved understanding of ankle dynamics in both sagittal and frontal planes during different maneuvers and by implementing strategies to account for these intricacies in prosthesis design.

A multi-axis ankle-foot prosthetic robot capable of generating torques in both the sagittal and frontal planes with impedance modulation similar to the human ankle may improve maneuverability and increase mobility. It is shown that unilateral below-knee amputees who use passive prostheses rely more on their hip joint and expend 20–30 % more metabolic energy compared to non-amputees at the same speed. As a result, their preferred speed of gait is 30–40 % lower than non-amputees [4, 5] and their compensatory gait strategies results in asymmetrical gait patterns that affect joints in both lower limbs [6–9]. Net positive work generated in the ankle contributes to propulsion in gait. It has been shown that a powered ankle-foot prosthesis reduces the metabolic costs of unilateral transtibial amputees during straight walking by providing sufficient power during push-off [10, 11]. However, studies of four representative daily activities show that turning steps may account for an average of 25 % of steps, ranging from 8 to 50 % of all steps depending on the activity [12], which amputees accomplish using different gait strategies than non-amputees. While a non-amputee relies on the hip movement in the coronal plane and moment generated in the ankle joint, an amputee using a passive prosthesis relies on hip extension in the sagittal plane [13–16]. During a turn, modulation of ankle impedance in sagittal and frontal planes plays a major role in controlling lateral and propulsive ground reaction forces in order to accelerate the body center of mass along the gait path; thus, during a step turn, lateral and propulsive impulses are larger compared to a straight step [17]. This difference will result in different gait strategies between amputees and non-amputees to compensate for the lack of propulsion in the passive prostheses to increase maneuverability [13]. This suggests that an ankle-foot prosthesis controllable in two planes, i.e. dorsiflexion-plantarflexion (DP) and inversion-eversion (IE) directions, may increase the mobility by providing more assistance in turning. Additionally, designing a feature that allows walking in arbitrary directions on slopes while conforming the foot to the ground profile and uneven surfaces may result in a more efficient gait.

Passive lower extremity prostheses do not store or generate energy. Understanding of the ankle's capability in impedance modulation and generating net positive work during the stance period of gait has influenced the design of new ankle-foot prostheses [18–21]. One design approach is based on storing energy during the heel strike and releasing it during the push-off before the trailing foot's heel strike. Collins and Kuo [22] developed a microprocessor-controlled artificial foot that limits the increase in metabolic cost to 14 % compared to 23 % that occurs with a passive prosthesis. The positive work by the prosthesis at the push-off partially compensates for the dissipative negative work at the heel strike of the trailing foot and lowers the redirection of the body's center of mass velocity [23–27]. On the other hand, there are powered prostheses capable of injecting energy to the system. Klute et al. developed a prototype using McKibben pneumatic actuators [28]. Sup et al. developed a powered transfemoral prosthesis with active knee and ankle joints, each with one controllable DOF in the sagittal plane [29–32]. The controller adjusts the impedance at a number of instants during gait by altering the neutral position of the ankle. Hitt et al. designed an ankle-foot prosthesis using a lightweight robotic tendon actuator that provided the majority of peak power for push-off [33, 34]. Au et al. developed an ankle-foot prosthesis [35–37] that later transitioned into a commercially available ankle-foot prosthesis, BiOM [38]. An adaptive muscle-reflex controller for this powered prosthesis was developed further by Eilenberg et al. using an ankle plantar-flexor model based on a Hill-type muscle and a positive force feedback reflex. A finite state machine determined the phase of the gait; hence, the appropriate ankle torques [39]. The controller in the BiOM allows for gait with different cadence over surfaces with different inclinations, e.g. uphill and downhill trajectories [40]. Other commercially available powered transtibial prosthesis are the Proprio foot from össur and the Elan from Endolite; however neither provides a net positive work during the stance period [41, 42]. BiOM provides the necessary energy during toe-off and generates a net positive work [43, 10] that has been shown to reduce the metabolic costs by 8.9–12.1 % at different gait speeds compared to a passive prosthesis. The improvements occurred for gait speeds between 1 and 1.75 m/s; however, it did not change the metabolic cost at 0.75 m/s, suggesting a possible optimal range of speed for its design [44]. The BiOM also increased the preferred gait speed by 23 % [44] and lowered loading of the intact leg during level-ground walking, which may lower the risk of secondary complications [45].

Because the ankle is a biomechanically complex joint with multiple DOFs, failure to incorporate full function of the ankle into prostheses design can inadvertently lead to secondary complications [46]. Mechanical impedance of a dynamic system determines the evoked torque to the motion perturbations and is a function of the stiffness, visco-elasticity, and inertia of the system. Ankle mechanical impedance in no load-bearing conditions has been studied in the sagittal plane [47–61].

Quasi-static ankle stiffness in both DP and IE were reported by Roy et al. [62], but coupling between these DOFs was not assessed. The ankle impedance during load-bearing conditions has also been studied. In the frontal plane, Saripalli et al. [63] studied the variation of ankle stiffness under different load-bearing conditions. Zinder et al. [64] studied dynamic stabilization and ankle stiffness in IE by applying a sudden perturbation in the frontal plane during bipedal weight-bearing stance. In the sagittal plane, the quasi-stiffness of the ankle has been studied and suggests humans change their reflex ankle stiffness in response to unpredicted perturbations [65]. Loram et al. determined that the intrinsic ankle stiffness during a quiet stance is almost constant with respect to ankle torque and suggested that the central nervous system contributes to the balance by modulating ankle stiffness especially with the triceps surae muscles in the sagittal plane [66, 67]. Sasagawa et al. made a similar conclusion with subjects standing on inclined surfaces moving forward and backward [68]. Ankle quasi-static stiffness was studied during quiet standing [69, 70] and locomotion [18, 20, 71]. Variations of ankle moment, ankle angle, and speed dependent hysteresis during gait cycles at different speeds was studied by Hansen et al. [21] . Also, dynamic stiffness of lower limbs during hopping and running was measured by Farley et al. [72, 73]. Recently, Rouse et al. developed a perturbation platform to estimate ankle impedance during the foot-flat phase of the stance period of gait in the DP direction [74–76].

The ankle's mechanical impedance in a single degree of freedom has been the focus of the studies in all of the prior work and the multidirectional characteristics of the ankle has not been addressed. The ankle joint is biomechanically complex and consists of multiple degrees of freedom. It's major anatomical axes are non-orthogonal with no intersection that could introduce a biomechanical coupling between DP and IE. Additionally, single DOF ankle movements are rare in normal lower limb actions and the control of multiple ankle DOFs presents unique challenges [77]. Therefore, understanding the directional impedance of the ankle requires a multivariable identification approach. Multivariable mechanical impedance of the human ankle in both DP and IE directions in stationary conditions was estimated by Rastgaar et al. [78, 79] for dynamic mechanical impedance and Lee et al. [80–83] for quasi-static mechanical impedance. Ho et al. also studied the directional variation of quasi-static mechanical impedance of ankle [84, 85]. Further, Lee et al. developed a method for estimation of time-varying mechanical impedance of the ankle during the entire stride length for the subjects walking on a treadmill [86]. Their study on ten unimpaired subjects showed consistent time-varying characteristics of ankle impedance during the entire stride in both sagittal and frontal planes.

In this chapter, we introduced the concept of a multi-axis powered ankle-foot prosthesis and showed the feasibility of this concept to the extent allowed by a proof of concept prototype. We first described the experiments for collecting the information on the range of motion (ROM) of the ankle during step turn and walking on straight path in both sagittal and frontal planes. The ankle displacements need to be studied since the mechanical impedance of the ankle is a dynamic operator that maps the time-history of angular displacements onto the corresponding time-history of torques at the ankle joint. Next, the design of the proof of concept prototype of a steerable ankle-foot prosthesis will be explained. Further, the design kinematics and its mechanical impedance in non-load bearing conditions will be evaluated and discussed.

4.2 Ankle Rotations During the Step Turns and Straight Steps

Straight walking requires a complex sequence of muscle activation to modulate the ground reaction forces to produce forward motion. Similarly, modulation of the reaction forces is required for turning the body [13]. Two different strategies that are commonly used for turning are the spin turn and the step turn. The spin turn consists of turning the body around the leading leg (e.g. turning right with the right leg in front). The step turn consists of shifting the body weight to the leading leg and stepping onto the opposite leg while still shifting the body weight (e.g. turning left with the right leg in front). The step turn is more stable since the base of support for body weight is wider [15] and for this reason it was used in this study. It has been shown that the step turn velocity, length, and width are considerably different than the straight walk with higher turning reaction forces [17]. Three-dimensional measurement of the ankle angles during step and spin turns have been previously studied [87]; however, it is of interest to study the ankle angular displacements during different phases of the stance period during step turns and comparing these results to the ankle angles during straight steps. Additionally, the collected data were used to evaluate the kinematic design of the ankle-foot prototype in reproducing the same trajectories. This will be discussed later in this chapter. Different approaches have been used to measure ankle angles such as using flexible electro-goniometer, electromagnetic tracking devices, and motion capturing cameras [14, 87, 17, 15, 88]. We used a motion capture camera system to track the three-dimensional rotations of the foot and tibia in stance periods during two gait scenarios: 1- walking on a straight path and 2–90 degree step turn.

The motion capture camera system consisted of eight cameras in a square formation covering a volume of about 16 cubic meters and an area of 12 square meters. The cameras emitted infrared light and captured the reflected light from reflectors mounted on the participants with a rate of 250 Hz. Five male subjects with no self-reported neuromuscular and biomechanical disorders were recruited for the experiments. The subjects gave written consent to participate in the experiment that was approved by the Michigan Technological University Institutional Review Board.

The subjects were instructed to walk at a normal pace and an audible metronome was synchronized to their number of steps per minute in an attempt to keep the walking speed constant. The preferred speed for the participants ranged from 88 to 96 steps per minute. They started walking from outside the field of view of the cameras while following a straight line marked on the floor. When they reached a reference point on the floor, they performed a 90° step turn to the left, pivoting on

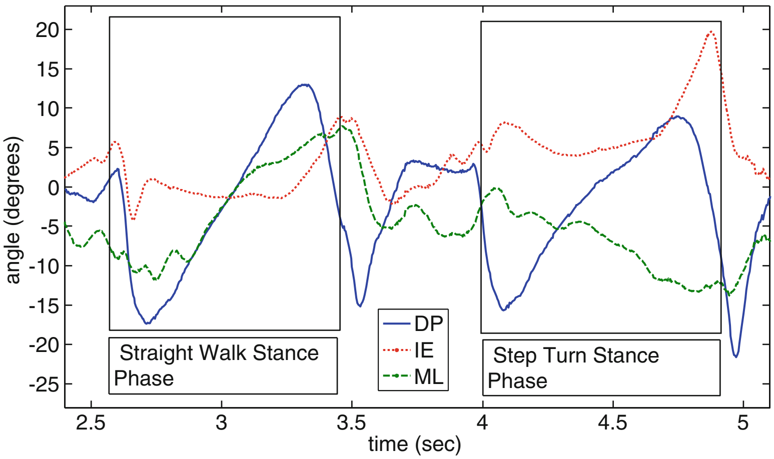

Fig. 4.1 A representative subject's ankle rotations in DP, IE, and ML directions during the straight walk and step turn

their right leg and continued walking straight until they were outside the field of view of the cameras. Each subject repeated the test nine times, after several training trials to increase the consistency of the trials. Time trajectories of the markers on the tibia and foot were used to estimate the ankle rotations.

The plots of DP, IE, and medial/lateral (ML) angles for a representative subject are shown in Fig. 4.1. The data for each test was divided into 6 phases (heel strike, flat foot, and toe-off for both straight and turning steps) and the averages of the DP, IE, and ML rotations of each phase were calculated for all 9 trials of 5 subjects (a total of 45 trials).

Table 4.1 shows the average ROM of the subjects during the straight step and step turn stance periods. The maximum and minimum angles and maximum angular velocities observed for the representative subject in Fig. 4.1 can also be seen in Table 4.1. Table 4.2 shows the average rotations and the difference in angles from the turning step to the straight step in each phase. The range of motion of each subject's ankle about the three axes of the ankle and their average rotations during the stance periods were calculated and used to find the averaged percent change from straight walk to step turn with respect to their ROM during the straight step (Table 4.2).

The duration of the combined phases of heel strike and loading response, mid stance, and terminal stance and pre-swing phases were determined and used to measure the average angles at each combined phase.

There was a modest decrease of ROM in DP direction during the step turn compared to the straight step. ROM in the IE direction increased by 23.8 % indicating the significance of the IE role during turning. A significantly smaller range of motion in ML may suggest a higher stiffness in that axis of rotation necessary to transfer the reaction forces from the ground to the body.

Table 4.1 ROM of ankle during the stance in straight walk and step turn

	ROM of straight step stance period (deg)		ROM of step turn stance period (deg)					
	Degrees	Standard error	Degrees	Standard error	% Change	Maximum angle[a]	Minimum angle[a]	Maximum angular velocity[a]
DP	33.9	0.65	31.6	0.62	−7.4	13.03°	−21.58°	120°/s
IE	15.69	0.52	20.6	1.06	23.8	19.72°	−4.248°	101°/s
ML	22.09	0.6	16.8	0.65	−31.9	7.69°	−13.75°	144°/s

[a]Representative subject

Table 4.2 Average angles at different phases of stance in straight step and step turn

	Straight step average (deg)	Standard error	Turning step average (deg)	Standard error	Angular change (deg)[a]	% Change[b]
DP heel Strike	−8.72	0.80	−9.68	0.95	−0.95	−3.0
DP flat foot	2.34	0.63	0.36	0.64	−1.98	−6.5
DP toe off	10.59	1.24	1.37	0.90	−9.22	−29.2
IE heel strike	−1.72	0.53	5.90	0.63	7.61	46.6
IE flat foot	−2.93	0.27	6.51	0.22	9.44	60.5
IE toe off	1.44	0.45	13.61	0.46	12.17	82.0
ML heel strike	−5.34	0.57	0.34	0.62	5.68	25.6
ML flat foot	−0.90	0.45	−3.55	0.41	−2.65	−12.8
ML toe off	5.53	0.32	−6.53	0.65	−12.06	−58.0

[a]Turning step angles – Straight step angles
[b]From straight to step turn with respect to individual straight walk ROM in stance period

As the step progressed through the gait cycle, noticeable differences were observed between the straight step and step turn for all subjects. DP displacement started at a similar initial angle as the straight step at the heel strike (−9.68° of dorsiflexion) but progressively showed less plantarflexion at toe-off (1.37° in step turn compared to 10.37° in straight walk). IE displacement started with 5.9° of inversion at heel strike and increased to 13.6° at toe-off during the step turn suggesting a gradual increase in inversion to lean the body toward the inside of the turn. At the heel strike of the step turn, ML displacement had an increase of 5.68° of medial rotation compared to straight walk that may suggest an anticipatory motion of the foot. The difference in lateral rotation during straight step and step turn at the toe-off increased to 12.06°.

4.3 Multi-axis Ankle-Foot Prototype

The result from the ankle rotations in three DOF suggested that a multi-axis mechanism in a prosthesis may enhance gait efficiency by adding control of ankle inversion/eversion during turning. This novel design is anticipated to enable the device to adapt to uneven and inclined ground surface condition and allow the amputees to benefit more from their prosthesis rather than using their hip joint; enabling a more natural gait with less stress in other joints.

Based on this concept, a prototype cable-driven ankle-foot prosthesis with two controllable degrees of freedom (Fig. 4.2) was designed to evaluate the feasibility of controlling a 2 DOF ankle joint. The design goals were to meet the ROM and angular velocity required for straight walk and step turn while providing sufficient torque for propulsion.

The device consisted of a pylon (A), two DC motors (E) and planetary gearheads (D) that are powered by two motor controllers (B) that receive signals from a DAQ

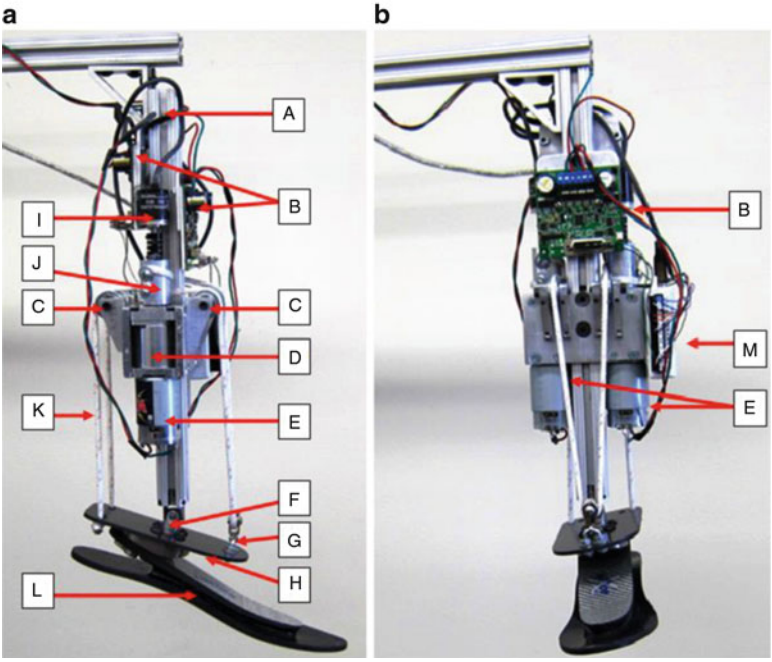

Fig. 4.2 Prototype of a multi-axis powered ankle-foot prosthesis (**a**) in plantarflexion and (**b**) in inversion

board (M) connected to a remote computer and two quadrature encoders (I). Two cable drums (J) transfer the required torque to the ankle through a nylon rope (K) that passes through two pulleys (C). The rope is looped around both the cable drums and secured to prevent slippage (Fig. 4.3). A universal joint (F) connects the pylon to the foot and an elastic carbon-fiber plate. The rope is attached to a carbon fiber plate (H) that is connected to a commercially available prosthetic foot (Otto Bock Axtion®) (L). In the aft side of the carbon fiber plate, the rope is mounted at both sides of the longitudinal axes of the foot. At the fore side, the rope passes through a pulley (G) that is connected to the carbon fiber plate by a universal joint. The mechanism is capable of both dorsiflexion-plantarflexion when the motors rotate in opposite directions and inversion-eversion when the motors rotate in the same direction. Also, any combination of DP and IE can be achieved by combining different amounts of rotations at each motor.

The proposed design with two controllable DOFs relies on the fact that three points are sufficient to define a plane in the space. As shown in Fig. 4.4, the three points (A, B, C) can be used to define rotations of the foot relative to the pylon about the X and Y axes that are equivalent to DP and IE, respectively. If the motors apply forces in the same directions, for example in the negative Y direction, points A and B will move downwards, while point C moves upwards, resulting in dorsiflexion. If the motors move in opposite directions, for example the right motor pull the rope

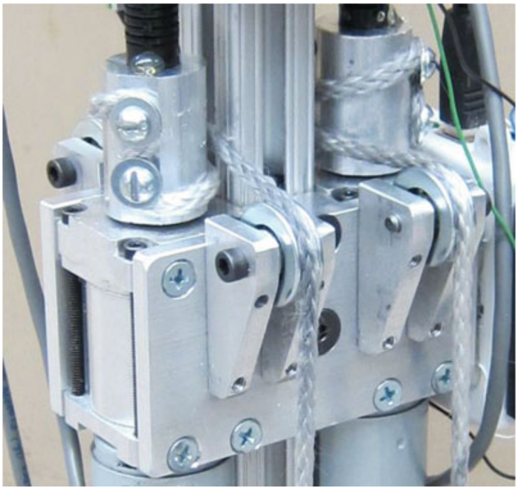

Fig. 4.3 Cable drum connection to avoid cable slippage

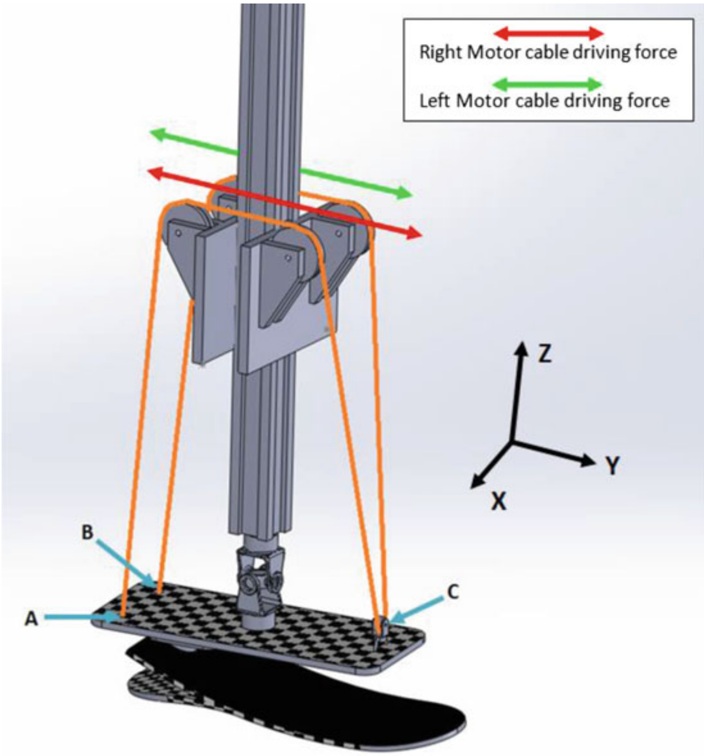

Fig. 4.4 A simplified drawing of the cable driven mechanism showing three interaction points A, B, and C between the cable, carbon fiber plate, and motor drive forces

in the positive Y direction and the left motor pulls the rope in negative Y direction, point A moves upwards, while point B moves downwards generating foot eversion. At point C, a pulley is mounted to the plate using a universal joint. Because point C is located on the axis of symmetry of the plate and the rope passes through the pulley at point C, no DP motion is generated. The carbon fiber plate is a fundamental component of the design. The carbon fiber plate acts as a spring element in series with the cable and the foot. The cable needs to be always in tension to assure proper control over the foot and keep the carbon fiber plate under a bending moment. This assures the cable has a sufficient tension over the ROM of the foot providing that it can be controlled to mimic the mechanical impedance of a human ankle.

Providing sufficient power and torque at the ankle joint without significant increase in the weight of the powered prostheses is a challenging issue. For example, Hitt et al. used two parallel actuators to increase the power output for walking in increased speed [33]. The steering mechanism proposed here also use two actuators; however, the design allows for generating a torque component in lateral plane. The cable driven design, besides the ability to control the ankle in two DOF, may provide a significant flexibility in managing the inertia of the ankle-foot prostheses too. A detailed description of the components used in this proof of concept prototype can be found in [89].

4.4 Evaluation of the Design Concept

The developed prototype has been evaluated for meeting two criteria. First, the design kinematics should be capable of regenerating the same ankle rotation as the human ankle during the stance and swing phases of gait. Second, the multivariable impedance of the prototype ankle needs to be comparable to the mechanical impedance of human ankle.

4.4.1 Kinematic Evaluation

Presently, two optical quadrature encoders (200 pulses per revolution) provide position feedback to a remote computer that uses a proportional plus rate controller to control the relative position of the foot with respect to the pylon. The controller uses a look-up table with recorded angles of the representative subject of the motion analysis experiment in both DP and IE. The input and output angles to the controller can be seen in Fig. 4.5 where the robot is moving at 50 % of the walking speed. For ease of comparison, the output plots have a time shift to remove the 80 milliseconds delay of the output. Also, all signals are filtered with a low-pass filter with a cutoff frequency of 5 Hz to remove sensor noise from the output signal. The current prototype was developed as a proof of concept to validate the design kinematics; therefore, faster motors and sensors with lower noise levels will be used in future designs.

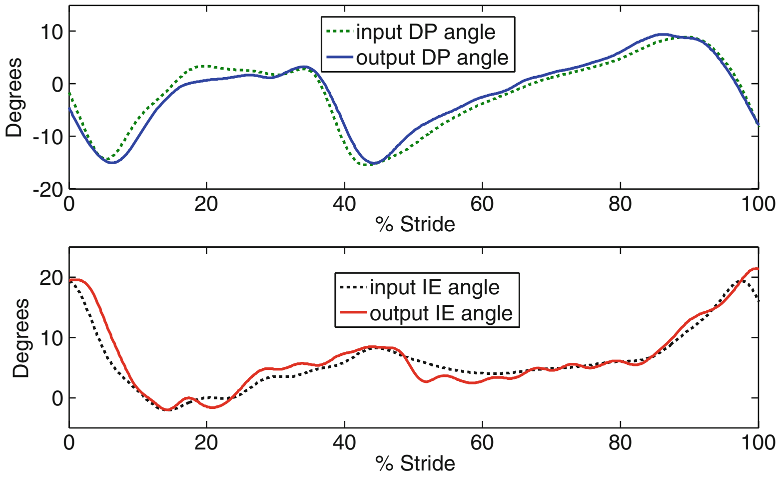

Fig. 4.5 Input and compensated output for time delay (80 ms) of the ankle-foot prosthesis during swing and stance periods of a step turn at 50 % of the walking speed with no load

4.4.2 Mechanical Impedance Estimation

Recently, hierarchical control strategies have been developed for impedance control of active prostheses [39, 30]. The higher level control identifies the gait cycle, and the lower level control regulates the actuators for a proper impedance characteristics. Following the same strategies, an ankle-foot prosthesis can be designed to have an initial mechanical impedance similar to a human's ankle. This may provide a faster modulation of the ankle impedance based on the state of the gait cycle.

The purpose of this evaluation was to identify the passive impedance of the prosthetic device and compare it to the impedance of human subjects. The impedance estimation experiment setup was similar to the procedure reported in [79, 78], where an Anklebot® was used to apply random torque perturbations to the ankle joint in DP and IE directions with a bandwidth of 100 Hz and record the provoked ankle angles. A stochastic system identification method was used to estimate the multivariable mechanical impedance of the ankle using the collected data. Similar procedures were used for estimation of passive mechanical impedance of the ankle-foot prosthesis while all its controllers were turned off. The experimental setup can be seen in Fig. 4.6, where the two devices were attached mechanically to each other. The Otto Bock Axtion® foot and its rubber foot shell were inserted in the same type of shoe used in human tests to ensure consistency in the experiments. Similarly, the same test was done on a representative human subject for comparison with the prosthesis. Impedance test of the human subject was performed with both relaxed muscles and 10 % MVC of the tibialis anterior following the procedures described in [79]. The EMG signals were monitored using a Delsys Trigno Wireless EMG System® with surface electrodes placed at the belly of the tibialis anterior. The EMG

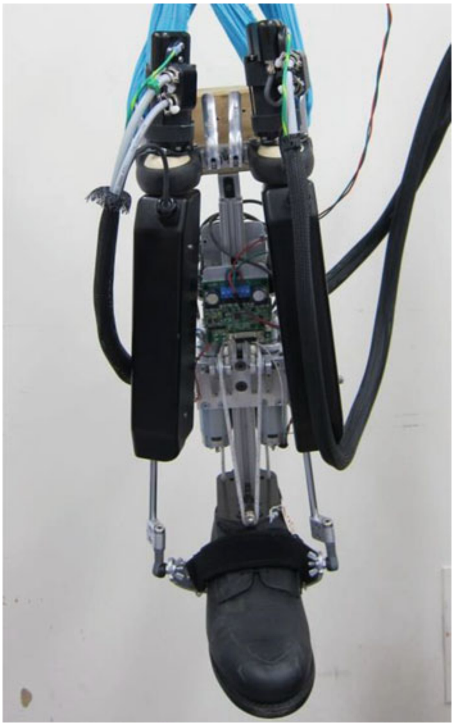

Fig. 4.6 Anklebot attached to the prosthetic foot to measure the mechanical impedance of the ankle-foot prosthesis

signal was sampled at 2 kHz and the root-mean-square value of a window of 13.5 ms of data calculated and displayed on a computer screen in order to provide a visual feedback to the participant for maintaining constant muscle activity. The results can be seen in Figs. 4.7 and 4.8.

Figure 4.7 shows the Bode plots of the mechanical impedances in DP direction for prototype prosthesis, human subject's ankle with relaxed muscles, and human subject's ankle with 10 % MVC. The quasi-static stiffness of the prototype prosthesis, which is the impedance magnitude at low frequencies, was 39.5 dB (94 N.m/deg) in DP at 1 HZ. Also, it shows a relatively linear impedance and phase over the frequency range of interest (0–5 HZ). The human subject showed similar stiffness in DP for the co-contraction testes and lower stiffness in passive test when compared to the prosthesis. IE impedance magnitude (Fig. 4.8) of the prosthesis was between the active and passive stiffness of the human sample with a value of 24.24 dB (16 N.m/deg) at 1 Hz.

While the maximum lifting force of the robot in the z axis was generated, the carbon fiber plate flexed due to the applied torque. Since the encoders read the cable displacement instead of foot angles, the controller perceived the deflection of the carbon fiber plate as an angular displacement of the foot. This caused the position controller to reduce the torque being applied prematurely, and thus the maximum lifting force was less than anticipated, although it was still powerful enough to lift a

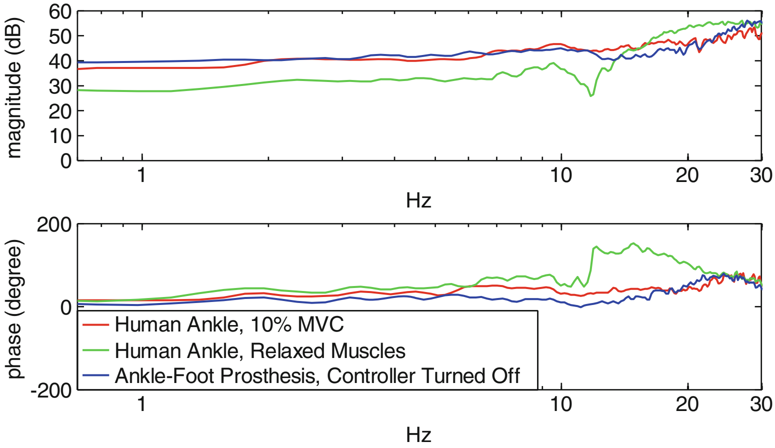

Fig. 4.7 Plots of the magnitude and phase of the impedance in DP rotation of the prosthetic robot and a human subject with relaxed muscles and 10 % cocontraction

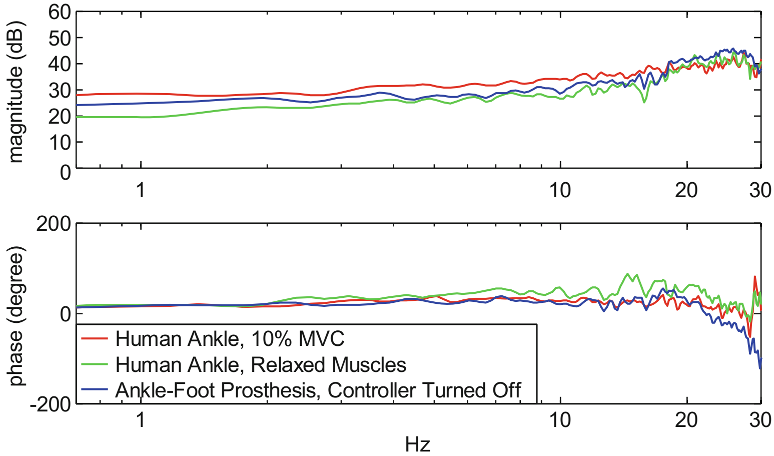

Fig. 4.8 Plots of the magnitude and phase of the impedance in IE rotation of the prosthetic robot and a human sample with relaxed muscles and 10 % cocontraction

72 KG person. Future designs will benefit from position sensors which can measure the foot angles directly to increase the precision of the position and the resulting torque.

Testing the range of motion in IE, it was found that the IE motion might become unstable when exceeds 62 degrees due to an external force. This is the equivalent of rolling the ankle, which is a common injury among active people and are mostly in inversion [63]. From the gait analysis experiment, it was seen that the maximum rotation in IE (Table 4.1) was 19.72°, and thus instability should not impose a significant issue during normal gait.

The current developments in control strategies for prostheses suggests that the control of the ankle joint in the ankle-foot prosthesis should mimic the time-varying impedance of the ankle in two DOF during different phases of stance period in different gait scenarios while providing the required torque. Recent work by Lee et al. and Rouse et al. [76, 86] are notable for estimating the time-varying ankle impedance during both swing and stance periods of gait along a straight path. To estimate the time-varying impedance of the ankle during a turning maneuver, a perturbing walkway may be necessary. The implemented mechanical design, although in early stages of development, showed anthropomorphic characteristics. The design was successful at mimicking human motion, and showed mechanical impedance similar to human ankle.

References

1. Health and Wellness for Persons with Disabilities Today (2007) Office of the Surgeon General https://www.ncbi.nlm.nih.gov/books/NBK44662/
2. A Roadmap for US Robotics, From Internet to Robotics: Computing Community Consortium (2013) http://www.us-robotics.us/reports/CCC%20Report.pdf.
3. Ziegler-Graham K, MacKenzie EJ, Ephraim PL, Travison TG, Brookmeyer R (2008) Estimating the prevalence of limb loss in the United States: 2005 to 2050. Arch Phys Med Rehabil 89(3):422–429
4. Colborne GR, Naumann S, Longmuir PE, Berbrayer D (1992) Analysis of mechanical and metabolic factors in the gait of congenital below knee amputees. Am J Phys Med Rehabil 92:272–278
5. Molen NH (1973) Energy/speed relation of below-knee amputees walking on motor-driven treadmill. Internationale Zeitschrift für angewandte Physiologie einschließlich Arbeitsphysiologie 31(3):173–185
6. Winter DA, Sienko SE (1988) Biomechanics of below-knee amputee gait. J Biomech 21(5):361–367
7. Skinner HB, Effeney DJ (1985) Gait analysis in amputees. Am J Phys Med Rehabil 64:82–89
8. Bateni H, Olney S (2002) Kinematic and kinetic variations of below-knee amputee gait. J Prosthet Orthot 14(1):2–13
9. Adamczyk PG, Kuo AD (2011) Asymmetry in Amputee Gait: the propagating effects of weak push-off. In: American Society of Biomechanics, Long Beach, CA
10. Herr HM, Grabowski AM (2010) Powered ankle-foot prosthesis improves metabolic demand of unilateral transtibial amputees during walking. In: American Society of Biomechanics, Long Beach, CA
11. Ferris AE, Aldridge JE, Sturdy JT, Wilken JM (2011) Evaluation of the biomimetic properties of a new powered ankle-foot prosthetic system. American Society of Biomechanics, Long Beach, CA
12. Glaister BC, Bernatz GC, Klute GK, Orendurff MS (2007) Video task analysis of turning during activities of daily living. Gait Posture 25(2):289–294
13. Ventura JD, Segal AD, Klute GK, Neptune RR (2011) Compensatory mechanisms of transtibial amputees during circular turning. Gait Posture 34:307–312
14. Orendurff MS, Segal AD, Berge JS, Flick KC, Spanier D, Klute GK (2006) The kinematics and kinetics of turning: limb asymmetries associated with walking a circular path. Gait Posture 23(1):106–111
15. Hase K, Stein RB (1999) Turning strategies during human walking. J Neurophysiol 81(6):2914–2922

16. Segal AD, Orendurff MS, Czerniecki JM, Schoen J, Klute GK (2011) Comparison of transtibial amputee and non-amputee biomechanics during a common turning task. Gait Posture 33(1):41–47. doi:10.1016/j.gaitpost.2010.09.021
17. Glaister BC, Orendurff MS, Schoen JA, Bernatz GC, Klute GK (2008) Ground reaction forces and impulses during a transient turning maneuver. J Biomech 41(4):3090–3093
18. Palmer M (2002) Sagittal plane characterization of normal human ankle function across a range of walking gait speeds. Massachusetts Institute of Technology, Cambridge, MA
19. Gates DH (2004) Characterizing ankle function during stair ascent, descent, and level walking for ankle prosthesis and orthosis design. Boston University, Boston
20. Davis R, DeLuca P (1996) Gait characterization via dynamic joint stiffness. Gait Posture 4(3):224–231
21. Hansena AH, Childress DS, Miff SC, Gard SA, Mesplay KP (2004) The human ankle during walking: implications for design of biomimetic ankle prostheses. J Biomech 37:1467–1474
22. Collins SH, Kuo AD (2010) Recycling energy to restore impaired ankle function during human walking. PLoS One 5(2)
23. Donelan JM, Kram R, Kuo AD (2002) Mechanical work for step-to-step transitions is a major determinant of the metabolic cost of human walking. J Exp Biol 205:3717–3727
24. Donelan JM, Kram R, Kuo AD (2002) Simultaneous positive and negative external work in human walking. J Biomech 35:117–124
25. Ruina A, Bertram JE, Srinivasan M (2005) A collisional model of the energetic cost of support work qualitatively explains leg sequencing in walking and galloping, pseudoelastic leg behavior in running and the walk-to-run transition. J Theor Biol 237(2):170–192
26. Kuo AD (2002) Energetics of actively powered locomotion using the simplest walking model. J Biomech Eng 124:113–120
27. Kuo AD, Donelan JM, Ruina A (2005) Energetic consequences of walking like an inverted pendulum: step-to-step transitions. Exerc Sport Sci Rev 33:88–97
28. Klute GK, Czerniecki J, Hannaford B (1998) Development of powered prosthetic lower limb. In: Proceedings of the 1st national meeting, Veterans Affairs Rehabilitation Research and Development Service, Washington, D.C.
29. Goldfarb M (2010) Powered robotic legs – leaping toward the future. National Institute of Biomedical Imaging and Bioengineering. http://www.nibib.nih.gov/news-events/newsroom/powered-robotic-legs-leaping-toward-future
30. Sup F, Bohara A, Goldfarb M (2008) Design and control of a powered transfemoral prosthesis. Int J Robot Res 27:263–273
31. Sup F, Varol HA, Mitchell J, Withrow TJ, Goldfarb M (2009) Preliminary evaluations of a self-contained anthropomorphic transfemoral prosthesis. IEEE ASME Trans Mechatron 14(6):667–676
32. Iv FCS (2009) A powered self-contained knee and ankle prosthesis for near normal gait in transfemoral amputees. Vanderbilt University, Nashville
33. Hitt J, Merlo J, Johnston J, Holgate M, Boehler A, Hollander K, Sugar T (2010) Bionic running for unilateral transtibial military amputees. In: 27th Army Science Conference (ASC), Orlando, Florida
34. Hitt JK, Sugar TG, Holgate M, Bellman R (2010) An active foot-ankle prosthesis with biomechanical energy regeneration. J Med Devices 4(1):011003
35. Au SK (2007) Powered ankle-foot prosthesis for the improvement of amputee walking economy. Massachusetts Institute of Technology, Cambridge, MA
36. Au S, Herr H (2008) Powered ankle-foot prosthesis. Robot Autom Mag 15(3):52–59
37. Au S, Weber J, Herr H (2009) Powered ankle-foot prosthesis improves walking metabolic economy. IEEE Trans Robot 25(1):51–66
38. BiOM (2013) Personal bionics http://www.biom.com/
39. Eilenberg MF, Geyer H, Herr H (2010) Control of a powered ankle–foot prosthesis based on a neuromuscular model. IEEE Trans Neural Syst Rehabil Eng 18(2):164–173
40. Bionic Technology with Powered Plantar Flexion (2012) http://www.iwalkpro.com/Prosthetists.html

41. The technology behind the PROPRIO FOOT® from Össur (2012) http://www.ossur.com/?PageID=15736
42. Endolite, élan (2012) http://www.endolite.com/products/elan
43. Au SK, Herr H, Weber J, Martinez-Villalpando EC (2007) Powered ankle-foot prosthesis for the improvement of amputee ambulation. In: International conference of the IEEE, Engineering in Medicine and Biology Society, Lyon
44. Herr HM, Grabowski AM (2012) Bionic ankle-foot prosthesis normalizes walking gait for persons with leg amputation. Proc Biol Sci 279(1728):457–464. doi:10.1098/rspb.2011.1194
45. Grabowski AM, D'Andrea S (2013) Effects of a powered ankle-foot prosthesis on kinetic loading of the unaffected leg during level-ground walking. J NeuroEng Rehabil 10(1):49
46. Gailey R, Allen K, Castles J, Kucharik J, Roeder M (2008) Review of secondary physical conditions associated with lower-limb amputation and long-term prosthesis use. J Rehabil Res Dev 45(1):15–30
47. Harlaar J, Becher J, Snijders C, Lankhorst G (2000) Passive stiffness characteristics of ankle plantar flexors in hemiplegia. Clin Biomech 15(4):261–270
48. Singer B, Dunne J, Singer K, Allison G (2002) Evaluation of triceps surae muscle length and resistance to passive lengthening in patients with acquired brain injury. Clin Biomech 17(2):151–161
49. Chung SG, Rey E, Bai Z, Roth EJ, Zhang L-Q (2004) Biomechanic changes in passive properties of hemiplegic ankles with spastic hypertonia. Arch Phys Med Rehabil 85(10):1638–1646
50. Rydahl SJ, Brouwer BJ (2004) Ankle stiffness and tissue compliance in stroke survivors: a validation of myotonometer measurements. Arch Phys Med Rehabil 85(10):1631–1637
51. Kobayashi T, Leung AKL, Akazawa Y, Tanaka M, Hutchins SW (2010) Quantitative measurements of spastic ankle joint stiffness using a manual device: a preliminary study. J Biomech 43(9):1831–1834
52. Lamontagne A, Malouin F, Richards CL (1997) Viscoelastic behavior of plantar flexor muscle-tendon unit at rest. J Orthop Sports Phys Ther 26(5):244–252
53. Hunter IW, Kearney RE (1982) Dynamics of human ankle stiffness: variation with mean ankle torque. J Biomech 15(10):742–752
54. Kearney RE, Hunter IW (1982) Dynamics of human ankle stiffness: variation with displacement amplitude. J Biomech 15(10):753–756
55. Kearney RE, Hunter IW (1990) System identification of stretch reflex dynamics. Crit Rev Biomed Eng 18:55–87
56. Weiss PL, Kearney RE, Hunter IW (1986) Position dependence of ankle joint dynamics—I. Passive mechanics. J Biomech 19(9):727–735
57. Weiss PL, Kearney RE, Hunter IW (1986) Position dependence of ankle joint dynamics—II. Active mechanics. J Biomech 19(9):737–751
58. Kearney RE, Stein RB, Parameswaran L (1997) Identification of intrinsic and reflex contributions to human ankle stiffness dynamics. IEEE Trans Biomed Eng 44(6):493–504
59. Kirsch RF, Kearney RE (1997) Identification of time-varying stiffness dynamics of the human ankle joint during an imposed movement. Exp Brain Res 114:71–85
60. Mirbagheri MM, Kearney RE, Barbeau H (1996) Quantitative, objective measurement of ankle dynamic stiffness: intra-subject reliability and intersubject variability. In: 18th annual international conference of the IEEE Engineering in Medicine and Biology Society, Amsterdam
61. Sinkjaer T, Toft E, Andreassen S, Hornemann BC (1998) Muscle stiffness in human ankle dorsiflexors: intrinsic and reflex components. J Neurophysiol 60(3):1110–1121
62. Roy A, Krebs HI, Williams DJ, Bever CT, Forrester LW, Macko RM, Hogan N (2009) Robot-aided neurorehabilitation: a novel robot for ankle rehabilitation. IEEE Trans Robot Automation 25(3):569–582
63. Saripalli A, Wilson S (2005) Dynamic ankle stability and ankle orientation. 7th symposium on footwear biomechanics conference, Cleveland, OH
64. Zinder SM, Granata KP, Padua DA, Gansneder BM (2007) Validity and reliability of a new in vivo ankle stiffness measurement device. J Biomech 40:463–467

65. Fitzpatrick RC, Taylor JL, McCloskey DI (1992) Ankle stiffness of standing humans in response to imperceptible perturbation: reflex and task-dependent components. J Physiol 454:533–547
66. Loram ID, Lakie M (2002) Human balancing of an inverted pendulum: position control by small, ballistic-like, throw and catch movements. J Physiol 540(3):1111–1124
67. Loram ID, Lakie M (2002) Direct measurement of human ankle stiffness during quiet standing: the intrinsic mechanical stiffness is insufficient for stability. J Physiol 545(3):1041–1053
68. Sasagawa S, Ushiyama J, Masani K, Kouzaki M, Kanehisa H (2009) Balance control under different passive contributions of the ankle extensors: quiet standing on inclined surfaces. Exp Brain Res 196(4):537–544
69. Winter DA, Patla AE, Rietdyk S, Ishac MG (2001) Ankle muscle stiffness in the control of balance during quiet standing. J Neurophysiol 85(6):2630–2633
70. Morasso PG, Sanguineti V (2002) Ankle muscle stiffness alone cannot stabilize balance during quiet standing. J Neurophysiol 88(4):2157–2162
71. Shamaei K, Sawicki GS, Dollar AM (2013) Estimation of quasi-stiffness and propulsive work of the human ankle in the stance phase of walking. PLoS One 8(3):e59935. doi:10.1371/journal.pone.0059935
72. Farley CT, Blickhan R, Saito J, Taylor CR (1991) Hopping frequency in humans: a test of how springs set stride frequency in bouncing gaits. J Appl Physiol 71:2127–2132
73. Farley CT, González O (1996) Leg stiffness and stride frequency in human running. J Biomech 29(2):181–186
74. Rouse EJ, Hargrove LJ, Peshkin MA, Kuiken TA (2011) Design and validation of a platform robot for determination of ankle impedance during ambulation. In: Conference proceedings of the IEEE Engineering in Medicine and Biology Society. Boston, MA, USA
75. Rouse E, Hargrove L, Perreault E, Kuiken T (2012) Estimation of human ankle impedance during walking using the Perturberator Robot. Paper presented at the fourth IEEE RAS/EMBS international conference on biomedical robotics and biomechatronics, Roma, Italy
76. Rouse E, Hargrove L, Perreault E, Peshkin M, Kuiken T (2013) Development of a robotic platform and validation of methods for estimating ankle impedance during the stance phase of walking. J Biomech Eng 135(8):1009-1–1009-8
77. Arndt A, Wolf P, Liu A, Nester C, Stacoff A, Jones R, Lundgren P, Lundberg A (2007) Intrinsic foot kinematics measured in vivo during the stance phase of slow running. J Biomech 40: 2672–2678
78. Rastgaar M, Ho P, Lee H, Krebs HI, Hogan N (2009) Stochastic estimation of multi-variable human ankle mechanical impedance. In: ASME dynamic systems and control conference, Hollywood, CA
79. Rastgaar M, Ho P, Lee H, Krebs HI, Hogan N (2010) Stochastic estimation of the multi-variable mechanical impedance of the human ankle with active muscles. In: ASME dynamic systems and control conference, Boston, MA
80. Lee H, Ho P, Krebs HI, Hogan N (2009) The multi-variable torque-displacement relation at the ankle. In: ASME dynamic systems and control conference, Hollywood, CA
81. Lee H, Ho P, Rastgaar M, Krebs HI, Hogan N (2010) Quantitative characterization of steady-state ankle impedance with muscle activation. In: ASME dynamic systems and control conference, Cambridge, MA
82. Lee H, Ho P, Rastgaar M, Krebs HI, Hogan N (2011) Multivariable static ankle mechanical impedance with relaxed muscles. J Biomech 44:1901–1908
83. Lee H, Ho P, Rastgaar M, Krebs HI, Hogan N (2014) Multivariable static ankle mechanical impedance with active muscles. IEEE Trans Neural Syst Rehabil Eng 22(1):44–52
84. Ho P, Lee H, Krebs HI, Hogan N (2009) Directional variation of active and passive ankle static impedance. Paper presented at the ASME dynamic systems and control conference, Hollywood, CA
85. Ho P, Lee H, Rastgaar M, Krebs HI, Hogan N (2010) The interpretation of the directional properties of voluntarily modulated human ankle impedance. In: ASME dynamic systems and control conference, Cambridge, MA

86. Lee H, Krebs HI, Hogan N (2012) Linear time-varying identification of ankle mechanical impedance during human walking. In: ASME 2012 5th annual dynamic systems and control conference, Fort Lauderdale, FL, USA
87. Taylor MJD, Dabnichki P, Strike SC (2005) A three-dimensional biomechanical comparison between turning strategies during the stance phase of walking. Hum Mov Sci 24:558–573
88. A Roadmap for US Robotics, From Internet to Robotics. (Computing Community Consortium, May 21, 2009). http://www.us-robotics.us/reports/CCC%20Report.pdf
89. Ficanha EM, Rastgaar M, Modirian B, Mahmoudian N (2013) Ankle Angles during Step Turn and Straight Walk: implications for the design of a steerable ankle-foot Prosthetic Robot. In: Dynamic systems and controls conference Stanford University, Palo Alto, CA

Chapter 5
Mimicking Human-Like Leg Function in Prosthetic Limbs

Martin Grimmer and André Seyfarth

Abstract Human upright locomotion is a complex behavior depending on manifold requirements. Bones, muscles, cartilage and tendons provide mechanical infrastructure. Central nervous commands, reflex mechanisms from the spinal cord level or also preflexes defined by actuator properties provide input to create motion patterns like walking or running. Due to dysvascularity, infections or traumatic events parts of the biological framework can get lost. Until the end of the twentieth century mostly passive structures were used to replace amputees lower limbs. Full functionality like in the biological system can not be provided because of missing sensory information and power source. Innovations in actuator, battery and micro electronics technology make it possible to improve prosthetic design. A first innovation was introduced with semi-active devices using microprocessor controlled dampers to modulate prosthetic joint behavior similar to isometric or eccentric muscle function. A further step is to power the joints to emulate concentric muscle function. Combined with ingenious control mechanisms this could potentially provide every possible movement task. Twenty-six powered prosthetic systems and further passive prototypes are presented in this work. Mechanical and control solutions are introduced. Amputee gait in various daily life situations using passive, semi-active and powered prostheses is compared. Areas for improvements are discussed.

Keywords Prosthetics • Human • Gait • Walking • Energy • Power • Biomechanics • Control • Spring

---

M. Grimmer (✉) • A. Seyfarth
Laufiabor Locomotion Lab, Technische Universität Darmstadt, Magdalenenstrasse 27, 64289 Darmstadt, Germany
e-mail: grimmer@sport.tu-darmstadt.de; seyfarth@sport.tu-darmstadt.de

P. Artemiadis (ed.), *Neuro-Robotics: From Brain Machine Interfaces to Rehabilitation Robotics*, Trends in Augmentation of Human Performance 2,
DOI 10.1007/978-94-017-8932-5_5,

Abbreviations

CE	contractile element
CIC	computational intrinsic control
CoM	center of mass
EMG	electromyography
ER	energy requirements
ESAR	energy storage and return
FPWS	fastest possible walking speed
GRF	ground reaction force
IEC	interactive extrinsic control
IL	intact limb
PE	parallel element
PEA	parallel elastic actuator
PP	peak power
PWS	preferred walking speed
RL	residual prosthetic limb
RoM	range of motion
SACH	solid ankle cushioned heel
SE	series element
SEA	series elastic actuator
TF	transfemoral
TT	transtibial
UPS	unidirectional parallel spring

5.1 Human Locomotion

Upright humanoid locomotion emerged about 6 million years ago [110]. The oldest humanoid footprints with evidence of bipedal locomotion are about 3.7 million years old [24]. As a result of evolutionary changes of the neural, the skeletal and the muscular system several upright human locomotion patterns were developed. In daily life commonly walking is performed. More dynamic gait patterns are skipping or running. A preferred walking speed is about 1.3 m/s [28]. Running, especially sprinting gives the possibility to move faster (up to 12.27 m/s, Usain Bolt, [137]) compared to walking (4.3 m/s, Vladimir Kanaykin, mean value of World Record 20 km Race Walking). While walking with passive carbon fiber prosthetic ankle joints, amputees have still a lack in performance compared to healthy people. Whereas in running with passive carbon fiber feet international scientists and sport officials discussing about advantages for amputee sprinters compared to healthy athletes.

In the following pages requirements for mimicking healthy humanoid gait patterns are presented. Current state of the art lower limb prosthetic technology is discussed. Newest prototypes to improve amputee gait are introduced. Mechanical and control solutions are presented and fields for improvements are discussed.

5.2 Prosthetics

First lower limb prosthetics were reported in an Indian sacred book called the Rig Veda that was written between 3500 and 1800 B.C. There it is mentioned that the leg of Queen Vishpla was amputated in a battle. Afterwards an iron leg was fitted to her to walk and to get her back to the battlefield [33]. Still 2000 A.C. war is a reason for amputations. The Annual Report of the Red Cross [169] reports 16,501 prosthetics manufactured in their 40 centers (14 selected countries) for 2001. 9,779 of them were made for mine victims. For the US Forces from 2000 to 2011, 6,144 traumatic amputations among 5,694 soldiers were realized. About 2,037 of them had major amputations like the loss of foot, hand or more [114]. In comparison 185,000 amputations are estimated for the US in total each year. In total 1.6 million people with lost limbs were estimated for the U.S. for 2005 [187]. Even higher numbers related to the population are documented in Germany. In the year 2003 about 61,000 amputations at 45,000 patients were made only for the lower extremity [65]. These values are including all surgeries including toe to whole leg amputations. The main reason for lower limb amputations in the United Kingdom is dysvascularity (72 %). Nearly half of it is related to diabetes mellitus. Also infections (8 %), trauma (7 %), neoplasia (3 %) or neurological disorder (1 %) can be a cause. In 4 % of cases no specified cause was identified. Other reasons together account for 5 % [157]. Lower limb referrals accounting more than 90 % of all new amputees. Fifty-three percent of them were transtibial amputees in the UK. Another 39 % are transfemoral amputees. The Amputee Statistical Database for the United Kingdom reports that over one half of the new amputees referred to prosthetics centers are aged over 65 and one fourth is over 75 years old. Only one fourth is younger than 54 years [157].

The function of prosthetics is on the one hand to provide a cosmetic part to cover the loss of the limb. On the other hand it should provide functionalities of the lost limb. For example with a lower limb prosthesis the amputee should be able to perform at least standing and slow walking. Additional functionalities for daily life are required. Two strategies are used to provide them for the amputees. Special prostheses for specific purposes like swimming [22] or running [176] were designed. A second way is to include more functions in existing prosthetic systems. For example, a special foot design with a manual ankle joint clutch makes it possible to use different kinds of shoes like sport shoes or high heels with one prosthetic foot (e.g. Runway, Freedom Innovations, [45]).

From an energetic point of view, prosthetics can be divided into three groups. Complete passive, semi-active and active devices. Complete passive devices are using passive clutch mechanisms, springs and dampers to mimic human gait behavior. They are the most common group. Semi-active devices are equipped with microprocessors to control the mechanical parts (e.g. hydraulic dampers) depending on gait phase. In the third group, active prosthetics can provide positive net work, mostly by motors, to assist the amputee in walking or climbing stairs.

5.3 Passive Prosthetics

5.3.1 Ankle Joint

5.3.1.1 Design Characteristics

Passive prosthetic ankle joints can be classified by their functionality. A first group are the non-elastic feet (e.g. SACH feet – solid ankle cushioned heel). Materials like wood and plastics are used to design them. Low costs make them still attractive for amputees and paying authorities. In third world countries manufacturing costs of less than US$150 can be realized for an artificial limb. For example in Vietnam the ICRC (International Committee of the Red Cross) estimated manufacturing costs of between US$38 and US$64 per polypropylene prosthesis [23].

A step further in functionality are ESAR (energy store and return) feet. They are able to store and release energy during the gait cycle by spring-like structures. Using the elastic capability of the forefoot they can mimic to some extend the function of the Achilles tendon which results in a more natural ankle joint behavior. For some prosthetic ankle joints one carbon heel part with a different stiffness than the forefoot (e.g. Vari-Flex – Ossur, [116]) is used to mimic the eccentric tibialis anterior muscle function during touch down. After loading this leaf spring during loading response, energy from unloading for shank forward rotation is provided. Composite materials are mainly used for designing the elastic structures in ESAR feet.

Another difference between prosthetic feet can be made by the provided degrees of freedom. SACH feet have a solid ankle and a cushioned heel. No ankle joint rotation is possible. Single axis feet like the 1H38 (Ottobock, [117]) providing one degree of freedom limited by soft or rigid bumpers. Multi-axial feet (e.g. Multiflex DR – Endolite, [38]) can move in more than one plane. Inversion or eversion and adduction or abduction can be realized. Adaptations to ground while walking curves or uneven terrain are possible. Potentially torsional forces for higher joints can be reduced. Similar functions can be provided by prosthetic torsion adapters integrated between foot and socket or artificial knee joint.

Quite often a lot of these functionalities are combined in one prosthetic foot design. For example the Echolon VT (Endolite, [38]) provides a heel and a forefoot spring. In addition it has a shock absorbing torsional element. To improve ground contact while Eversion or Inversion the forefoot spring has a separate left and a right part.

5.3.1.2 Gait Biomechanics

Asymmetries in abled-bodied gait could be identified by various gait studies [135]. Even more pronounced are asymmetries for unilateral amputees. Transfemoral amputations cause higher biomechanical differences between affected and unaffected leg than for transtibial amputees [113]. For the second group only the missing biological ankle joint effects the gait pattern. Differences in kinematics and kinetics can be identified between affected and unaffected side. Various gait studies on amputee gait showing the effects for different prosthetic feet [62, 128, 133, 164].

The natural Range of Motion (RoM) of the ankle joint while walking on a treadmill is between 20° and 38° increasing for speed from 0.5 to 2.6 m/s (Fig. 5.1). For running the RoM is between 26° and 40° considering speeds from 0.5 to 4 m/s (Fig. 5.2). For Sprinting values up to 50° are possible [86].

Using a passive prosthetic foot the RoM is about 16.8–21.2° for 1.35 m/s walking [125, 165]. 11–23° were reported in [63]. Thereby ESAR feet could almost double RoM in comparison to SACH feet that provided only up to 14° dorsiflexion. Prosthetic feet with mechanical ankle joint (Lager or 1H38, Otto Bock, [117]) can provide greater ROM than SACH or ESAR feet [125].

For amputees running with a Flex-foot (Ossur, [116]) at 2.7 m/s, a RoM of about 11° was achieved [136].

RoM is especially a topic on slopes or stairs. Limitations enforce compensating motion of the other leg joints. In [171] 8° ankle RoM was identified for unilateral amputees walking up a slope of 5° (SACH foot). The control group had a RoM of about 24°. Descending the same slope the amputees had an ankle RoM of about 9°, while the control group had about 20°. In addition ankle angle at touch down differs significant between the control and the amputee group.

The lag for amputee ankle joint RoM is caused by rigid prosthetic foot mechanisms. Softer mechanisms like ESAR feet could improve performance and may also increase stride length of the residual limb [63]. On the other hand the plantarflexion of a prosthetic ankle during push off is limited to the ankle rest position. Further changes in the ankle angle could only be realized by energy injecting systems. For realizing this in a passive device energy has to be stored first in another phase of the gait cycle.

In a novel semi-passive ankle prototype (Energy Recycling Foot, [21]) energy storage is realized during heel contact. Afterwards it is used to support push off. For push off in walking at preferred speed [28] between 0.2 and 0.29 J/kg of positive ankle work is required (Table 5.1). For a 75 kg person this would be about 15–22 J. In [184] the system returned about 19–25 J in unilateral amputees. The Energy Recycling Foot could double push of energy in comparison to a conventional prosthetic foot. Also net rate of metabolic consumption could be reduced from 23 %

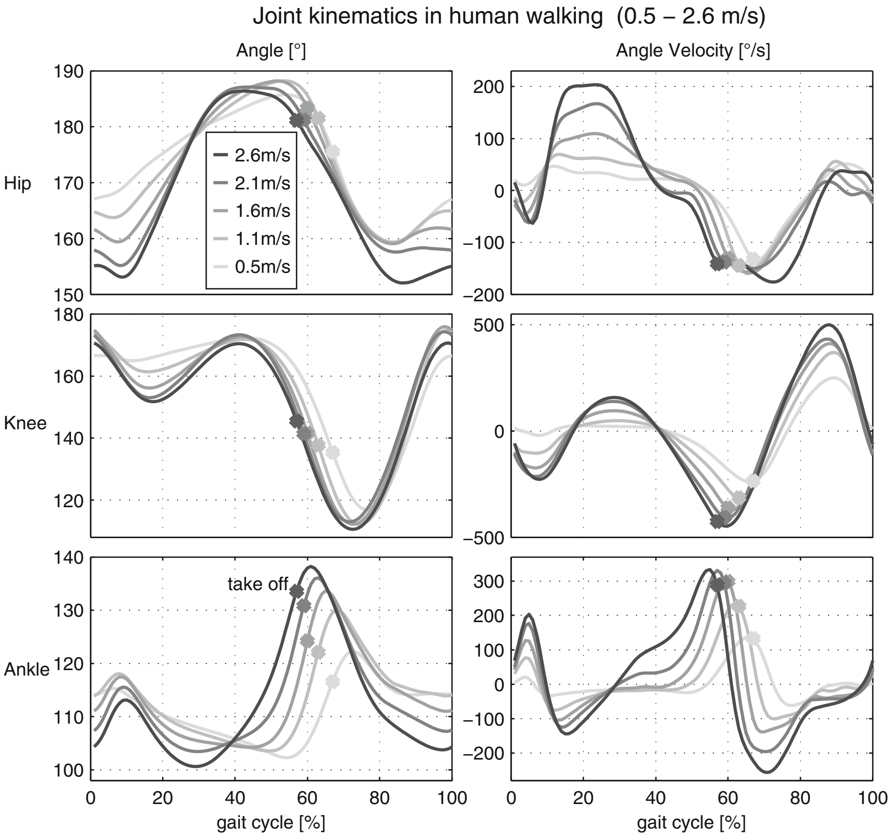

Fig. 5.1 Angle and angle velocity of human hip, knee and ankle in treadmill walking. Hip ankle is calculated between the seventh spine bone, trochanter major and a assumed rotational point at the knee (2 cm above the lateral meniscus at lateral femur condyle). Knee angle is calculated between trochanter major, the rotational point of the knee and the lateral malleolus. Ankle angle is calculated by the rotational point of the knee, the lateral malleolus and the fifth metatarsal joint of the foot. *Dots* are indicating take off for the individual speeds. Mean values of 21 subjects (25.4 years, 1.73 m, 70.9 kg) (Data from [94])

above normal (conventional prosthesis) to 14 % (Energy Recycling Foot) using a prosthetic simulator [21]. But more push off work not necessarily results in better gait performance. In [184] it was shown that with the same device softer spring stiffness values could improve positive push off work. This outcome was different to the results for the metabolic rate. It was best for a medium stiffness condition. As reasons excessive heel displacement and center of mass (CoM) collision losses were assumed.

Lower stiffness values also seem to reduce efficiency of the ESAR feet [43]. Similar tendencies could be identified by the hysteresis of different ESAR feet in a material testing machine [49].

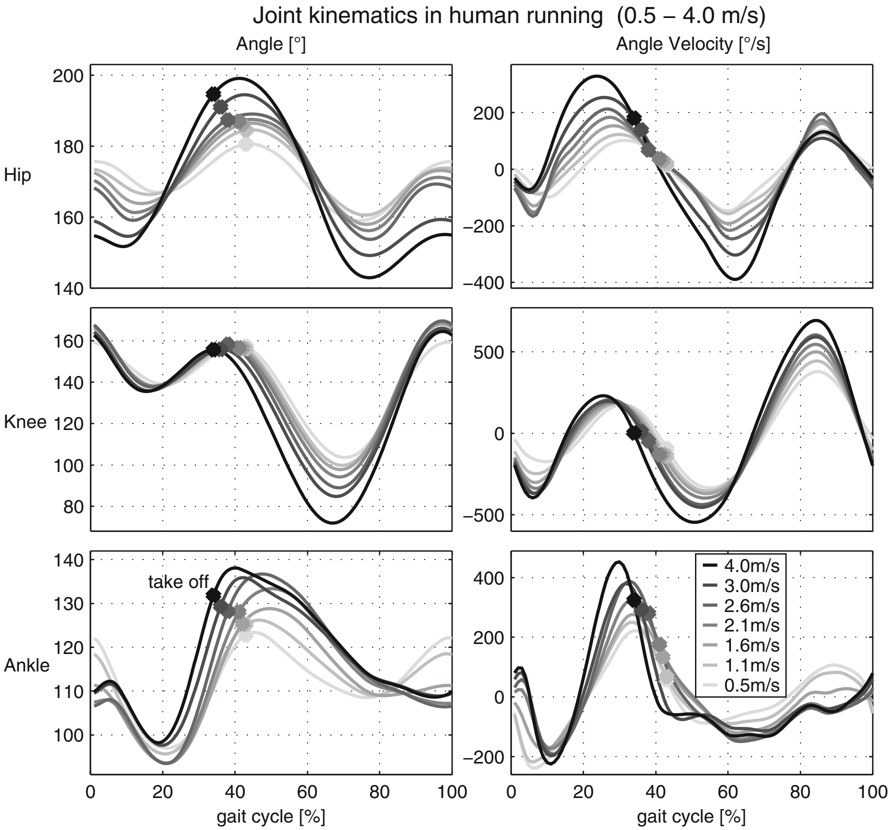

Fig. 5.2 Angle and angle velocity of human hip, knee and ankle in treadmill running. Mean values of 21 healthy subjects for speeds 0.5–2.6 m/s. Mean values of 7 subjects for 3 and 4 m/s (23.7 years, 1.8 m, 77.5 kg) (Data from [94]. For more information see caption of Fig. 5.1)

Table 5.1 Positive and negative peak power (W/kg) and work (J/kg) at the ankle joint during walking and running

Gait	Walking					Running						
Speed (m/s)	0.5	1.1	1.6	2.1	2.6	0.5	1.1	1.6	2.1	2.6	3.0	4.0
Positive peak power	0.9	2.0	3.2	4.3	4.6	5.3	6.0	6.1	7.1	8.7	10.0	14.1
Negative peak power	0.5	0.4	0.4	0.5	0.8	4.8	4.3	3.6	3.7	4.4	5.1	7.0
Positive work	0.12	0.20	0.29	0.45	0.54	0.54	0.60	0.60	0.64	0.70	0.80	0.98
Negative work	0.14	0.13	0.07	0.04	0.05	0.48	0.42	0.31	0.27	0.29	0.32	0.39

Transtibial amputees can get between 0.04 and 0.26 J/kg positive ankle work from their prosthesis during walking (Table 5.2). Medium values for preferred walking speed are about 0.06–0.11 J/kg (Table 5.2). Energy storage and release is increasing with walking speed [142, 148]. SACH feet can store and release less energy in comparison to ESAR feet [27, 53, 127, 142]. Efficiencies related to

Table 5.2 Energy, efficiency and peak power values for different passive prosthetic feet in transtibial (*TT*) and transfemoral (*TF*) amputees for walking (*W*) and running (*R*). For authors marked with ∗ energy and peak power values are estimated from published figures. Various studies used self-selected preferred walking speed (*PWS*)

Article	Prosthesis	Energy absorbed/ returned (J/kg)	Efficiency (%)	Peak power absorbed/ returned (W/kg)	Gait/ speed (m/s)	Subjects/ level of amputation
Czerniecki 1991 [27]	Flex Foot	0.45/0.38	84	6.7/5.5	R/2.8	5× TT
	Seattle Foot	0.49/0.25	52	8.2/4.1		
	SACH Foot	0.26/0.08	31	5.3/1.5		
Gitter ∗ 1991 [53]	Flex Foot	0.29/0.26	89	1.4/3.6	W/1.5	5× TT
	Seattle Foot	0.15/0.11	71	0.8/1.6		
	SACH Foot	0.1/0.04	39	0.5/0.7		
Seroussi ∗ 1996 [144]	Seattle Light Foot Mauch SNS Knee	0.09/0.07	75	0.39/0.6	W/PWS	8× TF
Silverman ∗ 2008 [148]	SACH or ESAR Foot	0.11/0.05	45	0.3/0.23	W/0.6	14× TT
		0.148/0.06	41	0.48/0.47	W/0.9	
		0.149/0.068	46	0.67/0.63	W/1.2	
		0.152/0.074	49	0.78/0.72	W/1.5	
Prince 1998 [127]	Golden Foot	0.27/0.11	41		W/0.9 to 1.4	5× TT
	Seattle Foot	0.17/0.064	39			
	SACH Foot	0.15/0.057	37			
Schaarschmidt (unpublished data from [139])	C-Walk	0.11/0.065	59	0.36/0.53	W/1.1	4× TF
Schneider 1993 [142]	Flex Foot			0.98/1.29	W/0.9	12× TT (children)
	SACH			0.57/0.29		
	Flex Foot			1.51/1.94	W/1.3	
	SACH			0.78/0.34		
Nolan 2000 [112]	Multiflex or SACH			0.81/0.86	W/1.2	4× TT
	Flex/Intelligent or Flex/Hydraulic			0.99/1.74	W/1.2	4× TF
Johansson 2005 [84]	Allurion Foot with				W/PWS	8× TF
	Rheo Knee			0.7/0.75		
	C-Leg			0.7/0.75		
	Mauch SNS			0.55/0.75		
Segal 2006 [143]	Dynamic Plus, C- Walk, LuXon Max with C-Leg			0.6/0.6	W/1.3	8× TF
	Seattle Light, Flex Foot with Mauch SNS			0.8/0.66	W/1.3	
Vanicek 2009 [165]	Multiflex, Variflex, Dynamic or Centerus Foot			Faller 0.55/0.4 Non Faller 0.4/0.45	W/PWS	11× TT

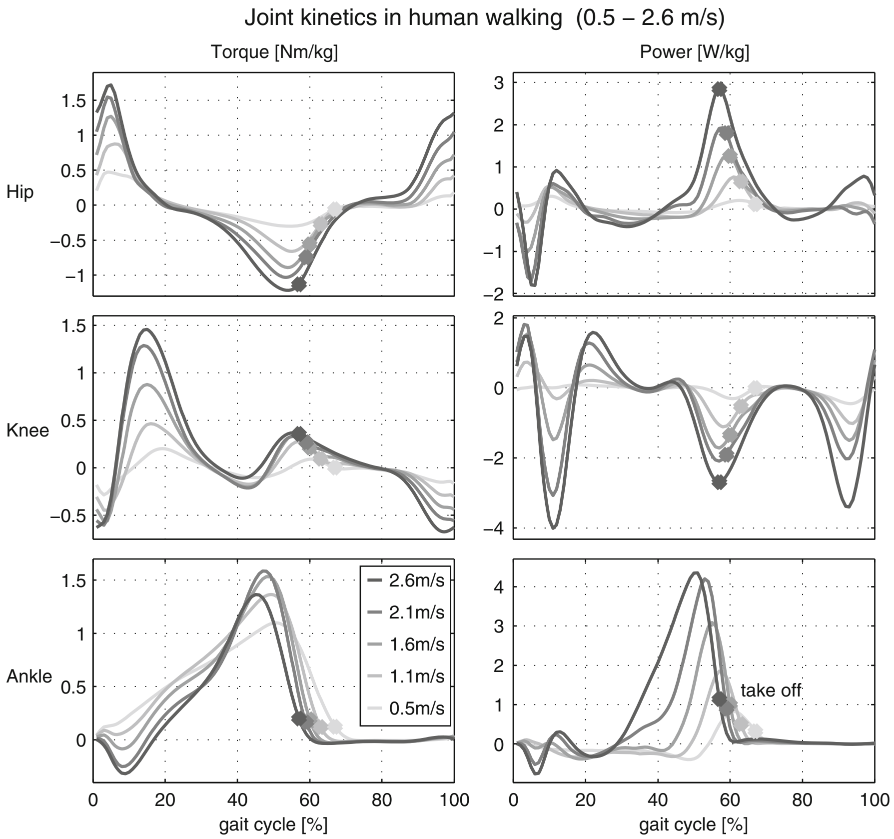

Fig. 5.3 Joint torque and power for human hip, knee and ankle in treadmill walking. Joint torques are calculated using inverse dynamics. Power is the product of joint velocity and joint torque. Both values are normalized to body mass. *Dots* are indicating take off for the individual speeds. Mean values of 21 subjects (25.4 years, 1.73 m, 70.9 kg) (Data from [94])

energy storage and dissipation and final push off recovery are between 39 and 89 %. Calculation methods [127] and material properties contribute to the wide range [49]. SACH feet seem to be less efficient than ESAR feet [27,53]. However nearly similar values were identified in [127] when comparing both designs.

When running (2.8 m/s) using walking feet a similar range for prosthetic foot efficiency (31–84 %) compared to walking (Table 5.2) was identified.

At the ankle joint PP around preferred walking speed in healthy subject gait is about 2.0–3.2 W/kg (Table 5.1, Fig. 5.3). In comparison 0.34–3.6 W/kg can be realized using prosthetic feet in transtibial amputees. Mean values for transfemoral amputees are about 0.6 W/kg (Table 5.2). Comparing amputation level much higher values could be identified for transtibial amputees [53, 142]. Similar to increasing energy storage and return also PP is increasing with speed [148].

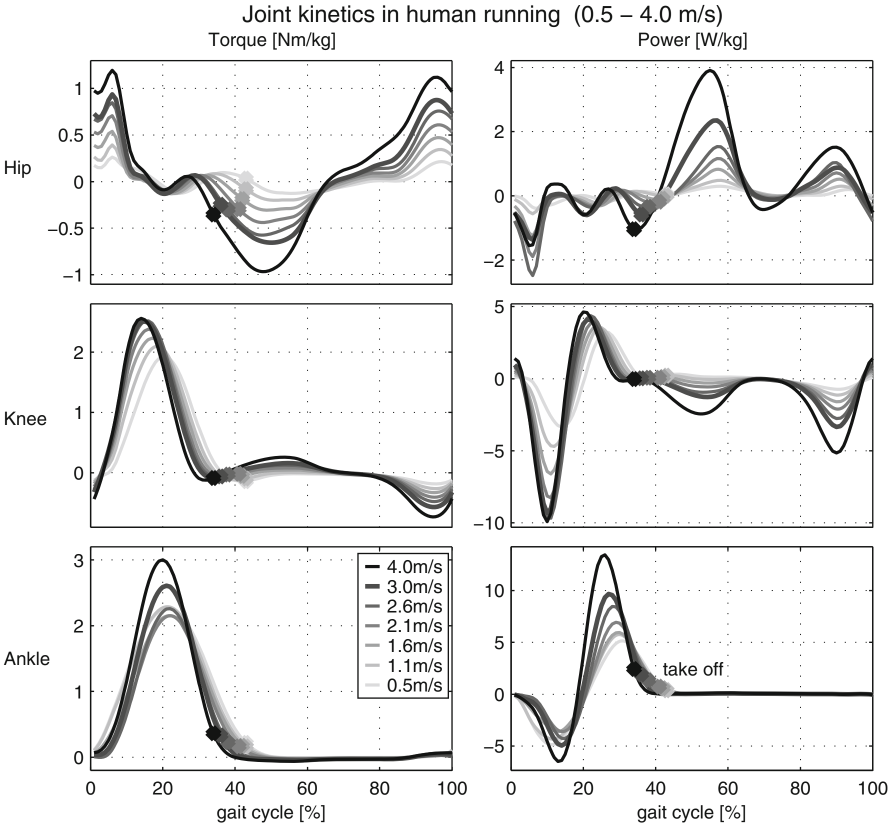

Fig. 5.4 Joint torque and power for human hip, knee and ankle in treadmill running. Mean values of 21 healthy subjects for speeds 0.5–2.6 m/s. Mean values of 7 subjects for 3 and 4 m/s (23.7 years, 1.8 m, 77.5 kg) (Data from [94]. For more information see caption of Fig. 5.3)

Highest PP values could be identified in running (e.g. 5.5 W/kg at 2.8 m/s [27]). At a similar speed healthy subjects would have a PP of about 9.4 W/kg (estimated from Table 5.1, Fig. 5.4).

Also when providing more positive work and higher PP, ambiguous outcomes for oxygen consumption with SACH feet in comparison to ESAR feet were identified by [63]. Only three out of nine studies showed an improved energy expenditure when using ESAR feet. Benefits seem to be possible for higher walking speeds [109, 141].

A reason for the discrepancy between oxygen consumption, positive work and PP could be a wrong timing and the wrong angular displacement of the leg segments at a certain event in comparison to non-amputees (Figs. 5.5 and 5.6). A primary contribution to the segment interaction could be created by biarticular structures coupling the joints. For example the gastrocnemius muscle has the potential for adjusting knee flexion and ankle plantarflexion during push off [166]. By this it could be possible to set push off direction in an appropriate manner.

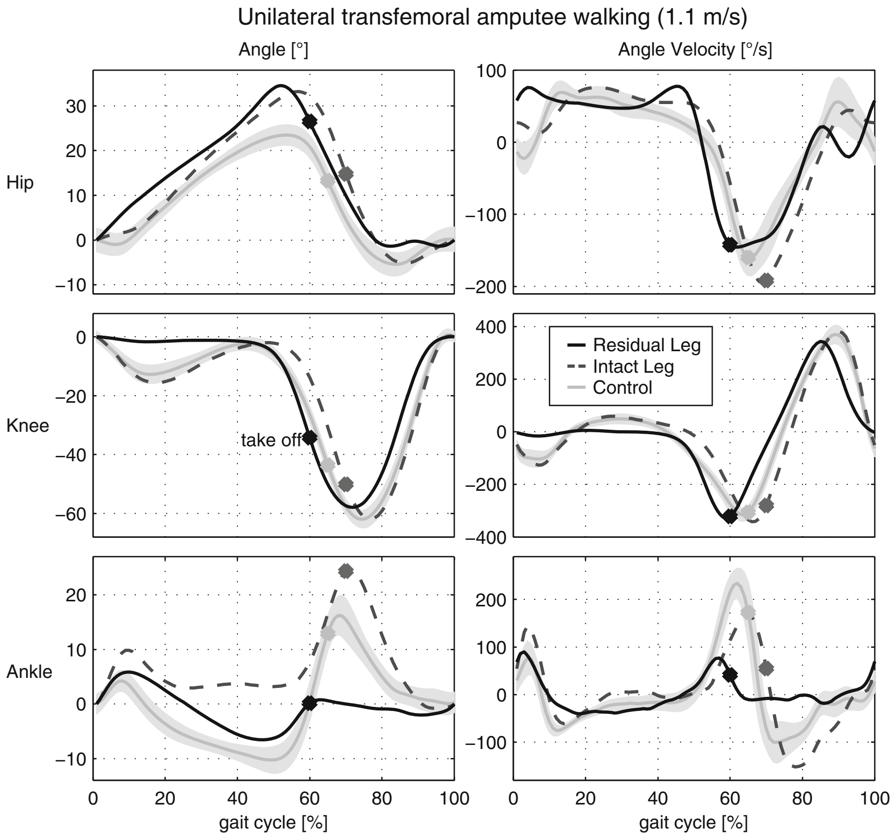

Fig. 5.5 Angle and angle velocity of human unilateral, transfemoral amputees for the hip, knee and ankle in walking at 1.1 m/s. The *solid black line* indicates the residual prosthetic leg (C-Leg knee and C-Walk foot, Otto Bock, [117]), the *dashed grey line* represents the intact amputee leg. *Dots* are indicating take off for the separate conditions. Reference data (*grey solid*, [94]) is presented with standard deviation. Amputee data is the mean value of 4 subjects taken from [139], (42.3 years, 1.86 m, 91.3 kg)

Ideas of biarticular structures, coupling the knee and the ankle joint, exist since the Hydra Cadence Knee in the late 1940s [177]. Already there the positive effects of the synchronized joints were reported. This concept is now used in a novel prototype to increase push off power in walking [161]. While extending the knee in flight phase the biarticular design enables to load a spring passively. This energy is released during take off and helps to bend the knee and to extend the ankle (plantarflexion). As a disadvantage this feature excludes the possibility of knee stance phase flexion. Due to the design the amputee has to walk with an extended knee, which is in contrast to the natural bending behavior used for shock absorption.

To overcome missing positive net work at the prosthetic ankle joint a compensating motion of the body is required. This results in 23 % higher oxygen consumption for speeds from 0.6 to 1.4 m/s compared to non-amputees. Variations

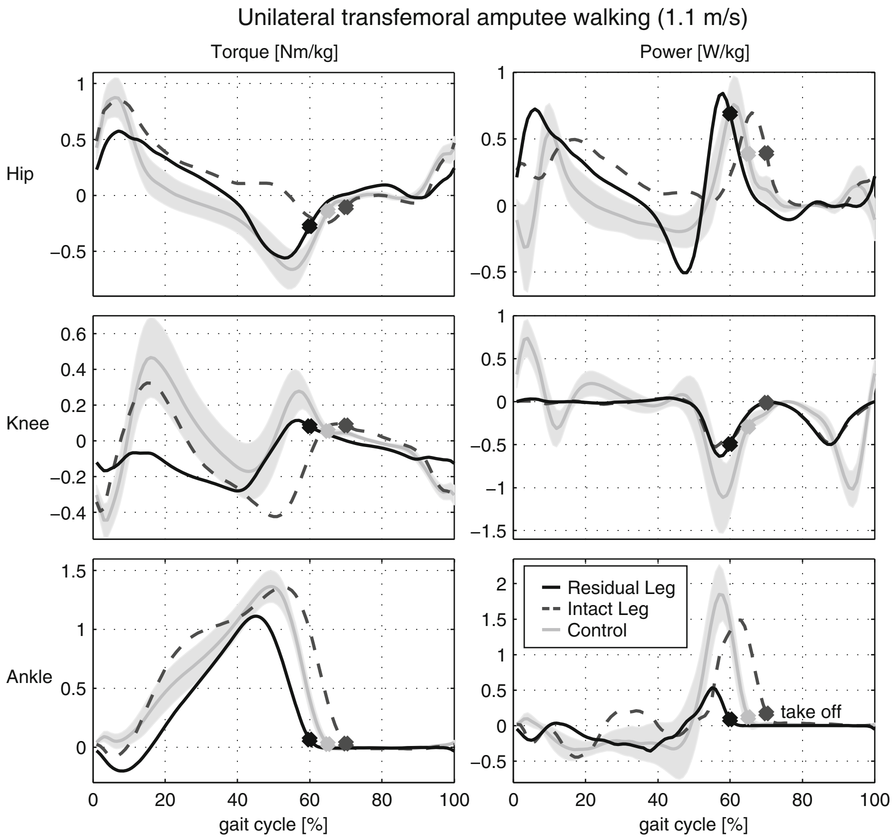

Fig. 5.6 Joint torque and power for human unilateral, transfemoral amputees for the hip, knee and ankle in treadmill walking at 1.1 m/s. Joint torques are calculated using inverse dynamics. Power is the product of joint velocity and joint torque. Both values are normalized to body mass. The *solid black line* indicates the residual prosthetic leg (C-Leg knee and C-Walk foot, Otto Bock, [117]), the *dashed grey line* represents the intact amputee leg. *Dots* are indicating take off for the separate conditions. Reference data (*grey solid*, [94]) is presented with standard deviation. Amputee data is the mean value of 4 subjects taken from [139], (42.3 years, 1.86 m, 91.3 kg)

could be possible by different alignments of the foot [141]. For the cost of transport (CoT) increased speed dependent (0.75–1.75 m/s) values between 11 and 25 % were identified for transtibial amputees [66].

In addition to no positive net work, higher metabolic rates, reduced RoM and reduced peak power further biomechanical characteristics could be identified caused by the artificial passive ankle joint.

Additional gait characteristics for transtibial amputees

- Reduced first vertical ground reaction force peak at residual limb (RL) [113]
- Reduced impulse at RL [113]

- Increased impulse at intact limb (IL) [113]
- Reduced stance time at RL [113]
- Increased stance time at IL [113]
- Increased swing time at RL [113]
- Reduced swing time at IL [113]
- Reduced lower preferred walking speed (18 %) [66]
- Reduced stride length [126]
- Increased EMG amplitude and duration for knee flexors and extensors at RL [126]
- Increased EMG for hip extensor in early stance phase [179]
- Increased early stance hip peak power, work and moment for compensation [148]

Further objects which are criticized by transtibial amputees testing ESAR and SACH feet can be found in [63].

5.3.2 *Knee Joint*

5.3.2.1 Design Characteristics

In contrast to the ankle joint, the knee joint performs more negative than positive work during level walking (Fig. 5.3). Thus it requires less actuation compared to the ankle joint. Dampers are able to modulate swing phase and by mechanical design knee is locked to secure stance phase. Using these features passive prosthetic knee joints can perform level walking at a similar level compared to semi-active devices [139].

There is a variety of mechanical features that differs between the passive joints. The number of axis (single, polycentric), the mechanism to lock the knee in stance phase or the way to provide damping during stance and swing are the most fundamental differences. First versions of hydraulic dampers were implemented in prosthetics in the late 1940s. A combination of hydraulic knee-ankle unit the Stewart-Vickers Hydraulic Above-Knee Leg, today known as the Hydra Cadence Knee, used a hydraulic mechanism to lock the knee at touch down. In addition it synchronized the behavior between the knee and ankle by a biarticular structure during the swing phase. In 1951 the Mauch S'n'S (Swing and Stance) system was developed by Henschke and Mauch. A hydraulic swing phase damper was introduced that worked together with a system to ensure stance phase [177]. In addition to hydraulics (e.g. 3R60, Otto Bock, [117]) also pneumatics (e.g. ESK, Endolite, [38]) are used. Both joints the 3R60 and the ESK are using different locking mechanisms. The 3R60 uses a polycentric joint that secures stance by geometry. The ESK is a single axis knee that uses a drum brake that works progressively in relation to the applied load. Further differences are components that allow yielding (up to 15° in 3R60, Modular Knee Joint booklet, Otto Bock, [117]) or to lock and unlock the knee joint manually for higher safety (e.g. 1M10, Proteor, [129]). A feasible set of knee components is offered for each level of activity by combining the required features in different combinations. As a result Otto Bock provides over 40 different knee joints (Modular Knee Joint booklet).

5.3.2.2 Gait Biomechanics

Transfemoral amputees suffer not only from the missing natural knee function. In addition they have to deal with the artificial ankle function. As a result asymmetric behavior is much more pronounced than for transtibial amputees [113]. This requires an increased step width in walking to keep balance in comparison to non-amputees [74]. Most of the transtibial characteristics (Sect. 5.3.1.2) are even more pronounced. In comparison to the artificial ankle joints RoM is not restricted for the knee joint (Knee angle Fig. 5.5) during walking in swing phase. Depending on Mobility Grade and preferred walking speed an adequate module can be applied. Otto Bock [117] provides joints with a range of 110–175° (Modular Knee Joint booklet). Especially devices with lower RoM values can cause discomfort during daily activities like sitting.

Kinematic deficits for the knee joint are found in the stance phase [84, 143, 144]. In addition no positive work is provided for a knee flexion during swing leg retraction [145]. Various prosthetic knee joints are locking the knee in an extended position at touch down. As a result natural shock reduction (elastic or damping) by the knee is not possible. Subsequently no or only little knee flexion during stance is possible for the amputee. Advanced passive knee joint technology provides solutions for the missing shock absorption. Individual adaptive spring-damper systems like in the EBS system (Otto Bock, [117]) allow stance phase flexion of up to 15°. Even though the technical feature to permit yielding is also implemented in the C-Leg, only a small part of the users is using it [84, 143, 144], (Fig. 5.5). Missing yielding could be explained by already existing movement patterns used to handle previous versions of passive knee joints. Also missing positive work which could be introduced by elastic or active components could explain it. Why to reduce vertical hip position by knee flexion when there is no mechanism in the knee joint to extend it again. This limitation could be compensated by muscle work of hip extensors or monoarticular artificial ankle plantarflexors.

Interestingly forward propulsion is mainly generated by the prosthetic limb. This phenomenon can be explained by the CoM behavior. The intact limb is increasing CoM height and by this the potential energy. During the contact of the prosthetic limb this energy is transformed into horizontal kinetic energy. The height of the CoM is decreasing. By this interaction of both limbs the prosthetic limb creates a net forward impulse without providing positive work at the knee or net positive work at the ankle joint [139].

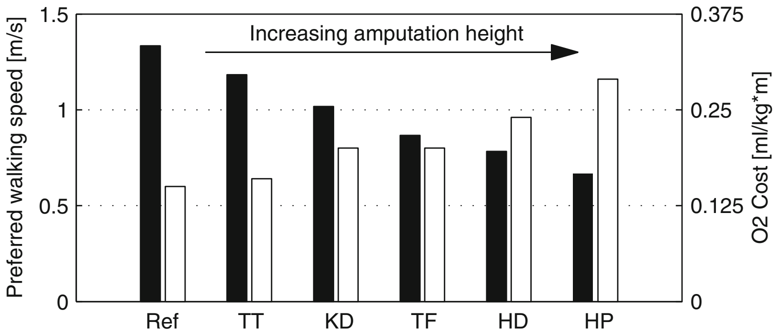

Fig. 5.7 Preferred walking velocity (*black*) and oxygen consumption (*white*) for different levels of amputation. *Ref* reference non amputee, *TT* transtibial, *KD* knee disarticulation, *TF* transfemoral, *HD* hip disarticulation, *HP* hemi-pelvectomy (Figure adapted from [174])

The resulting preferred walking speed for transfemoral amputees (1.04 m/s) is lower than for amputees with knee disarticulation (1.19 m/s, [13]). 1.45 m/s [13] or 1.41 m/s [66] were identified for control groups. In comparison to the transtibial amputees (18 % reduction) the preferred speed reduction would be about 27 % for transfemoral amputees. Waters and Mulroy [174] showed the opposing trend of oxygen consumption and preferred speed for different levels of amputation (Fig. 5.7). When amputees are forced to walk at similar speeds like non-amputees higher oxygen consumption during walking can also be identified. For transfemoral amputees the additional expenses are increasing with speed (0.6–1.4 m/s) by 55–64 %. In comparison to transtibial amputees (23 % higher than non-amputee) the increase is nearly tripled [141].

The reasons for this energetic increase are manifold. Compensating structures (muscles, tendons) to realize gait seem not to work at their most efficient operating point (e.g. muscle force – length relationship). Increased hip extensor torques were identified to be the reason for increased metabolic rates in different prosthetic alignments [141]. Higher extensor muscle activity [179] was mentioned as a reason in [141]. In addition the elastic behavior of the artificial ankle and the knee joint is not used in an appropriate way. Optimal stiffness values can decrease energetic requirements dramatically [58, 59]. Also biarticular couplings are missing (e.g. gastrocnemius), which could transfer energy between the joints. For saving energy, joint couplings seem to be highly beneficial [163]. Without, also loading these tendons in one phase of the gait cycle and releasing this energy in other parts is not possible. This would directly influence energetic effort. Furthermore with such two-joint structures also the coordination between the joints could be facilitated. Co-contraction of antagonistic muscles at the prosthetic and also at the contra-lateral site could help to stabilize gait without these structures. Also this would result in increased metabolic rates.

5.4 Semi-active Prosthetics

5.4.1 Ankle Joint

5.4.1.1 Design Characteristics

Compared to passive designs, semi-active feet provide an increased functionality. They are using passive mechanical principles controlled by active adjustable valves. Hydraulic concepts are used for the Raize ankle/foot system (Hosmer, [80]) or the élan foot (Endolite, [38]). The Raize ankle provides an adjustable planter/dorsiflexion range. In addition resistance is adaptable manually. Reduced damaging forces on the residual limb and greatly enhanced stability on slopes or slippery surfaces are promised [80]. Both mechanisms should provide better ground adaptation especially at inclines and declines. The élan foot uses sensor feedback as an input for adaptive control depending on slope during walking. Foot characteristics should be adapted to the most comfortable and energy efficient response. For this the hydraulics allow adjustments of up to 6° plantarflexion and 3° dorsalextension which adds to the RoM of the carbon foot. Twenty-four hours of operation should be possible.

5.4.1.2 Gait Biomechanics

The élan foot aims at supporting the push off while ascending slopes by stiffening the ankle damper at touch down. In addition, at descending slopes loading is reduced by a decreased ankle damping. This results in an increased RoM compared to simple carbon fibre feet and provides more stability.

5.4.2 Knee Joint

5.4.2.1 Design Characteristics

The most popular semi-active knee device is the C-Leg. After the introduction in 1997 over 40,000 (Advanced Prosthetic Knee Technology booklet, Otto Bock, [117]) of them were sold worldwide. Using different sensors (angle sensors, strain gauges) the knee joint can identify the gait phase. By this information and an individual patient depending gain adaptation of the prosthesis, the microprocessor can control the damping of a hydraulic joint. Primary targets like damping knee flexion or extension (negative knee power) in swing phase can be achieved (Fig. 5.6). However, the created patterns are only partially matching non-amputee data [84, 143, 144].

Using the compensatory mechanism of the hip extensor muscles, the Genium knee (Otto Bock, [117]) makes it possible to walk up stairs in an alternating stepping pattern. About 2 and 5 days of battery life are stated for the C-Leg and the Genium knee respectively. Up to 2 days of battery life are also envisioned for the Rheo Knee (Ossur, [116]). Damping is realized by a magnetorheological fluid. By varying the magnetic field intensity damping could be adapted comparable to the C-Leg. Similar technology is used in [106,107]. Other examples for microprocessor controlled knee joints are the Plié 2.0 (Freedom Innovations, [45]) or the Orion knee (Endolite, [38]). Both knees are working with hydraulic mechanisms. In addition the Orion uses a pneumatic system to control swing phase.

5.4.2.2 Gait Biomechanics

A key advantage for microprocessor controlled knee joints to purely mechanical devices is the possibility to adapt to different conditions. For instance an adaptation for different slopes or speeds can be realized.

In a comparison for level walking only little differences between a passive (Mauch SNS) and a semi-active prosthesis (C-Leg) could be identified [143]. Also when comparing 3R80 (passive) to the C-Leg at different speeds hardly any differences were observed [139]. Thus semi-active knee joints do not necessarily outperform passive mechanism at level walking in laboratory condition. More important seem to be non-steady daily life tasks as addressed in [158]. A daily activity test for amputees was used to compare passive with semi-active knee joints. Time was measured for different tasks. Using the semi active prosthesis all investigated scenarios were finished faster. A higher confidence of the users due to lower risk of falling could be a reason for this result [10, 11].

Passive knee joints like the 3R80 need a sufficient knee extension to be capable of supporting load. If this angle is not reached like when tripping on uneven ground the amputee would fall. Sensors in the semi-active knee joints can detect such events and provide an increased damping e.g. by closing the corresponding hydraulic valve. Such a mechanism can to some extend prevent from falling.

This can clearly increase the amputees confidence. It is of key importance since nearly 50 % of amputees (including transfemoral and transtibial amputees) suffer from the fear of falling [103]. About the same amount of amputees (50 %) are indeed falling at least once a year [55,87,103]. Nearly 20 % of the amputees needed medical care after falling [103]. A maximum of 15 falls for one amputee in the last year [55] illustrates the relevance of improving preventing aspects like handling training or more secure technology. Technology improvement could decrease the 12 % of falls that were reported to result from the prosthesis function alone and the 22 % related to the environment [87].

In [85] various tests were made to compare passive knee joints with a microprocessor controlled knee joint (C-Leg). Stumbles decreased by 59 % and falls by 64 % when using the C-Leg. Due to the higher self confidence (stumble recovery) and the possibility to adapt to different speeds [115, 143] improvements in walking speed on even and uneven terrain with semi-active knee prostheses are possible.

Benefits of microprocessor controlled knee joints

- Stumbles decreased 59 % [85]
- Falls decreased 64 % [85]
- Higher potential for security [10, 11]
- Increased PWS 8–15 % on even terrain [85, 115, 143]
- Similar oxygen costs for higher PWS [115]
- 3–5 % reduced metabolic rate [84]
- 75 m fastest possible walking speed (FPWS) on even terrain increased by 12 % [85]
- 38 m FPWS on uneven terrain increased by 21 % [85]
- 6 m FPWS on even terrain increased by 17 % [85]
- Performance score for stair descent increased [85]
- Faster placing and picking up of objects [158]
- Faster on slopes, stairs [158]
- Faster slalom walking speed while carrying objects [158]
- Decrease in hip work [84]
- Lower peak hip flexion moment at terminal stance [84]
- Reduction in peak hip power generation at toe-off [84]
- Increased symmetry between limbs [143]
- Less pronounced asymmetry between braking and propulsive impulses [139]

Further improvements in semi-active knee joints can potentially close the gap between healthy and amputee gait. New designs like the Genium knee (Otto Bock, [117]) mimic natural knee function better than the previous generations. Knee flexion angle during swing is independent of speed which is comparable to healthy gait (Fig. 5.1), [12]. A 4° preflexion of the Genium knee at touch down results in less asymmetry of step length. Increased stance phase flexion was found in 3 out of 11 subjects. Various additional benefits for daily life tasks like walking backwards, standing or walking on slopes or stairs were observed [9, 12].

5.5 Powered Prosthetics

Microprocessor controlled spring-damper systems at the knee or at the ankle joint can improve prosthetic technology and amputee performance. However, kinematic and kinetic gait analyses still show more asymmetric gait and higher oxygen consumption than in non-amputees. Continuous asymmetries in gait can cause long term sequelae [46, 131] which may result in even reduced living comfort and additional costs for the amputee or the health insurance company. To avoid this, further improvements in prosthetic technology are required.

Passive prosthetic devices can mimic eccentric or isometric muscle behavior (e.g. by dampers). They can also mimic elastic tendon like behavior by different kinds of springs. It is not possible to mimic concentric muscle behavior with passive systems. Including such an ability could provide additional functionality to a prosthetic system.

First steps toward powered prosthetics were realized with the Belgrade Above Knee Prosthesis (AKP) in the late 1980s [124]. The system used external power supply and control. DC motor technology was used to drive the knee joint. By the active knee amputee energy consumption could be reduced and maximum walking speed could be increased.

Twenty-five years later still only a few commercialized systems provide the possibility to inject energy and to create joint torques actively. Twenty-six systems including prototypes and commercialized systems are listed in Tables 5.3 and 5.4 (Appendix). Some of them have a couple of previous design generations. Non of the systems is addressing an active hip joint. So far only powered systems for ankle (Fig. 5.8a–j, r) and knee (Fig. 5.8k–r) are described in literature.

The first commercialized active foot is the Proprio Foot (Ossur, Fig. 5.8i). It has the possibility to lift the toe during swing phase to adapt to terrain and to prevent from trips or falling. Different sensors (accelerometer, angle sensor) detect the actual state (walking flat, stairs, slopes, sitting, standing) and set a linear actuator to the appropriate position corresponding to a defined ankle angle. For this motion events like take off or touch down are identified. To get a better pattern recognition also the last step is taken into account. A similar actuation concept was used for the prosthetic ankle concept introduced in [155].

A further commercialized concept for an active foot is from iWalk (Fig. 5.8f). They introduced the BiOM Power Foot, an active prosthesis to replace the ankle joint [83]. Achilles tendon like elastic function (spring) is combined with a motor that mimics calf muscle behavior. By this method not only swing phase adaptations like in the Proprio Foot but also active powered push off becomes possible.

Active motor support for the knee joint is provided in the Power Knee (Ossur, Fig. 5.8o). The first generation of the knee joint was launched in 2006. The second much more compact version is available since 2011. Knee extension while ascending stairs and slopes or also while standing up from sitting is supported by a motor. During sitting down or descending stairs and slopes the motor can dissipate energy. During take off the motor rises the heel actively for swing flexion. In addition it assists at stairs or slopes for positioning the knee adequately for touch down. Like in the BiOM Foot a spring is assisting the motor to some extend by storing energy in a specific phase (yielding, stance phase flexion) and releasing it later. The same approach is used in [102]. A powered knee joint prototype with an antagonistic SEA design (Fig. 5.8n) could increase amputee's average self-selected walking speed by 17 % from 1.12 to 1.31 m/s compared to a C-Leg. At fixed speed (1.3 m/s) metabolic costs decreased by 6.8 % using the powered prototype in comparison to the semi-active knee joint.

Fig. 5.8 Active prosthetics for the ankle (**a**–**j**) the knee (**k**–**q**) and for both joints (**r**). For a more detailed description see Table 5.3 for the ankle and Table 5.4 for the knee joints (Appendix)

Various powered prototypes (Tables 5.3 and 5.4) are in commercial or university development. Concepts are including single ankle and knee prosthetics but also approaches combining both joints actuated in one design. At the Vanderbilt University (Nashville) a combination of powered knee and ankle was developed [151], (Fig. 5.8r). The concept will be further developed and commercialized by Freedom Innovations [45].

A concept using electrical motors to do cheap design knee prosthetics is introduced in [82, 90], (Fig. 5.8l). The motor should not replicate torque profiles of walking or stair climbing but it should enable the person to flex or extend the knee in low load or no load conditions.

Powered ankle joints for walking (Odyssey Ankle, Fig. 5.8a) and running (Fig. 5.8c, d) were developed at Springactive [149] and Westpoint Military Academy [71] based on previous designs (Sparky, Fig. 5.8b) from the Arizona State University [8].

Walking should also be achieved with the PANTOE 1 (Fig. 5.8g) foot prosthesis developed at the Peking University [182, 186]. In addition to the common concepts an activated toe joint is integrated in the design.

A mixture of prosthetic and orthotic design is developed at the TU Darmstadt. The Powered Ankle Knee Orthoprosthesis (PAKO, Fig. 5.8j) should be used to evaluate elastic actuator design and control concepts for humanoid locomotion. Therefore a mechanism to change stiffness of a spring in the SEA is included in the design.

5.5.1 Mechanics

5.5.1.1 Actuator Concepts

All commercial available active prosthetics and the most of the prototypes using electrical motor technology for driving the ankle or the knee joint. In addition some of them include different kinds of elastic concepts. Series, parallel or unidirectional parallel alignments of motor and elastic element are used aiming at a reduction of motor requirements. Peak power (PP), which corresponds to motor size and energy requirements (ER), which defines battery size and operation time are characteristics to be decreased in comparison to direct drive (DD) systems.

Most of the active prosthetic prototypes try to mimic torque ankle profiles of the ankle and knee joint. Some of them are only acting with minimal power efforts [44, 155] to change for example ankle angle for ground clearance in flight phase or to adapt ankle angle to slopes.

In order to get a higher power density than in electrical motors also hydraulic or pneumatic actuators could be used. In [122] a design is introduced that provides energy injection for the ankle and the knee joint by linear hydraulic actuators driven by a single pump. So push off can be supported at the ankle, early swing at the knee and the ankle joint. During stair climbing and late swing the knee can be powered. A special feature of the prosthesis is to work in active mode or also as a semi-active device like the C-Leg.

Pneumatic actuation was demonstrated with the pleated pneumatic artificial muscles (PPAM) concept [170]. The system was able to produce required torques for an artificial ankle joint in walking. PPAM pressure was generated by a stationary compressor in the laboratory.

Using PPAM, a stiffness adaptation for different speeds was possible. Required stiffness was estimated by a linear regression on human ankle torque-angle curves.

Similar pneumatic concepts are used for experiments with orthotic structures [41, 138].

Pneumatic actuation can also be found in a knee prosthesis [175], (Fig. 5.8m). To become independent of external pneumatic supply this group investigates liquid propellants as energy source. The monopropellant, a reaction product of a catalytically decomposed liquid, should be able to provide large power output and long operation times. For a mobile solution the compact energy storage of the propellant will be beneficial [146].

The high power density of the pneumatic system [175] can help to improve prosthetic design. Similar advantages in power to weight ratio are identified for hydraulic solutions [34].

5.5.1.2 Spring Configurations

For the different leg joints and also different tasks optimal elastic actuator configurations can be identified. The challenge is to identify a most multifunctional solution that can provide benefits in various daily life activities. In terms of energy consumption the primary focus should be on the most common daily life activities like walking or just standing in place. But also energy and power requirements in stair climbing, standing up, sitting down, walking slopes or running could be included in the choice for an elastic actuation concept.

Inspired by muscle modeling different actuator solutions can be considered. Solutions with series elastic elements (SE) were used in [121]. Parallel elements (PE) to the contractile element (CE) were omitted in this study because many authors reported only negligible passive parallel forces. In contrast the Hill Model includes a SE and a PE. Different solutions exist with the CE and the SE together in parallel to the PE [183], (Fig. 5.9e) or only the CE in parallel to the PE [111], (Fig. 5.9c). In addition to the conventional elastic concepts unidirectional springs, coming into action at a defined condition (kinematic, kinetic), can be considered.

Such an approach is used in [151] where the spring comes into action at an ankle angle of about 5° of plantarflexion. The BiOM ankle prosthesis [37] includes an SEA in addition, to extend the system to a scheme similar to Fig. 5.9i. In an earlier version of the device the unidirectional spring is mentioned to be engaged at 0° [6]. A spring in series (Fig. 5.9b) with a much smaller stiffness than in the BiOM ankle is included in the Robotic Tendon approach of Sparky. Stiffness is defined using power

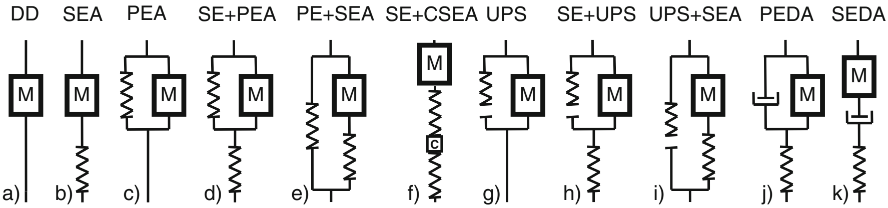

Fig. 5.9 Various concepts for elastic actuators combining a motor (*M*) with series (*SE*), parallel (*PE*) and/or unidirectional parallel (*UPS*) springs. In addition it could be possible to include clutches (*C*) or damping elements (**j** and **k**)

optimization calculations [76]. Especially the long lever arm between ankle joint and actuator causes this design difference [59]. In contrast, in the BiOM ankle series stiffness is chosen based on open-loop force bandwidth [6]. An extended version of the Robotic Tendon approach is introduced in [71, 140]. For running two parallel elastic actuators were included in the design to achieve the required power demands.

A series spring approach is also used for the AMP foot 2.0 [18], (Fig. 5.8e). In contrast to the approaches using motors with over 150 W the design requires only a 60 W motor. This solution is possible by combining two basic mechanisms. A series spring, which is decoupled from ankle motion, is loaded with a constant power by the small motor during the entire stance phase. A second spring is saving energy in a similar way like the forefoot part in ESAR feet. During push off the passive spring returns its energy. In addition a clutch is used to release the energy from the motor-spring combination (Fig. 5.9f). On the one hand this approach provides the advantage of less peak power requirements for the motor. This could potentially save space and weight if the required clutch mechanism is small enough. In contrast to the mechanisms used in [37] and [72] the energy return cannot be modulated in the same way. It is like a catapult that just releases the energy if the trigger is pulled. The interaction with the amputee must be programmed carefully to match desired patterns. To which extend this approach can handle different daily life situations like different speeds, slopes and stairs should be further investigated.

Two SEA's are used in the PANTOE 1 [182, 186]. The ankle prosthesis includes one SEA for ankle plantar and dorsiflexion. Another SEA modulates toe joint motion. It is envisioned that the active prosthetic toe joint can improve several biomechanical parameters for the foot like RoM, angle velocity and energy output. Higher walking speeds should be achieved in comparison to rigid foot design.

Systematic analysis on elastic actuator concepts that reduce energy requirements (ER) or peak power (PP) were published for the ankle [39, 59, 60, 173], the knee [58, 173] and the hip [173] joint. Methods for calculations base on [76]. In order to decrease power, actuator velocity or actuator force could be reduced. A series spring has the capability to decrease motor velocity. A parallel spring has the capability to reduce motor force.

Especially for the ankle joint high benefits could be identified for the motor when using a series spring with optimal stiffness in comparison to a direct drive. In terms of ER the mean advantage for five different speeds between 0.5 and

2.6 m/s was about 64.7 % for running and 25.8 % in walking using an SEA. A PEA (Fig. 5.9c) could reduce ER to less extent. 45 and 12.2 % were possible respectively. A combination of both elastic structures (SE+PEA, Fig. 5.9d) results in an energetic advantage of 52.8 % in running and 17.9 % in walking for the elastic actuator.

In terms of peak power highest reductions were identified for the SE+PEA system (81.8 %) in running. The force reduction by the parallel spring contributes most to reduce power requirements. A single PEA had already a mean advantage for the five speeds of 79 %. An SEA could reduce PP by 68.5 % in running.

For walking a similar trend was identified. An SE+PEA had highest benefits (70.4 %). Lower advantages were identified for the PEA (62.5 %) and the SEA (48.3 %).

Unidirectional parallel springs at the ankle joint (Fig. 5.9g–i) can have similar power advantages like the PEA. In addition it is possible for some speeds to get lower ER than in PEA [39].

At the knee joint energetic benefits of 5–29 % could be achieved by an SEA in comparison to a DD in walking (0.5–2.6 m/s). No or only little PP (high speeds up to 31 %) reductions were possible in walking, when considering that negative work has to be done by the motor (no passive damper or energy harvester to perform negative work). For running (0.5–4 m/s) energetic reductions of 40–71 % and PP reductions of 54–78 % were identified.

For the hip joint calculations on possible reductions were done for walking at 0.8 and 1.2 m/s. A PEA could reduce torque by 66 % for flexion and extension. A reduction of 53 % was identified at the hip for abduction and adduction [173]. Using an SEA 60 % reductions of torque could be identified for the same motion.

5.5.1.3 Damping

Next to springs also dampers can help to reduce actuator requirements in powered lower limb prosthetics. Negative joint power (Fig. 5.6) can be introduced by these passive prosthetic parts. Due to microprocessor controlled mechanisms damping ratio can be changed by semi-active prosthetic knee joints to adapt to variations in walking speed. Eccentric muscle function can be replaced. A similar function can be realized by a motor using energy for decelerating the motion. In contrast also energy harvesting could be possible for the same process. An energy harvester integrated in a single knee brace [32] could generate about 2.4 W while generative braking in the late swing phase. In [58] it was shown that using an SEA setup at the knee joint needs nearly no positive work in walking and running. Thus it could be possible to generate electricity at the prosthetic knee joint to use it for powering the artificial ankle joint. A similar idea to use damping work, store it and release it later to support push of is realized in a prosthetic foot prototype [21]. Damping work from impact during touch down is used. A similar damping function is realized in biology by the heel pad [48]. Additionally to the heel pad also wobbling masses are damping impacts in locomotion [118]. Similar systems are not included in current prosthetic designs. Partially shock absorbing elements are used to replace this function.

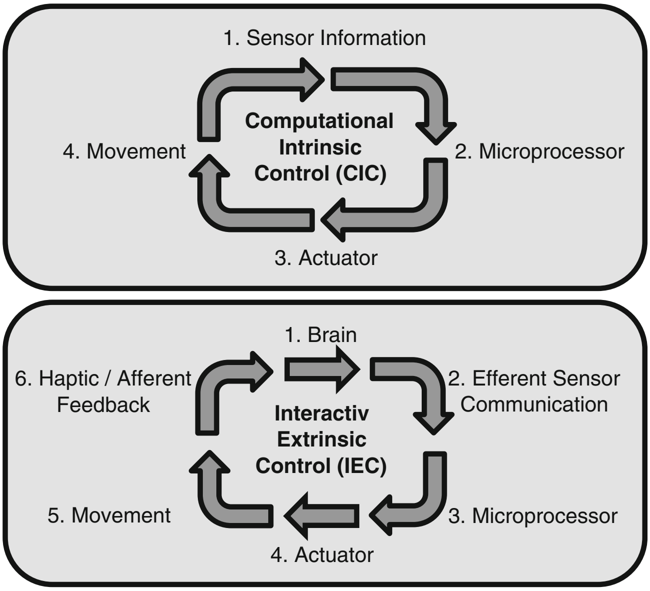

Fig. 5.10 Components of computational intrinsic control (*CIC*) and interactive extrinsic control (*IEC*) for prosthetic devices (Modified from [99])

For a prosthetic ankle joint similar to the eccentric phases of the knee joint it is possible to reduce energy requirements for a motor when using a damper. Possible operation phases are when replacing tibialis anterior function after touch down. Also while descending stairs negative work could be realized by a damper to mimic eccentric plantar flexor work. Eslamy et al. [40] predicted benefits of up to 50 % for PP and about 26 % for energy requirements using an SEA combined with a damper in comparison to a pure SEA (Fig. 5.9k). Similar concepts combining motors, springs and dampers for a powered ankle joint can be found in a patent from 2012 [67]. In level walking no benefits of a continuous acting damper could be identified for the evaluated systems [40]. Controllable dampers that are active only for some gait phases might change the results.

If the damper that assists the motor is only required for some phases of the gait cycle it should be switchable to avoid negative effects for other phases. A damper mimicking heel pad or wobbling mass function can be active the entire gait cycle.

5.5.2 Control

Control of prosthetic devices can be classified by the source of input data. On the one hand computational intrinsic control (CIC) on the other hand interactive extrinsic control (IEC) are possible [99], (Fig. 5.10). CIC has no connection to the user, whereas IEC allows a communication between brain and user. This interaction can happen on the efferent command but also on the afferent feedback site. A commonly used signal in commercial arm prosthetics at the efferent site is EMG (electromyography). But also other signals could be possible for interfacing the peripheral and central nervous systems with the prosthetic system [108]. At the afferent feedback site up to now no sensor signals are transferred back to the brain from the prosthetic parts itself. Only sensory organs from the remaining parts of the limb provide information. For example mechanoreceptors of the skin can provide prosthetic socket pressure information or existing knee muscles in transtibial amputees can give information about force and position. A main benefit of IEC can be to provide intent control signals already before the movement occurs. In contrast CIC can only react on current motion where for example classification algorithms detect the intention of the user. A reaction on current motion like in the CIC is also found naturally. Reflex like mechanisms can create basic motion patterns without brain interaction. In cat (decerebrated) and dog (decapitated) experiments it was shown that the spinal cord is able to produce reflex stepping after suppression of all afferent inputs from the brain [54, 147].

Thus it seems to be useful to have both approaches CIC and IEC combined in prosthetic control to get advantages of decentralized primary locomotion functions and in addition intend based control. Especially for cyclic motions like walking less brain control effort would be required with independent reflex like mechanisms. Using CIC or IEC different levels of prosthetic control are required. Referring to [151] the highest level is the intent recognizer that detects the basic movement behavior of the amputee. Activities like standing, climbing stairs, level or inclined walking can be distinguished. On a mid-level the movement control is realized. Here movement phase is detected and an appropriate output for the powered joint is created. At the low level torque, speed or position control is used to generate required motor trajectory.

Various concepts are used to detect users intent and generate required motion patterns. In the following some of them are explained with a focus on unique parts of each approach.

5.5.2.1 Muscle Reflex Control

Muscle reflex control can be a way to control a system independent from central motor commands [52]. Sensory feedback from muscle spindles and Golgi tendon organs is used as an input for an appropriate control output. These organs can measure length, speed or force in the biological actuators. In [52] it was shown that positive length and force feedback could be used to stabilize hopping in a computer simulation model. This basic idea is used and transferred to a complex multi-segmented bipedal muscle model [51]. The model is able to perform walking with human kinematics and dynamics, by using proprioreceptive feedback related to the body, muscle and ground interaction. Also it is able to deal with shallow slopes and small ground disturbances.

This concept is transferred to a powered ankle prosthesis [37]. An ankle angle sensor and an implemented spring force strain gauge can generate the input for the force and length feedback controller. Together with the strain gauge at the pyramid adapter the sensors detect also the gait phase and transitions to set a state machine (stance or swing). Joint torque is generated depending on torque delivered already by the mechanics (unidirectional parallel spring) to match human level walking. Using the neuromuscular model the intrinsic system characteristics will increase net work at the ankle when increasing speed [98].

5.5.2.2 Finite State Impedance Control

The finite state impedance control is used in a combined active knee and ankle prosthesis. A first version was implemented in a power-tethered pneumatically actuated prototype [150]. Later the control was implemented in a brushless motor driven design [151]. First an intent recognizer is detecting the amputees behavior. Prosthetic sensor data is compared to a database that classifies different activities like walking, sitting, standing or climbing stairs. For this classification a Gaussian Mixture Model is used [168]. In addition for example in walking a state machine is separating different phases of the gait cycle. For these phases an impedance is created to match human reference joint torque trajectories. By generating torque instead of position trajectories the controller should provide a more natural performance. The output signal is generated by the amputee and the prosthesis and not only by the prosthesis like in a position based control [151].

5.5.2.3 Phase Plane Control

Phase plane control of a robotic ankle joint was introduced in [75]. Various prosthetic prototypes are using this concept [71, 72]. The controller needs a gyro sensor at the tibia to measure shank rotational velocity. By integration, shank angle in relation to the ground is determined. A transfer function is used to eliminate integration errors. Using shank velocity and shank angle a phase plot can be generated. This was made for different step lengths in [75]. Another possibility is to do it for different speeds (Fig. 5.11). The radius of the polar curves can determine step length or gait velocity. The angle phi is used to determine gait percent. Both information are required to set the right motor position calculated by the robotic tendon approach [60, 76]. An advantage of this control approach is the possibility for automatic speed or step length adaptation during the gait cycle. When stopping walking shank velocity gets zero and the motor stops automatically. No states are required. Also backwards walking is possible with such a control approach. Slopes, stairs and uneven terrain can be handled by the interaction of the controller and the spring integrated in the mechanical design of the Sparky prosthesis.

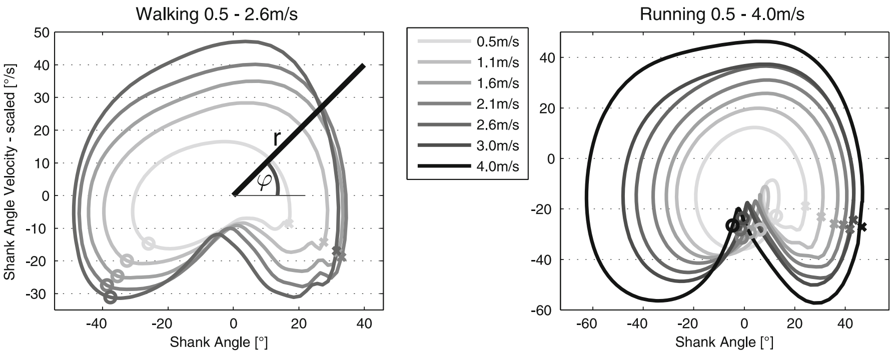

Fig. 5.11 Phase plane trajectories of shank velocity and shank angle for walking and running. Shank velocities are scaled (divided by 10) to create more functional graphs for calculating the Polar angle phi and the Polar radius r. Polar angle is used for gait percent determination. Polar radius for speed determination. Touch down is visualized by a cross, take off by a circle for each speed

5.5.2.4 Control Based on Residual Joints, Segments or Organs

In [120] a control method is introduced that uses the knee motion of a transtibial amputee to control ankle motion. For this a rotary potentiometer is measuring the knee angle that is used to calculate knee angle velocity. In addition a force sensor at the heel is used for contact information. Based on the sensory signals four states related to positive or negative velocity and heel contact or heel in flight phase can be defined. Based on the state ankle angle is adjusted. Depending on amputation level also thigh [159] or shank [75] can be instrumented with sensors to control the prosthetic leg. In [159] instead of a transfer function [75] data from accelerometers and a Kalman filter is used to eliminate drift when calculating segment angle.

A method to determine knee and ankle motion by measured hip behavior is introduced in [105]. Recursive Newton-Euler computation and inverse dynamics are used to obtain the joint behavior in walking.

Fuzzy logic as control approach is used for a motor driven knee joint [3, 14, 93]. As an input a potentiometer at the knee and an accelerometer at the femur was used.

Prosthetic control on the basement of eye motion was proposed in [35]. At the highest control level user intent like starting of walking, stopping or changing of speed can be transmitted to the prosthesis.

A neural network-based gait pattern classifier together with a rule-based gait phase detector was introduced in [96]. Inner socket forces of a transfemoral amputee were identified and used to establish a control scheme for a prosthetic foot.

5.5.2.5 EMG Based Control

EMG based control approaches for prosthetics are tested since the 1940s for arms and legs [7, 19, 36, 79]. Commercially available are so far only prosthetic arms.

EMG signals of upper arm muscles are used to flex or extend the elbow, for closing of the hand or also pronation of the wrist [25]. Various research groups try to use this biological signal also for powered prosthetic control at the knee [64, 78, 82] or also at the ankle [5]. EMG as a control signal for powered legs seems to be possible. Similar errors could be achieved while EMG based following of a trajectory with a prosthetic knee joint compared to a healthy knee [61].

A key problem in EMG control is safety. Especially with a prosthetic leg falls caused by measurement and classification errors could be possible. In [185] it was tested to which extend intent recognition errors based on EMG will influence safety of gait. For this purpose 0.1, 0.2 and 0.3 s lasting errors were applied in different phases of the gait. Errors applied used control signals for standing or ramp descent at level walking. For errors of 0.1 s no instability was reported. Also for longer error times during swing knee extension no critical safety issues were reported by the amputee. For 0.2 and 0.3 s during stance phase critical errors are reported. As a reason for the unsafe condition energetic differences between real and applied state were identified.

In [78] an impedance control approach was combined with myoelectric control signals. Evaluation of a single subject with transfemoral amputation showed robust and repeatable performance for ascending stairs. Using also an EMG based control, combined with the active ankle and knee prosthesis described by [91], in 2012 Zac Vawter climbed the 103 floors of Chicago's Willis Tower.

5.5.2.6 Neuromuscular: Mechanical Fusion

In addition to pure EMG based control also a fusion between biomechanical sensor signals (CIC) and EMG (IEC) could be possible. In [81] a classifier for gait was developed based on gluteal (2×) and residual thigh (9×) muscle EMG. Neuromuscular signals were combined with GRF and torques measured by a load cell on the prosthetic pylon. Insole pressure sensors were used for gait event detection. Using the combined method resulted in higher accuracy of gait mode prediction. Ninety-nine percent could be achieved in stance, 95 % in swing phase. To increase swing phase accuracy authors propose to add kinematic sensors. Transitions between different gait modes (obstacle crossing) were recognized using the sensor fusion with a sufficient prediction time.

Sensor fusion was also used in [30]. Here the desired knee angle was estimated based on gyro sensor and EMG data. The authors demonstrated that combining both signals could increase estimation precision and it reduces artifacts of purely EMG based control strategies [29].

5.5.2.7 Control with Sound Limb Signals

Prosthetic control with the sound limb named "echo control" was already discussed in [57]. In [5] it was tested if it is possible to generate motion patterns for a prosthetic foot by EMG signals of the residual limb. Both, a neural network based and a biomimetic based control approach could predict desired ankle movement patterns qualitatively. Using angle and angular velocity sensors of the sound limb [162] it was possible to control a prosthetic knee in walking. Ascending stairs was possible but required balance assistance. Descending was anticipated to be insecure and was less smooth compared to the C-Leg.

Grimes described that asymmetric behavior of the legs can cause problems in this approach [56]. Especially the sound limb of the amputee that is doing a compensating motion cannot be the reference for the residual limb. To overcome this problem healthy subject data was used in [162].

5.5.3 Prosthetic Challenges

Wearing a lower limb prosthesis causes several challenges in daily life situations. Less RoM, no power support, no direct control but also things like water proofed design can be a reason. For a comparison of passive and semi-active microprocessor controlled knee joints a daily activity performance test was developed [158]. Special test situations were created to be executed by the subjects. Tasks like normal walking, walking sideways, sitting down, standing up, carrying loads or also picking up objects are included. In addition tasks like dressing, putting on or taking off the prosthetic device are tested. The complexity of the test shows the requirements for a prosthetic development. Some of the requirements are addressed in the following subsections.

5.5.3.1 Terrain

Most prosthetic prototypes are first designed to be capable of standing and level walking. Due to additional daily life requirements like slopes, stairs or rough terrain further functionality should be included. Also tasks like standing up, sitting down, driving a bicycle or a car could be achievements to take into account.

Level ground: Level ground walking is one of the primary achievements for prosthetic design. Healthy people realize about 6,500 walking steps per day [160] with a preferred walking speed of about 1.3 m/s [28]. In comparison to passive prosthetic parts active ankle or knee joints should be able to reduce amputee metabolic costs, increase speed and reduce asymmetries in the gait pattern of the amputees.

With the BiOM ankle prosthesis ankle push off is supported. For a study of 11 amputees the ankle prosthesis generated significantly greater peak ankle power (35 %) in comparison to healthy controls [42]. In comparison to passive ESAR feet an increase of 125 % was possible. For a second study the increase of PP was about 54 % compared to an ESAR foot [97]. Referring to [184] higher peak power values, compared to normal condition, must not result in better gait performance. Using the motor also higher RoM could be achieved in comparison to the ESAR feet (30 %) [42]. However the control group was still 20 % better. The difference is caused by the ankle motion shortly after push-off. Here the healthy ankle joint is highly accelerated when leaving the ground. The fast stretching of the dorsal extensors is possible for muscles but for a prosthesis doing dorsal extension and plantarflexion by one structure it is hard to realize. High power values and less inertia would be required for the motor. The prosthesis is maybe not capable to mimic human behavior at this event. Also it could be possible that the desired motor trajectory is on a compromise solution to save energy at this point. The change of motor turning direction shortly after this event is strengthening the argument for a compromise solution. Here again higher power demands depending on required braking and acceleration of motor must be considered.

In addition to the effects at the ankle joint differences at knee and hip joint were identified for the control group and the powered prosthetic leg. Effects of a missing biarticular structure between ankle joint and knee joint are mentioned as a possible reason. Also higher ankle PP of the BiOM foot, compared to healthy subjects, could be a reason for pattern differences. In comparison to [6, 66] (5 and 23 % increase) an increase of about 6 % in self-selected walking speed from 1.32 to 1.4 m/s was identified using the powered foot compared to the ESAR foot [42]. Self selected walking speed also increased with the Sparky prototype compared to a passive foot [72] for one tested amputee. Desired ankle angle could be achieved in stance. In swing phase desired prosthetic ankle angle was reached too late. As a reason control properties can be assumed because electrical power consumption was not a limiting factor at this phase.

Typical amputee residual limb behavior with shorter stance and longer swing phases was not measured using the BiOM ankle. User recognition, reflected by the biomechanical data, resulted in higher user satisfaction using the powered foot.

Oxygen consumption in level walking could be reduced by 8.4 % using the BiOM ankle compared to an ESAR foot [97]. Fourteen percent reduction could be achieved in a study with a previous ankle design [6].

Self-selected walking speed was about 24 % higher for one transfemoral amputee using an powered knee combined with a powered ankle joint [151]. Level ground walking speed increased from 1.14 to 1.41 m/s. Peak power at the ankle joint was at about 250 W, about 50 W were realized at the knee joint. At the ankle 0.2 J/kg of net energy is delivered each step which is very close to non-amputee data (0.22 J/kg Table 5.1). In total 66 W (45 ankle, 18 knee, 3 embedded system) were required doing one step with powered knee and ankle for a 70 kg amputee. Using the 0.62 kg (lipo 29.6 V, 4,000 mAh) battery the prosthesis could be used over 9 km of powered level ground walking.

In comparison to most semi-active knee joints, stance phase flexion could be realized using the powered knee [151]. Positive power could be delivered. In contrast to [102] the system is not using springs at the knee joint to assist the motor. Partially negative joint power could be used to load the spring and to get positive power back to assist the motor. Additional reductions in energy requirements can potentially be achieved (see Sect. 5.5.1.2). Using an antagonistic SEA setup at the knee joint [102] in combination with an ESAR foot already results in metabolic reductions of about 7 %. Self-selected speed also increased with this setup from 1.12 to 1.31 m/s (+17 %) when using the active device compared to the C-Leg. Mean power consumption was about 11 W/gait cycle [100] for four subjects (mean weight 93.3 kg, mean speed 1.37 m/s). Even though the achieved knee angle – torque profiles are not similar to results achieved in [151] mean power requirements for the device using springs are 0.12 W/kg compared to 0.26–0.3 W/kg (1.42 m/s, 70 kg) when using direct drive. Contrary results for walking speed and metabolic costs were identified in [26] for the first version of the Power Knee. In a preliminary study with two amputees the powered device caused higher metabolics and reduced walking speed in comparison to the subjects with a semi-active prosthetic knee joint (C-Leg).

Slopes: Due to limited RoM and power generation amputees struggle to walk especially inclines [171]. Similar to level walking transtibial amputees show less deficits than transfemoral amputees [172]. To improve gait performance authors propose to improve control of prosthetic knee flexion without stability reductions. Using active prosthetics this criterion can be addressed. In order to set the right control slope has to be detected. Slope estimation could be realized by an accelerometer at the prosthetic foot [155]. An accuracy of 0.5–1.0° could be achieved for indoor experiments. Combining the accelerometer with a gyro sensor (at foot) resulted in an accuracy of about 1.5° [134]. Also strain sensors could be a possible solution. An error of about 1.5° was identified when using these sensors to detect the slope at various speeds [156]. Instead of placing sensors at the foot segment also other locations were considered. In [4] slope was estimated based on accelerometers placed at a waist belt. A neural network was trained and could predict slope with a standard deviation of about 2.3 %. The possibility to adapt to slopes was shown for an active knee and ankle prosthesis [152]. When a heel and a ball load sensors are detecting ground contact, slope angle is estimated by an accelerometer. 12, 15, and 17 J per stride were measured for the conditions level ground, 5° incline and 10° incline. For the active ankle-knee device 12.2 km of working range were estimated for level walking. Walking a slope of 5° or 10° would result in a decreased capability of 9.2 and 7.7 km respectively. Compared to the semi-active C-Leg the authors identified various differences when using the powered device in upslope walking.

- Stance knee flexion during heel strike and mid-stance
- Ankle plantarflexion during heel strike
- Ankle plantarflexion during push-off
- Increased knee flexion with increased slope after heel strike
- Net knee extension during stance phase
- Increasing bias towards ankle dorsiflexion with increasing slope

Stairs: How many stairs people climb each day hardly depends on living and working conditions. For a study among 2,539 men (mean age, 57 years) on longevity [92] 31 % of subjects reported less than 10 floors per week. Between 10 and 20 floors were reported by 20 %. Between 20 and 30 by 19 % and more than 35 floors by 30 %. Assuming a mean of 22 floors a week and 15 stairs per floor this would result in about 47 stairs a day. This value is less than the value reported in [130]. A group of 151 women (mean age, 43 years) reported 4.4 flights of stairs a day. At 15 stairs a flight this would be 66 stairs a day. In comparison to 6,500 walking steps per day [160] 47–66 stairs a day are only a very small amount. Ascending stairs requires a higher power effort than level walking [152]. Descending seems to need higher control effort because 76 % of stair falls happen while descending [154].

Stair ascent with a powered foot was analyzed in [2]. In comparison to an ESAR foot the powered version could improve peak plantarflexion and push off power. It was found that peak power did not differ between the prosthetic foot and the ankle joint of a control group. Surprisingly the hip strategy to support stair ascent used by transtibial amputees with a passive foot is not influenced by additional RoM and push off power. Hip strategy is characterized by increased prosthetic limb hip extensor torque and power, reduced knee torque and power and a more extended residual limb knee in stance phase [2]. A combination of powered knee and ankle was tested in stair ascent and descent [91]. The authors could show that using the powered prosthesis healthy gait was reflected better in comparison to a semi-active device (C-Leg). Similar characteristics were identified for the Power Knee in [180]. Without the possibility to inject energy knee extension at the semi-active knee joint in stair ascent is impossible. To ascent stairs a different strategy was used by the amputee including support of the hand rail [91]. Knee joint remained extended for the whole step. This causes high differences between healthy control, powered knee and the semi-active knee device. For stair descent less difference was identified for semi-active and powered knee joint whereas at the ankle joint the powered one showed much better performance in RoM.

Rough Terrain: Walking uneven terrain requires adaptation mechanisms for secure foot placement. This includes an angle adaptation to match ground slope that can vary with each step for example in rocky surfaces. Possible mechanisms for such adaptations could be active controlled or also passive like dampers or springs. To adapt contact area of the foot to the ground, a healthy foot can do inversion and eversion. For passive prosthetic feet this function could be partially represented by multiaxial joints or also splitted feet (Echolon VT). Powered solutions to increase amputee balance may provide additional benefits [119]. In [47] it is shown, that an amputee wearing a powered foot prosthesis providing plantarflexion, has a 10 % higher self-selected walking speed compared to an ESAR foot on a rocky surface. In comparison, on level ground a mean increase of about 5 % (three subjects) to 23 % (seven subjects) was identified in [6, 66].

5.5.3.2 Sitting Down – Sitting – Standing Up

Semi-active prosthetic knee joints like the C-Leg are able to secure sitting down by the mechatronic hydraulic stance phase safety system. The knee joint is damped to avoid collapse. In comparison standing up can not be supported by the passive mechanics of these devices. Intelligent mechanisms with springs, storing energy while bending the knees during sitting down, similar to the mechanism in [21], could potentially improve this. Standing up could be facilitated by powered knee devices. In [167] a finite state based impedance controller is designed to solve the specific task of sitting down and standing up. The subject reported easier standing up and he felt more support from the prosthesis compared to the C-Leg which he uses daily. Up to 0.7 W/kg of peak power was delivered by the powered knee during standing up and sitting down. Also the Power Knee (Ossur, [116]) can provide support in both sitting down and standing up. A comparison between C-Leg and Power Knee was made in [68]. The authors analyzed hip torques, knee torques and vertical GRF for symmetry at one subject. While standing up for all conditions except for GRF the Power Knee showed improvements. However, still high asymmetries between the sound limb and the residual limb exist. This outcome was approved in [69] where in addition to C-Leg and Power Knee also the Mauch-SNS was tested. Seven amputees for each joint were analyzed and compared to a seven subjects control group. While sitting down, a significant difference could only be identified for the prosthetics in GRF. The Power Knee showed best, the Mauch-SNS worst performance. While standing up a significant difference could only be identified for the hip torques. Also here, the Power Knee provides less asymmetric behavior. The authors concluded that with all three tested knee joints the transitional movement between sitting and standing is a one-legged task which probably increases the risk of injury or an accelerated degeneration to the sound limb.

A similar comparison with five C-Leg and five Power Knee users was done in [181]. The intact limb had higher average peak sagittal knee powers and vertical GRF for both prosthetic groups. During standing up peak knee power of the residual limb was greater for Power Knee users. In contrast to [68] but in line with [69] vertical GRF asymmetry was greater for the C-Leg. Few differences between both devices were identified.

As standing up is primary powered by the knee joint it is important to know that already significant differences between intact and residual limb exist for transtibial amputees [1]. Intact limb body weight support was about 64 % at seat off events. As a reason the authors assumed less muscular strength at the residual limb or limitations in ankle dorsal extension and plantar flexion.

While sitting it is important for the amputees to unlock the knee and move it freely. This provides higher comfort when choosing sitting position. Nearly all prosthetic knee devices include the feature to flex the knee joint within RoM.

5.5.3.3 Standing

While standing using a powered prosthesis the whole microcontroller – sensor system works to guarantee save changes in amputee behavior. This consumes about 3 W [151]. In addition motors have to create isometric behavior in the knee and the ankle joint consuming each also about 3 W. In total about 10 W are required only for standing. To reduce energy consumption in standing it could be an option to switch to a semi-active mode like envisioned in [89] for the low battery situations. Here like in the C-Leg only the microcontroller would consume energy in standing.

5.5.3.4 Prosthesis Mass

A design criterion for a prosthesis is its mass. Especially higher masses at the foot segment will increase hip joint torques during walking. In addition net metabolic rate will increase [15]. To avoid these effects similar or smaller segment masses should be achieved. To estimate the mass of partially missing segments (m_{seg}) of the lower limb the formula provided below can be used. It relies on the assumption that the thigh and the shank have the shape of a frustum with a relationship of the upper to the lower circle of 0.75. This relationship is introduced because of the segmental center of mass which is at about 37 % [20, 132] of the segment length from the proximal site.

$$m_{seg} = \frac{h_a}{h_t} * \frac{(1 - 0.25 * \frac{h_t - h_a}{h_t})^2 + (1 - 0.25 * \frac{h_t - h_a}{h_t}) * 0.75 + \frac{9}{16}}{\frac{37}{16}} * m_s * m_b \tag{5.1}$$

The required constant for the relative segmental mass m_s is 0.0435 for the shank and 0.1027 for the thigh [132]. To get the mass of completely missing segments the segmental mass m_s is multiplied by the body mass m_b. h_t represents the unaffected length of the shank for transtibial or of the thigh for transfemoral amputees. h_a is the missing length of the affected segment.

We now estimate m_{seg} for a transtibial amputee (mass = 75 kg, body height = 1.8 m) that should fit to the BiOM ankle prosthesis which has a build height of about 0.22 m. Referring to [178] the segmental height of the foot is about 0.039 times the body height. This would result in about 0.07 m height for the foot. The height of the shank is 0.246 times the body height what would be about 0.44 m for h_t. An amputation height of about 0.3 m (measured from ground) would result in an amputation of about 0.23 m (h_a) for the shank segment. Using Eq. 5.1 a missing shank mass of 1.5 kg can be assumed. For the foot, which has a segmental mass of 0.0147 of body mass, 1.1 kg can be assumed. To fulfill the requirements of mimicking human like masses for the design a total prosthetic mass (including socket, adapters, prosthetic foot) of 2.6 kg is predicted. The weight of the BiOM foot is about 2.4 kg including battery and foot cover.

5.5.3.5 Sound Level

Noise is one of the unsolved problems in powered prostheses. Electrical motors, ball screws and other mechanical parts produce motion related noise. Acoustical insulation of the mechanical system can decrease sound level. By this only the effect but not the cause would be addressed. Less system component friction and improvements in electrical motor design are design objects to address the reasons for sound level. On the other hand also different actuation mechanisms could be used. For example polymer artificial muscles [104] could be a potential solution. When using current technology also a compromise between gait imitation and sound level can be targeted. High accelerations of the motor are necessary to match human gait patterns with SEA. In addition hard braking and turning of motor direction will increase loudness. If desired trajectories are smoothed less peak power and energy would be required. In addition this method could potentially reduce the sound level.

5.5.3.6 Battery Runtime

Battery runtime is a limiting factor for powered prosthetics. The C-Leg and the Rheo Knee, both semi-active knee prostheses, have a runtime of 1–2 days depending on activity level. A similar runtime is envisioned with the partially powered Proprio Foot using a battery having 26.6 Wh. The Power Knee should provide a runtime of about 5–7 h using a battery capacity of 66.5 Wh (0.49 kg). All four systems use Lithium-Ion technology.

A former version of the BiOM Ankle is using a lithium polymer battery (0.22 kg) having an energy density of 165 Wh/kg. In a first study with three participants the prosthesis required about 31.4 J electrical energy per step to get 17.5 J per step net mechanical energy at 1.6 m/s walking speed [6]. This results in a system efficiency of 56 %. Using a 36.3 Wh (130.68 kJ) battery [37], about 4,162 steps could be realized consuming the 31.4 J [6] used by MIT's PowerFoot.

In daily life people realize about 6,500 walking steps per day [160] with a preferred walking speed of about 1.3 m/s [28]. As walking is one of the primary targets for powered prosthetics it can be a criterion for the dimensioning of a powered device. As the 6,500 steps are a result of two legs for unilateral amputees half of the steps need to be considered for the calculation of 1 day.

In addition ascending and descending of about 47–66 stairs and slopes should be considered. During these tasks ankle and knee joint behavior differs from level walking [31]. Thus it is required to estimate elastic actuator requirements similar to approaches used in [59] (ankle) and [58] (knee) for level walking and running.

Also while standing energy is required for a prosthetic device. For the electronics, the knee and the ankle motor a mean of 10 W was required in [151]. Assuming the value of about 295 min of standing a day [123], such a system needs 49.2 Wh only for this task. Less energy should be required while sitting or lying. Especially while lying motors require nearly no torque. About 3 W of electrical power consumption are measured for standing and walking for the electronics in [151]. As between these two tasks is only little difference a similar value can be assumed for the sitting or lying condition. These conditions are relevant because a huge amount of time (306 min) is spent for sitting (Fig. 5.12). Lying was executed for about 29 min. Both tasks together will need about 16.8 Wh at 3 W for 335 min. As level walking requires about 66 W for the powered knee and ankle joint and subjects performed about

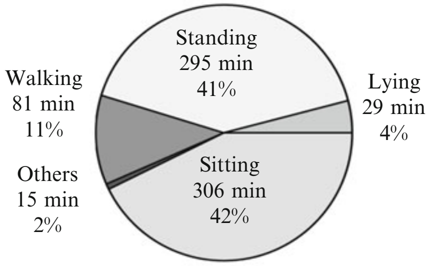

Fig. 5.12 Daily activity of healthy retired people with a mean age of 66 years. Activity was measured for 12 h after waking up (Modified from [123])

81 min each day [123], 89.1 Wh of battery is required for this task using a powered device at both legs. A single powered leg would require about 44.6 Wh. In total about 110.6 Wh are required to perform 1 day of a retired 66 years old person. This assumption is not including tasks like ascending or descending stairs or slopes which can increase requirements additionally. Actually the device is using a 118 Wh lithium polymer battery which could be potentially enough to perform 1 day for a retired person based on this estimation.

5.6 Technology Transfer

The technology developed for leg prosthetics could potentially also be used in other robotic designs, including exoskeletons or rehabilitation platforms like the Lokomat (Hocoma, [73]). Exoskeletons are powered orthotic systems which can assist people with muscle weakness or other deficits that affect locomotion. But also healthy people can potentially benefit from assistance similar to pedelecs or e-bikes. They allow to set an percentage to amplify the own power introduced to the bicycle. Especially at inclines or stair but also while carrying heavy loads a powered system could be beneficial. Systems like the Lokomat can be used to train people with a neurological or orthopedic impairment with a robotic orthosis operating the legs on a treadmill. Basically walking can be performed. Exoskeleton technology could be a way to provide flexible training conditions in each possible environment. A mobile device could also be used for locomotion training at home.

Also possible are combinations of powered or passive orthoses and prosthetics. This permits to include joint coupling structures that can transfer energy from a still existing to an artificial joint. With this, coordination in between the remaining limb and the artificial joints could be improved.

5.7 Summary and Outlook

Based on advances in motor, battery and microprocessor technology there is an increasing effort in developments of powered lower limb prosthetics over the last years. First active devices for replacing the knee or the ankle joint are already commercialized. Powered prosthetics have the potential to increase amputee performance compared to passive or semi-active devices. When comparing them to natural movements a lack can still be identified. Especially when changing between movement tasks or during non steady state motions systems get to their limits.

These deficits can result from the technical system. Biologically inspired highly efficient elastic design approaches can improve actuator performance. In contrast to semi-active and passive devices most powered prostheses are so far not including passive dampers. They could further reduce requirements. Instead of wasting energy by dampers the energy could also be harvested. By this especially at the knee energy could be stored and reused at the ankle joint to support push off.

Next to the hardware design, also control has to be improved. Anticipation of the environment and the selected movement task are key aspects for an appropriate control. Prosthetic devices should at least handle all basic tasks like ascending and descending stairs or slopes, walking and standing. Multiple types of controllers were developed to address these conditions. Sudden events like stumbling should be detected and handled similar to the way used in semi-active systems. An improved level of control should recognize user intention. Thus voluntary motions, like flexing the knee while sitting, could be performed. Also adaptations to walking speed or level of slope could be possible. Changes in movement tasks (from walking to stair climbing) could be initiated intuitively by the amputee. In contrast to intrinsic control (CIC), that reacts on current motion, a kind of pre-positioning of the joint similar to pre-activation in muscles would be possible.

A feature that is less addressed in prosthetics so far are adaptable mechanical properties in the prosthesis. Stiffness of elastic elements could be changed to reduce actuator requirements or to improve stability. Increased weight while carrying loads, different movement tasks or speeds could benefit from a variable mechanical design. Damping ratio could also be considered as a controllable parameter. These features should be combined with an intelligent control that is finding the optimal mechanical adjustment (“sweet spot”) for the individual subject. As an optimization criteria energy requirements or symmetry for cyclical motions could be considered.

So far only limited user adjustment of the prosthesis are possible for commercial systems. Control and by this system behavior is pre-designed by the developers. Partially an individual gait can be configured while calibrating the system using software tools like in the C-Leg. Damping ratio for different phases of the gait cycle can be changed. Adaptations are made by the orthopedic technician. A further step could be to provide a software where each amputee could calibrate the system on his own. To ensure security only a save region for possible changes in damping or power assistance should be considered. Exchange in internet communities could enhance user knowledge for creating their preferred personal settings. Even more potential would have an open source library of prostheses software based on predefined standards. Universities but also private people could work on improved control algorithms for various daily life conditions.

Up to now a valid comparison of different powered but also passive prosthetics is difficult. Different subjects, measurement setups or also amputation condition and histories make it hard to compare systems. Results presented in different papers are using various biomechanical parameters, different units and also different normalization. To evaluate prosthetic systems it would be beneficial to have an institute that evaluates prosthetic systems under well-defined conditions similar to the TÜV, Germany. Such an independent institute could provide sufficient data to health insurance companies regarding the benefits of different prosthetic systems. With this it could be easier and better justified to select an adequate prosthesis matching users requirements.

Appendix

Table 5.3 Overview on active prosthetic ankle developments

Device	Ankle, Odyssey, Springactive [149], USA – Picture: (a)
Actuator	Motor-parallel spring complex
Battery	External battery
Sensors	Motor encoder, gyro sensor
Control	Continuous control without states
Device	Ankle, Sparky, [70,72], Arizona State University and Springactive, USA – Picture: (b)
Actuator	Robotic Tendon (SEA), Maxon RE-40, 150 W, lead screw, planetary gear box
Battery	External battery
Sensors	Motor and ankle angle encoder, optical switch at heel or gyro sensor
Control	Position control or phase plane control [75]
Device	Bionic Foot, [71, 140], Military Academy West Point, USA – Picture: (c)
Actuator	Ankle, Robotic Tendon (SEA), 2× Maxon RE-40, lead screw
Battery	External battery
Sensors	Motor encoder, gyro sensor
Control	Phase plane control
Device	Ankle, Walk-Run Ankle, Springactive [149], USA (design) and TU Darmstadt, Germany (control) – Picture: (d)
Actuator	Elastic motor spring combination
Battery	External battery
Sensors	Motor encoder, gyro sensor, acceleration sensor
Control	For standing, walking, running and gait transitions
Device	Ankle AMP-Foot 2.0, [18] Vrije Universiteit Brussel, Belgium, about 2.5 kg – Picture: (e)
Actuator	Series spring and clutched SEA, Maxon RE 30, 60 W, transmission, ball screw
Battery	External power supply
Sensors	Force sensing resistor at toe and heel, strain gauges at two springs, two magnetic encoders at ankle joint,
Control	Nothing stated

(continued)

Table 5.3 (continued)

Device	Ankle, BiOM – Power Foot [6, 37], Massachusetts Institute of Technology and iWalk [83], USA – Picture: (f)
Actuator	SEA+UPS, Maxon EC-30, 200 W, 48 V at 24 V, belt drive transmission, ballscrew
Battery	0.22 kg lipo at 165 Wh/kg for 5,000 steps, internal
Sensors	Hall-effect ankle angle joint sensor, stain gauges for spring force, pyramid strain gauge for GRF, motor encoder
Control	Neuromuscolar reflex model
Device	Ankle and toe, PANTOE 1, [182, 186], Peking University, China, 1.47 kg – Picture: (g)
Actuator	Ankle – 83 W Faulhaber brushed DC, toe – 45 W Faulhaber DC, ballscrew
Battery	Li, 1 kg, external
Sensors	Motor angle encoder, touch and force sensor at heel and toe, potentiometer at ankle and toe joint, potentiometer for ankle spring displacement sensor
Control	Finite state control [182]
Device	Ankle, [153], Kanazawa Institute of Technology, Japan 3.8 kg including battery – Picture: (h)
Actuator	Unidirectional spring for controlling touch down plantarflexion with antagonistic unidirectional DD (assumed from figure), DC motor
Battery	Internal
Sensors	Ankle angle encoder
Control	Internal model control including last step, ankle angle position control
Device	Ankle, Proprio Foot, Ossur [116], Iceland, 1.5 kg with Pyramid and Foot cover – Picture: (i)
Actuator	Stepper motor
Battery	Lithium Ion 1,800 mAh, 14.8 V
Sensors	Accelerometers, ankle angle sensor
Control	Artificial intelligence including last step
Device	Ankle, [155], Halmstad University, Sweden – Picture: see publication
Actuator	DC motor, only powered in swing phase, ball screw
Battery	Nothing stated
Sensors	Accelerometer at foot for slope estimation and gait phase detection
Control	Finite state control
Device	Ankle, [170], Vrije Universiteit Brussel, Belgium – Picture: see publication
Actuator	Antagonistic pleated pneumatic artificial muscles (PPAM)
Battery	External power source
Sensors	Ankle joint angle encoder, footswitch at forefoot, midfoot and hindfoot, pressure sensor
Control	Feedforward torque control timed by foot switches
Device	Ankle, PAKO – Orthoprosthesis, Technical University Darmstadt, Lauflabor – Locomotion Lab, Germany – Picture: (j)
Actuator	SEA with variable stiffness, 1,025 W Thingap 2,320 brushless DC motor 80 V at 48 V
Battery	External power supply
Sensors	Knee and ankle joint encoder, SEA force sensor, GRF sensor in foot, gyro and accelerometer at shank
Control	Speed related phase plane control similar to [75]

Table 5.4 Overview on active prosthetic knee developments

Device	Knee, [88, 89, 122],University of California, USA – Picture: (k)
Battery	12× 2,000 mAh 15C lipo cells 36 V – 51 V in early version [88], 42–48 V in new design, internal
Actuator	Two linear hydraulic with one pump, Maxon EC-max 30 for pump – 40 W, low power valve motor
Sensors	Accelerometer and gyroscope at thigh, magnetic knee and ankle angle encoder, pressure sensor in hydraulic units, force transducer for sagittal plane moments and axial shank forces
Control	Finite state control
Device	Knee, [82,90], Islamic University of Technology and University of Dhaka, Bangladesh – Picture: (l)
Actuator	DD, 5 W DC motor for prototype, pulley
Battery	Nothing stated
Sensors	EMG at thigh, motor sensor
Control	EMG control
Device	Knee, [175], University of Alabama, USA, 3 kg – Picture: (m)
Actuator	Antagonistic pneumatic artificial muscles
Battery	External pneumatic supply, research on liquid propellant
Sensors	Force sensor (resistor) in foot for GRF, potentiometer knee, control valve and pressure sensors external
Control	Finite state impedance control similar to [151]
Device	Knee, [101, 102], Massachusetts Institute of Technology, USA, 3 kg – Picture: (n)
Actuator	Two antagonistic SEA's, Maxon RE40 extension, Maxon RE 30 flexion, belt drive, ball screw
Battery	6 cell 22.2 V Lipo, 0.15 kg
Sensors	Ankle angle encoder, motor encoder, spring compression by hall effect sensor, insole force resistor for heel and toe contact
Control	Finite state control
Device	Knee, Power Knee, Ossur [116], Iceland, 2.7 kg w/o battery – Picture: (o)
Actuator	DC motor, harmonic drive gearing system
Battery	50.4 V, 1,320 mAh, 66.5 Wh, 0.5 kg, 5–7 h runtime
Sensors	Gyro, Accelerometers, Torque meter, Ground contact sensor
Control	State machine
Device	Knee, [16, 17], Fraunhofer Institut Stuttgart, Germany – Picture: (p)
Battery	Nothing stated
Actuator	Faulhaber 4490, 48 V, 200 W, bevel-helical gearbox
Sensors	Gyro sensor, accelerometers
Control	Nothing stated
Device	Knee, [162], ETH Zurich, Switzerland – Picture: (q)
Actuator	Maxon RE 40, 150 W
Battery	External power supply
Sensors	Optical quadrature motor encoder, contralateral hip and knee angle and angle velocity sensor (goniometer, gyroscope)
Control	Complementary limb motion estimation (CLME)

(continued)

Table 5.4 (continued)

Device	Ankle and knee, 1st version [151], 2nd version [91], Vanderbilt University, USA, 4.3 kg (2nd) – Picture: (r)
Actuator	Motor+UPS at ankle, DD at knee, Maxon EC-30, 200 W, ballscrew (1st)
Battery	29.6 V, 4,000 mAh, 700 g, 115 Wh, internal (1st)
Sensors	Series uniaxial load cell in each actuator unit, potentiometers at ankle and knee joint, strain based sagittal plane moment sensor between socket and knee, strain gauges at foot and heel for GRF (1st)
Control	Finite state impedance control (1st)
Device	Knee, [95, 185], University of Rhode Island Kingston, USA – Picture: see publication
Actuator	Motor with parallel torsion spring – clutch mechanism, variable damper, Maxon RE 40, ball screw
Battery	External power supply
Sensors	Potentiometer for knee angle, motor encoder, 6 DOF load cell for GRF
Control	User intent recognition based on neuromuscular mechanical fusion, impedance control, finite state machine
Device	Knee, APK, [14, 93], University of Waterloo, Canada – Picture: see publication
Actuator	DD, Maxon RE 40, ballscrew
Battery	External power supply
Sensors	Potentiometer knee angle, accelerometer at femur, motor encoder
Control	Intelligent Fuzzy logic based control
Device	Ankle and knee proposed, [105], Dokuz Eylul University, Turkey – Picture: see publication
Actuator	DC motors
Battery	Nothing stated
Sensors	Nothing stated
Control	Hip angle based knee and ankle joint control
Device	Knee, [50], Hebei University of Technology, China – Picture: see publication
Actuator	Hybrid linear step motor, Haydon model 57000,
Battery	Nothing stated
Sensors	Nothing stated
Control	Central pattern generator
Device	Ankle and knee, [30],University of Brasilia and University of Oriente, Brazil and Cuba – Picture: see publication
Actuator	Nothing stated
Battery	Nothing stated
Sensors	EMG, Gyro
Control	Nothing stated
Device	Knee, [77, 78], 3.5 kg including electronics and battery – Picture: see publication
Actuator	Maxon RE 40 150 W, ball screw
Battery	4× 11.1-V, 2,000 mAh
Sensors	Load cell at knee for torque, knee potentiometer, pneumatic pressure sensors at heel and toe for ground contact, surface EMG at thigh muscles
Control	Finite-state linear impedance model based on EMG

References

1. Agrawal V, Gailey R, Gaunaurd I, Gailey R III, O'Toole C (2011) Weight distribution symmetry during the sit-to-stand movement of unilateral transtibial amputees. Ergonomics 54(7):656–664
2. Aldridge JM, Sturdy JT, Wilken JM (2012) Stair ascent kinematics and kinetics with a powered lower leg system following transtibial amputation. Gait Posture 36(2):291–295. Elsevier
3. Alzaydi AA, Cheung A, Joshi N, Wong S (2011) Active prosthetic knee fuzzy logic-PID motion control, sensors and test platform design. Int J Sci Eng Res 2:1–17
4. Aminian K, Robert P, Jequier E, Schutz Y (1995) Estimation of speed and incline of walking using neural network. IEEE Trans Instrum Meas 44(3):743–746
5. Au SK, Bonato P, Herr H (2005) An EMG-position controlled system for an active ankle-foot prosthesis: an initial experimental study. In: 9th international conference on rehabilitation robotics (ICORR 2005), Chicago, 2005. IEEE, pp 375–379
6. Au S, Weber J, Herr H (2009) Powered ankle–foot prosthesis improves walking metabolic economy. IEEE Trans Robot 25(1):51–66
7. Battye C, Nightingale A, Whillis J (1955) The use of myo-electric currents in the operation of prostheses. J Bone Jt Surg, British Volume 37(3):506–510
8. Bellman RD, Holgate MA, Sugar TG (2008) Sparky 3: design of an active robotic ankle prosthesis with two actuated degrees of freedom using regenerative kinetics. In: 2nd IEEE RAS & EMBS international conference on biomedical robotics and biomechatronics (BioRob 2008), Scottsdale, 2008. IEEE, pp 511–516
9. Bellmann M, Schmalz T, Ludwigs E, Blumentritt S (2012) Stair ascent with an innovative microprocessor-controlled exoprosthetic knee joint. Biomed Tech 57:435–444
10. Blumentritt S, Bellmann M (2010) Potenzielle Sicherheit von aktuellen nicht-mikroprozessor- und mikroprozessorgesteuerten Prothesenkniegelenken. Orthopädie-Tech nik 61:788–799
11. Blumentritt S, Schmalz T, Jarasch R (2009) The safety of C-Leg: biomechanical tests. JPO J Prosthet Orthot 21(1):2
12. Blumentritt S, Bellmann M, Ludwigs E, Schmalz T (2012) Zur biomechanik des mikroprozessorgesteuerten prothesenkniegelenks genium. Orthopädie Technik 01:24–35
13. Boonstra A, Fidler V, Eisma W (1993) Walking speed of normal subjects and amputees: aspects of validity of gait analysis. Prosthet Orthot Int 17(2):78–82
14. Borjian R (2009) Design, modeling, and control of an active prosthetic knee. Master's thesis, University of Waterloo
15. Browning RC, Modica JR, Kram R, Goswami A et al (2007) The effects of adding mass to the legs on the energetics and biomechanics of walking. Med Sci Sports Exerc 39(3):515
16. Budaker B (2012) Active driven prosthesis using a bevel helical gearbox in combination with a brushless DC-motor. In: Proceedings BMT 2012, 46. DGBMT Jahrestagung, Jena – track R. prevention and rehabilitation engineering, Jena
17. Budaker B (2012) Auslegung von Multidomänen-Systemen-Analyse, Modellierung und Realisierung von mechatronischen Systemen am Beispiel einer aktiven Knieprothese. Ph.D. thesis, Fraunhofer-Institut für Produktionstechnik und Automatisierung (IPA), Stuttgart
18. Cherelle P, Matthys A, Grosu V, Brackx B, Van Damme M, Vanderborght B, Lefeber D (2012) The AMP-Foot 2.0: a powered transtibial prosthesis that mimics intact ankle behavior. In: 9th national congress on theoretical and applied mechanics, Brussels
19. Childress DS (1985) Historical aspects of powered limb prostheses. Clin Prosthet Orthot 9(1):2–13
20. Clauser CE, McConville JT, Young JW (1969) Weight, volume, and center of mass of segments of the human body. Technical report, DTIC Document
21. Collins S, Kuo A (2010) Recycling energy to restore impaired ankle function during human walking. PloS One 5(2):e9307

22. Colombo C, Marchesin E, Vergani L, Boccafogli E, Verni G (2011) Design of an ankle prosthesis for swimming and walking. Procedia Eng 10:3503–3509
23. Coupland R (1997) Assistance for victims of anti-personnel mines: needs, constraints and strategy, vol 5. International Committee of the Red Cross, Geneva, pp 1–18
24. Crompton R, Pataky T, Savage R, D'Août K, Bennett M, Day M, Bates K, Morse S, Sellers W (2012) Human-like external function of the foot, and fully upright gait, confirmed in the 3.66 million year old laetoli hominin footprints by topographic statistics, experimental footprint-formation and computer simulation. J R Soc Interface 9(69):707–719
25. Cutti AG, Garofalo P, Janssens K, Davalli A, Sacchetti R, Cutti AG (2007) Biomechanical analysis of an upper limb amputee and his innovative myoelectric prosthesis: a case study concerning the otto bock "Dynamic Arm". Orthop-Tech Q (1):6–15
26. Cutti A, Raggi M, Garofalo P, Giovanardi A, Filippi M, Davalli A (2008) The effects of the 'Power Knee' prosthesis on amputees metabolic cost of walking and symmetry of gait-preliminary results. Gait Posture 28:S38
27. Czerniecki J, Gitter A, Munro C (1991) Joint moment and muscle power output characteristics of below knee amputees during running: the influence of energy storing prosthetic feet. J Biomech 24(1):63–65
28. Dal U, Erdogan T, Resitoglu B, Beydagi H (2010) Determination of preferred walking speed on treadmill may lead to high oxygen cost on treadmill walking. Gait Posture 31(3):366–369
29. Delis AL, Carvalho J, Seisdedos CV, Borges GA, da Rocha AF (2010) Myoelectric control algorithms for leg prostheses based on data fusion with proprioceptive sensors. In: Proceedings ISSNIP biosignals and biorobotics conference, Vitoria, 2010, pp 137–142
30. Delis AL, Carvalho JL, da Rocha AF, Nascimento FA, Borges GA (2011) Myoelectric knee angle estimation algorithms for control of active transfemoral leg prostheses. Intechopen.com
31. DeVita P, Helseth J, Hortobagyi T (2007) Muscles do more positive than negative work in human locomotion. J Exp Biol 210(Pt 19):3361
32. Donelan J, Li Q, Naing V, Hoffer J, Weber D, Kuo A (2008) Biomechanical energy harvesting: generating electricity during walking with minimal user effort. Science 319(5864):807–810
33. Duraiswami P, Orth M, Tuli S (1971) 5000 years of orthopaedics in India. Clin Orthop Relat Res 75:269
34. Durfee W, Xia J, Hsiao-Wecksler E (2011) Tiny hydraulics for powered orthotics. In: IEEE international conference on rehabilitation robotics (ICORR), Zurich, 2011. IEEE, pp 1–6
35. Duvinage M, Castermans T, Dutoit T (2011) Control of a lower limb active prosthesis with eye movement sequences. In: IEEE symposium on computational intelligence, cognitive algorithms, mind, and brain (CCMB), Paris, 2011. IEEE, pp 1–7
36. Dyck W, Onyshko S, Hobson D, Winter D, Quanbury A (1975) A voluntarily controlled electrohydraulic above-knee prosthesis. Bull Prosthet Res 10(23–26):169
37. Eilenberg M, Geyer H, Herr H (2010) Control of a powered ankle–foot prosthesis based on a neuromuscular model. IEEE Trans Neural Syst Rehabil Eng 18(2):164–173
38. Endolite. www.endolite.com
39. Eslamy M, Grimmer M, Seyfarth A (2012) Effects of unidirectional parallel springs on required peak power and energy in powered prosthetic ankles: comparison between different active actuation concepts. In: IEEE international conference on robotics and biomimetics (ROBIO), Guangzhou
40. Eslamy M, Grimmer M, Rinderknecht S, Seyfarth A (2013) Does it pay to have a damper in a powered ankle prosthesis? A power-energy perspective. In: IEEE international conference on rehabilitation robotics (ICORR), Seattle
41. Ferris DP, Czerniecki JM, Hannaford B et al (2005) An ankle-foot orthosis powered by artificial pneumatic muscles. J Appl Biomech 21(2):189
42. Ferris AE, Aldridge JM, Rábago CA, Wilken JM (2012) Evaluation of a powered ankle-foot prosthetic system during walking. Arch Phys Med Rehabil 93(11):1911–1918. Elsevier
43. Fey N, Klute G, Neptune R (2011) The influence of energy storage and return foot stiffness on walking mechanics and muscle activity in below-knee amputees. Clin Biomech 26(10):1025–1032

44. Fradet L, Alimusaj M, Braatz F, Wolf SI (2010) Biomechanical analysis of ramp ambulation of transtibial amputees with an adaptive ankle foot system. Gait Posture 32(2):191–198
45. Freedom Innovations. www.freedom-innovations.com
46. Gailey R, Allen K, Castles J, Kucharik J, Roeder M (2008) Review of secondary physical conditions associated with lower-limb amputation and long-term prosthesis use. J Rehabil Res Dev 45(1):15
47. Gates DH, Aldridge JM, Wilken JM (2013) Kinematic comparison of walking on uneven ground using powered and unpowered prostheses. Clin Biomech 28(4):467–472. Elsevier
48. Gefen A, Megido-Ravid M, Itzchak Y (2001) In vivo biomechanical behavior of the human heel pad during the stance phase of gait. J Biomech 34(12):1661–1665
49. Geil M (2001) Energy loss and stiffness properties of dynamic elastic response prosthetic feet. JPO J Prosthet Orthot 13(3):70
50. Geng Y, Yang P, Xu X, Chen L (2012) Design and simulation of active transfemoral prosthesis. In: 24th Chinese control and decision conference (CCDC), Taiyuan, 2012. IEEE, pp 3724–3728
51. Geyer H, Herr H (2010) A muscle-reflex model that encodes principles of legged mechanics produces human walking dynamics and muscle activities. IEEE Trans Neural Syst Rehabil Eng 18(3):263–273
52. Geyer H, Seyfarth A, Blickhan R (2003) Positive force feedback in bouncing gaits? Proc R Soc Lond Ser B Biol Sci 270(1529):2173–2183
53. Gitter A, Czerniecki J, DeGroot D (1991) Biomechanical analysis of the influence of prosthetic feet on below-knee amputee walking. Am J Phys Med Rehabil 70(3):142
54. Goltz F, Freusberg A, Gergens E (1875) Ueber gefässerweiternde nerven. Pflügers Arch Eur J Physiol 11(1):52–99
55. Greitemann B, Bui-Khac H (2006) Wie haufig sturzen an der unteren Extremitat amputierte Patienten? Medizinisch Orthopadische Technik 126(5):81
56. Grimes DL (1979) An active multi-mode above knee prosthesis controller. Ph.D. thesis, Massachusetts Institute of Technology
57. Grimes D, Flowers W, Donath M (1977) Feasibility of an active control scheme for above knee prostheses. J Biomech Eng 99:215
58. Grimmer M, Seyfarth A (2011) Stiffness adjustment of a series elastic actuator in a knee prosthesis for walking and running: the trade-off between energy and peak power optimization. In: IEEE/RSJ international conference on intelligent robots and systems (IROS), San Francisco. IEEE, pp 1811–1816
59. Grimmer M, Seyfarth A (2011) Stiffness adjustment of a series elastic actuator in an ankle-foot prosthesis for walking and running: the trade-off between energy and peak power optimization. In: IEEE international conference on robotics and automation (ICRA), Shanghai. IEEE, pp 1439–1444
60. Grimmer M, Eslamy M, Gliech S, Seyfarth A (2012) A comparison of parallel-and series elastic elements in an actuator for mimicking human ankle joint in walking and running. In: IEEE international conference on robotics and automation (ICRA), St. Paul, 2012. IEEE, pp 2463–2470
61. Ha KH, Varol HA, Goldfarb M (2011) Volitional control of a prosthetic knee using surface electromyography. IEEE Trans Biomed Eng 58(1):144–151
62. Hafner B (2005) Clinical prescription and use of prosthetic foot and ankle mechanisms: a review of the literature. JPO J Prosthet Orthot 17(4):S5
63. Hafner B, Sanders J, Czerniecki J, Fergason J (2002) Energy storage and return prostheses: does patient perception correlate with biomechanical analysis? Clin Biomech 17(5):325–344
64. Hargrove L, Simon AM, Finucane SB, Lipschutz RD (2011) Myoelectric control of a powered transfemoral prosthesis during non-weight-bearing activities. In: Proceedings of the 2011 MyoElectric controls/powered prosthetics symposium, Fredericton. Myoelectric Symposium
65. Heller G, Günster C, Swart E (2005) Über die Häufigkeit von Amputationen unterer Extremitäten in Deutschland about the frequency of lower limb amputations. Dtsch Med Wochenschr 130(28/29):1689–1690

66. Herr H, Grabowski A (2012) Bionic ankle–foot prosthesis normalizes walking gait for persons with leg amputation. Proc R Soc B Biol Sci 279(1728):457–464
67. Herr HM, Au SK, Dilworth P, Paluska DJ (2012) Artificial ankle-foot system with spring, variable-damping, and series-elastic actuator components. US Patent App. 13/348,570
68. Highsmith MJ, Kahle JT, Carey SL, Lura DJ, Dubey RV, Quillen WS (2010) Kinetic differences using a Power Knee and C-Leg while sitting down and standing up: a case report. JPO J Prosthet Orthot 22(4):237–243
69. Highsmith MJ, Kahle JT, Carey SL, Lura DJ, Dubey RV, Csavina KR, Quillen WS (2011) Kinetic asymmetry in transfemoral amputees while performing sit to stand and stand to sit movements. Gait Posture 34(1):86–91
70. Hitt JK, Bellman R, Holgate M, Sugar TG, Hollander KW (2007) The sparky (spring ankle with regenerative kinetics) project: design and analysis of a robotic transtibial prosthesis with regenerative kinetics. In: Design engineering technology conferences and computers in information and engineering conference (IDETC/CIE), Las Vegas. ASME
71. Hitt J, Merlo J, Johnston J, Holgate M, Boehler A, Hollander K, Sugar T (2010) Bionic running for unilateral transtibial military amputees. DTIC document
72. Hitt J, Sugar T, Holgate M, Bellman R (2010) An active foot-ankle prosthesis with biomechanical energy regeneration. J Med Devices 4:011,003
73. Hocoma. www.hocoma.com
74. Hof AL, van Bockel RM, Schoppen T, Postema K (2007) Control of lateral balance in walking: experimental findings in normal subjects and above-knee amputees. Gait Posture 25(2):250–258
75. Holgate M, Sugar T, Bohler A (2009) A novel control algorithm for wearable robotics using phase plane invariants. In: IEEE international conference on robotics and automation (ICRA), Kobe. IEEE, pp 3845–3850
76. Hollander K, Sugar T (2005) Design of the robotic tendon. In: Design of medical devices conference (DMD), Minneapolis
77. Hoover C, Fite K (2010) Preliminary evaluation of myoelectric control of an active transfemoral prosthesis during stair ascent. In: Proceedings ASME dynamic systems and controls conference, Cambridge. Paper no. DSCC2010-4158
78. Hoover CD, Fulk GD, Fite KB (2013) Stair ascent with a powered transfemoral prosthesis under direct myoelectric control. Trans Mechatron 18:1191–1200
79. Horn G (1972) Electro-control: am EMG-controlled A/K prosthesis. Med Biol Eng Comput 10(1):61–73
80. Hosmer. www.hosmer.com
81. Huang H, Zhang F, Hargrove LJ, Dou Z, Rogers DR, Englehart KB (2011) Continuous locomotion-mode identification for prosthetic legs based on neuromuscular–mechanical fusion. IEEE Trans Biomed Eng 58(10):2867–2875
82. Islam MR, Haque A, Amin S, Rabbani K (2011) Design and development of an EMG driven microcontroller based prosthetic leg. J Med Phys 4(1):107–114
83. iWalk. www.iwalkpro.com
84. Johansson J, Sherrill D, Riley P, Bonato P, Herr H (2005) A clinical comparison of variable-damping and mechanically passive prosthetic knee devices. Am J Phys Med Rehabil 84(8):563
85. Kahle JT, Highsmith M, Hubbard S (2008) Comparison of nonmicroprocessor knee mechanism versus C-Leg on prosthesis evaluation questionnaire, stumbles, falls, walking tests, stair descent, and knee preference. J Rehabil Res Dev 45(1):1
86. Kuitunen S, Komi P, Kyröläinen H et al (2002) Knee and ankle joint stiffness in sprint running. Med Sci Sports Exerc 34(1):166
87. Kulkarni J, Wright S, Toole C, Morris J, Hirons R (1996) Falls in patients with lower limb amputations: prevalence and contributing factors. Physiotherapy 82(2):130–136
88. Lambrecht BGA (2008) Design of a hybrid passive-active prosthesis for above-knee amputees. ProQuest LLC, Ann Arbor

89. Lambrecht BG, Kazerooni H (2009) Design of a semi-active knee prosthesis. In: IEEE international conference on robotics and automation (ICRA'09), Kobe, 2009. IEEE, pp 639–645
90. Latif T, Ellahi C, Choudhury T, Rabbani K (2008) Design of a cost-effective EMG driven bionic leg. In: International conference on electrical and computer engineering (ICECE 2008), Dhaka, 2008. IEEE, pp 80–85
91. Lawson B, Varol HA, Huff A, Erdemir E, Goldfarb M (2013) Control of stair ascent and descent with a powered transfemoral prosthesis. IEEE Trans Neural Syst Rehabil Eng 21(3):466–473. IEEE
92. Lee IM, Paffenbarger RS (2000) Associations of light, moderate, and vigorous intensity physical activity with longevity the Harvard Alumni Health Study. Am J Epidemiol 151(3):293–299
93. Lim J (2008) The mechanical design and analysis of an active prosthetic knee. University of Waterloo, Waterloo
94. Lipfert S (2010) Kinematic and dynamic similarities between walking and running. Verlag Dr. Kovac, Hamburg. ISBN:978-3-8300-5030-8
95. Liu M, Datseris P, Huang HH (2012) A prototype for smart prosthetic legs-analysis and mechanical design. Adv Mater Res 403:1999–2006
96. Mai A, Commuri S (2011) Gait identification for an intelligent prosthetic foot. In: IEEE international symposium on intelligent control (ISIC), Denver, 2011. IEEE, pp 1341–1346
97. Mancinelli C, Patritti BL, Tropea P, Greenwald RM, Casler R, Herr H, Bonato P (2011) Comparing a passive-elastic and a powered prosthesis in transtibial amputees. In: Annual international conference of the IEEE engineering in medicine and biology society (EMBC), Boston, 2011. IEEE, pp 8255–8258
98. Markowitz J, Krishnaswamy P, Eilenberg MF, Endo K, Barnhart C, Herr H (2011) Speed adaptation in a powered transtibial prosthesis controlled with a neuromuscular model. Philos Trans R Soc B Biol Sci 366(1570):1621–1631
99. Martin J, Pollock A, Hettinger J (2010) Microprocessor lower limb prosthetics: review of current state of the art. JPO J Prosthet Orthot 22(3):183–193
100. Martinez Villalpando EC (2012) Design and evaluation of a biomimetic agonist-antagonist active knee prosthesis. Ph.D. thesis, Massachusetts Institute of Technology
101. Martinez-Villalpando E, Herr H (2009) Agonist-antagonist active knee prosthesis: a preliminary study in level-ground walking. J Rehabil Res Dev 46:361–374
102. Martinez-Villalpando EC, Mooney L, Elliott G, Herr H (2011) Antagonistic active knee prosthesis. A metabolic cost of walking comparison with a variable-damping prosthetic knee. In: Annual international conference of the IEEE engineering in medicine and biology society (EMBC), Boston, 2011. IEEE, pp 8519–8522
103. Miller WC, Speechley M, Deathe B (2001) The prevalence and risk factors of falling and fear of falling among lower extremity amputees. Arch Phys Med Rehabil 82(8):1031–1037
104. Mirfakhrai T, Madden JD, Baughman RH (2007) Polymer artificial muscles. Mater Today 10(4):30–38
105. Mutlu L, Uyar E, Baser O, Cetin L (2011) Modelling of an under-hip prosthesis with ankle and knee trajectory control by using human gait analysis. In: World congress, Milano, vol 18, pp 9668–9673
106. Nandi G, Ijspeert A, Chakraborty P, Nandi A (2009) Development of adaptive modular active leg (AMAL) using bipedal robotics technology. Robot Auton Syst 57(6):603–616
107. Nandy A, Mondal S, Chakraborty P, Nandi G (2012) Development of a robust microcontroller based intelligent prosthetic limb. In: Contemporary computing. Springer, pp 452–462
108. Navarro X, Krueger TB, Lago N, Micera S, Stieglitz T, Dario P (2005) A critical review of interfaces with the peripheral nervous system for the control of neuroprostheses and hybrid bionic systems. J Peripher Nerv Syst 10(3):229–258
109. Nielsen DH, Shurr DG, Golden JC, Meier K (1988) Comparison of energy cost and gait efficiency during ambulation in below-knee amputees using different prosthetic feet-a preliminary report. JPO J Prosthet Orthot 1(1):24

110. Niemitz C (2010) The evolution of the upright posture and gait-a review and a new synthesis. Naturwissenschaften 97(3):241–263
111. Nigg BM, Herzog W, Herzog W (1994) Biomechanics of the musculo-skeletal system. Wiley, New York
112. Nolan L, Lees A (2000) The functional demands on the intact limb during walking for active trans-femoral and trans-tibial amputees. Prosthet Orthot Int 24(2):117–125
113. Nolan L, Wit A, Dudziński K, Lees A, Lake M, Wychowański M (2003) Adjustments in gait symmetry with walking speed in trans-femoral and trans-tibial amputees. Gait Posture 17(2):142–151
114. O'Donnell F, Brundage J, Wertheimer E, Olive D, Clark L (2012) Medical surveillance monthly report. vol 19, number 6. Technical report, DTIC Document
115. Orendurff MS, Segal AD, Klute GK, McDowell ML, Pecoraro JA, Czerniecki JM (2006) Gait efficiency using the C-Leg. J Rehabil Res Dev 43(2):239
116. Ossur. www.ossur.com
117. Ottobock. www.ottobock.com
118. Pain MT, Challis JH (2001) The role of the heel pad and shank soft tissue during impacts: a further resolution of a paradox. J Biomech 34(3):327–333
119. Panzenbeck JT, Klute GK (2012) A powered inverting and everting prosthetic foot for balance assistance in lower limb amputees. JPO J Prosthet Orthot 24(4):175–180
120. Parsan A, Tosunoglu S (2012) A novel control algorithm for ankle-foot prosthesis. In: Florida conference on recent advances in robotics, Boca Raton
121. Pierrynowski MR, Morrison JB (1985) A physiological model for the evaluation of muscular forces in human locomotion: theoretical aspects. Math Biosci 75(1):69–101
122. Pillai MV, Kazerooni H, Hurwich A (2011) Design of a semi-active knee-ankle prosthesis. In: IEEE international conference on robotics and automation (ICRA), Shanghai, 2011. IEEE, pp 5293–5300
123. Pitta F, Troosters T, Spruit MA, Probst VS, Decramer M, Gosselink R (2005) Characteristics of physical activities in daily life in chronic obstructive pulmonary disease. Am J Respir Crit Care Med 171(9):972–977
124. Popovic D, Tomovic R, Tepavac D, Schwirtlich L (1991) Control aspects of active above-knee prosthesis. Int J Man-Mach Stud 35(6):751–767
125. Postema K, Hermens H, De Vries J, Koopman H, Eisma W (1997) Energy storage and release of prosthetic feet part 1: biomechanical analysis related to user benefits. Prosthet Orthot Int 21(1):17–27
126. Powers CM, Rao S, Perry J (1998) Knee kinetics in trans-tibial amputee gait. Gait Posture 8(1):1–7
127. Prince F, Winter D, Sjonnensen G, Powell C, Wheeldon R (1998) Mechanical efficiency during gait of adults with transtibial amputation: a pilot study comparing the SACH, Seattle, and Golden-Ankle prosthetic feet. Development 35(2):177–185
128. Prinsen EC, Nederhand MJ, Rietman JS (2011) Adaptation strategies of the lower extremities of patients with a transtibial or transfemoral amputation during level walking: a systematic review. Arch Phys Med Rehabil 92(8):1311–1325
129. Proteor. www.proteor.com
130. Purath J, Michaels MA, McCabe G, Wilbur J (2004) A brief intervention to increase physical activity in sedentary working women une intervention ponctuelle en vue daccroitre lactivite physique chez les travailleuses sedentaires. CJNR (Can J Nurs Res) 36(1):76–91
131. Robbins C, Vreeman D, Sothmann M, Wilson S, Oldridge N (2009) A review of the long-term health outcomes associated with war-related amputation. Mil Med 174(6):588–592
132. Robertson DGE (2004) Research methods in biomechanics. Human Kinetics Publishers, Champaign
133. Rusaw D, Ramstrand N (2011) Motion-analysis studies of transtibial prosthesis users: a systematic review. Prosthet Orthot Int 35(1):8–19
134. Sabatini AM, Martelloni C, Scapellato S, Cavallo F (2005) Assessment of walking features from foot inertial sensing. IEEE Trans Biomed Eng 52(3):486–494

135. Sadeghi H, Allard P, Prince F, Labelle H (2000) Symmetry and limb dominance in able-bodied gait: a review. Gait Posture 12(1):34
136. Sanderson D, Martin P (1996) Joint kinetics in unilateral below-knee amputee patients during running. Arch Phys Med Rehabil 77(12):1279–1285
137. Sauren J, Lieby B et al (2010) Motion analysis of the 2009 men's 100 m world record. PhyDid B-Didaktik der Physik-Beiträge zur DPG-Frühjahrstagung
138. Sawicki GS, Ferris DP (2009) A pneumatically powered knee-ankle-foot orthosis (KAFO) with myoelectric activation and inhibition. J Neuroeng Rehabil 6(1):23
139. Schaarschmidt M, Lipfert SW, Meier-Gratz C, Scholle HC, Seyfarth A (2012) Functional gait asymmetry of unilateral transfemoral amputees. Hum Mov Sci 31(4):907–917. Elsevier
140. Schinder A, Genao C, Semmelroth S (2011) Methodology for control and analysis of an active foot-ankle prosthesis. In: Proceedings of the national conference on undergraduate research (NCUR) 2011, Ithaca College, New York, 31 Mar–2 Apr 2011, pp 2011–2018
141. Schmalz T, Blumentritt S, Jarasch R et al (2002) Energy expenditure and biomechanical characteristics of lower limb amputee gait: the influence of prosthetic alignment and different prosthetic components. Gait Posture 16(3):255
142. Schneider K, Hart T, Zernicke R, Setoguchi Y, Oppenheim W (1993) Dynamics of below-knee child amputee gait: SACH foot versus Flex foot. J Biomech 26(10):1191–1204
143. Segal A, Orendurff M, Klute G, McDowell M, Pecoraro J, Shofer J, Czerniecki J (2006) Kinematic and kinetic comparisons of transfemoral amputee gait using C-Leg® and Mauch SNS® prosthetic knees. J Rehabil Res Dev 43(7):857
144. Seroussi R, Gitter A, Czerniecki J, Weaver K (1996) Mechanical work adaptations of above-knee amputee ambulation. Arch Phys Med Rehabil 77(11):1209–1214
145. Seyfarth A, Geyer H, Herr H (2003) Swing-leg retraction: a simple control model for stable running. J Exp Biol 206(15):2547–2555
146. Shen X, Christ D (2011) Design and control of chemomuscle: a liquid-propellant-powered muscle actuation system. J Dyn Syst Meas Control 133(2):021,006–021,006
147. Sherrington CS (1910) Flexion-reflex of the limb, crossed extension-reflex, and reflex stepping and standing. J Physiol 40(1–2):28
148. Silverman A, Fey N, Portillo A, Walden J, Bosker G, Neptune R (2008) Compensatory mechanisms in below-knee amputee gait in response to increasing steady-state walking speeds. Gait Posture 28(4):602–609
149. Springactive. www.springactive.com
150. Sup F, Bohara A, Goldfarb M (2008) Design and control of a powered transfemoral prosthesis. Int J Robot Res 27(2):263–273
151. Sup F, Varol H, Mitchell J, Withrow T, Goldfarb M (2009) Self-contained powered knee and ankle prosthesis: initial evaluation on a transfemoral amputee. In: IEEE international conference on rehabilitation robotics (ICORR), Kyoto. IEEE, pp 638–644
152. Sup F, Varol HA, Goldfarb M (2011) Upslope walking with a powered knee and ankle prosthesis: initial results with an amputee subject. IEEE Trans Neural Syst Rehabil Eng 19(1):71–78
153. Suzuki R, Sawada T, Kobayashi N, Hofer E (2011) Control method for powered ankle prosthesis via internal model control design. In: International conference on mechatronics and automation (ICMA), Beijing. IEEE, pp 237–242
154. Svanström L (1974) Falls on stairs: an epidemiological accident study. Scand J Public Health 2(3):113–120
155. Svensson W, Holmberg U (2006) An autonomous control system for a prosthetic foot ankle. In: 4th IFAC symposium on mechatronic systems, Heidelberg, 2006. International Federation of Automatic Control (IFAC), pp 856–861
156. Svensson W, Holmberg U (2010) Estimating ground inclination using strain sensors with Fourier series representation. J Robot 2010:1–8
157. The amputee statistical database for the United Kingdom 2006/07 (2009). http://www.limbless-statistics.org/documents/Report2006-07.pdf

158. Theeven PJR (2012) Functional added value of microprocessor-controlled prosthetic knee joints. Ph.D. thesis, Maastricht University
159. Thomas G, Simon D (2012) Inertial thigh angle sensing for a semi-active knee prosthesis. In: Proceedings of the IASTED international symposia imaging and signal processing in health care and technology (ISPHT 2012), Baltimore. ACTA Press
160. Tudor-Locke C, Bassett J (2004) How many steps/day are enough?: preliminary pedometer indices for public health. Sports Med 34(1):1–8
161. Unal R, Carloni R, Behrens S, Hekman E, Stramigioli S, Koopman H (2012) Towards a fully passive transfemoral prosthesis for normal walking. In: 4th IEEE RAS & EMBS international conference on biomedical robotics and biomechatronics (BioRob), Rome, 2012. IEEE, pp 1949–1954
162. Vallery H, Burgkart R, Hartmann C, Mitternacht J, Riener R, Buss M (2011) Complementary limb motion estimation for the control of active knee prostheses. Biomedizinische Technik/Biomed Eng 56(1):45–51
163. Van den Bogert AJ (2003) Exotendons for assistance of human locomotion. Biomed Eng Online 2(17):1–8
164. van der Linde H, Hofstad CJ, Geurts AC, Postema K, Geertzen JH, Van Limbeek J et al (2004) A systematic literature review of the effect of different prosthetic components on human functioning with a lower-limb prosthesis. J Rehabil Res Dev 41(4):555–570
165. Vanicek N, Strike S, McNaughton L, Polman R (2009) Gait patterns in transtibial amputee fallers vs. non-fallers: biomechanical differences during level walking. Gait Posture 29(3):415–420
166. van Ingen Schenau Gv, Bobbert M, Rozendal R (1987) The unique action of bi-articular muscles in complex movements. J Anat 155:1
167. Varol H, Sup F, Goldfarb M (2009) Powered sit-to-stand and assistive stand-to-sit framework for a powered transfemoral prosthesis. In: IEEE international conference on rehabilitation robotics (ICORR), Kyoto. IEEE, pp 645–651
168. Varol HA, Sup F, Goldfarb M (2010) Multiclass real-time intent recognition of a powered lower limb prosthesis. IEEE Trans Biomed Eng 57(3):542–551
169. Verhoeff T (2002) ICRC physical rehabilitation programmes, annual report 2001
170. Versluys R, Lenaerts G, Van Damme M, Jonkers I, Desomer A, Vanderborght B, Peeraer L, Van der Perre G, Lefeber D (2009) Successful preliminary walking experiments on a transtibial amputee fitted with a powered prosthesis. Prosthet Orthot Int 33(4):368–377
171. Vickers DR, Palk C, McIntosh A, Beatty K (2008) Elderly unilateral transtibial amputee gait on an inclined walkway: a biomechanical analysis. Gait Posture 27(3):518–529
172. Vrieling A, Van Keeken H, Schoppen T, Otten E, Halbertsma J, Hof A, Postema K (2008) Uphill and downhill walking in unilateral lower limb amputees. Gait Posture 28(2):235–242
173. Wang S, van Dijk W, van der Kooij H (2011) Spring uses in exoskeleton actuation design. In: IEEE international conference on rehabilitation robotics (ICORR), Zurich. IEEE, pp 1–6
174. Waters RL, Mulroy S (1999) The energy expenditure of normal and pathologic gait. Gait Posture 9(3):207–231
175. Waycaster G, Wu SK, Xiangrong S (2011) Design and control of a pneumatic artificial muscle actuated above-knee prosthesis. J Med Devices 5(3):031003
176. Webster J, Levy C, Bryant P, Prusakowski P (2001) Sports and recreation for persons with limb deficiency. Arch Phys Med Rehabil 82(3):S38–S44
177. Wilson AB (1992) History of amputation surgery and prosthetics. In: Atlas of limb prosthetics: surgical, prosthetic, and rehabilitation principles. Mosby-Year Book, St. Louis, pp 3–16
178. Winter DA (2009) Biomechanics and motor control of human movement. Wiley, Hoboken
179. Winter DA, Sienko SE (1988) Biomechanics of below-knee amputee gait. J Biomech 21(5):361–367
180. Wolf EJ, Everding VQ, Linberg AL, Schnall BL, Czerniecki JM, Gambel JM et al (2012) Assessment of transfemoral amputees using C-Leg and Power Knee for ascending and descending inclines and steps. J Rehabil Res Dev 49(6):831–842

181. Wolf EJ, Everding VQ, Linberg AA, Czerniecki JM, Gambel COL (2013) Comparison of the Power Knee and C-Leg during step-up and sit-to-stand tasks. Gait Posture 38(3):397–402. Elsevier
182. Yuan K, Zhu J, Wang Q, Wang L (2011) Finite-state control of powered below-knee prosthesis with ankle and toe. In: World congress, Milano, vol 18, pp 2865–2870
183. Zajac FE et al (1989) Muscle and tendon: properties, models, scaling, and application to biomechanics and motor control. Crit Rev Biomed Eng 17(4):359
184. Zelik K, Collins S, Adamczyk P, Segal A, Klute G, Morgenroth D, Hahn M, Orendurff M, Czerniecki J, Kuo A (2011) Systematic variation of prosthetic foot spring affects center-of-mass mechanics and metabolic cost during walking. IEEE Trans Neural Syst Rehabil Eng 19(4):411–419
185. Zhang F, Liu M, Huang H (2012) Preliminary study of the effect of user intent recognition errors on volitional control of powered lower limb prostheses. In: Annual international conference of the IEEE engineering in medicine and biology Society (EMBC), San Diego, 2012. IEEE, pp 2768–2771
186. Zhu J, Wang Q, Wang L (2010) Pantoe 1: biomechanical design of powered ankle-foot prosthesis with compliant joints and segmented foot. In: IEEE/ASME international conference on advanced intelligent mechatronics (AIM), Montreal. IEEE, pp 31–36
187. Ziegler-Graham K, MacKenzie E, Ephraim P, Travison T, Brookmeyer R et al (2008) Estimating the prevalence of limb loss in the United States: 2005 to 2050. Arch Phys Med Rehabil 89(3):422

Chapter 6
Multi-directional Dynamic Mechanical Impedance of the Human Ankle; A Key to Anthropomorphism in Lower Extremity Assistive Robots

Mohammad Rastgaar, Hyunglae Lee, Evandro Ficanha, Patrick Ho, Hermano Igo Krebs, and Neville Hogan

Abstract The mechanical impedance of the human ankle plays a central role in lower-extremity functions requiring physical interaction with the environment. Recent efforts in the design of lower-extremity assistive robots have focused on the sagittal plane; however, the human ankle functions in both sagittal and frontal planes. While prior work has addressed ankle mechanical impedance in single degrees of freedom, here we report on a method to estimate multi-variable human ankle mechanical impedance and especially the coupling between degrees of freedom. A wearable therapeutic robot was employed to apply torque perturbations simultaneously in the sagittal and frontal planes and record the resulting ankle

M. Rastgaar (✉) • E. Ficanha
Department of Mechanical Engineering-Engineering Mechanics, Michigan Technological University, 815 MEEM Building, 1400 Townsend Dr., Houghton, MI 49931, USA
e-mail: rastgaar@mtu.edu

H. Lee
Department of Biomedical Engineering, Northwestern University, Evanston, IL, USA

Sensory Motor Performance Program, Rehabilitation Institute of Chicago, Chicago, IL, USA

P. Ho
Parian Logistics, Cambridge, MA 02139, USA

H.I. Krebs
Department of Mechanical Engineering, Massachusetts Institute of Technology, Cambridge, MA 02139, USA

Department of Neurology, University of Maryland School of Medicine, Baltimore, MD 21201, USA

N. Hogan
Department of Mechanical Engineering, Massachusetts Institute of Technology, Cambridge, MA 02139, USA

Department of Brain and Cognitive Sciences, Massachusetts Institute of Technology, Cambridge, MA 02139, USA

P. Artemiadis (ed.), *Neuro-Robotics: From Brain Machine Interfaces to Rehabilitation Robotics*, Trends in Augmentation of Human Performance 2,
DOI 10.1007/978-94-017-8932-5_6, © Springer Science+Business Media Dordrecht 2014

motions. Standard stochastic system identification procedures were adapted to compensate for the robot dynamics and derive a linear time-invariant estimate of mechanical impedance.

Applied to seated, young unimpaired human subjects, the method yielded coherences close to unity up to and beyond 50 Hz, indicating the validity of linear models, at least under the conditions of these experiments. Remarkably, the coupling between dorsi-flexion/plantar-flexion and inversion/eversion was negligible. This was observed despite strong biomechanical coupling between degrees of freedom due to musculo-skeletal kinematics and suggests compensation by the neuromuscular system. The results suggest that the state-of-the-art in lower extremity assistive robots may advance by incorporating design features that mimic the multi-directional mechanical impedance of the ankle in both sagittal and frontal planes.

Keywords Multi-variable mechanical impedance • Ankle impedance • Powered ankle-foot prosthesis • Directional • Impedance of ankle

6.1 Introduction

The mechanical impedance of the human ankle plays a major role in lower-extremity functions which involve mechanical interaction of the foot with a contacting surface, including shock-absorption during foot-strike or maintenance of upright posture. Precise quantitative measurement of ankle mechanical impedance may support deeper understanding of how the ankle supports these functions and other aspects of locomotion and its neural control, and may provide essential data for the design of improved therapeutic procedures to address deficiencies of balance and/or locomotion.

Recently, there have been a few lower extremity power prostheses that control the mechanical impedance at their joints. Notable examples are a transfemoral powered prosthesis by Sup et al. [1–4] and a transtibial powered prosthesis by Au et al. [5–7]. The former includes a controller that adjusts the impedance of the ankle and knee joints at different phases of gait. The latter, which later transitioned into the commercially available ankle-foot prosthesis BiOM, has an active ankle joint with a finite-state machine to generate appropriate ankle impedance and torque at each phase of gait [8, 9]. While both prostheses have advanced the state-of-the-art, their designs are confined to the sagittal plane. Even level walking in a straight line requires the ankle to function in both the sagittal and frontal planes. Additionally, normal daily activity includes more gait scenarios such as turning, traversing slopes, steering, and adapting to uneven terrain profiles. This suggests that the next advance in lower extremity assistive devices is to extend their design and control to the frontal plane. To do that, we need a better understanding of the multi-variable mechanical impedance of the human ankle, and that is the subject of this study.

Several prior studies have addressed ankle mechanical impedance. Lamontagne et al. [10] reported the viscoelastic behavior of relaxed ankle plantarflexors.

Other researchers compared dorsi-flexion/plantar-flexion (DP) ankle stiffness of unimpaired and neurologically-impaired subjects [11–15]. Dynamic compliance of the human ankle using band-limited Gaussian torque perturbations was estimated by Mirbagheri et al. [16]. Kearney and Hunter [17, 18] and Weis et al. [19, 20] used a similar system identification approach to estimate the passive and active dynamic stiffness of the ankle joint in DP. Also, Mirbagheri et al. [21] and Kearney et al. [22] used a similar method to estimate the intrinsic and reflexive components of ankle dynamic stiffness. Intrinsic and reflex contributions to ankle stiffness in dorsiflexion at different levels of voluntary muscle co-contraction were measured by Sinkjaer et al. [23]. Kirsch and Kearney [24] estimated ankle mechanical impedance in DP by superimposing small stochastic motion perturbations during a large stretch imposed upon active triceps surae muscles. Winter et al. [25], Morasso and Sanguineti [26], and Loram and Lakie [27, 28] measured the ankle stiffness during quiet standing. Davis and Deluca [29], Palmer [30], and Hansen et al. [31] measured ankle stiffness during locomotion.

All of these studies were confined to the sagittal plane. In the frontal plane, Saripalli and Wilson [32] studied the variation of ankle stiffness under different weight-bearing conditions. Zinder et al. [33] studied dynamic stabilization and ankle stiffness in the inversion/eversion direction (IE) by applying a sudden perturbation in the frontal plane at a time of upright posture during bipedal weight-bearing stance. Roy et al. estimated the ankle stiffness in both DP and IE for unimpaired subjects [34] and subjects with chronic hemiparesis [35] but coupling between these degrees of freedom was not assessed.

All of this prior work characterized ankle mechanical impedance in single degrees of freedom (DOF) and did not address the multi-variable character of the ankle. Yet the ankle is a biomechanically complex joint with multiple DOFs. Its major anatomical axes do not intersect and they are far from orthogonal, which could introduce a biomechanical coupling between DP and IE. Furthermore, single DOF ankle movements are rare in normal lower-extremity actions and the control of multiple ankle DOFs may present unique challenges [36]. In previous work by some of the authors [37–40], the multi-variable ankle mechanical impedance of young unimpaired subjects with maximally relaxed muscles was measured in static condition. In the study reported here, we extend the estimation to the dynamic condition. Preliminary reports of part of this work were presented in [41–43].

We chose to use stochastic frequency-domain methods to estimate ankle dynamic mechanical impedance. A singular advantage of this approach is that, although it requires an assumption of linear dynamics (which may be justified by assuming smoothness and using small perturbations) it requires no *a-priori* assumption about the order or dynamic structure of the system under investigation. In particular, it does not require the common assumption in previous work that ankle mechanical impedance is composed of inertia, damping, and stiffness, but is applicable to more complex, higher-order dynamics.

Stochastic excitation using hydraulic actuators has been used in prior research [18, 17, 22, 19–21, 23, 44]. Hydraulic actuators have intrinsically high output mechanical impedance, which cannot substantially be reduced by force feedback control, especially at higher frequencies, and that means they essentially impose motion perturbations [45, 46]. However, imposing motion perturbations requires care to avoid applying excessive force to subjects' joints.

Previously, we presented a multi-variable stochastic method to estimate upper extremity mechanical impedance by applying pseudo-random torque perturbations [47]. In the work reported here, we adapted that method to estimate human ankle mechanical impedance using Anklebot, a wearable robot designed for the study and treatment of the ankle [34]. The principal adaptation was to obviate direct force measurement by using an accurate characterization of the robot's dynamic behavior.

Remarkably, we found that, despite the non-orthogonality of the ankle joint's anatomical axes and the geometric complexity of its musculo-skeletal kinematics, the relaxed ankle's multivariable mechanical impedance is predominantly orthogonal and aligned with its principal axes in the sagittal and frontal planes.

6.2 Methods

6.2.1 Subject

This study reports the results on one young male subject with no reported biomechanical or neuromuscular disorder. This participant gave written informed consent to participate as approved by the Michigan Technological University institutional review board.

6.2.2 Experimental Setup

In general, we define ankle mechanical impedance as a dynamic operator that maps a time-history of angular displacement onto a corresponding time-history of torque. This dynamic operator was measured for DP and IE simultaneously using a wearable robot, Anklebot (Interactive Motion Technologies, Inc.), the device used in previous work [37–39, 41, 43, 42]. Described in detail in [34], it is backdrivable with low friction and allows human subjects to move the foot freely in three DOF relative to the shank. Of those, two DOF are actuated by two nearly-parallel linear actuators attached to the leg (through a shoe and knee-brace) and aligned approximately between the knee and the ball of the foot. The sum of the actuator forces generates a dorsi-flexion/plantar-flexion torque; their difference generates an inversion/eversion torque. Anklebot is able to apply actively controllable torques up to 23 N-m (DP) and 15 N-m (IE) simultaneously. Position information is provided by two linear incremental encoders (Renishaw) with a resolution of 5×10^{-6} m mounted on the traction drives. Torque is measured by current sensors (Burr-Brown 1NA117P), which provide a measure of motor torque with a nominal resolution of 2.59×10^{-6} N-m.

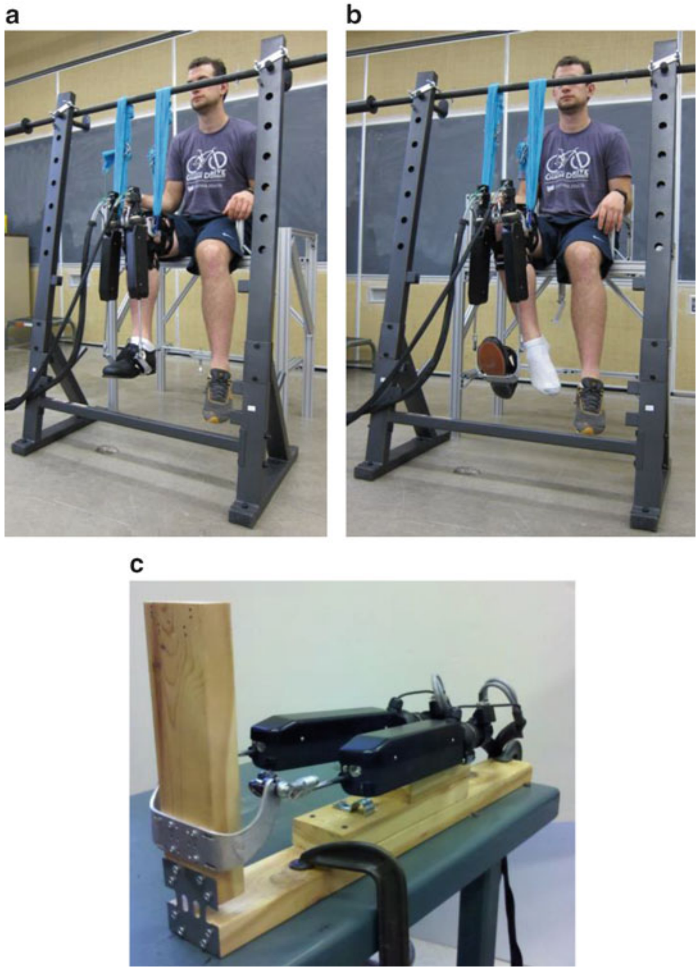

Fig. 6.1 Test setup. (**a**) Anklebot fully attached to a human subject while suspended using a compliant strap. (**b**) Anklebot partially attached to a human subject while suspended using a compliant strap. (**c**) Anklebot attached to ankle mockup

6.2.3 Experimental Protocol

Estimation of ankle mechanical impedance consisted of two steps. First, the subject was seated wearing a knee brace and the Anklebot (Fig. 6.1a). A proportional position controller prevented the ankle joint from drifting and guaranteed safe and stable data capture. Gains of 5, 10 or 15 N-m/rad were used in separate tests. With the subject's foot clear of the ground and his ankle gently held in a neutral position with the sole at a right angle to the tibia, subject was instructed to relax fully and allow the machine to move the foot. Two uncorrelated pseudo-random command voltage sequences with 100 Hz bandwidth and 60 s long, were applied simultaneously to the actuators to produce torque perturbations that rotated the subject's foot in all directions in the frontal and sagittal planes while remaining within the natural limits of the joint. Actuator displacements and command voltages were recorded. The second step repeated this procedure while the human subject was wearing the knee brace with the mounted Anklebot, except that the shoe was connected to the Anklebot actuators but was not worn by the human subject (Fig. 6.1b). This approach provided characterization of the apparatus dynamics including possible dynamic effects from the combined structure of the seat and human body.

To validate this procedure it was also applied to a physical "mockup" of the ankle, consisting of two wooden blocks, one corresponding to the shank, the other to the foot (Fig. 6.1c) and connected at right angles by a stainless steel plate weakened by slots. By design, the rotational stiffness of this plate was highly anisotropic to allow assessment of our method's ability to detect the directional structure of ankle impedance. The shank block was secured to a horizontal table. A connector similar to that used in the Anklebot shoes was secured to the foot block. To avoid plastic deformation of the steel plates, the magnitude of the random signals used with this mockup was 60 % of the magnitude used with human subjects. For comparison, the inertia of the foot block and the stiffness of the steel plate were estimated from their geometric and material properties.

6.2.4 Analysis Methods

The measured variables were the displacements X_L and X_R and commanded forces F_L and F_R in the left and right actuators, respectively. The ankle torques and angles were estimated from a kinematic model of the relation between actuator displacement and joint angular displacement depicted in Fig. 6.2:

$$\tau_{dp} = (F_R + F_L)\, x_{tr,len} \tag{6.1}$$

$$\theta_{dp} = \theta_{dp,offset} + \arctan\left(\frac{X_R + X_L}{2x_{tr,len}}\right) \tag{6.2}$$

$$\tau_{ie} = \frac{1}{2}(F_R - F_L)\, x_{tr,width} \tag{6.3}$$

$$\theta_{ie} = \theta_{ie,offset} + \arctan\left(\frac{X_R - X_L}{x_{tr,width}}\right) \tag{6.4}$$

where τ_{dp} and τ_{ie} are joint torques and θ_{dp} and θ_{ie} are angles in DP and IE directions, respectively. $\theta_{dp,offset}$ and $\theta_{ie,offset}$ are the angles at which the ankle will be centered with respect to the coronal and sagittal planes, respectively. In the experiments in

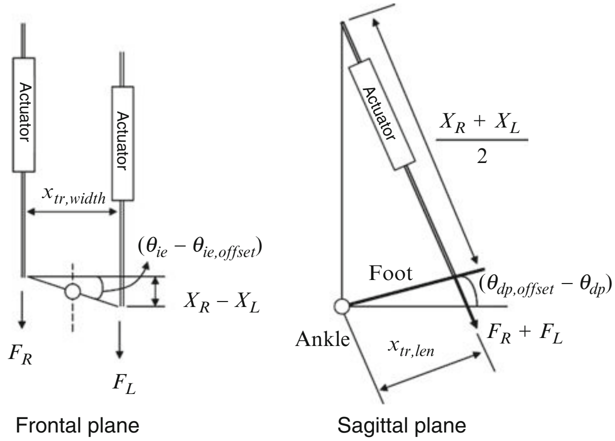

Fig. 6.2 Schematic of Anklebot and its geometrical parameters

this study, their values were zero. The other parameters in Eqs. 6.1, 6.2, 6.3, and 6.4 are described in Fig. 6.2.

Voltage inputs to the actuators generated forces that resulted in ankle motion. A "natural" or strictly proper description of this system is as a mechanical admittance (force input, motion output). Assuming linear dynamics, admittance $\mathbf{Y}(f)$ in DP-IE space is a 2×2 matrix of transfer functions.

$$\begin{Bmatrix} \theta_{dp} \\ \theta_{ie} \end{Bmatrix} = \mathbf{Y}(f) \begin{Bmatrix} \tau_{dp} \\ \tau_{ie} \end{Bmatrix} = \begin{bmatrix} Y_{11}(f) & Y_{12}(f) \\ Y_{21}(f) & Y_{22}(f) \end{bmatrix} \begin{Bmatrix} \tau_{dp} \\ \tau_{ie} \end{Bmatrix} \tag{6.5}$$

If this matrix is non-singular, its inverse is mechanical impedance, $\mathbf{Z}(f) = \mathbf{Y}^{-1}(f)$, a matrix of transfer functions relating input angles to output torques.

$$\begin{Bmatrix} \tau_{dp} \\ \tau_{ie} \end{Bmatrix} = \mathbf{Z}(f) \begin{Bmatrix} \theta_{dp} \\ \theta_{ie} \end{Bmatrix} = \begin{bmatrix} Z_{11}(f) & Z_{12}(f) \\ Z_{21}(f) & Z_{22}(f) \end{bmatrix} \begin{Bmatrix} \theta_{dp} \\ \theta_{ie} \end{Bmatrix} \tag{6.6}$$

A proportional controller with a diagonal gain matrix with identical elements prevented the ankle from drifting from its neutral position.

$$\boldsymbol{\tau} = \mathbf{K}\,(\boldsymbol{\theta}_o - \boldsymbol{\theta}) + \boldsymbol{\tau}_p \tag{6.7}$$

where $\boldsymbol{\tau} = \{\tau_{dp}\ \tau_{ie}\}^T$ is a vector of applied ankle torques, $\boldsymbol{\theta} = \{\theta_{dp}\ \theta_{ie}\}^T$ is a vector of ankle angles, $\mathbf{K}$ is a diagonal gain matrix that determines Anklebot stiffness that prevents the foot from drifting, subscript o denotes the neutral ankle angle, and subscript p denotes perturbation torques. The ankle and Anklebot form a multivariable closed-loop system.

$$\boldsymbol{\theta} = (\mathbf{1} + \mathbf{YK})^{-1}\mathbf{Y}\left(\mathbf{K}\boldsymbol{\theta}_o + \boldsymbol{\tau}_p\right) \tag{6.8}$$

The closed-loop admittance matrix is $\boldsymbol{\theta} = (\mathbf{1} + \mathbf{YK})^{-1}\mathbf{Y}\boldsymbol{\tau}_p$. The closed-loop impedance matrix is its inverse, $\boldsymbol{\tau}_p = \mathbf{Y}^{-1}(\mathbf{1} + \mathbf{YK})\boldsymbol{\theta} = (\mathbf{Z} + \mathbf{K})\boldsymbol{\theta}$, i.e.

$$\begin{Bmatrix} \tau_{dp} \\ \tau_{ie} \end{Bmatrix}_p = \begin{bmatrix} Z_{11}(f) + K & Z_{12}(f) \\ Z_{21}(f) & Z_{22}(f) + K \end{bmatrix} \begin{Bmatrix} \theta_{dp} \\ \theta_{ie} \end{Bmatrix} \tag{6.9}$$

The mechanical impedance of the system under test is

$$\mathbf{Z}(f) = \begin{bmatrix} Z_{11}(f) & Z_{12}(f) \\ Z_{21}(f) & Z_{22}(f) \end{bmatrix} = \begin{bmatrix} \frac{\tau_{dp}(f)}{\theta_{dp}(f)} - K & \frac{\tau_{dp}(f)}{\theta_{ie}(f)} \\ \frac{\tau_{ie}(f)}{\theta_{dp}(f)} & \frac{\tau_{ie}(f)}{\theta_{ie}(f)} - K \end{bmatrix} \tag{6.10}$$

where the impedance functions $\tau_x(f)/\theta_y(f)$ $x, y = dp, ie$ are determined from experimental measurements.

Although the system naturally behaves as a mechanical admittance, expressing it as a mechanical impedance simplifies separating the robot dynamics from the human ankle dynamics. The foot and shoe share the same motion, consequently the torque exerted by the actuator is the sum of the torques required to move the foot and shoe; the output mechanical impedance of the robot adds to the human ankle mechanical impedance. The human ankle mechanical impedance is obtained by subtracting the estimate for robot and shoe alone from the estimate for robot, shoe, and ankle as follows.

$$\mathbf{Z}\,|_{ankle} = \mathbf{Z}|_{ankle+Anklebot \;\; and \;\; shoe} - \mathbf{Z}\Big|_{Anklebot \;\; and \;\; shoe} \tag{6.11}$$

Frequency-domain stochastic methods were used to estimate the mechanical impedance matrices. Sixty seconds of data were sampled at 200 Hz yielding 12,000 samples. Welch's averaged, modified periodogram method of spectral estimation, as implemented in MATLAB was used to estimate one-sided auto- and cross-power spectral densities of the torque and angle sequences in the DP and IE directions. A periodic Hamming window with a length of 512 samples was used with an FFT length of 1,024 samples, yielding a spectral resolution of 0.195 Hz. Power spectral density functions were estimated by averaging their values calculated from 45 data windows with 50 % overlap (256 samples). The standard error of the impedance plots was determined by dividing the standard deviation of impedances at each frequency by $\sqrt{45}$. Elements of the mechanical impedance matrix are presented in Appendix as described in [48]. Moreover, partial coherence functions were estimated to measure the linear dependency between each input and output after removing the effects of the other inputs in the multivariable case (see Appendix).

6.3 Results

6.3.1 Validation Using the Ankle Mockup

Because of the modest torques applied to the physical mockup, its displacements were small (root-mean square actuator displacement was 2.5, 2.4 and 2.3 mm when proportional gains were 5, 10 and 15 Nm/rad, respectively) supporting a linear description of its dynamics. Figure 6.3a shows the partial coherences obtained when the stochastic estimation procedure was applied to the mockup in actuator coordinates (the forces and displacements of the actuators) with proportional gain 10 N-m/rad. The diagonal elements exhibited partial coherences greater than 0.8 at most frequencies from 0 to 50 Hz, averaging 0.86 in the DP and 0.89 in the IE directions over this range. The off-diagonal elements exhibited partial coherences typically greater than 0.8 from 0 to 20 Hz, decreasing to 0.6 at about 30 or 40 Hz and averaging 0.68 from X_R to F_L and 0.75 from X_L to F_R from 0 to 50 Hz. These results demonstrated that, despite the known nonlinearities of the Anklebot actuators (including static friction, primarily due to the traction drives, and "cogging" due to the permanent magnet motors [34]), the linear methods we used gave satisfactory results.

Figure 6.3b shows the partial coherences obtained when the recorded data were first transformed to DP-IE joint coordinates (as detailed in Eqs. 6.1, 6.2, 6.3 and 6.4) before applying the stochastic estimation procedure. Results obtained with four values of the proportional gain ($K = 0$, 5, 10 and 15 N-m/rad) are superimposed, showing that all yielded essentially identical results, along with the results obtained when the actuators were disconnected from the foot block (with $K = 5$ N-m/rad). In this case, the partial coherences of the off-diagonal elements declined to extremely low values, less than 0.2 at most frequencies, averaging less than 0.05 from θ_{ie} to τ_{dp} and from θ_{dp} to τ_{ie} from 0 to 50 Hz for all values of proportional gain. As shown by the partial coherences in Fig. 6.3a, this cannot be attributed to nonlinear dynamics but is due to low signal strength. By design, there is essentially no coupling between the DP and IE degrees of freedom of the mockup; its impedance matrix is essentially diagonal with zero entries in the off-diagonal positions. Confirming this account, the partial coherences of the diagonal elements increased, becoming greater than 0.8 and close to 0.9 at almost all frequencies between 0 and 50 Hz, averaging more than 0.9 from θ_{dp} to τ_{dp} and from θ_{ie} to τ_{ie}, respectively, over this range for all value of proportional gain, indicating that the diagonal elements of a linear model accounted for more of the data variance in joint coordinates.

Figure 6.4 shows Bode plots of the magnitude and phase of the actuator and mockup diagonal mechanical impedances. The impedance of the actuator alone was as expected. A permanent-magnet motor driven by a current-controlled amplifier is competently modeled as a force-controlled actuator retarded by an output impedance dominated by a combination of inertia and damping, and that

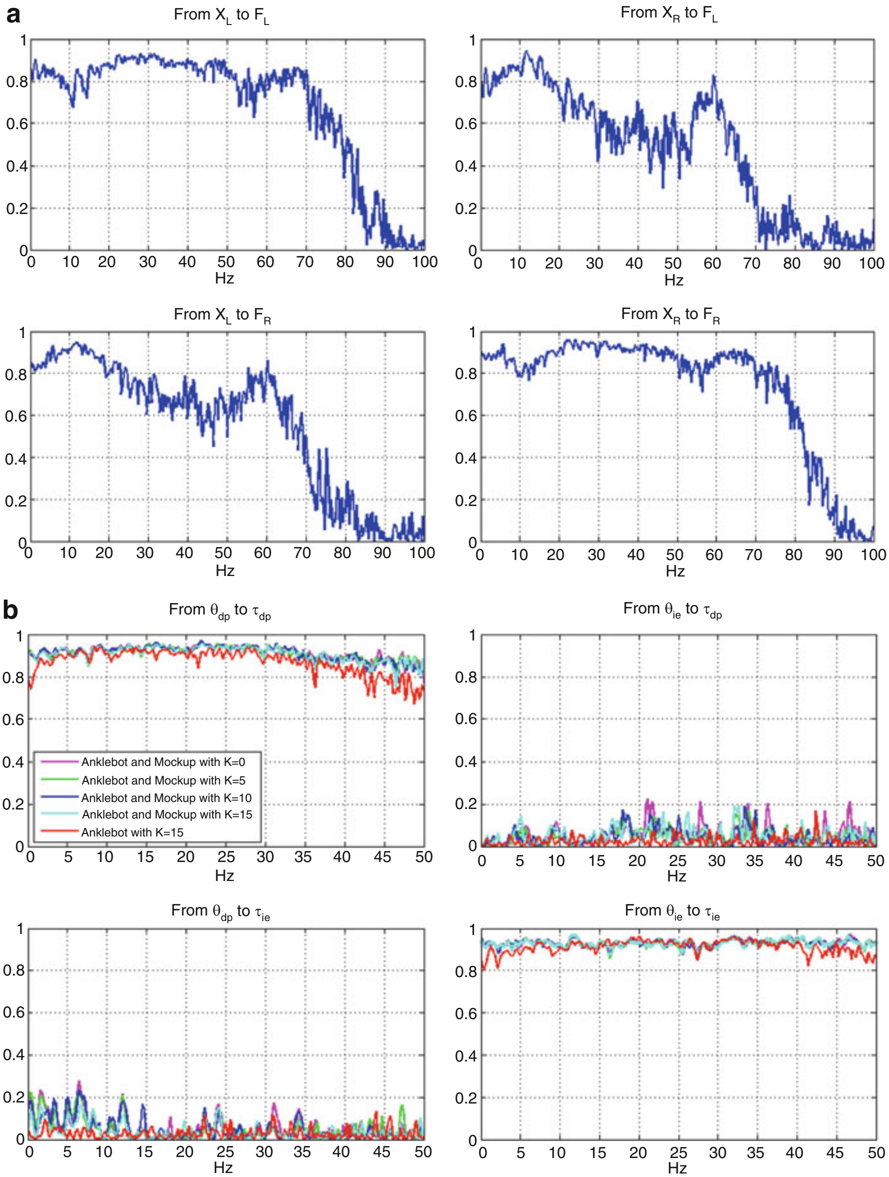

Fig. 6.3 Partial coherences of the mockup impedance matrix, (**a**) in actuator coordinates; (**b**) in joint coordinates

is consistent with these observations. The estimated mechanical impedance of the mockup was obtained by subtraction as described above. Results obtained with four values of the proportional gain, K, are superimposed, and demonstrate that the method was extremely insensitive to this parameter.

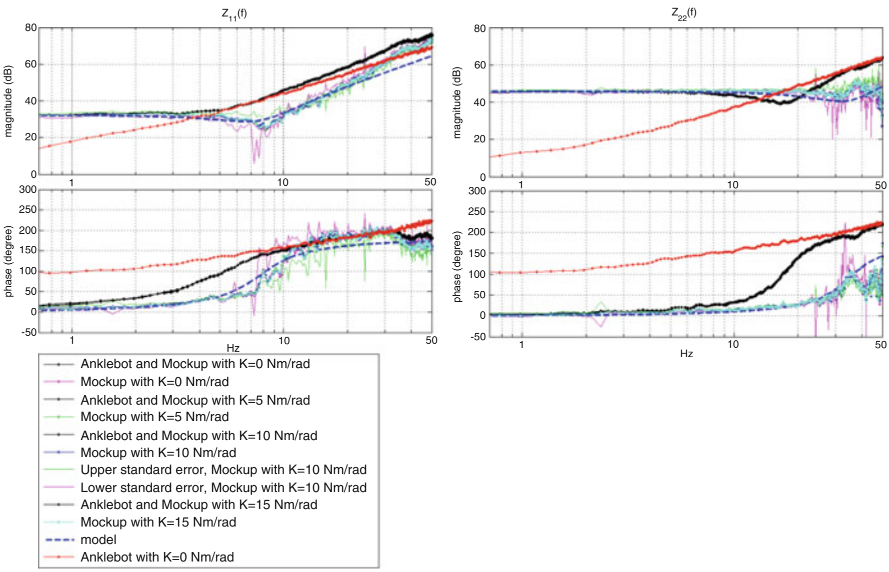

Fig. 6.4 Diagonal elements of the mockup impedance matrix in joint coordinates

A linear second-order model, based on the mockup physical parameters, is also superimposed. In DP the parameter values are inertia: 0.017 kg-m^2; damping: 0.4 N-m-s/rad; stiffness: 40.2 N-m/rad. Parameter values in IE are inertia: 0.004 kg-m^2; damping: 0.5 N-m-s/rad; stiffness: 191 N-m/rad. The model exhibited an undamped natural frequency at 7.7 Hz in DP.

In IE the undamped natural frequency appears to be at 34.8 Hz. However, in both DP and IE, the phase plots showed evidence of returning towards zero degrees, suggesting the presence of a dynamic zero, which may be due to un-modeled resonance, e.g., due to the metal bracket that was mounted on the foot block. As a result, the data at frequencies greater than 30 Hz should be interpreted with caution. Theoretical calculation of the foot block moment of inertia in the DP direction yielded 0.0176 kg-m^2, which differed from the DP model parameter by 3.4 %. Theoretical calculation of the steel plate stiffness in bending yielded 40.0 N-m/rad, which differed from the DP model parameter by 0.5 %.

6.3.2 Human Ankle Mechanical Impedance

6.3.2.1 Coherences

The torques applied to the ankle evoked small angular displacements (root-mean square displacement was 2.48° in DP and 2.70° in IE) consistent with linear analysis. Figure 6.5a shows a representative example of the partial coherences

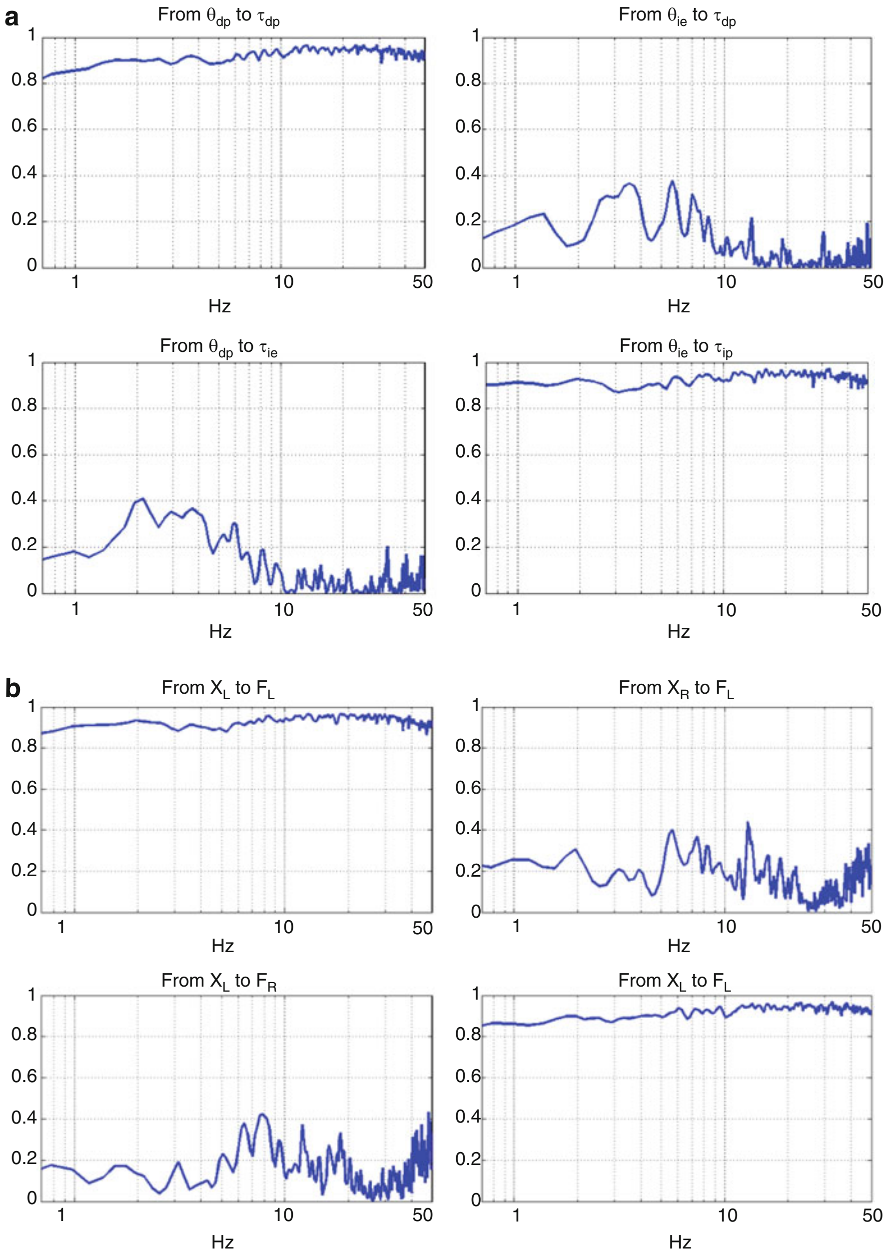

Fig. 6.5 Partial coherence plots of the diagonal elements of the impedance matrix for Anklebot attached to a human ankle with proportional gain $K = 10$ N-m/rad, (**a**) in joint coordinates; (**b**) in actuator coordinates

obtained when the stochastic estimation procedure was applied in joint coordinates. Over a frequency range from 0 to 50 Hz, both of the diagonal elements of the impedance matrix exhibited a partial coherence averaging 0.93, with a minimum of 0.84 at 0.78 Hz for Z_{11} and 0.87 at 3.12 Hz for Z_{21}. A proportional gain of $K = 10$ N-m/rad was used to prevent the ankle from drifting from its neural position. Almost identical results were obtained with proportional gains of $K = 5$ and 15 N-m/rad. In contrast, over the same frequency range the off-diagonal elements of the impedance matrix exhibited low coherence averaging 0.06. Below 10 Hz the off-diagonal partial coherence improved slightly, peaking at 0.41 at 2.15 Hz for Z_{12} and 0.37 at 5.6 Hz for Z_{21} but yielding averages over 0 to 10 Hz of 0.19 for Z_{12} and 0.20 for Z_{21}. As indicated from the validation tests, this indicates weak coupling between DP and IE throughout most of the frequency range.

Applying the stochastic estimation procedure in actuator coordinates improved the off-diagonal partial coherences (Fig. 6.5b), which averaged 0.18 from 30 to 50 Hz; 0.15 from 0 to 50 Hz; 0.15 from 0 to 30 Hz; and 0.22 from 0 to 10 Hz. However, the diagonal partial coherences remained high, averaging 0.93 from 0 to 50 Hz, indicating that a linear description with principal axes in the sagittal and frontal planes accounted for almost all of the data variance under these conditions.

6.3.2.2 Mechanical Impedance About Principal Axes

Figure 6.6 shows Bode plots of the diagonal impedance magnitude and phase in the DP and IE directions with their associated standard errors for this subject. Included in the plot are data obtained during both steps of the procedure, with and without the human subject. The estimated mechanical impedance of the ankle was obtained by subtraction of these complex vectors as described above.

At all frequencies, the mechanical impedance in DP was greater than in IE. For example, at low frequencies the impedance magnitude approached an asymptote from which the static impedance (i.e., stiffness) could be estimated. The stiffness in DP was 23.0 dB (14.1 N-m/rad), whereas the stiffness in IE was 17.1 dB (7.1 N-m/rad), 2.0 times smaller. This is consistent with results reported elsewhere [19, 20, 34, 37–39, 17, 18].

Figure 6.7 shows the directional variation of ankle impedance magnitude in DP-IE coordinates. The plots were generated by rotational transformation of the time-history of the torque and angle data from 0° to 90° in 5° increments before performing stochastic identification to find the ankle impedance in two orthogonal directions. To display the directional variation, the impedance magnitude was averaged over two frequency ranges: 0–3 Hz and 3–5 Hz, where the inertia makes minimal contribution to impedance. In the lowest frequency range (0–3 Hz) the average impedance magnitude was greater in DP than IE, resulting in a characteristic "peanut" shape. In the 3–5 Hz range the average impedance in the DP direction increased more than in the IE direction, accentuating this "peanut" shape. Interestingly, the peanut shape was not precisely aligned with the anatomical axes but tilted approximately 20° counter clockwise.

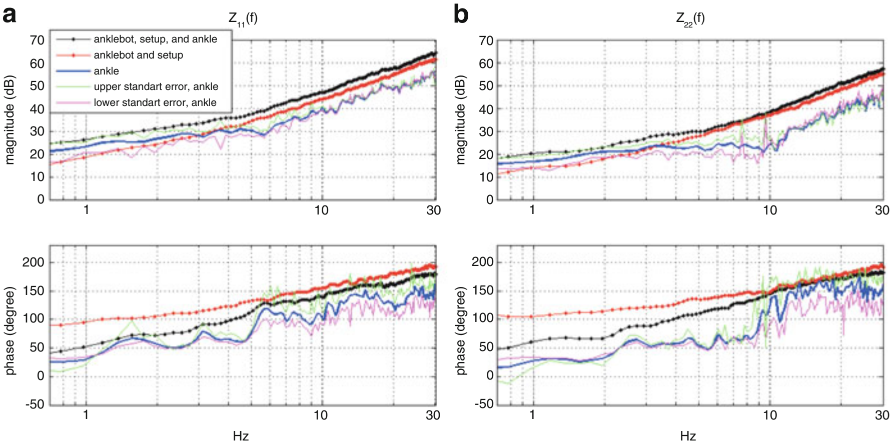

Fig. 6.6 Diagonal elements of the mechanical impedance matrix for Anklebot attached to a human ankle, Anklebot alone, and a human ankle with proportional gain $K = 10$ N-m/rad. (**a**) DP direction; (**b**) IE direction

Fig. 6.7 Spatial variation of ankle impedance magnitude over different frequency ranges. The radius represents impedance magnitude (Nm/rad). Angles 0°, 90°, 180°, and 270° correspond to eversion, dorsiflexion, inversion, and plantarflexion, respectively

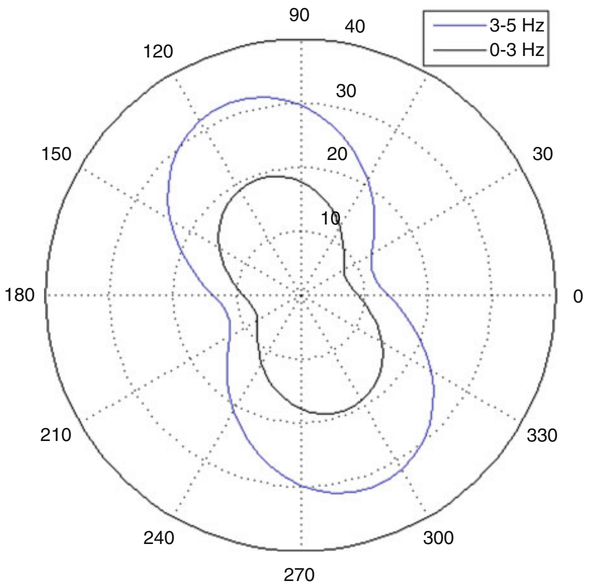

6.3.2.3 Low-Frequency Impedance

At lower frequencies, the mechanical impedance of the ankle passive tissues and lower extremity muscles was evident. To estimate a "break frequency" dividing these two regions, the intersection between a horizontal line through the mean low-frequency magnitude and a straight line least-squares best fit to the magnitude plot at higher frequencies was computed. In DP the mean magnitude between 0.7 and 5 Hz averaged 27.9 dB and the estimated break frequency averaged 5.8 Hz. In IE, the mean magnitude between 0.7 and 8 Hz averaged 22.0 dB and the estimated break frequency averaged 8.8 Hz.

Below this break frequency neither the magnitude nor phase plots were consistent with a simple damped spring, but indicated more complex dynamics. In DP there was a substantial increase of impedance magnitude in the vicinity of 3 Hz, with a corresponding increase of phase below this frequency and decline above it. In IE a similar phenomenon was observed, also in the vicinity of 3 Hz. The mean impedance magnitude in IE between 3 and 8 Hz was 23.1 dB. This exceeded the mean magnitude between 0.7 and 3 Hz, 19.7 dB. On average, the "mid-frequency" impedance magnitude exceeded the static impedance by a factor of 1.9.

Similar results were obtained in DP. The mean impedance magnitude in DP between 3 and 8 Hz was 29.6 dB. This exceeded the mean magnitude between 0.7 and 3 Hz, 26.6 dB. This "mid-frequency" impedance magnitude exceeded the static impedance by a factor of 2.0. Furthermore, the "mid-frequency" impedance magnitude in DP exceeded that in IE by a factor of 2.1.

6.3.2.4 High-Frequency Impedance

In both DOF there was clear evidence that, above the break frequencies, the magnitude plot increased with frequency, consistent with the expected predominance of inertial behavior. Purely inertial behavior corresponds to a slope of 40 dB/decade. In DP, a straight line least-squares best fit to the magnitude plot above 10 Hz yielded an average slope of 37.0 dB/decade. In IE, a straight line least-squares best fit to the magnitude plot above 10 Hz showed an average slope of 49.6 dB/decade.

Predominantly inertial behavior should also be accompanied by monotonic convergence of phase towards 180° with increasing frequency. However, though phase initially increased around the break frequencies, at still greater frequencies (in the vicinity of 20 Hz) it declined, indicating the presence of higher modes of vibration.

6.4 Discussion

This study presented a method for estimating the multi-variable mechanical impedance of the human ankle. The method was applied to one young male subject with no biomechanical or neurological disorders to identify his relaxed ankle mechanical impedance in DP and IE simultaneously.

Spatial variation of ankle impedance magnitude in the low frequency range was not precisely aligned with the anatomical axes but tilted approximately 20° counter clockwise. The maximum magnitude of the impedance in the DP direction can be achieved by projecting the maximum ankle impedance magnitude onto the

DP axis. It implies multiplying the maximum magnitude by cosine (20°) that is 0.94. This led to one unanticipated result of this study, that multivariable ankle mechanical impedance was predominantly oriented along axes in the sagittal plane (DP) and frontal plane (IE) with little coupling between these DOF. Using DP-IE joint coordinates, the diagonal elements of the mechanical impedance matrix exhibited partial coherences close to unity over a frequency range from 0 to as high as 60 Hz, indicating that a linear model of DP and IE impedance with zero cross-coupling would account for almost all of the variance in the data.

However, the musculo-skeletal anatomy of the human ankle is not simply organized along axes in the sagittal and frontal planes. Although the tibiotalar articulation (primarily responsible for dorsi-plantar flexion) may be approximated as a revolute joint with axis perpendicular to the sagittal plane (but see Ref. [49] for the single axis representation of the overall rotation of the ankle), the axis of the subtalar articulation (primarily responsible for inversion-eversion) is perpendicular to neither the sagittal nor frontal planes [36]. Furthermore, the lines of action of several musculo-tendon actuators (e.g., tibialis anterior, peroneus longus) lie neither in the sagittal nor frontal planes [50]. As a result, their tensions contribute both DP and IE torques simultaneously.

Given this biomechanical complexity, the lack of coupling we observed is remarkable. Ankle mechanical impedance arises from an interplay of skeletal, muscular and possibly neural factors, and contributes to several aspects of lower-limb function, including shock-absorption at foot-strike. The momentum absorbed by the leading leg at foot-strike is directed primarily in the plane of progression, the sagittal plane. Any coupling in the multivariable ankle mechanical impedance would re-direct this momentum to evoke displacement in the frontal plane, about the axis of lowest ankle impedance, eversion/inversion. It may, therefore, be advantageous to minimize the coupling between degrees of freedom. Hence the lack of coupling we observed may represent a functional adaptation of the ankle as a whole.

6.4.1 Dynamic Complexity of Ankle Mechanical Impedance

Although the Anklebot and its actuators include known nonlinearities, the linear methods used yielded a satisfactory and physically meaningful characterization of the mockup. In joint angle coordinates, the partial coherences for the off-diagonal elements of the impedance matrix were essentially zero—as they should have been, given the physical lack of coupling in the device.

Conversely, the partial coherences for the diagonal elements of the impedance matrix were close to unity at frequencies up to 40 Hz (Fig. 6.3b). Thus, despite the limitations of our apparatus, our methods were accurate over the frequency range of interest for studies of the biomechanics and neural control of the ankle.

The stochastic identification procedure we used exerted a random vibratory torque on the ankle. That vibratory input might have evoked abnormal neural activity which, in turn, may have affected the apparent mechanical impedance of the ankle. However, because we imposed a random vibratory torque, rather than motion, the "natural" low-pass character of the limb admittance resulted in a relative attenuation of ankle motion at higher frequencies and that may have mitigated this possible source of artifact. As matters turned out, the estimates of static mechanical impedance derived from the stochastic identification procedure used here corresponded well with independent measurements made using very slow ramp perturbations designed to minimize spurious activation of muscle spindles [37–39].

A pronounced deviation from second-order mass, spring and damper dynamics was observed at lower frequencies where inertial forces become insignificant and visco-elastic behavior predominates. We estimated a break frequency between "higher" and "lower" regions by intersecting a horizontal line through the low-frequency region (0.7–5 Hz in DP; 0.7 and 8 Hz in IE) with a straight line that best described the rate of magnitude increase at higher frequencies (10–30 Hz); the result was 5.8 Hz in DP and 8.8 Hz in IE. Substantially below these break frequencies, around 2–4 Hz, we observed a non-monotonic change of phase with frequency and a corresponding increase of impedance magnitude. The mean impedance magnitude in a "mid-frequency" region (3–5 Hz in DP and 3–8 Hz in IE) was substantially greater than the static stiffness of the joint: 1.9 times in IE and 2.0 times in DP.

We considered whether this phenomenon might be an artifact of our experimental apparatus and took steps to eliminate it. The lower limb and Anklebot were suspended from a highly compliant elastic support (the blue straps in Fig. 6.1a and b). As a result, resonant modes of vibration due to interaction between the lower limb and the frame supporting the subject were around 0.3 Hz, substantially lower than the frequency range we measured . In a further attempt to eliminate this possible artifact, the behavior of the Anklebot and shoe was measured without the human limb present (Fig. 6.1b) and the result subtracted from measurements with the limb present. Even though the Anklebot was arguably the dominant mass contributing to this resonance (it weighs $\sim$3.5 Kg) its frequency was lower with the limb present (around 0.15 Hz) that eliminated it as a possible artifact. On the other hand, the impedance magnitude plots from the experiment on the mockup did not show this "mid-frequency" phenomenon that led us to investigate the possible contribution of the shoe. An experiment similar to that depicted in Fig. 6.1a, b but using a foot block that could be fit tightly into the shoe did not show this phenomenon, indicating that our apparatus is unlikely to be a source of artifact. Nevertheless, whether the phenomenon we observed is an artifact of our methods or a property of human biomechanics remains to be resolved definitively in future work.

6.4.2 Ankle Mechanical Impedance in the Sagittal and Frontal Planes

The importance of minimizing coupling between sagittal and frontal plane motions was reinforced by our observation that ankle mechanical impedance in IE was substantially smaller than in DP. This is unsurprising at higher frequencies where inertia dominates, as the foot's moment of inertia about the DP axis is clearly greater than about the IE axis. However, IE mechanical impedance was also smaller at lower frequencies, resulting in similar break frequencies. This remarkable observation suggests that neuro-muscular mechanical impedance may have co-evolved with skeletal inertia to produce a dynamically uniform response to perturbations. Static impedance (stiffness) was smaller in IE than DP by more than a factor of two. Mid-frequency impedance was smaller in IE than DP by more than a factor of 3. Because the foot obviously has smaller inertia in IE than DP, this may simply reflect a functional preference to maintain a uniform dynamic response to perturbations in any direction—comparable transient perturbations would be resisted by comparable neuro-muscular responses. Of course, the validity of these speculations remains to be tested by further experimentation.

Although the data reported here were obtained with muscles relaxed, preliminary results with active muscles indicate a similar trend [51]. This is a clinically important finding and indicates the direction of rotation in which the ankle is most vulnerable. Lower frontal-plane mechanical impedance indicates a greater tendency for the foot to roll. Perturbations, e.g., from uneven ground, may evoke excessive displacement and possibly injury of the ankle. That is consistent with the observation that most ankle-related injuries occur in the frontal plane rather than in the sagittal plane [52].

In this chapter, we presented a method for estimating the multivariable mechanical impedance of the human ankle in non-load bearing conditions. This approach may provide information necessary for the design and development of the next generation of lower extremity assistive robots with more anthropomorphic ankle joint dynamics.

Modulation of ankle impedance is a significant characteristic of the human ankle during gait. However, considering the bandwidth limitations of actuators in the current state of technology, modulation of the impedance of an artificial ankle may be facilitated if the ankle joint is primarily designed with an intrinsic passive mechanical impedance similar to that of the human ankle. For example, a multi-axis ankle-foot prosthesis may have a passive mechanical impedance in both sagittal and frontal planes similar to human ankle impedance. Similarly, orthotic or exoskeletal assistive robots may be tailored for each individual user, such that the hybrid system of injured human ankle and assistive device possesses a passive mechanical impedance similar to the average unimpaired human ankle.

Incorporating design features that allow these devices to mimic the mechanical impedance of the human ankle in both sagittal and frontal planes may increase their weight and complexity; but this may be offset by their advantages. A more anthropomorphic ankle joint may improve gait dynamics and, as a result, lower the overall metabolic cost of gait, as well as reduce the occurrence of secondary injuries. Multi-axial orthotic and prosthetic ankle joints promise to allow better accommodation to terrains with different profiles of elevation and inclination. They also may offer better maneuverability that may, in turn, lead to increased mobility and hence improve general health and well-being.

Acknowledgments The authors would like to acknowledge the support of Toyota Motor Corporation's Partner Robot Division. H. Lee was supported in part by a Samsung Scholarship.

Appendix

Elements of the mechanical impedance matrix were found as described in [38].

$$\mathbf{Z} = \frac{1}{1-\gamma^2{}_{\theta_{dp}\theta_{ie}}}\begin{bmatrix} \frac{P_{\theta_{dp}\tau_{dp}}}{P_{\theta_{dp}\theta_{dp}}}\left(1-\frac{P_{\theta_{dp}\theta_{ie}}P_{\theta_{ie}\tau_{dp}}}{P_{\theta_{ie}\theta_{ie}}P_{\theta_{dp}\tau_{dp}}}\right) & \frac{P_{\theta_{ie}\tau_{dp}}}{P_{\theta_{ie}\theta_{ie}}}\left(1-\frac{P_{\theta_{ie}\theta_{dp}}P_{\theta_{dp}\tau_{dp}}}{P_{\theta_{dp}\theta_{dp}}P_{\theta_{ie}\tau_{dp}}}\right) \\ \frac{P_{\theta_{dp}\tau_{ie}}}{P_{\theta_{dp}\theta_{dp}}}\left(1-\frac{P_{\theta_{dp}\theta_{ie}}P_{\theta_{ie}\tau_{ie}}}{P_{\theta_{ie}\theta_{ie}}P_{\theta_{dp}\tau_{ie}}}\right) & \frac{P_{\theta_{ie}\tau_{ie}}}{P_{\theta_{ie}\theta_{ie}}}\left(1-\frac{P_{\theta_{ie}\theta_{dp}}P_{\theta_{dp}\tau_{ie}}}{P_{\theta_{dp}\theta_{dp}}P_{\theta_{ie}\tau_{ie}}}\right) \end{bmatrix} \tag{6.A.1}$$

where P_{xy} denotes the cross-power spectral density of two data sequences x and y (time sequences of input torques and output angles in the DP and IE directions) and $\gamma^2{}_{xy}(f)$ is the ordinary coherence function between two data sequences x and y defined as

$$\gamma^2{}_{xy}(f) = \frac{\left|P_{xy}(f)\right|^2}{P_{xx}(f)P_{yy}(f)} \tag{6.A.2}$$

A coherence function indicates linear dependency between two time sequences. In the multivariable case, the appropriate measure is partial coherence which measures the linear dependency between each input and output after removing the effects of the other inputs. The partial coherence matrix is defined as

$$\begin{aligned}\boldsymbol{\Omega}^2 &= \begin{bmatrix} \Omega^2{}_{11} & \Omega^2{}_{12} \\ \Omega^2{}_{21} & \Omega^2{}_{22} \end{bmatrix} \\ &= \begin{bmatrix} \frac{\left|P_{\theta_{dp}\tau_{dp}}P_{\theta_{ie}\theta_{ie}}-P_{\theta_{ie}\tau_{dp}}P_{\theta_{dp}\theta_{ie}}\right|^2}{P_{\theta_{ie}\theta_{ie}}P_{\theta_{ie}\theta_{ie}}P_{\theta_{dp}\theta_{dp}}P_{\tau_{dp}\tau_{dp}}\left(1-\gamma^2{}_{\theta_{ie}\theta_{dp}}\right)\left(1-\gamma^2{}_{\theta_{ie}\tau_{dp}}\right)} & \frac{\left|P_{\theta_{ie}\tau_{dp}}P_{\theta_{dp}\theta_{dp}}-P_{\theta_{dp}\tau_{dp}}P_{\theta_{ie}\theta_{dp}}\right|^2}{P_{\theta_{dp}\theta_{dp}}P_{\theta_{dp}\theta_{dp}}P_{\theta_{ie}\theta_{ie}}P_{\tau_{dp}\tau_{dp}}\left(1-\gamma^2{}_{\theta_{dp}\theta_{ie}}\right)\left(1-\gamma^2{}_{\theta_{dp}\tau_{dp}}\right)} \\ \frac{\left|P_{\theta_{dp}\tau_{ie}}P_{\theta_{ie}\theta_{ie}}-P_{\theta_{ie}\tau_{ie}}P_{\theta_{dp}\theta_{ie}}\right|^2}{P_{\theta_{ie}\theta_{ie}}P_{\theta_{ie}\theta_{ie}}P_{\theta_{dp}\theta_{dp}}P_{\tau_{ie}\tau_{ie}}\left(1-\gamma^2{}_{\theta_{ie}\theta_{dp}}\right)\left(1-\gamma^2{}_{\theta_{ie}\tau_{ie}}\right)} & \frac{\left|P_{\theta_{ie}\tau_{ie}}P_{\theta_{dp}\theta_{dp}}-P_{\theta_{dp}\tau_{ie}}P_{\theta_{ie}\theta_{dp}}\right|^2}{P_{\theta_{dp}\theta_{dp}}P_{\theta_{dp}\theta_{dp}}P_{\theta_{ie}\theta_{ie}}P_{\tau_{ie}\tau_{ie}}\left(1-\gamma^2{}_{\theta_{dp}\theta_{ie}}\right)\left(1-\gamma^2{}_{\theta_{dp}\tau_{ie}}\right)} \end{bmatrix}\end{aligned} \tag{6.A.3}$$

References

1. Goldfarb M (2010) Powered robotic legs—leaping toward the future. National Institute of Biomedical Imaging and Bioengineering
2. Sup F, Bohara A, Goldfarb M (2008) Design and control of a powered transfemoral prosthesis. Int J Robot Res 27:263–273
3. Sup F, Varol HA, Mitchell J, Withrow TJ, Goldfarb M (2009) Preliminary evaluations of a self-contained anthropomorphic transfemoral prosthesis. IEEE ASME Trans Mechatron 14(6):667–676
4. Sup F (2009) A powered self-contained knee and ankle prosthesis for near normal gait in transfemoral amputees. Vanderbilt University, Nashville
5. Au SK (2007) Powered ankle-foot prosthesis for the improvement of amputee walking economy. Massachusetts Institute of Technology, Cambridge
6. Au SK, Herr H (2008) Powered ankle-foot prosthesis. Robot Automat Magazine 15(3):52–59
7. Au SK, Weber J, Herr H (2009) Powered ankle-foot prosthesis improves walking metabolic economy. IEEE Trans Robot 25(1):51–66
8. BiOM (2013) Personal bionics. http://www.Biom.com/
9. Eilenberg MF, Geyer H, Herr H (2010) Control of a powered ankle–foot prosthesis based on a neuromuscular model. IEEE Trans Neural Syst Rehab Eng 18(2):164–173
10. Lamontagne A, Malouin F, Richards CL (1997) Viscoelastic behavior of plantar flexor muscle-tendon unit at rest. J Orthop Sports Phys Ther 26(5):244–252
11. Harlaar J, Becher J, Snijders C, Lankhorst G (2000) Passive stiffness characteristics of ankle plantar flexors in hemiplegia. Clin Biomech 15(4):261–270
12. Singer B, Dunne J, Singer K, Allison G (2002) Evaluation of triceps surae muscle length and resistance to passive lengthening in patients with acquired brain injury. Clin Biomech 17(2):151–161
13. Chung SG, Rey E, Bai Z, Roth EJ, Zhang L-Q (2004) Biomechanic changes in passive properties of hemiplegic ankles with spastic hypertonia. Arch Phys Med Rehab 85(10):1638–1646
14. Rydahl SJ, Brouwer BJ (2004) Ankle stiffness and tissue compliance in stroke survivors: a validation of myotonometer measurements. Arch Phys Med Rehab 85(10):1631–1637
15. Kobayashi T, Leung AKL, Akazawa Y, Tanaka M, Hutchins SW (2010) Quantitative measurements of spastic ankle joint stiffness using a manual device: a preliminary study. J Biomech 43(9):1831–1834
16. Gottlieb GL, Agarwal GC (1978) Dependence of human ankle compliance on joint angle. J Biomech 11(4):177–181
17. Hunter IW, Kearney RE (1982) Dynamics of human ankle stiffness: variation with mean ankle torque. J Biomech 15(10):742–752
18. Kearney RE, Hunter IW (1982) Dynamics of human ankle stiffness: variation with displacement amplitude. J Biomech 15(10):753–756
19. Weiss PL, Kearney RE, Hunter IW (1986) Position dependence of ankle joint dynamics—I. Passive mechanics. J Biomech 19(9):727–735
20. Weiss PL, Kearney RE, Hunter IW (1986) Position dependence of ankle joint dynamics—II. Active mechanics. J Biomech 19(9):737–751
21. Mirbagheri MM, Kearney RE, Barbeau H (1996) Quantitative, objective measurement of ankle dynamic stiffness: intra-subject reliability and intersubject variability. In: Proceedings of the 18th annual international conference of the IEEE Engineering in Medicine and Biology Society, Amsterdam
22. Kearney RE, Stein RB, Parameswaran L (1997) Identification of intrinsic and reflex contributions to human ankle stiffness dynamics. IEEE Trans Biomed Eng 44(6):493–504
23. Sinkjaer T, Toft E, Andreassen S, Hornemann BC (1998) Muscle stiffness in human ankle dorsiflexors: intrinsic and reflex components. J Neurophysiol 60(3):1110–1121
24. Kirsch RF, Kearney RE (1997) Identification of time-varying stiffness dynamics of the human ankle joint during an imposed movement. Exp Brain Res 114:71–85

25. Winter DA, Patla AE, Rietdyk S, Ishac MG (2001) Ankle muscle stiffness in the control of balance during quiet standing. J Neurophysiol 85:2630–2633
26. Morasso PG, Sanguineti V (2002) Ankle muscle stiffness alone cannot stabilize balance during quiet standing. J Neurophysiol 88(4)
27. Loram ID, Lakie M (2002) Direct measurement of human ankle stiffness during quiet standing: the intrinsic mechanical stiffness is insufficient for stability. J Physiol 545(3):1041–1053
28. Loram ID, Lakie M (2002) Human balancing of an inverted pendulum: position control by small, ballistic-like, throw and catch movements. J Physiol 540(3):1111–1124
29. Davis R, Deluca P (1996) Gait characterization via dynamic joint stiffness. Gait Posture 4(3):224–231
30. Palmer M (2002) Sagittal plane characterization of normal human ankle function across a range of walking gait speeds. Massachusetts Institute of Technology, Cambridge
31. Hansena AH, Childress DS, Miff SC, Gard SA, Mesplay KP (2004) The human ankle during walking: implications for design of biomimetic ankle prostheses. J Biomech 37:1467–1474
32. Saripalli A, Wilson S (2005) Dynamic ankle stability and ankle orientation. http://www.staffs.ac.uk/isb-fw/ISBFootwear.Abstracts05/Foot53.Saripalli.AnmkleStability.pdf
33. Zinder SM, Granata KP, Padua DA, Gansneder BM (2007) Validity and reliability of a new in vivo ankle stiffness measurement device. J Biomech 40:463–467
34. Roy A, Krebs HI, Williams DJ, Bever CT, Forrester LW, Macko RM, Hogan N (2009) Robot-aided neurorehabilitation: a novel robot for ankle rehabilitation. IEEE Trans Robot Autom 25(3):569–582
35. Roy A, Krebs HI, Bever CT, Forrester LW, Macko RF, Hogan N (2011) Measurement of passive ankle stiffness in subjects with chronic hemiparesis using a novel ankle robot. J Neurophysiol 105:2132–2149
36. Arndt A, Wolf P, Liu A, Nester C, Stacoff A, Jones R, Lundgren P, Lundberg A (2007) Intrinsic foot kinematics measured in vivo during the stance phase of slow running. J Biomech 40:2672–2678
37. Ho P, Lee H, Krebs HI, Hogan N (2009) Directional variation of active and passive ankle static impedance. Paper presented at the ASME dynamic systems and control conference, Hollywood
38. Lee H, Ho P, Krebs HI, Hogan N (2009) The multi-variable torque-displacement relation at the ankle. In: Proceedings of the ASME dynamic systems and control conference, Hollywood
39. Lee H, Ho P, Rastgaar M, Krebs HI, Hogan N (2011) Multivariable static ankle mechanical impedance with relaxed muscles. J Biomech 44:1901–1908
40. Lee H, Ho P, Rastgaar M, Krebs H, Hogan N (2013) Multivariable static ankle mechanical impedance with active muscles. IEEE Trans Neural Systems Rehab Eng. doi:10.1109/TNSRE.2013.2262689
41. Rastgaar M, Ho P, Lee H, Krebs HI, Hogan N (2009) Stochastic estimation of multi-variable human ankle mechanical impedance. In: Proceedings of the ASME dynamic systems and control conference, Hollywood
42. Lee H, Krebs HI, Hogan N (2011) A novel characterization method to study multivariable joint mechanical impedance. In: The fourth IEEE Ras/Embs international conference on biomedical robotics and biomechatronics, Roma
43. Lee H, Hogan N (2011) Modeling dynamic ankle mechanical impedance in relaxed muscle. In: Proceedings of the ASME 2011 dynamic systems and control conference, Arlington
44. van der Helm FCT, Schouten AC, Vlugt ED, Brouwn GG (2002) Identification of intrinsic and reflexive components of human arm dynamics during postural control. J Neurosci Methods 119:1–14
45. Buerger SP, Hogan N (2007) Complementary stability and loop-shaping for improved human-robot interaction. IEEE Trans Robot 23(2):232–244
46. Buerger SP, Hogan N (2010) Novel actuation methods for high force haptics. In: Zadeh M (ed) Advances in haptics. In-Tech Publishing, Vukovar
47. Palazzolo JJ, Ferrar M, Krebs HI, Lynch D, Volpe BT, Hogan N (2007) Stochastic estimation of arm mechanical impedance during robotic stroke rehabilitation. IEEE Trans Neural Syst Rehab Eng 15(1):94–103

48. Bendat JS, Piersol AG (1989) Random data analysis and measurement procedures. Wiley, Hoboken
49. Sancisi N, Parenti-Castelli V, Corazza F, Leardini A (2009) Helical axis calculation based on Burmester theory: experimental comparison with traditional techniques for human tibiotalar joint motion. Med Biol Eng Comput 47(11):1207–1217
50. Gray H (1973) Anatomy of the human body. Lea & Febiger, Philadelphia
51. Rastgaar M, Ho P, Lee H, Krebs HI, Hogan N (2010) Stochastic estimation of the multi-variable mechanical impedance of the human ankle with active muscles. In: Proceedings of the ASME dynamic systems and control conference, Boston
52. O'donoghue DH (1984) Treatment of injuries to athletes. Saunders Company, Philadelphia

Part II
Human-Machine Interfaces for Performance Augmentation

Chapter 7
Development of the Quantified Human

Morley O. Stone, Jack Blackhurst, Jennifer Gresham, and Werner J.A. Dahm

Abstract A *Sense-Assess-Augment (SAA)* framework – originally outlined by Galster and Johnson (Sense-assess-augment: a taxonomy for human effectiveness. Technical report. United States Air Force Research Laboratory, Wright-Patterson Air Force Base, 2013) and based loosely on the adaptive system framework of Feigh et al. (Hum Fact 54(6):1008–1024, 2012) – is presented for approaching augmentation of human performance. While the SAA framework has broad application across all three elements of human-computer interaction, including the machine, the human-machine interface, and the human operator, here we focus on its role for human performance augmentation. SAA begins with the human, sensing their physical, physiological, and psychological state. *Sensing* is the most mature piece of the SAA paradigm, because it leverages the considerable commercial investments in wearable sensors for athletics, healthcare, and human productivity. As a result, sensors exist or are in development that can measure a wide range of physiological parameters, such as brain activity, eye movement, skin temperature, and increasingly biological performance markers, such as blood glucose levels and molecules like orexin that indicate the onset of fatigue. *Assessment* involves aggregation of data from multiple sensors, algorithmic processing of the data, and correlation of the results to behaviors and actions of interest. The challenge is to empirically make sense of the data in relation to baselines that vary between and within individuals, and the needs of a task at hand that is shared by both human and machine and

M.O. Stone (✉) • J. Blackhurst
Air Force Research Laboratory, Wright-Patterson AFB, OH 45433, USA
e-mail: morley.stone@us.af.mil

J. Gresham
Florida Institute for Human and Machine Cognition, Ocala, FL, USA

W.J.A. Dahm
Security & Defense Systems Initiative (SDSI), Arizona State University, Tempe, AZ 85287-5604, USA

P. Artemiadis (ed.), *Neuro-Robotics: From Brain Machine Interfaces to Rehabilitation Robotics*, Trends in Augmentation of Human Performance 2,
DOI 10.1007/978-94-017-8932-5_7,

that may occur both in real time and across the human lifetime. Finally, based on the assessment, appropriate *augmentation* is delivered, which can take many forms, including redistribution of tasks from man to machine, changes in the operating environment, influences from external hardware, or even the growing use of “electroceuticals” – the use of electric stimulation to augment performance. The SAA framework provides a way of approaching human performance augmentation that is consistent with and leverages the emerging understanding of how humans can interact effectively with autonomous systems in an entirely new socio-technical dynamic.

7.1 Introduction

In 1961, President Kennedy issued a call to Congress and the Nation to put a man on the moon by the end of the decade. So started a decade of incredible advancements commensurate with the “space race”—catapulting computer science and engineering into a central developmental role. The previous decade, John McCarthy had coined the term “artificial intelligence” paving the way for the promise of robots, intelligent machines and other kinds of autonomous systems that would drastically reduce workload and the eliminate drudgery. Optimism abounded as nascent scientific and engineering fields were driven to the design of systems capable of transforming society as we knew it.

The pace of fulfillment on that promise has been astounding, though it has not unfolded as expected. In a mere five decades, computers and robots have become a fixture in everyday life. From robotic vacuum cleaners to wearable computers to the wholesale revamping of how we do our work, the push for smaller, faster, and more intelligent machines has been a success beyond expectation. What’s missing is the concurrent reduction in human workload. The effect has been dubbed the “autonomy paradox”, where the very systems designed to reduce the need for human operators require more manpower to support them. For example, unmanned aircraft carry cameras aloft without a crew, yet require multiple shifts of operators, maintainers and intelligence analysts on the ground to extract useful data. Current estimates for one particular system, the MQ-1/9, show that with nearly 20,000 h of full-motion video being collected each month, analysis personnel outnumber aircrew by 8 to 1 [1].

In recent decades, advancements in the human and biological sciences have been as rapid and transformative as the information and computer sciences. The Human Genome Project has provided a wealth of information that is already changing the way we think about medical care delivery and human performance. And the new White House BRAIN Initiative [2] brings with it the potential for breakthroughs in neuroscience, biology and computational science—much as President Kennedy’s space challenge did for computer science and engineering.

One could view the ongoing interaction and intersection of these transformative areas as the basis for increased speculation around the art-of-the-possible with respect to human performance augmentation (HPA). Below, we present a framework for HPA that borrows heavily from ongoing revolutions spanning mobile health (mHealth) to quantified self (QS) movements.

In this chapter, we discuss a Sense-Assess-Augment (SAA) framework for reviving the role of the human in the development of autonomous, interdependent systems. This will require research and development at each of the touch points: the machine, the human-machine interface, and the human operator. Artificial intelligence and autonomy is where much of the work on the machine is ongoing and much progress is being made. There is tremendous need and opportunity to improve the human side of the equation, and although we will discuss all three pieces of human-computer interaction (HCI), we shall devote most of our focus to human augmentation.

In order to understand the role of the human in future autonomous systems, it is important to draw a distinction between automation and autonomy. Automated processes are now common, particularly in areas like manufacturing, and involve execution and control of a narrowly defined set of tasks without human intervention. Automation is used when the parameters are well-defined and the environment is highly structured. In contrast, autonomous systems can perform tasks in an unstructured environment. Such a system is marked by two attributes: self-sufficiency—the ability to take care of itself—and self-directedness—the ability to act without outside control. Most technological developments today, including "unmanned" air systems, would still be more classified as automation rather than autonomy. For systems to become more autonomous, that is, more self-governing, they will require some type of basal reasoning capability. Reasoning is critical in order to deal with the main sources of brittleness in our systems today: dynamic, complex requirements and environments.

Reasoning, however, does not mean the machine acts alone. The question is not "what can machines do without us?" but "what can machines do with us?" Consider that it was not until the 1990s that the "I" in HCI switched from "interface" to "interaction [3]." It is only recently that adaptive computing based on the executive, affective, and conative state of the user has risen in prominence.

Unfortunately, as Aryeh Finegold noted in 1984, "One of the big problems is the tendency for the machine to dominate the human [4]." Sadly, despite our progress in fields such as artificial intelligence and autonomy over the last several decades, this is still true. This is due in large part to what we call the "leftover" principle of interface design, where the goal is to automate as much work as possible as the human adapts to whatever is leftover. This produces a rigid interaction lacking both in transparency and a bi-directional understanding of intent. The point is that the design parameters for an interdependent (not dependent) human-machine system look very different than a machine designed to maximize autonomy. Johnson et al. proposed [5] that interdependent systems should possess mutual awareness (context), consideration (adjustability) and the capability to support (reciprocation). This means we must design systems such that a machine not only provides support for others' dependence on it but can also deal with its own dependence on others.

7.2 Historical Context and Overview of the Sense-Assess-Augment Model

In 1948, Claude Shannon published his seminal work on information theory [6], describing an ideal communications system where all information sources have a source rate, and the channel through which the source's data travels has a capacity, both of which can be measured. Information can be transmitted only if the source rate does not exceed the channel's maximum capacity, now known as the Shannon limit. This had important implications with the advent of radar, one of the first exquisite pairings of man and machine, where in order to get the system to work at optimal levels, the operator had to be trained in how to discriminate the appropriate signal from an incredibly noisy background. By 1954, signal detection theory was being formally applied to the study of perception and recognition [7].

Shannon's work heralded the start of what psychologists now refer to as the cognitive revolution, spurring the idea that information processing could be used to describe the human as a system consisting of interacting subsystems, each of which operated with various capabilities and capacities. This was a time when the study of human performance was becoming increasingly interdisciplinary [8], with significant influences from the fields of psychology, linguistics, and computer science. As Proctor and Vu [9] put it: "Given the close relation of the information-processing approach to computers and artificial intelligence, and given the view that both humans and machines can be conceived of as being types of symbol manipulators, it seems only natural that the information-processing approach has provided a primary basis for understanding and analyzing human-computer interaction (HCI)." This not only allows for a common lexicon between those studying both humans and machines, but breaks the human-computer interaction into machine and human subsystems which can be analyzed either separately or together.

World War II also heralded a time of immense improvement in aircraft design, accompanied by a feverish rollout of new aircraft models. In that race to production, human factors issues were often overlooked. As an example, there were several known aviation mishaps, where pilots confused landing gear knobs with flaps. This is what spurred the innovative work of Lieutenant Colonel Paul Fitts. In 1954, he published what became known as Fitts' Law [10], a quantitative model relating the speed-accuracy trade-off associated with pointing, whereby targets that are smaller and/or further away require more time to acquire.

$$T = a + b \log_2(1 + \mathrm{D/W}) \tag{7.1}$$

With T equal to the average time required to complete the movement and D (distance) over W (width of target) as a proxy for accuracy; a and b are device dependent constants.

Fitts' law showed a linear relationship between task difficulty and movement time that has proved to be remarkably robust. Although there have been minor modifications since then, the mathematical relationship applies under a variety of conditions, with different limbs, and holds true even without overt motor movements [11]. More fundamentally, it advanced Shannon's work by providing the first empirical determination of the information capacity of the human motor system [12]. Providing a mathematically valid description of human performance was not only revolutionary for its time, it continues to be relevant and advantageous today.

Despite the cognitive revolution, much of the human sciences have remained rooted in empirical versus theory-driven studies. Indeed, as critical as the development and application of information theory has been, it has largely remained more descriptive than explanatory [13]. MacKenzie [14] stated that "despite being robust and highly replicable, Fitts' law remains an analogy waiting for a theory." In many ways, the real fruits of the cognitive revolution have yet to be picked. What distinguishes an engineering discipline is an objective feedback control mechanism. What's needed now is to "close the loop," where the physical and mental states of the operator are fed back into the machine, making the human a more seamless part of the overall system.

James Watson, in his explanation of the goals of behaviorism, says, "Its theoretical goal is the prediction and control of behavior [15]." Without that, as Donald Kennedy so aptly put it, neuro-imaging is akin to post-modern phrenology [16]. As Proctor and Vu stated in their review of Human Factors research progress, "One implication of an emphasis on paradigm shifts is that past research is of little relevance because it is from 'old' paradigms. This view is reinforced within human factors because the field deals with new, increasingly sophisticated technologies" [17].

What we propose in this chapter is a framework that reconciles the behaviorists' demand for objective data with the cognitive desire to understand mental processes directly. If one hopes to design human performance with the same precision as a circuit (or in concert with a circuit), a more quantitative, data-driven approach to human augmentation is needed.

With this in mind, we present the sense-assess-augment (SAA) framework [18], which is based loosely on the adaptive system framework originally proposed by Feigh et al. [19]. It begins with the human, sensing their physical, physiological, and psychological state. **Sensing** is the most mature piece of the paradigm, thanks to considerable commercial investment in athletics, healthcare, and productivity. Sensors exist or are in development that can measure a huge range of parameters, such as brain activity, eye movement, skin temperature, and biological performance markers, such as blood glucose levels or molecules like orexin that indicate the onset of fatigue. **Assessment** involves the interpretation of data from multiple, individual sensors and merging it into actionable information. The challenge is to empirically make sense of the data in relation to individual baselines and the needs of the task at hand. Ideally, this is a task shared by both human and machine and happens both in real time and across a lifetime. Finally, based on the assessment, the appropriate **augmentation** is delivered. Augmentation can take many forms, including the redistribution of tasks from man to machine, just in time or chronic uptake of drugs, external hardware, environmental changes, or even genetic engineering. We will discuss each of these pieces in more detail below.

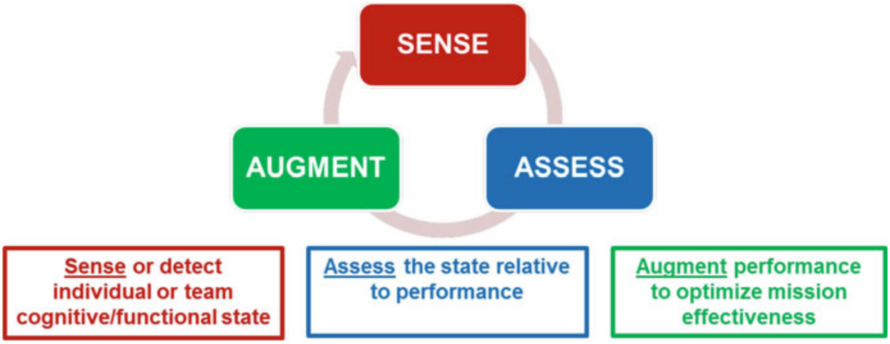

Fig. 7.1 Sense-assess-augment framework (From Galster and Johnson [18])

Each piece of the framework is critical to the design and deployment of human augmentation. Sensing without assessment is frustrating. It is, in fact, one of the most common complaints of consumers trying to make sense of the athletic, health, and productivity data they are collecting. Awash in a flood of data, many ask: what does the data mean and how do I alter my performance accordingly?

Augmentation without the sensing and assessment components is not only potentially dangerous, but breeds distrust among the public and policy-makers. For example, the Air Force pilots responsible for the friendly-fire deaths of Canadian troops in Afghanistan in 2003 implicated “go pills” as the cause of the accident. Although the official investigation found no contribution of the drug to the outcome, the public and media [20] were not persuaded. Physiological monitoring and assessment might have provided objective proof whether the cause was poor judgment by the pilot, a side effect of a widely used drug, or a combination of the two that stemmed from individual susceptibility.

Absent the framework described above, the sensing and augmentation communities have largely worked independently, and the assessment piece has lacked a research leader to make significant progress to bridge them. As we will discuss in detail, if there is one lesson learned from the decades of attempting to deliver the many promises of human performance augmentation, it is the necessity and interdependence of the three steps (Fig. 7.1).

7.2.1 Sense

In their article “Beyond Asimov: The Three Laws of Responsible Robotics [21],” Woods and Murphy proposed alternatives to Asimov’s classic laws of robotics, stating “The capability to respond appropriately—responsiveness—may be more important to human-robot interaction than the capability of autonomy.” An unfortunate case in point is the 2010 drone attack that killed 23 Afghan civilians. The primary cause of the accident cited by Air Force and Army officials was information overload [22]. In addition to keeping track of video from the drone, operators were also engaged in "dozens of instant-message and radio exchanges with intelligence analysts and troops on the ground." They failed to mentally account for the children that were part of the civilian assembly.

This is but one illustration that stems from a lack of shared perception between human and machine. There is not only a need, but now the opportunity, to push beyond simple measurements of human experimental feedback, such as filling out surveys or asking people, "Was your workload diminished or not?" Despite unprecedented technological advances, our ability to assess an individual's or team's physical, psychological, and physiological readiness is startlingly unsophisticated. We are blind, for example, to any number of problems that plague human operators:

- When boredom or data overload lead to prolonged lapses of attention
- When emotional resilience hits its breaking point
- When exhaustion or hunger degrade cognitive abilities

The emerging field of neuroergonomics aims to remedy this by decoding the functioning of a healthy brain at work [23]. The work is highly interdisciplinary, drawing from human factors, ergonomics, neuroscience, and machine learning to develop adaptive interfaces that sense and respond to changes in an individual's executive function, an umbrella term that refers to cognitive processes such as planning, working memory, task switching, initiative, and others. These studies are important because, as founder Parasuraman [24] explains, more traditional cognitive science and neuroscience work "often fails to capture the complexity and dynamics of behavior as it occurs naturally in everyday settings. In other cases, the tasks used in laboratory studies may have little or no relation to those confronting people in everyday life."

Another important milestone in personal sensing came in 2007, when two editors at Wired Magazine noticed that trends in life logging, personal genomics, location tracking, and biometrics were starting to converge. Gary Wolf, one of the founders of what became known as Quantified Self, stated "These new tools were being developed for many different reasons, but all of them had something in common: they added a computational dimension to ordinary existence." Today nearly anyone can record a half dozen physiological data streams in his quest to become fitter or healthier, including a log of alpha rhythms to diagnose sleep quality. For an elite athlete or corporate executive, the sky is the limit in terms of quantified physiological parameters. This made the development of unobtrusive, wearable, and robust sensors a commercial industry, enabling performance tracking at the individual level at a cost that would have been unfathomable just a decade ago.

The combination of neuroergonomics and individual tracking allows us to finally escape the tyranny of the "average user" which has dominated HCI philosophies. As discussed earlier, many protocols originate from Fitts and others, who examined the most complicated pairing of man and machine at that time—the airplane cockpit. The idea of an average user worked for pilots who simply had to distinguish between one knob or another on a panel and the time-accuracy trade-offs did not vary significantly across the population of users, given the right training. It was also fine for distinguishing the utility of a keyboard versus a mouse. The same cannot be said for today's information saturated, multi-tasking knowledge worker. There's huge variability in executive function between individuals, as well as differences that alter performance hour to hour, and from day to day. Thus, the complexity and the number of parameters that must now be optimized together fundamentally changes how we need to approach HCI.

Topol describes how individual tracking is already leading to massive changes in the approach to healthcare in his book *The Creative Destruction of Medicine* [25]. An example of particular relevance to HCI and the SAA model is blood glucose monitoring. Until a few years ago, the only way for diabetics to monitor their glucose levels in their day to day life was with finger sticks, using a device to lance one of the fingers to produce a drop of blood which must then be smeared onto a test-stick and read by a small device. This procedure is usually performed four times a day, is inconvenient, somewhat painful, but more importantly, still runs the risk of missing large spikes or drops due to food intake, exercise, or incorrect insulin dosages. Today, continuous glucose monitoring is possible with a sensor that samples glucose levels from the interstitial fluid just beneath the skin using a small, indwelling 27 gauge needle. The device still has its downsides, such as cost and the need to calibrate readings with finger sticks every 12 h. However, the sensor is robust enough that wearers can exercise and shower as normal. Topol describes additional sensors in development, noting "contact lenses can be embedded with particles that change color as the blood sugar rises or falls or the glucose level can be assessed through tears. Another imaginative solution has been dubbed a "digital tattoo" in which nanoparticles are injected to the blood that bind glucose, and emit a fluorescent signal that is quantified by a reader on a smart phone."

The challenge for HCI is to become equally imaginative in what to sense and how to sense it. The artificial intelligence and HCI communities have continued to focus on how the human can better access and utilize computer technology, without mention of how sensing of the human condition and capabilities might also augment the machine. For example, Sandberg writes, "What is new is the growing interest in creating intimate links between the external systems and the human user through better interaction. The software becomes less an external tool and more of a mediating 'exoself.' This can be achieved through mediation, embedding the human within an augmenting 'shell' such as wearable computers or virtual reality, or through smart environments in which objects are given extended capabilities [26]."

We now have the sensors and digital infrastructure to "remotely and continuously monitor each heart beat, moment-to-moment blood pressure readings, the rate and depth of breathing, body temperature, oxygen concentration in the blood, glucose, brain waves, activity, mood—all the things that make us tick [27]." And in response, we can imagine a machine that uses this information to asses the cognitive and affective state of its user and dynamically alter its level of automation and complexity in response. This is not a new idea—the field of human/brain-computer interface has sought such an adaptive interface since man became so dependent on his machine counterpart. But most of instruments used to examine mental workload today, such as electroencephalography (EEG), electrocorticography (ECoG), functional near-infrared spectroscopy (fNIRS), and functional magnetic resonance imagery (fMRI), were designed for laboratory use where issues of wearability, comfort, portability, and robustness are not an issue. In their review, Pickup et al. note [28], "The notion [of mental workload] has found widespread acceptance as of value in assessing the impact of new tasks, in comparing the effects of different or job interface designs and in understanding the consequences of different levels of automation." This highlights that much of the prior HCI work focused on initial design considerations rather than true adaptability.

Beyond simple user experience however, these instruments miss the more common and frequent sources of performance decrement, such as lack of sleep, low blood glucose, emotional distress, sickness, etc. Nor does it account for the growing source of information through mobile and social media. A recent survey [29] found that 75 % of workers access social media on the job from their personal mobile devices at least once a day (and 60 % access it multiple times a day). Without the ability to pinpoint the source of increased mental workload in real time, the proper augmentation strategy may not be implemented.

Biomarkers are essential to this endeavor. In addition to the readouts from EEG for example, peripheral measures largely associated with the autonomic nervous system have proven to be salient as well [30]. Biomarkers can mean different things: blood oxygen levels, eye movements, perspiration levels, posture, or any number of molecular metabolites.

Molecular monitoring has been aided significantly by the development of flexible, dissolvable electronics. Advances in electronics and microfluidics have led to the development of miniaturized "lab-on-a-chip" devices and unobtrusive wearable psychophysiologic sensors that can support the rapidly emerging need to instrument the user and monitor physical and mental states. This monitoring, when fed back into the machine system, can provide a "check engine light" for the operator as well as drive adaptive autonomy based on the real-time needs of the operator to improve overall sociotechnical team mission performance. Recent scientific studies have elucidated several molecular targets of opportunity. For example, the neuropeptide orexin A (hypocretin) has been implicated in arousal/alertness. Deficiency of orexin A results in narcolepsy, while other studies [31] suggest orexin is the central switch between sleep/wake states. Previously, monitoring this peptide in patients required a sample of cerebrospinal fluid—an impractical obstacle to widespread adoption. However, recent advances in biofunctionalized sensors have increased sensitivity for orexin detection over 3 orders of magnitude (pM levels) allowing for peptide detection in saliva—a more preferable biomatrix for sampling.

Another molecular target of opportunity is neuropeptide Y (NPY). This 36 amino acid peptide has been implicated in learning and memory and is produced by the hypothalamus. In one study [32], animals whose behavior was extremely disrupted by induced stress displayed significant down regulation of NPY in the brain, compared with animals whose behavior was minimally or partially disrupted and with unexposed controls. One-hour post-exposure treatment with NPY significantly reduced prevalence rates of extreme disruption and reduced trauma-cue freezing responses, compared with controls. Although most studies on NPY have been performed with rodents, there is accumulating data [33] from the genetic to the physiological to implicate NPY as a potential 'resilience-to-stress' factor in humans as well.

Diabetics are not the only ones who need to be concerned with blood glucose levels. Previous studies have not only shown decreased cognitive performance with low blood glucose, but that increasing blood glucose can partially compensate for decreases in procedural memory due to sleep deprivation [34], a condition that is increasingly common among workers across industries.

As mentioned, one of the biggest challenges is developing sensors that do not themselves impinge on human performance. Current "wet electrode" EEG monitoring, for example, is cumbersome enough to preclude its use except in the most extreme necessities where lapses in performance could mean loss of life (e.g. Flight traffic controllers). Arguably, the future of human performance monitoring may benefit most from advances in materials science, such as recent work [35] utilizing flexible, dissolvable, and unobtrusive electronics. Transient electronics, made of biocompatible metals and encased in silk, are meant to be implanted into the body, do their work for days, weeks, or even months, and then safely dissolve and resorb in the body.

In addition to measuring the human directly, we must also sense the environment to discover the right correlates to understand degraded executive function in context. Lighting, noise levels, and temperature can all impact cognitive function, and perhaps just as importantly, offer some the easiest of potential solutions.

7.2.2 Assess

Man's ability to understand is often outstripped by his ability to measure. Assessment of the context of the psychophysiologic and performance data represents a key underdeveloped area in many systems in need of future research. Knowledge of context and changes in context allow human team members to disambiguate underconstrained data that can have different meanings in different settings. Machine reasoning to understand sensor data related to environmental, system, task planning, and user physical and cognitive state will allow the system to share some level of perception with the human operator in the proper context. Fundamentally, assessment addresses three questions: who should augment, under what conditions, and how can we quantify the effects?

To better understand the challenge of assessment, consider the landmark work of Yerkes and Dodson [36], who in 1908 proposed a relationship between adverse reinforcement and discrimination learning in rats. What became known as the Yerkes-Dodson Law, popularized decades later in a review by Hebb [37], resembles an inverted, U-shaped curve, as shown below. The Hebbian version proposes that at low arousal, people are lethargic and perform badly. As arousal increases,

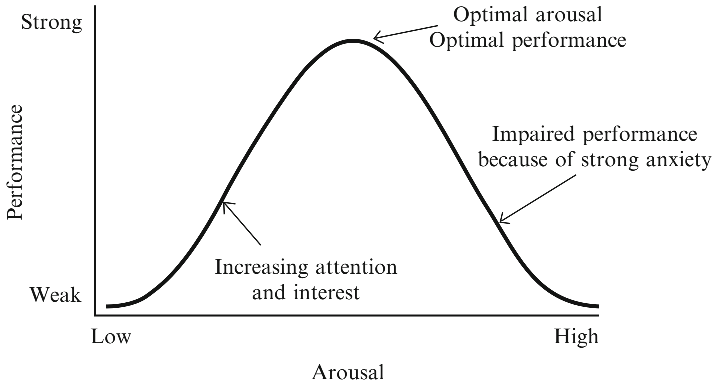

Fig. 7.2 Hebbian version of the Yerkes-Dodson law

performance also increases, but only to a point, after which increasing arousal actually decreases performance. Arousal in this context has often been equated with stress (Fig. 7.2).

Thus one might assume that, given the variety and robustness of sensors today, it should be straightforward to assess from physiological data when a user is experiencing less than optimal arousal in an operational setting and thus enhance the human or adjust the computer interface accordingly to maximize performance. However, there have been many criticisms of the Yerkes-Dodson Law, much of it relating to the misinterpretation [38] of the original work. For example, many modern references use terms such as arousal, stress, and performance, terms that were never used in the original paper and remain vague and un-quantified today. Nor was the original work, which was performed using rats, intended to extend to the relationship between stress and performance in humans. Even those experiments performed with rats produced notable exceptions to the expected curvilinear response. For example, as Easterbrook [39] describes in his paper on cue-utilization theory, “On some tasks, reduction in the range of cue utilization under high stress conditions improves performance. In these tasks, irrelevant cues are excluded and strong emotionality is motivating. In other tasks, proficiency demands the use of a wider range of cues, and strong emotionality is disorganizing. There seems to be an optimal range of cue utilization for each task.” Thus, Easterbrook goes on to explain, tasks can be considered complex if it involves attention to multiple cues and simple if it involves focused attention to a single cue. This may constitute Easterbrook’s definition of difficulty, but it is by no means widely accepted.

The problem extends throughout the human performance community, as well as medicine. In a now famous article, Ioannidis [40] suggested that much of what medical researchers conclude in their studies is misleading, exaggerated, or flat-out wrong. His conclusions are in keeping with the issues of the Yerkes-Dodson Law as well: (1) the smaller the studies, the less likely the research findings are to be true; (2) the smaller the effect, the less likely the research findings are to be true;

(3) the greater the financial and other interests, the less likely the research findings are to be true; (4) the hotter a scientific field (with more scientific teams involved), the less likely the research findings are to be true.

The appeal of the Yerkes-Dodson Law lies in its appeal to our intuition. We have all encountered cases where arousal, in the form of a cup of coffee or an impending deadline, allowed us to focus and perform better than we might have otherwise. Likewise, we have all experienced stress, in form of a cold or an overflowing email inbox, that appeared to degrade performance. What's missing from many of the studies today is the ability to determine the context of stress or arousal, and the patterns that link that context to individual performance. This is critical for determining whether augmentation is needed and the predicted improvement in performance based on the augmentation selected. Such an approach requires, at least initially, the fusion of much more sensory data from both the individual and the environment, than most research currently includes. As Tapscott and Williams warn [41], "When the devices we use to capture and process data are sparsely distributed and intermittently connected, we get an incomplete, and often outdated, snapshot of the real world."

The most common approach to pattern recognition is based on models, such as Markov models or neural networks, which provide some general knowledge of the system they are observing. However, both these approaches require large sets of training data in order to produce accurate results. For example, a study might monitor EEG channels combined with heart rate data as a participant is put through scenarios that are believed to represent low and high mental workload tasks. The training data establishes classification criteria for the two states. As the individual is then tested with real tasks, one sees attribution of low and high mental workload, typically with accuracy in the 80–85 % range. An issue manifests when baselining takes so long that the test subject enters a high stress, disengaged mental state before the experimental portion even begins. Thus, data which are supposed to indicate stress are already one or two standard deviations above baseline and thus little variation is seen in assessed response.

All of this data, however, is taken in a laboratory setting with very controlled parameters and tasks. If the characteristics of the data being analyzed deviate significantly from the training model, then previously learned data sets must be relearned along with the new data set. This means that without retraining, a model that relies on select EEG channels to produce impressive accuracy rates for a vigilance task, for example, often does not work well when applied to a different task in a different setting. This becomes even more problematic when you consider that the average worker engages in several tasks as part of his work, each of which may rely on a distinct assessment or augmentation. One task may require intense vigilance while another may require a mix of creativity, abstract thinking, and the ability to forecast. Today, a study that focuses on assessment of vigilance will be of little consequence to an assessment of creativity.

The answer then is not to collect less data, at least initially. The goal is to collect as much data as possible to discover the relevant performance patterns for each individual. This will likely require a data-driven algorithm that requires no a priori knowledge of the underlying system and can operate without a closed data set. The algorithm would be capable of learning and would include some or all of the following features:

1. Would not need to be tuned based on expected features in a data stream.
2. Able to learn and recognize patterns in an unlabeled data stream.
3. Works online—the process of learning and recognition would occur simultaneously without an offline training phase.
4. Quickly converges to recognize data patterns after only a few occurrences.
5. Finds patterns in nonlinear, nondeterministic, and non-Markovian systems.
6. Interpretable structure and produces an interpretable model.
7. Hierarchical pattern detection for the determination of context.

Such a system is particularly important when trying to merge sensor data across multiple time scales. Many parameters can be measured on an hourly or daily basis, but the trends that indicate the source of aberrations may not be apparent for months. For example, Sky Christopherson, a former Olympic cyclist turned technology CEO, started having health problems despite a lifetime of fitness and healthy eating. Because of his familiarly with personal tracking as an elite athlete, he started collecting a range of biomarkers and environmental data to discover where he could make significant, positive contributions to his health, including sleep, diet, stress, exercise, and traditional physiological measures such blood pressure. One of the most significant causes of stress was related to sleep quality, and only after collecting data for nearly 9 months did he notice trends that varied with the season. His assessment was that the real issue was room temperature that varied with outdoor temperature, so he installed a water-filled cushion on his bed that actively regulated body temperature year round. Although he implemented other changes, the effects were profound. He not only reversed his health issues, but in the process set a world cycling record at the age of 35—a feat previously thought biologically impossible due to declining testosterone levels [42].

It would also be desirable to add a predictive function to the learning algorithm. The simplest method for predicting the next state is based on the probability calculated by the number of times each state has been outputted from the system. Lacking a model for the underlying system itself, this approach might in fact be the only reasonable method of prediction. Future activities include enabling hierarchical and orthogonal learners to detect patterns of patterns, detecting spatial patterns within the model, determining similarity measurements between patterns, and incorporating visualizations of the model to assist human decision-makers in the post-processing step to identify meaningful and more nuanced patterns.

Performance assessments would ideally be quantified relative to an individual baseline collected over time. As we saw with the confusion around the Yerkes-Dodson Law, to say simply classify someone as tired or stressed provides little correlation to performance. But if it were possible to know, for example, when a someone's critical thinking ability decreased by 25 %, a better decision as to how and when to address the symptom of fatigue could be made. Nor should these assessments occur only at the tactical level. Supervisors and leaders are just as likely, if not more so, to be suffering from lack of sleep and exercise, poor nutrition, and information overload that can impair decision-making.

Initially, such a system might sound too complex to be manageable, much less design. However, Kurzweil's view of complexity in his book, *How to Create a Mind*, is undoubtedly relevant. He points out:

> We might ask, is a forest complex? The answer depends on the perspective you choose to take. You could note that there are many thousands of trees in the forest and that each one is different. You could then go on to note that each tree has thousands of branches and that each branch is completely different. Then you could proceed to describe the convoluted vagaries of a single branch. Your conclusion might be that the forest has a complexity beyond our wildest imagination. But such an approach would literally be a failure to see the forest for the trees. Certainly there is a great deal of fractal variation among trees and branches, but to correctly understand the principles of a forest you would do better to start by identifying the distinct patterns of redundancy with stochastic (that is, random) variation that are found there. It would be fair to say that the concept of a forest is simpler than the concept of a tree. [43]

Of course, there are challenges to such an approach as well. As the volume of raw data from various sensors increases, the problem of finding underlying sources within the information becomes more difficult and time consuming. Increasing the spatial resolution increases the number of data channels. Increasing the temporal resolution increases the sampling rate. Such a system would likely require long periods of data collection and analysis, along with input directly from the user, before it was capable of reliably recommending appropriate augmentation strategies.

This suggests that assessment not only needs to happen outside the laboratory, but likely outside the workplace as well. Just as "digital natives" expect to be tethered to their computing devices, those who grow up, literally, with assessment tools will find it just as normal to incorporate sensors both on and off the job to enhance performance. The growing Quantified Self movement indicates this change is already underway. This means that although assessments based primarily on self-learning algorithms will take longer to refine, the end result should be operationally robust for users who begin using them long before entering the workforce. A combination of model-based and self-learning algorithms may make sense in the interim.

So far, we've looked at assessment of a user's physical and cognitive states as they perform tasks, but assessment must also predict the best augmentation strategy and timing, as well as an evaluation of its performance enhancement. Determining returns on investment for augmentation might initially come from population studies of augmentation methods, which are then refined over time as a user implements them. But as Topol describes, there are radical variations in terms of effectiveness, even with vigorously tested substances such as commercial drugs. Part of the problem is a tendency to treat the signal, not the underlying cause (if it's even known). As an example, he discusses the cost-benefit analysis of prescribing statin drugs like Lipitor which lower blood cholesterol and which therefore presumably prevent heart disease [44], "So almost all patients will have a great blood test result with Lipitor.

But only 1 out of 100 without prior heart disease but at risk for developing such a condition will actually benefit. It therefore seems that the predominant benefit is cosmetic, normalizing an out-of-range blood test, at the risk of engendering side effects." It's not that Lipitor, the most widely prescribed drug in the world, isn't effective at lowering blood cholesterol. It's that lowering blood cholesterol doesn't lower the risk of heart disease in most of the population, despite the fact that the correlation exists precisely because of large population studies. Since nearly all measures that we can conceive of today are surrogate measures, the role of assessment is not only to recommend augmentation, but to determine its efficacy.

Perhaps one of the biggest returns on investment for assessment comes from harnessing the power of feedback loops. Some of the most intractable health problems—obesity, diabetes, smoking—have shown progress with biofeedback, with improvement outcomes typically in the range of 10 % [45]. In real terms, that means an obese 40-year-old man would spare himself 3 years of hypertension and nearly 2 years of diabetes by losing 10 % of his weight. Reducing traffic speeds by 10 % from 40 to 35 mph would cut fatal injuries by about half.

What has prevented biofeedback from becoming a mainstay of HCI or other systems is the ability to effortlessly collect and track personalized data. Thus, the assessment tools we have been discussing can now deliver information not in the raw-data form in which it was captured, but in a context that makes it emotionally resonant because it quantifies the consequence of not changing. This is why assessment cannot be the domain of the machine alone, and the currency must be information, not data. The goal is to have shared perception and to make joint decisions about augmentation strategies and timing.

7.2.3 Augment

The rising role of technology in our lives has led to a deep dependency, but not always a harmonious one. From "crackberry" addictions to "digital sabbaticals", there is a kind of begrudging "you can't live with it and you can't live without it" attitude that pervades the relationship between man and machine. The Air Force's Technology Horizons report warns, "Although humans today remain more capable than machines for many tasks, natural human capacities are becoming increasingly mismatched to the enormous data volumes, processing capabilities, and decision speeds that technologies offer or demand; closer human-machine coupling and augmentation of human performance will become possible and essential [46]."

One of the greatest difficulties in developing more adaptive human-computer interactions is that they must accommodate a broad set of tasks, environments, and users. Unlike the pilots in Fitts' experiments, computer users today vary considerably in their cognitive and physical capabilities. This is why future adaptations and augmentations must happen at the individual level, though this is not without its own set of challenges. We define augmentation in a functional sense as enhancing human performance above baseline levels and/or boosting performance to baseline levels after a decrement. Although augmentation strategies may include modifications to the operator, the human-machine interface, or the machine itself, it is important to understand that the desired end result is always focused on improved task outcomes or human performance.

The options for augmentation, once an assessment has determined it is necessary, are extensive. Augmentation may come from increased use of autonomous systems, interfaces for more intuitive and close coupling of humans and automated systems, and direct augmentation of humans via drugs or implants to improve memory, alertness, cognition, or visual/aural acuity. Important considerations when choosing among those options are: (1) machine versus human enhancement, (2) task specific versus lifetime enhancement of the user, and (3) potential trade-off considerations.

(1) Machine versus human augmentation: Most augmentation strategies being considered or deployed today focus on the man-machine interface. For example, in high workload or stressful situations, tasks may move from manual to autonomous control, less critical information may be removed from the display to help the user focus, or the employment of multi-sensory signals to avoid visual overload.

Virtual partners or assistants are another option to machine augmentation. An early example was Microsoft's Clippy, the paperclip that offered advice and access to help topics if you appeared confused. The problem was that Clippy had very limited assessment or interaction with the user and frequently became an annoyance. Advances in the ability to understand natural language and assessment technologies make modern versions more appealing. For example, IBM's supercomputer named Watson, famous for beating the best human contestants at the game Jeopardy!, is now being used as an important diagnostician and consultant to physicians. Watson can help manage the flood of data coming into a patient's electronic record while simultaneously scanning for recent and relevant publications in the literature that might alert a doctor to new therapies or trends. According to Sloan-Kettering, one of the first hospitals to use Watson, it would take at least 160 h of reading a week just to keep up with new medical knowledge as it's published, let alone consider its relevance or apply it practically. In tests, Watson's successful diagnosis rate for lung cancer is 90 %, compared to 50 % for human doctors [47]. It is not just the access to medical literature that's important, but also the computer's lack of cognitive bias in assessing it. It's estimated that one-third of hospital errors are due to misdiagnosis, one of which is anchoring bias, the human tendency to over-rely on the first pieces of information offered when making decisions [48].

On the human side, pharmaceuticals can be used to repair decrements in cognitive function, such as from sleep deprivation or prolonged vigilance, or increase natural capacities. For example, Modafinil and similar alertness or vigilance support pharmaceuticals have been studied extensively by the Army to support aviation operations. Although Modafinil has demonstrated utility in several DoD operational contexts, research now implies that may also offer benefit to sleep-deprived senior decision-makers, with research showing improved planning among their test subjects [49]. More recently, a study of sleep-deprived physicians found the drug improved their cognitive flexibility while reducing impulsive behavior [50].

Interestingly, Modafinil has also been shown to enhance working memory, especially at harder task difficulties for lower-performing subjects [51]. The mode of action is not yet understood, but part of what seems to happen is that Modafinil enhances adaptive response inhibition, making the subjects evaluate a problem more thoroughly before responding, thereby improving performance accuracy [52].

There are many challenges to the use of pharmaceuticals for performance enhancement. Many, of course, have undesirable side effects. More importantly, the current system for the development and approval of pharmaceuticals is geared towards treatment of disease, not augmentation of otherwise healthy individuals. This means that nearly all drugs for enhancement purposes are being prescribed by doctors for "off label" usage. Since drug companies can't market non-therapeutic benefits, tests are rarely run to prove effectiveness and safety of the product in individuals. In order for pharmaceuticals to play a more large-scale role in HCI strategies, current Federal Drug Administration regulatory schemes would need to be reformed. Fortunately, there are many augmentation alternatives outside of pharmaceuticals.

(2) Task specific versus lifetime augmentation: Task specific augmentation often focuses on adaptive interfaces that modulate the speed, amount, and visualization of information. On the human side, techniques such as noninvasive brain stimulation have shown to be effective at improving performance across a wide variety of tasks, presumably by either raising neuronal membrane and force action potential in the case of transcranial magnetic stimulation or altering neuron excitability in a region in the case of transcranial direct current stimulation [53].

Long term augmentation strategies are increasingly being investigated, primarily changes in diet and nutrition. The quantity and quality of dietary choices and distribution of nutrients throughout the day greatly impact muscle performance, body composition, cognitive performance, and feelings of energy or exhaustion. In addition, there is a rapidly expanding body of research showing an ever-increasing linkage between commensal (native gut) bacterial and overall human phenotype, from increased obesity to cognitive metabolites and immune responses [54].

Not surprisingly, effective metabolism is key to both physical and cognitive performance. A wide range of non-pharmaceutical substances are currently under investigation for their ability to enhance cognitive performance through regular ingestion over the long term. Among these are several where the mechanism of action is largely metabolic, such as leucine, creatine, and coenzyme Q10. Recently researchers at MIT and elsewhere have shown substantial cognitive benefits by the use of a newly developed magnesium compound, magnesium-L-threonate (MgT). In animal studies it has been demonstrated that increasing brain magnesium enhances synaptic plasticity in the hippocampus and leads to elevated learning abilities, working memory, and short- and long-term memory [55].

Another promising metabolic target is ketone bodies. Under normal conditions, the brain is totally dependent upon the metabolism of glucose to supply its metabolic energy. However, during starvation, the body normally produces ketone bodies that can then supply the majority of brain energy needs. Not only can ketone bodies replace glucose as the major energy substrate for the brain, the metabolism of ketones instead of glucose, increases the energy contained in the major cellular energy transmitter adenosine triphosphate (ATP [56]). The increased metabolic energy contained in ketone bodies (as opposed to glucose) was recently exploited in a DARPA-funded project (with NIH and Oxford) where a ketone ester was developed that can be administered as a food and which can improve cognitive and physical performance in animals and improve physical performance in humans. An experiment conducted at Oxford University with 22 elite British rowers showed remarkable improvements in performance including 10 season's best, 6 personal best, and 1 world's record an hour after ingestion of the ketone ester. Additionally, in animal studies, substantial improvements in cognitive performance have been seen and human studies are currently underway (personal communication by K. Clarke during DARPA presentation of research results, July 2012).

Another potential target for long term enhancement resides in the microbiome. The enteric nervous system, a collection of neurons in the gut often called "The Second Brain" in the popular press, contains some 100 million neurons, more than either the spinal cord or peripheral nervous system. Approximately 90 % of the nerve fibers in the primary visceral nerve (the vagus) carry information from gut to brain, not the other way around. Recent evidence supports the view that triggers and signals from the gut affect our emotions, decision-making, response to stress, immune response, and learning and memory.

The enteric microbiome of non-human organisms living in the human gut is thought to impact cognitive performance and emotional resilience. A recent study showed that mice receiving *Lactobacillus rhamnosus* were less anxious, performed better on tests for learning and memory, and had lower cortisol levels after stressful situations [57]. Supplemented mice also had atypical mRNA levels for 2 GABA receptors involved in decision-making and learning/memory. Severing the vagus nerve attenuated the effect, implying that commensal bacteria in the gut can have a direct effect on neurotransmitter receptors in the central nervous system in normal, healthy animals.

Nor is the effect limited to animal studies. Oral ingestion of probiotics, which often include *L. rhamnosus*, have also been effective in reducing psychological distress in otherwise normal, healthy humans, while antibiotic use may disturb the microbiome flora population distribution for a poorly understood length of time. In a clinical trial, volunteers participated in a double-blind, placebo-controlled, randomized group study with probiotics administered for 30 days and assessed with the Hopkins Symptom Checklist (HSCL-90), the Hospital Anxiety and Depression Scale (HADS), the Perceived Stress Scale, the Coping Checklist (CCL) and 24 h urinary free cortisol (UFC). Results indicate probiotic administration significantly alleviated psychological distress in volunteers, particularly as measured by the HSCL-90 scale [58].

(3) Potential trade-offs: Augmentation is unlikely to serve as a one-size-fits-all solution, and it's clear that trade-offs may be a consideration with certain cognitive enhancement strategies. For example, genetically engineered mice with extra copies of the NR2B gene have improved memories and learn faster, but they are also more susceptible to addiction and feel pain longer than normal mice [59]. In a documented case of a human with naturally and profoundly enhanced memory, the man was able to remember vast amounts of text on a single reading, even in a unfamiliar, foreign language, but was almost entirely unable to grasp metaphors, as his mind was so fixated on particulars [60]. This anecdotal evidence is in line with computer models that show that memory is actually optimized by slight imperfections, as they allow one to see connections between different but related events [61].

The New York Times also ran a series of essays by students who were otherwise considered healthy but began illicitly taking prescription medications such as Adderall and Ritalin to maintain their edge at competitive schools. These drugs are psychostimulants intended for treatment of attention deficit hyperactivity disorder (ADHD) and narcolepsy, but the essays reveal that those without the condition find benefits too. Students reported the drug provided an almost tunnel-vision like focus, reducing fatigue while reportedly [62] increasing reading comprehension, interest, and memory. But many also found the drugs deliver some unpleasant side effects, especially as they are often abused, such as anxiety, depression, sluggishness, and social withdrawal.

The difficulty is that in most cases, the neural mechanisms underlying cognitive enhancement, particularly in healthy individuals, is poorly understood. With psychostimulants, for example, it was only in 2012 that low-level, cognition-enhancing doses were shown to exert regionally-restricted actions, elevating extracellular catecholamine levels and enhancing neuronal signal processing preferentially within the prefrontal cortex [63]. Little data is available on how effective these neuro-enhancing agents are for non-ADHD users or on long-term side effects. This mismatch between the demand for cognitive enhancers and funded studies on their use may stem from a historical tendency to regulate rather than educate when it comes to human enhancement. The ability to understand the genetic basis for the varying effectiveness of augmentations is improving with technologies such as genome-wide association studies, which have been used to predict drug response based on individual genetic variations [64].

One potential solution to mitigating these trade-offs is to think about augmentation cocktails that make smaller changes across a spectrum of abilities, with the hope the cumulative effect is greater than the sum of its parts. As neuroscience unravels how the brain generates behaviors and integrates multiple kinds of information, such as memories, sensory information, and decisions, more targeted augmentation strategies can be developed. Optogenetics [65], a technique that allows researchers to selectively express or silence neurons in a temporally precise fashion using pulses of light, offers a bit of both. Not only is the technique being used to systematically explore how neural circuits contribute to cognition and behavior, but it has also been used in live animal studies to directly control behaviors such as reward seeking [66]. Nearly all of these options, however, are relatively long-term before they can be integrated into commercial workspaces. In the meantime, we must be aware that trade-offs may exist and they may not be known prior to use. In this regard, the assessment part of the paradigm becomes even more important.

7.3 Future Perspectives

Aristotle once said, “Those who know, do. Those who understand, teach.” Had Aristotle lived during the computer age, he might have concluded his final statement with the word “simulate” instead. At the Dartmouth Conference of 1956, where artificial intelligence (AI) was essentially born, it was proposed [67] “Every aspect of learning or any other feature of intelligence can in principle be so precisely described that a machine can be made to simulate it.” Indeed, the driving assumption of artificial intelligence is that when we have created a machine that can pass the Turing Test with flying colors, we will have laid bare the underpinnings that make the human mind possible. And while significant progress has been made in the creation of machines capable of performing like humans and sometimes better, it is fair to say that a coherent theory of the mind, particularly one that links the underlying biology with behavior, has lagged far behind.

Thus when Newell, one of the founding fathers of AI, grew frustrated with the progress of cognitive science in 1980 (and again in 1990), his proposed solution was shaped by the governing principles of AI. Anderson and Lebiere [68] describe Newell’s thoughts on the matter as thus, “He would point to such things as the ‘schools’ of thought, the changes in fashion, the dominance of controversies, and the cyclical nature of theories. One of the problems he saw was that the field had become too focused on specific issues and had lost sight of the big picture needed to understand the human mind.” In response, Newell made two contributions that would ultimately drive the field of computational cognition. First, he proposed a set of functional criteria for the evaluation of cognitive theories that forced researchers to break out of what Newell feared was a kind of theoretical myopia, where models explained their own results but made little sense in the greater context of what was already understood or observed. One can debate whether Newell’s criteria are the right ones (and many have), but the result has been the development of increasingly sophisticated cognitive architectures that combine psychological, and more recently neuroscientific [69], knowledge with developments from artificial intelligence to produce a powerful general-purpose engine of cognition.

Newell’s second major contribution was his four bands of cognition—the biological, the cognitive, the rational, and the social—that delineate the outcomes of cognition based on the speed at which they typically occur [70]. Each successive band captures the human experience at roughly 3 orders of magnitude greater than the previous (see Table 7.1). Newell thought the cognitive band was most relevant to a theory of cognitive architecture. Given the immaturity of neuroscience or even biology at the time, Newell can hardly be blamed for focusing on the more observable (and programmable) aspects of cognition, but it has had important consequences, namely the instantiation of symbolism as the primary basis of cognitive architectures. In 1980, he stated “symbolic behavior (and essentially rational behavior) becomes relatively independent of the underlying technology. Applied to the human organism, this produces a physical basis for the apparent irrelevance of the neural level to intelligent behavior [71].” And although more

Table 7.1 Newell's time scales of human action

Scale (s)	Time units	System	World (theory)
10^7	Months		Social band
10^6	Weeks		
10^5	Days		
10^4	Hours	Task	Rational band
10^3	10 min		
10^2	Minutes		
10^1	10 s	Unit task	Cognitive band
10^0	1 s	Operations	
10^{-1}	100 ms	Deliberate act	
10^{-2}	10 ms	Neural circuit	Biological band
10^{-3}	1 ms	Neuron	
10^{-4}	100 μs	Organelle	

recent architectures have penetrated into Newell's biological band, as Anderson explains, "the approach in cognitive psychology has largely been not to actually model the biological processes but rather to describe them at some level of abstraction. This level is called the subsymbolic level [72]." To use an analogy to computer systems, the assumption has been that to understand intelligent thought, we need to focus on the software, not the hardware that performs the calculations.

The comparison between biological and information systems turns out to be quite useful for examining concepts such as constraints, tradeoffs, and layered architectures. However, it must be noted that the delineation between hardware and software in computer systems is quite obvious, whereas in biological systems (including the brain), chemistry is involved at every level. In either case, Doyle and Csete effectively argue that "robust yet fragile" control systems are the key to understanding such complex systems [73]. They point out, "This enormous, hidden, cryptic complexity, driven by robustness, is both the greatest initial obstacle in using advanced information and control technologies as metaphors for biology and also ultimately, the key to important insights and theories." Thus, in order to fully capitalize on complexity, one must develop (1) a thorough understanding of the protocols that drive interaction between layers and modules, and (2) an understanding of robustness trade-offs which drive complexity.

This first point calls into question whether Newell's bands of the cognition, based on temporal duration, are the right hierarchy for architecture evaluation. The fact that existing architectures such as ACT-R and SOAR work as well as they do suggests the symbolic layer of cognition was likely the right starting point. Although researchers are successfully transcending multiple timescales as they model more complex tasks [74], this does not mean that a time-based hierarchy is the most productive one. For example, Sun 75et al. [75] have proposed four layers—physiological, componential, psychological, and social/cultural. At first glance, these appear remarkably similar to Newell's, but in this case are based on phenomena that occur rather than their duration (Table 7.2).

Table 7.2 Hierarchy of levels from [75]

Level	Object of analysis	Type of analysis	Computational model
1	Inter-agent processes	Social/cultural	Collections of agents
2	Agents	Psychological	Individual agents
3	Intra-agent processes	Componential	Modular construction of agents
4	substrates	physiological	Biological realization of modules

What is important is that these levels interact with and constrain one another in such a way that they cannot be studied solely in isolation. We do not presume that Sun's or anyone else's hierarchical layers necessarily offer the correct level of detail, however we agree with Sun et al. that "The capability, at least in principle, to map collective phenomenological properties all the way down to neural properties (or other detailed level descriptions) is an essential aspect of an effective theory of cognition in a sociocultural context. In contrast, the ability of a high-level theory to accurately model high-level phenomena is a necessary but not sufficient condition for effectiveness." It is not clear how an architecture based on Newell's time-based bands can achieve this. Moreover, if Doyle and Csete are correct that biology is optimized for robustness instead of efficiency, this suggests that a focus on the protocols that connect layers and provide "constraints that de-constrain" may be a better approach. Alderson and Doyle clarify, "In protocol-based architecture (PBA), the protocols (rules of interaction that persist) are more fundamental than the modules (which obey protocols and can change and diversify). PBAs facilitate coherent and global adaptation to variations in both components and the environments on a vast range of time scales despite implementation mechanisms that are largely decentralized and asynchronous [76]."

This point is particularly important for human performance augmentation, since it suggests hard theoretical limits to optimization. We think the SAA framework presented in this chapter will provide essential information for exploring and perhaps elucidating those limits. We argue this idea must be at the heart of good HCI, since we desire to understand not just how an individual human thinks, but how well they perform at any particular point in time. Further, we need cognitive models that allow us to simulate the effect of various augmentation strategies before implementing them. Alderson and Doyle conclude that managing or perhaps preventing the "robust yet fragile" complexity spiral is a key challenge, stating "Indeed, the emergence of complexity can often be seen as a spiral of new challenges and opportunities that organisms and/or technologies exploit, but which also lead to new fragilities, often from novel perturbations." We propose it is impossible to fully address this issue for the purposes of human performance augmentation without simulating more fully the biological body in which the mind resides, particularly the neurotransmitters and metabolites that play a key role in regulating cognition. We think the SAA framework combined with new mathematics and applications of control theory offer much hope in this regard.

References

1. Pocock C (2010) USAF Chief outlines UAVs' manpower needs. AINonline, February
2. http://www.nih.gov/science/brain/. Accessed 31 Jun 2013
3. Hinze-Hoare V (2007) The review and analysis of human computer interaction (HCI) principles. arXiv preprint arXiv:0707.3638
4. Woods DD (1985) Cognitive technologies: the design of joint human-machine cognitive systems. AI Mag 6(4):86–92
5. Johnson M, Bradshaw JM, Feltovich PJ, Jonker CM, van Riemsdijk B, Sierhuis M (2010) The fundamental principle of coactive design: interdependence must shape autonomy. In: De Vos M, Fornara N, Pitt JV, Vouros G (eds) Proceedings of the 6th international conference on coordination, organizations, institutions, and norms in agent systems (COIN@AAMAS'10). Springer, Berlin/Heidelberg, pp 172–191
6. Shannon CE (1948) A mathematical theory of communication. Bell Syst Tech J 27:379–423, 623–656
7. Tanner WP, Swets JA (1954) A decision-making theory of visual detection. Psychol Rev 61:401–409
8. Miller GA (2003) The cognitive revolution: a historical perspective. Trends Cogn Sci 7(3):141–144
9. Proctor RW, Vu KL (2006) The cognitive revolution at age 50: has the promise of the human information-processing approach been fulfilled? Int J Hum-Comput Interact 21(3):253–284
10. Fitts PM (1954) The information capacity of the human motor system in controlling the amplitude of movement. J Exp Psychol 47(6):381–391
11. Papaxanthis C, Schieppati M, Gentili R, Pozzo T (2002) Imagined and actual arm movements have similar durations when performed under different conditions of direction and mass. Exp Brain Res 143:447–452
12. Seow SC (2005) Information theoretic models of HCI: a comparison of the Hick-Hyman law and Fitts' law. Hum-Comput Interact 20:315–352
13. Sanders MS, McCormick EJ (1987) Human factors in engineering and design. McGraw-Hill, New York
14. MacKenzie IS (1992) Fitts' law as a research and design tool in human–computer interaction. Hum–Comput Interact 7:91–139
15. Watson JB (1913) Psychology as the behaviorist views it. Psychol Rev 20(2):158–177
16. Kennedy D (2005) Neuroimaging: revolutionary research tool or a post-modern phrenology? J Bioeth 5(2):19
17. Proctor RW, Vu KL (2010) Cumulative knowledge and progress in human factors. Annu Rev Psychol 61:623–651
18. Galster SM, Johnson EM (2013) Sense-assess-augment: a taxonomy for human effectiveness. Technical report. United States Air Force Research Laboratory, Wright-Patterson Air Force Base
19. Feigh KM, Dorneich MC, Hayes CC (2012) Toward a characterization of adaptive systems: a framework for researchers and system designers. Hum Factors 54(6):1008–1024
20. Borin E (2013) The U.S. Military needs its speed. WIRED (online). Available at: http://www.wired.com/medtech/health/news/2003/02/57434. Accessed 24 May 2013
21. Murphy R, Woods DD (2009) Beyond Asimov: the three laws of responsible robotics. IEEE Intell Syst 24(4):14–20
22. Shanker T, Richtel M (2011) In new military, data overload can be deadly. NY Times, 16 Jan 2011 (Online)
23. Parasuraman R, Rizzo M (2008) Neuroergonomics: the brain at work. Oxford University Press Inc, New York
24. Parasuraman R, Christensen J, Grafton S (2012) Neuroergonomics: the brain in action and at work. NeuroImage 59:1–3

25. Topol E (2011) The creative destruction of medicine: how the digital revolution will create better health care. Basic Books, New York
26. Savulescu J, ter Meulen R, Kahane G (2011) Enhancing human capacities (Kindle locations 2753–2755), Kindle edition. Wiley Publishing, New York
27. Topol E (2011) The creative destruction of medicine: how the digital revolution will create better health care (Kindle locations 199–201). Basic Books, New York
28. Pickup L, Wilson JR, Sharpies S, Norris B, Clarke T, Young MS (2005) Fundamental examination of mental workload in the rail industry. Theor Issues Ergon Sci 6:463–482
29. (2012) Social media & workplace collaboration. (e-book) SilkRoad, p 3. Available through: http://pages.silkroad.com/rs/silkroad/images/Social-Media-Workplace-Collaboration-SilkRoad-TalentTalk-Report.pdf
30. Estepp JR, Christensen JC (2011) Physiological cognitive state assessment: applications for designing effective human-machine systems. In: EMBC, 2011 annual international conference of the IEEE. Engineering in Medicine and Biology Society, pp 6538–6541
31. Tsujino N, Sakurai T (2009) Orexin/hypocretin: a neuropeptide at the interface of sleep, energy homeostasis, and reward system. Pharmacol Rev 61(2):162–176
32. Cohen H, Liu T, Kozlovsky N, Zohar J, Mathe' AA (2012) The neuropeptide Y (NPY)-ergic system is associated with behavioral resilience to stress exposure in an animal model of post-traumatic stress disorder. Neuropsychopharmacology 37(2):350–363
33. Sah R, Geracioti TD (2012) Neuropeptide Y and posttraumatic stress disorder. Mol Psychiatry 18(6):646–655
34. Herzog N, Friedrich A, Fujita N, Gais S, Jauch-Chara K et al (2012) Effects of daytime food intake on memory consolidation during sleep or sleep deprivation. PLoS One 7(6):e40298
35. Hwang SW, Tao H, Kim DH, Cheng H, Song JK et al (2012) A physically transient form of silicon electronics. Science 337:1630–1644
36. Yerkes RM, Dodson JD (1908) The relation of strength of stimulus to rapidity of habit formation. J Comp Neurol Psychol 18(5):459–482
37. Hebb DO (1955) Drives and the C.N.S. (conceptual nervous system). Psychol Rev 62(4):243–254
38. Hancock PA, Ganey HC (2003) From the inverted-U to the extended-U: the evolution of a law of psychology. J Hum Perform Extreme Environ 7(1):3
39. Easterbrook J (1959) The effect of emotion on cue utilization and the organization of behavior. Psychol Rev 66(3):183
40. Ioannidis JPA (2005) Why most published research findings are false. PLoS Med 2(8):e124
41. Tapscott D, Williams AD (2010) Macrowikinomics: new solutions for a connected planet. Penguin, New York, US
42. Quantified Self (2012) Sky Christopherson on the quantified athlete (Video online). Available at: http://quantifiedself.com/2012/05/sky-christopherson-on-the-quantified-athlete/
43. Kurzweil R (2012) How to create a mind: the secret of human thought revealed, Kindle edition. Penguin Group, New York, US
44. Topol E (2011) The creative destruction of medicine: how the digital revolution will create better health care, Kindle edition. Basic Books, New York, p 22
45. Goetz T (2011) Harnessing the power of feedback loops. Wired Mag 19(7)
46. Dahm WJA (2010) Technology horizons: a vision for air force science and technology during 2010–2030, vol 1. USAF HQ, Arlington, VA
47. Steadman I (2013) IBM's Watson is better at diagnosing cancer than human doctors. Wired UK (online). Available at: http://www.wired.co.uk/news/archive/2013-02/11/ibm-watson-medical-doctor. Accessed 1 May 2013
48. Cohn J (2013) The robot will see you now (online). Available at: http://www.theatlantic.com/magazine/archive/2013/03/the-robot-will-see-you-now/309216/. Accessed 1 May 2013
49. Turner DC, Robbins TW, Clark L, Aron AR, Dowson J, Sahakian BJ (2003) Cognitive enhancing effects of modafinil in healthy volunteers. Psychopharmacology 165(3):260–269
50. Sugden C, Housden CR, Aggarwal R, Sahakian BJ, Darzi A (2012) Effect of pharmacological enhancement on the cognitive and clinical psychomotor performance of sleep- deprived doctors: a randomized controlled trial. Ann Surg 255(2):222–227

51. Muller U, Steffenhagen N, Regenthal R, Bublak P (2004) Effects of modafinil on working memory processes in humans. Psychopharmacology 177(1–2):161–169
52. Savulescu J, ter Meulen R, Kahane G (2011) Enhancing human capacities (Kindle locations 2660–2664), Kindle edition. Wiley Publishing, New York
53. McKinley RA, Bridges N, Walters CM, Nelson J (2012) Modulating the brain at work using noninvasive transcranial stimulation. Neuroimage 59(1):129–137
54. Burnet PW (2012) Gut bacteria and brain function: the challenges of a growing field. Proc Natl Acad Sci 109(4):E175
55. Slutsky I, Abumaria N, Wu LJ, Huang C, Zhang L et al (2010) Enhancement of learning and memory by elevating brain magnesium. Neuron 65(2):165–177
56. Sato K, Kashiwaya Y, Kean CA, Tsuchiya N, King MT et al (1995) Insulin, ketone bodies, and mitochondrial energy transduction. FASEB J 9(8):651–658
57. Bravo JA, Forsythe P, Chew MV, Escaravage E et al (2011) Ingestion of Lactobacillus strain regulates emotional behavior and central GABA receptor expression in a mouse via the vagus nerve. Proc Natl Acad Sci 108(38):16050–16055
58. Messaoudi M, Lalonde R, Violle N, Javelot H, Desor D et al (2011) Assessment of psychotropic-like properties of a probiotic formulation (Lactobacillus helveticus R0052 and Bifidobacterium longum R0175) in rats and human subjects. Brit J Nutr 105(5):755–764
59. Tang Y-P, Shimizu E, Dube GR, Rampon C, Kerchner GA et al (1999) Genetic enhancement of learning and memory in mice. Nature 401(6748):63–69
60. Lehrer J (2009) Neuroscience: small, furry … and smart. Nature 461:862–864
61. McClelland JL (1995) Constructive memory and memory distortions: a parallel-distributed processing approach. In: Schacter D (ed) Memory distortion: how minds, brains, and societies reconstruct the past. Harvard University Press, Cambridge, pp 69–90
62. DeSantis AD, Webb EM, Noar SM (2008) Illicit use of prescription ADHD medications on a college campus: a multimethodological approach. J Am Coll Heal 57(3):315–324
63. Berridge CW, Devilbiss DM (2011) Psychostimulants as cognitive enhancers: the prefrontal cortex, catecholamines, and attention-deficit/hyperactivity disorder. Biol Psychiatry 69(12):e101–e111
64. Topol E (2011) The creative destruction of medicine: how the digital revolution will create better health care, Kindle edition. Basic Books, New York, p 88
65. Bernstein JG, Boyden ES (2011) Optogenetic tools for analyzing the neural circuits of behavior. Trends Cogn Sci 15(12):592–600
66. Stuber GD, Sparta DR, Stamatakis AM, van Leeuwen WA, Hardjoprajitno JE et al (2011) Excitatory transmission from the amygdala to nucleus accumbens facilitates reward seeking. Nature 475:377–380
67. Halpin H (2004) The semantic web: the origins of artificial intelligence redux. In: Third international workshop on the history and philosophy of logic, mathematics, and computation (HPLMC-04 2005)
68. Anderson JR, Lebiere C (2003) The Newell test for a theory of cognition. Behav Brain Sci 26:587–640
69. Anderson JR, Fincham JM, Qin Y, Stocco A (2008) A central circuit of the mind. Trends Cogn Sci 12(4):136–143
70. Newell A (1994) Unified theories of cognition, vol 187. Harvard University Press, Cambridge
71. Newell A (1980) Physical symbol systems. Cogn Sci 4:135–183
72. Anderson JR (2002) Spanning seven orders of magnitude: a challenge for cognitive modeling. Cogn Sci 26(1):85–112
73. Doyle JC, Csete M (2011) Architecture, constraints, and behavior. PNAS 108(3):15624–15630
74. Myers CW, Gluck KA, Gunzelmann G, Krusmark M (2010) Validating computational cognitive process models across multiple timescales. J Artif Gen Intell 2(2):108–127
75. Sun R, Coward LA, Zenzen MJ (2005) On levels of cognitive modeling. Philos Psych 18(5):613–637
76. Alderson DL, Doyle JC (2010) Contrasting views of complexity and their implications for network-centric infrastructures. IEEE Trans Syst Man Cyber A 40(4):839–852

Chapter 8
Effective Neural Representations for Brain-Mediated Human-Robot Interactions

Christopher A. Buneo, Stephen Helms Tillery, Marco Santello, Veronica J. Santos, and Panagiotis Artemiadis

Abstract Physical interactions between robots and humans are an integral part of many neurorobotic, neural prosthetic and rehabilitation robotics applications. It is generally acknowledged that such interactions can be enhanced by providing robots with advance knowledge of the *intentions* of human agents, e.g. their desired motor plans and goals in a given context. One potential source of these intentions are decoded neural signals obtained from the cerebral cortex, but precisely which cortical representations are most beneficial for facilitating effective human-robot interactions is unclear. Here we review the neural representations of movement plans in the cortex and discuss the potential utility of these representations for jointly performed motor actions, particularly manipulation tasks involving the hand and arm. Emphasis is placed on the coordinate frames used by different cortical areas to encode sensory- and motor-related variables. It is argued that *relative* coding of sensorimotor variables, a concept that has also recently been applied to robotic planning and control algorithms, might be particularly useful for facilitating joint actions of the hand and arm. More generally, discussion of the various neural representations will provide critical insight into how biological agents might better interact with robotic agents for the development of next-generation neural prosthetic systems and rehabilitation robots.

Keywords Brain-robot interface • Neural representation • Reference frame

C.A. Buneo (✉) • S. Helms Tillery • M. Santello
School of Biological and Health Systems Engineering, Arizona State University, Tempe, AZ 85287, USA
e-mail: cbuneo@asu.edu; stillery@asu.edu; marco.santello@asu.edu

V.J. Santos • P. Artemiadis
School for Engineering of Matter, Transport, and Energy, Arizona State University, Tempe, AZ 85287, USA
e-mail: veronica.santos@asu.edu; panagiotis.artemiadis@asu.edu

P. Artemiadis (ed.), *Neuro-Robotics: From Brain Machine Interfaces to Rehabilitation Robotics*, Trends in Augmentation of Human Performance 2,
DOI 10.1007/978-94-017-8932-5_8,

8.1 Introduction

In the last few decades, the field of robotics has witnessed tremendous growth, driven by advances in both hardware and software. Over the same time-frame, the field of neuroscience has seen a similar degree of advancement, due to methodological developments in neurobiology as well as disciplines essential to modern scientific inquiry such as computer science and engineering. The parallel development of robotics and neuroscience has spurred interest in engineering applications based on a combination of these two fields. This in turn has led to the establishment of entirely new disciplines including *neurorobotics (a.k.a. neurobotics)*, dedicated to the development of robotic control systems based on neuroscientific principles, *neural prosthetics*, devoted to systems (which may include robots) designed to replace motor, sensory and/or cognitive functions lost due to nervous system damage, and *rehabilitation robotics*, dedicated to the design of robotic systems (which may include nervous system input) for augmenting and/or stimulating recovery of sensory and motor function following nervous system damage.

The nature of neural representations is highly relevant to each of these nascent fields. For example, hypotheses regarding the sensorimotor transformations subserving motor behavior or cognitive processes such as decision making can be tested by instantiating neurorobots with computational elements modeled on the known properties of relevant neural representations. The extent to which the behavior of such neurorobots captures the essence of natural behavior can then be evaluated, leading to a refinement of hypotheses or the creation of new ones. Understanding the precise nature of neural representations is also critical for potentially endowing robots with the superb sensorimotor capabilities of humans, either for the purpose of enhancing interactions between robots and their environment, or for facilitating seamless robot-robot or human-robot interactions. Regarding the latter, understanding neural representations is most directly applicable for interactions that can be enhanced through the decoding and transmission of neural signals, as in prosthetic and rehabilitative applications facilitated by brain-machine interfaces [1–4].

In this chapter we discuss the nature of cortical representations of upper limb movements and their relevance to human-robot interactions. The goal is to identify the types of representations, and therefore brain regions, that are most suitable for facilitating cooperative manipulative tasks between humans and robots. We focus largely on activity related to movement planning, rather than movement execution. Planning activity is typically found in the association cortices of the brain and can represent simply the motor intentions of an agent, e.g. the desired goal of an action and the specific effector (eye, arm, etc.) that will be used to achieve that goal [5], or more detailed information such as desired kinematics and/or kinetics [6–10]. Importantly, and in consonance with the causal flow of robotic control schemes, planning activity precedes execution-related activity in the sensorimotor networks of the brain. As a result, planning activity can be provided to robotic agents in advance of an action, allowing predictive robot control schemes to augment reactive ones during the online performance of joint motor tasks.

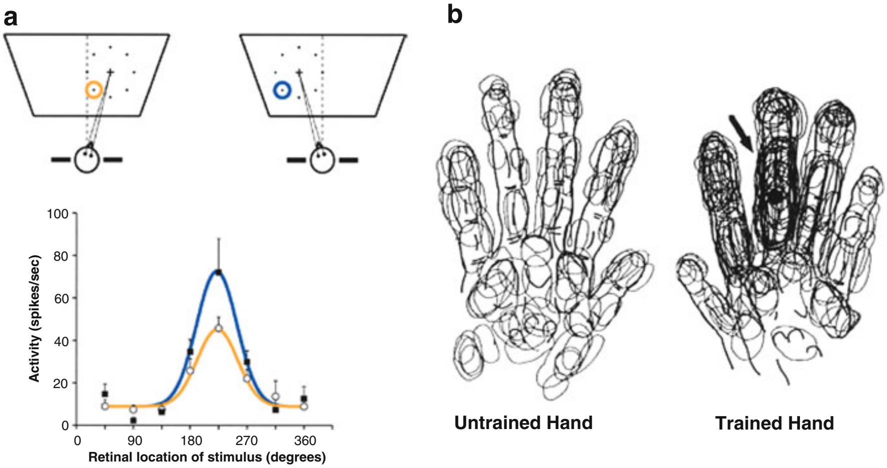

Fig. 8.1 Retinotopic (**a**) and somatotopic (**b**) receptive fields. (**a**). Responses of an idealized neuron encoding the locations of visual stimuli in retinotopic coordinates. Responses are characterized for different locations in allocentric (world-based) coordinates (*blue* and *yellow* circles) but the same locations in retinotopic coordinates by varying gaze direction in space. The response profiles (receptive fields) are similar in shape for the two gaze positions and are 'gain-modulated' by gaze direction, a common feature of neurons in association cortex [12]. (**b**). Tactile receptive fields of neurons in somatosensory cortical area 3b obtained from monkeys trained in a tactile frequency-discrimination task. The sizes, shapes and locations of receptive fields are shown for both the trained and untrained hand [13]

In reviewing and discussing planning activity, we focus almost entirely on the reference frames used by individual neurons and groups of neurons to encode spatial information relevant to movement planning. In the initial and final stages of sensorimotor processing, such reference frames are defined by the natural coordinates of the motor and sensory apparatus [11]. For example, visual information is initially encoded in the brain in a frame of reference defined by the receptive fields (the region of sensory space where a stimulus will elicit a change in activity) of photoreceptors in the two retinas. As a result, visual information can be said to be initially encoded in a 'retinotopic' frame of reference (Fig. 8.1). Similarly, tactile information is encoded in a frame defined by the receptive fields of sensory receptors in the skin (a 'somatotopic' frame of reference). Such elementary reference frames are typically retained in secondary and tertiary structures of the sensory hierarchy, but an interesting (and now well-explored) question concerns the reference frames used by the higher order association areas of the brain to encode spatial variables.

The reference frames used by association cortical areas are particularly interesting in the context of movement planning. Since these regions are multimodal in nature it is not evident a priori what reference frame(s) should be used to encode spatial information relevant to movement. For example, information about the current position of the arm must be taken into account to form a plan for a reaching movement. This information can be provided by both visual and somatosensory input. Additionally, motor-related association cortices of the brain typically receive both types of information. As a result, it is not immediately clear if arm position should be represented in a visually-based frame in these areas or in a body-centered one. It is also possible that a hybrid set of coordinates is used. Because of such questions, as well as the fact that (1) coordinate representations are thought to be a distinguishing feature of neurons and neuron populations in sensorimotor networks of the brain, and (2) reference frames and coordinate systems are also an integral part of robot planning and control schemes, we focus almost exclusively on this aspect of neural representations in our review.

In the future, the development of systems requiring intimate and extensive physical interactions between robots and humans, such as neural prosthetic and rehabilitation robotic systems, will benefit from knowledge gained by studying how two or more humans perform cooperative tasks. As a result, we will begin by providing a brief overview of what is known about the performance of such 'joint actions', as they are called in the neuroscience community, ending with a discussion of joint manipulative actions involving the hand and arm. We will then discuss the relevance of such studies for robot-robot and human-robot interactions. The point here is not to conduct an exhaustive review of human-robot interactions (HRI), as this is beyond the scope of this chapter, but merely to touch upon what is known about collaborative manipulation in HRI. Lastly, we will discuss what is known about the neural representations of hand and arm movements, with a particular emphasis on the coordinate frames for representing spatial variables, such as arm and target position.

8.2 Joint Actions in Humans

Joint actions involve two or more agents coordinating their behavior in space and time to perform a particular task [14]. The ability to engage in such behaviors, while not unique to humans, is most highly elaborated in our species. As pointed out by Tummolini and Castelfranchi [15], only humans have the capability to "create complex tools, structured symbol systems (i.e. language) and social institutions (i.e. government and marriage) as a means to facilitate such coordination and cooperation" [15]. However, most of what we currently know about "joint actions" still comes from studies in social contexts. Observations derived from these studies have led to the conclusion that the successful performance of joint actions in the social domain depends strongly (among other factors) upon the ability to predict the integrated effects of one's own and others' actions [16]. This is turn, requires the sharing of internal representations of both the task and mental state of others, a concept known as 'co-representation' [14, 17].

Joint actions are also an essential part of many motor-related activities of daily living; examples can be found in sport, as with the passing of a ball between two soccer teammates, art, as during ballroom dancing or the performance of a musical duet, and even rehabilitation, as when a therapist or rehabilitation robot assists a patient during therapeutic exercise. Despite their ubiquitous nature, comparatively little is known about joint actions in the sensorimotor domain. In recent years, research in this area has focused largely on three topics: co-representation (defined above), attentional and perceptual processes, and interpersonal (temporal) coordination [18].

Research on perceptual processes has been directed in part at understanding “motor resonance”, e.g. the idea that observation of someone else’s actions can facilitate the recruitment of corresponding motor representations in observers [19]. Recent findings suggest that even in the absence of contextual information, subjects are able to infer the intentions of others from information derived from movement [20]. For example, Sartori et al. [21] video-recorded reach-to-grasp movements performed under conditions in which subjects were either intending to cooperate with a partner, compete against an opponent, or perform an action individually. When the video clips were presented to “observer” participants in an intention discrimination task, all three scenarios (cooperative, competitive and individual) were found to be discriminable by the observers [21]. This was true even when visual information about the terminal phases of movement and object contact were occluded. This supports the idea that intent can be inferred even from visual information present in the early stages of a motor action.

Interest in interpersonal coordination is comparatively long standing and has recently expanded from a focus on rhythmic movements [18, 22] to include analyses of non-rhythmic activities [23–25]. For example, Braun and colleagues [24, 25] have recently studied intra- and inter-personal coordination in a virtual rope-pulling game and found evidence for both cooperative and non-cooperative (competitive) behaviors. That is, when two different subjects performed the game together, behavior tended toward a competitive strategy, whereas when individual subjects performed the same task alone but bimanually, behavior tended to be more cooperative. Such results are consistent with a “Nash equilibrium solution”, a concept derived from classical game theory, which predicts that in a two-person game each player will choose a strategy that ensures that neither player has anything to gain by altering their own strategy [26]. Overall, this work suggests that the performance of some joint action tasks can be analyzed successfully within a game theoretic framework.

Research on co-representation addresses how and when two agents are able to form internal representations of tasks and each other’s actions [27]. Co-representation is often studied using a variant of the classical “Simon task,” in which subjects are required to respond to stimuli using responses that are either spatially congruent or incongruent with the stimuli [28]. The “Simon effect” refers to the phenomenon that behavioral reaction times of single subjects are slower for the spatially incongruent responses, as when pushing a button with the right hand in response to a stimulus appearing in left visual space. Interestingly, the same effect can be observed when the Simon task is performed jointly by two subjects. In the basic form of these experiments, each subject is typically responsible for one of the two responses, e.g. one subject for left button presses and one for right button

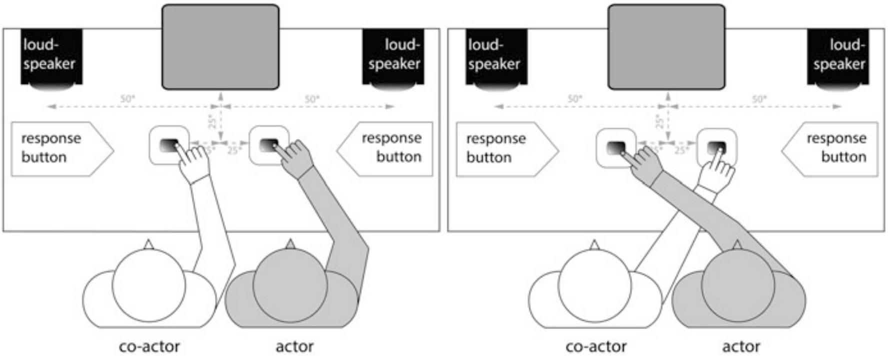

Fig. 8.2 Illustration of an auditory version of the Social Simon task [30]. Subjects performed a reaction time task requiring button presses in response to auditory stimuli. Responses were generated using either a crossed (*right*) or uncrossed configuration of the actors' arms

presses. The resulting differences in reaction time that are observed in such tasks is commonly referred to as the "social Simon Effect" [27].

The concept of co-representation and its underlying neural representation is naturally tied to the issue of frames of reference. That is, in forming an internal representation of a joint action, do subjects use the same frame of reference to plan their behavioral responses and if so which reference frame is used? Some investigators have addressed this question using a variant of the social Simon task. For example, in a recent study by Welsh [29], dyads (pairs of subjects) performed the social Simon task standing side-by-side and with their inside or outside hands placed in either a crossed or uncrossed configuration [29]. Welsh found that the social Simon effect was observed in all of these conditions. In other words, the presence of a social Simon effect appeared to be dependent only upon the spatial location of the response keys, and not the relative locations of the subjects in space or the configurations of the responding hands. This has been interpreted as reflecting a preference for 'external, response-based coordinates', i.e. visual or allocentric (world-centered) coordinates, in planning joint actions [30], though other work suggests that internal (body-centered) frames can also be used in different contexts [31].

The Welsh study raises the question of whether the apparent dominance of external frames in joint action is related to the use of predominantly visual stimuli. Dolk et al. [30] recently addressed this issue in sighted and congenitally blind dyads using a variant of the social Simon task that involved responses made to auditory stimuli with the arms either crossed or uncrossed [30] (Fig. 8.2). These investigators found that the social Simon effect was observed in both the arms crossed and uncrossed conditions in sighted individuals, but only in the uncrossed condition for the congenitally blind subjects. This study affirmed the importance of external frames in governing behavioral responses in joint action but also suggested that the type of external reference frame used for planning joint actions is determined by experience. That is, congenitally blind individuals appear to use both response-based and "agent-based" external frames, while sighted individuals tend to use predominantly the former.

In a recent study with particular relevance to human-robot interaction, electroencephalography signals (EEGs) were recorded from the brain while pairs of subjects performed a joint Simon task [32]. Here subjects made left and right keyboard presses to targets presented either on the right or left side of a computer screen. In one condition subjects performed the task under the belief that they were interacting with a biological agent situated in another room, while in another condition they were told they were performing the task with a computer. In both conditions however, responses of their partner were actually randomly generated by the same computer program. Interestingly, reaction times followed the predictions of the social Simon effect, *only* in the condition where subjects believed they were acting with a biological agent. In addition, these behavioral differences were reflected in the patterns of EEG activity. These results reinforce the notion that the perceived agency of co-actors influences the representation of planned motor actions in the brain.

8.3 Joint Manipulative Actions of the Hand and Arm

Cooperative, manipulative actions such as pouring liquids into a hand-held glass, turning a large crank or wheel, and transferring of objects between hands ("hand-overs") are examples of common joint actions performed between human agents and between humans and humanoid robots [33] (Fig. 8.3). However, little information exists on precisely how such actions are planned controlled and even

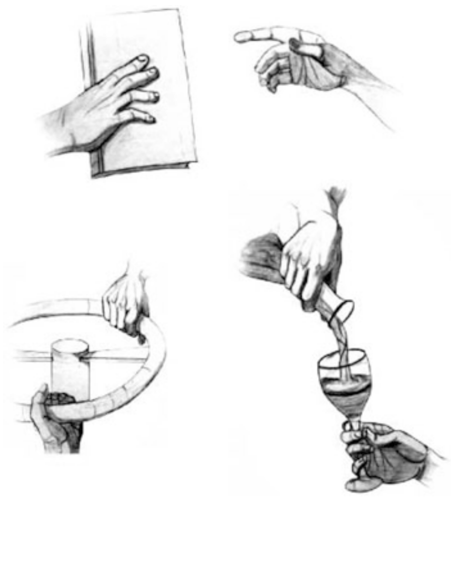

Fig. 8.3 Examples of joint manipulative actions of the hands [33]

less information is available regarding how they are represented in the brain. For example, despite the ubiquitous nature of handovers, surprisingly few studies have addressed the planning of these actions in humans and their underlying coordinates. Studies have focused instead on such features as the endpoint kinematics of the hander and receiver [34, 35], the relationship between grip force and load force [36], handover duration [37], and the reaction times of the receiver and spatial position of the handover [38–40].

Although handovers have not received a lot of attention to date, these actions are similar in many ways to more well-characterized tasks typically performed by single agents such as reach-to-grasp (RTG). That is, both handovers and RTG involve the following constituent actions: (1) reaching or transport of the hand, (2) orienting of the hand, and (3) hand preshaping (prior to receiving in a handover task or grasping in an RTG task). As a result, object handovers can be thought of as an extension of RTG to the domain of joint actions. These similarities suggest that the relatively large literature on RTG can be used to gain preliminary insight into the behavioral and neural correlates of the joint action of handovers.

A large number of RTG studies in humans have examined the coordinate frames underlying reach planning. As discussed earlier, reach planning requires a comparison between the hand's current position and the position of the target. In situations where the target and hand can be viewed, both positions can be coded with respect to the current gaze direction. Throughout this review we will use the term "eye-centered" to refer to this coding scheme though the terms "viewer-centered", "gaze-centered", or "fixation-centered" have also been used [41–43]. Hand position can also be defined in the hybrid body/arm frame defined by the proprioceptors. It is commonly thought that planning is facilitated by transforming hand and target position into the same set of coordinates (cf. [44]), but precisely which frame is used remains controversial. Evidence for both eye- and/or body-centered coordinates exists in the literature [41, 45–49].

One simple explanation for these disparate results is that the choice of frame is context dependent, with eye-centered coordinates being used in conditions where at least some visual information about both hand and target position is available. For example, when subjects make reaching movements to remembered targets with some visual feedback of the hand, their constant and variable errors suggest that planned reach vectors are computed in a visual or eye-centered frame [42, 45, 49] (Fig. 8.4). This result is consistent with findings that reach plans are dynamically updated in eye coordinates following saccadic eye movements [46], regardless of the sensory modality used to cue these movements [50]. It is also consistent with findings that generalization patterns following local visuomotor perturbations of the fingertip are consistent with eye-centered coordinates [51]. Providing a neurorobotics perspective on the matter, Tuan and colleagues have reported that a planning scheme based on eye-centered coordinates is more robust to sensory biases and delays than schemes based purely on body-centered coordinates, emphasizing the advantage of eye coordinates in certain contexts [52].

A somewhat different story emerges when subjects are required to make reaching movements to remembered target locations with little or no visual feedback of the

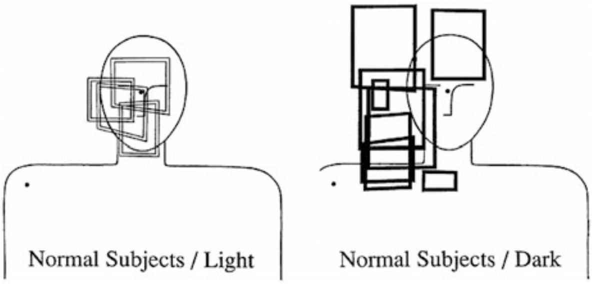

Fig. 8.4 Behavioral evidence supporting context dependent reference frames for reach planning [45]. Each box represents the 95 % confidence limits on the presumed origin of the coordinate system used for planning reaching movements to remembered targets. Data from four subjects in fully-lighted conditions (*left*) and eight subjects in dark conditions are shown. In the light (i.e. with vision of the hand), the origin is centered around the approximate line of sight, while in the dark the origin is biased for most subjects toward the right shoulder

arm. Here, patterns of constant and variable errors support a coordinate system for planning that is at least partially body-centered [42, 45, 49]. Interestingly, similar trends are observed when subjects make movements without delay to visible targets (not remembered ones) but without online visual feedback of the hand [53]. Results such as these suggest that the coordinate frame(s) used to plan human reaching movements are context-dependent, being determined in part by the extent and reliability of relevant visual feedback, particularly regarding the arm [49, 54–59]. Note that this conclusion is also in agreement with a recent study of the social Simon effect, which pointed to context-dependent frames for planning joint actions [31].

The above considerations for representations and frames of reference involved with pointing or reaching are likely to apply to RTG, where proximal limb motion is coupled with hand shaping to grasp an object, i.e., preshaping. Hand preshaping could be considered a process through which object geometry and grasp affordances, expressed in a world-centered frame of reference, drive a sensorimotor transformation leading to the alignment of hand and object frames of reference, culminating in a close match between the opposition axis (i.e., the line connecting the tips of the thumb and index finger [60]) and the graspable axis of an object, or between hand shape and object shape. Rather than addressing this process directly, behavioral studies have mostly focused on the sensory mechanisms underlying the time course of hand shape modulation to object shape. One of the main questions addressed by these studies is the extent to which continuous visual feedback of the hand and/or the object is required to coordinate finger movements leading to a stable grasp at the end of the reach. One possible scenario consists of computing an ‘error’ signal arising from visually-perceived object shape versus hand shape, until the hand can conform to the object at contact. An alternative scenario might involve vision, but not necessarily on a continuous basis. Specifically, object shape visually perceived at reach onset might be sufficient to drive the coordination of finger movement throughout the reach. Behavioral evidence supports the latter scenario, indicating that whole-hand shaping occurs in a similar fashion regardless of whether visual feedback of the object is present or absent during the reach [61]. Interestingly, removing tactile feedback at the end of the reach when reaching to grasp a visible virtual object also leads to a similar hand shaping observed when reaching to grasp a physical object [61]. A follow-up study confirmed these observations by showing that hand preshaping occurs in a similar fashion regardless of whether vision of the hand *and* object is allowed [62]. Although these observations do not rule out a role for online visual feedback for hand preshaping, they demonstrate that vision of the object prior to initiating a reach is sufficient to drive the spatial and temporal coordination of finger movements in preparation for a grasp.

As with hand preshaping, relatively few RTG studies have focused on the planning and control of hand orientation. Here we define hand orientation as a rotation about the long axis of the forearm, in order to distinguish it from rotations of the opposition axis. The relative lack of attention given to examination of hand orientation is unfortunate, as orienting is a critical component of dexterous manipulation and yet involves fewer mechanical degrees of freedom and muscles than hand preshaping. Although most real world manipulation tasks require precise coordination of both orienting and preshaping, the relative biomechanical simplicity of hand orienting makes it more amenable to study in the laboratory than hand preshaping, particularly with regard to coordinate representations. In addition, damage to certain regions of the cerebral cortex appears to be associated with specific deficits in orienting the hand. For example, patients with optic ataxia resulting from damage to the parietal lobe have also been shown to exhibit difficulty in orienting their hand to match the orientation of a target slot [63]. Similarly, patients with damage to the lateral occipital and parasagittal occipitoparietal cortex have been shown to demonstrate deficits in perceiving the orientation of a visual stimulus during orientation-matching tasks [64]. These studies point to a disruption of the high level sensorimotor transformations required for planning appropriate final wrist orientations following damage to parietal and occipital regions of the brain.

Behavioral studies examining hand orientation have shown that during RTG actions, final hand orientation is influenced by several factors including: (1) the direction of reaching, (2) the initial and final postures of the upper arm before and after the reach, (3) the spatial location and orientation of the target, and (4) the optimal grasp axis of the target object [64–78]. In addition, studies involving reaches to objects that unexpectedly change orientation suggest that orienting the hand involves a process whereby a final desired orientation is compared to the initial (or current) hand orientation to compute a desired change in orientation [67, 79]. This suggests that planned changes in orientation are encoded in a relative, rather than absolute, frame of reference at least somewhere in the sensorimotor structures responsible for RTG. As will be demonstrated below, this idea resonates with some recent robotic planning and control schemes and also with recent neurophysiological investigations of eye-hand coordination in the primate brain.

8.4 Joint Manipulative Actions: A Robotics Perspective

As discussed above, handovers serve as an excellent example of joint manipulative actions performed by human agents. Handovers are also a critical action for robots that cooperate closely with humans and, as with other joint actions, successful performance of these handovers depends critically on communication cues exchanged both before and during the action [80]. For example, Cakmak and colleagues [81] examined robot-to-human handovers and demonstrated that both spatial (pose) or temporal aspects of the robot motion can fail to adequately convey the intent of the robot, leading to delayed or failed acceptance of the object by a human collaborator [81]. They proposed addressing these issues by incorporating spatial and temporal motion cues that distinguish handovers from other manipulative actions, and found that temporal cues were particularly useful for enhancing the fluency of handovers. Expression of robot intent has also been explored using body movements, facial expressions and speech [82–84] though not in the context of handovers.

As a result of these and other observations, considerable effort has been put into providing robots and humans with the means to better decode each other's intentions. For example, Grigore and colleagues [85] showed that the success rate of robot-to-human handovers can be improved by providing the robot with the ability to interpret the human's current gaze orientation and therefore their locus of attention [85]. Similarly, Huber and colleagues [37] showed that robot-to-human handovers can be facilitated by using robot motion profiles that are consistent with observed human motion profiles. In this study, robot-to-human handovers were examined using both a humanoid and industrial robot [37]. In addition, two different velocity profiles for robot arm motion were used: a trapezoidal velocity profile in joint coordinates and a minimum jerk profile in Cartesian (endpoint) coordinates, the latter being inspired by observations of human reaching movements [86]. Reaction times of the human subjects were found to be shorter for the minimum jerk profiles, regardless of whether the robot was humanoid or industrial, indicating that human preferences for biomimetic motion influence the ability to infer robot intent. Preferences have also been observed with respect to the approach direction of a mobile robot partner and the height and distance of the object being passed [87].

The study of joint manipulative actions between robots and humans has generally ignored the issue of which coordinate frame or frames might best represent these tasks. At least in the laboratory setting, the position and orientation (pose) of the robot and human hands are defined with respect to different absolute frames. For example, for humanoid robots this frame might be fixed to the head or torso of the robot while for humans this frame might be defined with respect to the coordinate system of a motion tracking device. However, effective cooperation on manipulation tasks requires the robot and human to react in real-time to their collaborator's motion, a feature that is not straightforward to implement using representations involving absolute poses. As a result of these and other difficulties, Adorno and colleagues [33] developed an approach to representing cooperative manipulative tasks by means of the *relative* configuration between the human's and the robot's hands [33]. This approach has the advantage of allowing a large set of tasks, including handovers, to be represented in a similar fashion, and in a manner that is invariant with respect to the physical location of the robot and human/motion tracker in space. Perhaps most importantly, this approach is noteworthy because it resonates with psychophysical studies of the control of human hand orientation during RTG tasks and, as discussed below, with neurophysiological studies of eye-hand coordination tasks.

8.5 Neural Representations of Joint Actions

While significant progress has been made in understanding joint motor actions from a behavioral perspective, almost nothing is known about their corresponding neural correlates [88]. Recent modeling work has emphasized the potential role of the putative mirror neuron system (MNS) in mental state inference, a key component of joint action [89]. The MNS is a group of frontal (ventral premotor) and parietal regions (mainly the anterior intraparietal area) that are believed to play a role in motor learning by observation as well as other high-level cognitive, sensory, and motor functions essential for joint action [19, 90, 91]. Inferring mental states, i.e. knowledge of the required task and goal, during joint actions is highly dependent upon communication cues exchanged between interacting agents. These cues can be provided by visual feedback, in the case where one actor simply observes the other, or by both visual and haptic feedback, in the case where tasks involve physical interaction. Oztop et al. [89] proposed a computational model of mental state inference in the context of pure visual observation. In this model, inference is facilitated by defining task goals and objectives in *visual* coordinates, which is in accordance with both recent human [47, 92–95] and animal studies [96, 97]. In this scenario, actions such as reaching are defined simply as difference vectors in visual coordinates. This has the advantage of allowing the actions of both the actor and observer to be treated in a nearly equivalent manner by the observer's motor planning apparatus, thereby simplifying the inference process.

While this model is elegant in its simplicity, it is currently unclear how well the model can be generalized to conditions of physical interaction involving both visual and haptic feedback, which are not always congruent or equally reliable [98]. The model of Oztop and colleagues could, in principle, be extended to this context if a mechanism existed to transform haptic information from the hybrid arm/body-centered coordinates of proprioceptive and tactile feedback to the natural coordinates of visual processing (eye coordinates), an idea that is not without precedence [57, 99–103]. However, it is also possible that integration is achieved using the principles of optimal cue integration, which does not require transformation of feedback into a common reference frame and would directly take into account the relative reliabilities of the sensory cues [104, 105].

In agreement with the work of Oztop et al. [89], recent fMRI studies in humans point to the MNS as a potential neural substrate for many joint actions [106, 107].

An important element to models such as the one proposed by Oztop et al. is the idea of simulation. To predict the actions of an observed agent, one could use the same neural systems that underlie movement planning to simulate the movements of others and thereby deduce the intentions of an observed act. Consistent with this idea, activation has been observed in the cortical areas associated with the MNS both when subjects balance a bar and when they observe a bar being balanced [108]. When extended to joint action, i.e. the subjects cooperating with another agent in balancing the bar, activation in the same cortical areas was further facilitated. This would be consistent with the MNS having a special involvement in joint action.

While studies such as these suggest a significant contribution of the MNS to joint action, these studies may be limited by focusing too carefully on shared corresponding actions. Kokal et al. [106] pointed out that the examination of joint action should be expanded to include the coding of complementary, as well as corresponding, actions. For example, if two people are engaging in a hand-off, one agent is presenting and releasing an object, while the other agent is receiving and grasping. Thus, a neural system which participates in joint action needs to be more flexible than simply coding the same action irrespective of the actor. Kokal and colleagues constructed a set of joint action tasks in which the two agents either performed the same motion, or opposite and complementary movements to achieve the joint goal. Under these conditions conjugate and complementary tasks facilitated activity not only in the fronto-parietal areas conventionally associated with the MNS, but also in additional cortical areas in the occipital and parietal lobes. Thus, while the mirror neuron system is likely an important element in the neural architectures which subserve joint action, it may not be the only element recruited during joint action performance.

Although human imaging studies have provided crucial information regarding the anatomical loci of joint action representations, methods such as fMRI are unable to shed light on precisely *how* these actions are represented at the level of single neurons or small ensembles. However, single and multi-unit studies in non-human primates are ideally suited for probing such representations. Neurons in the MNS have some of the properties one would expect of neurons that participate in a joint action system. In particular, neurons in both the posterior parietal cortex (PPC) and ventral premotor cortex (PMv) have been shown to exhibit similar activity for both motor execution and observed action. In each of these cortical regions, neurons have been observed which encode elements of grasp, including the configuration and orientation of objects that are about to be grasped and the hand configuration that is being used to carry out those grasps [109, 110]. That these neurons have similar coding for actual grasps and observed grasps is evidence for their participation in joint actions. Especially notable in the context of joint action is the observation that many neurons in PMv appear to encode implied actions [111]. When vision of the final phase of an observed grasp task is blocked, some neurons in PMv still code the unseen grasp, suggesting that they were in fact being used to simulate and predict the movements of other agents.

An important principle in the neural representation of task space is effector independence: neurons in networks coding for task performance should show aspects of

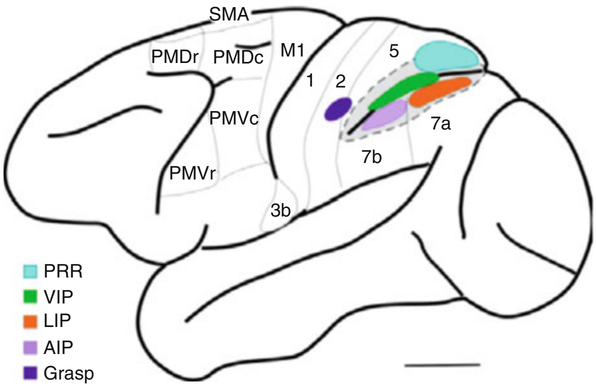

Fig. 8.5 Lateral view of the macaque monkey brain, highlighting many of the areas discussed in this review [113]. *PRR* parietal reach region, *VIP* ventral intraparietal area, *LIP* lateral intraparietal area, *AIP* anterior intraparietal area, *Grasp* area 2 grasp –related area, *M1* motor cortex, *SMA* supplementary motor area, *PMDr* dorsal premotor cortex, rostral subdivision, *PMDc* dorsal premotor cortex, caudal subdivision, *PMVr* ventral premotor cortex, rostral subdivision, *PMVc* ventral premotor cortex, caudal subdivision, *PMVr* (also referred to as F5) represents the frontal node of the mirror neuron system in monkeys, *AIP* and area *PFG* represent the parietal node [19], the latter corresponding roughly to what is labeled 7b in this figure

coding that do not depend on the effector performing the task. Simultaneous multi-unit chronic recordings in PPC and PMv during feeding tasks suggest there are a number of similarities in the way that observed and executed tasks are coded, but there is also one important difference [112]. The coding of observed action in PMv appears to have an element of effector-dependence, whereas the coding of observed action in posterior parietal cortex has a measure of effector independence. This kind of task-focused encoding is closer to reflecting the quality of flexibility that Kokal et al. [106] suggested should be an additional hallmark of neuronal systems that support joint actions. To date, however, there have not been reports of recordings undertaken specifically with the goal of gaining insight into the neural coding of joint actions.

Other more dorsally-situated parts of the premotor and parietal cortices, including the dorsal premotor cortex (PMd), parietal area 5, the medial intraparietal area and parietal area V6A (Fig. 8.5), have been shown to be involved in integrating visual, somatosensory and motor signals in support of goal-directed actions such as reaching and grasping and in the forming of motor "intentions", i.e. high level plans for movement [96, 114–118]. These regions could therefore also play a role in the planning and/or execution of joint actions. Activity in these areas is similar in many respects. Being association areas of the cortex, neurons in the parietal and premotor regions often exhibit both sensory- and motor-related responses. In addition, many neurons exhibit responses that reflect higher-order cognitive processes such as movement planning. Movement planning is typically examined using some form of memory-guided delayed response task [119]. Such tasks involve training animals to withhold their response to a presented cue for periods lasting as long as several seconds, then cueing them to make the appropriate response. The benefit of such tasks for understanding sensorimotor processing is the following: by incorporating a delay period, activity related to planning a motor response can be temporally dissociated from both simple sensory responses to the presented instructional cue and the processes involved in movement execution, including sensory feedback.

Delayed response tasks have provided evidence for movement planning processes in a number of arm and hand movement related areas of the frontal cortex. Moreover, evidence for the planning of both kinematic and dynamic (kinetic) variables has been uncovered. For example, neurons in areas such as the motor cortex (M1), dorsal premotor cortex (PMd) and supplementary motor area (SMA), have been shown to represent high-level parameters of upcoming movements, including movement direction, amplitude and speed, during the delay periods of delayed response tasks [120–125]. These same areas appear to represent the impending dynamics associated with arm movements, consistent with a role in the planning of kinetic variables such as endpoint forces or torques [8–10, 126]. Regarding the encoding of kinematics, a particularly noteworthy study is one by Hocherman and Wise [6]. These investigators trained animals to move between identical starting and goal locations but using different (curved) trajectories and found that the activity of some neurons differentiated among such trajectories [6]. In this way, these investigators were the first to show that the *planning* of detailed movement trajectories can be represented in the discharge of cortical neurons.

In the parietal cortex, the origin of activity occurring during the memory period of delayed response tasks has proven to be much more controversial, with some interpreting this activity as reflecting previous sensory events or attention-related phenomena rather than planning [127]. However, several studies have now provided strong evidence that this activity is viewed in part as reflecting plans for impending movements [118, 128–132]. Regarding arm movements specifically, activity in medial intraparietal area (MIP) and area 5 appears to be consistent with transforming information about target positions and the current position of the hand into a desired movement vector [57, 97, 133]. Recent TMS, imaging, and clinical studies in humans are largely consistent with this view [47, 93–95, 134]. The specific coordinate frames thought to underlie these computations are discussed in detail below.

What about more detailed aspects of movement plans? Torres et al. [7] recently reported the results of a study where animals planned and executed a block of direct (point-to-point) reaches between two locations on a curved, vertical surface, then attempted to move between those same locations in the presence of an obstacle. Moving in the presence of the obstacle required the animals to use very different movement trajectories to complete the task and, in this way, memory activity for the same starting position and target position but different movement paths could be compared. This design was similar to that of Hocherman and Wise [6] except that in that study, the different trajectories were explicitly instructed using a visually-presented path while in the study by Torres et al. [7], no such instruction was provided. Nevertheless, animals gradually adopted stereotyped trajectories that allowed them to successfully avoid the obstacles. Moreover, memory activity in MIP very clearly distinguished between trajectories planned in the presence and absence of the obstacle, with the activity of some cells being enhanced when the obstacle was present and others being suppressed. The findings support the idea that MIP plays an important role in movement planning, and moreover, that it is involved not only in specifying high level movement parameters such as movement direction and amplitude, but in mapping these plans into corresponding movement trajectories.

8.6 Coordinate Representations for Reaching: Parietal Cortex

The coordinate representations for reaching have been studied most extensively in the parietal lobe, particularly its more posterior subdivision, the PPC. This makes sense as the PPC is an association area of the brain that receives information from multiple sensory modalities and, in addition, projects to frontal lobe areas more directly involved in control of the arm. The PPC is also known to play a role in high-level aspects of movement planning. In addition to previously described evidence, damage to this area results in a number of sensorimotor deficits that are consistent with the idea that the PPC plays a role in transforming sensory information into motor output. Among these disorders is optic ataxia, characterized by misreaching to visual targets. Importantly, patients with this disorder do not exhibit an inability to move their arms or to perceive the locations of visual stimuli but demonstrate a specific deficit in linking motor and sensory representations together to guide movements [63].

In non-human primates, the coordinate frames underlying arm movement planning and execution have been studied by training animals to reach under conditions where arm and/or target positions are held constant in one frame of reference (e.g. with respect to the body) while simultaneously being varied in other frames (e.g. eye or head-centered coordinates). The underlying assumption of this design is that neurons encoding spatial variables in one frame of reference should be unaffected by changing their location in another frame of reference. For example, the activity of a neuron encoding information in body-fixed coordinates should remain invariant if the position of the hand and target remain fixed with respect to the body (even if body position is changed in space) and should, therefore, be unaffected by manipulating the direction of gaze, which alters the position of the hand and target with respect to the eye.

Such experimental manipulations were first used to explore the coordinate frames of arm movement related activity in the parietal reach region (PRR), a part of the PPC located within the bank of the intraparietal sulcus which largely overlaps the previously identified MIP and V6A. In initial experiments, reach targets were varied in arm and eye coordinates on individual trials by varying the starting position of the arm and point of visual fixation [96] (Fig. 8.6). Surprisingly, the activity of many

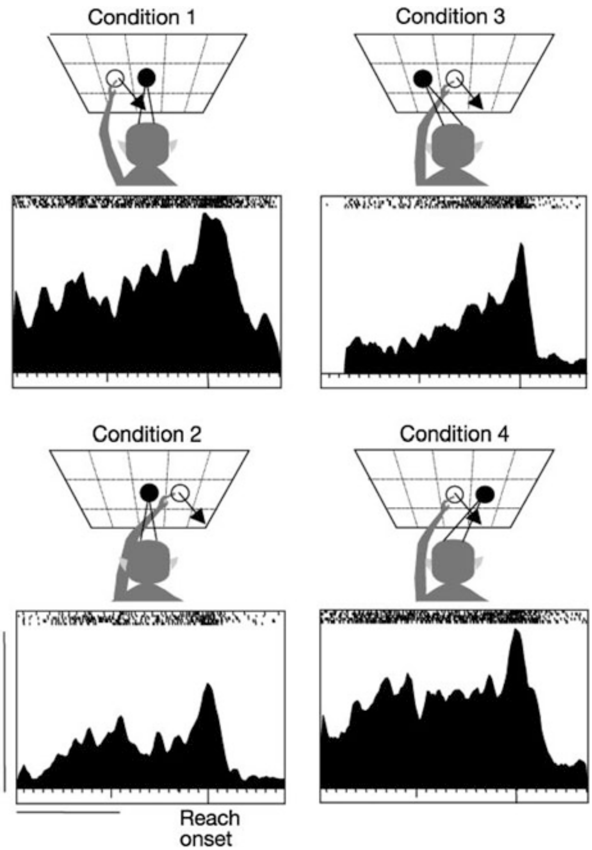

Fig. 8.6 Mixed or hybrid reference frames for reaching in the PPC [97]. Responses of a single neuron in an experiment where initial hand location and/or gaze direction were varied on a trial-by-trial basis. Responses were most similar under conditions where hand locations and target locations were identical with respect to gaze (i.e. conditions 1 and 4 and also conditions 2 and 3), despite the fact that these corresponded to different locations with respect to the body/space. Such responses could be interpreted as reflecting a hybrid representation encoding target location in both eye- and hand-centered coordinates

neurons in this movement-related area was invariant when target locations were identical in an eye-fixed reference frame (i.e. with respect to where the animal was fixating), rather than an arm or body-fixed frame. It should be noted however that the activity of a subset of neurons in this area was *also* modulated by changing the position of the arm. Importantly, changing arm position did not alter the coordinate frames used to encode target position. That is, such neurons were still 'tuned' to the position of the target in eye-coordinates; changing the position of the arm simply scaled the responses of the neuron up or down (cf. Fig. 8.1a). Interestingly, the extent of this scaling did not depend on the position of the arm with respect to the body or in space, but depended instead on the location of the hand with respect to gaze. Thus, many PRR neurons appear to encode information about the location of both the hand and target in eye-fixed coordinates and could, therefore, be considered to be encoding (at least implicitly) the required movement vector in an eye-centered reference frame as well [57, 97, 135].

The coordinate frames for reaching have subsequently been investigated in other areas of the PPC as well. In one such study, responses were examined in the caudal part of area 5, immediately adjacent to the intraparietal sulcus [97]. Using the identical experimental paradigm employed by Batista et al. [96], it was found that most neurons did not encode reach-related variables in any single reference frame; rather, the responses of these neurons were more consistent with a mixed or hybrid representation reflecting both eye- and arm-centered coordinates (Fig. 8.6). More specifically, the tuning of these neurons varied when either arm position *or* eye position was varied but, similar to PRR, was most consistent when the initial hand position and target position were identical with respect to gaze direction. This conclusion was confirmed in a subsequent experiment employing a wider range of target locations and hand positions arranged along the horizontal dimension. Lastly, additional analyses showed that this representation was workspace invariant and did not appear to depend on vision of the hand prior to reaching [133].

One limitation of the experimental paradigms employed by Batista et al. [96] and Buneo et al. [97] is that target position, arm position and eye position were not *independently* varied. More recent studies of neural reference frames in the PPC and dorsal premotor cortex have addressed these limitations by independently varying the position of the eyes, arm, and target along a horizontal axis. For example, Bremner and Andersen [136] recently examined the reference frames for reach-related activity in the dorsal subdivision of area 5, more rostral (anterior) to the part of area 5 examined by Buneo et al. [97]. They found that neurons in this area do not appear to use eye-fixed coordinates at all; rather they appear to largely encode the difference between the current target and hand locations (the movement vector) in a gaze-independent manner [136].

Thus, neurons within the PPC appear to use more than one reference frame to encode reach-related variables. More recent work is also consistent with this idea [137, 138] but it is currently unclear whether cells coding in different reference frames are arranged in a systematic gradient within the PPC or whether they are largely intermingled. For example, evidence from studies performed independently in different subdivisions of the PPC suggests that the reference frame(s) used by an individual neuron depends on that neuron's precise location within the PPC, with more caudal regions using eye coordinates [96], more rostral regions using motor- or arm-centered coordinates [136], and intermediate regions using both reference frames to encode the same variables [97]. However, other work suggests a non-systematic and idiosyncratic arrangement of neural reference frames [138], similar to what has been reported in PMdc (see below).

It is important to note that even a relatively orderly arrangement in space would not necessarily imply a sequential activation of these neural subdivisions in the form of a "wave" of activity that advances across the cortical surface. In fact, neurons in each subdivision of the PPC (as well as areas of the frontal lobe to which they are connected) appear to be activated simultaneously once the reach plan is instantiated [96, 97, 124, 129, 139, 140]. Moreover, each subdivision of the PPC appears to use the same reference frame(s) throughout the completion of a reach task [141]. As discussed above, PRR neurons appear to encode the reach exclusively in eye-coordinates, even during reach execution, while area 5 uses both eye- and arm-centered coordinates. This suggests that each stage of the coordinate transformation for reaching coexists simultaneously within the PPC and can potentially be independently read-out or decoded by other brain areas or by implanted neural interfaces.

Thus far we have discussed movement representations in the PPC in terms of extrinsic variables such as arm endpoint location and target location. Ultimately, however, some form of intrinsic (i.e. joint/muscle-based) representation is required by the motor system of the arm. In other words, simply knowing the direction and distance to move the hand is insufficient to specify an adequate control signal for the arm. This is due to the fact that the arm is biomechanically complex, with redundancy in both its mechanical degrees of freedom and available force-generating elements (muscles) at a given joint. As a result, either the movement vector representation in the PPC already reflects intrinsic coordinates or regions downstream of the PPC (in the frontal lobe) must be responsible for converting an extrinsic movement representation derived from PPC activity into an intrinsic representation required to control the arm.

Some findings suggest that both extrinsic and intrinsic representations of reaching movements coexist in the PPC [7, 142]. For example, Torres et al. [7] recently reported that during a memory-guided reaching task, the same population of MIP neurons accurately predicted impending movement trajectories in both endpoint and joint coordinates. Similarly Scott et al. [142] showed that the preferred movement directions of area 5 neurons change when arm configuration is altered but hand position and target position in space are held constant. While these findings suggest that the movement representation in area 5 is similar to those in frontal lobe reach areas, it should be noted that area 5 neurons do not appear to encode the time course of kinetic variables (such as endpoint forces) in the same way as M1 neurons [143]. This could indicate that the PPC preferentially encodes kinematic variables rather than kinetic ones, as suggested by Kalaska and colleagues [144]. Alternatively, the apparent mixing of extrinsic and intrinsic reach variables such as force could reflect a role for the PPC in estimating arm position based on vision, proprioception, and previous motor commands [57].

8.7 Coordinate Representations for Reaching: Premotor Cortex

In non-human primates, the issue of coordinate frames has also been investigated fairly extensively in the dorsal premotor cortex (PMd). Batista et al. [145] examined this issue in the caudal portion of PMd (PMdc) using an experimental paradigm similar to that used by Batista et al. [96] and Buneo et al. [97]. Here animals reached to targets on a touch screen using one of four combinations of initial hand and eye position [145]. Although many neurons did not appear to encode reach targets in any clear reference frame, some neurons appeared to encode reach targets in eye-centered coordinates and others in arm-centered coordinates, the latter

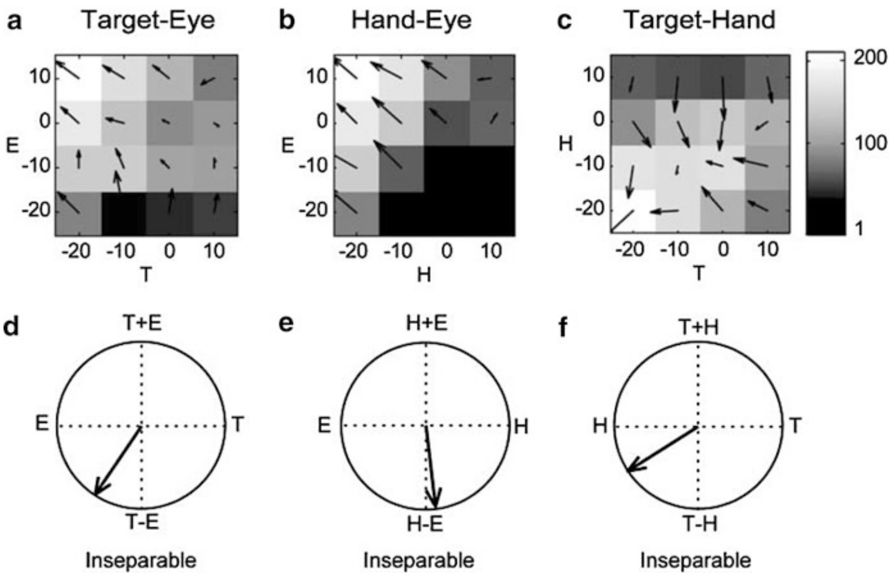

Fig. 8.7 Relative coding of spatial information in PMdr [146]. Responses of a single neuron in an experiment where initial hand location (H), target location (T) and/or gaze direction (E) were independently varied on a trial-by-trial basis. (**a**–**c**): Average firing rates plotted as a function of (**a**) gaze direction and target location, (**b**) gaze direction and hand location, and (**c**) hand and target location. Neurons encoding a given combination of variables inseparably can be said to be coding their relative position. This neuron encodes each combination of variables inseparably and can therefore be said to encode the relative positions of the hand, target and direction

being consistent with a representation of the movement vector. The activity of the remaining neurons was more consistent with a mixture of reference frames, being influenced by both the eye- and arm-centered locations of targets or by both hand and eye position. This latter group of neurons is similar to what was reported in area 5 by Buneo et al. [97]. More generally, the findings of Batista et al. [145] suggest that a multitude of reference frames are used to represent reach-related spatial information in PMdc, similar to what has been reported in the PPC.

Examination of more rostral portions of PMd (PMdr) reveals a somewhat different story [146]. Pesaran et al. [146] trained animals to reach to targets on a touch screen while independently varying the hand, eye and target positions along a single spatial dimension (see also Bremner and Andersen [136]). Although some PMdr neurons were consistent with an encoding of reach targets in either eye or hand coordinates, many neurons encoded these locations using more than one reference frame, similar to what has been reported in area 5 and PMdc. However, the paradigm used here also revealed two other important types of responses: (1) some cells were found to encode the *relative* position of the hand and eye and (2) in some of these neurons such “hand-eye” responses were combined with responses specifying target locations in eye and hand coordinates (Fig. 8.7). Thus, in PMdr, neurons can be found that encode one or more (and in some cases all) of the following vector quantities: target position relative to the hand, target position relative to the eye, and eye and hand position relative to each other. In this way, PMdr can be thought to encode the relative positions of the hand, eye and target.

A relative position code possesses several advantages over those based on absolute positions and orientations. For example, in such a scheme a given configuration of the hand, eye, and target would correspond to the same neural activity, regardless of the absolute positions of these variables in space [146]. As a result, such representations can be said to be naturally *position-invariant*. These types of representations can also be considered to be *invertible*, in that they allow a movement in eye-coordinates to be converted directly to hand-coordinates and back again [57, 146]. Why then would some parts of the premotor cortex use relative position codes and some not? The fact that more caudal regions such as PMdc (which lies immediately adjacent to the motor cortex) do not use relative position codes could simply reflect that such codes must be broken down into simpler ones (at least in part) before individual commands to move the eyes and arms can be specified and delivered to the appropriate effectors. As a result PMdc could be specifying information about arm movements in coordinates that are more intrinsic to the arm, such as joint angles or muscle activity.

The results from PMdr described above indicate that, in non-human primates, neurons can be identified that encode the relative *positions* of important task-related variables. Interestingly, evidence for relative coding of spatial variables has also been identified in areas of the human brain involved in visual processing [147]. Relative coding has also been used in robotics to represent the difference between the positions of agents engaged in actions across long distances [148] or, as indicated earlier, as the difference between the *configurations* of two effectors, e.g. the hands and arms of two agents engaged in tasks requiring interactive, dexterous manipulation [33]. Such schemes have been shown in some situations to be more computationally efficient than those employing absolute positions and configurations [149, 150]. Thus, if populations of neurons can be found in PMdr or other planning areas that encode the difference between the current and desired arm pose (position and orientation), these areas could play a critical role in the representation and facilitation of joint manipulative actions performed by human and robot agents.

8.8 Coordinate Representations for Hand Preshaping and Orienting

As in the behavioral domain, few neurophysiological studies have examined the coordinate frames involved in the planning of hand preshaping. This is likely due to a number of factors. First, monitoring hand kinematics during complex RTG tasks is considerably more challenging than monitoring corresponding arm kinematics, and is particularly challenging in non-human primates due to their smaller hands and aversion to tactile stimuli resulting from motion tracking markers and gloves. Second, the kinematics and dynamics of hand movements themselves are highly complex, involving many more mechanical degrees of freedom and muscles than arm movements. In addition, neural coding of finger movements is also highly complex, with single neurons being activated for a large range of movement types and, conversely, simple movements involving neurons that are distributed over a large part of the motor cortex [151]. These last two factors increase the difficulty associated with, for example, relating neural activity to digit placement in one or more reference frames. Lastly, defining an appropriate reference frame to describe finger movements and their associated neural activity can itself be a challenge [152]. Nonetheless, several frames could potentially be tested and disentangled including object-centered, world-centered and even visual frames [89, 153].

The neural correlates of final hand orientation (and, in some cases, grip type) have recently been probed in subdivisions of both the frontal and parietal cortices [109, 110, 117, 154]. The coordinate frames underlying this activity have largely been ignored, though some have investigated related issues such as sensitivity to the presence/absence of visual cues [117, 155]. The exception to this is the work of Kakei and colleagues who examined the responses of neurons in PMv in a task where muscle activity, direction of joint movement and direction of movement in extrinsic space were dissociated [156]. In contrast to previous findings in motor cortex, they found that nearly all of the recorded PMv neurons encoded the direction of hand-orienting movements in extrinsic rather than intrinsic (joint- or muscle-based) coordinates. It remains to be seen however if this extrinsic representation is more consistent with world-, eye-, or body-centered frames of reference.

8.9 Summary and Conclusions

In summary, multiple lines of evidence point to the fact that spatial variables relevant to reaching (and, perhaps, some aspects of grasp as well) are encoded using both absolute (eye-centered, body-centered) and relative coordinates in the association cortices of the brain. As discussed above, relative position codes can be considered to be both *position-invariant* and *invertible,* and representations employing such codes may, therefore, prove to be more tractable for neuroprosthetic and neurorobotic applications than representations based purely on absolute codes. For example, using an absolute eye-centered representation as the basis for a brain-robot interface would require a continuous tracking of gaze direction in order to correctly decode the activity. This could be accomplished using signals obtained from eye-tracking glasses, or directly from gaze-related signals embedded in the neural activity. In fact, it has been shown that the decoding of the desired reach endpoint in PMd is more accurate when eye position is accounted for by a neural prosthetic system, even when eye position is estimated directly from the neural activity [157]. In many planning areas, however, other positional signals may be present which, if left unaccounted for, could adversely affect decoding performance. In fact, failing to account for arm position also results in substantial reductions in decoding accuracy in PMd [157]. Similarly, if neurons in PMd are modulated by head position signals, then head position might also need to be accounted for in a decoder algorithm in order to maximize accuracy. Although in principle these signals could also be estimated directly from neural activity and accounted for in a decoding algorithm, doing so could prove to be challenging, particularly in the temporal domain. In addition, accounting for these signals would seem to require sampling from enough neurons such that all combinations of target, hand and body position signals are represented. This problem may be magnified by the fact that, in order to avoid the curse of dimensionality, not all combinations of these variables may be represented within a single population, but rather in only partially overlapping subpopulations [158].

In contrast, brain-robot interfaces based in areas that encode planned movements in relative coordinates would not require accounting for eye-, hand- or other body part-related signals in order to function correctly. For example, cells encoding only the relative positions of the hand and target (T−H; see Fig. 8.7) would specify the planned movement vector, regardless of the position of the hand with respect to the eyes, body, or space. This type of representation could be used by a robot-based decoder to infer the motor intent of a human subject with which a robot is cooperating and could do so regardless of the absolute positions of the human and robot arms in the workspace. However, as pointed out by Batista et al. [157], if the same set of neurons also encodes other difference vectors, such as the relative positions of the eye and target [146], the effectiveness of such a system might be limited. That is, it might prove challenging to isolate activity related to the relative positions of the hand and target (T−H), from activity related to the relative positions of the hand and eye (H−E). This issue can be avoided if distinct populations of neurons can be identified that encode predominantly one type of difference vector (such as T−H), as appears to be the case in area 5 [136].

An optimal representation for facilitating joint manipulative actions between robots and humans should specify not simply the planned change in endpoint position but the planned change in arm pose or, alternatively, the relative position and orientation between the arms of the human and robot. This is due to the fact that simply knowing the trajectory in endpoint space would be insufficient information to predict critical aspects of the transfer and manipulation of objects, including the directions of applied forces and torques. Unfortunately, it is currently unclear whether neurons in association areas of the brain encode relative configurations. This hypothesis seems highly likely though given that neurons in these areas have been shown to encode relative *positions* [97, 133, 136, 146] and are also modulated by changes in arm configuration [7, 142]. Future experiments should be aimed at a more direct assessment of the responses of such neurons during joint manipulative tasks.

References

1. Collinger JL, Wodlinger B, Downey JE, Wang W, Tyler-Kabara EC, Weber DJ, McMorland AJC, Velliste M, Boninger ML, Schwartz AB (2013) High-performance neuroprosthetic control by an individual with tetraplegia. Lancet 381(9866):557–564. doi:10.1016/s0140-6736(12)61816-9
2. Fukuda O, Tsuji T, Kaneko M, Otsuka A (2003) A human-assisting manipulator teleoperated by EMG signals and arm motions. IEEE Trans Robot Autom 19(2):210–222. doi:10.1109/tra.2003.808873
3. Hochberg LR, Bacher D, Jarosiewicz B, Masse NY, Simeral JD, Vogel J, Haddadin S, Liu J, Cash SS, van der Smagt P, Donoghue JP (2012) Reach and grasp by people with tetraplegia using a neurally controlled robotic arm. Nature 485(7398):372–375. doi:10.1038/nature11076
4. Artemiadis P, Kyriakopoulos K (2010) EMG-based control of a robot arm using low-dimensional embeddings. IEEE Trans Robot Autom 26(2):393–398
5. Andersen RA, Buneo CA (2002) Intentional maps in posterior parietal cortex. Annu Rev Neurosci 25:189–220
6. Hocherman S, Wise SP (1991) Effects of hand movement path on motor cortical activity in awake, behaving rhesus monkeys. Exp Brain Res 83(2):285–302
7. Torres EB, Quian Quiroga R, Cui H, Buneo CA (2013) Neural correlates of learning and trajectory planning in the posterior parietal cortex. Front Integr Neurosci 7:1–20
8. Xiao J, Padoa-Schioppa C, Bizzi E (2006) Neuronal correlates of movement dynamics in the dorsal and ventral premotor area in the monkey. Exp Brain Res 168(1–2):106–119. doi:10.1007/s00221-005-0074-2
9. Padoa-Schioppa C, Li CSR, Bizzi E (2002) Neuronal correlates of kinematics-to-dynamics transformation in the supplementary motor area. Neuron 36(4):751–765
10. Padoa-Schioppa C, Li CSR, Bizzi E (2004) Neuronal activity in the supplementary motor area of monkeys adapting to a new dynamic environment. J Neurophysiol 91(1):449–473. doi:10.1152/jn.00876.2002
11. Soechting JF, Flanders M (1992) Moving in 3-dimensional space – frames of reference, vectors, and coordinate systems. Annu Rev Neurosci 15:167–191. doi:10.1146/annurev.neuro.15.1.167
12. Salinas E, Sejnowski TJ (2001) Gain modulation in the central nervous system: where behavior, neurophysiology, and computation meet. Neuroscientist 7(5):430–440
13. Recanzone GH, Merzenich MM, Jenkins WM (1992) Frequency discrimination training engaging a restricted skin surface results in an emergence of a cutaneous response zone in cortical area 3a. J Neurophysiol 67:1057–1070
14. Sebanz N, Bekkering H, Knoblich G (2006) Joint action: bodies and minds moving together. Trends Cogn Sci 10(2):70–76. doi:10.1016/j.tics.2005.12.009
15. Tummolini L, Castelfranchi C (2006) Introduction to the special issue on cognition, joint action and collective intentionality. Cogn Syst Res 7(2–3):97–100. doi:10.1016/j.cogsys.2006.01.003
16. Sebanz N, Knoblich G (2009) Prediction in joint action: what, when, and where. Top Cogn Sci 1(2):353–367. doi:10.1111/j.1756-8765.2009.01024.x
17. Tomasello M, Carpenter M, Call J, Behne T, Moll H (2005) Understanding and sharing intentions: the origins of cultural cognition. Behav Brain Sci 28(5):675–691. doi:10.1017/s0140525x05000129
18. Obhi SS, Sebanz N (2011) Moving together: toward understanding the mechanisms of joint action. Exp Brain Res 211(3–4):329–336. doi:10.1007/s00221-011-2721-0
19. Rizzolatti G, Sinigaglia C (2010) The functional role of the parieto-frontal mirror circuit: interpretations and misinterpretations. Nat Rev Neurosci 11(4):264–274. doi:10.1038/nrn2805

20. Becchio C, Manera V, Sartori L, Cavallo A, Castiello U (2012) Grasping intentions: from thought experiments to empirical evidence. Front Hum Neurosci 6:117. doi:10.3389/fnhum.2012.00117
21. Sartori L, Becchio C, Castiello U (2011) Cues to intention: the role of movement information. Cognition 119(2):242–252. doi:10.1016/j.cognition.2011.01.014
22. Richardson MJ, Marsh KL, Isenhower RW, Goodman JRL, Schmidt RC (2007) Rocking together: dynamics of intentional and unintentional interpersonal coordination. Hum Mov Sci 26(6):867–891. doi:10.1016/j.humov.2007.07.002
23. Pecenka N, Keller PE (2009) Auditory pitch imagery and its relationship to musical synchronization. In: Dalla Bella S, Kraus N, Overy K, Pantev C, Snyder JS, Tervaniemi M, Tillman B, Schlaug G (eds) Neurosciences and music III: disorders and plasticity, vol 1169, Annals of the New York academy of sciences. Blackwell, Boston, pp 282–286. doi:10.1111/j.1749-6632.2009.04785.x
24. Braun DA, Ortega PA, Wolpert DM (2009) Nash equilibria in multi-agent motor interactions. Plos Comput Biol 5(8):e1000468. doi:10.1371/journal.pcbi.1000468
25. Braun DA, Ortega PA, Wolpert DM (2011) Motor coordination: when two have to act as one. Exp Brain Res 211(3–4):631–641. doi:10.1007/s00221-011-2642-y
26. Nash JF (1950) Equilibrium points in N-person games. Proc Natl Acad Sci U S A 36(1):48–49. doi:10.1073/pnas.36.1.48
27. Sebanz N, Knoblich G, Prinz W (2003) Representing others' actions: just like one's own? Cognition 88(3):B11–B21. doi:10.1016/s0010-0277(03)00043-x
28. Hommel B (2011) The Simon effect as tool and heuristic. Acta Psychol 136(2):189–202. doi:10.1016/j.actpsy.2010.04.011
29. Welsh TN (2009) When $1+1=1$: the unification of independent actors revealed through joint Simon effects in crossed and uncrossed effector conditions. Hum Mov Sci 28(6):726–737. doi:10.1016/j.humov.2009.07.006
30. Dolk T, Liepelt R, Prinz W, Fiehler K (2013) Visual experience determines the use of external reference frames in joint action control. PLoS One 8(3):e59008. doi:10.1371/journal.pone.0059008
31. Liepelt R, Wenke D, Fischer R (2013) Effects of feature integration in a hands-crossed version of the Social Simon paradigm. Psychol Res-Psychologische Forschung 77(2):240–248. doi:10.1007/s00426-012-0425-0
32. Tsai CC, Kuo WJ, Hung DL, Tzeng OJL (2008) Action co-representation is tuned to other humans. J Cogn Neurosci 20(11):2015–2024. doi:10.1162/jocn.2008.20144
33. Adorno BV, Bo APL, Fraisse P, Poignet P (2011) Towards a cooperative framework for interactive manipulation involving a human and a humanoid. In: Robotics and automation (ICRA), 2011 IEEE international conference on, 9–13 May 2011. IEEE, Piscataway, pp 3777–3783. doi:10.1109/icra.2011.5979787
34. Shibata S, Tanaka K, Shimizu A (1995) Experimental analysis of handing over. In: IEEE international workshop on robot and human communication. IEEE, Piscataway, pp 53–58
35. Kajikawa S, Ishikawa E (2000) Trajectory planning for hand-over between human and robot. In: Proceedings of the 2000 IEEE international workshop on robot and human interactive communication, Osaka, Japan. IEEE, Piscataway, pp 281–287
36. Chan W, Parker C, Van der Loos H, Croft E (2012) Grip forces and load forces in handovers: Implications for designing human-robot handover controllers. In: Human robot interaction 2012, Boston, pp 9–16
37. Huber M, Rickert M, Knoll A, Brandt T, Glasauer S (2008) Human-robot interaction in handing-over tasks. In: Proceedings of the 17th IEEE international symposium on robot and human interactive communication, Munich, Germany. IEEE, Piscataway, pp 107–112
38. Glasauer S, Huber M, Knoll A, Brandt T (2010) Interacting in time and space: investigating human-human and human-robot joint action. In: Proceedings of the 19th IEEE international symposium on robot and human interactive communication, Viareggio, Italy. IEEE, Piscataway, pp 252–257

39. Huber M, Knoll A, Brandt T, Glasauer S (2009) Handing over a cube spatial features of physical joint-action. In: Strupp M, Buttner U, Cohen B (eds) Basic and clinical aspects of vertigo and dizziness, vol 1164, Annals of the New York academy of sciences. Blackwell, Boston, pp 380–382. doi:10.1111/j.1749-6632.2008.03743.x
40. Huber M, Kupferberg A, Lenz C, Knoll A, Brandt T, Glasauer S (2013) Spatiotemporal movement planning and rapid adaptation for manual interaction. PLoS One 8(5):e64982. doi:10.1371/journal.pone.0064982
41. Crawford JD, Medendorp WP, Marotta JJ (2004) Spatial transformations for eye-hand coordination. J Neurophysiol 92(1):10–19
42. McIntyre J, Stratta F, Lacquaniti F (1997) Viewer-centered frame of reference for pointing to memorized targets in three-dimensional space. J Neurophysiol 78(3):1601–1618
43. Shadmehr R, Wise SP (2005) The computational neurobiology of reaching and pointing. The MIT Press, Cambridge, MA
44. Pouget A, Deneve S, Duhamel JR (2002) A computational perspective on the neural basis of multisensory spatial representations. Nat Rev Neurosci 3(9):741–747
45. Flanders M, Helms-Tillery SI, Soechting JF (1992) Early stages in a sensorimotor transformation. Behav Brain Sci 15:309–362
46. Henriques DY, Klier EM, Smith MA, Lowy D, Crawford JD (1998) Gaze-centered remapping of remembered visual space in an open-loop pointing task. J Neurosci 18(4):1583–1594
47. Khan AZ, Crawford JD, Blohm G, Urquizar C, Rossetti Y, Pisella L (2007) Influence of initial hand and target position on reach errors in optic ataxic and normal subjects. J Vis 7(5):8.1–8.16. doi:10.1167/7.5.8
48. McGuire LMM, Sabes PN (2009) Sensory transformations and the use of multiple reference frames for reach planning. Nat Neurosci 12(8):1056–1061. doi:10.1038/nn.2357
49. McIntyre J, Stratta F, Lacquaniti F (1998) Short-term memory for reaching to visual targets: psychophysical evidence for body-centered reference frames. J Neurosci 18(20):8423–8435
50. Pouget A, Ducom JC, Torri J, Bavelier D (2002) Multisensory spatial representations in eye-centered coordinates for reaching. Cognition 83(1):B1–B11
51. Vetter P, Goodbody SJ, Wolpert DM (1999) Evidence for an eye-centered spherical representation of the visuomotor map. J Neurophysiol 81(2):935–939
52. Tuan MT, Soueres P, Taix M, Girard B (2009) Eye-centered vs. body-centered reaching control: a robotics insight into the neuroscience debate. Paper presented at the IEEE international conference on robotics and biomimetics, Guilin, China
53. Carrozzo M, McIntyre J, Zago M, Lacquaniti F (1999) Viewer-centered and body-centered frames of reference in direct visuomotor transformations. Exp Brain Res 129:201–210
54. Engel KC, Flanders M, Soechting JF (2002) Oculocentric frames of reference for limb movement. Archives Italiennes De Biologie 140(3):211–219
55. Heuer H, Sangals J (1998) Task-dependent mixtures of coordinate systems in visuomotor transformations. Exp Brain Res 119(2):224–236
56. Sober SJ, Sabes PN (2005) Flexible strategies for sensory integration during motor planning. Nat Neurosci 8(4):490–497
57. Buneo CA, Andersen RA (2006) The posterior parietal cortex: sensorimotor interface for the planning and online control of visually guided movements. Neuropsychologia 44(13):2594–2606. doi:10.1016/j.neuropsychologia.2005.10.011
58. Buneo CA, Soechting JF (2009) Motor psychophysics. In: Squire LR (ed) Encyclopedia of neuroscience, vol 5. Elsevier, Oxford, pp 1041–1045
59. Sabes PN (2011) Sensory integration for reaching: models of optimality in the context of behavior and the underlying neural circuits. In: Green AM, Chapman CE, Kalaska JF, Lepore F (eds) Enhancing performance for action and perception: multisensory integration, neuroplasticity and neuroprosthetics, Part I, vol 191, Progress in brain research. Elsevier, Amsterdam, pp 195–209. doi:10.1016/b978-0-444-53752-2.00004-7
60. Paulignan Y, Frak VG, Toni I, Jeannerod M (1997) Influence of object position and size on human prehension movements. Exp Brain Res 114(2):226–234. doi:10.1007/pl00005631

61. Santello M, Flanders M, Soechting JF (2002) Patterns of hand motion during grasping and the influence of sensory guidance. J Neurosci 22(4):1426–1435
62. Winges SA, Weber DJ, Santello M (2003) The role of vision on hand preshaping during reach to grasp. Exp Brain Res 152(4):489–498. doi:10.1007/s00221-003-1571-9
63. Perenin MT, Vighetto A (1988) Optic ataxia: a specific disruption in visuomotor mechanisms. I. Different aspects of the deficit in reaching for objects. Brain 111(Pt 3):643–674
64. Goodale MA, Milner AD, Jakobson LS, Carey DP (1991) A neurological dissociation between perceiving objects and grasping them. Nature 349(6305):154–156
65. Darling WG, Miller GF (1993) Transformations between visual and kinesthetic coordinate systems in reaches to remembered object locations and orientations. Exp Brain Res 93(3):534–547
66. Dyde RT, Milner AD (2002) Two illusions of perceived orientation: one fools all of the people some of the time; the other fools all of the people all of the time. Exp Brain Res 144(4):518–527. doi:10.1007/s00221-002-1065-1
67. Fan J, He JP, Tillery SIH (2006) Control of hand orientation and arm movement during reach and grasp. Exp Brain Res 171(3):283–296. doi:10.1007/s00221-005-0277-6
68. Gentilucci M, Daprati E, Gangitano M, Saetti MC, Toni I (1996) On orienting the hand to reach and grasp an object. Neuroreport 7(2):589–592. doi:10.1097/00001756-199601310-00051
69. Marotta JJ, Medendorp WP, Crawford JD (2003) Kinematic rules for upper and lower arm contributions to grasp orientation. J Neurophysiol 90(6):3816–3827. doi:10.1152/jn.00418.2003
70. Mamassian P (1997) Prehension of objects oriented in three-dimensional space. Exp Brain Res 114(2):235–245. doi:10.1007/pl00005632
71. Roby-Brami A, Bennis N, Mokhtari M, Baraduc P (2000) Hand orientation for grasping depends on the direction of the reaching movement. Brain Res 869(1–2):121–129. doi:10.1016/s0006-8993(00)02378-7
72. Soechting JF, Flanders M (1993) Parallel, independent channels for location and orientation in sensorimotor transformations for reaching and grasping. J Neurophysiol 70(3):1137–1150
73. Torres EB, Zipser D (2002) Reaching to grasp with a multi-jointed arm. I. Computational model. J Neurophysiol 88(5):2355–2367
74. Torres EB, Zipser D (2004) Simultaneous control of hand displacements and rotations in orientation-matching experiments. J Appl Physiol 96(5):1978–1987. doi:10.1152/japplphysiol.00872.2003
75. Tunik E, Frey SH, Grafton ST (2005) Virtual lesions of the anterior intraparietal area disrupt goal-dependent on-line adjustments of grasp. Nat Neurosci 8(4):505–511. doi:10.1038/nn1430
76. van Doorn H, van der Kamp J, Savelsbergh GJP (2005) Catching and matching bars with different orientations. Acta Psychol 120(3):288–306. doi:10.1016/j.actpsy.2005.05.005
77. Gosselin-Kessiby N, Kalaska JF, Messier J (2009) Evidence for a proprioception-based rapid on-line error correction mechanism for hand orientation during reaching movements in blind subjects. J Neurosci 29(11):3485–3496. doi:10.1523/jneurosci.2374-08.2009
78. Gosselin-Kessiby N, Messier J, Kalaska JF (2008) Evidence for automatic on-line adjustments of hand orientation during natural reaching movements to stationary targets. J Neurophysiol 99(4):1653–1671. doi:10.1152/jn.00980.2007
79. Desmurget M, Prablanc C (1997) Postural control of three-dimensional prehension movements. J Neurophysiol 77(1):452–464
80. Strabala K, Lee MK, Dragan A, Forlizzi J, Srinivasa SS, Cakmak M, Micelli V (2013) Towards seamless human-robot handovers. J Hum Robot Interact 1(1):1–23
81. Cakmak M, Srinivasa SS, Lee MK, Kiesler S, Forlizzi J (2011) Using spatial and temporal contrast for fluent robot-human handovers. In: Proceedings of the 6th international conference on human-robot interaction, Lausanne, Switzerland. ACM Press, New York, pp 489–496

82. Nakata T, Sato T, Mori T (1998) Expression of emotion and intention by robot body movement. In: Proceedings of the international conference on intelligent autonomous systems. IOS press, Amsterdam
83. Schulte J, Rosenberg C, Thrun S (1999) Spontaneous, short-term interaction with mobile robots in public places. In: Proceedings of ICRA. IEEE, Piscataway
84. Jee E, Jeong Y, Kim CH, Kobayashi H (2010) Sound design for emotion and intention expression of socially interactive robots. Intell Serv Robot 3(3):199–206
85. Grigore EC, Eder K, Pipe AG, Melhuish C, Leonards U (2013) Joint action understanding improves robot-to-human object handover. In: Intelligent robots and systems 2013. IEEE, Piscataway, pp 1–8
86. Hogan N, Flash T (1987) Moving gracefully – quantitative theories of motor coordination. Trends Neurosci 10(4):170–174
87. Koay K, Sisbot E, Syrdal D, Walters M, Dautenhahn K, Alami R (2007) Exploratory study of a robot approaching a person in the context of handing over an object. In: Multidisciplinary collaboration for socially assistive robotics, Stanford, CA, pp 18–24
88. Bekkering H, de Bruijn ERA, Cuijpers RH, Newman-Norlund R, van Schie HT, Meulenbroek R (2009) Joint action: neurocognitive mechanisms supporting human interaction. Top Cogn Sci 1(2):340–352. doi:10.1111/j.1756-8765.2009.01023.x
89. Oztop E, Wolpert D, Kawato M (2005) Mental state inference using visual control parameters. Cogn Brain Res 22(2):129–151. doi:10.1016/j.cogbrainres.2004.08.004
90. Fabbri-Destro M, Rizzolatti G (2008) Mirror neurons and mirror systems in monkeys and humans. Physiology 23(3):171–179. doi:10.1152/physiol.00004.2008
91. Jastorff J, Begliomini C, Fabbri-Destro M, Rizzolatti G, Orban GA (2010) Coding observed motor acts: different organizational principles in the parietal and premotor cortex of humans. J Neurophysiol 104(1):128–140. doi:10.1152/jn.00254.2010
92. Fernandez-Ruiz J, Goltz HC, DeSouza JFX, Vilis T, Crawford JD (2007) Human parietal "reach region" primarily encodes intrinsic visual direction, not extrinsic movement direction, in a visual-motor dissociation task. Cereb Cortex 17(10):2283–2292. doi:10.1093/cercor/bhl137
93. Vesia M, Yan XG, Henriques DY, Sergio LE, Crawford JD (2008) Transcranial magnetic stimulation over human dorsal-lateral posterior parietal cortex disrupts integration of hand position signals into the reach plan. J Neurophysiol 100(4):2005–2014. doi:10.1152/jn.90519.2008
94. Beurze SM, Toni I, Pisella L, Medendorp WP (2010) Reference frames for reach planning in human parietofrontal cortex. J Neurophysiol 104(3):1736–1745. doi:10.1152/jn.01044.2009
95. Beurze SM, Van Pelt S, Medendorp WP (2006) Behavioral reference frames for planning human reaching movements. J Neurophysiol 96(1):352–362. doi:10.1152/jn.01362.2005
96. Batista AP, Buneo CA, Snyder LH, Andersen RA (1999) Reach plans in eye-centered coordinates. Science 285:257–260
97. Buneo CA, Jarvis MR, Batista AP, Andersen RA (2002) Direct visuomotor transformations for reaching. Nature 416(6881):632–636. doi:10.1038/416632a
98. Ernst MO, Banks MS (2002) Humans integrate visual and haptic information in a statistically optimal fashion. Nature 415(6870):429–433
99. Azanon E, Longo MR, Soto-Faraco S, Haggard P (2010) The posterior parietal cortex remaps touch into external space. Curr Biol 20(14):1304–1309. doi:10.1016/j.cub.2010.05.063
100. Tillery SIH, Flanders M, Soechting JF (1991) A coordinate system for the synthesis of visual and kinesthetic information. J Neurosci 11(3):770–778
101. Tillery SIH, Flanders M, Soechting JF (1994) Errors in kinesthetic transformations for hand apposition. Neuroreport 6(1):177–181
102. Tillery SIH, Soechting JF, Ebner TJ (1996) Somatosensory cortical activity in relation to arm posture: nonuniform spatial tuning. J Neurophysiol 76(4):2423–2438
103. Buneo CA, Andersen RA (2002) effects of gaze angle and vision of the hand on reach-related activity in the posterior parietal cortex. In: Program no 62.3. 2002 Abstract viewer/itinerary planner. Washington, DC

104. Buneo CA, Apker GA, Shi Y (2011) Probing neural correlates of cue integration. In: Trommershauser J, Kording K, Landy MS (eds) Sensory cue integration. Oxford University Press, New York/Oxford, pp 317–332
105. Gu Y, Angelaki DE, DeAngelis GC (2008) Neural correlates of multisensory cue integration in macaque MSTd. Nat Neurosci 11(10):1201–1210
106. Kokal I, Gazzola V, Keysers C (2009) Acting together in and beyond the mirror neuron system. Neuroimage 47(4):2046–2056. doi:10.1016/j.neuroimage.2009.06.010
107. Kokal I, Keysers C (2010) Granger causality mapping during joint actions reveals evidence for forward models that could overcome sensory-motor delays. PLoS One 5(10):e13507. doi:10.1371/journal.pone.0013507
108. Newman-Norlund RD, Bosga J, Meulenbroek RGJ, Bekkering H (2008) Anatomical substrates of cooperative joint-action in a continuous motor task: virtual lifting and balancing. Neuroimage 41(1):169–177. doi:10.1016/j.neuroimage.2008.02.026
109. Fluet MC, Baumann MA, Scherberger H (2010) Context-specific grasp movement representation in macaque ventral premotor cortex. J Neurosci 30(45):15175–15184. doi:10.1523/jneurosci.3343-10.2010
110. Baumann MA, Fluet MC, Scherberger H (2009) Context-specific grasp movement representation in the macaque anterior intraparietal area. J Neurosci 29(20):6436–6448. doi:10.1523/jneurosci.5479-08.2009
111. Umilta MA, Kohler E, Gallese V, Fogassi L, Fadiga L, Keysers C, Rizzolatti G (2001) I know what you are doing: a neurophysiological study. Neuron 31(1):155–165. doi:10.1016/s0896-6273(01)00337-3
112. Fujii N, Hihara S, Iriki A (2008) Social cognition in premotor and parietal cortex. Soc Neurosci 3(3–4):250–260. doi:10.1080/17470910701434610
113. Kaas JH, Gharbawie OA, Stepniewska I (2011) The organization and evolution of dorsal stream multisensory motor pathways in primates. Front Neuroanat 5:34. doi:10.3389/fnana.2011.00034
114. Andersen RA, Cui H (2009) Intention, action planning, and decision making in parietal-frontal circuits. Neuron 63(5):568–583. doi:10.1016/j.neuron.2009.08.028
115. Buneo CA (2010) Neural representations of intended movement. In: Koob G, Le Moal M, Thompson R (eds) Encyclopedia of behavioral neuroscience, vol 2. Elsevier, Oxford, pp 356–361
116. Andersen RA, Buneo CA (2002) Intentional maps in posterior parietal cortex. Annu Rev Neurosci 25:189–220. doi:10.1146/annurev.neuro.25.112701.142922
117. Raos V, Umilta MA, Gallese V, Fogassi L (2004) Functional properties of grasping-related neurons in the dorsal premotor area F2 of the macaque monkey. J Neurophysiol 92(4):1990–2002. doi:10.1152/jn.00154.2004
118. Fattori P, Kutz DF, Breveglieri R, Marzocchi N, Galletti C (2005) Spatial tuning of reaching activity in the medial parieto-occipital cortex (area V6A) of macaque monkey. Eur J Neurosci 22(4):956–972. doi:10.1111/j.1460-9568.2005.04288.x
119. Hikosaka O, Wurtz RH (1983) Visual and oculomotor functions of monkey substantia nigra pars reticulata. III. Memory-contingent visual and saccade responses. J Neurophysiol 49(5):1268–1284
120. Kurata K, Wise SP (1988) Premotor cortex of rhesus-monkeys: set-related activity during 2 conditional motor tasks. Exp Brain Res 69(2):327–343
121. Shen LM, Alexander GE (1997) Neural correlates of a spatial sensory-to-motor transformation in primary motor cortex. J Neurophysiol 77(3):1171–1194
122. Moran DW, Schwartz AB (1999) Motor cortical representation of speed and direction during reaching. J Neurophysiol 82(5):2676–2692
123. Crammond DJ, Kalaska JF (2000) Prior information in motor and premotor cortex: activity during the delay period and effect on pre-movement activity. J Neurophysiol 84(2):986–1005
124. Messier J, Kalaska JF (2000) Covariation of primate dorsal premotor cell activity with direction and amplitude during a memorized-delay reaching task. J Neurophysiol 84(1):152–165

125. Churchland MM, Afshar A, Shenoy KV (2006) A central source of movement variability. Neuron 52(6):1085–1096. doi:10.1016/j.neuron.2006.10.034
126. Li CSR, Padoa-Schioppa C, Bizzi E (2001) Neuronal correlates of motor performance and motor learning in the primary motor cortex of monkeys adapting to an external force field. Neuron 30(2):593–607
127. Colby CL, Goldberg ME (1999) Space and attention in parietal cortex. Annu Rev Neurosci 22:319–349
128. Snyder LH, Batista AP, Andersen RA (1997) Coding of intention in the posterior parietal cortex. Nature 386(6621):167–170
129. Battaglia-Mayer A, Ferraina S, Mitsuda T, Marconi B, Genovesio A, Onorati P, Lacquaniti F, Caminiti R (2000) Early coding of reaching in the parietooccipital cortex. J Neurophysiol 83(4):2374–2391
130. Quiroga RQ, Snyder LH, Batista AP, Cui H, Andersen RA (2006) Movement intention is better predicted than attention in the posterior parietal cortex. J Neurosci 26(13):3615–3620
131. Battaglia-Mayer A, Mascaro M, Caminiti R (2007) Temporal evolution and strength of neural activity in parietal cortex during eye and hand movements. Cereb Cortex 17(6):1350–1363
132. Cui H, Andersen RA (2007) Posterior parietal cortex encodes autonomously selected motor plans. Neuron 56(3):552–559. doi:10.1016/j.neuron.2007.09.031
133. Buneo CA, Andersen RA (2012) Integration of target and hand position signals in the posterior parietal cortex: effects of workspace and hand vision. J Neurophysiol 108(1):187–199. doi:10.1152/jn.00137.2011
134. Beurze SM, de Lange FP, Toni I, Medendorp WP (2007) Integration of target and effector information in the human brain during reach planning. J Neurophysiol 97(1):188–199
135. Chang SWC, Papadimitriou C, Snyder LH (2009) Using a compound gain field to compute a reach plan. Neuron 64(5):744–755. doi:10.1016/j.neuron.2009.11.005
136. Bremner LR, Andersen RA (2012) Coding of the reach vector in parietal area 5d. Neuron 75(2):342–351. doi:10.1016/j.neuron.2012.03.041
137. McGuire LMM, Sabes PN (2011) Heterogeneous representations in the superior parietal lobule are common across reaches to visual and proprioceptive targets. J Neurosci 31(18):6661–6673. doi:10.1523/jneurosci.2921-10.2011
138. Chang SWC, Snyder LH (2010) Idiosyncratic and systematic aspects of spatial representations in the macaque parietal cortex. Proc Natl Acad Sci U S A 107(17):7951–7956. doi:10.1073/pnas.0913209107
139. Battaglia-Mayer A, Ferraina S, Genovesio A, Marconi B, Squatrito S, Molinari M, Lacquaniti F, Caminiti R (2001) Eye-hand coordination during reaching. II. An analysis of the relationships between visuomanual signals in parietal cortex and parieto-frontal association projections. Cereb Cortex 11(6):528–544
140. Russo GS, Backus DA, Ye SP, Crutcher MD (2002) Neural activity in monkey dorsal and ventral cingulate motor areas: comparison with the supplementary motor area. J Neurophysiol 88(5):2612–2629
141. Buneo CA, Batista AP, Jarvis MR, Andersen RA (2008) Time-invariant reference frames for parietal reach activity. Exp Brain Res 188(1):77–89. doi:10.1007/s00221-008-1340-x
142. Scott SH, Sergio LE, Kalaska JF (1997) Reaching movements with similar hand paths but different arm orientations. 2. Activity of individual cells in dorsal premotor cortex and parietal area 5. J Neurophysiol 78(5):2413–2426
143. Hamel-Paquet C, Sergio LE, Kalaska JF (2006) Parietal area 5 activity does not reflect the differential time-course of motor output kinetics during arm-reaching and isometric-force tasks. J Neurophysiol 95(6):3353–3370. doi:10.1152/jn.00789.2005
144. Kalaska JF, Cohen DAD, Prudhomme M, Hyde ML (1990) Parietal area-5 neuronal-activity encodes movement kinematics, not movement dynamics. Exp Brain Res 80(2):351–364
145. Batista AP, Santhanam G, Yu BM, Ryu SI, Afshar A, Shenoy KV (2007) Reference frames for reach planning in macaque dorsal premotor cortex. J Neurophysiol 98(2):966–983
146. Pesaran B, Nelson MJ, Andersen RA (2006) Dorsal premotor neurons encode the relative position of the hand, eye, and goal during reach planning. Neuron 51(1):125–134

147. Hayworth KJ, Lescroart MD, Biederman I (2011) Neural encoding of relative position. J Exp Psychol-Hum Percept Perform 37(4):1032–1050. doi:10.1037/a0022338
148. Desai JP, Ostrowski JP, Kumar V (2001) Modeling and control of formations of nonholonomic mobile robots. IEEE Trans Robot Autom 17(6):905–908. doi:10.1109/70.976023
149. Dissanayake M, Newman P, Clark S, Durrant-Whyte HF, Csorba M (2001) A solution to the simultaneous localization and map building (SLAM) problem. IEEE Trans Robot Autom 17(3):229–241. doi:10.1109/70.938381
150. Taylor CJ, Spletzer J (2007) A bounded uncertainty approach to cooperative localization using relative bearing constraints. In: Proceedings of the 2007 IEEE/RSJ international conference on intelligent robots and systems, San Diego, CA. IEEE, Piscataway
151. Santello M, Baud-Bovy G, Jorntell H (2013) Neural bases of hand synergies. Front Comput Neurosci 7:23. doi:10.3389/fncom.2013.00023
152. Georgopoulos AP, Pellizzer G, Poliakov AV, Schieber MH (1999) Neural coding of finger and wrist movements. J Comput Neurosci 6(3):279–288. doi:10.1023/a:1008810007672
153. Selen LPJ, Medendorp WP (2011) Saccadic updating of object orientation for grasping movements. Vis Res 51(8):898–907. doi:10.1016/j.visres.2011.01.004
154. Fattori P, Breveglieri R, Marzocchi N, Filippini D, Bosco A, Galletti C (2009) Hand orientation during reach-to-grasp movements modulates neuronal activity in the medial posterior parietal area V6A. J Neurosci 29(6):1928–1936. doi:10.1523/jneurosci.4998-08.2009
155. Theys T, Srivastava S, van Loon J, Goffin J, Janssen P (2012) Selectivity for three-dimensional contours and surfaces in the anterior intraparietal area. J Neurophysiol 107(3):995–1008. doi:10.1152/jn.00248.2011
156. Kakei S, Hoffman DS, Strick PL (2001) Direction of action is represented in the ventral premotor cortex. Nat Neurosci 4(10):1020–1025
157. Batista AP, Yu BM, Santhanam G, Ryu SI, Afshar A, Shenoy KV (2008) Cortical neural prosthesis performance improves when eye position is monitored. IEEE Trans Neural Syst Rehabil Eng 16(1):24–31
158. Pouget A, Dayan P, Zemel R (2000) Information processing with population codes. Nat Rev Neurosci 1(2):125–132. doi:10.1038/35039062

Chapter 9
Assisted Computer Interaction for Users with Weak Upper Limb Motion

Nikos G. Tsagarakis and Darwin G. Caldwell

9.1 Introduction

Computer assisted therapy is one of the most promising new techniques for those suffering from physical and neurological dysfunction. As a result recently there has been a considerable body of work directed towards the development of rehabilitation and power/motion coordination systems based on assistive robotic devices [1, 2]. These devices range from manipulandums and simple power orthoses to exoskeletal systems [3–13] and aim to assist in all areas of physical therapy, for instance, to recover from different injuries, to compensate for various disabilities, or to provide motion coordination/assistance and performance evaluation [14–24]. Some of these pathological conditions such as; Parkinson's disease, Muscular Dystrophy, Muscle Ataxia and Cerebral Palsy have symptoms such as reduced strength, restricted or irregular (jerky) movements, poor motion coordination and a continuum of impairments involving spasms and tremors. Often these physical impairments can make it difficult or impossible for sufferers to interact with computer generated environments using conventional mouse type interfaces [25, 26] limiting their scope to take advantage of developments in computer technology for work, educational, entertainment and social purposes. This has a significant impact on life and work opportunities. Assistive robotic devices may help to ameliorate these difficulties for this group. For interactions with a computer generated environment, the efficacy of various human machine interfaces such as force feedback mouse [27, 28] has been evaluated in GUI interaction tasks. Velocity dependent force feedback has

N.G. Tsagarakis, Ph.D. (✉)
Department of Advanced Robotics (ADVR), Istituto Italiano di Tecnologia (IIT-Genova), Via Morego 30, Genova 16163, Italy
e-mail: nikos.tsagarakis@iit.it

D.G. Caldwell, Ph.D.
Department of Advanced Robotics, Istituto Italiano di Tecnologia (IIT), Via Morego 30, Genova 16163, Italy

P. Artemiadis (ed.), *Neuro-Robotics: From Brain Machine Interfaces to Rehabilitation Robotics*, Trends in Augmentation of Human Performance 2,
DOI 10.1007/978-94-017-8932-5_9,

been evaluated in a number of other studies to damp erratic motions [29, 30]. It has been shown that increasing the viscous damping helps to reduce the level of sudden motions but at the same time resistance to voluntary movement may occur.

Following similar path this work has the goal to improve the capability and efficiency of people with motion impairments arising from the pathological disorder muscle ‘Ataxia’, while interacting with computer generated environments using a conventional mouse interface. Ataxia (from Greek *ataxia*, meaning *failure to put in order*) is unsteady and clumsy motion of the limbs or trunk due to a failure of the gross coordination of muscle movements. It is a relatively rare disorder with about 20,000 cases in Europe and North America (1/50,000). While the term ataxia is primarily used to describe this set of symptoms, it is sometimes also used to refer to a family of disorders. It is not, however, a specific diagnosis [31]. Symptoms usually appear between the ages of 5 and 15 and involve: poor muscle tone and weak muscles; difficulty making rapid changes in muscle tension; undershooting or overshooting of a target trajectory.

The third symptom is not only due to the failure of the gross motion coordination and control, but is also a physical consequence of the first two symptoms. Weak muscle tone or inability to rapidly change the muscle tension prevents the subjects from perceiving the expected motion effect of their effort, leading to overshooting of the target trajectory. Subjects, consequently, apply greater effort to generate satisfactory motions which often results in overshooting trajectories. These symptoms can make the use of computer keyboard and mouse devices difficult or even impossible.

This work explores the application of a 2-dimensional haptic device as an assistive robotic aid to minimize the effects of the pathological absence of motor control in the upper limb in impaired users when using a mouse. The reduction in the undershooting is achieved by assisting the execution of movement to compensate for the poor muscle tone. This allows the impaired subjects to generate motions with less effort which in consequence reduces the possibility of overshooting. The end-tip of the device has been attached to a traditional mouse interface to form the complete mouse motion assistive interface. The device details and its assistive control strategy are described. The assistive functionality of the system is validated in tracking tasks using a human subject with failure of the gross coordination of the upper limb muscle movements – ‘Muscle Ataxia’. Experimental results demonstrate that with this system the capability of the impaired subject to track predefined trajectories within a computer generated 2D is significantly improved.

9.2 Description of the Assistive Haptic System

9.2.1 System Configuration

The custom assistive haptic device developed in this work is shown in Fig. 9.1. It is a five bar pantograph system with its dimensions (links) specified to permit the end-tip of the device to cover the field of motion usually found in mouse based interactions.

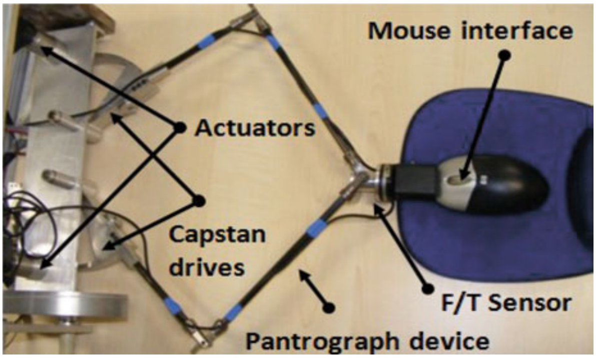

Fig. 9.1 The planar pantograph haptic system integrated with a mouse

Table 9.1 Specifications of the planar haptic device

Property	Value
Actuator	40 W DC motors
Position resolution	<0.05 mm
Back-drivable friction	<0.2 N
Peak force	26 N
Continues stall force	3.9 N
Workspace	340 × 250 mm

The device is powered by two precious metal brushed 40 W DC-motors from Portescap (Model 25GT2R82-222E) through capstan cable transmissions which provide a 26:1 gearing ratio with minimum friction and excellent back drivability (back-drivable friction is below 0.2 N). Incremental encoders at the joints monitor the position changes of the device tip, while torque sensors measure the torque at each motor output shaft. The specifications of the device are shown in Table 9.1.

The haptic system end-tip has been interfaced with a mouse to form the assistive interface for the GUI based interactions. To monitor the exchange of forces between the assistive system and user's hand a force sensor has been installed between the mouse and the haptic device. The cost of the prototype haptic device is 1300€ excluding the cost of the 6DOF F/T sensor (5,000€). This additional cost of the force torque sensor can be significantly reduced by replacing it with a two axis load cell with a cost of approximately 500€. Although a 2DOF load cell is sufficient the 6DOF sensor was used in this study as it was already available in our laboratory.

9.2.2 Device Kinematics

The kinematic configuration of the assistive haptic device is presented in Fig. 9.2. The position vector of the device tip with respect to the base frame $O(\mathbf{x_o}, \mathbf{y_o}, \mathbf{z_o})$ is denoted by $\mathbf{x_t}$. We can obtain $\mathbf{x_t}$ as a function of the active joint angles $q_i,\ i = 1, 2$ and the upper link angle q_u:

Fig. 9.2 The kinematic geometry of the haptic device

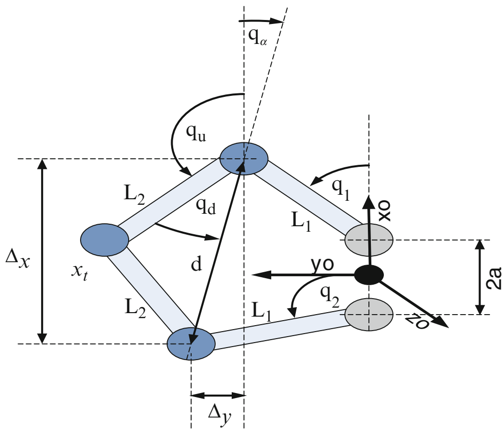

$$\mathbf{x_t} = \begin{bmatrix} \mathrm{a} + \mathrm{L}_1 \cos(\mathrm{q}_1) + \mathrm{L}_2 \cos(\mathrm{q}_\mathrm{u}) \\ \mathrm{L}_1 \sin(\mathrm{q}_1) + \mathrm{L}_2 \sin(\mathrm{q}_\mathrm{u}) \end{bmatrix} \tag{9.1}$$

where L_1, L_2 are the lengths of links and a is the location, along the X-axis, of the proximal joints of the inner links with respect to the base frame. The upper link angle q_u can be determined using the geometry of the five bar mechanism $q_u = \pi - q_d - q_\alpha$.

The angle q_d can be computed from the triangle formed by the outer links and the line joining the distal joints of the inner links $q_d = \arccos\left(\frac{d}{2L_2}\right)$ while angle q_α is given by $q_\alpha = \arctan\left(\frac{\Delta y}{\Delta x}\right)$. L_2, d and $\Delta x, \Delta y$ represent the length of the distal link, the length of the line joining the distal joints of the inner links and the x, y distances between the distal joints of the inner links respectively. Substituting q_u in (9.1) and directly differentiating the final expression of the forward kinematics yields the device Jacobian which relates the handle tip velocity to the two active joint velocities.

$$\dot{\mathbf{x}}_\mathbf{t} = \mathbf{J}\dot{\mathbf{q}} \tag{9.2}$$

The dynamic behavior of the haptic device is finally described by:

$$\mathbf{D}(\mathbf{q})\ddot{\mathbf{q}} + \mathbf{C}(\mathbf{q}, \dot{\mathbf{q}}) + \mathbf{F}(\dot{\mathbf{q}}) + \mathbf{J}^\mathbf{T}\mathbf{F_d} = \boldsymbol{\tau} \tag{9.3}$$

where the newly introduced notations describe: $\boldsymbol{\tau}$ the generalized joint torque vector, $\mathbf{D}(\mathbf{q})$ the inertia matrix, $\mathbf{C}(\mathbf{q}, \dot{\mathbf{q}})$ the coriolis/centripetal vector, $\mathbf{F}(\dot{\mathbf{q}})$ the friction vector, $\mathbf{F_d}$ is the force that the device generates at the end-tip and $\mathbf{J}^\mathbf{T}$ is the transpose Jacobian of the haptic device.

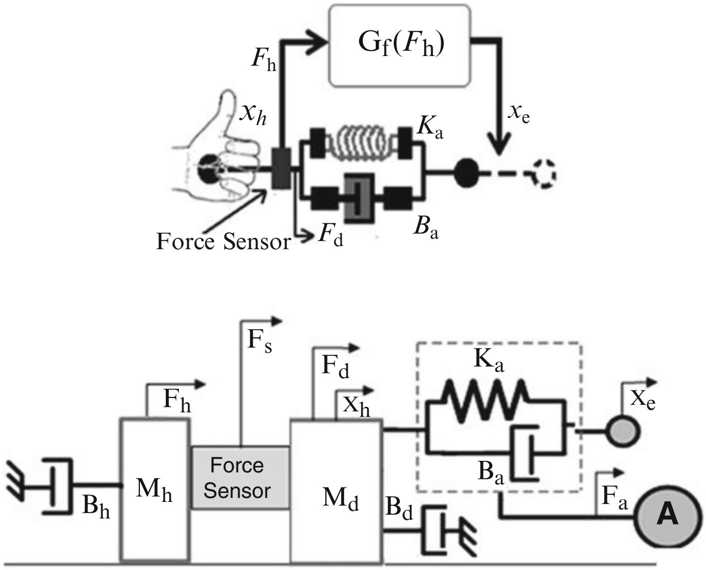

Fig. 9.3 User hand/device interaction diagram (*top*) and conceptual 1DOF linear model of the proposed assistive/suppression control law (*bottom*)

9.2.3 Assistive Control Scheme

The haptic device and its control scheme aims to aid a subject with motion coordination difficulties to interact with GUIs using a mouse by assisting the movements in the trajectory regions where motion is weak. We introduce the assistive control for the haptic device by initially considering the 1DOF linear mechanical system shown in Fig. 9.3.

The extension of the concept to the full system will be discussed in the next section. In Fig. 9.3, mass M_h and damper B_h resemble the mass and damping properties of the human forearm and hand segments (mouse motions are primary generated by the movement of the elbow, wrist and finger joints). The user mass/damper block is fixed to the device end-tip through a force sensor which monitors the forces exchanged between the user and the haptic device. The device itself is represented by the mass/damper network denoted by M_d and B_d. The spring/damper arrangement indicated by K_a, B_a is a virtual spring/damper group which is attached to the device tip at its one end point and represents the assistive control network. The remaining notations introduced in Fig. 9.3 are; F_h the force applied by the user, F_d the force provided by the device, F_s the force measured by the sensor, F_a the force generated by the actuator *A*, X_h the current device end-tip position and X_e the assistive network (K_a, B_a) grounding position which is dynamically updated according to the user effort and intended motion.

9.2.3.1 Assistive Controller Description

Let now assume that the subject's hand is applying a force F_h through the mouse, while the haptic device is exerting a force F_d. The difference between these two forces is measured as the force sensor $F_s = F_h - F_d$. To provide the assistive functionality the amplitude and the direction of the assistive force needs to be determined. It is reasonable to use the direction of F_h to determine the direction of the user's intended motion. The force applied by the user F_h can then be computed from the measured force F_s as follows:

$$F_h = F_s + F_d \tag{9.4}$$

To generate an assistive force in the user's intended direction of movement, the assistive control network, represented by the spring/damper group (K_a, B_a) is used. One end of this virtual spring/damper system is rigidly linked to the device end-tip, while its second end is free to move; its position X_e is determined using the user's effort and intended motion. In particular, the desired position X_e of the assistive network grounding end point is updated using the user force F_h. This can be written as:

$$X_e = G_f\, F_h \tag{9.5}$$

where G_f represents the transfer function between the force exerted by the user and the grounding end point position. A possible transfer function G_f which can be used is the simple integrator $G_f = \frac{K_f}{s}$. The motivation behind the simple integrator is based on the idea that the accumulation of forces applied by the user can give a good indication/estimation of the user motion intention/direction and therefore it can be used to update X_e towards this direction. Other transfer function candidates include double integrators or other higher order controllers which could in addition permit shaping of the frequency response, e.g. preventing any tremor noise from entering the estimation of the intention of motion. As ataxia subjects do not suffer for this kind of tremor noise a simple integrator was experimentally proved (see section IV) to be adequate in this case.

The perturbation of the free end of assistive spring/damper network will trigger the generation of forces attracting the device end-tip towards the position X_e of the free end-point. In other words the device will generate a force F_d pulling towards X_e, which from the user's point of view will be perceived as a force assisting his/her movement (the direction of the perturbation of X_e has been selected to coincide with the direction of the user's applied force F_h). The pulling force is determined by the properties of the virtual assistive spring/damper (K_a, B_a) and is written as:

$$F_d = G_a\,(x_e - x_h) \quad \text{with} \quad G_a = B_a s + K_a \tag{9.6}$$

To exert the assistive force F_d at the device tip we select an actuator control signal as follows:

$$F_a = u = F_d + G_d x_h = G_a (x_e - x_h) + G_d x_h \tag{9.7}$$

where the term $G_d x_h$ with $G_d = M_d s^2 + B_d s$ is added to compensate for the device dynamics. This pulling force F_d together with the force applied by the user F_h, drives the position of the pair (Haptic device + user's hand) X_h towards X_e. It can be written:

$$x_h = \frac{F_h + F_d}{G_h} \tag{9.8}$$

where $G_h = M_h s^2 + B_h s$ resembles the mass and damping properties of the human hand/finger segments. By injecting F_h, F_d from (9.5) and (9.6) into (9.8) the position X_h can be obtained as a function of X_e.

$$x_h = \frac{F_h + F_d}{G_h} = \frac{\frac{X_e}{G_f} + G_a (x_e - x_h)}{G_h} = \frac{\frac{1}{G_f} + G_a}{G_h + G_a} x_e \tag{9.9}$$

Similarly by substituting X_h and X_e from (9.5) and (9.8) in (9.6) the assistive force F_d developed by the device can be derived as a function of the human applied force F_h.

$$F_d = G_a (x_e - x_h) = \frac{G_a G_f G_h - G_a}{G_h + G_a} F_h \tag{9.10}$$

Substituting G_h, G_a and G_f into (9.9) and (9.10) x_h and F_d can be obtained as a function of the device, the human arm and the assistive network parameters.

9.2.3.2 Stability Analysis and Assistive Gain Selection

The characteristic equation of the transfer functions in (9.9) and (9.10) is

$$G_h(s) + G_a(s) = M_h s^2 + (B_h + B_a) s + K_a$$

This characteristic equation is subject to change due to variations in $G_h(s)$. This is due to the variability in the mass and damping coefficients of the human arm M_h and B_h. If $(B_h + B_a) > 0$ and $K_a > 0$, then $G_h(s)$ is Hurwitz. We may write:

$$\frac{K_a}{M_h} = \omega_n^2 \text{ and } \zeta = \frac{B_h + B_a}{2 M_h \omega_n} = \frac{B_h + B_a}{2\sqrt{M_h K_a}} \tag{9.11}$$

where ω_n is the natural frequency for a stable, second-order, closed-loop system and ζ is the damping ratio. Through the control parameters of the assistive spring network (K_a, B_a), we have independent regulation of the natural frequency and damping ratio. We choose a desired $\zeta = \sqrt{2}/2$ such that the system is underdamped. Therefore from (9.11) we can obtain:

$$\zeta = \frac{B_h + B_a}{2\sqrt{M_h K_a}} \Rightarrow B_a = \sqrt{2M_h K_a} - B_h \tag{9.12}$$

The parameters of the assistive control law (K_a, B_a) are selected by considering the desired system bandwidth and damping ratio. Since the system and controller are used as a mouse based motion assistive device it is sensible to select the (K_a, B_a) gains such that the bandwidth of the system is greater than the maximum motion frequency during mouse based interaction movements (1–2 Hz). For this simulation study a bandwidth of ~ 5 Hz ($\omega_n = 30$ rad/s) was considered for the 1DOF system presented in Fig. 9.3. The assistive network parameters were determined from (9.11) and (9.12) as $K_a = 10$ N/cm and $B_a 30$ N s/cm. The mass and damping properties of the human hand/finger were set as $M_h = 1$ Kg, $B_h = 0$. The level of damping at the wrist and finger joints during voluntary movements is greatly affected by many factors the most important of which are; the mean level of muscle activation and the angular velocity of the joint [30]. Therefore, the value of the joint damping is a highly uncertain parameter with its maximum level being of an order greater than the minimum. Various studies [32–35] reports damping ratios for the forearm joints (elbow, wrist and finger joints) in the range of 0.1–1.0. By setting $B_h = 0$ the worst case condition in terms of system stability (hand/finger represented by a pure mass) is applied.

9.2.3.3 Assistive Controller Validation

To test the assistive control scheme, simulation studies were carried out on the 1DOF system shown in Fig. 9.3. The gain parameters used were those reported in the previous section. Here, a step like force input lasting for 0.2 s as shown in Fig. 9.4 (top graph) was used to trigger the 1DOF system.

The top graph in Fig. 9.4 depicts the resultant perturbation of the grounded end of the assistive spring/damper group X_e and the dynamic behaviour of X_h towards X_e (dashed line). The displacement of X_e triggers the generation of force which pulls the device tip X_h towards the position X_e.

The attracting force F_d plotted against the force applied by the human F_h is shown in the following graph, Fig. 9.4. It increases with the application of the human force F_h to assist the motion and declines as soon as the human force is removed and the device position X_h reaches the target point X_e. The fourth graph in Fig. 9.4 presents the ratio $\frac{F_h}{F_d}$ which can be seen as the reciprocal of the assistive ratio. A high value indicates the absence of assistive forces, while low values reveal their existence. It can be seen that the reciprocal of the assistive ratio is high during the application of the human force, but rapidly declines indicating the rise of the assistive force component.

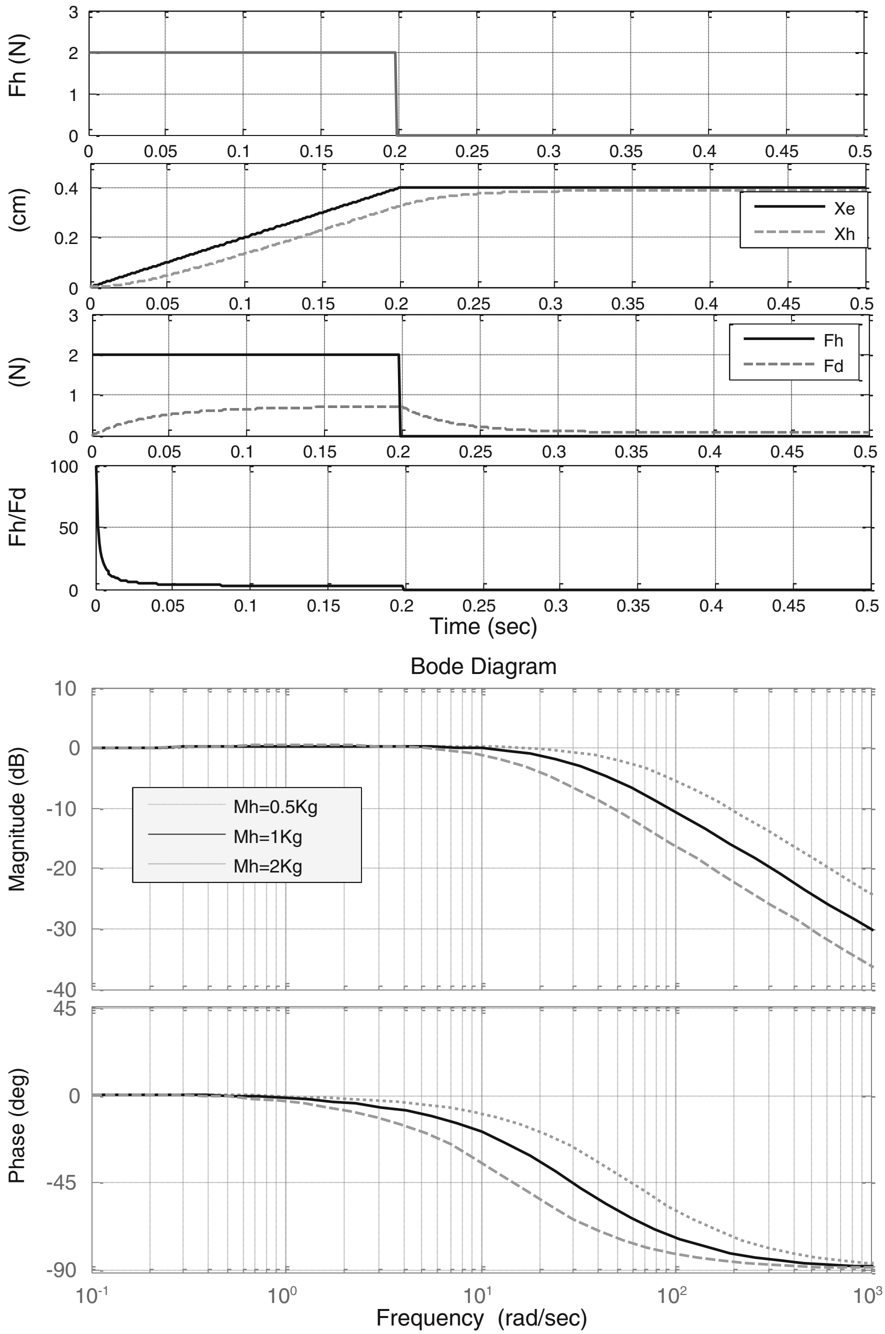

Fig. 9.4 The simulated responses of the 1DOF assistive control system

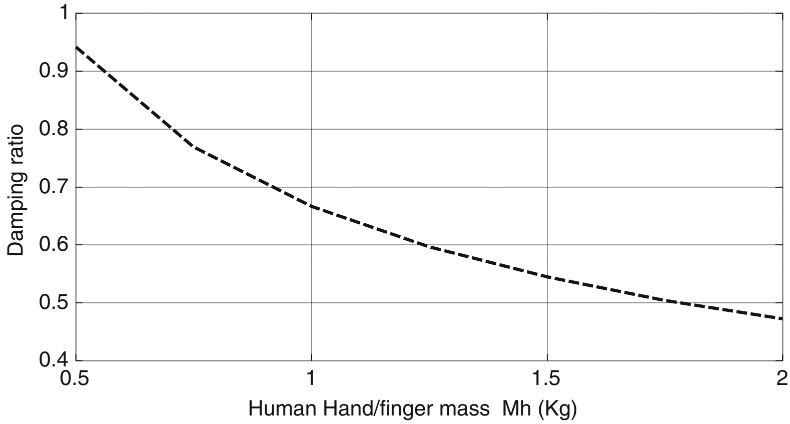

Fig. 9.5 Damping ratio of $\frac{x_h}{x_e}$ dynamics as a function of hand/finger mass M_h

The Bode diagram in Fig. 9.4 presents the effect of the variation of the mass of the human hand/finger ($0.5\text{ Kg} < M_h < 2\text{ Kg}$) to the bandwidth of $\frac{x_h}{x_e}$ dynamics demonstrating a bandwidth of ~ 5 Hz (30 rad/s) for a nominal mass of $M_h = 1\text{Kg}$. In Fig. 9.5 the variation of the damping ratio of $\frac{x_h}{x_e}$ dynamics is presented as a function of the mass of the human hand/finger M_h. These simulation results demonstrate the potential of the proposed scheme as an assistive controller when triggered by the application of the human force.

9.3 Assistive Controller for the Haptic Device

The overall dynamic behaviour of the haptic device is described by (9.3). This equation can also be used to describe the interaction between the subject and the haptic device. Considering the scenario shown in Fig. 9.6, where the subject's hand is attached to the device tip, $\mathbf{F_h}$ denotes the two dimensional force vector that the subject exerts on the planar device tip and $\mathbf{F_d} = -\mathbf{F_h}$ is the planar force vector that the device applies back to the subject as a consequence of the displacements of the device tip. Suppose now that $\mathbf{Z}_a$ is the system desired output mechanical impedance which governs the force $\mathbf{F_h}$ felt by the user. To make the coupled pair's (Haptic Device + subject's hand) motion follow the desired impedance dynamics, the following expression must be applied.

$$\mathbf{F_h} = \mathbf{M_a}\ddot{\mathbf{x}}_\mathbf{h} + \mathbf{B_a}\dot{\mathbf{x}}_\mathbf{h} + \mathbf{K_a}\left(\mathbf{x_h} - \mathbf{x_e}\right) \tag{9.13}$$

To be consistent with the 1DOF system presented in Fig. 9.3, $(\mathbf{M_a}, \mathbf{B_a}, \mathbf{K_a})$ represent the inertia, damping and stiffness matrix coefficients of the desired impedance $\mathbf{Z_a}$ while $\mathbf{x_e}$ is the impedance equilibrium position vector (equivalent

Fig. 9.6 The user interacting with the planar haptic device

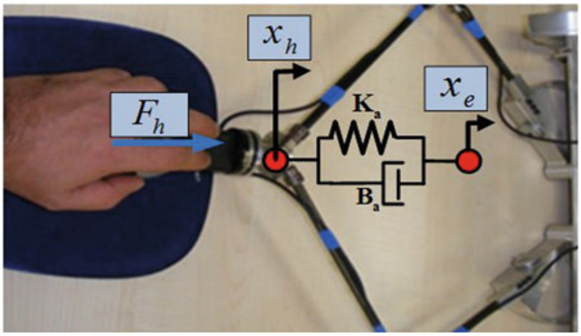

to the grounding end point of the assistive network of the 1DOF system presented in the previous section) and $\mathbf{x_h}$ is the position of subject's hand and device end tip.

Having specified the desired behaviour of the system, the control law can be derived by eliminating $\ddot{\mathbf{x}}_\mathbf{h}$ and $\ddot{\mathbf{q}}$ from equations (9.3) and (9.13). To do this the following equations, which relate the velocities and accelerations of the assistive haptic device end-point with the velocities and accelerations in joint space are introduced.

$$\ddot{\mathbf{x}}_\mathbf{h} = \mathbf{J}\ddot{\mathbf{q}} + \dot{\mathbf{J}}\mathbf{q} \tag{9.14}$$

Solving (9.13) and (9.14) for $\ddot{\mathbf{x}}_\mathbf{h}$ and $\ddot{\mathbf{q}}$ respectively gives:

$$\ddot{\mathbf{x}}_\mathbf{h} = \mathbf{M}_\mathbf{a}^{-1}\left\{\mathbf{F_h} - \mathbf{B_a}\dot{\mathbf{x}}_\mathbf{h} - \mathbf{K_a}\left(\mathbf{x_h} - \mathbf{x_e}\right)\right\} \tag{9.15}$$

$$\ddot{\mathbf{q}} = \mathbf{J}^{-1}\left(\ddot{\mathbf{x}}_\mathbf{h} - \dot{\mathbf{J}}\mathbf{q}\right) \tag{9.16}$$

Combining, (9.3), (9.15), and (9.16) $\ddot{\mathbf{q}}$ can be eliminated to give:

$$\mathbf{D}\left(\mathbf{q}\right)\mathbf{J}^{-1}\left(\mathbf{M}_\mathbf{a}^{-1}\left(\mathbf{F_h} - \mathbf{B_a}\dot{\mathbf{x}}_\mathbf{h} - \mathbf{K_a}\left(\mathbf{x_h} - \mathbf{x_e}\right)\right) - \dot{\mathbf{J}}\dot{\mathbf{q}}\right) + \mathbf{G}\left(\mathbf{q}\right) = \tau - \mathbf{J^T}\mathbf{F_d} \tag{9.17}$$

To keep the cartesian inertia of the device unchanged we select:

$$\mathbf{M_a} = \mathbf{J}^{-1}\mathbf{D}\mathbf{J}^{-\mathbf{T}} \tag{9.18}$$

The choice of keeping the Cartesian inertia unchanged is based on the fact that the device design itself (low gear reduction which reduces the amplification of the actuator inertia) and the materials used (lightweight carbon fibre structures and Ergal7075 aluminium joints) for the realization result in a very light and small inertia device (apparent mass on the device tip is below 130 g). Furthermore the combination of the low apparent physical inertia with slow motions and low accelerations which are relevant to this application mean the inertial forces felt by the user can be neglected without any significant compromise. Considering also slow movements typical in mouse based interaction and that $\mathbf{F_d} = -\mathbf{F_h}$, equation (9.17) gives

$$\boldsymbol{\tau} = -\mathbf{J}^{\mathbf{T}} \left(\mathbf{B_a}\dot{\mathbf{x}}_{\mathbf{h}} + \mathbf{K_a} \left(\mathbf{x_h} - \mathbf{x_e}\right)\right) + \mathbf{G}\left(\mathbf{q}\right) \tag{9.19}$$

Since the haptic system is a planar device (9.19) can be further reduced by eliminating the gravity term $\mathbf{G}(\mathbf{q})$.

$$\boldsymbol{\tau} = -\mathbf{J}^{\mathbf{T}} \{(\mathbf{B_a}\dot{\mathbf{x}}_{\mathbf{h}} + \mathbf{K_a} \left(\mathbf{x_h} - \mathbf{x_e}\right)) \tag{9.20}$$

Equation (9.20) describes the impedance control law for the haptic device where $\mathbf{K_a}$ and $\mathbf{B_a}$ are 2×2 diagonal stiffness and damping matrices. Similarly to the 1DOF system presented in Fig. 9.3, these matrices depend on the desired assistive dynamics. Under the assistive control mode the haptic system should apply assistive force signals depending on the subject's desired motion, therefore, the user intention of motion is required. To detect the user's intention, a force torque (F/T) sensor is mounted between the mouse and the tip of the planar device. This sensor monitors the force signals applied by the user and based on these force signals the desired position vector of the impedance equilibrium $\mathbf{x_e}$ is updated in (9.20). The following formula was used to derive the new desired position vector $\mathbf{x_e}$ using the measured force signal.

$$\Delta \mathrm{x}_{\mathrm{e}}^{\mathrm{i}} = \left\{ \begin{array}{rr} \mathrm{k}_{\mathrm{f}}^{\mathrm{i}} \left(\mathrm{F}_{\mathrm{h}}^{\mathrm{i}} - \mathrm{a}^{\mathrm{i}}\right) & \mathrm{F}_{\mathrm{h}}^{\mathrm{i}} > \alpha^{\mathrm{i}} \\ 0 & \alpha^{\mathrm{i}} < \mathrm{F}_{\mathrm{h}}^{\mathrm{i}} < \alpha^{\mathrm{i}} \\ \mathrm{k}_{\mathrm{f}}^{\mathrm{i}} \left(\mathrm{F}_{\mathrm{h}}^{\mathrm{i}} + \mathrm{a}^{\mathrm{i}}\right) & \mathrm{F}_{\mathrm{h}}^{\mathrm{i}} < \alpha^{\mathrm{i}} \end{array} \right\} \quad \mathrm{i} = 1, 2 \tag{9.21}$$

$$\mathrm{x}_{\mathrm{e}}^{\mathrm{i}} = \mathrm{x}_{\mathrm{e}-1}^{\mathrm{i}} + \Delta \mathrm{x}_{\mathrm{e}}^{\mathrm{i}}, \quad \mathrm{i} = 1, 2 \tag{9.22}$$

where $\mathrm{F}_{\mathrm{h}}^{\mathrm{i}}$, $\mathrm{k}_{\mathrm{f}}^{\mathrm{i}}$ and a^{i} are the i components of the force vector applied by the operator, the sensitivity constant, and the noise dead band constant vectors respectively. By injecting the desired position vector derived from (9.22), into (9.20) assistive forces augmenting the user desired actions/motions can be generated that are governed by the stiffness matrix $\mathbf{K_a}$ of the impedance network. The damping matrix $\mathbf{B_a}$ of the impedance filter helps to damp erratic movements towards the direction of motion. A block diagram of the control scheme expressed by equations (9.20, 9.21, and 9.22) is shown in Fig. 9.7. In this diagram ${}^{\mathbf{e}}\mathbf{F_h}$ represents the estimated force applied by the user, ${}^{\mathbf{r}}\mathbf{F_d}$ is the desired force that should exerted by the device, ${}^{\mathbf{r}}\boldsymbol{\tau}_{\mathrm{d}}$ is the desired torque command, and ${}^{\mathbf{e}}\mathbf{F_d}$ is the force generated by the device approximated from (9.3) given the output state of the system $(\boldsymbol{\tau}, \ddot{\mathbf{q}}, \dot{\mathbf{q}}, \mathbf{q})$. It is evident that the force $\mathbf{F_h}$ used in (9.21) to derive the new position $\mathbf{x_e}$ cannot be directly measured. The estimated component ${}^{\mathbf{e}}\mathbf{F_h}$ is derived from the approximated force applied by the device ${}^{\mathbf{e}}\mathbf{F_d}$ and the force measured by the force sensor $\mathbf{F_s}$ as follows:

$${}^{\mathbf{e}}\mathbf{F_h} = \mathbf{F_s} + {}^{\mathbf{e}}\mathbf{F}_{d} \tag{9.23}$$

9.4 *Experimental* Evaluation and Discussion

A series of experiments were conducted to evaluate the performance of the impedance assistive control scheme.

9.4.1 Assisting the Execution of Free Path Trajectories

The first experiments aimed to validate the functionality of the assistive control scheme in Fig. 9.7 and evaluate its ability to provide different assistive force levels. During these trials one healthy subject manipulated the device without any constraints, and executed a number of free path trajectories.

The execution of these trajectories under the assistive mode of operation required the tuning of the assistive control scheme. The inertial matrix $\mathbf{M_a}$ of the desired impedance was set according to (9.18) to maintain the Cartesian inertia of the haptic system at the original level. The tuning of the assistive network matrices $\mathbf{K_a} = \begin{bmatrix} \mathrm{k} & 0 \\ 0 & \mathrm{k} \end{bmatrix}, \mathbf{B_a} = \begin{bmatrix} \mathrm{b} & 0 \\ 0 & \mathrm{b} \end{bmatrix}$ was based on both simulations studies and experimental manual tuning procedures. As a starting point we consider a bandwidth of ~ 5 Hz, ($\omega_n \sim 30$ rad/s) and a damping ratio of $\zeta = \sqrt{2}/2$ for the assistive response of the 2DOF system presented in Fig. 9.6. Fine tuning of the stiffness and damping

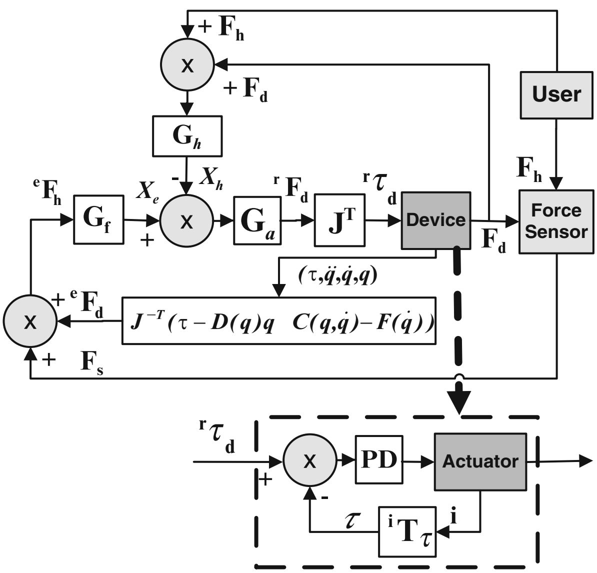

Fig. 9.7 Diagram of the proposed assistive control

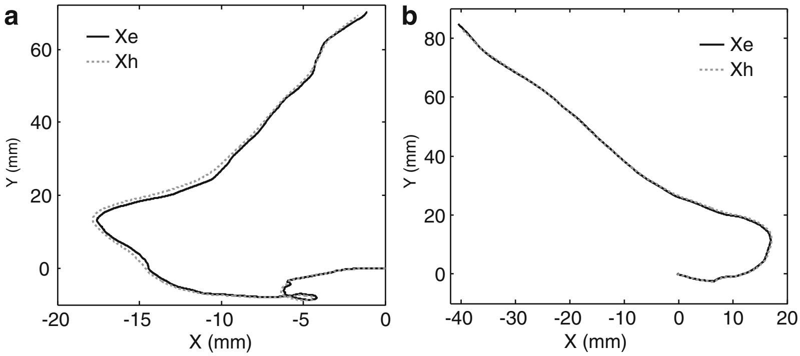

Fig. 9.8 Unconstraint trajectories executed under the assistive mode for (**a**) $k_f = 1$ and (**b**) $k_f = 2$

matrixes was performed by a series of trials where adjustments of the ($\mathbf{K_a}, \mathbf{B_a}$) were made while the healthy subject manipulated the device in the XY plane to reach randomly indicated target locations. Overshooting of the trajectories was measured at the target locations but it was not visually shown to the subjects (overshooting of the cursor was visually removed by attracting the cursor image to the target location despite the fact that the real measured trajectory may overshoot the target location).

The tuning of the assistive network was then performed manually based on the amplitude of the overshooting at the two target point locations and the level of the assistive forces applied during the motion from one target point to the other (higher assistive forces tended to increase overshooting). Feedback provided from the subject regarding the comfort and feeling during the tuning procedure was also taken into account. The time required for the gain adjusting procedure was 5–10 min approximately. The scalar values of the diagonal stiffness and damping matrixes ($\mathbf{K_a}, \mathbf{B_a}$) were adjusted to $\mathbf{K_a} = \begin{bmatrix} \mathrm{k} & 0 \\ 0 & \mathrm{k} \end{bmatrix}, \mathbf{B_a} = \begin{bmatrix} \mathrm{b} & 0 \\ 0 & \mathrm{b} \end{bmatrix}$ with $\mathrm{k} = 7$ N/cm and $\mathrm{b} = 35$ N s/cm compromising between overshooting user comfort, and assistance (equivalent bandwidth and damping ratio of the $\frac{x_h}{x_e}$ dynamics are ~ 3.2 Hz, ($\omega_n \sim 20$ rad/s) and $\zeta = 0.87$).

Control of the assistive force levels was achieved by modulation of the G_f in (9.5) through the matrix $\mathbf{K_f} = \begin{bmatrix} \mathrm{k_f} & 0 \\ 0 & \mathrm{k_f} \end{bmatrix}$. Two of the executed paths for $\mathrm{k_f} = 1$ and $\mathrm{k_f} = 2$ are shown in Figs. 9.8 and 9.9. Figure 9.8a presents the trajectory generated for $k_f = 1$ using the force applied by the user $\mathbf{F_h}$ (last row of Fig. 9.9a). The computation of the user forces was achieved using (9.23) and through the monitoring of force applied to the force sensor $\mathbf{F_s}$ (top row of Fig. 9.9a) and the force generated by the device ${}^{\mathbf{e}}\mathbf{F_d}$ (last row of Fig. 9.9a) which was computed from the measurement of the device state ($\boldsymbol{\tau}, \ddot{\mathbf{q}}, \dot{\mathbf{q}}, \mathbf{q}$).

The individual X and Y components of the assistive impedance equilibrium trajectory $\mathbf{x_e}$ as well the user hand trajectory $\mathbf{x_h}$ are presented in the middle row of Fig. 9.9a. The assistive functionality of the system and its control scheme can

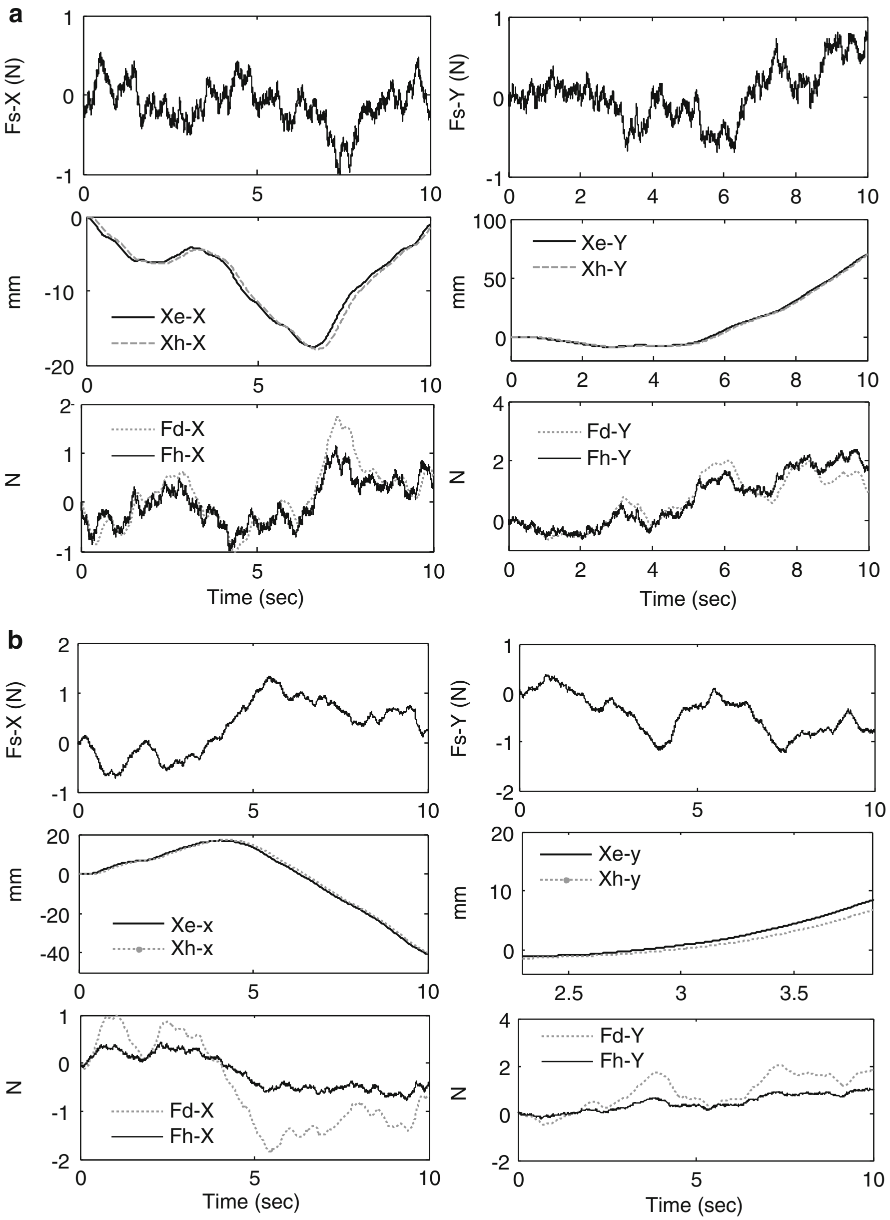

Fig. 9.9 The X, Y trajectories, subject forces and assistive forces generated by the device for the two trajectories of Fig. 9.8 for (**a**) $k_f = 1$ and (**b**) $k_f = 2$

Fig. 9.10 Subject manipulating the mouse attached on the assistive haptic device

be observed in the last row of Fig. 9.9a which shows the forces applied by the user and the forces generated by the device. The ratio between the forces generated by the device and those applied by the user can be regulated by tuning the matrix $\mathbf{K_f}$. Figure 9.8b presents a second trajectory performed with $k_f = 2$. Fig. 9.9b shows the corresponding user and device forces generated and the resulting trajectory components. In this second case as can be seen in the bottom row of Fig. 9.9b the ratio between the device forces generated in response to the user applied forces is higher, indicating greater assistance. For both levels of k_f the resultant trajectories are smooth, as predicted in the simulations used for the tuning of $(\mathbf{K_a}, \mathbf{B_a})$ with no evidence of forced oscillations.

9.4.2 Improving the Tracking Performance

The second set of trials involved a subject suffering from muscle ataxia. The purpose of these experiments was to evaluate if the assistive functionality demonstrated in the first (able bodied) experiment can aid the ataxia impaired subject to interact better with a computer generated environment by reducing the effect of undershooting/overshooting behavior.

The test subject was a regular computer user and possessed the ability to manipulate the mouse in a somewhat good manner but with difficulties in the accurate target tracking, e.g. moving a vertical or horizontal slider or selecting an item from a drop down menu. During this experiment, the subject, sitting in front of a computer display, manipulated the mouse attached to the tip of the haptic device and performed a number of tracking experiments with and without the use of the assistive control scheme, Fig. 9.10.

A target tracking task required the subject to follow an on-screen target pattern with a cursor which was controlled by manipulating the mouse at the tip of the haptic device in a manner similar to computer mouse input. Two tracking patterns were used; a diagonal line and a 90 deg edge. In the first phase of this experiment no haptic assistance was provided.

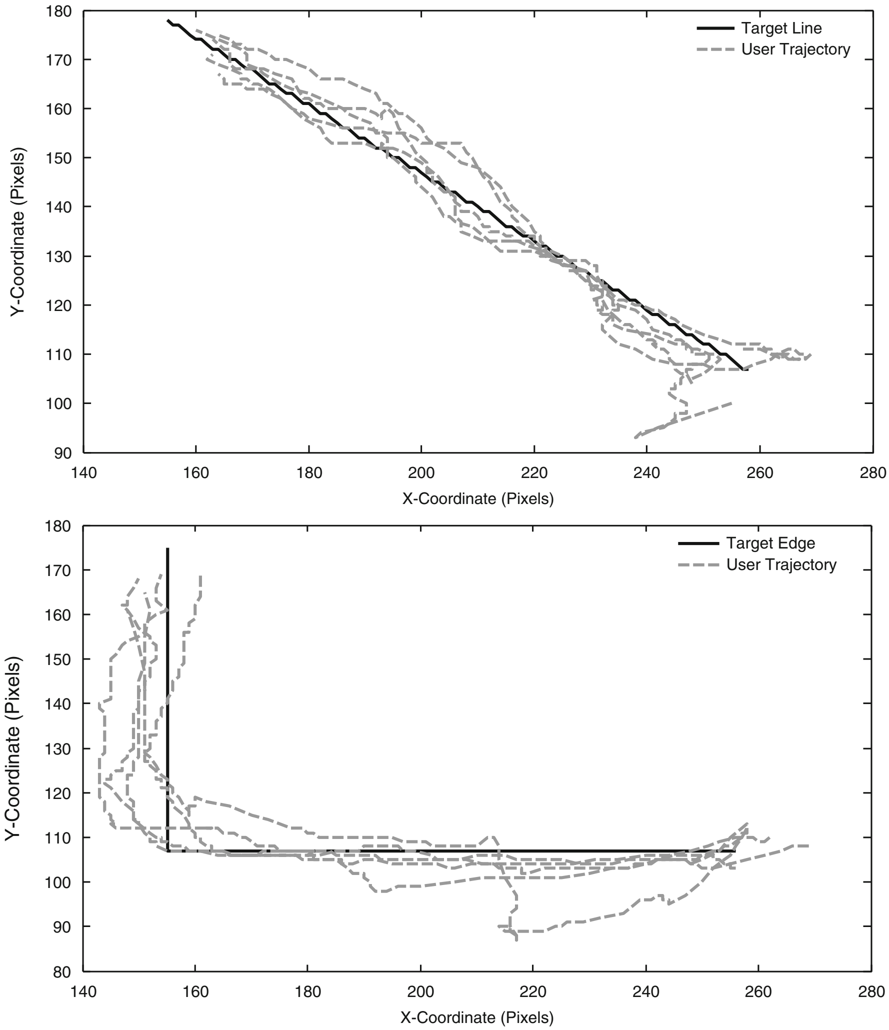

Fig. 9.11 Line and edge tracking performance of the muscle ataxia impaired subject

To demonstrate the tracking difficulties of the muscle ataxia subject the same experiment was also repeated with the healthy subject. Both the impaired subject and healthy subject were asked to track the line and edge patterns several times as quickly as they could. Observing the impaired subject trajectory in Fig. 9.11, there is clearly evidence of erratic motions during the execution of the task. Comparing the performance of the muscle ataxia subject with that demonstrated by a typical healthy subject, Fig. 9.12, the tracking difficulty of the impaired subject can be confirmed.

Following these initial without assistance trials, the haptic device was set to assistive mode and the same tracking tasks were executed by the impaired subject.

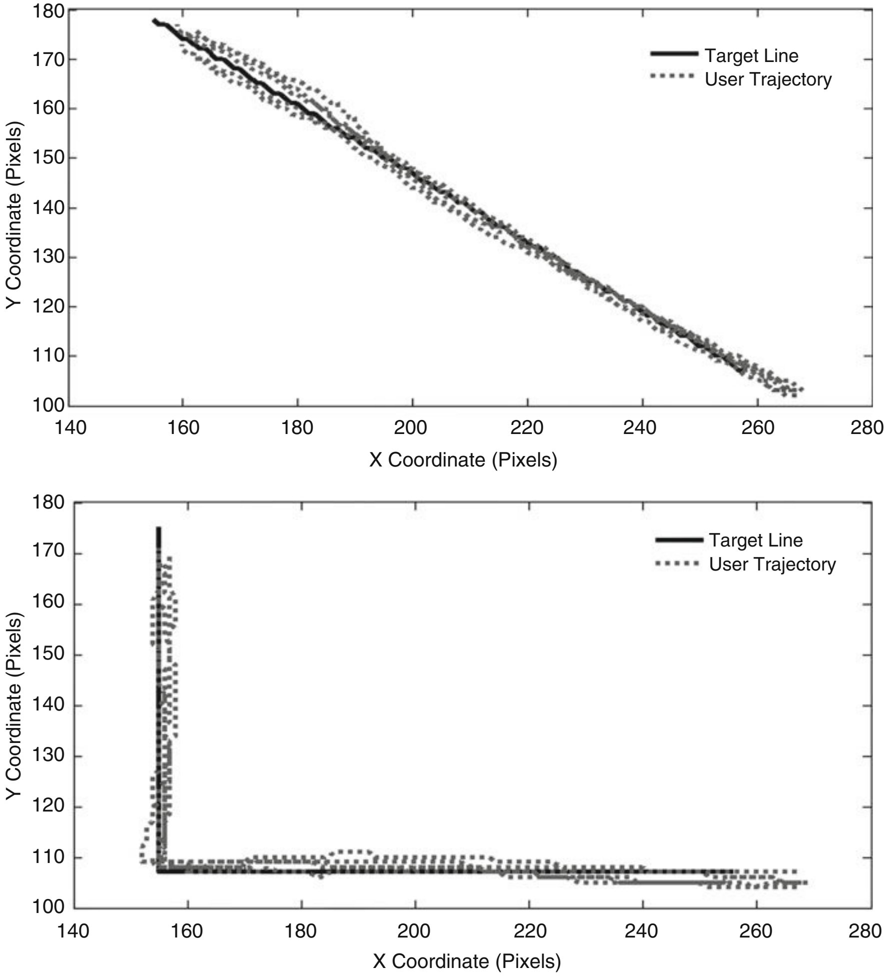

Fig. 9.12 Line and edge tracking performance of a typical healthy subject

The assistive network parameters were tuned with a procedure similar to that described in section IV-A. The scalar values of the diagonal stiffness and damping matrixes, matrixes $\mathbf{K_a}$ and $\mathbf{B_a}$ were adjusted accordingly (k = 7 N/cm and b = 50 N s/cm) with $k_f = 1$. Figure 9.13 presents the trajectory for the line and the edge tracking tasks. It can be seen that the amplitude of the sudden motions has been reduced with the application of the assistive control.

Comparing the performance of these trajectories with those in Fig. 9.11 obtained without (WO) the assistance, it can be seen that in the case of the edge pattern, the Mean Error distance of the trajectories, Fig. 9.14a, has been significantly reduced (by 40 %) with (W) the provision of the assistive control. We perform a *t*-test

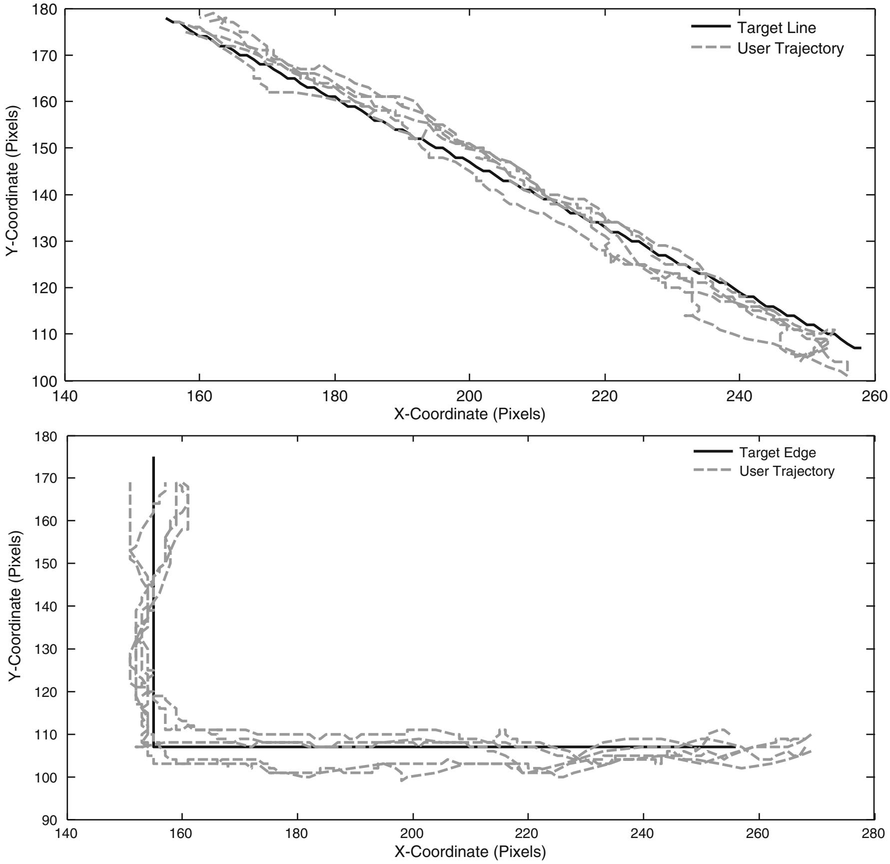

Fig. 9.13 Line and edge tracking performance of the impaired subject with assistive control

between the means of the error distances of the tracking trajectories without assistance and of those with assistance. The *t*-test indicated significant differences on the mean distance errors under the two modes of operation $(p = 0.026, t_{(4)} = 3.43)$. The average of the means of the error distance for the trajectories performed under the assistive mode was lower than that of the trajectories without assistance $\overline{X}\,(W/WO) = 10.92/16.72$, Fig. 9.14b. In terms of execution time the impaired subject was, in addition, able to complete the task in less time (19 % reduction) compared to the time needed in the case of the unsupported trajectory, t(W/WO) = 14.72/18.13 s. In the case of the line target similar trends were observed. The overall trajectory is also smoother and more regular with fewer and smaller jerks or spasms.

Figure 9.15a shows the means of the distance error for the line pattern in the no assistive and assistive mode demonstrating considerable accuracy improvements. The t-test between the means also revealed noteworthy variations between the

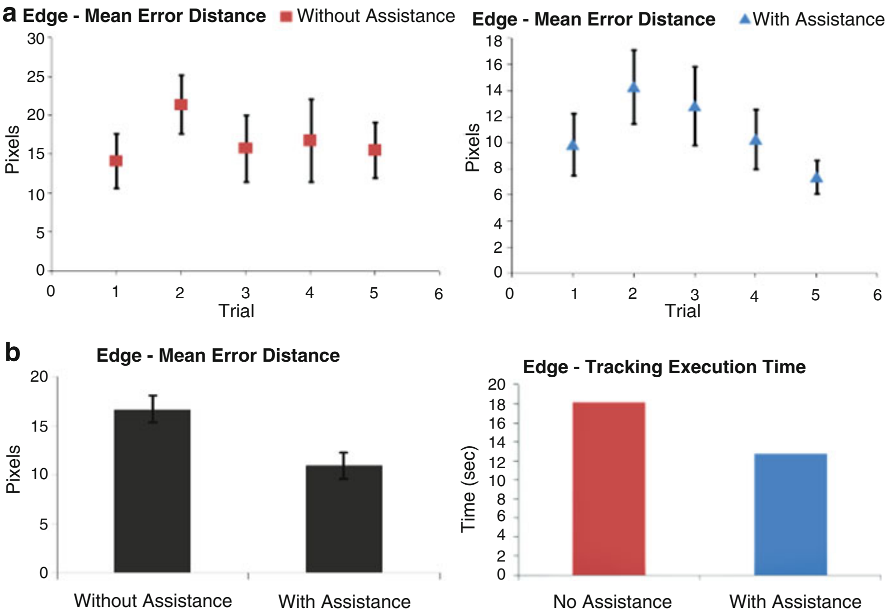

Fig. 9.14 Edge tracking performance: (**a**) Mean and standard deviation of the error distance for the different trials without and with assistance, (**b**) Average of means of the error distance and average execution time with and without assistance

means under the two modes of operation, $(p = 0.011, t_{(4)} = 4.45)$. The average of the means of the error distance for the trajectories performed under the assistive mode was also considerably lower (by almost 60 %) than those of the trajectories without assistance $\overline{X}\,(W/WO) = 5.89/16.08$, Fig. 9.15b. In terms of execution time the subject was able to complete the task in less time (40 % reduction) compared to the time needed in the case of the unsupported trajectory, $t(W/WO) = 7.71/12.89$ s. These results indicate that the system and control scheme have the potential to improve the tracking performance of muscle ataxia impaired subjects. By providing assistive forces collinear with the forces applied by the subject, the system helped the impaired user to improve their tracking performance, both in accuracy and execution time.

9.5 Conclusion

Computer assisted therapies are a significant potential training tool for many conditions but they do rely on the ability to efficiently interact with the computer. In conditions such as Muscle Ataxia this efficient interaction is not possible. A 2DOF pantograph planar device was developed to assist impaired subjects with poor

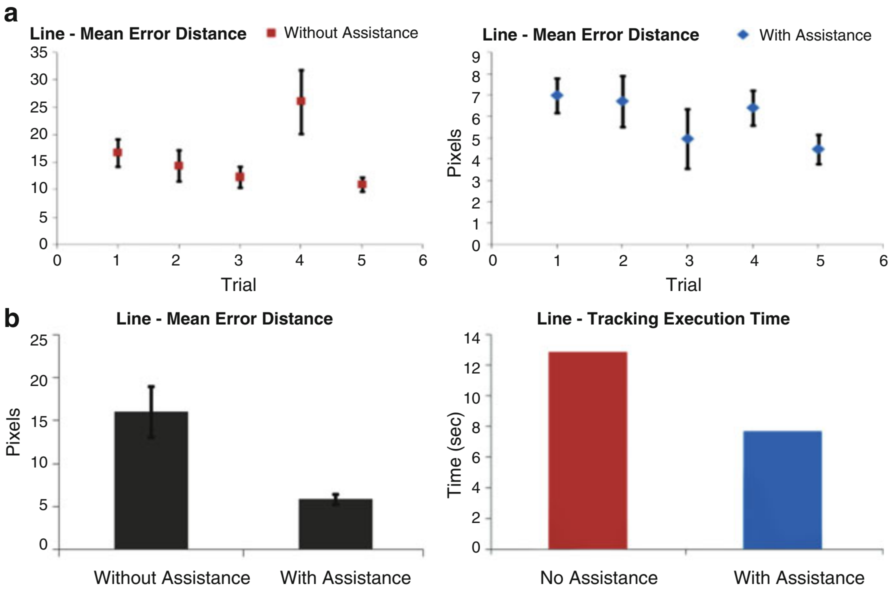

Fig. 9.15 Line tracking performance: (**a**) Mean and standard deviation of the error distance for the different trials without and with assistance, (**b**) Average of means of the error distance and average execution time with and without assistance

muscle tone and weak muscles to interact with a computer generated environment using a mouse interface. The device control scheme was designed to assist the impaired subject to complete a tracking task with higher accuracy and in less time. The overall system was evaluated with experimental trials performed by a healthy and an impaired subject suffering from muscle ataxia. In particular, the benefits of the motion assistance on the trajectory tracking were evaluated by experiments where the impaired subject performed 2-dimensional tracking tasks. With assistance the tracking performance of the impaired subject improved in terms of the execution time (19 % reduction for edge pattern and 40 % reduction for the line pattern). In terms of accuracy the reduction of the mean of the distance error of the tracking trajectory from the target path was statistically significant with $\overline{X}\,(W/WO) = 10.92/16.72$ for the edge pattern and $\overline{X}\,(W/WO) = 5.89/16.08$ for the line trajectory. These results indicate that the proposed assistive setup has a good potential in improving the hand/arm motion of the muscle ataxia subjects by reducing the trajectory overshooting trends.

Following the above promising output, future work will focus on improving the system hardware optimizing, size, portability and cost. Further trials are also foreseen for the near future to assess the application of the system in other pathological conditions including; Parkinson's disease, Muscular Dystrophy, and Cerebral Palsy. These disabilities are typically associated with symptoms such as reduced strength, restricted or irregular jerky movements, poor motion coordination and a continuum of impairments involving spasms and tremors. Further extensions of the assistive controller may include the use of electromyography (EMG) signal to intrinsically monitor and extract the user intention/direction of motion which will drive the device assistance effort.

References

1. Hillman M (2003) Rehabilitation robotics from past to present – a historical perspective. In: Proceedings of the international conference on rehabilitation robotics, Daejeon, Korea, April 2003
2. Burgar CG, Lum PS, Shor PC, Van der Loos HFM (2000) Development of robots for rehabilitation therapy: the Palo Alto VA/Stanford experience. J Rehabil Res Dev 37(6):663–673
3. Oblak J, Cikajlo I, Matjacic Z (2010) Universal haptic drive: a robot for arm and wrist rehabilitation. IEEE Trans Neural Syst Rehabil Eng 18(3):293–302
4. Caldwell DG, Tsagarakis NG, Kousidou S, Costa N, Sarakoglou Y (2007) Soft' exoskeletons for upper and lower body rehabilitation – design, control and testing. J Humanoid Robot: Spec Issue Act Exoskeleton 4(3):549–573
5. Spencer SJ, Klein J, Minakata K, Le V, Bobrow JE, Reinkensmeyer DJ (2008) A low cost parallel robot and trajectory optimization method for wrist and forearm rehabilitation using the Wii. In: Proceedings of the 2008 IEEE EMBS conference on biorobot, 2008, Scottsdale, pp 869–874
6. Rosen M, Arnold A, Baiges I, Aisen M, Eglowstein S (1995) Design of a controlled-energy-dissipation-orthosis (CEDO) for functional suppression of intention tremors. J Rehabil Res Dev 32(1):1–16
7. Brown M, Tsagarakis NG, Caldwell DG (2003) Exoskeletons for human force augmentation. Ind Robot 30(6):592–602
8. Carignan CR, Naylor MP, Roderick SN (2008) Controlling shoulder impedance in a rehabilitation arm exoskeleton. In: Proceedings of the IEEE ICRA 2008, Pasadena, CA, pp 2453–2458
9. Tsagarakis NG, Caldwell DG (2003) Development and control of a 'soft-actuated' exoskeleton for use in physiotherapy and training. Auton Robot Spec Issue Rehabil Robot 15:21–33
10. Kong K, Jeon D (2006) Design and control of an exoskeleton for the elderly and patients. IEEE/ASME Trans Mechatron 11(4):428–432
11. Kousidou S, Tsagarakis NG, Caldwell DG, Smith C (2006) Assistive exoskeleton for task based physiotherapy in 3-dimensional space. In: Proceedings of the IEEE/RAS-EMBS international conference on biomedical robotics and biomechatronics, 2006 (BioRob 2006). Pisa, Italy, pp 266–271
12. Kousidou S, Tsagarakis NG, Smith C, Caldwell DG (2007) Task-orientated biofeedback system for the rehabilitation of the upper limb. In: Proceedings of the 10th international conference on rehabilitation robotics, (ICORR). Noordwijk, Netherlands, pp 376–384
13. Gupta A, O'Malley MK (2006) Design of a haptic arm exoskeleton for training and rehabilitation. IEEE/ASME Trans Mechatron 11:280–289
14. Nef T, Mihelj M, Colombo G, Riener R (2006) ARMin – robot for rehabilitation of the upper extremities. In: Proceedings of the 2006 IEEE international conference on robotics and automation, Orlando, Florida, May 2006, pp 3152–3157
15. Kim DJ, H-Knudsen R, Culver-Godfrey H, Rucks G, Cunningham T, Portée D, Bricout J, Wang Z, Behal A (2012) How autonomy impacts performance and satisfaction: results from a study with spinal cord injured subjects using an assistive robot. IEEE Trans Syst Man Cybern A Syst Hum 42(1):2–14
16. Rosati G, Gallina P, Masiero S (2007) Design, implementation and clinical tests of a wire-based robot for neurorehabilitation. Trans Neural Syst Rehabil Eng 15(4):560–569

17. Kahn LE, Zygman ML, Rymer WZ, Reinkensmeyer DJ (2006) Robot-assisted reaching exercise promotes arm movement recovery in chronic hemiparetic stroke: a randomized controlled pilot study. J Neuroeng Rehabil 3:12
18. Uemura M, Kanaoka K, Kawamura S (2006) Power assist system for sinusoidal motion by passive element and impedance control. In: Proceedings of the IEEE ICRA, Orlando, Florida, May 2006, pp 3935–3940
19. Volpe BT, Krebs HI, Hogan N et al (2000) A novel approach to stroke rehabilitation: robot-aided sensorimotor stimulation. Neurology 54(10):1938–1944
20. Magee JJ, Betke M, Gips J, Scott MR, Waber BN (2008) A human–computer interface using symmetry between eyes to detect gaze direction. IEEE Trans Syst Man Cybern A Syst Hum 38(6):1248–1261
21. Cesqui B, Micera S, Mazzoleni S, Carrozza MC, Dario P (2006) Analysis of upper limb performance of elderly people using a mechatronic system. In: Proceedings of the international conference on biomedical robotics and biomechatronics, Pisa, pp 365–370
22. Rocon E, Ruiz AF, Brunneti F, Pons JL (2006) On the use of an active wearable exoskeleton for tremor suppression via biomechanical loading. In: Proceedings of the 2006 IEEE international conference on robotics and automation, Orlando, Florida, May 2006. pp 3140–3145
23. Koeneman EJ, Schultz RS, Wolf SL, Herring DE, Koeneman JB (2004) A pneumatic muscle hand therapy device. Conf Proc IEEE Eng Med Biol Soc 4:2711–2713
24. Krebs HI, Volpe BT, Williams D, Celestino J, Charles SK, Lynch D, Hogan N (2007) Robot-aided neurorehabilitation: a robot for wrist rehabilitation. IEEE Trans Neural Syst Rehabil Eng 15:327–335
25. Trewin S, Pain H (1999) Keyboard and mouse errors due to motor disabilities. Int J Hum-Comput Stud 50(2):109–144
26. Dennerlein JT, Yang MC (2001) Haptic force feedback devices for the office computer: performance and musculoskeletal loading issues. Hum Factors 43(2):278–286
27. Hasser S, Goldenberg C, Martin A, Rosenberg K (1998) User performance in a GUI pointing task with a low-cost force feedback computer mouse. In: Proceedings of the ASME Dynamic Systems and Control Division. American Society of Mechanical Engineers, New York, pp 151–156
28. Hwang F, Keates S, Langdon P, Clarkson PJ (2003) Multiple haptic targets for motion impaired users. In: Proceedings of the CHI 2003, Fort Lauderdale, pp 41–48
29. Beringhause S, Rosen M, Haung S (1989) Evaluation of a damped joystick for people disabled by intention tremor. In: Proceedings of the RESNA 12th annual conference, New Orleans, pp 41–42
30. Morrice B, Becker W, Hoffer J, Lee R (1990) Manual tracking performance in patients with cerebellar incoordination – effects of mechanical loading. Can J Neurol Sci 17(3):275–285
31. Delatycki MB, Williamson R, Forrest SM (2000) Friedreich ataxia: an overview. J Med Genet 37:1–8
32. Milner TE, Cloutier C (1990) Damping of the wrist joint during voluntary movement. Exp Brain Res 122:309–317
33. Becker JD, Mote CD (1990) Identification of a frequency response model of joint rotation. J Biomech Eng 112:1–8
34. Hajian AZ, Howe RD (1997) Identification of the mechanical impedance at the human finger tip. J Biomech Eng 119:109–114
35. Lacquaniti F, Licata F, Soechting JF (1982) The mechanical behaviour of the human forearm in response to transient perturbations. Biol Cybern 44:35–46

Part III
Rehabilitation Robotics

Chapter 10
Robotic Systems for Gait Rehabilitation

Aline Marian Callegaro, Ozer Unluhisarcikli, Maciek Pietrusinski, and Constantinos Mavroidis

Abstract Human walking is impaired by various neurological diseases such as stroke. Gait restoration is a major goal in neurological rehabilitation following stroke. Robotic devices have been developed to assist locomotor training improving gait function and thus a stroke survivor's independence. This chapter presents robotic systems that have been developed specifically for gait rehabilitation providing pelvic, hip and/or knee motion assistance. Robotic systems allow clinicians to increase the duration, intensity and specificity of treatment compared to traditional physical therapy. These factors could result in a faster and increased level of recovery of functional capability thus leading to an improvement of patient's level of independence and quality of life. In addition, robotic systems could be used to reduce the number of physical therapists involved in the treatment of each patient. In fact, there is great interest in robot-assisted rehabilitation for partially automating such therapy, to enable just one physical therapist to administer gait training instead of at least two. A major limitation in the use of robotic systems for gait rehabilitation is their high cost. Currently, commercially available robotic solutions for automation of gait rehabilitation physical therapy cost between \$60,000 and \$300,000 and thus very few clinical facilities can afford them. In addition, low cost robotic devices

A.M. Callegaro (✉)
CAPES Foundation, Ministry of Education of Brazil, Brasília DF 70.040-020, Brazil

Product and Process Optimization Laboratory, Graduate Program in Industrial Engineering, Engineering School, Federal University of Rio Grande do Sul, 99 Osvaldo Aranha Avenue, 90035190 Porto Alegre, RS, Brazil
e-mail: nimacall@gmail.com

O. Unluhisarcikli • M. Pietrusinski • C. Mavroidis (✉)
Department of Mechanical and Industrial Engineering, 334 Snell Engineering Center, Northeastern University, 360 Huntington Avenue, Boston, MA 02115, USA
e-mail: ozer.unluhisarcikli@gmail.com; maciekdp1@gmail.com; mavro@coe.neu.edu

P. Artemiadis (ed.), *Neuro-Robotics: From Brain Machine Interfaces to Rehabilitation Robotics*, Trends in Augmentation of Human Performance 2,
DOI 10.1007/978-94-017-8932-5_10,

for gait rehabilitation could be used by post-stroke survivors at home, in order to accelerate and intensify the rehabilitation process and improve the therapeutic outcomes.

Keywords Rehabilitation robotics • Gait rehabilitation • Motor learning

10.1 Introduction

Human walking is a process of locomotion in which the erect, moving body is alternatingly supported by one leg after the other [1]. The degrees of freedom (DoFs) of the lower limbs are determined by the degrees of freedoms of each one of the leg joints i.e. hip, knee, ankle and feet joints. The knee is a basic determinant of limb stability during the stance phase, where the flexion and extension of the knee is used for progression. Some diseases impair the patients' walking ability. Stroke can cause a central neurological lesion in the brain motor areas which impairs the motor control, consequently resulting in spastic paralysis: muscle weakness, impaired selective control, emergence of primitive locomotor patterns, and spasticity [2].

Each year, 795,000 people experience a new or recurrent stroke in the United States [3]. Stroke survivors need rehabilitation because of the neurological impairment. Restoration of gait is a major goal in neurological rehabilitation following stroke, because it is decisive for the aspired social and vocation reintegration [4]. It can be quite difficult for physical therapists to train a stroke survivor in walking due to posture and balance problems, that may result in falls and potential injuries to patients [5] due to deficient equilibrium reflexes [4]. Providing a safe and controlled environment for stroke survivors is very important. Therefore a wide range of strategies and assistive devices have been developed for this purpose. The approaches used in gait rehabilitation after stroke include neurophysiologic and motor learning techniques, robotic devices, Functional Electrical Stimulation (FES), and Brain-Computer Interfaces (BCI) [6].

Rehabilitation robotics comprises any robot technology in the medical field that has as goal to help people gain control over parts of their body that can no longer be controlled due to a disease or traumatic injury [7]. Robot-assisted gait training was introduced in the late 1990s [8]. Robotic devices are designed to assist locomotor training, improving gait function and independence in individuals following a stroke. They aim at recovering a physiological gait pattern to complete repetitive walking training safety, especially in patients with significant weakness [9]. An important point is that interaction forces and torques can be measured with sensors, making it possible to quantitatively assess the level of motor recovery, and controlled repetitive training can be realized at a reasonable cost [5].

Several lower extremities rehabilitation devices have been developed in the last decade for gait training during walking [10]. Robots have the potential to provide accessible, precise, and physiological gait patterns, adapted and reproduced with higher accuracy [11], making it possible to test and optimize the biomechanical gait pattern (speed, step length, amplitude) in order to get an optimal effect [12, 13]. In addition, patient progress can be monitored and training sessions can be longer without the force limitations and inconsistency of conventional human-regulated therapy, relieving strain on therapists [14].

This chapter aims at presenting the state of the art in rehabilitation robotics for lower extremities, specifically robotic devices for gait rehabilitation. Robots developed for lower limb rehabilitation can be classified based on their mechanical structure as (a) end-effector devices and (b) as exoskeletons [15]. An end-effector lower limb rehabilitation robotic device has indirect control of the patient's limbs by applying forces on the patient body using a structure that includes the system's actuators outside the patient's body. The lack of a common kinematic space between the patient and the robot may cause safety issues; such as moving the patient's limbs to an uncomfortable (or even dangerous) configuration, or collision between the patient and the robot. They are rather preferred in unique systems that target a specific purpose. An exoskeleton is a mechanical structure that includes the actuators worn by an operator. Anthropomorphic exoskeletons attempt to mimic the kinematic structure of the human skeleton. As they work in parallel with the user's limbs, mechanical limits can be implemented directly, and the risk of collisions is eliminated. However, the joints should be accurately aligned with that of the user to prevent shear forces.

10.2 End-Effector Type Lower Limb Rehabilitation Robotic Devices

A device called Ambulation-assisting Robotic Tool for Human Rehabilitation (ARTHuR), developed at the Biomechatronics Laboratory of the University of California at Irvine is an end-effector type robotic system that incorporates moving coil forcers. ARTHuR is a backdriveable and flexible machine, which can be used by people with different sized legs [16].

Another end-effector type gait rehabilitation robot is the HapticWalker that is a scalable and modular robotic walking simulator comprising a hybrid parallel-serial kinematic structure with programmable-footplates. The patient's feet are attached to individual foot-modules, each containing a 6-DoF force/torque sensor and a footplate. The HapticWalker can simulate walking, climbing upstairs and climbing downstairs by controlling the position of the footplates [17]. The robot's kinematic architecture and highly dynamic drives allow natural walking movements, training arbitrary gait trajectories of daily life with unrestricted leg motion and muscle activation [18].

The gait robot G-EO System (EO, latin: I walk) is based on the end-effector principle, and was designed to enable stroke patients perform the repetitive practice of floor walking, stair climbing and stair descending, as shown in Fig. 10.1. A novel control strategy allows training in adaptive mode [20, 21]. Harness secured patients

Fig. 10.1 Gait Robot G-EO System (Reha Technology AG [19]) (Published with permission from Reha Technology AG)

stand on two three DoF foot plates connected by a pivoting arm to two moving sledges, whose trajectories are completely programmable. The foot's forward motion is given by the movement of the principal sledge, which is connected to the transmission belt of the linear guide. The forward and backward excursion of the principal sledge controls the step length. A completely programmable drive fixed on the arm transfers the rotation through a transmission belt to an external axle, which is aligned to the ankle, controlling the plantar- and dorsiflexion during the stepping. The device has two DoFs for the control of the Center of Mass (CoM) [21].

The Pelvic Assist Manipulator (PAM) developed at the University of California at Irvine is a pneumatic robot for measuring and manipulating pelvic motion during stepping with a Body Weight Support (BWS) system over a treadmill [22]. The PAM allows naturalistic motion of pelvis, which is actuated by six pneumatic cylinders, that combined with a nonlinear force-tracking controller, provides backdrivability and large force output. Two cylinders lie coplanar in the horizontal plane, and the third cylinder lies in an oblique plane to provide upward forces. The system has five DoFs, providing control of three translations (side-to-side, forward-and-back, up-and-down) and two rotations (pelvic rotation, and pelvic obliquity). One rotation cannot be controlled, that of pelvic tilt. The PAM can act as a teach-and-replay device with a Proportional and Derivative (PD) position controller driving the pelvis onto the reference trajectory specified with or without a therapist's help. Footswitches detect the gait timing and a feedback control algorithm adjusts the play-back speed of the gait pattern in real-time to help synchronizing the robotic assistance during stepping by unimpaired subjects, even when the subjects change their step size and period [23].

The Pneumatically Operated Gait Orthosis (POGO) was also developed at the University of California at Irvine together with the PAM, to provide assistance to the lower limbs. The POGO attaches to and works with PAM, preventing buckling of the knee during the stance phase of the naturalistic walking motion [22].

A robotic trainer called Natural and TUneable rehabilitation gait system (NaTUre-gaits), has been developed in Singapore for over the ground walking rehabilitation [24]. This device consists of a pair of Robotic Orthoses (RO) connected to a Pelvic Arm (PA) and mounted on a Mobile Platform (MP) [25]. The RO provides gait locomotion assistance for lower limbs, the PA provides actuated assistance for five pelvic movements (three translational and two rotational) and the BWS is provided during walking by using one single mechanism. The MP allows over the ground walking. A pelvic motion active BWS (pa-BWS) control strategy was developed for NaTUre-gaits to provide an active BWS, promoting active patient participation during the rehabilitation for a better therapeutic outcome. The scheme also aims at driving the pelvis along a reference trajectory for a natural gait [26]. Each motion is achieved by a linear sliding mechanism, actuated by a Direct Current (DC) servo motor [27].

The 6-DoF gait rehabilitation robot allows patients to exercise their walking velocity on various terrain types and navigate for diverse walking training in Virtual Environment (VE) through upper and lower limb connections, by estimating the interaction torques between the human and the upper limb device. This robot is composed of an upper limb device, as sliding device, two footpad devices, and a body support system. The footpad device on the sliding device generates three DoFs spatial motion in the sagittal plane for each foot. The upper limb device allows users to swing their arms naturally through the use of a simple pendulum link with a passive prismatic joint. Synchronized gait patterns for this robot are designed to represent a normal gait with upper and lower limb connections. In addition, the patient is able to navigate in the VE [28].

The MIT-Skywalker (Fig. 10.2) is a device developed for gait therapy based on the concept of passive walkers and the natural dynamics of the lower extremity to deliver more "ecological" therapy [30]. The fast donning and doffing alongside its dynamic principles and ecological intervention are the advantages of this device. A camera-based closed loop control facilitates safe and efficient control of the device, providing an effective and interactive gait therapy program, based on the real-time information of the patient's leg motion [29].

The cable-driven robotic gait training system CaLT is a highly backdrivable, compliant robotic gait training system that gives patients the freedom to voluntarily move their legs in a natural gait pattern during body weight supported treadmill. It

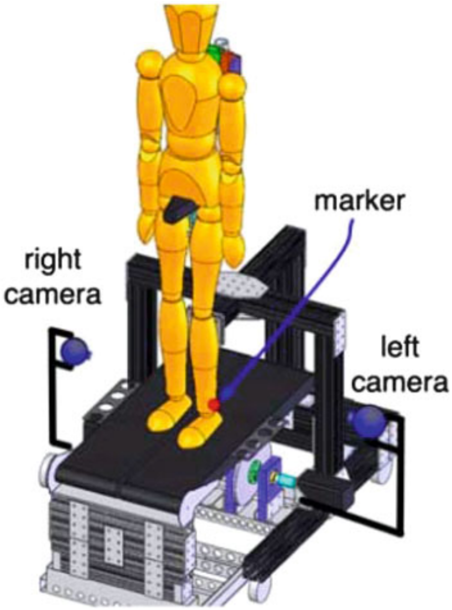

Fig. 10.2 The MIT-Skywalker platform [29] (Published with permission from Prof. Hermano Igo Krebs, Massachusetts Institute of Technology, Cambridge, MA)

was designed to encourage active involvement of subjects in the treatment and allow freedom for subjects to control their stepping performance during treadmill training. The device provides a controlled assistance or resistance force to assure stable stepping and maximize patient effort; as well as to allow step-to-step variation in leg kinematics. This device applies forces to legs at the ankle level during treadmill stepping and studies have shown that with such therapy it is possible to improve the locomotor function in people with Spinal Cord Injury [31] and in patients post-stroke through robotic-assisted treadmill training [32].

A modular light-weight robotic system called STRING-MAN was developed by researchers at the Institute for Production Systems and Design Technology IPK in Berlin, Germany to assist in locomotion recovery therapy and gait training. This powerful robotic system provides functions for improving gait rehabilitation outcomes, especially those relevant to the restoration of posture balancing and gait motor functions. STRING-MAN combines modular wire robot components, advanced artificial muscle drives, reliable, and dynamically controlled weight-suspension and balancing system. This robotic structure is able to control the patient's posture in six DoFs and allows the patient's own initiative by using force or impedance control. Patients can autonomously perform gait recovery training in the early rehabilitation stage, because the system has the ability to adjust the interaction control from totally passive to completely active [33].

Another robotic device for gait and balance training is the KineAssist (Fig. 10.3) that focuses on increasing the level of challenge to a patient's ability to maintain balance during gait training, permitting the direct involvement of a Physical

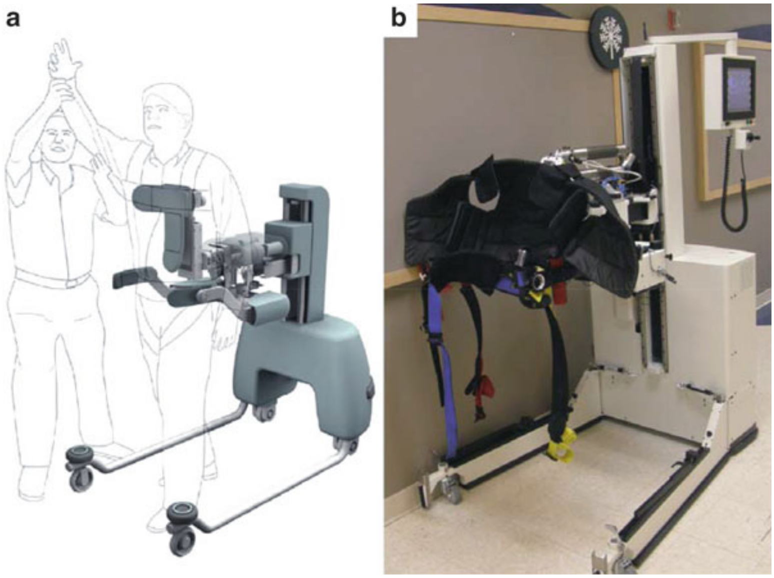

Fig. 10.3 (**a**) Artist's rendition of the KineAssist in use with a physical therapist [34]; (**b**) KineAssist device (Published with permission from The Rehabilitation Institute of Chicago)

Therapist. The KineAssist is microprocessor controlled, and uses control methodology developed for haptic displays. The motion of the mobile base is powered while the patient's intent for motion is detected by passive sliders and integrated force sensors positioned in the pelvic support. Control algorithms move the base in response to a patient's forces and motions. This actuated device provides Partial Body Weight Support (PBWS) and postural torques at the trunk, and allows many DoFs of the trunk as well as the pelvis. The KineAssist leaves the patient's legs accessible to a physical therapist during walking. The device follows a patient's walking motion over-ground in forward, rotation, and sidestepping directions and prevents falls. This device has seven programmable operation modes, ranging from low level setting for patients with impaired mobility on a basic functional level, to more advanced setting [34].

Two types of gait rehabilitation robot systems called "WHERE-I" and "WHERE-II" (Fig. 10.4) were developed by researchers of the Korean Advanced Institute of Science and Technology. WHERE-I is a mobile manipulator based on electrical BWS mechanism, whereas WHERE-II is a mobile vehicle with a one-link manipulator and a pneumatic BWS mechanism. Each system consists of four main subsystems: a mobile base, an actuated BWS, an intention analysis system, and a safety system. Both systems have electrical actuators for height adjust and ultrasonic sensors for safety. Three of the six axes of motion at the pelvis that are involved in walking are inhibited. These devices can move forward/backward and can rotate in place. The BWS system unloads and controls the up-and-down motion [35].

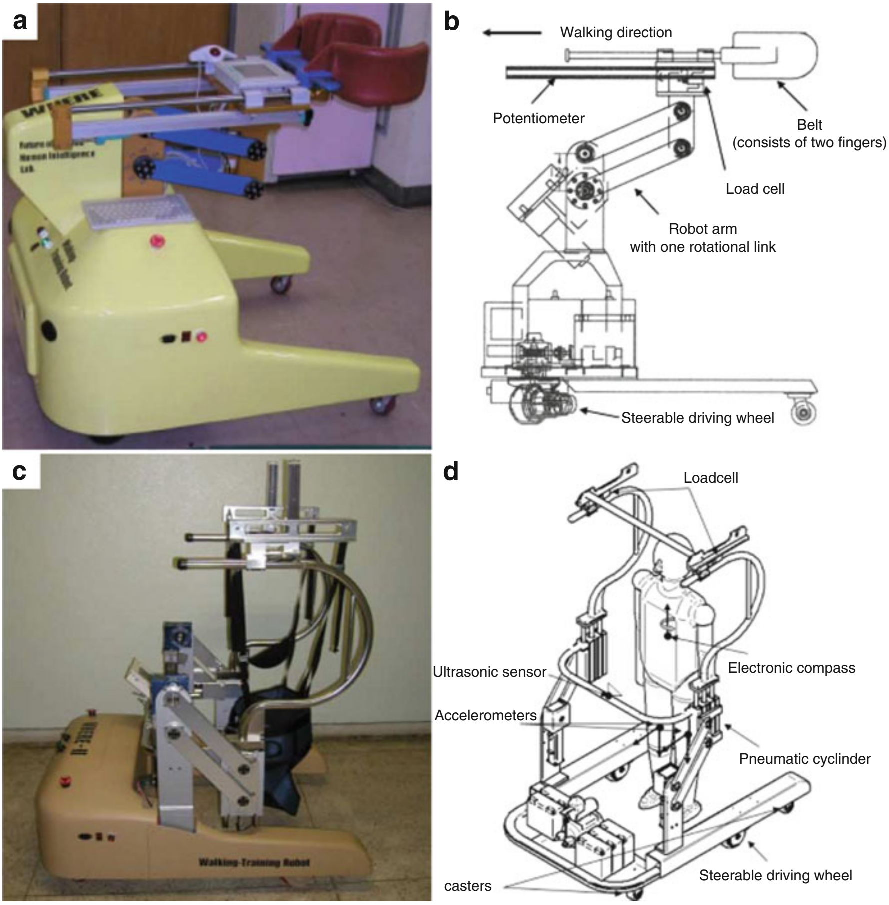

Fig. 10.4 (**a**) WHERE-I prototype; (**b**) WHERE-I CAD drawing; (**c**) WHERE-II prototype; (**d**) WHERE-II CAD drawing [35] (Published with permission from Dr. Kap-Ho Seo)

10.3 Exoskeleton Type Lower Limb Rehabilitation Robotic Devices

The Driven Gait Orthosis (DGO) is a rehabilitation robot developed at the Rehabilitation Center ParaCare, of the University Hospital Balgrist in Zurich (Switzerland). The DGO performs locomotor training for paraplegic patients (Spinal Cord Injury – SCI) and post-stroke survivors. The device is adjustable to individual needs, has a BWS system and four DoFs. A position controller regulates actuators at the knee and hip joints in the sagittal plane. The first version of the DGO with position control strategies did not allow voluntary active movements of the patient [12, 36]. A new version had a cooperative control architecture based on impedance

Fig. 10.5 Lokomat®Pro [37] (Published with permission from Hocoma, Switzerland)

control that allowed patients to accomplish free walking movements. Impedance control motivates patients and accelerates the rehabilitation progress [13]. The DGO was commercialized as the 'Lokomat®' – Enhanced Functional Locomotion Therapy with Augmented Performance Feedback by the Swiss company Hocoma (http://www.hocoma.com/). The Lokomat®Pro (Fig. 10.5) offers different tools for a convenient assessment of the main problems of neurologic patients: patient's walking endurance comparison between several training sessions, evaluation of the mechanical stiffness of the patient's joints while passively moving the legs in a specific pattern, evaluation of the isometric force, and the range of motion used during a passive or active movement without support by the Lokomat drives [37]. The Lokomat is irrefutably the most recognized gait rehabilitation system. The patient's hips and knees are actuated in the sagittal plane via DC motors coupled to ball screws. A spring-based passive foot lifter helps with ankle dorsiflexion during swing. However, the pelvis is only allowed to translate in the frontal plane. Its therapy methods rely on repetition and task-oriented training.

The gait rehabilitation robot called LOPES (LOwer Extremity Powered ExoSkeleton), shown in Fig. 10.6, was developed at the University of Twente in Netherlands [38]. LOPES is using an impedance controller and is basically a combination of an exoskeleton robot for the lower limbs and an externally located end-effector robot for the pelvis, allowing a total of eight DoFs. The exoskeleton has three rotational joints per leg: two at the hip (abduction/adduction and flexion/extension) and one at the knee (flexion/extension) [39, 40]. All motions of the ankle, and vertical translation of the pelvis are allowed, but not actuated. The

Fig. 10.6 LOPES exoskeleton (Published with permission from the University of Twente)

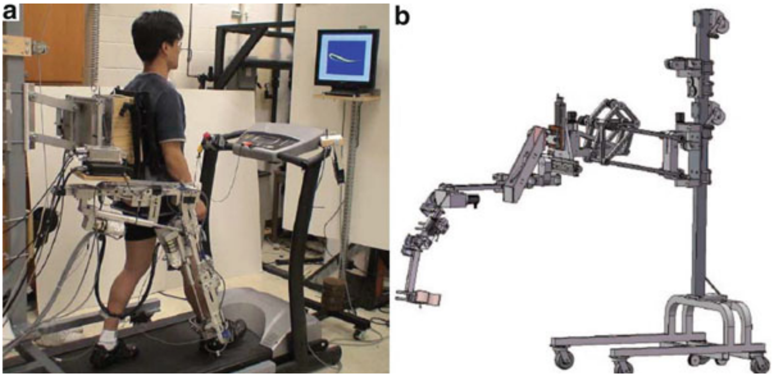

Fig. 10.7 (**a**) Active limb exoskeleton (ALEX) [41]; (**b**) ALEX II device [42] (Published with permission from Professor Sunil Agrawal)

LOPES allows free leg motions and a free 3D translation of the pelvis, maintaining the fundamental instability of upright standing and walking [39].

The Active Limb Exoskeleton I and II (ALEX I and ALEX II), shown in Fig. 10.7 are devices developed at the University of Delaware. ALEX I is a motorized exoskeleton, which modulates the foot trajectory using motors at the hip (for flexion/extension and abduction/adduction) and the knee (for flexion/extension), and a force field at the foot which helps in gait training. Alex's flexible design allows ankle dorsiflexion/plantarflexion and inversion/eversion motions [5, 10, 41, 43–45]. This device has three types of controllers: trajectory tracking PD controller; set-point PD controller; and force-field controller [5]. ALEX I can only be worn on the right side while ALEX II can be used on the subject's right or left leg, and allows several adjustments, improving fit to the user [42].

A unilateral and supportive arm for ankle assistance, BWS and human-robot interaction was developed by researchers of the Vrije Universiteit Brussel in Belgium. This exoskeleton has three DoFs (one DOF joint for ankle, knee and hip). Only the knee joint is powered by pleated pneumatic artificial muscles. A strap-on the footplate helps with actuator force transfer during stance and for better fitting. A Proxy-based Sliding Mode Control (PSMC) is used as a trajectory-tracking based approach to gait training of SCI patients with poor motor control. It was proposed in view of the system's safety requirements and envisaged compliant behavior [46].

The Tibion® PK100 bionic leg orthosis (now called the AlterG Bionic Leg), commercialized by the Tibion Corporation (now part of AlterG, http://www.tibion.com/), is a wearable, portable and lightweight (constructed of carbon fiber) device for rehabilitation of patients affected by neurological conditions such as stroke. This powered leg orthosis includes a high-torque actuator, electronics, sensors, and embedded firmware. This battery powered device supplies the force to assist or resist leg extension and flexion. The device provides multiple modes of operation including automatic assistance, manual assistance, continuous passive motion and robotic therapy for the knee. The biomechanical algorithms make use of information from pressure sensors in the foot in order to determine when the patient requires extra assistance or high forces for active assistance during sit-to-stand transfers, stair ascent/descent, and walking.

The Active Knee Rehabilitation Orthotic System (ANdROS), shown in Fig. 10.8, developed in Prof. Mavroidis' Laboratory at Northeastern University in Boston, MA is a wearable and portable assistive tool for gait rehabilitation and monitoring of people with motor control deficits due to a neurological ailment, such as stroke. ANDROS reinforces a desired gait pattern by continually applying a corrective torque around the knee joint, commanded by an impedance controller. A sensorized yet unactuated brace worn on the unimpaired leg is used to synchronize the playback of the desired trajectory based on the user's intent. The device is mechanically grounded through two Ankle Foot Orthoses (AFOs) rigidly attached to the main structure, that help reduce the weight perceived by the user [47].

ANdROS has the potential to control the knee joint in a way that is similar to the Lokomat system. However, *ANdROS* could be made available at a small fraction of the cost of the Lokomat system therefore allowing clinical centers to make extensive use of this robotic system at a cost compatible with the healthcare system. Besides, patients could wear them during extended periods of time therefore allowing for more intense rehabilitation leading to faster recovery of ambulatory function. Even though *ANdROS* may look similar to Tibion Bionic Leg as both are fully portable and can apply torques at the knee joint, their functions and intended training is very

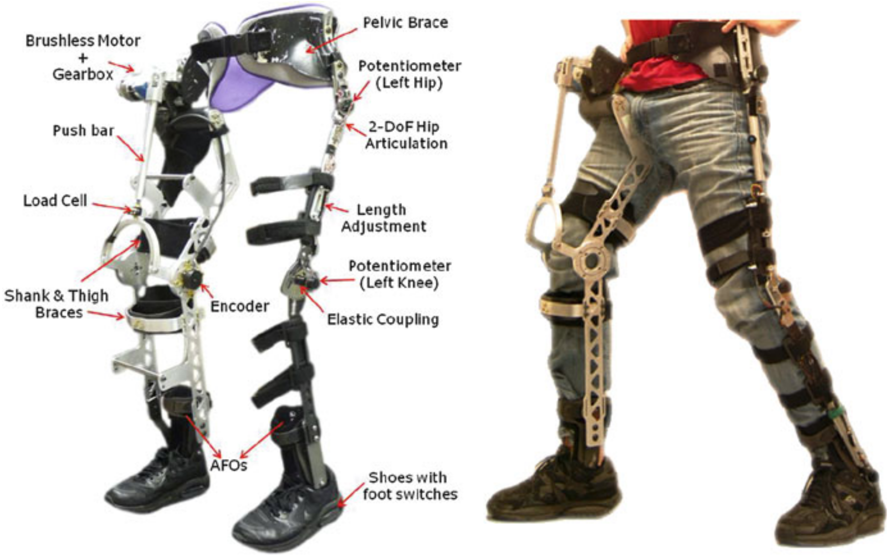

Fig. 10.8 Active knee rehabilitation orthotic system (ANdROS) (Published with permission from Prof. Mavroidis, Northeastern University, Boston, MA)

different. Tibion's Bioninc Leg has been designed to provide active knee assistance during sit-to-stand, stair ascent/descent, and over ground walking while *ANdROS* reinforces a desired gait pattern by applying a force field to the patient's impaired leg during over the treadmill training.

The Robotic Gait Rehabilitation (RGR) Trainer Fig. 10.9 was developed to target secondary gait deviations (i.e. gait abnormalities that result from compensatory movements associated with a primary gait abnormality in patients post-stroke). Using an impedance control strategy and a linear electromagnetic actuator, this 1 DOF robotic device generates a force field that affects the obliquity of the pelvis (rotation of the pelvis around the anteroposterior axis) via a lower body exoskeleton while the patient ambulates on a treadmill. The RGR Trainer applies a moment to the pelvis in the frontal plane, to affect the pelvic obliquity angle. The RGR Trainer features low mechanical complexity, while allowing all the natural motions of the pelvis with its ten DoFs. The single linear electromagnetic actuator employs impedance control and human-machine synchronization to generate corrective forces as a response to deviations from pre-determined pelvic obliquity trajectories. The corrective force fields are applied onto the subject via a lower body exoskeleton, which, as the authors claim, can effectively transfer forces to the pelvis. Preliminary healthy human subject testing, such as the ones shown in Fig. 10.10, demonstrated that the *RGR Trainer* can effectively guide the pelvis in the frontal plane via force fields to alter pelvic obliquity [48, 49].

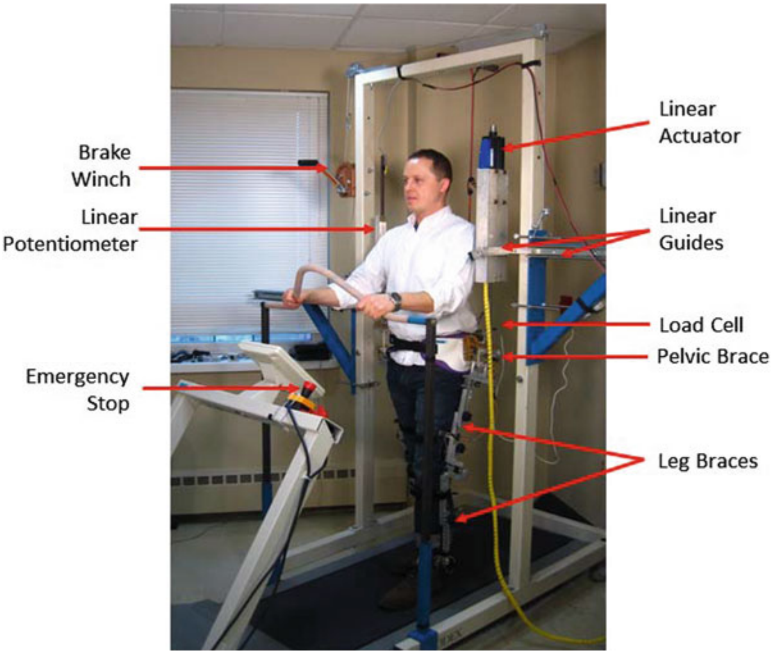

Fig. 10.9 Robotic gait rehabilitation (RGR) trainer (Published with permission from Prof. Mavroidis, Northeastern University, Boston, MA)

10.4 Conclusions

During the past decade, the field of physical medicine and rehabilitation has witnessed an increasing interest for the clinical use of robotic systems. *Robotic systems allow clinicians to increase the duration, intensity and specificity of treatment compared to traditional physical therapy*. These factors could result in a faster and increased level of recovery of functional capability thus leading to an improvement of patient's level of independence and quality of life. Consequently, individuals who undergo therapy using robotic systems could do better than patients who receive traditional physical therapy. Robotic rehabilitation is particularly appealing in patients with conditions such as spinal cord injury, stroke, and traumatic brain injury. A major goal of therapy for these patients is to achieve motor recovery. Increasing the duration, intensity and specificity of therapy – as it is possible by leveraging robotic systems for rehabilitation – is in tune with this goal. Therefore, clinicians treating patients with the above-mentioned conditions have paid a great deal of attention to robotic systems for physical therapy (particularly those devoted to gait retraining) and some of these systems have been already adopted in clinical practice.

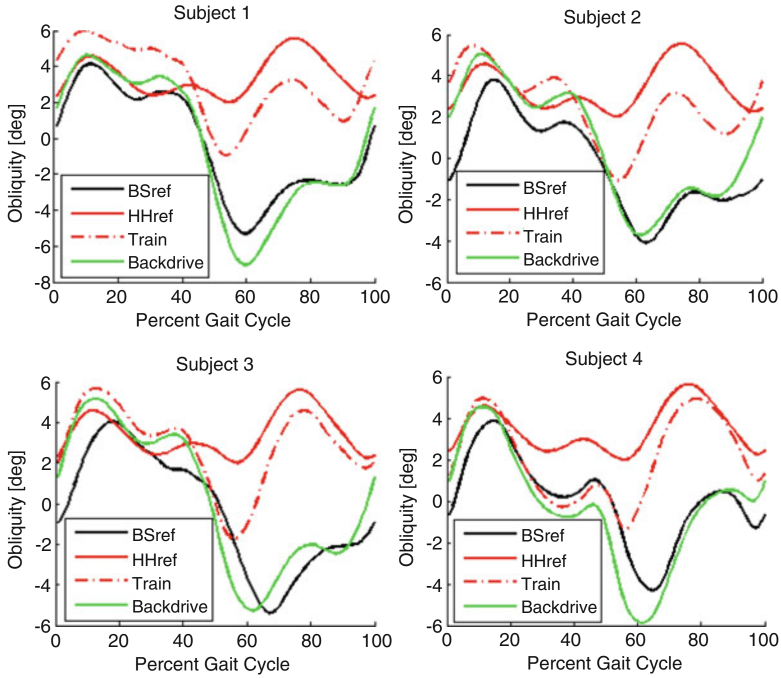

Fig. 10.10 Results of hip-hike training experiments. Four subjects were instructed to follow the *RGR Trainer*, as it guided their pelvic obliquity to first match 'HHref' (desired hip-hiking reference) by applying a force field to the subject's pelvis area and then 'BSref' (baseline – average trajectory of healthy subjects) by applying a zero-force field, producing thus the lines 'Train' and 'Backdrive' responses respectively (Published with permission from Prof. Mavroidis, Northeastern University, Boston, MA)

In this chapter we presented various robotic systems that have been proposed for gait rehabilitation after stroke and other neurological diseases. We classified these systems into two types: exoskeletons and end-effectors. While most of these systems represent unique engineering designs and offer many new possibilities for gait training after stroke, they also have important limitations that do not allow their widespread use in clinical practice. Recently we performed an extensive survey in clinical facilities about the use of robotic systems in gait rehabilitation. Over the course of 7 weeks we interviewed almost 80 clinicians (Physical Therapists (PT), PT aides, Physiatrists), Physical Therapy Academics, Directors of Rehab, Directors of Stroke, PT Supervisors and Managers at a variety of institutions, including Inpatient Rehab Facilities (IRFs), Outpatient Clinics, Skilled Nursing Facilities (SNFs) and Long Term Acute Care Facilities (LTACs). In the next paragraph we will report some of the findings of this survey regarding the needs and problems that currently exist with robotic therapy in gait rehabilitation.

Currently commercially available robotic solutions for automation of physical therapy cost between $60,000 and $300,000. It is obvious that very few facilities worldwide can afford them. This high cost of existing robotic systems for gait rehabilitation is a huge hurdle that needs to be overcome so that robotic systems become widely accepted in clinical facilities. During our survey, we found out that there is a need for simple, cost-effective robotic devices for leg advancement in gait training, because manual facilitation very often requires 2 or 3 PTs or PT aides working in unison, which is very costly to the clinical facility. The existing commercially available high-end robotic devices for gait rehabilitation are certainly impressive, but they have major limitations: the patient setup time can take 15 min (up to 20 min during the first session), which is significant when the total training session lasts only 30 or 45 min. These devices are highly restrictive to natural gait kinematics, they can only administer gait training over treadmill, and they are complicated to operate, requiring a trained full time staff person. What clinicians are missing is a simple and easy to use robotic tool which can assist them in advancing the legs of the patient during gait training over the treadmill and over the ground. This tool needs to apply guidance forces and torques to the leg(s) while not impeding all of the natural gait kinematics.

Moreover, an extensive literature research on rehabilitation robotics has demonstrated the advantages of robot-supported therapy [7]. A key design objective for lower limb robotic systems is to develop a mechanism that can better reflect the real movement of human lower limbs during walking. However, including all DoFs which can be found on a human lower limb in a robotic mechanism is almost impossible and not cost effective. Because of this, it is important to focus on rehabilitation goals of specific injuries in a specific neurological area. Therefore we need several robotic devices for gait rehabilitation each one targeting different joints (e.g. ankle, knee, hip etc.). Some therapists have pointed out that sagittal plane control during initial gait rehabilitation is sufficient for the patient. Having extra DoFs for the patient to control would create a burden to the patient. Because of this, certain joint movements of the patient during gait rehabilitation are locked without over-constraining the natural walking dynamic [50]. However, each gait rehabilitation phase has different goals, i.e. it is important to improve the sagittal plane control, but it is also very important to recuperate the functional movements for the subject to be able to return to his personal and professional life that depends also on other movement planes.

The interactive participation of the patient should also be considered in gait rehabilitation because it can accelerate the rehabilitation process, emphasizing the importance of assistive robots. The self-corrected gait monitoring by devices provide objective information about the gait pattern, can motivate patients to correct their gait based on the visual feedback information. Thus, developing a virtual environment, with a friendly and positive interface, is important during the rehabilitation process. It conveys a variety of information to therapists that can identify limitations in flexibility, strength and motor control and thus focus on the treatment by specific exercises for strengthening, flexibility and motor learning [51].

It is obvious that robotic gait rehabilitation devices are very important. However, as we have discussed in this section, currently available systems for robotic gait rehabilitation have many important limitations. Therefore, a lot of research needs to be performed and new robotic systems for gait rehabilitation need to be developed so that they are widely use in the clinical practice. Robotic gait rehabilitation is a very exciting filed that combines societal benefit with engineering innovation.

References

1. Inman VT, Ralston HJ, Frank T (1981) Human walking. Williams & Wilkins, Baltimore
2. Perry J, Burnfield JM (2010) Gait analysis: normal and pathological function, 2nd edn. Slack Incorporated, Thorofare, New Jersey
3. Roger VL, Go AS, Lloyd-Jones DM, Benjamin EJ, Berry JD, Borden WB, Bravata DM et al (2011) Heart disease and stroke statistics – 2012 update: a report from the American Heart Association. Circulation 125:e2–e220. doi:10.1161/CIR.0b013e31823ac046
4. Hesse S (2008) Treadmill training with partial body weight support after stroke: a review. NeuroRehabilitation 23:55–65
5. Banala SK, Agrawal SK, Scholz JP (2007) Active Leg Exoskeleton (ALEX) for gait rehabilitation of motor-impaired patients. In: Proceedings of the IEEE international conference on rehabilitation robotics, 10th edn, Noordwijk, pp 401–407. doi:10.1109/ICORR.2007.4428456
6. Belda-Lois J-M, Horno SM, Bermejo-Bosch I, Moreno JC, Pons JL, Farina D, Iosa M et al (2011) Rehabilitation of gait after stroke: a review towards a top-down approach. J Neuroeng Rehabil 8:66. doi:10.1186/1743-0003-8-66
7. Aliverti A, Frigo C, Andreoni G, Baroni G, Bonarini A, Cerveri P, Crivellini M et al (2011) Functional evaluation and rehabilitation engineering. IEEE Pulse 2:24–34. doi:10.1109/MPUL.2011.941520
8. Swinnen E, Duerinck S, Baeyens JP, Meeusen R, Kerckhofs E (2010) Effectiveness of robot-assisted gait training in persons with spinal cord injury: a systematic review. J Rehabil Med 42:520–526. doi:10.2340/16501977-0538
9. Tefertiller C, Pharo B, Evans N, Winchester P (2011) Efficacy of rehabilitation robotics for walking training in neurological disorders: a review. J Rehabil Res Dev 48:387–416
10. Agrawal SK, Banala SK, Fattah A, Sangwan V, Krishnamoorthy V, Scholz JP, Hsu W-L (2007) Assessment of motion of a swing leg and gait rehabilitation with a gravity balancing exoskeleton. IEEE Trans Neural Syst Rehabil Eng 15:410–420. doi:10.1109/TNSRE.2007.903930
11. Beyl P, Van Damme M, Van Ham R, Versluys R, Vanderborght B, Lefeber DP (2008) An exoskeleton for gait rehabilitation: prototype design and control principle. In: Proceedings of the IEEE international conference on robotics and automation, Pasadena, pp 2037–2042. doi:10.1109/ROBOT.2008.4543506
12. Colombo G, Joerg M, Schreier R, Dietz V (2000) Treadmill training of paraplegic patients using a robotic orthosis. J Rehabil Res Dev 37:693–700
13. Colombo G, Wirz M, Dietz V (2001) Driven gait orthosis for improvement of locomotor training in paraplegic patients. Spinal Cord 39:252–255
14. Ichinose WE, Reinkensmeyer DJ, Aoyagi D, Lin JT, Ngai K, Edgerton VR, Harkem SJ, Bobrow JE (2003) A robotic device for measuring and controlling pelvic motion during locomotor rehabilitation. In: Conference proceedings of the IEEE Engineering in Medicine and Biology Society, 25th edn, vol 2, Cancun, pp 1690–1693. doi:10.1109/IEMBS.2003.1279715
15. Unluhisarcikli O (2012) Human-robot interaction control of neurorehabilitation robots. Ph.D. thesis, Northeastern University
16. Reinkensmeyer DJ, Wynne JH, Harkema SJ (2002) A robotic tool for studying locomotor adaptation and rehabilitation. In: Proceedings of the annual conference and annual fall meeting of the Biomedical Engineering Society, 24th edn, vol 3, Houston, pp 2353–2354. doi:10.1109/IEMBS.2002.1053318

17. Schmidt H, Hesse S, Bernhardt R, Kruger J (2005) HapticWalker – a novel haptic foot device. ACM Trans Appl Percept 2:166–180. doi:10.1145/1060581.1060589
18. Hussein S, Schmidt H, Volkmar M, Werner C, Helmich I, Piorko F, Krüger J et al (2008) Muscle coordination in healthy subjects during floor walking and stair climbing in robot assisted gait training. In: Conference proceedings of the IEEE Engineering in Medicine and Biology Society, 30th edn, Vancouver, pp 1961–1964. doi:10.1109/IEMBS.2008.4649572
19. Rehab Technology AG (2012) Rehab technology: for a better life (G-EO system). http://www.rehatechnology.com/. Accessed 20 Apr 2013
20. Tomelleri C, Waldner A, Werner C, Hesse S (2011) Adaptive locomotor training on an end-effector gait robot: evaluation of the ground reaction forces in different training conditions. In: Proceedings of the IEEE international conference on rehabilitation robotics, Zurich, pp 5975–5492. doi:10.1109/ICORR.2011.5975492
21. Hesse S, Waldner A, Tomelleri C (2010) Innovative gait robot for the repetitive practice of floor walking and stair climbing up and down in stroke patients. J Neuroeng Rehabil 7:30. doi:10.1186/1743-0003-7-30
22. Aoyagi D, Ichinose WE, Harkema SJ, Reinkensmeyer DJ, Bobrow JE (2007) A robot and control algorithm that can synchronously assist in naturalistic motion during body-weight-supported gait training following neurologic injury. IEEE Trans Neural Syst Rehabil Eng 15:387–400
23. Aoyagi D, Ichinose WE, Harkema SJ, Reinkensmeyer DJ, Bobrow JE (2005) An assistive robotic device that can synchronize to the pelvic motion during human gait training. In: Proceedings of the IEEE international conference rehabilitation robotics, 9th edn, Chicago, pp 565–568. doi:10.1109/ICORR.2005.1502026
24. Wang P, Low KH, Lim PH, Tow A (2011) Effects of ground contact for overground walking on a robotic gait trainer. In: Proceedings of the IEEE international conference on robotics and biomimetics, Phuket Island, pp 895–900. doi:10.1109/ROBIO.2011.6181401
25. Wang P, Low KH, Tow A (2011) Synchronized walking coordination for impact-less footpad contact of an overground gait rehabilitation system: NaTUre-gaits. In: Proceedings of the IEEE international conference on rehabilitation robotics, Zurich, pp 1–6. doi:10.1109/ICORR.2011.5975353
26. Luu TP, Lim H-BB, Qu X, Low KH (2011) Pelvic motion assistance of NaTUre-gaits with adaptive body weight support. In: Proceedings of the Asian control conference, 8th edn, Kaohsiung, pp 950–955
27. Lim H-BB, Luu TP, Hoon KH, Qu X, Tow A, Low KH (2011) Study of body weight shifting on robotic assisted gait rehabilitation with NaTUre-gaits. In: Proceedings of the IEEE/RSJ international conference on intelligent robotics and systems (IROS), San Francisco, pp 4923–4928. doi:10.1109/IROS.2011.6094849
28. Yoon J, Novandy B, Yoon C-H, Park K-J (2010) A 6-DOF gait rehabilitation robot with upper and lower limb connections that allows walking velocity updates on various terrains. IEEE ASME Trans Mechatron 15:201–215. doi:10.1109/TMECH.2010.2040834
29. Artemiadis PK, Krebs HI (2010) On the control of the MIT-Skywalker. In: Conference proceedings of the IEEE Engineering in Medicine and Biology Society, 32nd edn, Buenos Aires, pp 1287–1291. doi:10.1109/IEMBS.2010.5626407
30. Artemiadis PK, Krebs HI (2011) On the potential field-based control of the MIT-Skywalker. In: Proceedings of the IEEE international conference on robotics and automation, Shanghai, pp 1427–1432. doi:10.1109/ICRA.2011.5980063
31. Wu M, Hornby TG, Landry JM, Roth H, Schmit BD (2011) A cable-driven locomotor training system for restoration of gait in human SCI. Gait Posture 33:256–260. doi:10.1016/j.gaitpost.2010.11.016
32. Wu M, Landry JM, Yen SC, Schmit BD, Hornby TG, Rafferty M (2011) A novel cable-driven robotic training improves locomotor function in individuals post-stroke. In: Conference proceedings of the IEEE Engineering in Medicine and Biology Society, 33rd edn, Boston, pp 8539–8542. doi:10.1109/IEMBS.2011.6092107

33. Surdilovic D, Zhang J, Bernhardt R (2007) STRING-MAN: wire-robot technology for safe, flexible and human-friendly gait rehabilitation. In: Proceedings of the IEEE international conference on rehabilitation robotics, 10th edn, Noordwijk, pp 446–453. doi:10.1109/ICORR.2007.4428463
34. Peshkin M, Brown DA, Santos-Munne JJ, Makhlin A, Lewis E, Colgate JE, Patton J et al (2005) KineAssist: a robotic overground gait and balance training device. In: Proceedings of the IEEE international conference on rehabilitation robotics, 9th edn, Chicago, pp 241–246. doi: 10.1109/ICORR.2005.1501094
35. Seo K-H, Lee J-J (2009) The development of two mobile gait rehabilitation systems. IEEE Trans Neural Syst Rehabil Eng 17:156–166
36. Colombo G, Jorg M, Dietz V (2000) Driven gait orthosis to do locomotor training of paraplegic patients. In: Conference proceedings of the IEEE engineering in Medicine and Biology Society, 22nd edn, vol 4, Chicago, pp 3159–3163. doi:10.1109/IEMBS.2000.901556
37. Hocoma AG (2007) Lokomat® – enhanced functional locomotion therapy with augmented performance feedback [cited 2012 August 6th]. http://www.hocoma.com/en/products/lokomat/. Accessed 8 Mar 2013
38. Veneman JF (2007) Design and evaluation of the gait rehabilitation robot LOPES. Ph.D. thesis, University of Twente
39. Veneman JF, Kruidhof R, Hekman EEG, Ekkelenkamp R, Van Asseldonk EHF, van der Kooij H (2007) Design and evaluation of the LOPES exoskeleton robot for interactive gait rehabilitation. IEEE Trans Neural Syst Rehabil Eng 15:379–386. doi:10.1109/TNSRE.2007.903919
40. Ekkelenkamp R, Veneman JF, van der Kooij H (2007) LOPES: a lower extremity powered exoskeleton. In: Proceedings of the IEEE international conference on robotics and Automation, Roma, pp 3132–3133. doi:10.1109/ROBOT.2007.363952
41. Banala SK, Kim SH, Agrawal SK, Scholz JP (2009) Robot assisted gait training with Active Leg Exoskeleton (ALEX). IEEE Trans Neural Syst Rehabil Eng 17:2–8. doi:10.1109/TNSRE.2008.2008280
42. Winfree KN, Stegall P, Agrawal SK (2011) Design of a minimally constraining, passively supported gait training exoskeleton: ALEX II. In: Proceedings of the IEEE international conference on rehabilitation robotics, Zurich, pp 1–6. doi:10.1109/ICORR.2011.5975499
43. Banala SK, Agrawal SK, Kim SH, Scholz JP (2010) Novel gait adaptation and neuro-motor training results using an Active Leg Exoskeleton (ALEX). IEEE ASME Trans Mechatron 15(2):216–225
44. Kim SH, Banala SK, Agrawal SK, Krishnamoorthy V, Scholz JP (2010) Robot-assisted modification of gait in healthy individuals. Exp Brain Res 202:809–824
45. Stegall P, Winfre K, Agrawal SK (2012) Degrees-of-freedom of a robotic exoskeleton and the human adaptation to templates of new gait. In: Proceedings of the IEEE international conference on robotics and automation, Saint Paul, MN
46. Beyl P, Van Damme M, Van Ham R, Lefeber D (2008) Design and control concepts of an exoskeleton for gait rehabilitation. In: Proceedings of the IEEE RAS EMBS international conference on biomedical robotics biomechatronics, 2nd edn, Scottsdale, pp 103–108. doi:10.1109/BIOROB.2008.4762874
47. Unluhisarcikli O, Pietrusinski M, Weinberg B, Bonato P, Mavroidis C (2011) Design and control of a robotic lower extremity exoskeleton for gait rehabilitation. In: Proceedings of the IEEE/RSJ international conference on intelligent robots and systems (IROS), San Francisco, pp 4893–4898. doi:10.1109/IROS.2011.6094973
48. Pietrusinski M, Cajigas I, Goldsmith M, Bonato P, Mavroidis C (2010) Robotically generated force fields for stroke patient pelvic obliquity gait rehabilitation. In: Proceedings of the IEEE international conference on robotics and automation, Anchorage, pp 569–575. doi:10.1109/ROBOT.2010.5509872
49. Pietrusinski M, Cajigas I, Severini G, Bonato P, Mavroidis C (2013) Robotic gait rehabilitation trainer. IEEE ASME Trans Mechatron 19(2):490–499

50. Lim H-BB, Hoon KH, Low KH, Soh YC, Tow A (2008) Pelvic control and over-ground walking methodology for impaired gait recovery. In: Proceedings of the IEEE international conference on robotics and biomimetics, Bangkok, pp 282–287. doi:10.1109/ROBIO.2009.4913017
51. Bae J, Kong K-C, Byl N, Tomizuka M (2009) A mobile gait monitoring system for gait analysis. In: Proceedings of the IEEE international conference on rehabilitation robotics, 11th edn, Kyoto, pp 73–79. doi:10.1109/ICORR.2009.5209621

Chapter 11
Enhancing Recovery of Sensorimotor Functions: The Role of Robot Generated Haptic Feedback in the Re-learning Process

Lorenzo Masia, Maura Casadio, Valentina Squeri, Leonardo Cappello, Dalia De Santis, Jacopo Zenzeri, and Pietro Morasso

Abstract The term Robotic Rehabilitation defines a class of machines employed for different scenarios, ranging from therapeutic and assistive applications to robots devoted to neuroscience, behavioral research, and cognitive aspects. The first use of such technology dates back to early 1990s, with a relatively long history and it remains linked to the idea that robots, even with a certain degree of autonomy, must be directly controlled by humans while the interaction must be opportunely regulated in order to promote motor recovery or independent living. These devices are designed for individuals with neuromotor and cognitive disabilities to provide rehabilitative exercises or assistance for activity of daily living. They are also measurement systems i.e. they can incorporate sensors for monitoring kinematic and kinetic interaction with subjects such as movement, force or inertial sensors, or for detecting EMG signals to trigger the assistance or to provide – in more complex architectures – Functional Electric Stimulation (FES) to promote motor activity. In this chapter we will focus on therapeutic robots, which are usually employed to perform rehabilitation protocol, describing in details the most widely used control architectures, the implementation of rehabilitation exercises to restore specific motor functions and the measures of the corresponding performance.

Keywords Robot aided rehabilitation • Proprioception recovery • Assistive control • Motor adaptation • Stroke rehabilitation • Cerebral palsy

---

L. Masia (✉)
School of Mechanical and Aerospace Engineering, Nanyang Technological University, Singapore
e-mail: Lorenzo.masia@ntu.edu.sg

M. Casadio
Department of Informatics, Bioengineering, Robotics and Systems Engineering,
University of Genoa, Genoa, Italy

V. Squeri • L. Cappello • D. De Santis • J. Zenzeri • P. Morasso
Department of Robotics, Brain and Cognitive Sciences, Italian Institute of Technology,
Genoa, Italy

P. Artemiadis (ed.), *Neuro-Robotics: From Brain Machine Interfaces to Rehabilitation Robotics*, Trends in Augmentation of Human Performance 2,
DOI 10.1007/978-94-017-8932-5_11,

11.1 Introduction

The term Robotic Rehabilitation defines a class of machines employed for different scenarios, ranging from therapeutic and assistive applications to robots devoted to neuroscience, behavioral research, and cognitive aspects. The first use of such technology dates back to early 1990s, with a relatively long history and it remains linked to the idea that robots, even with a certain degree of autonomy, must be directly controlled by humans while the interaction must be opportunely regulated in order to promote motor recovery or independent living. These devices are designed for individuals with neuromotor and cognitive disabilities to provide rehabilitative exercises or assistance for activity of daily living. They are also measurement systems i.e. they can incorporate sensors for monitoring kinematic and kinetic interaction with subjects such as movement, force or inertial sensors, or for detecting EMG signals to trigger the assistance or to provide – in more complex architectures – Functional Electric Stimulation (FES) to promote motor activity. In this chapter we will focus on therapeutic robot, which are usually employed to perform rehabilitation protocol and aimed to restore motor function. These kind of robots can be programmed to deliver different robot-assisted exercises; according to the taxonomy suggested by Marchal-Crespo and Reinkensmayer [56], there are three main approaches based on the interaction between the machine and the subject:

- Assistive: the robot provides forces in order to facilitate subjects' movements. The regulation of the assistance is mainly based on subjects' performance and clinical status.
- Virtual reality and haptic simulation of activities of daily living: in this paradigm the subjects interact via robotic devices with virtual environments characterized by a variety of objects. The haptic rendering can be defined as the process of generating contact force by a device in order to create the illusion of touching a virtual object.
- Challenge-based: this approach mainly based on previous motor adaptation studies; the robot generates structured force fields or feedback, which perturb or oppose resistance to subjects' movements or augmented motor error, thus promoting the reorganization of their residual movement abilities.

These approaches are not mutually exclusive and we can combine them. There are several examples of rehabilitative protocols employing the aforementioned categories of controllers; the choice is correlated with several scenarios, ranging from the pathology and the residual movement capacity of the patients to the type of robotic device in use and therefore its hardware/software configuration. Classification for rehabilitation robots can be based also on mechanical design and control architecture. According to the mechanical structure classification, devices can be grouped into two types: endpoint robots and exoskeletons. There is also a third class of devices based on cable suspension architecture, but we do not include them in this chapter because of their completely different control strategy for limb manipulation. Endpoint robots have a single connection point with the

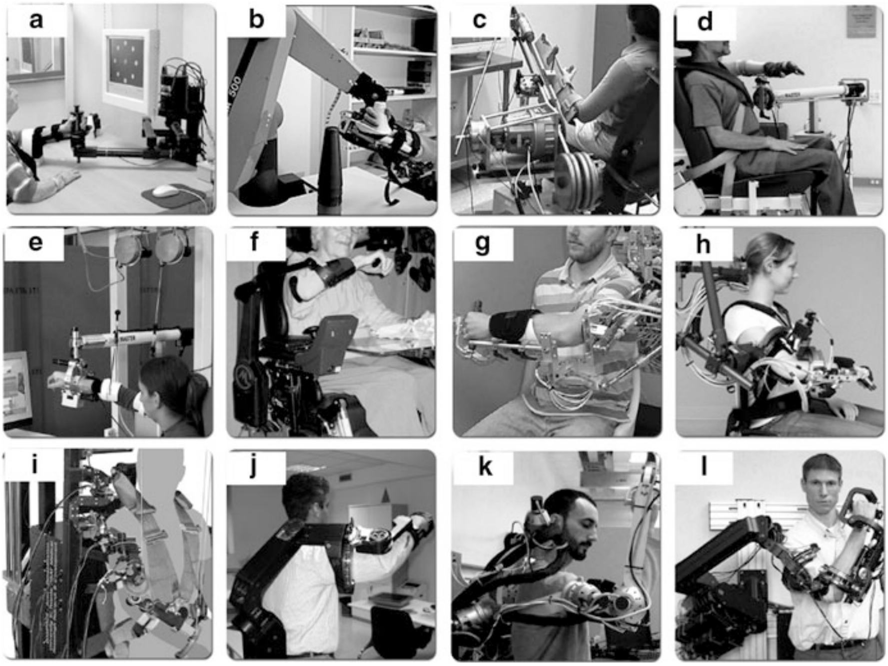

Fig. 11.1 Examples of different manipulator architecture for upper limb rehabilitation. For the serial mirrored manipulator. (**a**) MIT Manus [1]; (**b**) MIME [2]; (**c**) ARM Guide [3]; (**d**) ACT 3D [4]; (**e**) Gentle-S [5]; (**f**) Armon [6]. Exoskeletal architectures. (**g**) Pneu WREX [7]; (**h**) ARMin [8]; (**i**) Dampace [9]; (**j**) L-EXOS [10]; (**k**) MGA exoskeleton [11]; (**l**) CADEN 7 [12]

subjects' body e.g. hand, foot, wrist, etc. This connection limits the control over individual joint axes; subjects hold the end-effector (handle) of the robotic device and move in virtual environments, while the device deliver assistance or resistance or perturbations by generating structured force fields. Exoskeletons are external skeletons placed over the limb and mostly powered by actuators on the joints. Therefore, they do not control directly only a single endpoint, but also (a subset of) joints, e.g. for the arm – shoulder, elbow, wrist, etc., at the cost of more complex mechanics. For an overview of existing examples of exoskeletons and endpoint manipulators for the upper limb refer to Fig. 11.1.

The robotic devices can be grouped also considering the control architecture. The initial applications in the robotic rehabilitation field employed industrial manipulators opportunely controlled. However, due to their inherent high power/weight ratio and some critical issue related to safety, engineers decided to design a different class of devices where the specific requirements were oriented toward an enhancement of human-robot interaction. This new class of haptic devices is based on force reflecting controllers designed to provide realistic rendering of the simulated environment and therefore to generate different mechanical impedance at the end effector. This is guaranteed by the power of the actuation, however a more powerful

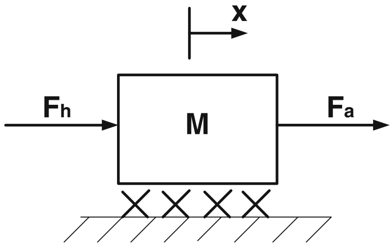

Fig. 11.2 Simplified model of a haptic actuators

electromechanical actuator tends to be heavier. Larger and powerful actuators can deliver a high force at the end effector, but they also increase the friction and inertia perceived by the human operator. Contrarily, small motors can guarantee a very backdrivable design, but they deliver a limited range of haptic rendering. That's why in haptics the choice of actuation is a crucial design specification, which is driven by the overall structure of the device, including the control architecture. There are several solutions adopted for the implementation of haptic control scheme, but the most widely used can be mainly summarized in the class of impedance and admittance controllers.

In order to understand how the two mentioned control architectures work, Fig. 11.2 depicts a simplified model of a one degree of freedom actuator, where F_h and F_a are respectively the force exerted by the human and the actuators. Writing down the equation of motion of the entire system, there is also the force related to the intrinsic mechanical impedance Z due to the friction of the mechanism and the inertial contribution of the moving mass of the mechanism.

$$\left(ms^2 + bs\right) x - F_a = F_h \tag{11.1}$$

The maximum force that the haptic device can deliver is strictly related to the maximum level of the haptic rendering the human operator can perceive; this concept is explained with the introduction of the definition of transparency [13] of an haptic device which is the ratio of the impedance as the input source of the haptic interface Z_{in} and the actually perceived output impedance Z_{out} of the device.

$$T = \frac{Z_{in}}{Z_{out}} \tag{11.2}$$

The principle of transparency is strictly related to the concept of back-drivability, and a transparency close to unity means that the source of the mechanical impedance is not altered by the mechanics of the device [13]: the action of the actuator is perceived at the end effector in a pristine way by the operator. Colgate [14] provided another important contribution to the comprehension of the mechanism of haptic rendering, describing the Z_{width} as the difference between the maximum load Z_{max} and the perceivable friction and inertia at the free space movement Z_{min}.

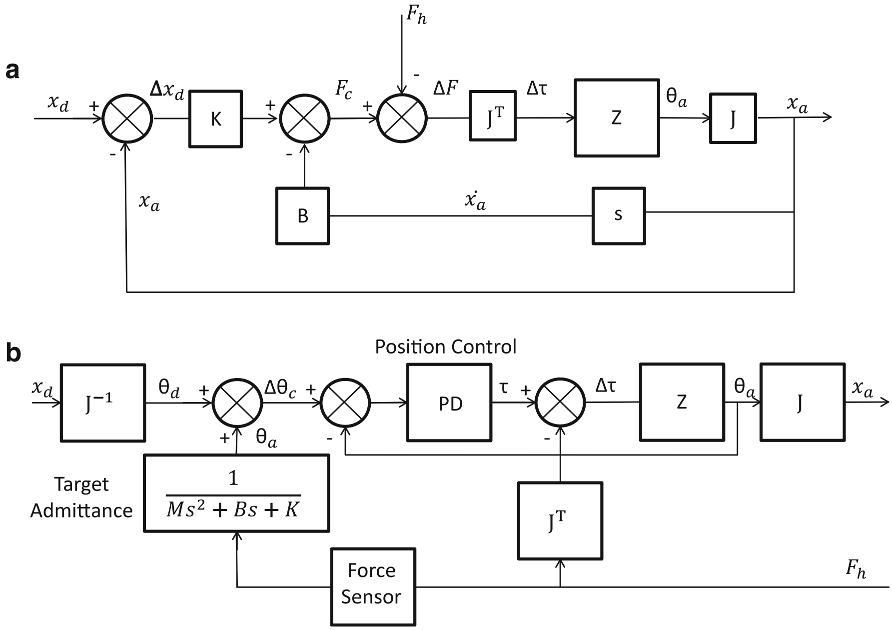

Fig. 11.3 (**a**) Impedance control scheme. (**b**) Admittance control scheme

$$Z_{width} = Z_{\max} - Z_{\min} \tag{11.3}$$

Both Z_{width} and transparency T are complex operators, which are related to many factors and are strictly dependent on the frequency characteristics of the device and associated control architecture. In haptics and all the applications related to human robot interaction there are two main controllers that are used and they are strictly correlated with the specific feature of the hardware on which they must be implemented: generally speaking the main characteristics which drives the choice between different control schemes is the intrinsic mechanical impedance of the hardware referred as *Z*. For a very back-drivable device (with a very low value of Z) the preferred controller is the simple **Impedance control scheme**: the loop of an impedance controller does not require any force sensor to detect the interaction forces at the end effector exchanged between the operator and the device, because due to the back-drivable mechanism the motion of the operator is the parameter by which the control action is generated. Observing Fig. 11.3a the control effort is computed by comparing the desired position x_d with the actual position x_a; the force generated by the impedance controller is, in most of the applications, the sum of a proportional and derivative actions as reported in the following formula.

$$F_c = K\,(x_d - x_a) - B\dot{x}_a \tag{11.4}$$

The computed force F_c is then summed to the force exerted by the human and converted into joint torques. The overall impedance felt by the user, i.e. the transfer function between the robot motion X_a and the hand force F_h is a combination of the programmed impedance and the dynamics of the robot Z. Therefore, this control scheme is only applied when robot dynamics is negligible in comparison to the target impedance generated by the controller action. Open-loop impedance controllers are easy to implement, and are widely used in robotic rehabilitation. Devices like MIT-Manus [1], 'Braccio di Ferro' [15], ATR's Parallel direct drive air-magnet Floating Manipulandum (PFM) [16] and vBot [17] all use this control scheme.

Admittance control scheme (see Fig. 11.3b) is mainly based on two nested control loops and it is implemented when the mechanical impedance perceived at the end effector of the device is high and therefore the system does not result in a back-drivable solution. In the outer loop the human-generated force, measured by a force/torque sensor, is translated into a robot movement through a 'target admittance' block, which specifies the desired behavior of the manipulator at the interface with the subject.

In other words, the target admittance block reflects the desired haptic behavior by generating a desired device position θ_a; the generated position is then compared with a desired θ_d and sent to an inner loop control consisting in a position controller, for example a PID (as in the figure a PD), which is used to drive the system in the configuration generated by the admittance outer loop. The robot is transformed into a position (displacement) generator where the position is the response of second order linear model corresponding to the target admittance block. The inner loop is generally implemented by the servos of the motor at a very high speed (>3 kHz). The outer loop can be updated at lower speeds to limit the computational burden.

Admittance control is used in devices with low levels of back-drivability; an example is the HapticMASTER (Moog, USA) [18], which is a widely used device in the field of neurorehabilitation and neuroscience; see, for instance, the ACT3D [4] and GENTLE/S [5] systems. Whereby the user exerts a force on the device, the device reacts by generating the appropriate displacement.

Overall, the two proposed control schemes behave in similar way and the final purpose is imposing a dynamic behavior to the end effector, which mainly depends on the computational action of the software, hiding the intrinsic mechanical impedance of the hardware. The difference between the two solutions is in the parameters used for the generation of the control efforts: while the impedance controller receives as input the motion flow generated by the human interaction with the end effector, feeding back a force computed by the controller, contrarily the admittance control is based on the acquisition of the interaction forces between the human and the device. The presence of the force sensor at the end effector in the admittance control scheme is therefore crucial for the generation of the desired haptic rendering, which is primarily computed as a desired position from the admittance target block and successively translated into a force by the inner position loop. It is clear from these considerations that the admittance controller results in a more complex architecture with respect to the impedance one, for the presence of the sensor employed to acquire the force and the two nested loop which must be opportunely tuned for respecting stability. Furthermore, if on one side the admittance controller allows for a wider Z_{width} because is usually implemented on powerful robotic devices able to deliver high force and torque ranges, on the other side the presence of force sensors and the necessity of very high gain parameters in the control loop has the disadvantage of being intrinsically less safe in case of failure with respect to the impedance controller where the control loop is extremely simplified and the back-drivability of the mechanical structure is still able to assure a good level of haptic rendering and an intrinsically safe gentle interaction. In other terms, impedance control is generally more *robust* than admittance control in most applications and implementations.

11.2 Measures of Performance and Recovery

About 80 % of stroke survivors are unable to perform activities of daily living (ADL) due to an abnormal disturbed sensory feedback or motor control of the upper limb on the paretic side [19, 20] associated to sensory distortions, which manifests through a reduction of tactile or afferent feedback, or as the opposite, through hypersensitivity and lack of control.

The loss of motor control is classified in typical neurological impairments by the following phenomena:

- Muscle weakness limits the maximum potential output force of a muscle [21]. It is caused by the damage to motor cortex neurons or their corticospinal projections, decreasing the activation of spinal motor neurons controlling the muscles.
- Hyperactive reflexes can resist or even reverse desired movements. The expression of hyperactive reflexes is felt as increased muscle tone or joint resistance when it depends on the muscle-length feedback [22, 23]. When dependent on the muscle speed feedback, the effects are described as spasticity [24].
- Abnormal muscle synergies express themselves through a loss of independent joint control, where involuntary co-activation of muscles occurs over multiple joints [25, 26]. For example, when attempting to reach up and out for an object on a shelf, the abduction torque in the shoulder causes an involuntary flexion of the elbow, reducing the achievable reaching distance of the hand [4].
- Muscle atrophy is a decrease in muscle mass and the results of muscle disuse over time [27]. The loss of neural activation leads to a slow wasting away of the affected muscle fibers, thereby contributing to long-term muscle weakness.
- Increased joint stiffness is due to changes in muscle and tendon properties. These changes are a result from permanent muscle activity due to abnormal muscle coactivation patterns or spasticity.

The immediate effects after a stroke can range from losing all voluntary muscle activation, to having no noticeable effects on limb movements. Spontaneous recovery can bring back some original motor function, but this takes many months to level out [28].

Several stroke assessment scales are used to more precisely assess the need for medical treatment and assistance, and to monitor functional recovery. The following scales all capture some of the mental and motor impairments in stroke survivors:

- Barthel Index (BI): measures independent functioning and mobility in daily life.
- Functional Independence Measure (FIM): measures sensitivity and comprehensiveness in daily life.
- Chedoke-McMaster Stroke Assessment (CMSA): measures impairment and activities of daily life.
- Motor Activity Log (MAL): measures arm usage.
- Modified Ashworth Scale (MAS): measures muscle tone.
- Tone Assessment Scale (TAS): measures muscle tone.
- Modified Tardieu Scale (MTS): measures muscle tone
- Motor Assessment Scale (MAS): measures performance of functional tasks.
- Fugl-Meyer Assessment (FMA): measures motor and joint function and sensation.
- Action Research Arm Test (ARAT): measures ability to handle different objects.
- Nine Hole Peg Test (NHPT): measures fine manual dexterity.
- Wolf Motor Function Test (WMFT): measures time-based upper extremity performance.

These scores are placed in order of level of detail given. The top scales only yield an indication of the care and assistance needed. The bottom scales measure the dexterity of the upper paretic limbs, and are most useful for upper-extremity research. Of these, the FMA [29] is a well-designed, feasible clinical examination based on the general stages of recovery [30]: these stages cover different course of the pathology form an initial stage when the subject is unable to voluntarily move his/her limb, an intermediate stage when synergies are corrupted due to the presence of spasticity and a final one when movement still appears clumsy, but spasticity is reduced and the subject can voluntarily control the motion performing simple actions. It has been widely tested in the stroke population, but due to the amount of time it takes to administer, it is mostly used by scientists, not by therapists or physicians. The ARAT and NHPT have been suggested as faster and more accurate assessments to measure dexterity [31]. While for quantifying muscle tone, the MTS seems the most objective measuring the stretch reflex induced by an angular movement of each joint in its range of motion at different velocities [32].

A problem for most of these clinical scales is their non-linearity, lack of resolution, and inter-rater reliability. Some scales have only six possible levels, and when different examiners administer the test, the results may vary as well. Robots are now used in research environments to obtain more accurate measurements [33–35]; the capacity of a haptic device to acquire multiple data relying on various sensors can drive towards a unified approach to the use of robotic rehabilitation not only as a mere exercising machine, but also as an instrument able to quantify and qualify the pathological conditions. There are several parameters that can be detected during robot therapy; most of the works in literature uses kinematic data to characterize motor learning and motor recovery. The paradigms of the experiments are mainly (most widely used) characterized by point-to-point movements starting from a position in the workspace and reaching a target with or without assistance of the robotic interface. Observation of the kinematics usually consists in an offline analysis of trajectories over the course of the different phases of the protocol. Each trajectory during reaching tasks is a movement that can gather information of the capacity of the subject to interpret the task and successively control his/her limb. Analysis usually aims to characterize each trajectory by the following parameters:

– Lateral deviation (*LD*): it is defined as the deviation from the straight line that connects the initial position to the target, evaluated at the time of peak velocity or also the max deviation over the entire trajectory to the target. Positive and negative errors correspond to leftward and rightward lateral deviations, respectively [36].
– Acceleration peak: it is the highest value of the acceleration profile. This indicator, if associated with movement direction, can provide a polar plot that we expect to be asymmetric, as suggested in a previous study [37] that analyzes the anisotropy of the inertial properties of both the human and robot arms.
– Aiming error: it is the angular deviation from ideal trajectory (the straight line that connects the starting point to the target), evaluated 300 ms after movement onset; it a indicator which is mainly used to evaluate the feedforward effort to movement.
– Jerk metric: the jerk is the derivative of the acceleration and allows measuring the level of smoothness during a movement, which resulted to be a characteristic of coordinated and healthy movements [38–41].
– Directional analysis: it is usually performed for each of the previously defined variables, in order to highlight the interplay between the effect of the assisting/deviating robotic action and the capacity of the subject to generalize the movements in the arm workspace [42, 43].
– Learning Index: the degree of adaptation to the action of a robotic device during a motor learning or motor recovery exercise. Usually these index is computed by observing the force field effect on the lateral deviation by means of the following formula [44] that takes into account the values of lateral deviations in the force-field and catch trials while the force field generated by the robotic device is suddenly and randomly removed (LD_{ff} and LD_{catch})

$$LI = \frac{|LD_{catch}|}{|LD_{catch}| - |LD_{ff}|} \tag{11.5}$$

Other kinds of measures consider not the kinematic, but the dynamics of the movements. Most of the devices employed in rehabilitation are equipped with force/torque sensors, which allow detecting the interaction between the device and the patient. Although kinematic data provide a more generalized characterization of the movements, the force exchanged between the end effector and the subject's limb can be used to have a deeper insight of the modulation of motor commands during human robot interaction. This is the case of the stiffness measurements: the pioneering technique for stiffness estimation was based on the acquisition of muscular restoring force resulting from a small imposed displacement [45]: the new experimental method used a computer controlled mechanical interface (planar manipulandum) to measure and plot the conservative elastic force field associated to the posture of the arm by observing the steady-state force responses to a series of separate one-dimensional 'step' perturbations imposed from different directions. The main outcome was that endpoint stiffness of the human arm in the horizontal plane is characterized by directional properties that depend on limb geometry. Robot generated force impulses have been used to estimate stiffness during multijoint movements [46–52] and a successive experiment by Burdet et al. [53] strengthens the robustness of this technique by implementing an algorithm able to modulate the hand displacement on a predictive algorithm of the unperturbed trajectory.

The question arises as to whether is possible to have a continuous information of the muscular stiffness level during robot therapy, and gather some insights on how the central nervous system is able to modulate muscular activation while manipulating external environment. Recently Piovesan et al. [54, 55]. made a fist attempt in this direction, proposing a new and fast method for measuring the arm impedance of people with neuromotor disabilities during robot assisted movements. This methodology was tested with a stroke survivor's population. The results showed that the performance improvements produced by minimally assistive robot training are associated with decreased viscosity and stiffness in stroke survivors' paretic arm and these mechanical impedance components are partially modulated by visual feedback. In their review Marchal-Crespo and Reinkensmeyer [56] highlighted that it is necessary to find 'improved models of human motor recovery to provide a more rational framework for designing robotic therapy control strategies'. While musculoskeletal models have been extensively used for personalizing rehabilitation treatments [57], only recently some studies proposed computational models of neuromotor recovery. Some of these models describe the subjects' capability to execute a task e.g. [58, 59] modeled the time course of the performance during training. Others models investigated how assistive forces [60] or more in general training [61] influence voluntary control, thus neuromotor recovery. Some of these models [62–64] were incorporated in the robotics controllers to personalize the intervention and to automatically regulate the exercise according to subjects' residual ability, the progress of the disease, and the improvement due to the on-going therapy.

Another class of models focuses on the recovery process at the cortical level [65–67] studying how focal cortical lesions determine the reorganization at the neural and motor levels. Several studies investigated muscle activation highlighting that muscles participate to the production of movements in well-defined functional groups – called "synergies" – activated by the descending cortical commands. A recent study [68] has suggested that muscle synergies can be considered as physiological markers of motor cortical damage and can be used to characterize and understand motor impairment in stroke survivors. Finally there are models that look at both the cortical and the behavioral levels [69–71] describing how in motor skill learning tasks voluntary movements induce cortical and subcortical reorganization.

These recent studies opened the new field of computational rehabilitation and have a far reach potential both with respect to a better understanding of the mechanisms underlying the recovery process and with respect to the optimization of the rehabilitative intervention.

11.3 Learning Adaptation and Rehabilitative Exercises

As suggested by recent reviews [72–74], neural plasticity is recognized as the fundamental property of the human brain that must be exploited in order to achieve significant improvements in neuromotor rehabilitation of the upper-limb. This somehow clashes with the conventional view among clinicians that the recovery margin is close to null when the stroke survivor becomes “chronic”. It is then necessary to revise the conception and design of robot therapy in order to promote neural plasticity and enhance motor learning/re-learning. The underlying fundamental problem that must be faced in order to achieve such goal is that the main “cybernetic” effect of the neurological insult is to break the intrinsic coherence of purposive actions, namely the causal relation between *intended actions, actual movements*, and the corresponding *feedback reafference* (see Fig. 11.4 for a graphical representation of this concept): the *motor program* that drives the *muscles* in agreement with a given *task* can successfully unfold its control patterns only if the sensory consequences of the control patterns (the *sensory reafferences*) match the expected motion patterns. The same criterion of coherence impinges upon the validity of the task planner: if the expected and the actually measured motion patterns do not fit than the task description and the related motor program must be changed.

The neurological damages that characterize stroke patients do not allow them to achieve the cybernetic coherence of purposive actions typical of healthy subjects. Rehabilitation treatments provided by human or technological operators has the purpose of helping the patients to recover a minimum of cybernetic coherence

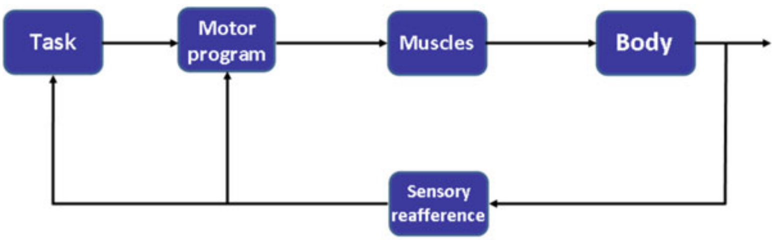

Fig. 11.4 Cybernetic structure of purposive actions in healthy subjects

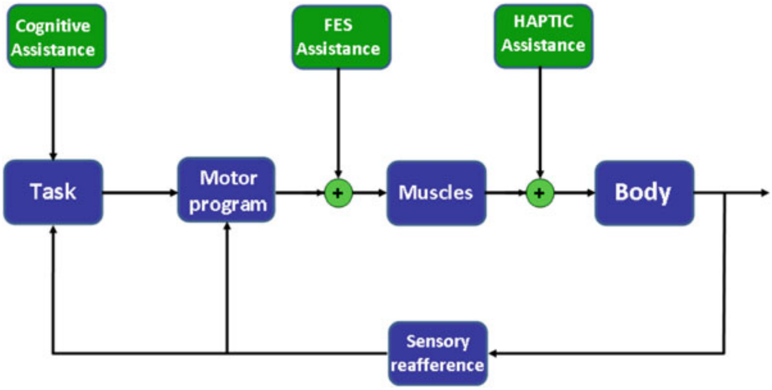

Fig. 11.5 Possible types of assistance in pathological conditions

by providing suitable assistance patterns. In general, three types of assistance can be envisaged, as sketched in Fig. 11.5. (1) *Cognitive assistance*, characterized by procedural, declarative and motivational aspects; (2) *Electrical assistance (FES)*, i.e. direct electrical stimulation of weakly activated muscle groups; (3) *Haptic assistance*, i.e. physical interaction of a human or robot therapist which consists of modulated patterns of assistive/resistive forces, associated with an optimally regulated mechanical impedance of the therapist.

Frequently, cognitive assistance has been developed in the framework of immersive or semi-immersive visual virtual reality. However, if used alone, it must be limited to individuals with a rather low level of impairment, namely patients who are able to carry out a goal-directed movement; in intermediate cases, it has been shown that a specific type of non-adaptive physical assistance, for example partial compensation of gravity (Armeo Spring Hocoma, AG, Switzerland) can be helpful. In more severe cases, in which the subjects are unable to carry out simple reaching movements in some directions (for example center-out movements to distant targets, on the border of the workspace) or have a strongly reduced RoM (Range of Motion) these movements must be supported by carefully regulated assistance. The purpose of such assistance is not to carry out the movements in place of the subject, as it happens in prosthetic devices. On the contrary, the issue is to train the subject is such a way that he/she can re-learn the control patterns that are necessary to perform the movement. The physiological prerequisite of functional recovery by means of training is the availability of neural plasticity and the main issue that must be faced by the designer of rehabilitation technologies is to use design principles that allow recruiting such plasticity in an efficient manner. There are two main dangers that must be taken into account: (1) the danger of *spasticity* and (2) the danger of *slacking* [60]. The first danger suggests to use smooth assistance patterns, in order to avoid strong acceleration peaks that may induce exaggerated reflex reaction and thus determine muscular hypertonus and worsens the level of spasticity. For this reason it is important to integrate, in the electrical/haptic assistance protocol, mechanisms for on-line detection of the mechanical impedance of the arm which is a sensitive indicator of excessive tonic activities induced by treatment (see later sections of this chapter). The second danger, which consists of the general tendency of human subjects to over-rely on external help, behaving as greedy optimizers of error and effort, suggests to modulate the level of assistance to the minimum level required for allowing to carry out the planned action without time constraints, i.e. in a self-paced manner. This is equivalent to attempt to trigger the assisting patterns upon positive detection of the *intention to move*. In other words, the regulation of assistance should avoid the imposition of passive movements because in such case the physiological coherence of the plan-effort-reafference circle is not reinforced: avoiding (unidirectional) Passive Mobilization (PM) is the main avenue to promote (bidirectional) haptic interaction.

On the other hand, passive mobilization can help contrasting the deterioration of the thixotropic properties of the collagen matrix of the muscle tissue that is a secondary consequence of the functional immobilization of the paretic limbs of stroke survivors. Thus, although some degree of passive mobilization is acceptable in a treatment routine (see also the technique of *dynamic splinting*, discussed in a coming section of the chapter), the majority of it must be based on smooth and minimized patterns of assistance, triggered by the detected intention to move. In fact, task oriented training has emerged as a leading concept in clinical practice. In other words, it is not movement per se, obtained for example by means of passive mobilization, which is effective in recruiting plastic adaptation, but minimally assisted movements associated with a task and volitional effort.

The intention to move, even in severely motor impaired subjects, can be detected directly or inferred/promoted indirectly. Examples of the former approach are provided by the "contralateral-homonymous paradigm" [75] or by "body machine interfaces" that extract motor intentionality even from extremely reduced mobility [76]. Another direct approach to the detection of intentionality is based on the analysis of brain activity, which is known to occur in anticipation of overt actions, in the so called preparation time. For example, event-related de-synchronization signals from cortical activity have been proved to be reliable and effective triggers of electrical assistance for the fast recovery of foot drop [77]. In contrast, EMG-triggered or cyclically delivered FES, in absence of a trigger of the intention to move, is totally ineffective for the recovery of voluntary control [78, 79]. Figure 11.6 depicts the aforementioned solutions. The indirect approach to the detection of intentionality is a typical topic in HRI (Human-Robot Interaction) and in the study of interacting *dyads*. It is known indeed that people often perform actions that involve a direct physical coupling with another person, for example when cooperating in the manipulation of a large and heavy object. This is a problem of coordination through physical interaction, which has some analogy to the interaction between a human or a robotic therapist with a motor impaired individual. It has been found that dyads produce much more overlapping forces than individuals, especially for tasks with higher coordination requirements [80], thus suggesting that dyads amplify their forces to generate a haptic information channel. In the case of robotic rehabilitation such haptic information channel can be facilitated by

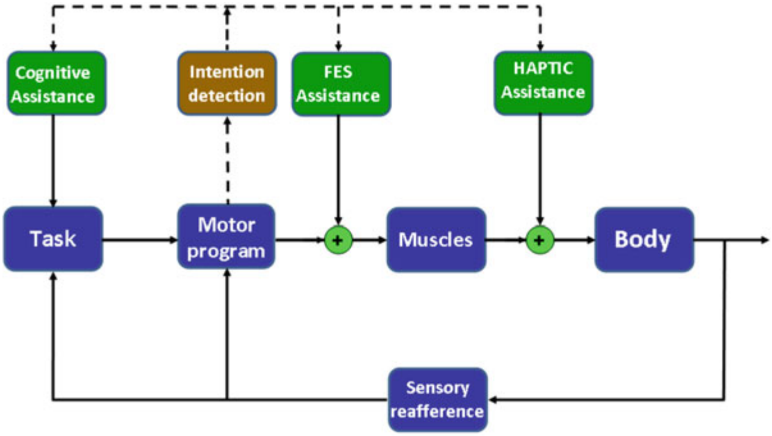

Fig. 11.6 Triggering channels of assistance with intention detection

different techniques, such as oscillatory or pulsed assistance patterns, as explained in following sections of the chapter. In general, it is safe to say that in the near future the different assistance channels will need to be integrated. Indeed, rehabilitation of individual with neuromotor disabilities is a complex process that requires a "division of labour", exploiting the pros of a method for compensating the cons of another. In particular, electrical assistance seems to be more appropriate for specific muscles or small muscle groups, whereas it is unfeasible for movements that involve multiple degrees of freedom. In contrast, haptic assistance delivered by a robot or exoskeleton is more naturally suited for coordinated movements of proximal and distal movements of the arm, although it is ill-suited for more functional movements, typical of the activities of daily life, such as picking a bottle and filling a glass. This is where human assistance, by an experienced physiotherapist, is more appropriate. On the other hand, the degree of success of such "precious" and "expensive" human intervention is greatly enhanced if electrical/robot assistance training has allowed the patient to recover basic control functionalities, such as range of motion, speed, force that are the prerequisite for achieving functional movements.

11.4 Results and Case Studies

In the present chapter we will report some examples of using haptic devices designed and developed the Motor Learning and Robotic Rehabilitation Laboratory of the Istituto Italiano di Tecnologia. The first section will be dedicated to some applications for proximal arm (elbow and shoulder) and body machine interface with special emphasis to assistive control and visual feedback design. The second part of the case studies will be focused on rehabilitation of distal upper limb in particular the wrist.

11.4.1 Case Study 1: Pulsed Assistance

This study [81] aims at evaluating a new paradigm of minimal haptic assistance designed to aid stroke survivors in a reaching task. We proposed to combine a force field that is continuous in time with a pulsed component, which is characterized by sequences of a smooth impulse (0.2 s) followed by a refractory phase (0.3 s) having a repetition frequency of 2 Hz. For each subject we estimated the level of minimal assistive force that the robot has to provide to keep him/her stable in different positions of the workspace. This value corresponds to the maximum assistive force that the robot applied during the reaching task, in which the continuous component contributes for 50 % of the total amplitude while the remaining 50 % is the impulse peak amplitude. As a consequence, the assistance average value over an impulse period is much inferior (∼30 %) to the minimal assistance estimated value. This choice makes the task more challenging for the subjects and is aimed to avoid the phenomenon known as s*lacking*. Moreover, the inclusion of a transient component in the force feedback should enhance the mechanoreceptors phasic response and hence favor proprioceptive awareness.

The protocol was designed in order to promote the active execution of large outward movements. Five 'far' targets (T) were arranged at a distance of 26 cm from a starting position (S) for center-out movements. Three intermediate targets (I) were added for the return movements, at distance of 13 cm from S, as shown in Fig. 11.7 (left panel). The task consisted of reaching one target, chosen randomly in the set of points, with a threshold of 2 cm. Reaching sequences followed the scheme: S → T → I → S. After a reaching movement was completed, a 1 s delay was introduced before presenting a new target in the sequence. We tested two conditions, i.e. vision (V) and no-vision (NV). In both cases haptic feedback was provided and in vision condition a screen displayed the target and current hand position by means of colored circles. The protocol included two sessions on 2 separate days: a familiarization session and a test session that comprised two evaluation blocks and one training block. In the training block of trials the subjects had to complete a total of 6 target-sets (3 with vision, 3 without vision); each target-set consisted of 30 outward movements (S → T) and 60 inward movements (T → I and I → S), for a total of 90 movements. The evaluation blocks aimed at estimating the minimal assistance level.

Five stroke survivors (all females, age 45.6 ± 12.5) participated in this study. The inclusion criteria were: (1) diagnosis of a single, unilateral stroke verified by brain imaging; (2) sufficient cognitive and language abilities to understand and follow instructions; (3) chronic condition (at least 1 year after stroke); (4) stable clinical conditions for at least 1 month before being enrolled in this study. All subjects underwent clinical evaluations before starting the present study. The average Ashworth score was 1.6 ± 0.4 (range 0–4), the average Fugl-Meyer score was 30.4 ± 15.4 (range 0–66).

Subjects' trajectories throughout the training appeared to be fragmented in a series of sub-movements. Nonetheless, we observed a substantial performance

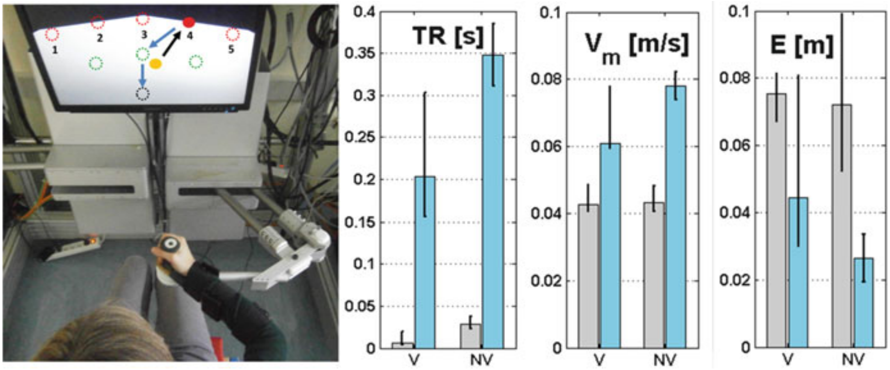

Fig. 11.7 *Left panel*: Pulsed assistance task. *Red circles* are the possible target locations, *green ones* are the intermediate targets and the *black circle* is the starting point. *Yellow filled circle* represents the current hand position while the *red filled one* the active target. *Right panel*: *Bar graphs* showing the median performance indicators values relative to the first (*grey*) and the last (*light blue*) trial

improvement throughout the training session in the NV condition: the *mean speed* (V_m) of movement increased (V: 0.011 ± 0.018 (0.044, −0.029) [m/s], NV: 0.029 ± 0.033 (0.131, −0.029) [m/s]) and there is accordingly an increment in duration of the first sub-movement compared to the total movement time *T-ratio* (TR, range [0,1]) in the NV condition (V: −0.163 ± 0.476 (0.310, −1) [s], NV: 0.332 ± 0.393 (0.965, −0.521) [s]). At the end of the training, subjects improved their precision in reaching the targets, especially in NV trials, thus the end-point error (E) decreased during the training (V: 0.006 ± 0.030 (0.082, −0.077) [m], NV −0.059 ± 0.069 (0.091, −0.205) [m]). Figure 11.7 (right panel) shows V_m, TR, E for one of the subjects. These results highlighted that the minimal level of assistance required was consistently reduced at the end of the session (1.27 ± 1.58 (0.04, −3.45) [N]) for most of the subjects.

11.4.2 *Case Study 2: Integrating Proprioceptive Assessment with Proprioceptive Training*

Multisensory integration of the information from muscle spindles, Golgi tendon organs, joint and cutaneous receptors of the arms allows the human brain to be aware of the relative position of the two hands as well as their positions in the peripersonal space, in the absence of visual feedback. This integration capacity is crucial for conceiving and carrying out purposive actions in everyday life, but is frequently impaired in stroke patients [82]. This is a strong obstacle for the recovery of sensorimotor functions. Clinical observations suggest that intact position sense following stroke strongly correlates with motor recovery of the paretic arm and is predictive of long term motor recovery [83]. Until now, the capacity to discriminate the relevant features of the deficits is limited.

A recent work by Dukelow et al. used the KINARM device [84], by fitting each arm of the subjects in one of two exoskeletons: one arm was passively placed in one of nine positions, in one half of the workspace, and the subject was told to actively mirror-match the other arm in the contralateral hemi space. This procedure provides a quantitative assessment of the *limb position sense* in the joint configuration space.

We propose an alternative method [85], based on a bimanual manipulandum [86]. The subject is asked to actively match the hand position of the paretic arm with the healthy arm, using a set of 17 test points, balanced in the two halves of the workspace. In other words, matching is performed in the extrinsic peri-personal space and is assessed the *hand position sense*. Since *proprioceptive assessment* should always be integrated with *proprioceptive training*, in order to provide adaptive assistance, we propose also a robot treatment mechanism that uses the same set of 17 target points, balanced in the peripersonal workspace, with the difference that in this case the non-paretic hand (passively placed by the robot in 1 of the 17 test points) is the target of the paretic hand and the motion of the arm is robot-assisted by a smooth force field.

Summing up, during *proprioceptive assessment* the position of the paretic hand is the target of the un-assisted healthy arm, whereas during *proprioceptive training* the position of the healthy hand is the target of the robot-assisted paretic arm. When the target is reached, in either modality, the brain of the user is informed that efferent and afferent signals are matched and we believe that this is likely to be a powerful reinforcement mechanism for the recovery of sensorimotor functions. The two interactive modalities of proprioceptive assessment and training were implemented and preliminary tests were carried out with a single, severely impaired patient (female, 28 years old, FMA, arm section = 12/66; WOLF Motor Function Test = 20/85; Modified Ashworth Scale: 2/4) and three controls.

Figure 11.8 shows the relevant results about the assessment procedure of the hand position sense, for the two groups of subjects. The graphs on the left part refer to the patient and the graphs on the right part refer to one of the controls.

Figure 11.8a shows, in the background (light gray), the test points, arranged as a polar lattice, where robot keeps the tested hand (paretic hand for the patient and non-dominant hand for the controls) as targets for the other hand. On top of this graph there is the lattice of matched positions, i.e. the positions achieved by second robot at the end of the matching movement. The two polar lattices are well matched in the control subject, as expected, which means that his position sense is accurate and the corresponding representation of the peripersonal space is isotropic. On the contrary, the space representation of the patient is strongly shrieked, with a strong deficit in the forward direction.

The middle pair of graphs (Fig. 11.8b) shows complementary metric information: the average positional error for each test point. In the control subject the error is quite small and rather uniform, suggesting that his space representation is well matched to the proprioceptive stimuli, both in topological and metric terms. In the patient the

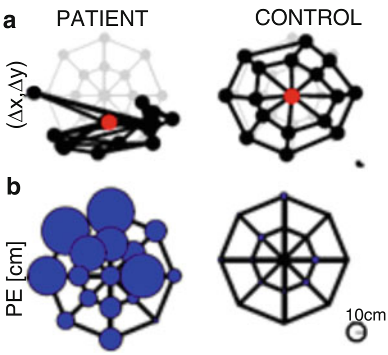

Fig. 11.8 Assessment of the hand position sense. (**a**) Polar lattice of the test points (*gray dots*) and of the matched points (*black dots*), with the corresponding barycenter (*red dot*); Δx, Δy refer to the shift of the barycenter of the lattice with respect to the nominal center. (**b**) Average positional errors (PE) over the lattice of test-points, represented by means of circles with a radius proportional to the error. "PATIENT" corresponds to the single tested subject; "CONTROL" corresponds to one of the healthy subjects (Intersubject variability is rather small, for the controls, compared with the patient)

Table 11.1 Indicators of proprioceptive training

	Parameters	Patient
1	Time to target, *TT* [s]	7.19 ± 0.14
2	Matching positional error, *PE* [cm]	3.78 ± 0.22
3	Magnitude of the assistive force, *AF* [N]	2.98 ± 0.18
4	Magnitude of the holding force, *HF* [N]	6.08 ± 0.23

most deficient part is the left forward part, where *PE* is much greater than in the other areas of the workspace.

All together, the graphs of Fig. 11.8 show in qualitative terms the massive impairment of the space representation of the patient, induced by the defective hand position sense, in topologic and metric terms, in comparison with the control subject.

Table 11.1 shows quantitative evaluation of the *proprioceptive training*: the average amount of time required to reach the target (*TT*); the average magnitude of the positional error (*PE*) at the end of the assisted motion, the average magnitude of forces that were involved in the training phase (AF); then the holding force (*HF*) needed to maintain the paretic arm on the matching position for 1 s.

This new technique is well accepted even by a severely impaired patient and the fatigue associated with the attentional load is not excessive. More in general there are open questions about the role of the hand position sense that need to be addressed in order to design optimal robot training: how important is monitoring the hand position sense before and during treatment? Which levels of accuracy of the hand position sense should be reached in order to achieve given levels of motor function?

11.4.3 Case Study 3: Cerebral Palsy

It is known that healthy adults can quickly adapt to a novel dynamic environment, generated by a robotic manipulandum as a structured disturbing force field. The brain injury resulting in cerebral palsy (CP) occurs early in neurodevelopment or birth accident, whereas stroke occurs generally in adult life. There are many scientific results, which suggest that plasticity is greater in the developing brain than in the mature one [87, 88]. Despite evidences that are observable in adults, the ability of CP subjects to deal with the central planning issues associated with control of arm is still an open question. The recovery mechanisms in children are quite different from adults [89], due to their higher plasticity and because the limbs control ability is age-related. The goals of the presented study [90] were twofold: (1) to ascertain if impaired children affected by CP preserve the ability to adapt to a force field; (2) to investigate which differences in kinematics between CP and Control groups lead to an unequal learning rate. We believe that these findings may suggest new therapies, as it has been demonstrated in healthy adult stroke survivors [56, 91, 92].

We adapted the protocol already used with adults, which employs a velocity dependent viscous field (Fig. 11.9a), and compared the performance of a group of subjects affected by congenital Cerebral Palsy (CP group, seven subjects) with a Control group of unimpaired age-matched children. The protocol included a familiarization phase (FA), during which no force was applied (80 randomized center out movements), a force field adaptation phase (CF) (160 center out movement), and a wash-out phase (WO) in which the field was removed (80 randomized center out movements). During the CF phase the field was shut down in a number of randomly selected “catch” trials (40 catch trials), which were used in order to evaluate the “learning index” for each single subject and the two groups. We also measured the *Learning Index* as described in the previous section “Measure of performance”. Lateral deviation, was evaluated for each trajectory during the three training phases and compared. Figure 11.9b shows the trajectories (form the center to the peripheral targets) during the entire experiment for two representative subjects form the CP and control group. For both subjects the effects to the force field are evident (CF phase, red trajectories), although the unimpaired subject learns to compensate the force in a more effective manner performing straighter trajectories. Catch trials in the CF phase (blue lines) reveal the presence of an anticipatory strategy and after effects in the WO phase indicates the compensation activity of the force field continues after the robot dynamics is removed.

If we consider the lateral deviation evaluated at the population level during the FA phase the movements of the CP subjects were more curved, displaying greater and variable lateral error (Fig. 11.9c); over the course of the CF phase both groups showed a decreasing trend in the pointing error and an after-effect at the beginning of the wash-out, but the CP group had a non significant adaptation rate suggesting that CP subjects have reduced ability to learn to compensate external robot generated dynamics. Moreover, a strong indication of the reduced adaptation of the CPs is

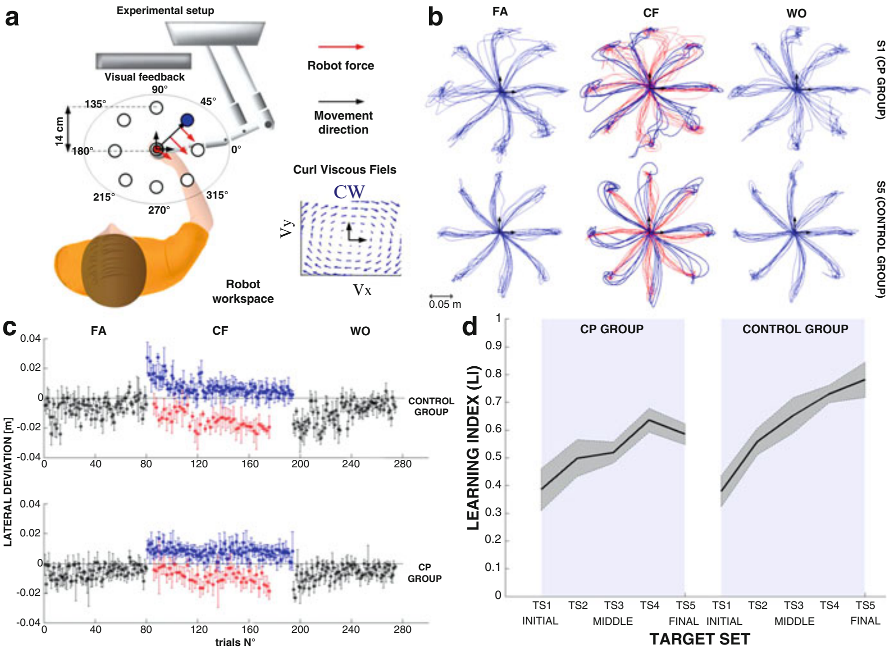

Fig. 11.9 (**a**) Experimental setup: The elliptical workspace of the robot is included in the reachable workspace of the subject. The shoulder of the subject is aligned with the center of the workspace of the robot. The subjects were pre-tested in order to check if they were able to reach all the targets presented during the experiment. A clockwise (CW) curl viscous field was used. (**b**) Trajectories during the different experimental phases for two representative subjects, from the CP **b**) and Control group. The *blue traces* correspond to movements with no disturbing field: all trials in the Familiarization phase (FA) and Wash-Out (WO) phase and catch trials in the Curl Viscous Field Adaptation phase (CF). The *red traces* correspond to movements affected by the disturbing force during the CF phase. (**c**) Trend of adaptation for the CP group (*bottom*) and control group (*top*) over the different target-sets; it refers to all the trials where *black dots* are average values of lateral deviation for all the subjects during familiarization and wash-out, while *blue* and *red* are referred to lateral deviation during force field adaptation and catch trials respectively. *Error bars* for each value refer to standard error over all subjects. (**d**) Learning index for CP and Control groups for five different target sets (TS). Each learning index value is computed as the average of eight catch trials, taking into account the corresponding directions, when the force field is active in the CF phase. *Solid lines* indicate mean value and *dashed lines* indicate standard error

clearly shown by the learning index (LI) depicted in Fig. 11.9d. The LI corrects for possible difference in performance due to differences in the action of the force field; if adaptation occurs, during force field the lateral deviation decreases while its value increases for the trajectories performed during catch trials due to the higher compensatory action by the CNS. Figure 11.9d shows that in the control group LI grows monotonically, in the initial learning, and this behavior is followed by an exponential trend, as expected for a short term adaptation experiment. In contrast, in the CP group LI is characterized by a lower increasing trend, with an early saturation, which implies a reduced learning capability. Spatial abnormalities in children affected by congenital cerebral palsy may be related not only to disturbance in motor control signals generating weakness and spasticity, but also to an inefficient control strategy which is not based on a robust knowledge of the dynamical features of their upper limb. This lack of information could be related to the congenital nature of the brain damage and may contribute to a better delineation of therapeutic intervention.

11.4.4 Case Study 4: Body Machine Interface

The idea of the Body-Machine Interface (BMI see [93–94] for a recent review) has been recently revisited with the specific goal of mapping the residual motor skills of the users into efficient patterns of control for external devices with assistive or/and rehabilitative purposes [95, 96]. The development of a BMI is based on the following key concepts:

- Collecting a broad spectrum of residual signals from the body (muscle or brain activities, movements, forces, etc.);
- Translating the body-derived signals onto BMI commands, encoding subjects' state, impairment and residual abilities and providing the impaired users with a continuous or discrete signal space operated directly by the combination of residual body abilities
- Adaptively changing the body-device map based on the user's residual abilities and preferences.
- Encoding information of the subject's state of motion and interaction with the environment into appropriate sensory feedback.

BMIs may promote two concurrent processes of learning: while – on one hand – the users practice controlling a device, the interface – on the other hand – modifies itself based on the user's status and performance. Because of its adaptive nature, a broad population of individuals with different types and degrees of disability can take advantage of the interface. A first attempt to build a BMI based on these concepts was reported in studies where healthy controls and spinal cord injured subjects used their upper body movements to engage in exercises that required different operational functions such as controlling a keyboard for playing a videogame, driving a simulated wheelchair in a virtual reality (VR) environment, and piloting a cursor on a screen for reaching targets [94]. The signals from the body were collected non-invasively by using infrared cameras that recorded the movements of small wireless infrared markers (Fig. 11.10). During an initial calibration procedure, subjects performed self-selected and self-paced upper body motions. The variance of these movements in the space of body motion signals was extracted by a standard statistical technique (Principal Component Analysis, PCA). Then, the two highest principal eigenvectors of the body signals were used to project the high dimensional signal space of the body movements in the two dimensional space of the cursor

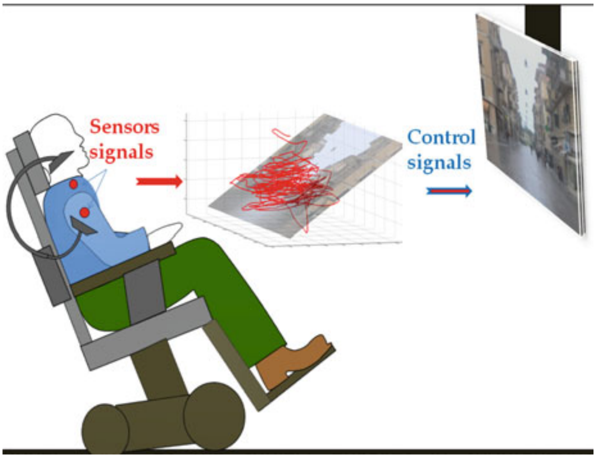

Fig. 11.10 Interface concept. The subject's movements are detected by infrared markers (*red dots*) placed on the upper body. As the subject engages in spontaneous movements, the sensor signals define a point moving in a high dimensional space (here represented as 3D). The calibration procedure establishes a correspondence between the plane that captures the highest amount of signal variance with the plane of the display, where the sensor signals are represented as a *moving cursor*

motion in the computer screen, thus establishing a linear correspondence from the subspace of maximal mobility to the space of control signals. Since there are multiple body configurations corresponding to each cursor position, subjects may choose a broad spectrum of body motions to perform different tasks. Unimpaired control subjects and SCI individuals exploited their movement redundancy and found repeatable and stable correlations of movement signals, established both by the presence of biomechanical constraints and by new learned patterns of coordination consistent with the representation of extra personal space, as already observed in previous studies focused on remapping of fingers movements [96, 97]. This first prototypes of BMI systems have been developed based on "assistive" goals, such as simplifying the control of electrically powered wheelchairs and the related learning process. Machine learning methods are investigated to remove the burden of learning from the impaired subjects to shift it instead toward the BMI. However these earlier studies highlighted also an important secondary outcome for the SCI subjects that were involved in a multisession training: an improvement on movement coordination, range of motion and forces generation by the upper body. This provides us with a proof of concept that the assistive goal can be combined with the rehabilitative goals. In this framework, the BMI has a far reaching potential. It targets residual movement capacity into a specific operational function, which makes this system capable of striking a natural balance between ease of device control and exercise of underutilized muscles to prevent atrophy and enhance the recovery process. Moreover it is also possible to create a transformation from body

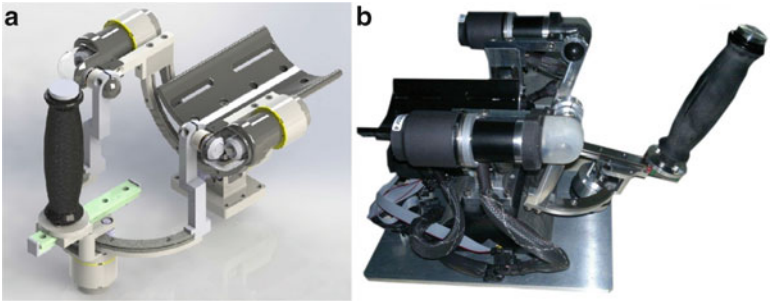

Fig. 11.11 Wrist robot. (**a**) CAD model and (**b**) physical device

motions to a “command” space that emphasizes degrees of freedom, which are more difficult to operate. This would likely facilitate strengthening a subject’s weaker muscle combination. It is now possible to aim at extending and enriching BMIs with rehabilitation capabilities by using their double potential and overcoming the separation between assistive and rehabilitative devices.

11.4.5 Case Study 5: Restoring Wrist Motor Function

In the present section we introduce the study on how to use a wrist exoskeleton [98, 99] to deliver rehabilitation to chronic stroke subjects (Fig. 11.11). The wrist robot is a three DOFs (Degrees Of Freedom) manipulandum which was developed for motor control study and rehabilitation: it allows full range of motion for the human wrist and is fully backdrivable, in order to allow the design of experiments in which a low end-point impedance is a key aspect. When a subject attempts to backdrive the robot, the interaction forces must be small enough to give the sensation as no device was connected.

The range of motion (ROM) of the three DOFs almost matches the ROM of a normal wrist: 65°/70° (F/E), 15°/30° (A/A), 90°/90° (P/S), in a typical human subject, vs. ±72° (F/E), 45°/27° (A/A), ± 80° (P/S), in the wrist robot. The robot is driven by four brushless motors which were chosen in such a way to compensate for the weight of the device, provide sufficient lifting force of the subject’s wrist (in case of rehabilitation) and overcome muscular force in case of isometric quasi maximal contraction. The maximum torque values are: 1.53 Nm (F/E); 1.63 Nm (A/A); 2.77 Nm (P/S). Angular rotations on the three axes are measured by means of digital encoders with a resolution of 4098 bit/turn. The system is integrated with a virtual reality environment (VR) in order to provide a visual feedback to the user. The control architecture is based on three control loops: (1) an inner loop, running at 7 kHz in the motor servos; (2) an intermediate loop running at 1 kHz on a real time kernel that updates the current reference of each motor; (3) an external loop running at 100 Hz for the visual virtual reality and user interface. The PC is equipped with an Analog and Digital I/O PCI card (Sensoray, model 626), in which we use the following channels: (a) Four 14 bit D/A channels for commanding the reference values of the motor currents; (b) Four 24-bit counters for receiving the repetition signals of the digital encoders.

11.4.6 Case Study 6: Chronic Stroke Wrist Rehab

Despite distal arm impairment after brain injury is an extremely disabling consequence of neurological damage, most studies on robotic therapy are mainly focused on recovery of proximal upper limb motor functions, routing the major efforts in rehabilitation to shoulder and elbow joints. In the present study we developed a novel therapeutic protocol aimed at restoring wrist functionality in chronic stroke patients by means of a haptic three DoFs (Degrees of Freedom) robot used to quantify motor impairment and assist wrist and forearm articular movements: flexion/extension (FE), abduction/adduction (AA), pronation/supination (PS). This preliminary study [100] involved nine stroke patients, from a mild to severe level of impairment. Therapy consisted in ten 1-h sessions over a period of 5 weeks: subjects were required to complete a tracking task starting from the neutral position of their wrist joint and trying to increase the amplitude of the oscillations over the course of each session. The novelty of the approach was the adaptive control scheme which trained wrist movements with slow oscillatory patterns of small amplitude and progressively increasing bias, in order maximize the recovery of the active range of motion: this approach was used for the three wrist joints separately and the range of motion was measured at the beginning (T0), at the end of the therapy (T1) and 3 months after the end of the robotic protocol (follow up at T2) (Fig. 11.12a). During a given block of trials, the harmonic motion of the target is described by the following equation:

$$\vartheta_T(t) = \vartheta_{\mathit{off}\_BN} + A \cdot \cos(2\pi\ t/T) \tag{11.6}$$

where $\vartheta_{\mathit{off}\_BN}$ is the angular offset used in the Nth Block (BN stands for Block Number), T is the oscillation period, and A is its amplitude; at each time instant, θ_T is compared with the angular position θ of the exercised DoF (Fig. 11.12b). We used slow oscillations of small amplitude of the targets, in order to increase progressively the achieved RoM: T = 4 s and A = 5 deg. During a trial, the target motion was broken into two ‘clipped’ semi-oscillations, while the robot provided an adaptive assistive torque: after one semi-oscillation the target was stopped if the tracking error (the absolute value of $\theta_T - \theta$) exceeded a threshold of 2 deg waiting for the subject’s assisted motion to re-enter the threshold above, with a deadline of 4 s. If the deadline was not met the trial were considered ‘unsuccessful’. Successful trials were rewarded with a pleasant acoustic signal, allowing subjects to online follow his/her progress. If the five trials of a block were successfully completed, the block counter *BN* was increased by one and the angular offset $\vartheta_{\mathit{off}\_BN}$ was increased by $\Delta\vartheta_{\mathit{off}} = A = 5deg$, thus initiating the next block (Fig. 11.12c).

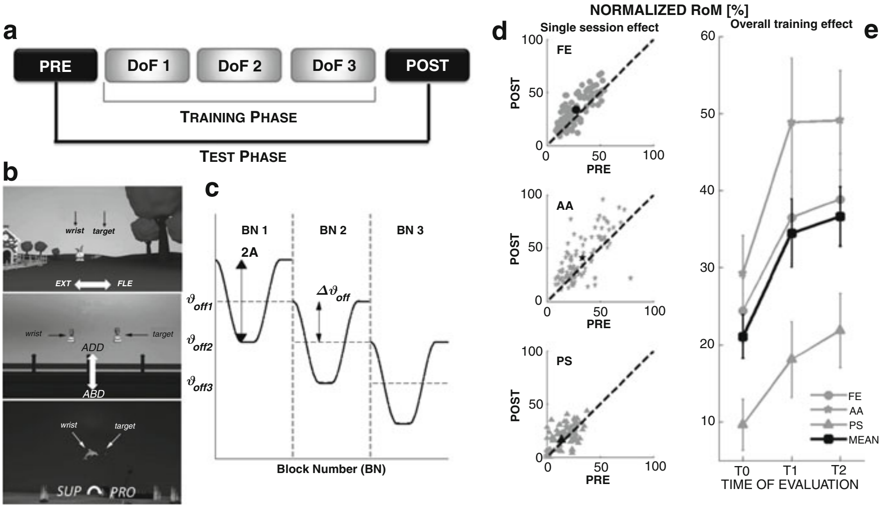

Fig. 11.12 (**a**) **Scheme of the training sessions.** Each session consists of two test modules (one at the beginning and one at the end of the session) and three training modules, in which one DoF is assisted by the robot and the other two inactive DoFs are constrained in the anatomical neutral position by means of mechanical holders. The order of training of the three DoFs is randomized. (**b**) **Visual rendering, specific for each DoF**. Against a DoF-specific background, subjects receive in real time the visual feedback on the motion of the target and the active DoF, respectively. (**c**) **Harmonic-clipped motion of the target**. The five oscillations of the first block occur around an angular offset (θ_{off1}), evaluated in the initial part of the test phase. The second block is activated if and when the first one is successfully terminated, with an offset angle which is shifted by an amount equal to the oscillation amplitude. During a given block, the five oscillations are 'clipped' in the sense that at the end of each semi-oscillation the target is stopped if the tracking error exceeds a threshold. There is a deadline for the subject to re-enter a window of tolerance: if it is not met, the current training module is aborted and the next one is initiated. (**d**) **Single session effect on the normalized RoM**. Normalization is carried out with respect to the entire range allowed by the device for each DoF: FE, AA, PS, respectively. *Symbols* in each graph represent the performance of a subject in a single session, PRE vs. POST, for a given DoF: each graph contains 90 points, that is 9 subjects × 10 sessions. A data point located above the equality line (*dashed*, with a slope of 45°) indicates that a subject had a higher RoM value in the POST than in the PRE test phase, meaning an increased RoM at the end of the single therapy session. The opposite would hold for a point below the equality line The *black markers* represent group means. (**e**) **Overall training effect on the normalized RoM**. Time series evolution of the population means (±SE) during the whole ten training and test procedure, for each DoF (*grey symbols*) and overall averaged performance (*black symbol*). **T0**: before training; **T1**: end of training; **T2**: at follow-up

We measured at the beginning and at the end of each therapeutic session and for the whole therapy, for each DoF, the RoM of the subjects by asking them to actively oscillate back and forth a given DoF in such a way to achieve the largest possible range; the robot encoders were used for the measurements, with no robotic assistance. The measures were normalized with respect to the entire RoM allowed by the device and we evaluated (1) the *single-session effect*, by comparing the estimated values before (PRE) and after (POST) training sessions (Fig. 11.12d), and (2) the *overall training effect*, by plotting the average population values against the three reference times T0, T1, T2 (Fig. 11.12e).

As regards the single-session effect, Fig. 11.12d, which plots PRE (initial) vs. POST (final) RoM values of all the subjects for each DoF, clearly shows that most of subjects' performance fell above the dashed equality line, i.e. POST > PRE: 67 out of 90 ROM measurements (74.4%) for the FE task, 65 out of 90 (72.2 %) for the AA task, and 59 out of 90 (65.5 %) for the PS task. This is also confirmed by the analysis of the normalized RoM population mean (depicted as black markers): 30.12 ± 1.17 % (POST) vs. 24.58 ± 0.97 % (PRE). A three-way ANOVA (10 SESSION $\times$ 3 DoF $\times$ 2 TIME) revealed significant differences between the three measures within a single session ($F(1,8) = 17.956$, $p = 0.00285$), with a short term benefit for each training. As regards the effect observed for over the course of the training, Fig. 11.12e shows the evolution of the normalized RoM estimates from the first session (T0), to the last session (T1) and then to the follow up test (T2). As observable the trend in improvement from the beginning of the end of the therapy is positive for the three DoFs and the follow up shows (FE, AA, PS) revealed significant differences among the three DoFs ($F(2,16) = 22.28$, $p = 0.00002$), where AA showed the highest value of restored RoM (42.36 ± 4.16 %), FE a lower percentage (33.26 ± 3.25 %) and the PS a quite limited improvement (16.53 ± 2.64 %) of the entire allowed joint's excursion. Moreover, also the TIME of EVALUATION factor was statistically significant ($F(2,16) = 15.80$, $p = 0.00016$) highlighting that the RoM increased between T0 and T1 (post-hoc analysis by Newman-Keuls; $p = 0.000522$) and improvements were present in the follow-up too (T0 vs. T2, $p = 0.000389$; T1 vs. T2, $p > 0.05$). The experimental results of this preliminary clinical study provide enough empirical evidence for introducing the novel progressive, adaptive, gentle robotic assistance of wrist movements in the clinical practice, consolidating the evaluation of its efficacy by means of a controlled clinical trial. Results were confirmed by clinical evaluation: FMA score reported a significant improvement (average of 9.33 ± 1.89 points), revealing a reduction of the upper extremity motor impairment over the sessions; moreover, a detailed component analysis of the score hinted at some degree of motor recovery transfer from the distal, trained parts of the arm to the proximal untrained parts. WOLF showed an improvement of 8.31 ± 2.77 points, highlighting an increase in functional capability for the whole arm. The active RoM displayed a remarkable improvement. Moreover, a 3-months follow up assessment reported long lasting benefits in both distal and proximal arm functionalities.

11.5 Final Remarks

Although Robotic Rehabilitation is a young discipline, the interest demonstrated by the international community is noticeable with an increasing number of publication and dedicated conferences. Several devices are right now evolved into commercial products and clinical applications report beneficial effects of such kind of technology. Despite all, a multidisciplinary approach to the problem of motor recovery and neurorehabilitation is far to come and research streams remains always oriented toward their respective disciplines. If on one side the interest of engineers in developing more efficient devices is boosting the diffusion of such kind of technologies, on the other side the deep comprehension of the mechanisms beyond neural plasticity and cortical reorganization after neurological illnesses still remains prerogative of the neurophysiologists. The main limitation lies in the role of the technology, which is mostly relegated to an ancillary part of the medical sciences. This limitation can be overcome by designing experimental paradigm based on the synergy between clinical and robotic results: the main example can be identified in the use of robotic set up and functional imaging (FMRI) to test the benefits of robotic before and after therapy. The introduction of extensive and large scale clinical trials is driven towards the main effort to provide clinicians with novel technology for rehabilitation and to develop a unified Robotic Evaluation Metric to qualify and quantify the different components of motor recovery in the patients treated by robot-aided techniques. Outcomes on patient's performance and related mechanisms during training are used not only to assess the rate of improvement over time, but also to develop predictive models of functional status at discharge.

References

1. Hogan N, Krebs HI, Sharon A, Charnnarong J (1995) Interactive robotic therapist. US Patent 5,466,213
2. Burgar CG, Lum PS, Shor PC, van der Loos HFM (2000) Development of robots for rehabilitation therapy: the Palo Alto VA/Stanford experience. J Rehabil Res Dev 37(6):663–673
3. Reinkensmeyer DJ, Takahashi CD, Timoszyk WK, Reinkensmeyer AN, Kahn LE (2000) Design of robot assistance for arm movement therapy following stroke. Adv Robot 14(7):625–637
4. Sukal TM, Ellis MD, Dewald JP (2007) Shoulder abduction-induced reductions in reaching work area following hemiparetic stroke: neuroscientific implications. Exp Brain Res 183:215–223
5. Loureiro R, Amirabdollahian F, Topping M, Driessen B, Harwin WS (2003) Upper limb robot mediated stroke therapy – Gentle/s approach. Auton Robot 15(1):35–51
6. Herder JL, Vrijlandt N, Antonides T, Cloosterman M, Mastenbroek PL (2006) Principle and design of a mobile arm support for people with muscular weakness. J Rehabil Res Dev 43(5):591–604
7. Sanchez RJ, Liu J, Rao S, Shah P, Smith R, Rahman T, Cramer SC, Bobrow JE, Reinkensmeyer DJ (2006) Automating arm movement training following severe stroke: functional exercises with quantitative feedback in a gravity-reduced environment. IEEE Trans Neural Syst Rehabil Eng 14(3):378–389
8. Nef T, Mihelj M, Riener R (2007) ARMin: a robot for patient-cooperative arm therapy. Med Biol Eng Comput 45(9):887–900
9. Stienen AHA, Hekman EEG, Helm FCT, Prange GB, Jannink MJA, Aalsma AMM, Kooij H (2007) Dampace: dynamic force-coordination trainer for the upper extremities. In: IEEE 10th International Conference on Rehabilitation Robotics, ICORR 2007, pp 820–826
10. Frisoli A, F Rocchi F, Marcheschi S, Dettori A, Salsedo F, Bergamasco M (2005) A new force-feedback arm exoskeleton for haptic interaction in virtual environments. In: Proceedings of 1st WHC'05, pp 195–201

11. Carignan C, Tang J, Roderick S (2009) Development of an exoskeleton haptic interface for virtual task training. In: Proceedings of IEEE/RSJ international conference on intelligent robots and systems, pp 3697–3702
12. Perry JC, Rosen J, Burns S (2007) Upper-limb powered exoskeleton design. IEEE ASME Trans Mech 12(4):408–417
13. Lawrence DA (1993) Stability and transparency in bilateral teleoperation. IEEE Trans Robot Automat 9(5):624–637
14. Colgate JE, Brown JM (1994) Factors affecting the Z-width of a haptic display. Proc IEEE Int Conf Robot Automat 4:3205–3210, 8–13 May 1994
15. Casadio M, Morasso PG, Sanguineti V, Arrichiello V (2006) Braccio di Ferro: a new haptic workstation for neuromotor rehabilitation. Technol Health Care 13:1–20
16. Gomi H, Kawato M (1997) Human arm stiffness and equilibrium-point trajectory during multi-joint movement. Biol Cybern 76(3):163–171
17. Howard IS, Ingram JN, Wolpert D (2009) A modular planar robotic manipulandum with end-point torque control. J Neurosci Methods 181(2):199–211
18. Van der Linde RQ, Lammertse P, Frederiksen E, Ruiter B (2002) The HapticMaster, a new high-performance haptic interface. In: Proceedings of the EuroHaptics 2002, Edimbourg, Ecosse, 8–10 July 2002, 5 pp
19. Lemon RN (2008) Descending pathways in motor control. Annu Rev Neurosci 31:195–218
20. Rosamond W, Flegal K, Furie K, Go A, Greenlund K, Haase N, Hailpern SM, Ho M, Howard V, Kissela B, Kittner S, Lloyd-Jones D, McDermott M, Meigs J, Moy C, Nichol G, O'Donnell C, Roger V, Sorlie P, Steinberger J, Thom T, Wilson M, Hong Y, AHA committees (2008) Heart disease and stroke statistics–2008 update: a report from the American Heart Association Statistics Committee and Stroke Statistics Subcommittee. Circulation 117(4):e25–e146
21. Harris JE, Eng JJ (2007) Paretic upper-limb strength best explains arm activity in people with stroke. Phys Ther 87(1):88–97
22. Pomeroy VM, Dean D, Sykes L, Faragher EB, Yates M, Tyrrell PJ, Moss S, Tallis RC (2000) The unreliability of clinical measures of muscle tone: implications for stroke therapy. Age Ageing 29(3):229–233
23. Powers RK, Marder-Meyer J, Rymer WZ (1990) Quantitative relations between hypertonia and stretch reflex threshold in spastic hemiparesis. Ann Neurol 23(2):115–124 (1998)
24. Lance JW (1990) What is spasticity? Lancet 335(8689):606
25. Dewald JP, Pope PS, Given JD, Buchanan TS, Rymer WZ (1995) Abnormal muscle coactivation patterns during isometric torque generation at the elbow and shoulder in hemiparetic subjects. Brain 118(2):495–510
26. Dewald JPA, Beer RF (2001) Abnormal joint torque patterns in the paretic upper limb of subjects with hemiparesis. Muscle Nerve 24(1):273–283
27. Hafer-Macko CE, Ryan AS, Ivey FM, Macko RF (2008) Skeletal muscle changes after hemiparetic stroke and potential beneficial effects of exercise intervention strategies. J Rehabil Res Dev 45(2):261–272
28. Mirbagheri MM, Rymer WZ (2008) Time-course of changes in arm impairment after stroke: variables predicting motor recovery over 12 months. Arch Phys Med Rehabil 89(8):1507–1513
29. Fugl-Meyer AR, Jaasko L, Leyman I, Olsson S, Steglind S (1975) The post-stroke hemiplegic patient. I. A method for evaluation of physical performance. Scand J Rehabil Med 7(1):13–31
30. Twitchell TE (1951) The restoration of motor function following hemiplegia in man. Brain 74(4):443–480
31. Kwakkel G, Kollen BJ, Krebs HI (2008) Effects of robot-assisted therapy on upper limb recovery after stroke: A systematic review. Neurorehabil Neural Repair 22(2):111–121
32. Mehrholz J, Wagner K, Meissner D, Grundmann K, Zange C, Koch R, Pohl M (2005) Reliability of the modified Tardieu scale and the modified Ashworth scale in adult patients with severe brain injury: a comparison study. Clin Rehabil 19(7):751–759

33. Colombo R, Pisano F, Micera S, Mazzone A, Delconte C, Carrozza MC, Dario P, Minuco G (2008) Assessing mechanisms of recovery during robot-aided neurorehabilitation of the upper limb. Neurorehabil Neural Repair 22(1):50–63
34. Dipietro L, Krebs HI, Fasoli SE, Volpe BT, Hogan N (2009) Submovement changes characterize generalization of motor recovery after stroke. Cortex 45:318–324
35. Ellis MD, Sukal T, Demott T, Dewald JPA (2008) Augmenting clinical evaluation of hemiparetic arm movement with a laboratory-based quantitative measurement of kinematics as a function of limb loading. Neurorehabil Neural Repair 22(4):321–329
36. Patton JL, Phillips-Stoykov ME, Stojakovich M, Mussa-Ivaldi FA (2006) Evaluation of robotic training forces that either enhance or reduce error in chronic hemiparetic stroke survivors. Exp Brain Res 168:368–383
37. Flanagan JR, Lolley S (2001) The inertial anisotropy of the arm is accurately predicted during movement planning. J Neurosci 21:1361–1369
38. Rohrer B, Fasoli S, Krebs HI, Hughes R, Volpe B, Frontera WR et al (2002) Movement smoothness changes during stroke recovery. J Neurosci 22(18):8297–8304
39. Rohrer B, Fasoli S, Krebs HI, Volpe B, Frontera WR, Stein J et al (2004) Submovements grow larger, fewer, and more blended during stroke recovery. Motor Control 8(4):472–483
40. Rohrer B, Hogan N (2003) Avoiding spurious submovement decompositions: a globally optimal algorithm. Biol Cybern 89(3):190–199
41. Rohrer B, Hogan N (2006) Avoiding spurious submovement decompositions II: a scattershot algorithm. Biol Cybern 94:409–414
42. Malfait N, Shiller DM, Ostry DJ (2002) Transfer of motor learning across arm configurations. J Neurosci 22:9656–9660
43. Mattar AA, Ostry DJ (2007) Modifiability of generalization in dynamics learning. J Neurophysiol 98:3321–3329
44. Hwang EJ, Donchin O, Smith MA, Shadmehr R (2003) A gain-field encoding of limb position and velocity in the internal model of arm dynamics. PLoS Biol 1(2):E25
45. Mussa-Ivaldi FA, Hogan N, Bizzi E (1985) Neural, mechanical, and geometric factors subserving arm posture in humans. J Neurosci 5:2732–2743
46. Shadmehr R, Mussa-Ivaldi FA, Bizzi E (1993) Postural force fields of the human arm and their role in generating multijoint movements. J Neurosci 13:45–62
47. McIntyre J, Mussa-Ivaldi FA, Bizzi E (1996) The control of stable arm postures in the multijoint arm. Exp Brain Res 110:62–73
48. Gomi H, Kawato M (1997) Human arm stiffness and equilibrium point trajectory during multijoint movement. Biol Cybern 76:163–171
49. Tsuji T, Morasso P, Goto K, Ito K (1995) Human hand impedance characteristics during maintained posture in multi-joint arm movements. Biol Cybern 72:475–485
50. Lacquaniti F, Carrozzo M, Borghese NA (1993) Time-varying mechanical behavior of multijointed arm in man. J Neurophysiol 69:1443–1464
51. Dolan JM, Friedman MB, Nagurka ML (1990) A testbed for measurement of human arm impedance parameters. In: Proceedings of the IEEE conference on system engineering, pp 123–126
52. Dolan JM, Friedman MB, Nagurka ML (1993) Dynamic and loaded impedance components in the maintenance of human arm posture. IEEE Trans Syst Man Cybern 23:698–709
53. Burdet E, Osu R, Franklin DW, Milner TE, Kawato M (2000) A method for measuring hand stiffness during multi-joint arm movements. J Biomech 33:1705–1709
54. Piovesan D, Pierobon A et al (2012) Measuring multi-joint stiffness during single movements: numerical validation of a novel time-frequency approach. PLoS One 7(3):e33086
55. Piovesan D, Morasso P, Giannoni P, Casadio M (2013) Arm stiffness during assisted movement after stroke: the influence of visual feedback and training. In: IEEE transactions on neural systems and rehabilitation engineering, Zurich, Switzerland, 29th June, 1st July
56. Marchal-Crespo L, Reinkensmeyer DJ (2009) Review of control strategies for robotic movement training after neurologic injury. J Neuroeng Rehabil 6:20

57. Fregly BJ, Boninger ML, Reinkensmeyer DJ (2012) Personalized neuromusculoskeletal modeling to improve treatment of mobility impairments: a perspective from European research sites. J Neuroeng Rehabil 9:18
58. Colombo R, Pisano F, Micera S, Mazzone A, Delconte C, Carrozza MC, Dario P, Minuco G (2008) Assessing mechanisms of recovery during robot-aided neurorehabilitation of the upper limb. Neurorehabil Neural Repair 22:50–63
59. Colombo R, Sterpi I, Mazzone A, Delconte C, Minuco G, Pisano F (2010) Measuring changes of movement dynamics during robot-aided neurorehabilitation of stroke patients. IEEE Trans Neural Syst Rehabil Eng 18:85
60. Emken JL, Benitez R, Sideris A, Bobrow JE, Reinkensmeyer DJ (2007) Motor adaptation as a greedy optimization of error and effort. J Neurophysiol 97:3997–4006
61. Casadio M, Sanguineti V (2012) Learning, retention, and slacking: a model of the dynamics of recovery in robot therapy. IEEE Trans Neural Syst Rehabil Eng 20(3):286–296. doi:10.1109/TNSRE.2012.2190827
62. Vergaro E, Casadio M, Squeri V, Giannoni P, Morasso P, Sanguineti V (2010) Self-adaptive robot training of stroke survivors for continuous tracking movements. J Neuroeng Rehabil 7:13
63. Wolbrecht ET, Chan V, Reinkensmeyer DJ, Bobrow JE (2008) Optimizing compliant, model-based robotic assistance to promote neurorehabilitation. IEEE Trans Neural Syst Rehabil Eng 16:286–297
64. Squeri V, Sterpi I, Basteris A, Casadio M, Pisano F, Colombo R, Sanguineti V (2012) Robot therapy for severely impaired stroke survivors: toward a concurrent regulation of task difficulty and degree of assistance. In: 4th IEEE RAS/EMBS international conference on biomedical robotics and biomechatronics (BioRob2012), pp 1026–1031
65. Butz M, Van Ooyen A, Worgotter F (2009) A model for cortical rewiring following deafferentation and focal stroke. Front Comput Neurosci 3:10
66. Goodall S, Reggia JA, Chen Y, Ruppin E, Whitney C (1997) A computational model of acute focal cortical lesions. Stroke 28:101–109
67. Reinkensmeyer DJ, Iobbi MG, Kahn LE, Kamper DG, Takahashi CD (2003) Modeling reaching impairment after stroke using a population vector model of movement control that incorporates neural firing-rate variability. Neural Comput 15:2619–2642
68. Cheung VC, Turolla A, Agostini M, Silvoni S, Bennis C, Kasi P, Paganoni S, Bonato P, Bizzi E (2012) Muscle synergy patterns as physiological markers of motor cortical damage. Proc Natl Acad Sci U S A 109:14652–14656
69. Han CE, Arbib MA, Schweighofer N (2008) Stroke rehabilitation reaches a threshold. PLoS Comput Biol 4:e1000133
70. Reinkensmeyer DJ, Guigon E, Maier MA (2012) A computational model of use-dependent motor recovery following a stroke: optimizing corticospinal activations via reinforcement learning can explain residual capacity and other strength recovery dynamics. Neural Netw 29–30:9
71. Takiyama K, Okada M (2012) Recovery in stroke rehabilitation through the rotation of preferred directions induced by bimanual movements: a computational study. PLoS One 7:e37594
72. Krebs HI, Hogan N (2012) Robotic therapy: the tipping point. Am J Phys Med Rehabil 91(11, suppl 3):S290–S297
73. Mehrholz J, Hädrich A, Platz T, Kugler J, Pohl M (2012) Electromechanical and robot-assisted arm training for improving generic activities of daily living, arm function, and arm muscle strength after stroke. Cochrane Database Syst Rev 6:CD006876
74. Morasso P (2012) Towards an integrated approach to multimodal assistance of stroke patients based on the promotion of intentionality. In: Pons JL, Torricelli D, Pajaro M (eds) Converging clinical and engineering research on neurorehabilitation, Biosystems & biorobotics. Springer, Berlin/Heidelberg, pp 23–27

75. Osu R, Otaka Y, Ushiba J, Sakata S, Yamaguchi T, Fujiwara T, Kondo K, Liu M (2012) A pilot study of contralateral homonymous muscle activity simulated electrical stimulation in chronic hemiplegia. Brain Inj 26:1105–1112
76. Casadio M, Pressman A, Acosta S, Danzinger Z, Fishbach A, Mussa-Ivaldi FA, Muir K, Tseng H, Chen D (2011) Body machine interface: remapping motor skills after spinal cord injury. In: Proceedings of the 12th IEEE international conference on rehabilitation robotics, Zurich, Switzerland, 29th June, 1st July
77. Takahashi M, Takeda K, Otaka Y, Osu R, Hanakawa T, Gouko M, Ito K (2012) Event related desynchronization-modulated functional electrical stimulation system for stroke rehabilitation: a feasibility study. J Neuroeng Rehabil 9:56
78. de Kroon JR, Jzerman MJI (2008) Electrical stimulation of the upper extremity in stroke: cyclic versus EMG-triggered stimulation. Clinical Rehabil 22:690–697
79. Meilink A, Hemmen B, Seelen H, Kwakkel G (2008) Impact of EMG-triggered neuromuscular stimulation of the wrist and finger extensors of the paretic hand after stroke: a systematic review of the literature. Clin Rehabil 22:291–305
80. van der Wel RPRD, Knoblich G, Sebanz N (2011) Let the force be with us: Dyads exploit haptic coupling for coordination. J Exp Psychol Hum Percept Perform 37(5):1420–1431
81. De Santis D, Masia L, Morasso P, Squeri V, Zenzeri J, Casadio M, Giannoni P, Riva A (2013) Pulsed assistance: a new paradigm of robot training. In: Proceedings of the 13th IEEE international conference on rehabilitation robotics, Zurich, Switzerland, 29th June, 1st July
82. Smith DL, Akhtar AJ, Garraway WM (1983) Proprioception and spatial neglect after stroke. Age Ageing 12:63–69
83. de Weerdt W, Lincoln NB, Harrison MA (1987) Prediction of arm and hand function recovery in stroke patients. Int J Rehabil Res 10:110–112
84. Dukelow SP, Herter TM, Moore KD, Demers MJ, Glasgow JI, Bagg SD, Norman KE, Scott SH (2010) Quantitative assessment of limb position sense following stroke. Neurorehabil Neural Repair 24:178–187
85. Squeri V, Zenzeri J, Morasso P, Basteris A (2011) Integrating proprioceptive assessment with proprioceptive training of stroke patients. In: IEEE International Conference on Rehabilitation Robotics (ICORR), Zurich, Switzerland, 29th June, 1st July, pp 1–6
86. Casadio M, Sanguineti V, Squeri V, Masia L, Morasso P (2010) Inter-limb interference during bimanual adaptation to dynamic environments. Exp Brain Res 202(3):693–707
87. Berlucchi G, Buchtel HA (2009) Neuronal plasticity: historical roots and evolution of meaning. Exp Brain Res 192:307–319
88. Rosenkranz K, Kacar A, Rothwell JC (2007) Differential modulation of motor cortical plasticity and excitability in early and late phases of human motor learning. J Neurosci 27:12058–12066
89. Farmer SF, Harrison LM, Ingram DA, Stephens JA (1991) Plasticity of central motor pathways in children with hemiplegic cerebral palsy. Neurology 41:1505
90. Masia L, Frascarelli F, Morasso P, Di Rosa G, Petrarca M, Castelli E, Cappa P (2011) Reduced short term adaptation to robot generated dynamic environment in children affected by congenital hemiparesis. J Neuroeng Rehabil (JNER) 8:28
91. Aisen ML, Krebs HI, Hogan N, McDowell F, Volpe BT (1997) The effect of robot-assisted therapy and rehabilitative training on motor recovery following stroke. Arch Neurol 54:443–446
92. Casadio M, Giannoni P, Morasso P, Sanguineti V (2009) A proof of concept study for the integration of robot therapy with physiotherapy in the treatment of stroke patient. Clin Rehabil 23:217–228
93. Casadio M, Ranganathan R, Mussa-Ivaldi FA (2012) The body-machine interface: a new perspective on an old theme. J Mot Behav 44:419–433
94. Casadio M, Pressman A et al (2011) Body machine interface: remapping motor skills after spinal cord injury. In: Proceedings of the 12th IEEE international conference on rehabilitation robotics, Zurich, Switzerland, 29th June, 1st July

95. Casadio M, Pressman A et al (2010) Functional reorganization of upper-body movement after spinal cord injury. Exp Brain Res 207:233–247
96. Liu X, Mosier KM et al (2011) Reorganization of finger coordination patterns during adaptation to rotation and scaling of a newly learned sensorimotor transformation. J Neurophysiol 105:454–473
97. Mosier KM, Sceidt RA et al (2005) Remapping hand movements in a novel geometrical environment. J Neurophysiol 94:4362–4372
98. Masia L, Casadio M, Sandini G, Morasso P (2009) Eye-hand coordination during dynamic visuomotor rotations. PLoS One 4(9):e7004
99. Masia L, Squeri V, Burdet E, Sandini G, Morasso P (2012) Wrist coordination in a kinematically redundant stabilization task. IEEE Trans Haptics 5(3):231–239
100. Squeri V, Masia L, Giannoni P, Sandini G, Morasso P (2014) Wrist rehabilitation in chronic stroke patients by means of adaptive, progressive robot-aided therapy. In: IEEE transactions on neural systems and rehabilitation engineering, vol 22, pp 312–325

Chapter 12
Robotic Assistance for Cerebellar Reaching

David I. Grow, Amy J. Bastian, and Allison M. Okamura

Abstract Robotic instruments allow precise measurements and interventions to understand and treat human motor deficits. These same tools may be used to design model-based and patient-specific robotic assistance and rehabilitation paradigms. This approach could lead to an increased understanding of the brain and improved patient outcomes. We illustrate this paradigm with two studies in which generic and patient-specific models are used to provide reaching assistance with a robotic exoskeleton, the KINARM. These studies involve patients with cerebellar ataxia who make reaching movements that are irregularly curved, over- or undershoot targets, and are more variable than those of healthy people. Two assistive methods are explored. In the first, a patient-specific change in arm dynamics predicted to assist each patient is utilized. The results suggest this approach may improve the reaching of some cerebellar patients and not for others. The second method employs force channels, which improved reaching movements for all patients. However, neither method showed evidence of motor learning; i.e. there was no maintenance of improved movement after the assistive forces were removed.

Keywords Robotic assistance • Rehabilitation • Cerebellar ataxia

D.I. Grow (✉)
New Mexico Tech, 801 Leroy Pl., Socorro, NM 87801 USA
e-mail: dgrow@nmt.edu

A.J. Bastian
Kennedy Krieger Institute, Baltimore, MD, USA

Johns Hopkins University, Baltimore, MD, USA
e-mail: bastian@kennedykrieger.org

A.M. Okamura
Stanford University, Stanford CA, USA
e-mail: aokamura@stanford.edu

P. Artemiadis (ed.), *Neuro-Robotics: From Brain Machine Interfaces to Rehabilitation Robotics*, Trends in Augmentation of Human Performance 2,
DOI 10.1007/978-94-017-8932-5_12,

12.1 Introduction

Damage to the cerebellum results in ataxia, or a lack or coordination of volitional movements [1, 3, 13, 28, 33]. Point-to-point movements are often composed of an initial movement that under or overshoots the target (dysmetria), followed by a series of erroneous attempts at correction (intention tremor) [5]. In addition, cerebellar patients have difficulty adapting to changes in environment dynamics [8, 10, 19, 20, 24, 31]. People with ataxia almost always have normal strength. Cerebellar ataxia is difficult to treat; there are no medications that reliably reduce ataxia, making physical therapy and exercise the primary intervention. There is a need to understand the mechanisms of ataxia more completely to drive the development of rational physical therapy-based rehabilitation strategies. In this chapter, we present two methods for robotic assistance of cerebellar reaching (dynamic augmentation and force channels), and report their impact on the reaches of cerebellar patients, both during and after assistance.

12.1.1 Rehabilitation Robotics

The field of rehabilitation robotics involves the use of automatically controlled mechanisms to provide therapy and assistance to humans with disabilities [35]. As an alternative to human-only therapy, these devices permit: (1) consistent therapy without tiring; (2) precise measurements of behavior to quantify motor deficits and recovery; and (3) implementation of therapy paradigms not possible by a human therapist [20,30,31,35]. A wide variety of rehabilitation robots have been developed. One way to categorize these devices is by the way in which they physically connect to the user. One class are manipulandums – robots for upper-extremity therapy that connect to the user through a handle. An example of such a device that has been used extensively for clinical applications is the InMotion Arm Robot (originally called the MIT Manus). This device has undergone 20 years of development and has been used in research studies involving patients with stroke, cerebral palsy, and other neurological conditions [2, 12, 17].

Another class of rehabilitation robotic devices are exoskeletons, which couple to the user through multiple contact areas. An example of this type of device is the Lokomat by Hocoma, which is a lower-body exoskeleton and treadmill for gait therapy [36]. This device measures the user's gait and automatically augments the user's stride to provide individualized training.

Ideally, a rehabilitation robot would be able to provide many different forms of mechanical input, such as assisting, resisting, perturbing, and stretching, based on the subject's real-time response.

12.1.2 Robot-Assisted Rehabilitation Approaches

A robotic device can be programmed to apply forces that assist or resist the movements of the user. Assistive devices have been developed to extend the strength and dexterity of injured or diseased users as they walk, grasp objects, and perform other activities of daily living. Resistive devices, on the other hand, are used to retrain patients or minimize the undesired consequences of unintended motor activity.

Some common assisting methods include (1) passive motion, in which the robot moves the subject through a desired pattern, (2) active assistance, in which a subject-initiated movement is subsequently guided by the robot, (3) active constraint, or force channel, which allows subject motion only towards a target, and (4) mirror image, in which the less impaired arm motion is measured and used to guide motion of the more impaired arm [18].

Resistance to motion is achieved by a control law that increases forces opposing the subject's desired motion with speed and/or proximity to the target, such as a linear damping field [32]. Related to resistance training, feedback distortion can also be used in isometric and isotonic conditions to alter a subject's perception of therapeutic exercises [7]. Other work has exploited the after-effect of training forces (i.e. adaptation) that magnify original errors [11, 25]. With the capability to record motions and forces automatically, robotic systems can provide objective data to quantify how specific deficits change during training [35], as well as identify the mechanism of the deficit [20, 31].

12.1.3 Robot-Assisted Study of Neurological Impairments

Robots have also been used to study neurological impairments. Scheidt and Stoeckmann used a robot joystick to show that cerebral stroke subjects could use normal strategies based on error history to adapt movement, though not as efficiently as controls [27]. Patton et al. found that error-enhancing robot therapy improves reaching in stroke subjects more than control strategies that assist movement [25]. In contrast, subjects with cerebellar ataxia have been shown to be slowed or unable to adapt arm movements to novel forces, suggesting a deficient internal model of limb dynamics [20]. Interestingly, cerebellar subjects could correct on-line errors using feedback mechanisms, but could not adapt feedforward control mechanisms from trial to trial [31]. Subjects with Huntington's disease showed the reverse pattern, demonstrating that control mechanisms have distinct neural bases. Robotic devices can also be used to estimate human arm dynamics, as in [23].

12.2 Methods

The feasibility of uncovering cerebellar function and discovering a model of ataxia is bolstered by the availability of high-fidelity robotic exoskeletons. The field of robotics provides powerful tools for understanding the function of the cerebellum and other brain areas because it allows us to quantify and affect mechanical features of movement in a way not possible by direct human observation and manipulation. Here, we describe the robotic exoskeleton used in our experiments, our patient population, and two experiments (dynamic augmentation and force channels) that provide assistance to enhance cerebellar reaching.

12.2.1 KINARM Robot Motor and Controller Performance Characterization

In order to rigorously examine hypotheses about the function of the cerebellum, we require knowledge of actual limb dynamics and precise measurements of user reaching performance. Our studies used the KINARM robotic exoskeleton (Fig. 12.1, BKIN Technologies, Kingston, ON). The KINARM is an adjustable exoskeleton that permits bimanual shoulder and elbow rotation in the horizontal plane. This device has been used to acquire behavioral data during reaching [29]. In [15], a kinematic and dynamic model of the human arm and robot were developed and populated with parameter values obtained through direct measurement, system identification, and use of anthropometric tables. This provides a relationship between motor effort and movement.

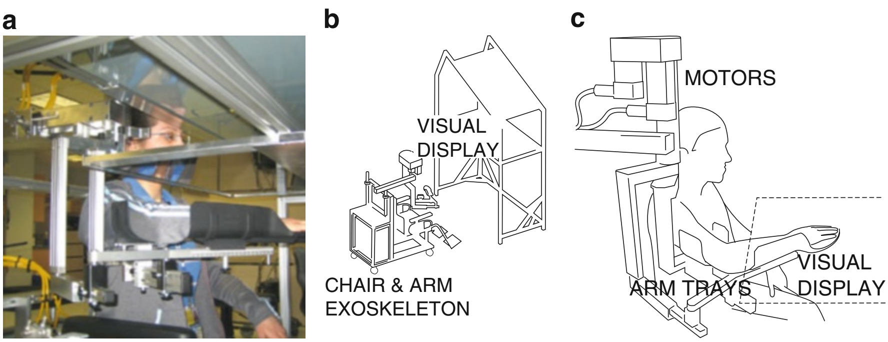

Fig. 12.1 The KINARM robot (**a**) used in this study has a two-degree-of-freedom planar exoskeleton for each arm (only right arm shown for clarity). The user sits in a chair (**b**) that is positioned so that the user's hand location and targets are visible on a horizontal display. The seat height, linkage lengths, and arm tray positions are adjusted for each user (**c**). Special care is taken to ensure that the rotational axes of the human shoulder and elbow are coincident with the corresponding joints of the KINARM. An advantage of the exoskeletal nature of the robot is that robot linkage and human arm kinematic parameters are determined simultaneously

The motors of the KINARM are controlled in an open-loop fashion. In order to understand the limits of the system's performance, we characterized the ability of motor controllers to follow a desired torque trajectory. Accurate calibration of motor gains is critical for accurate rendering of dynamic forces. For example, consider attempting to render arm inertia (mass matrix with non-negative scalars a, b, and c) while the shoulder and elbow motors have the non-unity gains ζ_1 and ζ_2. This torque scaling results in a corresponding scaling of the mass matrix:

$$\begin{bmatrix} \tau_{1_{act}} \\ \tau_{2_{act}} \end{bmatrix} = \begin{bmatrix} \zeta_1 a & \zeta_1 b \\ \zeta_2 b & \zeta_2 c \end{bmatrix} \begin{bmatrix} \ddot{\theta}_1 \\ \ddot{\theta}_2 \end{bmatrix}. \tag{12.1}$$

If $\zeta_1 \neq \zeta_2$, then the mass matrix is no longer symmetric – in essence, it no longer corresponds to any physically realistic inertia. In such a case, there would be no symmetry between the interaction torques of connected joints. A one-dimensional analog is a mass that feels heavier when moved forward than when moved backward.

12.2.1.1 Static Performance

To calibrate the static motor gains, the peak motor torque for each link was measured using a single-axis, hand-held digital force gauge (SHIMPO model FGV-50XY, Japan). The sensor was mounted tangentially to the robot link and coupled via a fitting that could not transmit substantial torque to the linkage. Thus, the reaction torque is the measured force multiplied by the moment arm. The torque trajectory was repeated four times at five different amplitudes for each motor.

12.2.1.2 Single-Joint Dynamic Performance

Next, the motor controller's performance while commanding velocity- or acceleration-dependent loads (viscosity/inertia) was characterized. The velocity, $\dot{\theta}$, and acceleration, $\ddot{\theta}$, signals are derived from a high-resolution encoder signal that is discretely differentiated. The process of differentiation scales the high-frequency (noise) content of a signal. To mitigate this effect, a running-average digital filter was used. This window must be larger to filter the acceleration signal compared to velocity.

The actual output torques were measured using an ATI Mini40 force/torque sensor (ATI Industrial Automation, Inc., Apex, NC; SI-20-1 calibration) mounted as before while the robot forearm was manipulated manually to follow a roughly sinusoidal position trajectory. The accuracy of the rendering was assessed by comparing the torques and kinematics using ordinary-least-squares regression [16]. If the desired coefficients for friction and inertia are f_b and I, the appropriate torque command τ_{com} is given by (12.2). Even when rendering only inertial or viscous forces, the robot's inherent inertia and friction contribute to the force/acceleration relationship. As such, objective function (12.3) was used in all cases.

$$\tau_{com} = f_b\dot{\theta} + I\ddot{\theta} \tag{12.2}$$

$$\begin{bmatrix} \tau(t_1) \\ \tau(t_2) \\ \tau(t_3) \\ \vdots \end{bmatrix} = \begin{bmatrix} \theta(t_1) & \dot{\theta}(t_1) \\ \theta(t_2) & \dot{\theta}(t_2) \\ \theta(t_3) & \dot{\theta}(t_3) \\ \vdots & \vdots \end{bmatrix} \begin{bmatrix} f_b \\ I \end{bmatrix} \tag{12.3}$$

12.2.1.3 Multi-joint Dynamic Performance

In the first experiment, the KINARM is used to render the change in arm inertia predicted to help each patient. With active use of the robot, the mass matrix is composed of:

$$M_\theta = M_{human\ arm} + M_{robot\ linkage} + M_{rendered}. \tag{12.4}$$

Excessive noise or delay of the acceleration signal may result in poor rendering or instability. To reduce the noise and delay of the acceleration signal, two 2g 3-axis accelerometers (Crossbow Technology, Inc., San Jose, CA) were incorporated into each arm. Though substantially reduced, the residual noise presents an increasing challenge to system performance as the magnitude of the rendered inertia increases. Predicting whether some amount of rendered inertia will be achievable is a formidable problem because it depends on the robot setup and the patient's size, muscle tone, movement pattern, etc. As such, the rendered inertia must be gradually increased ($\epsilon \rightarrow 1$ in (12.5)) while the onset of noise or instability is monitored. It can be shown that any value of $0 < \epsilon < 1$ results in a qualitatively similar change to the total inertia ellipse – the eigenvectors, which determine the ellipse orientation, remain unchanged.

$$M_{rendered} = \epsilon \begin{bmatrix} \Delta a & \Delta b \\ \Delta b & \Delta c \end{bmatrix} \tag{12.5}$$

12.2.2 Human Subjects

Patients with damage to the cerebellum but no signs of sensory loss or extracerebellar damage were recruited. The severity of each patient's cerebellar impairment was determined using the International Cooperative Ataxia Rating Scale (ICARS) [34]. Table 12.1 lists cerebellar subjects ordered by the ICARS kinetic functions subscore, which assesses voluntary limb movements. Scores range from 0 (normal)

Table 12.1 Subject characteristics

Subject	Sex	Dominant hand	Age (years)	Height (m)	Weight (kg)	Diagnosis[a]	Limb score
Cerebellar 1	M	R	75	1.63	77	Stroke	13/52
Cerebellar 2	F	R	52	1.58	51	Stroke	15/52
Cerebellar 3	F	R	20	1.68	64	Trauma	18/52
Cerebellar 4	F	R	65	1.68	61	Sporadic	18/52
Cerebellar 5	M	L	37	1.78	123	SCA8	20/52
Cerebellar 6	M	R	56	1.80	90	SCA6,8	23/52
Cerebellar 7	M	L	57	1.70	96	ADCA	25/52
Cerebellar 8	F	R	69	1.70	68	Sporadic	23/52

[a]Spinocerebellar ataxia (SCA) diagnoses are described in [4]

to 52 (severe). Subject diagnosis is based on medical history, family history, and a neurological examination. The cause of ataxia may be abrupt damage to cerebellar tissue (stroke or trauma), genetic diseases (ADCA, SCA6, and SCA8), or unknown (sporadic) [4]. All subjects gave informed consent to the protocols approved by the Johns Hopkins Medical Institutions Review Board.

12.2.3 Methods of Robot Assistance

The anisotropic nature of arm inertia and other dynamic effects necessitate a non-trivial calculation of the muscle activity needed to reach rapidly in a given direction. It has been hypothesized that the cerebellum plays a key role in planning such movements and that damage to the cerebellum results in a degradation of the ability of the motor control system to plan these movements, accounting for the characteristic misdirection of observed arm movements [5, 6, 21, 22, 26]. The first assistive method explores this possibility in the attempt to derive an optimal, patient-specific assistance method. The second method applies a simple and generic method for assistance. As mentioned in Sect. 12.1, the cerebellum is thought to play a key role in accounting for (adapting to) changes in the dynamics. As such, subsequent to practicing with both of these assistive methods, additional null trials were incorporated into the experimental protocols to search for evidence of adaptation.

12.2.3.1 Assistance Method 1: Dynamics Augmentation

Phase 1: Identifying Optimal Augmentation

In [15], the KINARM robot was used to record the movements of cerebellar patients (Cerebellar 1–8, Table 12.1) performing a targeted reaching task. This task focused on early movement because the role of the cerebellum is most observable during early movement. Subjects made center-out movements through 1 cm diameter targets at a 3 cm radius within a 350–650 ms window. Offline analysis of this data and the arm dynamic model were used to test various hypotheses proposed in the literature about the role of the cerebellum, all of which assume that the cerebellum functions as an internal model of limb dynamics for planning movements. It follows that damage to the cerebellum results in movements that do not properly account for arm dynamics. If this error is known, the potential exists for predicting reaching errors during early movement (before movement feedback is available).

During early movement, arm dynamics can be approximated as (12.6) [14, 15]. The parameters a, b, c, and d are all non-negative scalars, the first three relating to mass properties and the last relating to centripetal and Coriolis forces.

$$\begin{bmatrix} \tau_1 \\ \tau_2 \end{bmatrix} = \begin{bmatrix} a & b \\ b & c \end{bmatrix} \begin{bmatrix} \ddot{\theta}_1 \\ \ddot{\theta}_2 \end{bmatrix} + \begin{bmatrix} 0 & -2d & -d \\ d & 0 & 0 \end{bmatrix} \begin{bmatrix} \dot{\theta}_1^2 \\ \dot{\theta}_1 \dot{\theta}_2 \\ \dot{\theta}_2^2 \end{bmatrix} \tag{12.6}$$

Knowledge of each patient's arm dynamics allows inverse dynamic calculations to identify torque trajectories to each target. Because of the movements start from rest and are rapid, the magnitude of the acceleration greatly exceeds that of the velocity for the movements recorded. As such, the trajectories are insensitive to variations in d and so the computer simulations searched for a perturbation over the reduced set, $\{a, b, c\}$, that when used in forward dynamic simulations with the torque trajectories, optimally reduced reaching errors. Perturbations of this type are equivalent to reshaping and reorienting the arm inertia ellipse [9]. Though no change to arm dynamics was found that fully removed errors, patient-specific perturbations were found that resulted in a reduction in root-mean-squared directional reaching errors of 41 % averaged over 7 cerebellar patients.

Phase 2: Applying Prescribed Augmentation

A subset of these patients were available to return to perform a follow-up experiment to apply the dynamic augmentations predicted to most improve reaches. The KINARM robot was controlled to effectively reshape and/or increase or decrease the arm inertia. Three particular subjects were selected because distinct optimal perturbations were predicted and their ataxia severities spanned those of the group. These perturbations are summarized in Table 12.2 (columns 2–5). It follows that the opposite perturbation (i.e. $\{\Delta a, \Delta b, \Delta c\}$ vs. $\{-\Delta a, -\Delta b, -\Delta c\}$) would significantly hinder reaching performance, which could be a resistive approach to neurorehabilitation (see Sect. 12.1.2).

The task in this phase was nearly identical except that the center-out movements were to, not through, targets at a 10 cm, not 3 cm, radius. The more distant spacing of these targets compared to those in the Phase 1 task was chosen to permit

Table 12.2 A perturbation predicted to help patients was applied during a reaching task. The predicted optimal change in arm inertia, characterized by ellipse eccentricity, size, and orientation, for each subject is summarized along with the extent to which reaching performance is predicted to improve. The effect of applying the opposite perturbation (e.g. to reduce mass rather than add) was also explored with the goal of resisting rather than assisting movement. The full perturbation could not always be applied for stability reasons. During practice trials, conservatively safe values of ϵ (12.5) for each patient and for both the perturbation expected to help and hinder performance were determined and are also listed, ϵ_{help} and ϵ_{hinder}, respectively

Subject	Δ eccentricity (%)	Δ size (%)	Δ orientation (deg)	Predicted error reduction (%)	ϵ_{help}	ϵ_{hinder}
Cerebellar 1	−34	−61	1	37.5	0.8	0.8
Cerebellar 5	−14	−47	5	62.5	1.0	0.75
Cerebellar 6	−39	−99	2	62.9	0.3	0.3

investigation of the method's effect on movement both before and after peripheral feedback can be used. Another subtle difference compared to the preliminary studies is that four, rather than eight, targets were used to obtain a greater number of reaches to each target.

At the beginning of each trial, the subject moved to a center position (shoulder at 35°, elbow at 90°). After a slight delay, one of four targets appeared randomly, to which subjects were directed to move within a 200–550 ms time window. Trials were divided into five blocks (Fig. 12.2). Movement duration feedback was given to the subjects in the form of color coding: the target turned blue if reached late, red if early, or green if on time. At the end of each trial, the actual hand path taken was shown to subjects. All trials were analyzed, whether or not the timing criteria were met.

To ensure that the robot would remain stable throughout the experiment, the magnitude of the inertia perturbation, ϵ, was gradually increased towards the desired magnitude while patients practiced the target reaching movements until the onset of instability was detected. This detection was done using digital scopes that report the joint accelerations and motor commands where the onset of instability was evident well before it was perceptible to the subject, resulting in a conservative limit. For the patients tested, the level of perturbation rendered varied from $\epsilon = 30$–$100\,\%$ (12.5). Force levels and dynamic perturbations are given in Table 12.2, columns 6 and 7.

Reaching performance was measured using lateral deviation Δ_{err} of the finger at 150 ms (12.7), where the finger location and target vectors are **p** and **t**, respectively (Fig. 12.3). It is computed as:

$$\Delta_{err} = \left\| \mathbf{p}(150) - \frac{\mathbf{p}(150) \cdot \mathbf{t}}{\|\mathbf{t}\|^2} \mathbf{t} \right\|. \qquad (12.7)$$

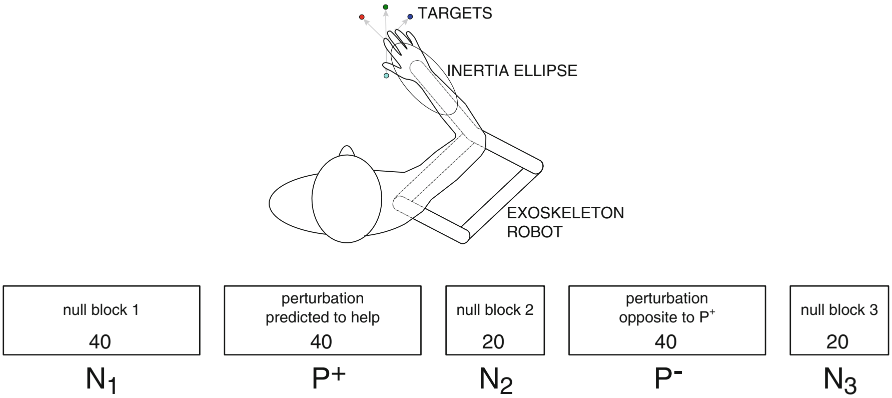

Fig. 12.2 Horizontal reaching task with augmented arm inertia. During the null blocks $\{N_1, N_2, N_3\}$, the robot is passive as the patient moves to one of four targets, the blocks containing 40, 20, and 20 trials, respectively. During the first perturbation block P^+, the robot augments arm inertia in a manner predicted to help as the subject makes a total of 40 reaches to 4 targets. The second perturbation block P^- is identical except the robot augments arm inertia with the opposite sign

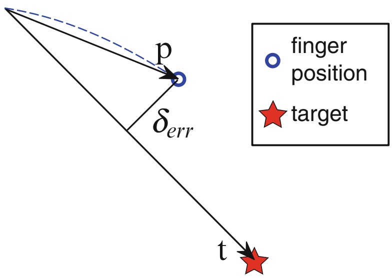

Fig. 12.3 Depiction of error metric: lateral deviation of the finger position from the target path (12.7)

12.2.3.2 Assistance Method 2: Force Channel Rendering

This potential reaching assistance method applies force channels designed to improve reaching performance by enforcing the coordination needed to follow a straight path. Furthermore, these channels are used in an attempt to elicit use-dependent learning, or improvements in both the straightness of the path (lateral error) and the ability to stop at the target (overshoot error) subsequent to channel reaching.

Six cerebellar patients performed this experiment (Cerebellar 2 and 4–8 in Table 12.1). Because it has been reported that use-dependent learning is stronger when the non-dominant arm is trained, that arm was tested whenever possible. The one exception was the case of Cerebellar 6, whose non-dominant arm had a reduced range of motion. Also, Cerebellar 5 was available to have both arms tested.

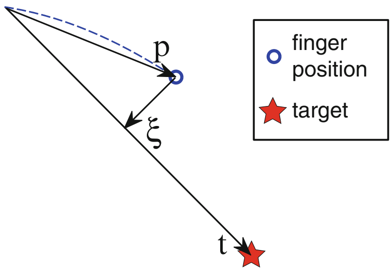

Fig. 12.4 The KINARM robot is used to render force channels that assist a user in moving in a straight direction to targets. The force generated is perpendicular to and scales linearly with deviation from the desired path (12.8)

Force channels were rendered by the KINARM to provide a simple form of assistance during reaching. These channels act as virtual walls to constrain movement by applying a forces perpendicular to the desired direction of movement. The forces are smooth and allow the subject to maintain complete control over the speed of movement. Figure 12.4 illustrates the relationship between finger position, target location, and the spring-like force generated. Given the positions of the finger, $\mathbf{p}$, and target, $\mathbf{t}$, the channel force with stiffness k_c in Cartesian space is given by:

$$\boldsymbol{\xi} = \frac{\mathbf{p} \cdot \mathbf{t}}{\|\mathbf{t}\|^2}\,\mathbf{t} - \mathbf{p}$$
$$\mathbf{f} = k_c\,\boldsymbol{\xi}. \tag{12.8}$$

As before, subjects were directed to make point-to-point movements. At the beginning of each trial, the subject moved to a center position (shoulder at 35°, elbow at 90°). After a slight delay, a target appeared in one of four radial targets, again 10 cm away and to be reached within a 200–550 ms window with as straight a movement as possible. Using the same color-coding as in the augmentation experiment and by showing a trace of the actual movement path after each reach, subjects were given feedback after each reach about timing and movement accuracy, respectively. Spatial feedback was given after each reach. All trials were analyzed, whether or not the timing criteria were met. Two experimental protocols were used to address questions about reaching direction, prolonged training, and generalization of learning. The organization of each protocol and the differences between them are given in Fig. 12.5.

Reaching performance during null and force-channel blocks was measured using four metrics:

M_1: Path length is computed by integrating changes in finger position over the duration of movement:

$$\text{path}_{err} = \sum_n \|\mathbf{p}(n) - \mathbf{p}(n-1)\|\,. \tag{12.9}$$

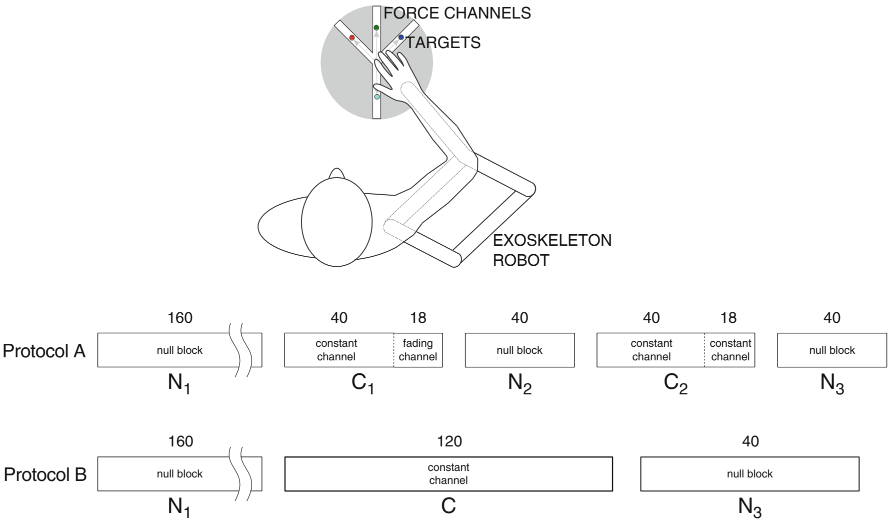

Fig. 12.5 Horizontal reaching task with force channels. One of four targets with 1 cm diameter appear in pseudo-random order at 10 cm from start position. In Protocol A there are seven blocks with $\{160, 58, 40, 58, 40\}$ trials each. Three null (robot passive) blocks $\{N_1, N_2, N_3\}$ are separated by force channel (robot active) blocks. During the first channel block C_1, the robot generates a force channel and the subject makes 40 reaches *only to the 12:00 target* followed by 18 more reaches while the channel is gradually removed. The second channel block C_2 is identical except that the force channel remains at full strength for 58 reaches. During these channel blocks assistance is only provided for the 12:00 direction. By looking at other directions during null trial blocks, evidence of learning generalization is sought. In Protocol B there are three blocks with $\{160, 120, 80\}$ trials each. Two null blocks are separated by a channel block where force channels are rendered to *each* of the four targets. Another difference from Protocol A is the extended length of the training blocks to investigate whether learning would arise from prolonged training

M_2: Maximum lateral deviation throughout the trial is computed by:

$$\Delta_{err} = \arg\max_{n} \left\| \mathbf{p}(n) - \frac{\mathbf{p}(n) \cdot \mathbf{t}}{|\,\mathbf{t}\,|^2}\,\mathbf{t} \right\|. \tag{12.10}$$

M_3: Lateral deviation at 150 ms is computed as described previously (12.7).

M_4: Overshoot is computed by finding the finger position at the first velocity zero crossing, $\mathbf{p}(n_0)$, and computing the displacement of this point from the target (Fig. 12.6):

$$\eta_{err} = \left\| \mathbf{t} - \arg\max_{n \le n_0} \|\mathbf{p}(n)\| \right\|. \tag{12.11}$$

Differences in performance between null and channel trial blocks were checked for statistical significance using a Kruskal-Wallis non-parametric test. This test

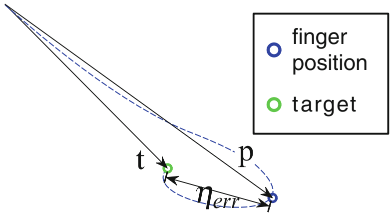

Fig. 12.6 Depiction of the overshoot error metric: the distance between the target and the point of maximum excursion (12.11). We only consider the portion of movement until the first zero-crossing

is well suited to these data because the variability of the error metrics tends to change significantly during channel trials, violating the sphericity assumption of the Analysis of Variance (ANOVA).

12.3 Results

12.3.1 Motor and Controller Performance Characterization

12.3.1.1 Static Performance

For each commanded torque amplitude and for each motor, four torque measurements were taken and averaged. Linear regression of this data yields a calibration coefficient for each motor (Fig. 12.7). Each slope is inverted to determine the appropriate gain to apply to the motor torque command (e.g. a slope of 0.95 prescribes a 1.05 gain). Fortunately, the motor gains are all within 10 % of unity. This degree of miscalibration does appear to vary in time, but can be accounted for by scaling commanded torques accordingly in software. The appropriate adjustments in motor gains were determined from the open-loop, near-static conditions shown in Fig. 12.7 by taking the inverse of the slopes.

12.3.1.2 Single-Joint Dynamic Performance

Even after calibration, the open-loop torque controller may not be linear under non-static conditions. From Fig. 12.8, it is clear that the open-loop performance is inaccurate if the frequency content exceeds 7 Hz.

In the case of a perfect sinusoidal position trajectory, the velocity and acceleration signals are scaled versions of the position with phase shifts of 90° and 180°, respectively. Because inertial forces are rendered by simply scaling the acceleration signal, the same delay persists. Thus, this delay makes rendered inertial forces behave increasingly like viscosity. The overall delay in the system is appreciable and in fact, when attempting to render inertia, a least-squares regression of the resulting forces are identifies increases in both inertia and damping. A smaller filter (and thus

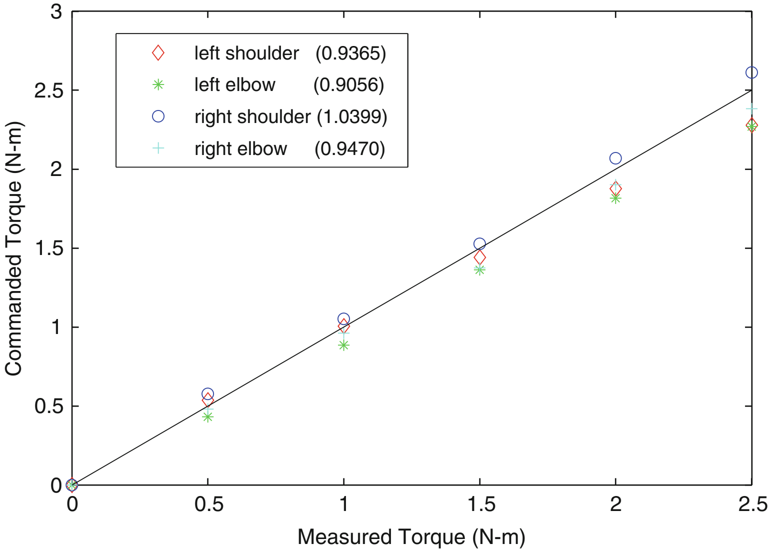

Fig. 12.7 Measured vs. commanded torque trajectories were recorded as sinusoidal torque trajectories were commanded to each of the four motors (From this data, calibration factors were determined)

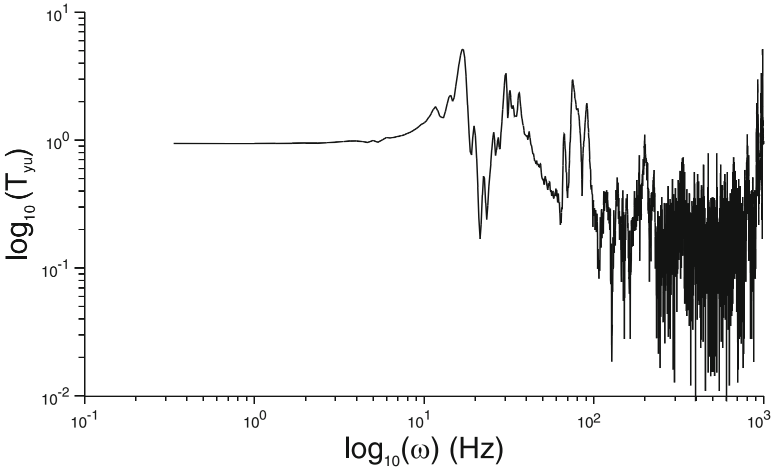

Fig. 12.8 The ratio of angular acceleration to commanded torque T_{yu} at the elbow joint is plotted as a function of angular frequency. Note the near unity gain for low frequencies and degraded (non-unity gain) at higher frequencies

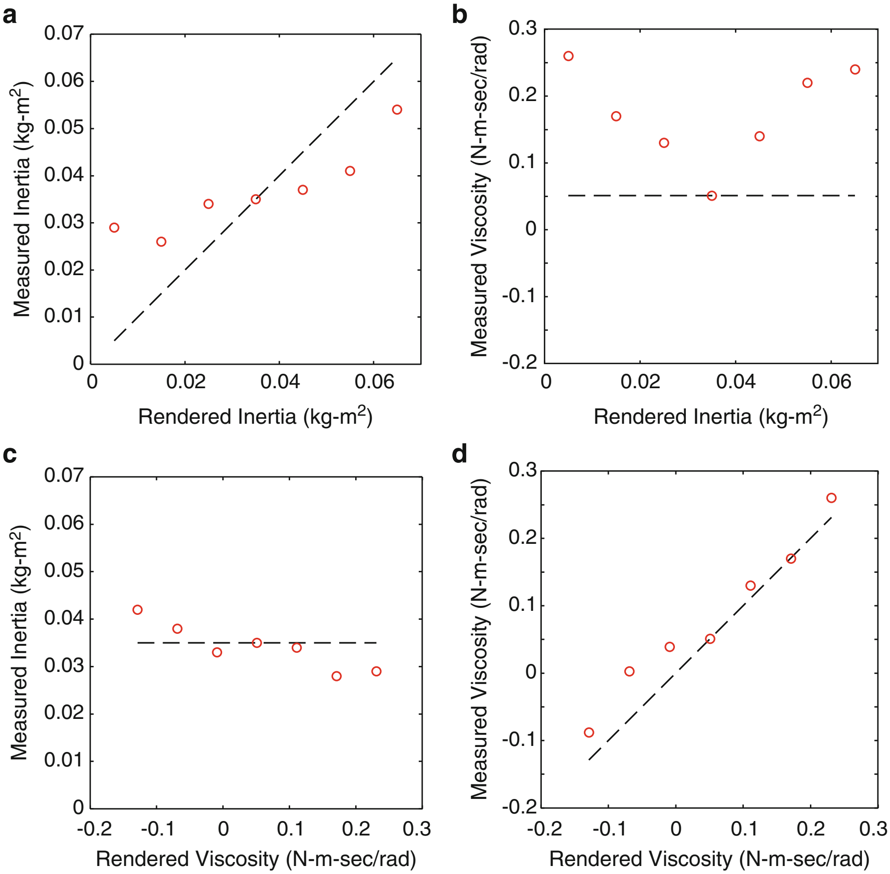

Fig. 12.9 The ability of the robot to render viscous and inertial torques is investigated. In (**a**), virtual inertia is added by the robot increasing and decreasing the base inertia in steps of 0.01 kg-m^2. In (**b**), an undesired effect on the forearm viscosity while rendering inertia is shown. In (**c**), an undesired effect on the forearm inertia while rendering viscosity is shown. In (**d**), virtual viscosity is added by the robot increasing and decreasing the base viscosity in steps of 0.03 N-m-s/rad

smaller delay) applied to the velocity signal results in forces that are identified as being nearly pure viscosity of the target magnitude, the identified inertia remaining relatively constant across rendered viscosity magnitudes (Fig. 12.9). In Fig. 12.10, the raw data used for regression are shown. The individual data points in each of the sub-figures are of no particular significance – they are specific to the manual perturbations applied. However, the covariance of the points is significant. If the dynamics consist of inertia only, an angular acceleration vs. torque point cloud will have a nonzero slope that corresponds to the inertia and the angular velocity vs. torque point cloud will have a zero slope. The opposite is true if the dynamics consist only of viscosity. If both inertia and viscosity are present, both clouds will have a

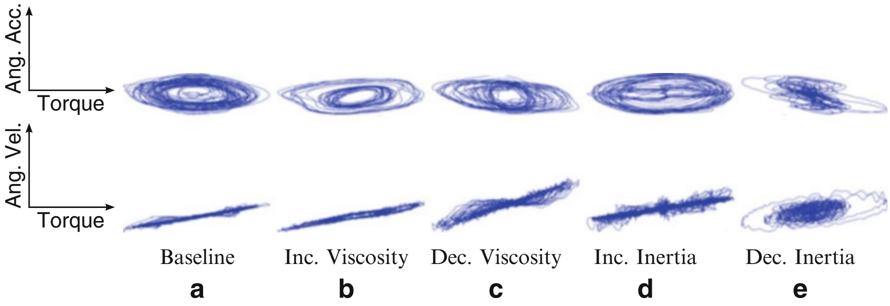

Fig. 12.10 The elbow joint of the robot is manipulated manually while various dynamic effects are rendered. The collected data are used for dynamic parameter identification. Representative data is shown to conceptually illustrate the process of regression: (**a**) baseline condition (robot passive), robot adds (**b**) or subtracts (**c**) viscosity, and robot adds (**d**) or subtracts (**e**) inertia

Table 12.3 Inertia values about shoulder and elbow joints at baseline and as measured during the rendering of reduced inertia compared to that desired change in inertia

	Joint	Baseline (kg-m^2)	Desired change (kg-m^2)	Measured change (kg-m^2)
Left	Shoulder	0.1313	−0.0500	−0.0377
	Elbow	0.0387	−0.0150	−0.0068
Right	Shoulder	0.1313	−0.0520	−0.0377
	Elbow	0.0387	−0.0142	−0.0068

nonzero slope. This procedure was duplicated with the other arm, and then at the shoulder of each arm. The results of rendering reduced inertia at each of the four joints are summarized in Table 12.3.

12.3.1.3 Multi-joint Dynamic Performance

As in the one-dimensional case, inertia rendering fidelity is affected by filter delay. The measured versus commanded torques while rendering various simple dynamic perturbations are shown in Fig. 12.11.

12.3.2 Assistance Method 1: Dynamics Augmentation Results

Data collected from the patients are included in several figures that follow. The hand paths and errors are shown for each of the five trial blocks. Because reach direction is the movement feature of interest, lateral deviations at 150 ms are shown both as block averages and for individual reaches. The individual data for Cerebellar 5, who has moderate ataxia, is shown in Fig. 12.12. It is evident that the patient benefited from the prescribed perturbation in effect (reduced lateral deviations). Similarly, the

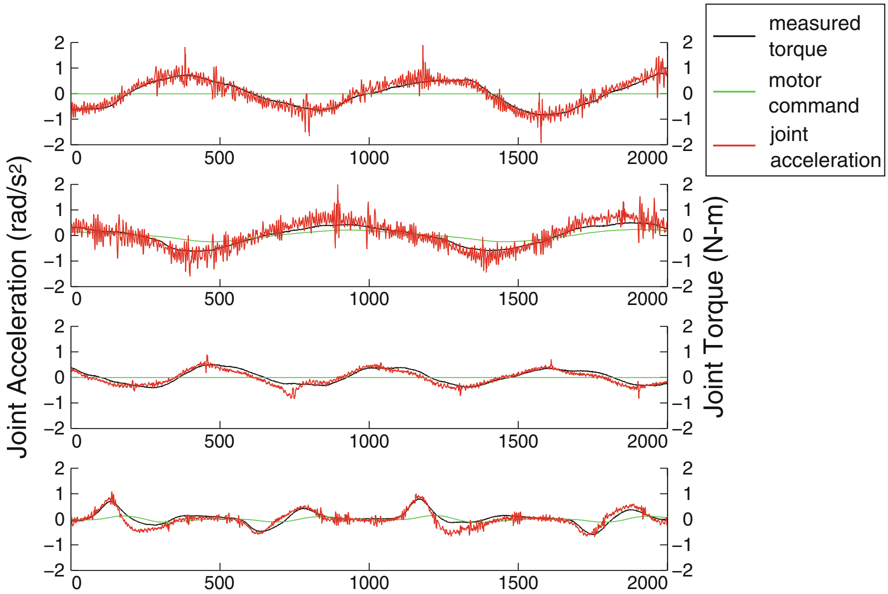

Fig. 12.11 Measured acceleration vs. commanded torque trajectories. During passive perturbations (row 1, shoulder and row 3, elbow), the acceleration and the torque measured via a force/torque sensor are linearly dependent. During active perturbations (row 2, shoulder and row 4, elbow), the motor command can be seen to lag the acceleration. This delay is more profound for rapid (row 4) movements

opposite perturbation resulted in degraded movement performance. The results for Cerebellar 1 (mild ataxia) and 6 (severe ataxia) are not as consistent across direction, but show a similar trend [15].

12.3.3 Assistance Method 2: Force Channel Results

The data were analyzed according to each of the four error metrics ($M_1 - M_4$) and differences in performance were checked for statistical significance. Representative recorded movements and performance measurements for subjects tested under Protocol A and Protocol B are included in Figs. 12.13 and 12.14, respectively. Summaries of the results including statistical test outcomes are given in Figs. 12.15 and 12.16.

During channel blocks, performance was significantly improved (Table 12.4). Error metrics M_2 and M_3 decreased in all four directions in both Protocols A and B. Significant improvement in overshoot error was observed in the 12:00 and 6:00 directions under Protocol A. We also found a significant improvement in path length for the 12:00 target under Protocol A (Table 12.4).

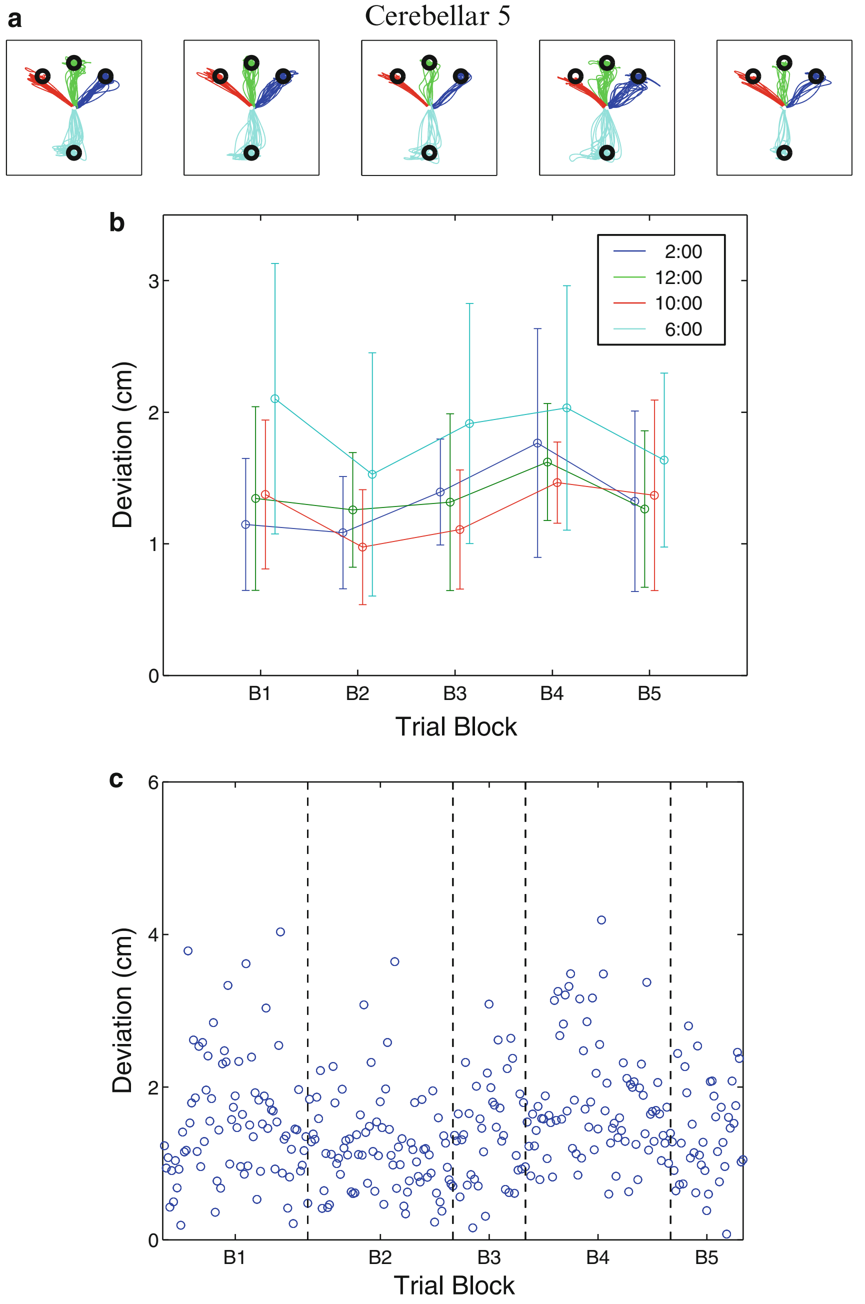

Fig. 12.12 Cerebellar Subject 5 makes targeted reaching movements to four targets while the robot provides Assistance Method 1. The task is divided into five blocks. The first, third, and fifth are null blocks where the robot is passive. During the second block, the robot affects arm dynamics in a manner predicted to help. During the fourth block, the opposite change in dynamics is made, which we expect to hinder performance. Hand paths and errors are color coded by direction

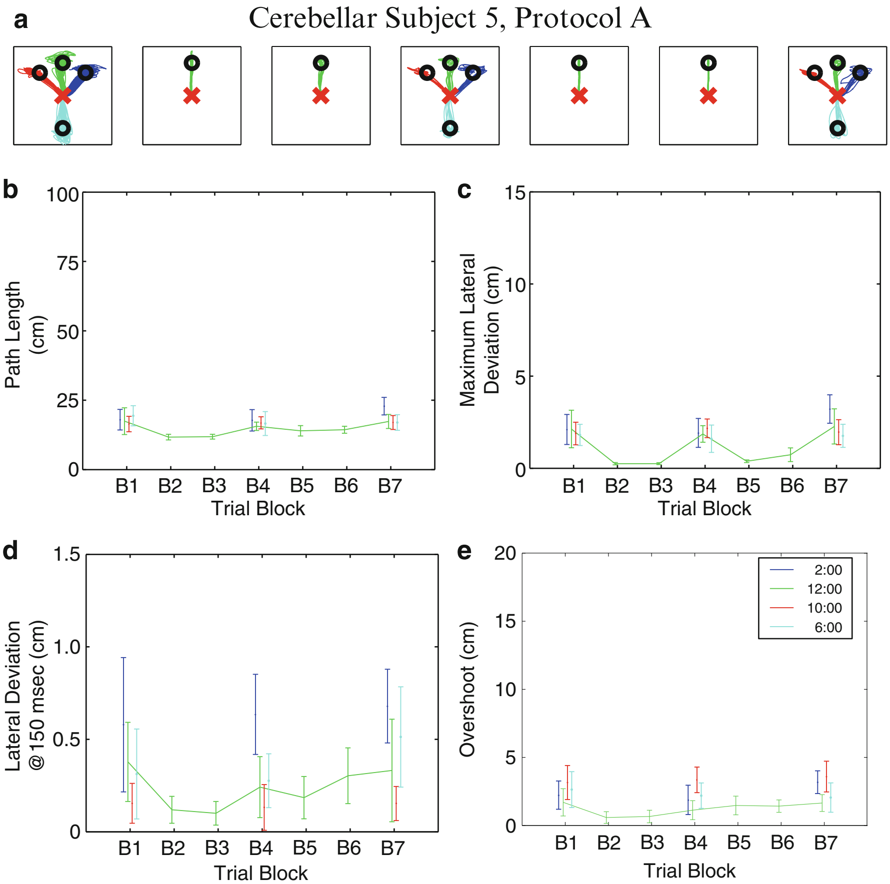

Fig. 12.13 Cerebellar Subject 5 makes targeted reaching movements to four targets while the robot provides assistance Method 2, Protocol A. The task is divided into seven blocks. The first, fourth, and seventh are null blocks where the robot is passive and subjects move to each of the four targets. During the second, fifth, and sixth blocks, the robot renders a force channel that assists the patient in moving in a straight path to the 12:00 target only. During the third block, the force channel begins at full strength and is reduced linearly to zero strength over the course of the block. Reaching performance is measured using the error metrics described in Sect. 12.2.3.2. Hand paths and errors are color coded by direction

Learning would be evidenced by residual improvements in performance after the removal of force channels. However, whether the force channel was removed gradually (Protocol A, $B_3 \rightarrow B_4$) or abruptly (Protocol A, $B_6 \rightarrow B_7$ or Protocol B, $B_2 \rightarrow B_3$) no learning was identified (Table 12.5).

We also looked for generalization by comparing performance in the non-trained directions (2:00, 10:00, and 6:00) after a block of channel trials. We found no evidence of generalization according to any of the error metrics (Table 12.6).

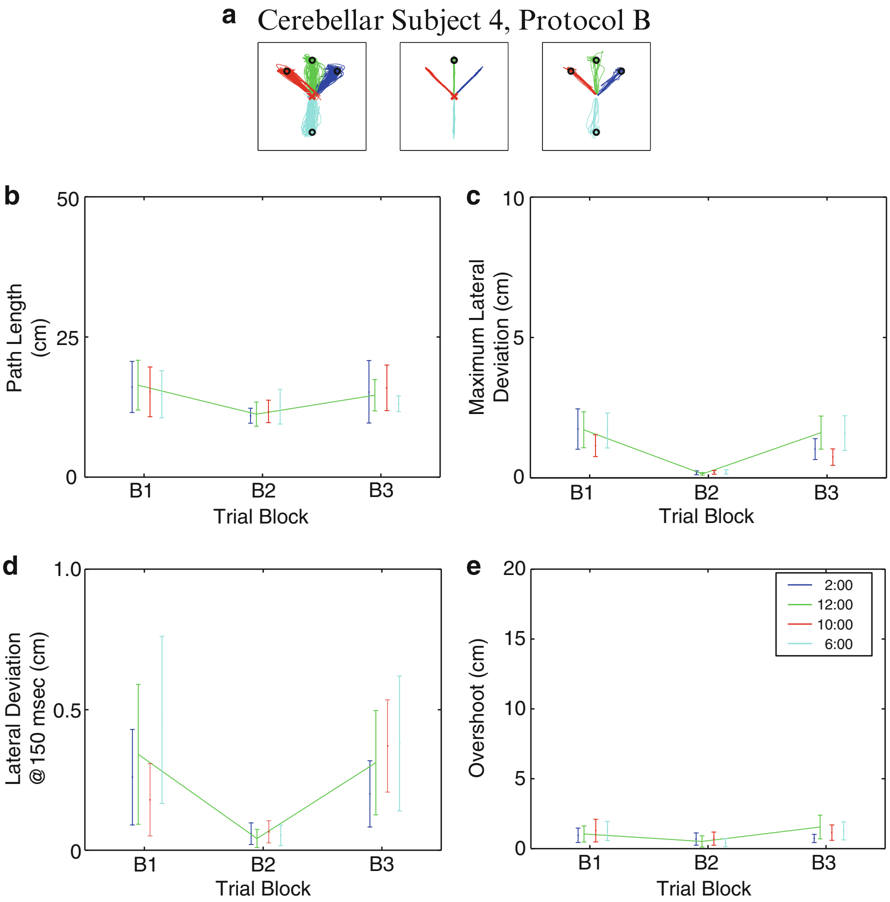

Fig. 12.14 Cerebellar Subject 4 makes targeted reaching movements to four targets while the robot provides assistance Method 2, Protocol B. The task is divided into three blocks. The first and third are null blocks where the robot is passive. During the second block, the robot renders a force channel that assists the patient in moving in a straight path to the target. Reaching performance is measured using the error metrics described in Sect. 12.2.3.2. Hand paths and errors are color coded by direction

12.4 Discussion

12.4.1 Motor and Controller Performance Characterization

The fidelity of dynamic forces rendered by the KINARM was characterized in detail. For this particular robot, the ability to render inertia was somewhat limited, although the performance is linear up to approximately 7 Hz. Performance was

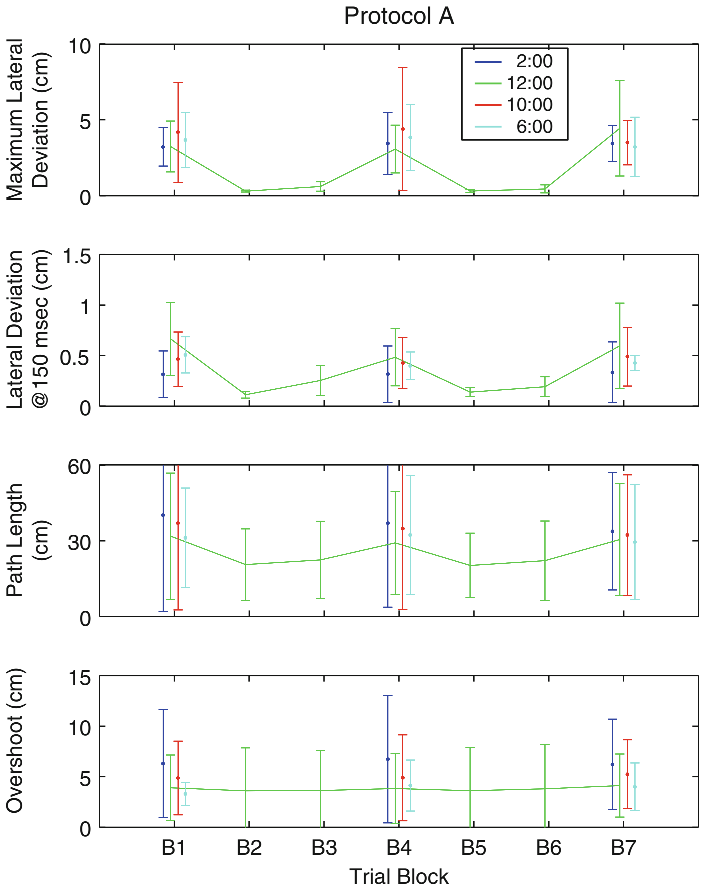

Fig. 12.15 Summary of force channel results under assistance Method 2, Protocol A. Three patient data sets are averaged. Four metrics are used to measure performance – maximum lateral deviation from the straight path (first row), lateral deviation at 150 ms from the straight path (second row), path length (third row), and overshoot (fourth row). The only direction in which statistically significant changes in performance were observed is the 12:00 direction. Hand paths and errors are color coded by direction

increased with the addition of accelerometers and tuned digital filters. We designed controllers and instrumentation, and validated the ability of the robot to render desired acceleration-dependent forces. The quality of the dynamic forces rendered was sufficient, and, when necessary, the magnitude of dynamics perturbations were reduced in scale to ensure patient safety and controller stability. Robot friction parameters were identified, but were found to contribute insignificantly to the overall dynamics.

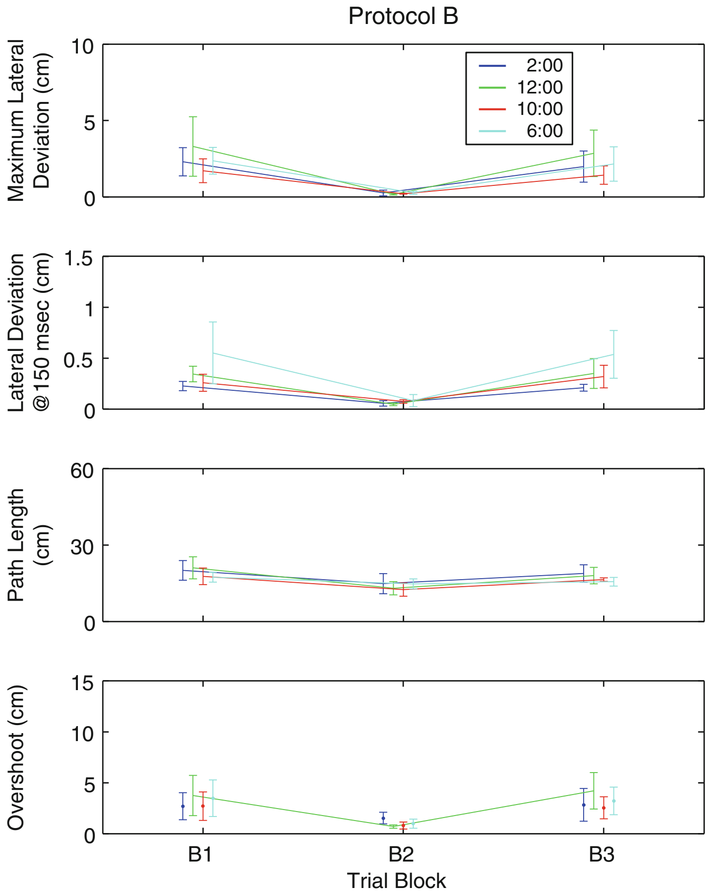

Fig. 12.16 Summary of force channel results under assistance Method 2, Protocol B. Four patient data sets are averaged. Four metrics are used to measure performance – maximum lateral deviation from the straight path (first row), lateral deviation at 150 ms from the straight path (second row), path length (third row), and overshoot (fourth row). Hand paths and errors are color coded by direction

12.4.2 Assistance Method 1: Dynamics Augmentation

Patient-specific changes in arm dynamics predicted to assist in making straight reaching movements were tested in this study. The results suggest this dynamics augmentation approach may improve the reaching of some cerebellar patients and not others. There was no evidence of motor learning.

The mildly impaired patient, Cerebellar 1, demonstrated near-control-like reaching performance in all five blocks. Even during B_2 and B_4 when substantial perturbations were applied, the patient performed nearly as well as control subjects.

Table 12.4 Nonparametric test p-values are listed for various metrics and reaching directions (p-values less than 0.05 are printed in boldface). In this test, errors during the null blocks are compared to errors during channel blocks ($\{B_1, B_4, B_7\}$ vs. $\{B_2, B_3, B_5, B_6\}$ under Protocol A and $\{B_1, B_3\}$ vs. B_2 under Protocol B). Significant improvements in performance were observed as patients reached in force channels

Protocol A $\{B_1, B_4, B_7\}$ vs. $\{B_2, B_3, B_5, B_6\}$				
Direction	M_1 (path length)	M_2 (max lateral dev)	M_3 (dev at 150 ms)	M_4 overshoot
12:00	0.2752	**0.0495**	**0.0495**	0.5127
Protocol B $\{B_1, B_3\}$ vs. B_2				
Direction	M_1	M_2	M_3	M_4
2:00	0.2482	**0.0209**	**0.0209**	0.3865
12:00	**0.0433**	**0.0209**	**0.0209**	**0.0209**
10:00	0.0833	**0.0209**	**0.0209**	0.1489
6:00	0.1489	**0.0209**	**0.0209**	**0.0433**

Table 12.5 Nonparametric test p-values are listed for various metrics and reaching directions. In this test, errors during the null blocks are compared to each other ($\{B_1, B_4, B_7\}$ under Protocol A and $\{B_1, B_3\}$ under Protocol B). No evidence of use-dependent learning was observed

Protocol A B_1 vs. B_4 vs. B_7				
Direction	M_1 (path length)	M_2 (max lateral dev)	M_3 (dev at 150 ms)	M_4 overshoot
12:00	0.9565	0.7326	0.7326	0.9565
Protocol B B_1 vs. B_3				
Direction	M_1	M_2	M_3	M_4
2:00	0.3865	0.3865	0.3865	0.7728
12:00	0.1489	0.3865	1	0.7728
10:00	1	0.5637	0.5637	0.7728
6:00	0.1489	0.7728	1	1

Table 12.6 Nonparametric test p-values for various metrics and reaching directions. In this test, errors to the non-trained reaching directions during the null blocks $\{B_1, B_4, B_7\}$ under Protocol A are compared to each other. Generalization of use-dependent learning was not observed

Protocol A B_1 vs. B_4 vs. B_7				
Direction	M_1 (path length)	M_2 (max lateral dev)	M_3 (dev at 150 ms)	M_4 overshoot
2:00	0.5866	0.8752	0.9565	0.9565
10:00	0.7326	0.9565	0.4298	0.8371
6:00	0.7326	0.9565	0.6703	0.9565

This indicates that some capacity for motor adaptation remains for this subject and a potentially substantial subset of the patient population. This contradicts one of our key assumptions made during the computer simulations used to find the optimal perturbation: in accordance with the many studies which have shown impaired motor adaptation among cerebellar patients, the simulations assumed cerebellar patients repeat the same pattern of muscle activity during early movement. Violations of this assumption would result in a perturbation that will not remain optimal over time. Real-time optimization of this perturbation might result in further improvement for patients capable of motor adaptation.

For the moderately impaired patient, Cerebellar 5, performance improved with the P^+ perturbation and degraded with the P^- perturbation, as predicted (lateral deviation decreased 16 % with P^+ and increased 19 % with P^-). These results suggest that this model-based approach may be useful, at least for some subset of patients. However, more experiments must be done to better understand the efficacy of this approach.

With the severely impaired patient, Cerebellar 6, no clear pattern was observed. Though this method can only address the repeated misdirection, or bias, in reaching, ataxia results in both misdirected and highly variable movements. This subject's movements were particularly variable and it is possible that the robot's effect on reaching dynamics does not exceed some critical, noise-dependent threshold. We also suspect that this patient's shoulder injury may obscure these results.

12.4.3 Assistance Method 2: Force Channel

In this second study, the robot was used to render force channels to constrain arm movements during reaching. This study also explored how the ordering of null (robot passive) and channel (robot active) trial blocks affected motor learning. The force channels resulted in significant improvements in reaching performance in the directions both parallel and orthogonal to the force channel. There was no evidence that reaching practice in these channels results in improved reaching performance after the channels were removed.

It may be seen as a trivial observation that force channels had a significant effect of decreasing lateral deviation – this is precisely the function of the channel. However, the presence of force channels also had an effect on overshoot in the 12:00 and 6:00 directions. In other words, patients not only made straighter movements, but in two of the four directions, demonstrated improvement in the direction orthogonal to the channels. This is analogous to the observation that cerebellar subjects are less impaired when making single-jointed movements [5], in that the channels simplify motor control requirements.

Our failure to observe learning is consistent with many other cerebellar studies. Indeed, a common theme in cerebellar studies is that error-based or use-dependent learning mechanisms are difficult to elicit. We found that the gradual removal of the force channel did not produce a measured effect.

12.5 Conclusions

The first assistance method explored here utilizes the KINARM exoskeleton to apply the optimal augmentation in dynamics for specific cerebellar patients. In essence, the goal is to "add back in" the aspects of limb control that have been lost for each cerebellar subject. It appears that this targeted, assistive approach may work for some patients. This work could be extended by improving the fidelity and range of dynamic perturbations that the robot can stably render. This could possibly increase the number of patients and the degree to which each is assisted by this method.

This approach could lead to a "soft" rehabilitation strategy in which wearable devices are used to change effective limb dynamics in a manner that exactly counters the original movement deficit, thus providing patient-specific, unconstrained robotic assistance or training for movement control. An approach like this would be especially useful as correcting faulty cerebellar patient movements through motor learning has proven elusive [10, 19, 20, 31]. These results inspire the design of new assistance strategies for patients with cerebellar damage using patient-specific augmentations to arm dynamics. Critically, such an approach could improve reaching performance without knowing the patient's intended direction of movement a priori.

The motor behavior does, at least for some cerebellar patients, change in the presence of an altered dynamic environment. One approach to account for this is to apply a prescribed perturbation, measure performance, recalculate the optimal perturbation, and iterate. Faster simulation and optimization may enable this approach in future work.

The second assistive method uses force channels and explores task designs that might elicit use-dependent learning with cerebellar patients. The KINARM is able to stably render stiff force channels that significantly improve reaching performance. However, reaching performance returned to baseline after the channels were removed. We also were not able to detect generalization of learning – practice in a force channel had no effect of subsequent reaching behavior in other directions.

The design of effective training protocols for cerebellar subjects is certainly a challenge given the reality of their loss of brain function. However, much redundancy does exist in the human motor control system and other learning mechanisms might be engaged through clever task design. The importance of informed task design is critical given the logistical difficulty in recruiting patients with a very specific condition. In parallel to these efforts, wearable devices could be designed to implement assistive strategies to improve patients' quality of life by assisting them with activities of daily living.

These studies demonstrate the use of robotic instruments for precise measurements and interventions to understand and treat human motor deficits. In particular, the capacity to affect the dynamics of the human arm in an arbitrary manner allowed for a direct test of a popular hypothesis about cerebellar function and is something that could not be practically achieved with any other instrument. The approach of designing model-based and patient-specific robotic assistance and rehabilitation paradigms could lead to an increased understanding of the brain and improved patient outcomes.

References

1. Adams R, Victor M (1993) The cerebellum. Principles of neurology. McGraw-Hill, OH
2. Aisen M, Krebs H, Hogan N, McDowell F, Volpe B (1997) The effect of robot-assisted therapy and rehabilitative training on motor recovery following stroke. Arch Neurol 54(4):443–446
3. Ataxia (2013) The mayo clinic. http://www.mayoclinic.com/health/ataxia/DS00910. Accessed 13 May 2013
4. Ataxias: General Classification (2013) Neuromuscular. neuromuscular.wustl.edu/ataxia/aindex.html. Accessed 13 May 2013
5. Bastian A, Martin T, Keating J, Thach W (1996) Cerebellar ataxia: abnormal control of interaction torques across multiple joints. J Neurophys 76:492–509
6. Bastian A, Zackowki K, Thach W (2000) Cerebellar ataxia: torque deficiency or torque mismatch between joints? J Neurophysiol 83(5):3019–3030
7. Brewer B, Fagan M, Klatzky R, Matsuoka Y (2005) Perceptual limits for a robotic rehabilitation environment using visual feedback distortion. Trans Neural Syst Rehabil Eng 13:1–11
8. Diedrichsen J, White O, Newman D, Lally N (2010) Use-dependent and error-based learning of motor behaviors. J Neurosci 30(15):5159–5166
9. Dolan J, Friedman M, Nagurka M (1993) Dynamic and loaded impedance components in the maintenance of human arm posture. IEEE Trans Syst Man Cybern Syst 23(3):698–709
10. Earhart G, Fletcher W, Horak F, Block E, Weber K, Suchowersky O, Melvill J (2002) Does the cerebellum play a role in podokinetic adaptation? Exp Brain Res 146(4):538–542
11. Emken J, Reinkensmeyer D (2005) Robot-enhanced motor learning: accelerating internal model formation during locomotion by transient dynamic amplification. Trans Neural Sys Rehabil Eng 13(1):33–39
12. Fasoli S, Fragala-Pinkham M, Hughes R, Hogan N, Krebs H, Stein J (2008) Upper limb robotic therapy for children with hemiplegia. Am J Phys Med Rehabil 87:929–936
13. Ghez C, Thach W (2000) The cerebellum. In: Kandel E, Schwartz J, Jessell J (eds) Principles of neural science. McGraw-Hill, New York
14. Gomi H, Kawato M (1997) Human arm stiffness and equilibrium-point trajectory during multi-joint movement. Biol Cybern 76(3):163–171
15. Grow D (2011) Robot-assisted modeling and rehabilitation strategies for cerebellar Ataxia. Dissertation, Johns Hopkins University
16. Hollerbach J, Khalil W, Gautier M (2008) Model identification. In: Sciliano B, Khatib O (eds) Springer handbook of robotics. Springer, New York, pp 321–342
17. Krebs H, Volpe B, Aisen M, Hogan N (2000) Increasing productivity and quality of care: robot-aided neuro-rehabilitation. J Rehabil Res Dev 37(6):639–652
18. Lum P, Burgar C, Shor P, Majmundar M, Van der Loos M (2002) Robot-assisted movement training compared with conventional therapy techniques for the rehabilitation of upper-limb motor function after stroke. Arch Phys Med Rehabil 83(7):952–959
19. Martin T, Keating J, Goodkin H, Bastian A, Thach W (1996) Throwing while looking through prisms: I. Focal olivocerebellar lesions impair adaptation. Brain 119:1183–1198
20. Maschke M, Gomez C, Ebner T, Konczak J (2004) Hereditary cerebellar ataxia progressively impairs force adaptation during goal-directed arm movements. J Neurophys 91(1):230–238
21. Massaquoi S, Hallett M (1996) Kinematics of initiating a two-joint arm movement in patients with cerebellar ataxia. Can J Neuro Sci 23(1):3–14
22. Miall R, Weir D, Wolpert D, Stein J (1993) Is the cerebellum a Smith predictor? J Motor Behav 25:203–216
23. Mobasser F, Hashtrudi-Zaad K (2006) A method for online estimation of human arm dynamics. Paper presented at the 28th EMBS, New York, 31 Aug–3 Sept 2006
24. Morton S, Bastian A (2006) Cerebellar contributions to locomotor adaptations during splitbelt treadmill walking. J Neurosci 26(36):9107–9116

25. Patton J, Stoykov M, Kovic M, Mussa-Ivaldi F (2006) Evaluation of robotic training forces that either enhance or reduce error in chronic hemiparetic stroke survivors. Exp Brain Res 168(3):368–383
26. Pigeon P, Bortolami S, DiZio P, Lackner J (2003) Coordinated turn-and-reach movements. I. Anticipatory compensation for self-generated coriolis and interaction torques. J Neurophys 89(1):276–289
27. Scheidt R, Stoeckmann T (2007) Reach adaptation and final position control amid environmental uncertainty after stroke. J Neurophys 97(4):2824–2836
28. Schweighofer N, Arbib M, Kawato M (1998) Role of the cerebellum in reaching movements in humans: I. Distributed inverse dynamics control. Eur J Neurosci 10(1):86–94
29. Scott S (1999) Apparatus for measuring and perturbing shoulder and elbow joint positions and torques during reaching. J Neurosci Methods 89:119–127
30. Smith E (2004) Robotic compensation of cerebellar ataxia. Thesis, Massachusetts Institute of Technology
31. Smith M, Shadmehr R (2005) Intact ability to learn internal models of arm dynamics in Huntington's disease but not cerebellar degeneration. J Neurophys 93(5):2809–2821
32. Stein J, Krebs H, Frontera W, Fasoli S, Hughes R, Hogan N (2004) Comparison of two techniques of robot-aided upper limb exercise training after stroke. Am J Phys Med Rehabil 83(9):720–728
33. Topka H, Konczak J, Schneider K, Boose A, Dichgans J (1998) Multi-joint arm movements in cerebellar ataxia: abnormal control of movement dynamics. Exp Brain Res 119(4):493–503
34. Trouillas P et al (1997) International cooperative ataxia rating scale for pharmacological assessment of the cerebellar syndrome. J Neuro Sci 145(2):205–211
35. Van der Loos H (1995) VA/Stanford rehabilitation robotics research and development program: lessons learned in the application of robotics technology to the field of rehabilitation. IEEE Trans Rehabil Eng 3(1):46–55
36. Westlake K, Patten C (2009) Pilot study of lokomat versus manual-assisted treadmill training for locomotor recovery post-stroke. J Neuroeng Rehabil 6(1):8–18

Chapter 13
A Human Augmentation Approach to Gait Restoration

Dino Accoto, Fabrizio Sergi, Nevio Luigi Tagliamonte, Giorgio Carpino, and Eugenio Guglielmelli

Abstract Impaired gait can be restored to its physiological level using wearable robotic systems acting alongside human lower limbs and providing assistive forces that adapt to the residual sensory-motor capabilities of the wearer. Such systems can be used as assistive aids (to overcome disabilities or age-related impairments) or as rehabilitation tools (to restore physical and neurological abilities through proper training). In order to elicit physiological gait as a behavior emerging from the interaction between the robot and the user, the robot morphology must be considered as an open design variable, thus relaxing the constraint of using basically anthropomorphic architectures. This chapter deals with several design aspects related to this approach for the development of lower limbs wearable robots. In particular, it analyzes kinematic compatibility issues, possible topological connections among robotic elements, morphological optimization of robot properties, actuation solutions with series compliance, interaction control schemes and user's intention detection strategies. Pilot tests on a novel non-anthropomorphic device, developed according to the proposed approach, are presented as a case-study, exemplifying the main design aspects described within the chapter.

Keywords Assistive and rehabilitation robotics • Wearable robotics • Exoskeleton • Compliant actuator • Physical human-robot interaction

D. Accoto (✉) • N.L. Tagliamonte • G. Carpino • E. Guglielmelli
Università Campus Bio-Medico di Roma, via Alvaro del Portillo 21, 00128 Rome, Italy
e-mail: d.accoto@unicampus.it; n.tagliamonte@unicampus.it; g.carpino@unicampus.it; e.guglielmelli@unicampus.it

F. Sergi
Rice University, Houston, TX 77005, USA
e-mail: fabs@rice.edu

P. Artemiadis (ed.), *Neuro-Robotics: From Brain Machine Interfaces to Rehabilitation Robotics*, Trends in Augmentation of Human Performance 2,
DOI 10.1007/978-94-017-8932-5_13,

13.1 Human-Robot Symbiosis

Wearable robots (WRs) aim at supplementing the function of a limb (active orthoses and augmenting devices) or to replace it (prostheses). Wearability does not necessarily imply that the robot is ambulatory, portable or autonomous [1]. Historically, the earliest device resembling a WR was described by Yagn in the U.S. Patent granted in 1890 [2]. This wearable device, intended to augment human running and jumping capabilities, consisted of long bow/leaf springs operating in parallel to the legs, cyclically storing and releasing elastic energy according to gait phases. Several years later, General Electric Co. developed the concept of human-amplifiers (*Hardiman* project, 1966–1971).

Exoskeletons constitute a subset of WRs with specific characteristics. An exoskeleton is effectively defined in Dollar and Herr [3] as "*an active mechanical device that is essentially anthropomorphic in nature, is worn by an operator and fits closely to his or her body, and works in concert with the operator's movements*". In an anthropomorphic structure, robot kinematics is not a free design parameter. Conversely, WRs can be designed so to have a non-anthropomorphic kinematic structure. In fact, WRs are not just robots designed around the human body, so to obtain an as safe as possible physical Human-Robot Interaction (pHRI). Rather, the level of interaction between the WR and the human body should be advantageously pushed ahead by designing the WR so that a *symbiotic interaction* occurs between it and the human body. The adjective "symbiotic" refers to the intimate physical interaction between the human body and the robotic artifact, building upon the human capabilities in order to lead to useful *emergent behaviors*, assisting or augmenting the selected human performance (Fig. 13.1).

Specifically, *design for symbiosis* is intended as a kind of design for emergence aiming at producing dynamic behaviors, by augmenting wearer's residual motor capabilities, as useful to a given purpose (e.g. restoring proper motor abilities in chronic subjects, of whom elderly people are the most socially relevant example).

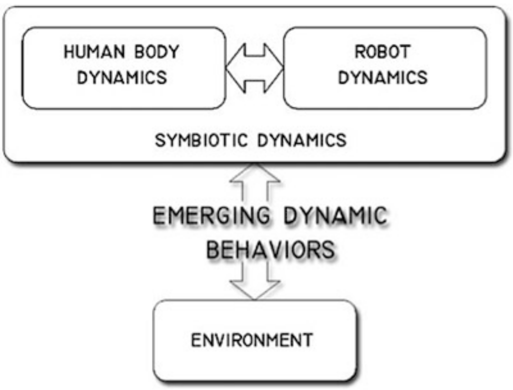

Fig. 13.1 Emerging behaviors, arising from the coupled dynamics of human body and robotic structure interacting with the environment, help the execution of a complex task with low computational efforts. Low-level adaptations to the environment are managed by the intrinsic properties of the mechanical structure of the robot (preflexes)

It is also desirable that the mechanical structure of the WR is capable of managing the low-level issues related to the interaction with the environment by exhibiting proper zero-delay, intrinsic responses (i.e. preflexes) to a perturbation [4]. The ability of a mechanical structure of producing useful emergent behaviors and of adapting itself to external perturbations through preflexes can be seen as whole as a form of *structural intelligence*, as an instantiation of *embodied intelligence*.

The concept of embodied intelligence highlights how intelligence benefits also from the physicality of an agent, where the term *physicality* is meant to catch as a whole the dynamic, kinematic and somesthetic properties of an organism and the typology of its possible interactions with the environment. Indeed, it is recognized [5] that the embodiment of an agent has implications on the information theoretic processes (e.g. by effectively structuring the sensory inflow from the environment) and that morphology itself can perform computation through physical interactions (i.e. morphological computation). Robots designed to exploit embodied intelligence are frequently simpler, more robust and adaptive than those based on the classical interaction control paradigm.

These concepts formulated in artificial intelligence and computer science are often strictly related with biological observations of animal behavior, especially in locomotion, that focus on the intimate connections among intelligence, morphology and performance. As shown in Kubow and Full [4], the lowest level of intelligence is completely physical, as it consists in the ability of neuro-musculoskeletal systems to present zero-delay, intrinsic responses to a perturbation [6]. Preflexes are useful for performing low-level tasks, such as stabilization and feedforward locomotion control. As an example, the cockroach *Blaberus discoidalis* is able to scramble over randomically distributed obstacles up to three times its body height without significantly slowing down [7]. Such striking performance cannot be achieved by a feedback-based, centralized sensory-motor control, because the required adaptation to the environment is too quick. On the contrary, robust locomotion is achieved mainly through a basically feedforward pattern applied to a properly tuned mechanical system. Such principles have been implemented in the development of a highly efficient hexapedal robot capable of sensorless robust locomotion at speeds up to 2.5 body lengths/s [8].

On a higher level, recent studies on biped robots have shown that even complex tasks, such as walking, may arise from the intrinsic dynamics of a machine during its interaction with the environment. Studies on passive walking show that bipedal walking, normally obtained through computationally demanding feedback control algorithms, can emerge from an accurate tuning of the dynamical properties of a purely mechanical system, without any feedback control [9, 10]. The performance obtained through this methodology produces a gait that appears to be more biomimetic under both the energetic and kinematic standpoints. In particular, it has been demonstrated that the energetic efficiency of such mechanisms is closer to that of the human body, while existing bipedal walking robots are about 30 times more energy demanding [11]. Moreover, experiments performed on physical simulation environments have shown that it is possible to optimize, via a coupled evolutionary process, both the morphological properties of a robot and its controller, with mutual benefits for both, in terms of reduced complexity and enhanced efficiency [12].

The two examples mentioned above demonstrate that better performance, with lower computation cost and with simpler and lighter structures, can be achieved if the potentialities of structural intelligence are properly harvested and exploited. Till now, such concepts have been explored and applied to the development of robots inspired by a large variety of biological systems, such as mammalians, fishes and insects. On the contrary, the human body has been poorly investigated from the structural intelligence standpoint, while this is a promising new route toward the development of useful machines intended for the strict interaction with humans, such as robots for rehabilitation, assistance and functional restoring for elderly and disabled people.

In the scenarios where the robot and the human body are strictly interacting, the design of the artificial system must take into account the dynamics of the biological counterpart, which is highly variable and actively tuned by the human sensory-motor system. When strict physical interaction occurs, the dynamics of the human body and that of the robotic artifact are strongly coupled. If the robot is meant to compensate for lost body functionalities, such as proper gait generation, the proposed approach consists in finding how the robotic system must be designed to take advantage of the variable biomechanical properties of the human body.

The objective is to design the robotic system in such a way that the dynamics of the human body, especially in the case of impaired or elderly subjects, and that of the robot during interaction, symbiotically benefit from each other, eliciting emergent dynamic behaviors, which favor the execution of the desired task.

The nature and the level of symbiosis, that can be effectively attained, depend on the specific employed design methods and tools and on their capability to accurately predict the kind of interaction that the user and the robot would establish, depending from the morphological and control properties of the latter.

The engineering of a specific dynamical interaction is still an open research objective. Indeed, it requires simulation tools not yet available, which should be capable to accurately model personal motor styles, human motor control strategies and time-dependent, subject-specific self-adaptations to the robot. Nonetheless, as presented in the following sections, the concept of structural intelligence can be effectively exploited to design a WR with a diverse structure, better ergonomics (i.e. intrinsically capable of solving micro- and macro- misalignments issues), better dynamical properties (e.g. limited inertial effects associated to the swinging of actuators), and good backdrivability.

The approach, in which embodied intelligence is taken a step further to embrace also the potentialities of structural intelligence, is radically new, as better highlighted by the analysis of the state of the art in the field of WRs, as summarized in the following section.

13.2 Wearable Robots for Gait Restoration

A substantial push in the advancements of the field of wearable robots for human performance augmentation has been provided by the program promoted by the US Defense Advanced Research Projects Agency (DARPA), called Exoskeletons for Human Performance Augmentation (EHPA), started in 2001, which encouraged the development of exoskeletons helping soldiers to carry backpacks during operative missions. The *Berkeley Lower Extremity Exoskeleton* (*BLEEX*) has been developed by prof. Kazerooni and his group at the University of California [13]. BLEEX features three Degrees Of Freedom (DOFs) at the hip, one at the knee, and three at the ankle. Of these, four are actuated: hip flexion/extension, hip abduction/adduction, knee flexion/extension, and ankle flexion/extension. Of the non-actuated joints, the ankle inversion/eversion and hip rotation joints are spring-loaded, and the ankle rotation joint is completely free [14].

After the first prototypal version of the system, the Berkeley Robotics & Human Engineering Laboratory worked on new versions of the device for military applications developing the *ExoHiker* and the *ExoClimber* systems, tailored for load carrying during overground walking or during slopes ascent. The third generation of their exoskeletal system, the *Human Universal Load Carrier* (*HULC*) has reduced bulkiness and weight, since structural parts are titanium made. Interestingly, the HULC is claimed to be the first system able to provide a reduction in the order of 5–15 % of the metabolic cost associated to overground walking.

Sarcos (recently purchased by Raytheon) has developed an exoskeleton also based on hydraulic actuation. The exoskeleton (*Sarcos XOS*) has been designed to encompass the entire body. The XOS robot includes 30 actuated DOFs and is controlled using a number of multi-axis force-moment transducers that are located between the feet, the hands and the torso of the operator and the machine [15]. However, the largest drawback of this device is the lack of a mobile power source. A quasi-passive exoskeleton, the *MIT exoskeleton*, has been designed in the Biomechatronics Group at the Massachusetts Institute of Technology Media Laboratory by the group of prof. Hugh Herr. This concept seeks to exploit the passive dynamics of human walking in order to create a lighter exoskeletal device [11], which demonstrated an increased energetic efficiency when compared to conventional walking machine designed through a kinematically anthropomorphic design and controlled via Zero Moment Point (ZMP) technique [16, 17]. The group of prof. Yoshiyuki Sankai at the University of Tsukuba (Japan) developed an exoskeleton targeted for both performance-augmenting and rehabilitative purposes [18, 19]. The leg structure of the full-body *HAL-5* exoskeleton powers the flexion/extension of hip and knee joints via a DC motor with harmonic drive placed directly on the joints. The ankle dorsi/plantar flexion DOF is passive. The HAL-5 system utilizes a number of sensing modalities: skin-surface EMG electrodes, placed below the hip and above the knee on both the anterior (front) and posterior (back) sides of the wearer's body; potentiometers for joints angles measurement, ground reaction force sensors, a gyroscope and accelerometer mounted on the backpack for torso posture estimation. HAL-5 is currently commercialized by the spinoff company Cyberdine (Tsukuba, Japan).

Compared to human augmentation devices, *mobile medical exoskeletons* are intended for assistive and/or rehabilitative purposes. Improving the quality of life of wheelchair users is the aim of the *Ekso*, designed and commercialized by the Ekso Bionics (Berkeley, CA, US), intended for people with lower extremity weakness or paralysis due to neurological disease or injury (spinal cord injuries, multiple sclerosis, Guillain Barré syndrome).

Founded in 2001 and originally operating under the auspices of the Technion Seed (Technion, Institute of Technology, Israel), Argo Medical Technologies has developed a robotic ambulation system for wheelchair users named *ReWalk*, assisting only the movements in the sagittal plane. The ankle joint is not actuated.

Different from Ekso and ReWalk, *REX*, produced by REX Bionics (Auckland, New Zealand), is an anthropomorphic lower body orthosis designed for sit-to-stand, stair ascend and overground walking, without the use of crutches. The system does not use sensors to sense the intention of the user but uses a joystick for the user to control the exoskeleton. The system has been validated with healthy subjects, and for sit-to-stand of wheelchair users.

The *Vanderbilt powered orthosis* [20] is a powered lower-limb orthosis intended for Spinal Cord Injured (SCI) individuals. Differently from the previous mentioned devices, it neither includes a portion worn over the shoulders, nor a portion under the shoes. The orthosis is intended to be used in conjunction with a standard ankle foot orthosis, which provides support at the ankle and prevents foot drop during swing.

Treadmill-based WRs are mainly used as rehabilitation platforms capable of (partially) supporting patient weight and of providing assistance in performing therapeutic exercises, usually according to the *Assist-As-Needed (AAN)* paradigm.

Lokomat, developed by Hocoma (Volketswil, Switzerland), assists hip and knee movements in the sagittal plane while the ankle joint is not supported. Similarly, the *LOPES* (*LOwer-extremity Powered ExoSkeleton*) is a treadmill-based wearable robotic device for gait training and assessment of motor function in stroke patients [21] developed at University of Twente by the group led by prof. Herman van der Kooij. It is comprised of two parts: the adjustable lightweight frame for pelvic control actuating the two horizontal pelvis translations and the exoskeleton leg with four actuated DOFs per each leg which assist hip flexion/extension, adduction/abduction, knee flexion/extension and ankle dorsi/plantar flexion. All the actuated DOFs are based on series elastic actuation, consisting of a servomotor, a flexible Bowden cable transmission and a force feedback controller. This solution implies that the actuators are used as force (and torque) sources and allow impedance control of the robot. Impedance control with this kind of setup can be used in both high impedance control (resembling position control) and zero impedance control.

The *AutoAmbulator* [22] by Healtsouth Corp. (AL, USA) essentially consists of an electrically actuated anthropomorphic device supporting hip and knee movements in the sagittal plane.

The *Pelvic Assist Manipulator* (*PAM*) and *Pneumatically Operated Gait Orthosis* (*POGO*) are pneumatic robots that compliantly assist in gait training. PAM can assist in five DOFs of pelvic motion, while POGO can assist the hip/knee flexion/extension [23]. The devices can be used in a back-drivable mode to record a desired stepping pattern that is manually specified by human trainers, then replay the pattern with compliant assistance. During compliant replay, the devices automatically synchronize the timing of the replayed motions to the inherent variations in the patient's step timing, thereby maintaining an appropriate phase relationship with the patient.

In some systems developed in the last years the principles of structural intelligence can be glimpsed. In Krut et al. [24], Mokhtarian et al. [25], Vallery et al. [26] passive spring-based balancers dynamically sustain the body weight during walking. In the *MIT SkyWalker* [27], passive walkers have provided inspiration to define gait rehabilitation strategies that promote natural legs dynamics during the swing phase. Another interesting example is the *Elastic exoskeleton* [28], developed at University of Michigan, where leaf springs provide intrinsic elasticity and allow an optimized human-robot energy exchange during running. In *KNEXO* [29] the principles of bioinspiration, as a form of embodied intelligence, has been exploited in the actuation system; the agonistic/antagonistic configuration of two pleated pneumatic artificial muscles has been adopted to actuate a knee orthosis for gait assistance.

The problem of assessing if, how and how much the findings achieved in the field of pseudo-passive bipedal walking can be transferred to the field of WRs for the lower limbs consists of a very tough challenge. Despite of that, the literature suggests that possible improvements of the performances of WRs can be provided by "opening" the design of the mechanical subcomponent, and not just focusing on novel control schemes or aspects related to actuators power efficiency or intrinsic safety.

These considerations suggest that WRs performances can benefit from a careful design of robot morphology, which is open in the case of non-anthropomorphic WRs, and can allow to achieve a better dynamical interaction with the human body and with the environment.

13.3 Non-anthropomorphic Design: From Topological Analysis to Morphological Optimization

The problem of optimal kinematic synthesis of non-anthropomorphic WRs may be very unpractical to be tackled by the conventional insight-driven engineering approach, due to the large number of open parameters involved in the design. This task can be simplified by automatic tools in support of the designer.

In the last decade, evolutionary programming has been applied to solve the problem of co-designing both the mechanics and the control of mobile artificial machines, by just defining the basic building blocks of the structure and the rules to connect them [30, 31]. This open-ended design methodology has the advantage that it can lead to unexpected design solutions. However, such kind of methods implies that the entire design process is completely demanded to the tool, which can autonomously decide to switch to a more complex structure during the optimization phase so to increase the fitness of the best individuals.

The authors are pursuing a systematic approach for the kinematic synthesis of WRs, based on a three-step process. The first step requires the exhaustive search of all independent generalized solutions for a WR design problem; the subsequent step consists of the selection among the pool of admissible solutions; finally, a candidate solution is optimized in terms of its morphological parameters, to satisfy a multi-objective fitness function.

This three-step strategy appears more reliable compared to open-ended kinematic optimization approaches, since optimization algorithms, acting on a fixed parameter space, are simpler and converge faster. Compared to the "brute-force" approach followed in [30], this strategy guarantees that only a reduced subset of solutions are evaluated, i.e. those kinematically compatible with the human body. Additionally, this strategy assures *completeness*: all relevant generalized solutions (i.e. topologies) are considered before producing the final design. The only drawback of the approach consists in the fact it requires the a-priori knowledge of the independent topologies having desired kinematic properties. No standard design tool was available for this specific problem of the design of a non-anthropomorphic WR for gait assistance, and then a major methodological step has been focused on development of ad-hoc computational tools, adapted from the general case of mechanism design.

13.3.1 Exhaustive Kinematic Synthesis of Non-anthropomorphic Wearable Robots

As a first step, it is important to define an efficient encoding, which allows the representation of the kinematic structure of a WR connected to a given human limb, which is modeled as a generalized serial chain. Since the aim is to evaluate also the mobility of the human limbs connected to the robot, the parallel kinematic chain, consisting of both robot links and human limbs, is considered. The most generalized level of abstraction at which such structure can be described is the *topology* level, which defines only the number of links and the connections among them.

13.3.1.1 Kinematic Structure Encoding and Topologies Enumeration

Under some reasonable hypotheses [32], many properties of mechanisms kinematics, such as the number of DOFs, are entirely determined only by the topology of the kinematic chain and unaltered by the geometry of its links. At this level of

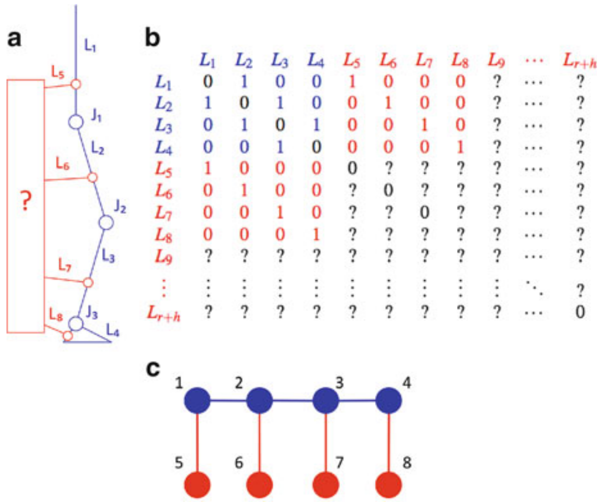

Fig. 13.2 Structural representation (**a**), generalized TAM (**b**) and graph representation (**c**) of the problem of structural synthesis of robotic orthoses for a planar WR for the lower limbs. Human articulations and segments are in *blue*, while robot links and joints are in *red*. In the adjacency matrix, the *blue color* is used to represent entries which describe the connectivity of human limbs, while the *red color* represents fixed entries

abstraction, the classical (graph)-(kinematic chain) analogy introduced in [33] can be employed, where graph vertexes correspond to the links of the chain and edges correspond to the joints. A graph can then be encoded through the Topology vertex-vertex Adjacency Matrix (TAM): a binary symmetric matrix of order n (where n corresponds to the number of links) where the element a_{ij} equals to 1 if link i and link j are connected through a joint, and to 0 otherwise.

As a first assumption, we decide to focus on planar kinematic chains composed of only revolute joints, for the assistance of the lower limb, modeled as a serial chain with three DOFs (hip, knee and ankle) moving in the sagittal plane. It is then unnecessary to discriminate on the type of joint connecting each link; hence the representation is complete in the description of kinematic chains topology, allowing the conversion of a problem of kinematic synthesis into a problem of graphs enumeration. The mentioned assumption limits the relevance of the methodology for the design of assistive WRs for the lower limbs, since the hip and the ankle joints have spatial movements. However, it can be noticed that, during ground walking, most of the power of the lower limbs is provided by actuation of movements in the sagittal plane, which is therefore the dominant plane during human locomotion [34].

The graph enumeration problem is graphically represented in Fig. 13.2, which depicts the structural representation, the graph representation and the corresponding TAM of the kinematic chain comprising both human segments and robot links. The process of enumerating kinematic chains consists of three successive steps: (i) *enumeration of graphs with the desired mobility*, (ii) *pruning of isomorphic (*i.e. *non-independent) solutions and*, (iii) *pruning of non-kinematic compatible solutions*. The mentioned steps will be described in more detail in the following.

Each kinematic solution can be represented by a graph with $h + r$ edges, where h corresponds to the number of body segments (four in our case) and r corresponds to the number of robot links.

The complete list of independent kinematic solutions can be derived from the frame of the basic TAM shown in Fig. 13.2b. Any topology can be encoded by a binary string of length l, where:

$$l = h\,(r - h) + \frac{r\,(r - 1)}{2} \tag{13.1}$$

However, not any combination of parameters is adequate, since we are interested only in kinematic chains with a given number of DOFs. For a given planar kinematic chain with n links and f joints with one DOF, the total number of degrees of freedom (DOFs) is obtained by using the Kutzbach criterion [35]:

$$DOFs = 3\,(n - 1) - 2f \tag{13.2}$$

From (13.2), given any number of links and a desired number of DOFs, the kinematic chain can contain only a fixed number of joints. Since each joint between links i and j corresponds to a 1 in the (i, j) position of the corresponding TAM, the problem of enumeration of all topologies with a desired mobility can be converted into the problem of exhaustively listing the binary strings of length l, with a fixed number of ones.

13.3.1.2 Degeneracy and HR-Degeneracy Testing

A further selection over the list of enumerated topologies is performed, in order to filter out the kinematic chains which:

1. contain rigid or over-constrained sub-chains;
2. correspond to disconnected graphs (i.e. not all graphs vertices are connected by a path);
3. impair the motion of human joints.

A standard degeneracy testing algorithm has been implemented to recognize and discard rigid sub-chains (such as three links-three joints and five links-six joints sub-chains). Kinematic chains containing at least one sub-chain with zero or negative DOFs according to Kutzbach formula (e.g. three links-three joints and five links-six joints sub-chains) are considered as degenerate solutions and are then eliminated. Additionally, disconnected mechanisms (i.e. such that there is not a path connecting each couple of vertices of the corresponding graph) are eliminated with a purposively developed algorithm, which verifies the existence of a path between each couple of vertices.

Furthermore, an additional test was introduced so to exclude those solutions where a subset of p human joints is part of a subchain with less than p DOFs. In this case the robot would impair human movements by imposing unnatural kinematic constraints. This test is called *HR-degeneracy* test (*Human-Robot degeneracy* test) since it applies to kinematic chains including both human and robot structures. The test is performed by recognizing the presence of sub-chains where two adjacent human joints are constrained in a one-DOF sub-chain, or where all three adjacent human joints are constrained in a two-DOFs sub-chain. The exhaustive list of such HR-degenerate primitives (reported in Fig. 13.2) could be obtained by adapting results coming from standard atlases of kinematic chains [36] and was re-obtained in a previous work concerning the enumeration of orthoses for a one-DOF human joint [37].

13.3.1.3 HR-Isomorphism Testing

Since the chosen method is based on the enumeration of suitable matrices of adjacencies, an explicit isomorphism test is required to guarantee mutual independence of set of enumerated solutions. Two kinematic chains K_1 and K_2 are said to be isomorphic if there exists a one-to-one correspondence between links of K_1 and K_2 such that any pair of links of K_1 are jointed if and only if the corresponding pair of links of K_2 are jointed. This means that from the graph corresponding to K_1 one can obtain the graph corresponding to K_2 by only relabeling link numbers.

A function defined on a kinematic chain is called an *index of isomorphism* if any given pair of kinematic chains is isomorphic if and only if the corresponding values of the function are identical. The *index of isomorphism* used in the present work is the characteristic polynomial of the Extended Adjacency Matrix (EAM) $A^{(d)}$ of order d, as also suggested in [38]. In [38] it is demonstrated that the simultaneous evaluation of the characteristic polynomial of both $A^{(0)}$, $A^{(1)}$ and $A^{(2)}$ has a reliability of 100 % for kinematic chains consisting of up to 11 links. This technique for isomorphism detection shows to be a very good compromise between reliability and computational efficiency, since it requires a polynomial time for assessing isomorphism.

However, when applying the isomorphism test to kinematic chains including both human segments and robot links, any kind of isomorphism test produces false-positives, because robot and human links would be treated the same way. This happens because isomorphism tests are "blind" with respect to the special condition which involves considering both human segments and robot links as part of a unique kinematic chain. A false positive happens any time the permutation, which maps one graph into the other, affects any of the human joints. From the perspective of designing a WR aimed at a certain kind of interaction with each of the human joints, such solutions correspond to actual different WR topologies and must not be discarded. An example of two isomorphic but not HR-isomorphic solutions is shown in Fig. 13.3. To recognize such kind of solutions, a modified version of the isomorphism test has been introduced and named *HR-isomorphism* test (since it applies to kinematic chain including both human and robot structures). This test basically consists of assessing, after a classical characteristic polynomial-based

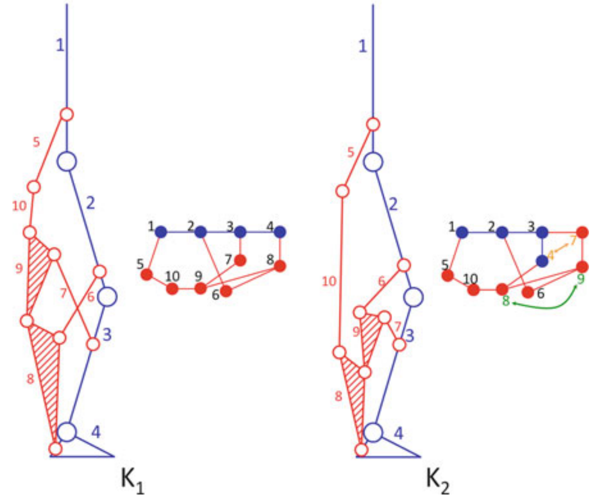

Fig. 13.3 Two isomorphic but not HR-isomorphic solutions. The permutation mapping K_1 into K_2 is given by the permutation vector [1 2 3 7 5 6 4 9 8]. This permutation maps link 4 (i.e. foot) into robot link 7. It can be noticed that local kinematic properties around each human joint (for example DOFs of the subchain including the hip, the knee and the ankle joints) are different in the two kinematic chains

isomorphism test, whether one of the permutations p_{adm} contained in a properly defined set P_{adm} is responsible for mapping one kinematic chain into another. Every permutation vector contained in the P_{adm} set is of the form $p_{adm}(i) = [1\ 2\ 3\ 4\ \mathrm{perms}_i(5{:}n)]$, where the function $perms_i$ provides the i^{th} element of the set of permutations of the elements in the input array.

13.3.2 Application to a Two-DOF Lower Limbs Wearable Robot for Hip and Knee Assistance

The developed method is applied to the design of the LENAR (Lower-Extremity Non-Anthropomorphic Robot) for hip and knee assistance in the sagittal plane. A design optimization is carried out to minimize static torques demanded to actuators to provide gait assistance. Due to the considerations reported above, the following hypotheses/constraints are imposed:

1. robot kinematic design is not fixed a-priori and can be possibly non-anthropomorphic;
2. only solutions involving revolute joints are considered;
3. the desired number of DOFs of the parallel structure, comprising both human segments and robot links, is two;
4. simultaneous and independent movements of the hip and the knee joints must not be constrained (i.e. the structure must not to impose unnatural kinematic constraints to the addressed human joints).

The method described in Sect. 13.3.1 allowed to exhaustively list all the independent kinematic structures of planar kinematically-compatible wearable hip-knee robotic orthoses, respecting the constraints reported above. Ten generalized

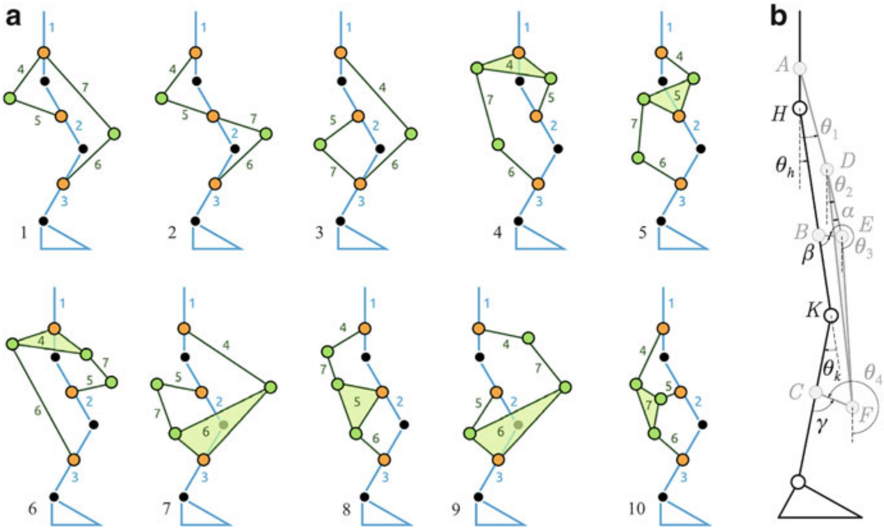

Fig. 13.4 (**a**) Arbitrary structural representation of the ten generalized solutions for the design problem addressed. Human segments are reported in blue, and human articulations are reported in *black*. Robot joints are reported in *orange* (on attachment sites) and in *green* (Adapted from [39]). (**b**) Kinematic scheme of the selected WR design (*black*), worn by a subject (*gray*). Actuated joints are joints A and joint D, that guarantee controllability of hip posture and knee posture with two DOFs

solutions (topologies) are admissible in the considered design problem, as shown in Fig. 13.4. Such solutions represent the most synthetic form of describing the mechanical optimization problem described so far.

We applied a heuristic topology selection criterion based on a static ergonomics principle: correct force interaction in WRs is based on the transfer of forces to human segments only in the direction orthogonal to the bones. If the connection between a human segment and the robot is implemented through a binary passive link (i.e. with two passive revolute joints at its extremities), static forces applied on the human segments are necessarily directed along the connection link axis.

No forces along the orthogonal direction can be present, since no torque can be applied by passive joints. If said passive link is orthogonal to the human segment to which it is connected, the transfer of forces can be statically optimized based on simple geometric considerations (i.e. the attached link must be orthogonal to the addressed segment). Using this criterion, we investigated which of the ten topologies in Fig. 13.4 allowed links 5 and 6 (respectively connected to the thigh and shank) to be completely passive and orthogonal to human segments (labeled with 2 and 3). Three topologies (4, 6 and 10) guarantee in principle such condition, while still allowing independent control of hip and knee movements by actuating the two remaining joints. Topology 10 was finally selected, since it allows to reduce size and weight and to better distribute masses and inertias along the lower limb. A schematic of the resulting kinematic chain is shown in Fig. 13.4b.

13.3.2.1 Morphological Optimization of a Non-anthropomorphic Wearable Robot for Hip-Knee Assistance During Gait

A model of the chosen generalized solution was developed, as described in more detail in Sergi et al. [40], allowing to calculate the torques required to actuators to guarantee a physiological gait [34], for a generic set of parameters defining the structure shown in Fig. 13.4b. By using the mentioned model, morphological optimization was carried out, using a custom scalar fitness function, designed in order to take into account known limitations of actuators purposively developed for this wearable robot (Sect. 13.4), and in order to guarantee a high desired level of ergonomics of force interaction.

Using standard walking datasets reporting kinematic variables of level-ground walking (hip and knee angles $\theta_h(t)$ and $\theta_k(t)$), as well as inverse-dynamics calculated equivalent torques exerted by subjects (hip and knee torques $\tau_h(t)$ and $\tau_k(t)$), the corresponding actuator torques $\tau_{m1}(t)$ and $\tau_{m2}(t)$ and interaction forces at the points of contact *A, B* and *C* could be calculated. In particular, the components of interaction forces in contact points *B* (shank) and *C* (thigh) were decoupled into the component perpendicular to the connected body segment F_{perp} and the component parallel to it F_{shear}.

Workspace maximization was introduced as another optimization objective. In particular, increasing robustness of the design with respect to kinematic singularities was a highly sought design target, considered the specific application of the parallel WR. To this aim, passive angles values were individually checked for parallelism throughout the entire planar workspace of the robot. The occurrence condition of a singular configuration was that the angle between two passive links fell below a threshold, set to 30 ° in the optimization. Singularity is signaled by a binary variable $sing(\theta_h,\theta_k)$. The posture at which a singular configuration occurred was taken into account, by specifying a singularity weighting function $w_{sing}(\theta_h,\theta_k)$, designed to take into account the distance between the posture at which a singular configuration was detected and the nominal trajectory of the hip and knee joints during nominal gait, as shown in Fig. 13.5.

In order to account for both actuator limits on the maximum applicable torque, to avoid transfer of excessive interaction force along the supported segment axis and to increase robustness of the design with respect to singularities, the following scalar transfer functions were defined:

$$\begin{aligned} fitness_\tau &= \max\left(\tau_{m1}(t), \tau_{m2}(t)\right)/\tau_{max} \\ fitness_F &= \max\left(F_{sh,B}(t), F_{sh,C}(t)\right)/F_{max} \\ fitness_{sing} &= \sum_i \sum_j sing\left(\theta_{h,i}, \theta_{k,j}\right) \cdot w_{sing}\left(\theta_{h,i}, \theta_{k,j}\right), \end{aligned} \tag{13.3}$$

having defined the normalization values $\tau_{\max} = 50$ Nm and $F_{\max} = 30$ N. Solutions with singularities within the closed region defined by hip and knee profiles

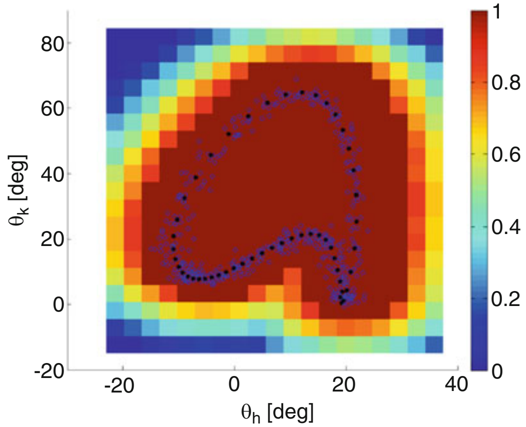

Fig. 13.5 Colormap of the weighting function w_{sing} used for weighting the occurrence of a singular posture during optimization. The weighting function is normalized in the range [0, 1] and assumes highest values inside the closed region defined by level-ground walking, in hip and knee angle coordinates, and degrades to smaller values, for postures more distant from an admissible posture during walking

during overground walking were discarded during optimization, and the remaining solutions were evaluated using the composite scalar fitness function, defined as:

$$fitness = fitness_{\tau} + fitness_{F} + fitness_{sing}. \tag{13.4}$$

A hybrid optimization strategy has been employed in order to explore the nine-dimensional space. The optimization algorithm consists of the consecutive application of a Genetic Algorithm (GA)[1] and a deterministic constrained non-linear optimization (CNLO)[2] method (using MATLAB fmincon function). The latter was used to perform a local optimization, using the best individual produced by the Genetic Algorithm as starting point. The fittest solution was selected for the final design, and the resulting relevant functions considered in the optimization are described in Fig. 13.6. The optimized solution requires a peak actuator torque of 52 Nm for level-ground walking of a subject with mass 80 kg, compared to peak hip and knee torques, calculated via inverse kinematics, equal to 48 Nm. Furthermore, the maximum shear force transferred to the supported body segments equals 21 N. The optimized solution was fabricated and integrated with custom designed actuators, as detailed in the next sections.

[1]GA parameters: Population Size: 40, Max Generations: 100, Scattered Crossover with Fraction: 0.8, Elite count: 2, Migration Fraction: 0.4, Migration Interval: 5, Stall Generations Limit: 15, Function Tolerance: 10^{-5}.

[2]The "active-set" algorithm was used. Maximum number of iterations: 100, Parameters Termination Tolerance: 10^{-9}.

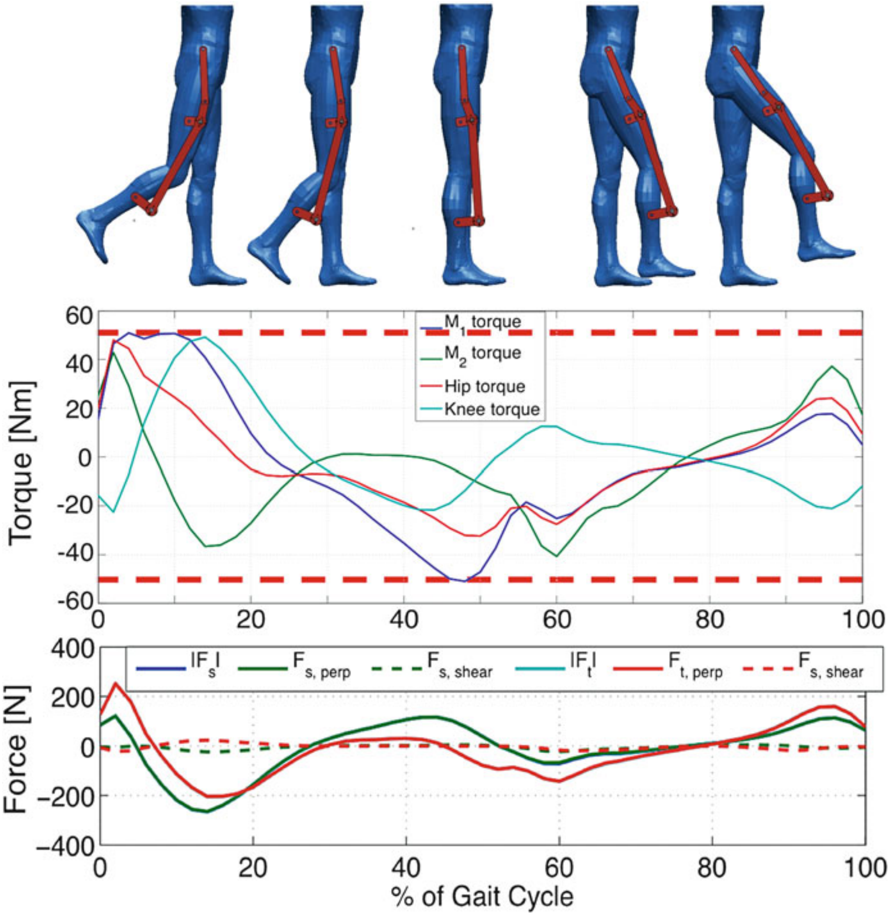

Fig. 13.6 (*Top*) Poses of the mechanism during different phases of a walking cycle. Profiles of (*middle*) actuator torques and (*bottom*) forces at the attachment points *B* (shank) and *C* (thigh), for the optimized solution corresponding to the inverse dynamics simulation of the system, for level-ground walking of a subject with mass equal to 80 kg

13.4 Compliant Actuators and Joints

The need of a safe pHRI is crucial in assistive WRs, which are not required to simply move the limbs according to prescribed patterns, but should offer an amount of assistance adapted to the residual motor capabilities of the subjects. In this case a high level of biomechanical compatibility and dynamical adaptability is desirable. These machines have to be as transparent as possible to the active motion of the users and to provide assistance as needed in conditions where they are not able to complete a prescribed motor task. The need to stably and robustly regulate human-robot dynamic interaction, also on the basis of the variable level of assistance

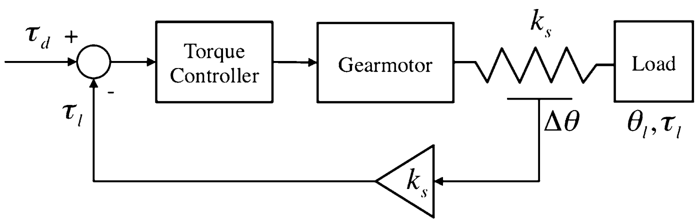

Fig. 13.7 Torque control scheme for a rotary SEA. τ_d represents the desired torque, k_s the stiffness of the series elastic element, $\Delta\theta$ the spring deflection, τ_l the output torque and θ_l the output angle

required by the subjects, entails the use of actuators operating in an ideal force (or torque) mode control. This implies theoretical zero output impedance (i.e. perfect back-drivability) and high force (torque) control fidelity.

The smart inclusion of springs in the mechanical structure can effectively reduce both the power and energy requirements demanded to an actuator [41, 42]. This is because a spring can store and release energy efficiently during cyclic repetitive tasks. Reproducing passive elastic properties of human and animal joints can also enormously improve the energetic efficiency of legged robot, especially in the case of running and hopping machines, as demonstrated in pioneer works in the early 1980s both in simulation and in prototypal implementations [43].

The interposition of a compliant element between an actuator and its load was originally presented in Pratt and Williamson [44] and Pratt et al. [45]. The proposed prototype, named Series Elastic Actuator (SEA), was a linear actuator. A number of rotary systems have been developed in recent years [40, 46–53] (Fig. 13.8).

SEAs provide several advantages:

- shock tolerance;
- motor inertia is decoupled from the output link;
- the compliant element protects the motor and gearbox in case of impacts;
- output torque/force can be calculated from the measure of the elastic element deflection;
- the effects of stiction, friction, backlash and other non-linearities are reduced;
- work and power output of the actuator can be increased if an appropriate series elasticity is selected according to a specific task;
- in cyclical and/or explosive tasks efficient energy storage/release can be achieved;
- the high-frequency impedance of the actuator is limited to the stiffness of the elastic element.

Rotary SEAs are typically torque-controlled, using the representative control scheme depicted in Fig. 13.7. In this general scheme, the spring deflection $\Delta\theta$ provides an estimate of the torque exerted by the actuator τ_l; this measure is used as feedback signal for torque control.

The stiffness of the series elastic element must be carefully selected in order to trade-off between performances, adaptability and safety. Moreover, the dimensions

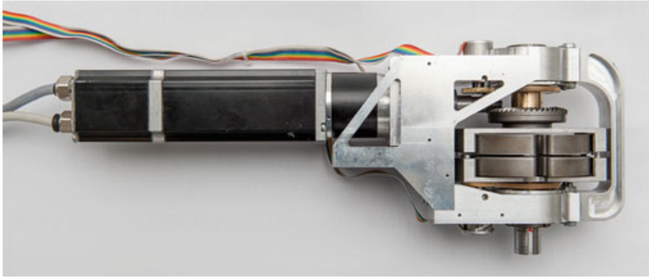

Fig. 13.8 Rotary SEA developed for the LENAR Peak torque: 55 Nm; torque control bandwidth: 5.0 Hz. The custom-designed spring pack has a rotary stiffness of 272.3 Nm/rad. The interaction force is measured with a quantization of 2.6×10^{-2} Nm, using two 15 bit absolute encoders

and weight of the spring have to be reduced as much as possible, especially for wearable robotics applications. In order to be included in a torque control scheme, a compliant element for a SEA is then required to be verified against the maximum output torque supplied by the actuator and to possibly provide a linear torque vs. rotation relationship both in static and dynamic conditions to guarantee an accurate torque estimation and consequent control performance. Several solutions in literature have been proposed to overcome these design challenges. To implement the desired output torsional stiffness some authors have adopted linear compression springs to mimic a torsional stiffness [50, 54–56], while others have used compliant elements embedded in the transmission train or custom torsional springs directly connected to the load [46, 47, 49, 57].

Nevertheless, series elasticity causes a degradation of performances in terms of control bandwidth with respect to traditional rigid actuation systems [58]. This limitation can be overcome using elastic elements whose properties can be varied during operation. The aim of independently regulating motion and impedance field to improve performances as well as stably controlling robots interaction forces with external agents have steered to the development of *Variable Stiffness/Impedance Actuators (VSA/*VIA*)*, which are obtained by means of redundant actuation solutions [59, 60], i.e. including a number of active elements higher than the number of actively controlled DOFs.

Finally, impedance may be tuned by resorting to passive joints, with tunable mechanical impedance [61, 62].

13.5 Control

The control of WRs must assure that users' limbs are not forced towards harmful configurations and that no dangerous forces are imparted. Additionally, user's motion intentions have to be accommodated, shaping the action of the robot around subject's residual sensory-motor capabilities, behavior and motor style.

To this aim traditional stiff position-controlled robots and pre-defined motion patterns become inadequate and interaction control schemes, underlying proper force modulation, intention recognition and adaptation features have to be adopted. This is even more critical if a restoration of physiological behaviors based on subject-specific features is targeted.

13.5.1 Interaction Control

Conventional approaches to achieve direct or indirect force modulation [63] include: (i) *Explicit (or direct) force control* [64]: a force servo is implemented since the desired force is directly regulated closing a force feedback loop. (ii) *Stiffness* and *damping control* [65]: where a virtual spring or damper is created around an equilibrium position. (iii) Impedance control [66], generalizes the concepts of stiffness and damping controls. The position and velocity are commanded to follow an equilibrium trajectory and the controller modulates robot behavior as a viscoelastic or as a second-order system (if also virtual inertial contribution is considered). Control gains, setting virtual stiffness, damping and inertia, directly correlate with stability and bandwidth. (iv) *Hybrid position/force control* [67] combines position control, employed in unconstrained directions, with force control in interaction with external agents (e.g. obstacles). More sophisticated control algorithms can be basically considered as an evolution of these basic schemes.

In kinesthetic robotics [68] an alternative to impedance control is constituted by admittance control, which consists in measuring interaction forces to display desired admittance through position servos. This strategy allows displaying high virtual stiffness and mass but it asks for high positioning bandwidth, and hence for high-power and high-impedance actuators. Impedance controlled robots typically lack performance in kinesthetic display of high impedance but this is not critical in robotic physical assistance since no extremely stiff contact or large mass/inertia have to be displayed. For these reasons impedance control is commonly preferred.

Impedance control allows variable deviation from reference trajectory depending on the user's performances and provides comfortable assistance since robots are not perceived as too rigid or obtrusive. Therefore, high-impedance mode is used when the subjects need a high level of assistance and, in the worst case, they are completely unable to move (a predefined kinematic pattern has to be rigidly imparted). On the other hand, in low-impedance mode the subjects must be guided and assisted with a weak intervention and without altering their natural motion. Ideally they should not be hindered when null impedance is set and the robot is desired to be fully transparent. In the control of WRs these two opposite behaviors have to be guaranteed, both for therapeutic reasons in rehabilitation scenarios and for adaptation to different levels of disability in assistance applications.

The stability of interaction control schemes depends on the dynamic characteristics of the robot and of the interacting system. Pioneering studies on direct force control of manipulators explored sources and solutions to instabilities caused by interactions with the environment (*coupled instability*) [69, 70]. In Colgate and Hogan [69] it was shown that a robot, which is stable when no interaction occurs (*isolated stability*), can exhibit unstable behaviors when interacting with passive environments, such as springs or masses. A simplified analysis on linear, time-invariant systems in Colgate and Hogan [69] showed that a (force) feedback controlled plant is stable during interaction if it has the interaction port behavior of a passive system, i.e. the transfer function of the impedance at the interaction port is a positive real function. This condition basically quantifies the concept that the system, for any time period, cannot deliver more energy at its interaction port than that introduced into it. This condition is valid for interactions with arbitrary stable, passive environments. Passivity-based control laws guarantee robust performance with respect to uncertainties and they can be used for a safe pHRI [71]. Even though passivity criterion ensures stability only with passive environments, the successful interaction with the human motor system (basically non-passive because of time delays in sensory feedback loops) is due to the limited frequency content and energy production of active human motion [72]. Hence, since the magnitude of human limbs impedance is quite bounded, passivity criterion, as stability measure, may be often regarded as overly conservative.

13.5.2 Control of Compliant Actuators

Impedance control demands actuators to be ideal force/torque sources. To this aim, it is useful to decouple the dynamics of the actuator and the load by intentionally interposing a compliant element. The introduced series elasticity complicates both the actuator design and control, reducing the controllable bandwidth due to saturation effects that limit the maximum achievable motor velocity in deflecting the spring [58].

Different approaches to SEA control have been proposed in literature. First solutions were based on the regulation of motor current with feed-forward compensation of motor inertia [73]. Current regulation was replaced by position control in Pratt et al. [74] while in Wyeth [55] a velocity loop nested in an external torque loop was proposed, thus considering the motor as an ideal velocity source. In Kong et al. [75] torque regulation was based on a PD controller coupled to a disturbance observer that compensated for model errors and plant variations. A similar model-based approach was presented in Grun et al. [76].

Passivity conditions for the control of SEAs based on inner velocity control loop was derived in Vallery et al. [77]. It was demonstrated that for stiffness-controlled SEA, the maximum renderable stiffness equals the physical stiffness of the series elastic element, if conservative demands for passivity are to be met.

13.5.3 Robot Adaptation and Intention Detection

WRs have to adapt to cognitive and motor capabilities of the users. In the case of assistance for motor (e.g. gait) restoration, residual functions have to be taken into account, similarly to what happens in neuro-rehabilitation, where the active participation of the subject is crucial to optimize motor recovery (AAN paradigm, [78, 79]). On the other side, a non negligible factor is also the adaptation of the user to the external robotic agent: the human learning capability causes a re-modulation of muscular activity to cope with and benefit from the external assistive actions exerted by the robot [80] reducing the effort in performing a task but simultaneously keeping the control of the device. Therefore, human-robot coupled adaptation is fundamental mechanism to be taken into account.

From these considerations it is clear that strategies to detect user's intention and to synchronously adapt robot behavior in a natural and smooth fashion are strongly needed. A possible intention detection strategy consists in using interfaces with the central or peripheral nervous system ([81]; Velliste et al.). Nevertheless, these solutions are highly invasive and implants are not yet sufficiently reliable/durable.

A number of controllers based on the measurements of electromyographic signals (EMG) have been explored [82–84]. These controllers estimate the muscular force, and consequently the joint torque, from EMG measurements, using model-based [85] or model-free [86] approaches, and provide assistive torques as a fraction of the one to be exerted by the subject. EMG-based approaches can pose some issues in terms of signal acquisition, subject-specific calibrations (intra and extra experimental sessions), electrode positioning, and skin condition. Moreover, model-based torque estimation is computationally demanding, sensitive to subject anatomy and to electrodes placement. Anyhow, compared to inverse dynamics techniques, EMG-based methods do not require dynamic models of the limbs and of their interaction with the environment/robot.

Another interesting approach to predict the limbs motion consists in extracting kinematic anticipatory information from the movements of different body district using wearable sensors. In particular, biomechanical and motor control studies evidenced that the movements of the human body segments are dynamically coupled [87] (e.g. postural stability during walking can only be achieved by the upper and lower body coordination). For example, the upper body (especially head and arms) motion has a natural anticipatory informative content with respect to locomotion activities, which can be exploited to improve the detection of human intention and to regulate the controllers of WRs, thus achieving simpler and more natural adaptation to the human. In the field of gait analysis, wearable sensors have quickly advanced and networks able to perform even complex tasks, such as fall detection, have been developed [88]. In the same way it is possible to estimate voluntary intention to start and stop walking. When gait is initiated, the user objective changes from staying in a stationary position to achieving the balance needed to stabilize walking. Gait termination is characterized, on the other hand, by increased braking forces of the lead foot and by a reduction of trail foot push-off during the final steps. Based on these kinds of information, in Novak et al. [89] a method to detect gait initiation and termination using inertial measurement units, sensorized insoles and machine learning algorithms was presented.

Another promising and non-invasive approach, useful in case of periodic motion, consists in predicting movements directly from the observation of joint kinematics [90]. The strategy exploits the concept of motor primitives, i.e. the idea that complex motor behaviors can be described as the composition of simple elementary blocks. A non-linear dynamical system can be derived able to synchronize itself with complex human movements with a finite set of parameters. This system is based on Adaptive Frequency Oscillators (AFOs), mathematical tools developed in Righetti et al. [91] for many applications [92]. An AFO is expressed as a dynamical system characterized by a limit cycle. Its parameters (amplitude, frequency, phase, etc.) can adapt to an external input, such as the human kinematics, thus reflecting the real-time user intention about the performed movement. This approach has been successfully used to control upper and lower body exoskeletons [93].

13.6 Experimental Tests with a Compliant Non-anthropomorphic WR

In this section we report on tests exemplifying the main aspects presented in the previous sections. In the tests, performed on healthy subjects, a stiffness-controlled non-anthropomorphic robot with SEAs establishes a symbiotic interaction with the user, by predicting walking kinematics through the observation of residual voluntary movements (further details can be found in Tagliamonte et al. [94]).

The LENAR, depicted in Fig. 13.9, is composed (for each leg) of: (i) Supporting links, whose kinematic structure been designed starting from the optimization process described in Sect. 13.3. (ii) Two rotary SEAs connected to joints A and D; (iii) Cuffs at the pelvis level (joint A), at the thigh level (joint B) and at the leg level (joint C). The segment EF can be manually adjusted to make robot kinematics to be compatible with different users. Other regulations (position of the joints A, B and C on the pelvis cuff, the thigh cuff and the leg cuff respectively) are allowed by sliders.

The treadmill-based platform is shown in Fig. 13.10. The WR is suspended to a support system able to passively compensate its weight, without introducing resonance frequencies so to minimize the inertia perceived by the subjects. Cables are used to connect the weight balancing system to the pelvis cuff. Hip and torso rotations are unconstrained.

Each of the four SEAs is torque-controlled. The employed control scheme is based on the cascaded approach proposed in Vallery et al. [95], and described in Sect. 13.5. The robot is stiffness-controlled in the joints space. The torque for each actuated joint (right r and left l leg) is set as:

$$\tau_{mi,d}(t) = -k_{mi}\,[\theta_{mi}(t) - \theta_{mi,d}(t)] \tag{13.5}$$

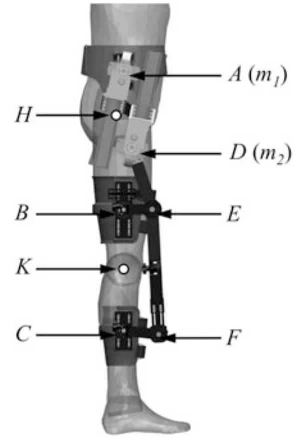

Fig. 13.9 Blank circles, *H* and *K*, represent the human hip and knee joints respectively. *A* and *D* are the actuated robotic joints, also indicated as m_1 and m_2

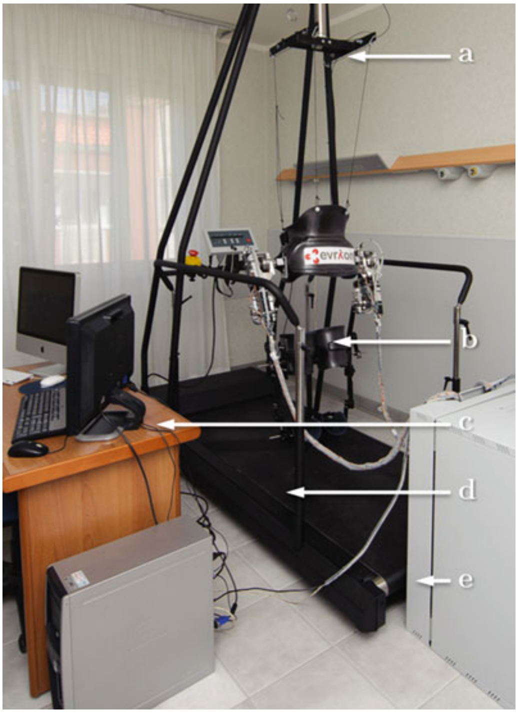

Fig. 13.10 Treadmill-based platform. (**a**) Robot weight support system; (**b**) Wearable robot; (**c**) Control station; (**d**) Treadmill; (**e**) Electronic rack

with θ_{mi} and $\theta_{mi,d}$ actual and desired actuators rotations respectively, k_{mi} the virtual stiffness ($i = 1, 2$).

The block scheme of the control of a single SEA is represented in Fig. 13.11.

Assistive torques are provided following the approach proposed in Ronsse et al. [93], based on a pool of AFOs, which learn periodic joints angles $\theta(t)$ in steady-

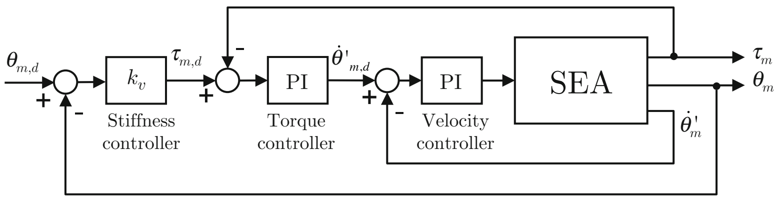

Fig. 13.11 SEA control scheme. τ_m, θ_m are the output torque and angle respectively; $\dot{\theta}_m$ is the motor velocity. Torque controller generates a desired velocity value $\dot{\theta}_{m,d}$ as set-point for the velocity controller. Stiffness controller generates a desired elastic torque with virtual stiffness k_v

state conditions. In addition, the oscillators are coupled to a non-linear filter, a sum of weighted Gaussian-like kernels as a function of the phase. An iterative local regression continuously learns the weights to estimate joint angle $\widehat{\theta}^*(t)$. Therefore, joint angle at a time corresponding to $\Delta\phi$ phase lead in the future $\widehat{\theta}^{*,\Delta\phi}(t)$ is derived. For each joint the assistive torque is calculated as in (13.5) by setting $\theta_{mi,d} = \widehat{\theta}_{mi}^{*,\Delta\phi}$. With this approach the user is attracted by elastic torques towards her/his estimated future kinematic status, having the possibility to continuously adapt the frequency and the amplitude/shape of the attractive pattern.

Experimental tests were performed to assess torque tracking capabilities of the SEAs. The output shaft of each actuator was connected to a torque sensor to measure torques delivered, while measuring spring deflections. Torques and deflections data were fitted, obtaining a stiffness of 270.2 ± 3.1 Nm/rad. Torque control regulation was evaluated by connecting the output shaft of the SEA to the frame (i.e. considering the deflection of the elastic element without any external load disturbances). The transfer function between desired and actual torque was determined by using a non-parametric identification method [96] and setting as desired torque a waveform with a flat spectrum in the range 0.1–10 Hz and peak torque 15 Nm. An almost flat transfer function was found, with an amplitude attenuation of 3 dB at about 6.5 Hz.

To estimate the order of magnitude of the torques needed to actuate the robot in the free space, physiological walking movements were produced with the robot not worn. Results demonstrated that necessary torques were lower than 12 % of the maximum allowable of the actuators (mainly gravitational and friction effects had to be compensated since the test was performed at slow walking speed) while the remaining 88 % is available to provide physical assistance.

A voluntary healthy subject (male, 28 years old, height 180 cm, body mass 80 kg), was asked to walk on the treadmill wearing the robot suspended to the weight support system. Cuffs were fastened to minimize their relative motion during trials but also to assure user's comfort. Before the tests, the subject was asked to freely walk at a self-selected walking speed for 10 min (robot unpowered) to get familiar with the device.

Back-drivability tests aimed at evaluating robot intrinsic transparency, i.e. at verifying that a human subject can walk physiologically even though the robot is

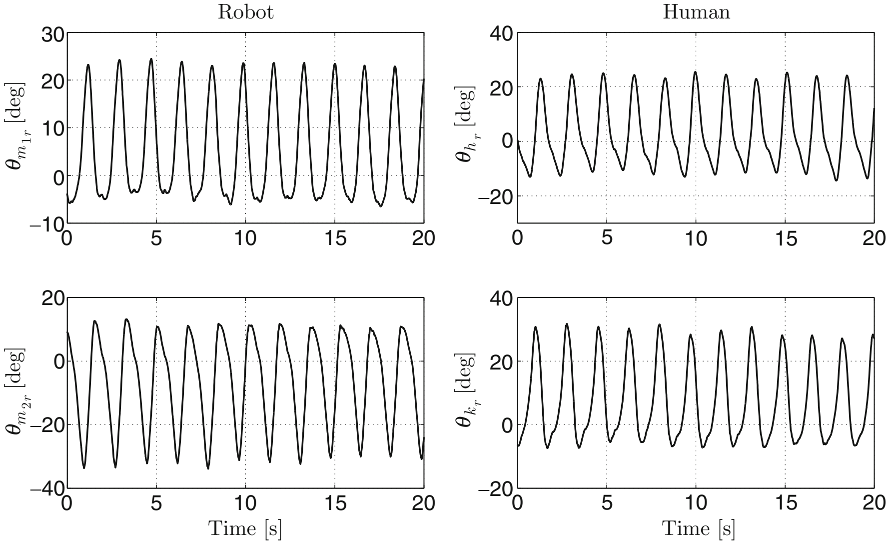

Fig. 13.12 Robot actuator and human joint rotations for the back-drivability test performed at a walking speed of 2.5 km/h. Representative data for the right leg, in steady-state conditions, are reported

unpowered. For this test, actuators were turned off and the user had to back-drive the robot at different walking speeds (2.0, 2.5 and 3.0 km/h). Robot actuated joints rotations (θ_{mir} and θ_{mil}, $i = 1, 2$) and human-robot interaction torques in the robot joint space (τ_{mir} and τ_{mil}, $i = 1, 2$) were recorded; angles (θ_h and θ_k) and torques (τ_h and τ_k) in human joint space were calculated. In Fig. 13.12 robot actuators and human joints angles of the right leg are reported for a representative test at a walking speed of 2.5 km/h. The Gait Cycle (GC) for this test (calculated averaging on ten periods) is 1.71 s. Interaction torques for the same test, average and standard deviation calculated on ten cycles, are reported in Fig. 13.13 in human joint domain.

Back-driving torques were found to be in the order of 10 Nm (i.e. 15–20 % of torques delivered by human joints during overground walking). This result demonstrates the low mechanical impedance of the actuated joints (SEAs).

In assistance tests the subject was initially asked to walk freely at a self-selected walking speed (2.5 km/h), with robot actuators switched off. In this phase, AFOs could learn kinematics in the robot joint space $\widehat{\theta}^*_{mi}$ and calculate it with a predefined phase lead in the future (set to 10 % of the gait cycle). A representative kinematic prediction is reported in Fig. 13.14.

Estimated kinematics only requires few gait cycles to converge to the actual profiles. In Fig. 13.15 torques delivered by the four actuators during assistance test are depicted. At $t = 24.5$ s assistance is enabled and virtual stiffness is set as $k_{mil} = k_{mir} = k_v$ (i =1, 2). Then, its value is manually changed as reported in the lower graph of the Fig. 13.15. Modifying virtual elasticity corresponds to changing

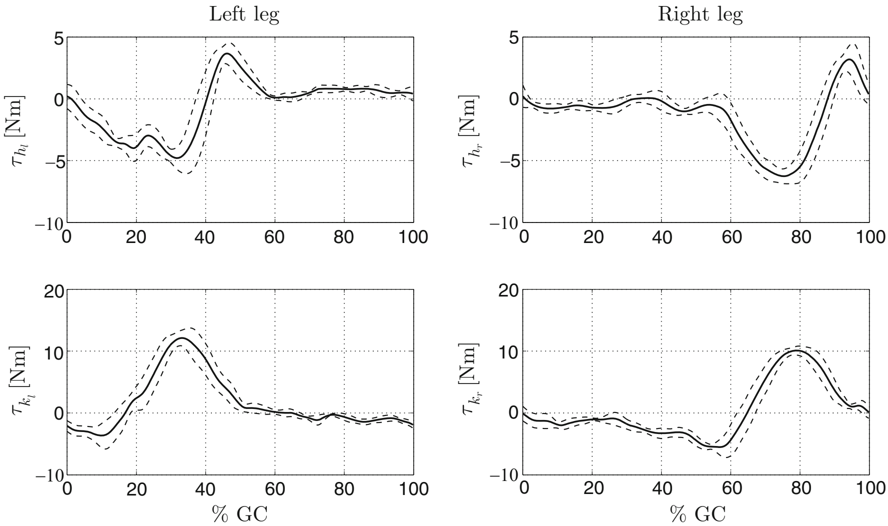

Fig. 13.13 Human-robot interaction torques in the human joint space (as a function of the percentage of the GC) for the back-drivability test performed at a walking speed of 2.5 km/h. Data are averaged over ten gait cycles. Solid line: mean torque; dashed lines: standard deviation

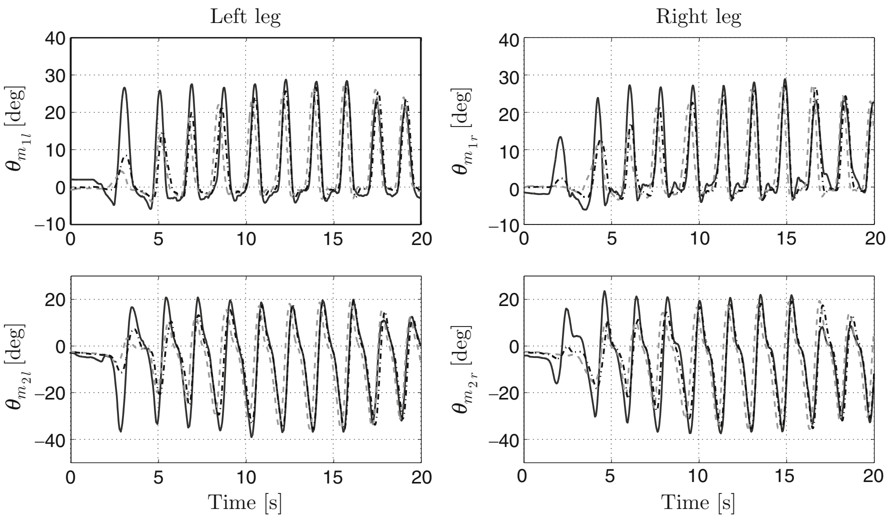

Fig. 13.14 AFO-based kinematic estimation in the robot joint space with actuators switched off during a test at 2.5 km/h walking speed. *Solid line*: measured angle; *dashed black line*: estimated angle; *dashed gray line*: predicted (shifted) angle. The phase shift is set to 10 % of the GC

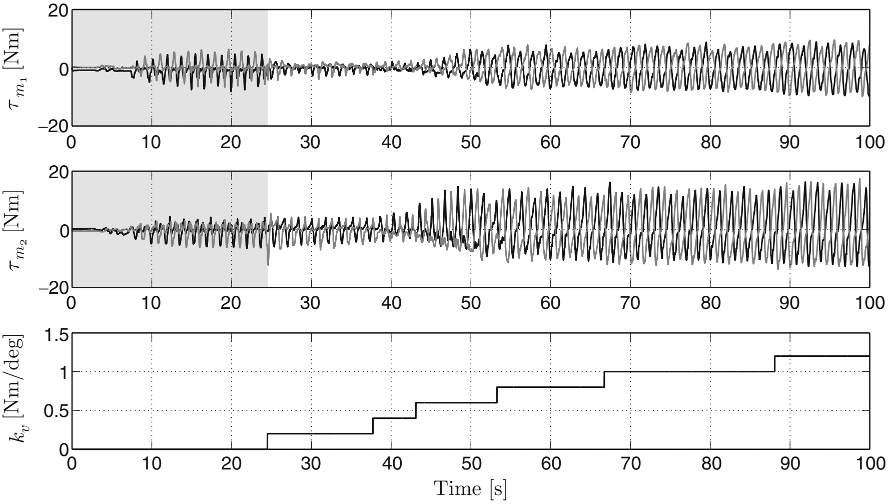

Fig. 13.15 Actuator torques delivered during the assistance test. *Black line*: right leg; *Gray line*: left leg; *Gray band*: unassisted mode (actuators powered off). At $t = 24.5$ s assistance is enabled. Virtual stiffness was manually changed as reported in the lower graph

assistance level, since the robot produces physical support with a more or less rigid behavior. Starting from the case of disabled actuators, interaction torques initially reduced for low values of assistance, then increased, producing assistance.

13.7 Conclusions

Design is a creative activity, inherently centered on the designer's technical insights. Whereas conventional design methodologies are effective in several application fields for robotics technology, a number of issues arise in the case of WRs, since they have to cope with the human body own dynamics, influenced by a number of concurrent biomechanical, physiological and neurological factors, sometimes not yet completely understood.

An emerging design paradigm for robotic systems is based on Embodied Intelligence, i.e. on the idea of introducing some level of morphological computation in the structural subsystem of a mechatronic machine. This approach tends to allocate some basic control function to the "body" of the robot, for simplifying the higher levels of control and reducing the need for embedded sensors and computational units.

The concept of Embodied Intelligence also applies to the human body, which can be considered as one of the most advanced examples of 'biomechatronic' system capable of performing useful morphological computation to improve its own performance while interacting with the environment. This appears particularly evident in the case of walking, where the biomechanics of the lower limbs and the synchronized movements of the arms assure smooth periodic energy exchanges between the muscular springs, the body mass and the environment, leading to limit cycles which correspond to proper walking patterns. This concept has been, and is being, intensively investigated for the development of walking bipedal robots, where the design of a mechanical structure, endowed with the proper dynamics, greatly simplifies the achievement of desired behaviors.

In the case of WRs, the human body and the robot have to be treated as a symbiotic system, where the biological and the artificial components dynamically interact with each other (e.g. exchanging assistive forces) and, as a single whole, with the external environment. In this scenario, the artificial component has to be designed so that the symbiotic compound system (human + robot) exhibits the desired emerging behaviors, such as a physiologically restored gait. Since this behavior is elicited, and not imposed by the machine, this approach intrinsically builds upon the residual motor capabilities of the user. In this sense, gait restoration in elderly and/or disabled people is obtained by augmenting the (possibly limited) residual capabilities of the user. This approach, inherently open-ended since the topology/morphology of the robot has to be considered as a design variable, is computation intensive, and relies on modeling and optimization tools. As such, also the model of the biological component (i.e. the user) is central. The development of such a model still appears as a major research challenge, deserving intense efforts.

Indeed, the open-ended design approach needs to take into account biomechanical constraints, such as kinematic compatibility, and technological limitations in the fabrication of the actual device. In this chapter these aspects were addressed presenting methods to enumerate possible human-compatible topological solutions and to optimize morphological parameters. Technological actuation solutions exploiting intrinsic compliance were presented. Interaction control schemes and intention detection strategies were also discussed.

As a case-study of the presented design aspects, some pilot tests on a newly developed non-anthropomorphic robot were reported, demonstrating some of the potentialities of the novel design methodology proposed by the Authors. In this regards, re-engineering the traditional machine design cycle in order to exploit the potentialities of Embodied Intelligence can be considered as a major, novel and promising research avenue, whose exploration is only at its beginning.

References

1. Pons JL (2008) Wearable robots: biomechatronic exoskeletons. Wiley, Chichester
2. Yagn N (1890) Apparatus for facilitating walking, running and jumping. US Patent 420179
3. Dollar AM, Herr H (2007) Active orthoses for the lower-limbs: challenges and state of the art. Transport 1:968–977
4. Kubow T, Full RJ (1999) The role of the mechanical system in control: a hypothesis of self-stabilization in hexapedal runners. Phil Trans R Soc Part B 354:849–861

5. Pfeifer R, Lungarella M, Iida F (2007) Self-organization, embodiment, and biologically inspired robotics. Science 318:1088–1093. doi:10.1126/science.1145803
6. Brown IE, Loeb GE (2000) Biomechanics and neuro-control of posture and movement. Springer, New York
7. Full RJ, Tu MS (1990) Mechanics of six-legged runners. J Exper Biol 148:129–146
8. Cham JG, Bailey SA, Cutkosky MR (2000) Robust dynamic locomotion through feedforward-preflex interaction. In: ASME International Mechanical Engineering Congress & Exposition (IMECE 2000), Orlando, Florida, November 5–10, pp 5–10
9. Collins S, Wisse M, Ruina A (2001) A three-dimensional passive-dynamic walking robots with two legs and knees. Int J Robot Res 20:607–615
10. Mcgeer T (1990) Passive dynamic walking. Int J Robot Res 9(2):62–81
11. Collins S, Ruina A, Tedrake R, Wisse M (2005) Efficient bipedal robots based on passive-dynamic walkers. Science 307:1082–1085. doi:10.1126/science.1107799
12. Matsushita K, Yokoi H, Arai T (2006) Pseudo-passive dynamic walkers designed by coupled evolution of the controller and morphology. Robot Autonomous Syst 54:674–685. doi:10.1016/j.robot.2006.02.016
13. Kazerooni H, Steger R, Huang L (2006) Hybrid control of the Berkeley lower extremity exoskeleton (BLEEX). Int J Robot Res. doi:10.1177/0278364906065505
14. Zoss A, Kazerooni H, Chu A (2006) Biomechanical design of the Berkeley lower extremity exoskeleton (BLEEX). IEEE/ASME Trans Mechatronics 11:128–138
15. Jacobsen SC (2007) On the development of XOS, a powerful exoskeletal robot. In: IEEE/RSJ International Conference on Intelligent Robots and Systems, October 29–November 2, San Diego, USA
16. Vukobratovic M, Borovac B (2004) Zero-moment point – thirty five years of its life. Int J Human Robots 1:157–173
17. Vukobratovic M, Juricic D (1969) Contribution to the synthesis of biped gait. IEEE Trans Biomed Eng 16:1–6. doi:10.1109/TBME.1969.4502596
18. Kawamoto H, Lee S, Kanbe S, Sankai Y (2003) Power assist method for HAL-3 using EMG-based feedback controller. In: IEEE International Conference on Systems, Man and Cybernetics, Waikoloa, Hawaii, USA, October 10–12, 2005. ISBN 0-7803-9298-1, vol 2, pp 1648–1653
19. Suzuki K, Kawamura Y, Hayashi T et al (2006) Intention-based walking support for paraplegia patient. In: 2005 IEEE International Conference on Systems, Man and Cybernetics, Waikoloa, Hawaii, USA, October 10–12, 2005. ISBN 0-7803-9298-1, vol 3, pp 2707–2713
20. Farris R, Quintero H, Goldfarb M (2011) Preliminary evaluation of a powered lower limb orthosis to aid walking in paraplegic individuals. In: IEEE transactions on neural systems and rehabilitation engineering, p 1, doi: 10.1109/TNSRE.2011.2163083
21. Veneman J, Kruidhof R, Hekman E et al (2007) Design and evaluation of the LOPES exoskeleton robot for interactive gait rehabilitation. IEEE Trans Neural Syst Rehabil Eng 15:379–386. doi:10.1109/TNSRE.2007.903919
22. Fisher S, Lucas L, Thrasher TA (2011) Robot-assisted gait training for patients with hemiparesis due to stroke. Top Stroke Rehabil 18:269–276. doi:10.1310/tsr1803-269
23. Aoyagi D, Ichinose WE, Harkema SJ et al (2007) A robot and control algorithm that can synchronously assist in naturalistic motion during body-weight-supported gait training following neurologic injury. IEEE Trans Neural Syst Rehabil Eng 15:387–400. doi:10.1109/TNSRE.2007.903922
24. Krut S, Benoit M, Dombre E, Pierrot F (2010) MoonWalker, a lower limb exoskeleton able to sustain bodyweight using a passive force balancer. In: 2010 IEEE international conference on robotics and automation (ICRA), Anchorage, Alaska, May 3–8, pp 2215–2220
25. Mokhtarian A, Fattah A, Agrawal SK (2010) A novel passive pelvic device for assistance during locomotion. In: 2010 IEEE international conference on robotics and automation (ICRA), Anchorage, Alaska, May 3–8, pp 2241–2246

26. Vallery H, Duschau-Wicke A, Riener R (2010) Hiding robot inertia using resonance. In: 2010 annual international conference of the IEEE engineering in medicine and biology society (EMBC), August 31–September 4, 2010, Buenos Aires, Argentina, pp 1271–1274
27. Bosecker CJ, Krebs HI (2009) MIT-Skywalker. In: 2009 IEEE international conference on rehabilitation robotics, ICORR 2009, 23–26 June 2009, Kyoto, Japan, pp 542–549
28. Cherry MS, Kota S, Ferris DP (2009) An elastic exoskeleton for assisting human running. In: Proceedings of the ASME 2009 international design engineering technical conferences & computers and information in engineering conference, IDETC/CIE 2009, August 30, San Diego, USA, pp 1–12
29. Beyl P, Knaepen K, Duerinck S et al (2011) Safe and compliant guidance by a powered knee exoskeleton for robot-assisted rehabilitation of gait. Adv Robot 25:513–535
30. Lipson H, Pollack JB (2000) Automatic design and manufacture of robotic lifeforms. Nature 406:974–978
31. Sims K (1994) Evolving virtual creatures. In: Proceedings of the 21st annual conference on computer graphics and interactive techniques, New York, pp 15–22
32. Dobrjanskyj L, Freudenstein F (1967) Some applications of graph theory to structural analysis of mechanisms. J Eng Ind-Trans ASME Ser B 89:153–158
33. Mruthyunjaya TS (2003) Kinematic structure of mechanisms revisited. Mech Mach Theory 38(4):279–320
34. Winter DA (1999) Biomechanics and motor control of human gait: normal, elderly and pathological, 2nd edn. University of Waterloo Press, Waterloo
35. Kutzbach K (1929) Mechanische Leitungsverzweigung. Maschinenbau, der Betrieb
36. Ding H, Huang Z (2007) A unique representation of the kinematic chain and the atlas database. Mech Mach Theory 42(6):637–651
37. Sergi F et al (2010) A systematic graph-based method for the kinematic synthesis of non-anthropomorphic wearable robots. In: 2010 IEEE conference on Robotics Automation and Mechatronics (RAM), pp 100–105
38. Sunkari RP (2006) Structural synthesis and analysis of planar and spatial mechanisms satisfying Gruebler's degrees of freedom equation. Department of Mechanical Engineering, University of Maryland, College Park
39. van den Kieboom J, Sergi F, Accoto D, Guglielmelli E, Ronsse R, Ijspeert AJ (2011) Co-evolution of morphology and control of a wearable robot for human locomotion assistance exploiting variable impedance actuators. Procedia Comput Sci 7:223–225
40. Sergi F, Accoto D, Carpino G et al (2012) Design and characterization of a compact rotary series elastic actuator for knee assistance during overground walking. In: 2012 4th IEEE RAS EMBS international conference on biomedical robotics and biomechatronics (BioRob), 24–27 June, Rome, Italy, pp 1931–1936
41. Hurst J, Rizzi A (2004) Physically variable compliance in running. CLAWAR, Springer-Verlag, www.springeronline.com
42. Raibert MH, Tello ER (1986) Legged robots that balance. IEEE Expert 1:89. doi:10.1109/MEX.1986.4307016
43. Raibert MH (1984) Hopping in legged systems – modeling and simulation for the 2D one-legged case. IEEE Trans Syst Man Cybernetics 14:451–463
44. Pratt G, Williamson M (1995) Series elastic actuators. Proc IEEE/RSJ IROS 1:399–406
45. Pratt GA, Willisson P, Bolton C, Hofman A (2004) Late motor processing in low-impedance robots: impedance control of series elastic actuators. In: American control conference, Boston, pp 3245–3251, 30 June–2 July 2004
46. Kong K, Bae J, Tomizuka M (2011) A compact rotary series elastic actuator for human assistive systems. In: IEEE/ASME transactions on mechatronics, pp 1–10, ISSN: 1083-4435, doi: 10.1109/TMECH.2010.2100046
47. Lagoda C, Schouten A, Stienen A et al (2010) Design of an electric series elastic actuated joint for robotic gait rehabilitation training. In: 2010 3rd IEEE RAS and EMBS international conference on biomedical robotics and biomechatronics (BioRob), 26–29 September, Tokyo, Japan, pp 21–26, doi: 10.1109/BIOROB.2010.5626010

48. Sensinger J, Weir R (2008) User-modulated impedance control of a prosthetic elbow in unconstrained, perturbed motion. IEEE Trans Biomed Eng 55:1043–1055. doi:10.1109/TBME.2007.905385
49. Stienen A, Hekman E, Ter Braak H et al (2010) Design of a rotational hydroelastic actuator for a powered exoskeleton for upper limb rehabilitation. IEEE Trans Biomed Eng 57:728–735. doi:10.1109/TBME.2009.2018628
50. Tsagarakis N, Laffranchi M, Vanderborght B, Caldwell D (2009) A compact soft actuator unit for small scale human friendly robots. In: 2009 IEEE international conference on robotics and automation, ICRA'09, 12–17 May, Kobe, Japan, pp 4356–4362, doi: 10.1109/ROBOT.2009.5152496
51. Veneman J, Ekkelenkamp R, Kruidhof R et al (2005) Design of a series elastic- and Bowden cable-based actuation system for use as torque-actuator in exoskeleton-type training. In: 2005 9th international conference on rehabilitation robotics, ICORR 2005, June 28–July 1, Chicago, Illinois, pp 496–499, doi: 10.1109/ICORR.2005.1501150
52. Wyeth G (2006) Control issues for velocity sourced series elastic actuators. In: Proceedings of Australasian conference on robotics and automation 2006, December 6–8, Auckland, New Zealand
53. Accoto D, Carpino G, Sergi F, Tagliamonte NL, Guglielmelli E (2013) Design and characterization of a novel high-power series elastic actuator for a lower limb robotic orthosis. Int J Adv Robot Syst 10:359
54. Veneman JF, Ekkelenkamp R, Kruidhof R et al (2006) A series elastic- and Bowden-cable-based actuation system for use as torque actuator in exoskeleton-type robots. Int J Robot Res 25:261–281. doi:10.1177/0278364906063829
55. Wyeth G (2008) Demonstrating the safety and performance of a velocity sourced series elastic actuator. In: Proceedings of the IEEE international conference on robotics and automation, 19–23 May, Pasadena, CA, USA, pp 3642–3647, doi: 10.1109/ROBOT.2008.4543769
56. Yoon S, Kang S, Kim S et al (2003) Safe arm with MR-based passive compliant joints and visco-elastic covering for service robot applications. In: Proceedings of the 2003 IEEE/RSJ international conference on intelligent robots and systems (IROS 2003), 27–31 October, Las Vegas, USA, vol 3, pp 2191–2196, doi: 10.1109/IROS.2003.1249196
57. Carpino G, Accoto D, Sergi F et al (2012) A novel compact torsional spring for series elastic actuators for assistive wearable robots. J Mech Design 134:121002. doi:10.1115/1.4007695
58. Robinson D (2000) Design and analysis of series elasticity in closed-loop actuator force control. PhD dissertation, Massachusetts Institute of Technology (MIT), Cambridge
59. Van Ham R, Sugar T, Vanderborght B et al (2009) Compliant actuator designs. IEEE Robot Automat Mag 16:81–94. doi:10.1109/MRA.2009.933629
60. Tagliamonte NL, Sergi F, Accoto D et al (2012) Double actuation architectures for rendering variable impedance in compliant robots: a review. Mechatronics 22:1187–1203. doi:10.1016/j.mechatronics.2012.09.011
61. Accoto D, Carpino G, Tagliamonte NLT, Sergi F et al (2012) pVEJ: a modular passive viscoelastic joint for assistive wearable robots. In: 2012 IEEE international conference on robotics and automation (ICRA), 14–18 May, St. Paul, Minnesota, USA, pp 3361–3366
62. Carpino G, Accoto D, Di Palo M et al (2011) Design of a rotary passive viscoelastic joint for wearable robots. In: 2011 IEEE international conference on rehabilitation robotics (ICORR), June 29–July 1, Zurich, Switzerland, pp 1–6
63. Siciliano B, Sciavicco L (2009) Robotics: modelling, planning and control. Springer-Verlag London
64. Whitney DE (1987) Historical perspective and state of the art in robot force control. Int J Rob Res 6:3–14. doi:10.1177/027836498700600101
65. Salisbury JK (1980) Active stiffness control of a manipulator in Cartesian coordinates. In: 1980 19th IEEE conference on decision and control including the symposium on adaptive processes, 10–12 December, Albuquerque, NM, vol 19, pp 95–100, doi: 10.1109/CDC.1980.272026
66. Hogan N (1985) Impedance control: an approach to manipulation: Parts I, II, and III. J Dyn Syst Measure Control 107:1–24

67. Raibert MH, Craig JJ (1981) Hybrid position/force control of manipulators. Trans ASME J Dyn Syst Meas Contr 102:126–133
68. Adams RJ, Hannaford B (2002) Control law design for haptic interfaces to virtual reality. IEEE Trans Control Syst Technol 10:3–13. doi:10.1109/87.974333
69. Colgate E, Hogan N (1989) An analysis of contact instability in terms of passive physical equivalents. In: Proceedings of the 1989 IEEE international conference on robotics and automation, 14–19 May, Scottsdale, AZ, USA, vol 1, pp 404–409
70. Eppinger S, Seering W (1987) Understanding bandwidth limitations in robot force control. In: Proceedings of the 1987 IEEE international conference on robotics and automation, 31 March–3 April, Raleigh, NC, USA, pp 904–909
71. Albu-Schaffer A, Ott C, Hirzinger G (2007) A Unified Passivity-based Control Framework for Position, Torque and Impedance Control of Flexible Joint Robots. The International Journal of Robotics Research 26:23–39. doi:10.1177/0278364907073776
72. Hogan N (1989) Controlling impedance at the man/machine interface. In: Proceedings of the 1989 IEEE international conference on robotics and automation, 14–19 May, Scottsdale, AZ, USA, vol 3, pp 1626–1631
73. Pratt G, Williamson M (1995) Series elastic actuators. Intelligent robots and systems 95. In: Proceedings of the 1995 IEEE/RSJ international conference on human robot interaction and cooperative robots, 5–9 August, Pittsburgh, Pennslyvania, USA, vol 1, 399–406, doi: 10.1109/IROS.1995.525827
74. Pratt G, Willisson P, Bolton C, Hofman A (2004) Late motor processing in low-impedance robots: impedance control of series-elastic actuators. In: Proceedings of the 2004 American control conference, 30 June–2 July, Boston, MA, vol 4, pp 3245–3251, doi: 10.1109/ACC.2004.182786
75. Kong K, Bae J, Tomizuka M (2009) Control of rotary series elastic actuator for ideal force-mode actuation in human–robot interaction applications. IEEE/ASME Trans Mechatronics 14:105–118. doi:10.1109/TMECH.2008.2004561
76. Grun M, Muller R, Konigorski U (2012) Model based control of series elastic actuators. In: 2012 4th IEEE RAS EMBS international conference on biomedical robotics and biomechatronics (BioRob), 24–27 June, Rome, Italy, pp 538–543
77. Vallery H, Ekkelenkamp R, Van der Kooij H, Buss M (2007) Passive and accurate torque control of series elastic actuators. In: Proceedings of IEEE IROS, IEEE/RSJ International Conference on Intelligent Robots and Systems, October 29–November 2, San Diego, USA, pp 3534–3538
78. Krebs HI, Hogan N, Aisen ML, Volpe BT (1998) Robot-aided neurorehabilitation. IEEE Trans Rehabil Eng 6:75–87. doi:10.1109/86.662623
79. Schaechter J (2004) Motor rehabilitation and brain plasticity after hemiparetic stroke. Progress Neurobiol 73:61–72
80. Gordon KE, Ferris DP (2007) Learning to walk with a robotic ankle exoskeleton. J Biomech 40:2636–2644. doi:10.1016/j.jbiomech.2006.12.006
81. Rossini PM, Micera S, Benvenuto A et al (2010) Double nerve intraneural interface implant on a human amputee for robotic hand control. Clin Neurophysiol 121:777–783. doi:10.1016/j.clinph.2010.01.001
82. Kiguchi K, Iwami K, Yasuda M et al (2003) An exoskeletal robot for human shoulder joint. IEEE/ASME Trans Mechatronics 8:125–135
83. Lenzi T, De Rossi SMM, Vitiello N, Carrozza MC (2012) Intention-based EMG control for powered exoskeletons. IEEE Trans Biomed Eng 59:2180–2190. doi:10.1109/TBME.2012.2198821
84. Rosen J, Brand M, Fuchs MB, Arcan M (2001) A myosignal-based powered exoskeleton system. IEEE Trans Syst Man Cybernetics Part A Syst Hum 31:210–222. doi:10.1109/3468.925661
85. Cavallaro EE, Rosen J, Perry JC, Burns S (2006) Real-time myoprocessors for a neural controlled powered exoskeleton arm. IEEE Trans Biomed Eng 53:2387–2396. doi:10.1109/TBME.2006.880883

86. Kinnaird CR, Ferris DP (2009) Medial gastrocnemius myoelectric control of a robotic ankle exoskeleton. IEEE Trans Neural Syst Rehabil Eng 17:31–37. doi:10.1109/TNSRE.2008.2008285
87. Dietz V, Fouad K, Bastiaanse CM (2001) Neuronal coordination of arm and leg movements during human locomotion. Eur J Neurosci 14:1906–1914. doi:10.1046/j.0953-816x.2001.01813.x
88. Rueterbories J, Spaich EG, Larsen B, Andersen OK (2010) Methods for gait event detection and analysis in ambulatory systems. Med Eng Phys 32:545–552. doi:10.1016/j.medengphy.2010.03.007
89. Novak D, Reberšek P, De Rossi SMM, Donati M, Podobnik J, Beravs T, Lenzi T, Vitiello N, Carrozza MC, Munih M (2013) Automated detection of gait initiation and termination using wearable sensors. Med Eng Phys 35(12):1713–1720. doi:10.1016/j.medengphy.2013.07.003
90. Ronsse R, Vitiello N, Lenzi T et al (2011) Human-robot synchrony: flexible assistance using adaptive oscillators. IEEE Trans Biomed Eng 58:1001–1012. doi:10.1109/TBME.2010.2089629
91. Righetti L, Buchli J, Ijspeert AJ (2006) Dynamic Hebbian learning in adaptive frequency oscillators. Physica D Nonlinear Phenom 216:269–281. doi:10.1016/j.physd.2006.02.009
92. Righetti L, Buchli J, Ijspeert AJ (2009) Adaptive frequency oscillators and applications. Open Cybernetics Syst J 3:64–69. doi:10.2174/1874110X00903020064
93. Ronsse R, Lenzi T, Vitiello N et al (2011) Oscillator-based assistance of cyclical movements: model-based and model-free approaches. Med Biol Eng Comput 49:1173–1185. doi:10.1007/s11517-011-0816-1
94. Tagliamonte NL, Sergi F, Carpino G et al (2013) Human-robot interaction tests on a novel robot for gait assistance. In: IEEE International Conference on Rehabilitation Robotics (ICORR), 24–26 June 2013, Seattle, WA, pp. 1–6.
95. Vallery H, Veneman J, Van Asseldonk E et al (2008) Compliant actuation of rehabilitation robots: benefits and limitations of Series Elastic Actuators. IEEE Robot Automat Mag 15:60–69. doi:10.1109/MRA.2008.927689
96. Pintelon R, Schoukens J (2001) System identification: a frequency domain approach. IEEE Press, New York

Chapter 14
Home-Based Rehabilitation: Enabling Frequent and Effective Training

Kyle B. Reed, Ismet Handžić, and Samuel McAmis

Abstract Rehabilitation studies have recently demonstrated that the amount of time spent training is one of the most important factors in one's ability to regain motor control. The methods employed need to be effective, but individuals need to spend significant amounts of time retraining. One of the most effective ways to enable more training time is for rehabilitation to occur in one's home so individuals have adequate access to it and there is no cost associated with traveling to the clinic. There are several challenges that need to be overcome to make home rehabilitation more common; for example adapting the methods from the clinical setting to the home setting, ensuring safety, and providing motivation. This chapter outlines existing technologies for upper and lower limb rehabilitation and how they could be adapted for use in one's home. Although many types of disabilities would benefit from home-based rehabilitation, this discussion will focus on traumatic brain injuries, specifically stroke related. Many of the methods that could be used at home for stroke would also have application for helping in other circumstances.

Keywords Home-based rehabilitation • Low-cost therapy • Stroke rehabilitation • Robotic therapy • Upper-limb • Lower-limb

14.1 Introduction

The saying "practice makes perfect", although a cliché, adequately describes a good rehabilitation method. The more a person with a traumatic brain injury, such as stroke, is able to practice, the better their motor relearning will be [1].

K.B. Reed (✉) • I. Handžić • S. McAmis
Department of Mechanical Engineering, University of South Florida, Tampa, FL, USA
e-mail: kylereed@usf.edu; ihandzic@mail.usf.edu; smcamis@mail.usf.edu

P. Artemiadis (ed.), *Neuro-Robotics: From Brain Machine Interfaces to Rehabilitation Robotics*, Trends in Augmentation of Human Performance 2,
DOI 10.1007/978-94-017-8932-5_14,

However, patients are dissatisfied with their options for training after they are discharged from the rehabilitation hospital/clinic [2], and 85 % of patients would prefer a home-based rehabilitation solution [3]. The ability to train at home means individuals can train more often, which leads to better results in motor relearning [4] and can maintain individuals' ability to perform activities of daily living [5, 6]. These studies indicate that appropriate methods need to be further developed to enable home-based rehabilitation to improve functional ability after discharge.

The fundamental idea of rehabilitation is to effect a relatively permanent change in the brain that allows continued use of the affected limb(s). Ideally, an individual would regain the full use of his/her impaired abilities following rehabilitation. However, this is not always feasible depending on the nature of the impairment. The literature suggests several holistic outcome measures that could be considered ideal for the individuals; for example, finding satisfaction with his/her life, contributing to society more than he/she is dependent on it, and being able to maintain physical and mental health [7, 8].

In the near future, rehabilitation *could* consist of a mix of home-based therapy and regular but less frequent visits to the clinic. During the clinic visits, the physical therapist would discuss any issues with the patient, and a functional assessment device would evaluate the subject's abilities, such as demonstrated by Schweighofer et al. [9] and Fluet et al. [10]. The physical therapist would prescribe the appropriate home-based therapy to be used daily. The home-based rehabilitation would include an engaging interaction, such as a game, to maintain the individual's interest. The data and video from each home-based session would be securely sent to the therapist at the clinic where it would be automatically evaluated by software, therapists, or both, as deemed appropriate. Non-compliance or non-use would be followed up with a phone call or earlier clinic visit. Due to the low-cost and availability of the rehabilitation, the therapy could continue until the individual was satisfied with their ability to independently perform activities of daily living [8]. Many of the technologies to enable this vision exist, but there is a severe shortage of effective and clinically validated home-based methods that would enable the home-based portion to take place for individuals with moderate impairment.

Specifically for stroke, many methods of rehabilitation are able to generate positive results, but there is no clear evidence for the superiority of any one specific approach [11]. A growing amount of literature suggests that the fundamental problem is not the methods employed, but the lack of adequate training for extended periods of time [1, 12, 13]. Thus, home-based rehabilitation that is widely and affordably available will benefit the many individuals looking for continued training [3].

One of the most common robotic rehabilitation systems, the MIT-Manus [14], is estimated to cost around $15,000 per patient for 36 weeks, which is slightly higher than intensive non-robotic therapy and usual care [15]. To use it, individuals must go to the clinic, which incurs additional cost and time of the individuals not explicitly measured in the study. A home-based method would only incur a one-time cost that would enable rehabilitation for an extended period of time (possibly years) with a small recurring cost for monitoring, whereas clinic-based methods will continue to incur costs throughout the treatment. Even with home-based methods, occasional clinic visits would be expected but would be significantly less frequent than a clinic-based solution.

There are many individuals that could benefit from home-based therapy. More than 795,000 Americans experience a new or recurrent stroke each year and more than 6 million individuals have survived a stroke and are living with the debilitating after-effects [16]. Most individuals with a stroke are left with limited functional ability of the upper limb; 40 % have moderate functional impairment and 15–30 % have a severe disability [17]. The estimated costs associated with strokes in 2010 were $73.7 billion [16]. Annually, an estimated 1.7 million Americans suffer a Traumatic Brain Injury (TBI), with 275,000 requiring hospitalization [18]. Approximately 43 % of TBIs requiring hospitalization result in long term disability [19] resulting in over 3.2 million Americans currently living with a disability as a result [20]. The lifetime costs associated with TBI in the year 2000 was $60.4 billion [21].

14.2 Traditional Therapy

Conventional therapies, such as the Bobath method [22] and proprioceptive neuromuscular facilitation technique [23], have been commonly used for stroke rehabilitation. Forced use [24] and the more recently developed Constraint-Induced Movement Therapy [25] binds the sound arm and forces the individual to use only the paretic limb, which aids in cortical re-mapping of neurons from damaged to functional brain cells [26]. One advantage of forced use is that the learning occurs directly during the tasks that are to be learned and can be implemented during home therapy. However, forced use is unable to provide assistance, so it works only on individuals with high motor function.

Traditional physical therapy will often retrain a patient's movements by a therapist physically holding the patient's limb and assisting the motion. The motions are imparted to the patient and the patient is able to feel some of the resulting forces. However, the dynamics of the physical therapist and patient are coupled, which results in motions that are not exactly as intended and the forces are not as expected due to the redundant dynamics of two people [27, 28]. The exact dynamics of this physical interaction between therapist and patient is an open question and studies with healthy subjects have shown the need for further study of the topic. In a study with relatively simple dynamics, Glynn et al. [29] examined how two participants cooperatively moved a cursor through a virtual maze. The participants had difficulty separating the force feedback of the device from the other member's forces. Several other studies have examined similar physical interactions: two individuals will naturally escalate their forces when told to apply the same force as was applied to them since they perceive externally and self-generated forces differently [30], but training can partially alleviate this effect [31]; individuals will unknowingly use constraints, possibly their partner, to generate a force in the desired direction since certain directions are easier to generate force in [32]; two people physically interacting will perform faster than either individual alone [33]; and two people cooperatively performing a task will subconsciously specialize their motions so each person takes on a different part of the task [34].

There are two main challenges in bringing traditional therapy home. First, it is not exactly clear what forces and motions are being conveyed by the physical therapist. The lack of a fundamental understanding of this interaction could potentially be limiting all realms of physical therapy. Second, there is no physical therapist at home to perform the rehabilitation, which raises several additional concerns. One of the proposed solutions is robotic therapy, discussed in the next section.

14.3 Robotic Therapy

Robotic technologies have been used to provide rehabilitation to individuals with low motor function since therapy is time-consuming and requires significant effort from physical therapists. Patients can also use robotic devices for longer and more frequent periods of time in the clinics.

One of the earliest robotic upper limb rehabilitation systems developed is the MIT-Manus [14], shown in Fig. 14.1. The MIT-Manus can operate in several planar reaching modes: assisting users, passively sensing motions, or by responding to the user's motions. The results of several independent clinical trials showed that robotic training with the MIT-Manus helped 372 persons with stroke to improve upper extremity motor function [36]. Similarly, the Assisted Rehabilitation and Measurement Guide is an active-assistive robotic device that also showed the benefit of robotic training for people with a stroke [37]. Force feedback devices have also been used to quantify the performance of a patient for use in measuring

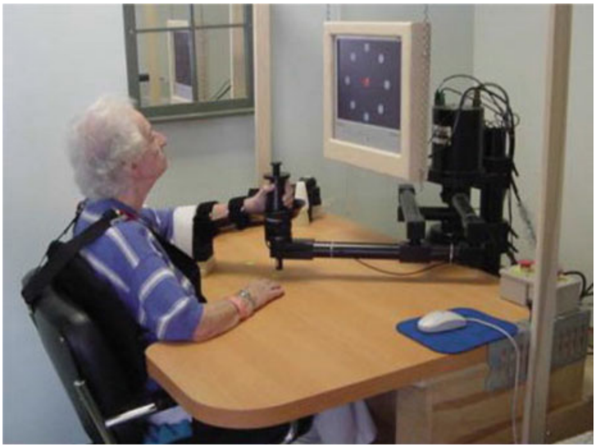

Fig. 14.1 MIT Manus, one of the earliest robotic upper limb rehabilitation systems (Figure reproduced from [35] under the Creative Commons Attribution License)

improvement and possibly prescribing treatments [10]. However, recent review papers have stated that it is unclear whether robotic methods have the potential to produce greater benefits than conventional techniques when practiced for the same amount of time [12, 13]. The amount of training is one of the most important factors for functional recovery after stroke [1, 38, 39].

Robot guided therapy can either use assistive or resistive methods and it is not currently clear which is more effective. In active assistance training, a therapist or robot assists the patient through the desired motion. The benefits of active assistance include stretching the muscles and connective tissues, reinforcing a normal pattern of motion, and allowing the patient to practice more complex tasks [13]. Active assistance also allows for an increase in the intensity of training, since with assistance, more motions may be completed in less time. However, the "guidance hypothesis" suggests that motor learning could actually be decreased when the individual is physically guided since the individual learns how to interact with the therapist or device and not necessarily how to generally move their arm [13, 40]. It is possible that the patient is subconsciously only performing a portion of the task and not learning the other necessary muscle activations [41].

Resistive training methods work to facilitate rehabilitation by making task completion more difficult during training by applying forces that resist or perturb the motion. Individuals moving in a force field that perturbs their motion will adapt to generate forces that counteract the field, resulting in a normal motion within the field [1]. The adaptation will persist for a short time after the field is removed. This after-effect has led to error enhancement training, in which the errors that an individual makes during a motion are exaggerated. Once the disturbance is removed, the after-effect results in a more correct motion, however the corrected motion typically only persists for a short amount of time [42].

One reason the after-effects only last a short amount of time is the dual-rate learning process [43, 44]. The motor output is the summation of a fast learning process, which adapts quickly to new patterns and also forgets quickly, and a slow learning process which adapts over many repeated interactions, but shows prolonged after-effects. The after-effects generated as a result of resistive training are largely due to the slow learning process, but the quick fall off of the effects is the fast learning process adapting quickly. To modify the generated motions permanently, the slow learning process must be involved repeatedly. However, simply making the training sessions longer on each day does not increase the effectiveness since time is needed between sessions to allow for motor consolidation [45, 46]. Longer sessions several times a week are unlikely to make a significant difference, but shorter sessions practiced everyday are likely to be most effective. However, this has not been confirmed since most of the rehabilitation studies train for only 3 days a week. It is costly and time consuming to bring a person in everyday for the study and for long-term rehabilitation. Thirty minutes performed in the home each day would not be so difficult to perform and would involve less overall time spent training each week, particularly if transportation time is included.

There are several challenges that need to be overcome before these robotic methods can be used in the home. Cost is a significant issue that will be helped partially by economies of scale and decreasing cost of parts, but these costs will only come down so far. The methods need to be reevaluated to determine the most fundamental type of rehabilitation that can be used to generate the result. As opposed to developing more complicated and expensive robots that only incrementally improve the rehabilitation, some of the effort should focus on finding the methods that provide 90 % of the benefit at 10 % of the cost. The less complicated devices could also use less powerful motors, which would inherently provide a safer environment for rehabilitation; safety is critical to a home-based solution.

14.4 Visual and Haptic Feedback

One major problem of many rehabilitation programs is the transference of learning between tasks, specifically from the rehabilitation therapy to activities of daily living. The use of visual and haptic feedback has been studied to overcome this problem. One study examined the effects of displaying patient motion collected from an electromagnetic motion capture system during training sessions and showed significant gains after 15 one-hour sessions [47], however no control subjects were used for comparison. In video capture virtual reality, the mirror images of patients' motions have been displayed interacting in a virtual environment. These systems have been tested in a large number of studies, but have focused on presence and enjoyment rather than rehabilitation outcomes [48]. One example is shown in Fig. 14.2. The enjoyment is an important aspect of home-based rehabilitation as it directly relates to motivation and the likelihood that an individual will continue with the training. Virtual and augmented reality for use in rehabilitation has been a popular subject of recent research, however further study is needed to determine the long-term efficacy of virtual reality in rehabilitation [49, 50].

Fig. 14.2 An example of a rehabilitation game to encourage movements that are appropriate for motor relearning (Figure reproduced from [48] under the Creative Commons Attribution License)

Haptic force feedback through a Phantom Omni [51] and a Rutgers Master II glove [52] have also been shown to help transfer stroke patient rehabilitation improvements to activities of daily living. The use of exoskeletons for force feedback providing a control force to the palm of the user's hand [53] as well as gravity support exoskeletons [54] have shown significant improvements in clinical measures of stroke patients. Haptic guidance using vibration motors on the arms have recently been shown to be as effective as visual feedback for correcting motions [55]. In another study looking at targeted force-based movement, haptic feedback was shown to lead to improved ease of use and success in accurately completing the virtual finger-pointing task, but the task with haptic feedback was slower [56].

Methods based on simple haptic and visual methods are ideal for home use since they are cheap and easy to use. The downside of them is that they are unable to provide any significant force assistance, so they are not going to be effective for moderate to severely impaired individuals. However, it is unlikely that home-based rehabilitation would ever be appropriate for individuals with severe impairment as they will likely need additional supervision and care.

14.5 Upper Limb Rehabilitation

This section will look specifically at methods for upper-limb rehabilitation and discuss prospects for expanding the effectiveness of home-based methods.

14.5.1 Home Based Rehabilitation Methods

As discussed earlier, the ability to train more often leads to better results in motor relearning [4]. Home-based methods have been shown to help maintain individuals' ability to perform activities of daily living [5, 6]. There are several methods that have been adapted for home use, but they are limited to individuals with mild impairments. Ideally, moderately impaired individuals would also be able to benefit from home-based rehabilitation.

The SMART system [57] incorporates a motion tracking system to monitor performance of daily tasks and rehabilitation exercises, an online database that allows therapists to monitor patient performance, and a visual feedback system that therapists may use to provide instruction. Java Therapy [58] uses a commercially available force feedback joystick and a suite of online games to provide therapy and evaluation. Another home computer based method is UniTherapy, which uses a force feedback joystick and steering wheel [59,60] and has been validated in clinical trials [61, 62]. These home-based methods, however, use a home computer with

Fig. 14.3 The MOTOmed® is a arm cycling device with passive, motor-assisted, or active resistive options (Figure reproduced with permission)

limited accessories that can only provide limited assistance forces and have a limited workspace. These methods are able to provide some benefit, but the rehabilitation effect is limited to people who have relatively high motor function. The challenge is to develop safe and affordable rehabilitation for individuals with moderate impairment.

The commercially available MOTOmed arm cycling training device (Fig. 14.3) targeted towards stroke, multiple sclerosis, hypertension, cerebral paresis and Parkinson's disease, offers a home-based rehabilitation option. For a relatively low price, patients can perform daily rehabilitative cycling exercises within the comfort of their home. MOTOmed can be customized to be used passively, motor-assisted, or active resistively. Rhythmic Arm cycling has shown to increase upper limb performance [63] and reduces arm spasticity [64, 65].

14.5.2 Bimanual Rehabilitation

Self-rehabilitation using bimanual rehabilitation is ideal for home-based stroke therapy since much of the required force could be provided by the person's sound limb and minimal, or no, external assistance would be required from a caregiver or a motor. The idea behind bimanual rehabilitation is that an individual assists his own paretic arm with his sound arm through an external physical coupling. Neither a physical therapist nor a robot can determine the exact path a person wants his arm to move as well as the person can. When an individual moves both the paretic and sound arms at the same time, the same signal is sent from the brain to the arms and, since the arms are constrained to move together, the proprioceptive feedback will be similar between the two sides of the brain. Burgar et al. hypothesize that bimanual symmetric exercise will enhance recovery by stimulating the ipsilateralcorticospinal pathways [66], which is similar to the

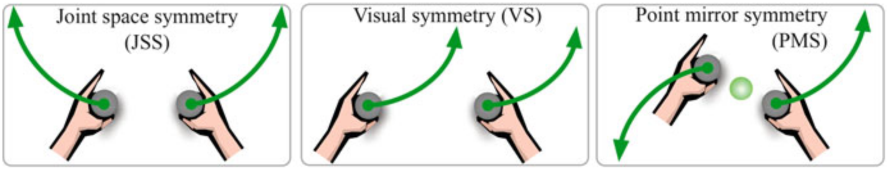

Fig. 14.4 There are three common symmetric motions in which bimanual rehabilitation is typically performed: joint-space symmetry (*JSS*) where the joint angles are mirrored; visual symmetry (*VS*) where the hands move through the same visual path; and point mirror symmetry (*PMS*) where the hand motions are mirrored about a point in space

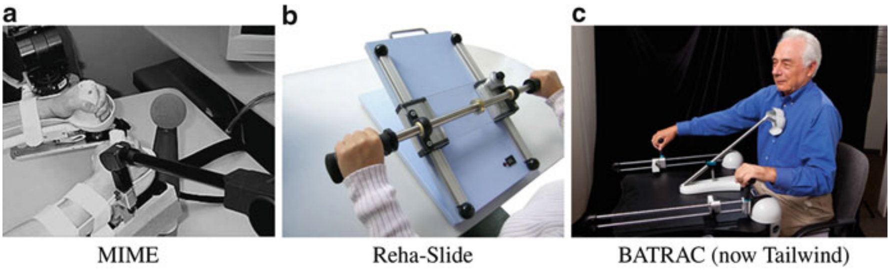

Fig. 14.5 Several of the devices that have been used for bimanual rehabilitation. The general idea of bimanual rehabilitation is that an individual assists his own paretic arm with his sound arm through an external physical coupling (Subfigure (**a**) reproduced from [48] under the Creative Commons Attribution License. Subfigures (**b**) and (**c**) reproduced with permission)

hypothesis by Wolf et al. [67] that bimanual therapies could target the ventromedial brain stem pathways. The fundamental idea is that duplicating the efferent and afferent signals will retrain the motor pathways on the paretic side.

Many devices have implemented bimanual motions in a subset of the coupling modes shown in Fig. 14.4. In Joint Space Symmetry, the joint angles for the left and right arms are identical, resulting in hand motions that are mirrored about the sagital plane. In Visual Symmetry, both hands move in the same absolute direction in the visual reference frame. VS occurs in many daily activities, such as moving a large object with both hands. In Point Mirror Symmetry, the hand motions are mirrored about a point in space, much like turning a steering wheel.

14.5.2.1 Robotic Bimanual Rehabilitation

Robotic bimanual rehabilitation uses a robotic device to assist an individual in making bimanual motions, some of which are shown in Fig. 14.5. The Mirror Image Movement Enabler (MIME) mirrors the position of the sound arm to the paretic arm using a large industrial robot, the PUMA 500 [66], but the study did not clearly identify the effectiveness of bimanual rehabilitation since subjects used a combination of unimanual and bimanual training [1]. Whereas the MIME focuses on mirroring the overall position of the hands, the BiManuTrack mirrors the flexion of the forearm and wrist and has shown positive results similar to the MIME [68] and to unimanual therapy [69].

Although these devices have been shown to be effective, they are limited to hospital and clinical settings. In recent years simpler passive devices have been developed that are well-suited for home-use rehabilitation.

14.5.2.2 Passive Bimanual Rehabilitation

Passive bimanual rehabilitation devices rely solely on the patient to generate motions, and do not provide assistive forces. Some of these devices have no physical coupling and rely entirely on the impaired arm to generate motions, while others physically link the hands, allowing one arm to assist the other.

BATRAC incorporates one such device where individuals independently move their hands along a linear track with in-phase and out-of-phase motions [70]. BATRAC has shown results similar to dose-matched therapeutic exercises [71]. A commercially available version of the BATRAC device, called Tailwind, is available and may be suited to home-use, although home use trials have not been conducted.

The Reha-Slide [72] implements bimanual motions only in the visual reference frame. The hands are linked by a rigid mechanism that allows an adjustable amount of friction. The entire effort to move the handles, including friction, is controlled by the sound side, The Reha-Slide is simple and demonstrated some improvement, but was not as effective as the BiManuTrack.

The ImAble system includes two devices that couple motions in a visually symmetric frame [73]. The Able-B supports the impaired arm against gravity while allowing the unimpaired arm to assist in making horizontal motions. The Able-X consists simply of a rigid handlebar with a motion sensitive game controller. The devices are used to interact with a suite of virtual reality computer games and have shown positive improvements in a pilot study [73]. The Able-X is commercially available for home use, however its home use efficacy has not been studied.

14.5.2.3 Compliant Bimanual Rehabilitation

The preceding devices have shown bimanual rehabilitation to be effective, but each only used one symmetry mode and either a rigid coupling or no coupling. However, for healthy individuals, certain motion types are easier to duplicate in one symmetry mode than another [74, 75]. These results indicate that the coupling symmetry mode and stiffness could affect the effectiveness of bimanual rehabilitation. Healthy individuals could recreate bimanual motions more easily in VS if the task was a rapid, unpredictable motion, but could recreate rhythmic motions more easily in JSS [76].

For bimanual rehabilitation, a completely rigid coupling may cause the individual to entirely rely upon their sound arm for all motions [13, 40] whereas a coupling that is too soft would completely eliminate the effect of the coupling, which would prevent individuals with low motor function from benefitting from this training method. With a flexible coupling, the paretic limb will have some assistance, but will apply at least a minimal amount of force, and the assistance force can gradually decrease throughout training. As discussed in Sect. 14.3, allowing the individual to gradually adapt will likely train the individual better than an all-or-nothing approach.

To directly compare the rehabilitation efficacy of different bimanual symmetry modes and coupling stiffnesses, a Compliant Bimanual Rehabilitation Device (CBRD) has been developed. This device allows the hands to be coupled in JSS, VS, or PMS, with a wide range of coupling stiffnesses, from 100 to 2,000 N/m. Preliminary results have shown that the CBRD can couple the motions of two healthy individuals in a task that simulates hemiparesis [77, 78]. This study also showed that the CBRD may improve bimanual task performance of healthy individuals.

14.6 Lower Limb Rehabilitation

Most survivors of stroke, persons suffering from traumatic brain injury, paraplegia, tetraplegia, multiple sclerosis, cerebral palsy, or hydrocephalus are known to suffer from motor deficits, including hemiparesis. Hemiparesis in the lower limb leads to hemiparetic gait, which is characterized by an asymmetric walking pattern [79, 80]. Hemiparetic gait typically includes asymmetries in walking coordination measures, such as step length and double support. In other words, the placement and timing of each foot are not equal on the two sides. The rehabilitation techniques used for this target population can be categorized as one of the following:

- Classic gait Rehabilitation (Neurophysiological and Motor Learning)
- Robotic Devices
- Functional Electrical Stimulation

There are generally not as many methods available for home-based lower-limb rehabilitation as there are for upper-limb due to the added complications related to balance and stability when standing/walking. Below is a description of existing methods and how they could be adapted for the home.

14.6.1 Classic Gait Rehabilitation for Hemiparesis

Currently, the most common gait rehabilitation techniques are classic methods, but robotic devices are gaining acceptance [81]. Classic gait rehabilitation mainly includes preparatory exercises, such as calisthenics, mild stretching, range of motion exercises [82, 83], and guidance/assistance of the limb position while walking over

Fig. 14.6 The Lokomat® is a gait-assistive device with a built-in body weight support system (Picture: Hocoma, Switzerland)

even ground in conjunction with a physical therapist. Classic gait rehabilitation has two subcategories: neurophysiological techniques and motor learning techniques. In the neurophysiological rehabilitation approach, such as Bobath [22] and the Brunnstrom method [84], the patient is the passive recipient of the physiotherapist's corrective and assistive movements [85]. Motor learning approaches, such as the Perfetti method [86], are quite the opposite in that they emphasize active patient participation [87]. Although these are two distinct approaches to hemiparetic gait rehabilitation, in practice each method is customized for each specific situation and patient. For these two categories, no method has been explicitly developed for gait rehabilitation [88]. While overground gait training still persists to be the most commonly used method for patients who are unable to walk independently [89], States et al. [90] indicate that there seems to be no distinct benefits caused by this method. It is suggested that a combination of methods, such as the use of body weight supported treadmill training [91], is a more effective approach [92]. An example of a body weight supported training in combination with guided therapy is shown in Fig. 14.6.

Home-based motor imagery exercises for gait rehabilitation can also be an effective tool to improve walking performance in patients. Motor imagery is a cognitive operation that increases brain activity in neuronal cortical networks [93], or in other words, motor imagery is a meditation technique that focuses on the visualization of proper limb movement. Dunsky et al. [94] studied the effects of motor imagery exercises on 17 hemiparesis patients over a period of 3 months. As a result, walking speed increased by 40 % with gains retained at the 3-week follow up. Also, a significant increase in stride length, cadence, and single-support time of the affected limb was reported along with a significant decrease in double-support time. A comprehensive review of imagery exercises for gait rehabilitation [95] reveals similar positive effects, however further clinical studies with strong designs and larger groups are needed for confirmation of these positive findings. If validated, motor imagery would be suitable for home-based therapy that could include a large range of individuals.

Fig. 14.7 The MOTOmed® is a passive, motor-assisted, or active resistive cycling training device (Figure reproduced with permission)

14.6.2 Robotic Devices for Hemiparesis Rehabilitation

Classic gait rehabilitation methods alone are unable to restore a normal walking pattern in many stroke patients [96] and are progressively used in conjunction with robotic devices. There are several advantages in the use of robotic devices for gait rehabilitation: reduction of physical assistance and therapy cost, data acquisition, measurement and assessment, and repeatability [3]. Studies indicate that introducing robotic devices into gait rehabilitation results in improved endurance, lower-limb balance, functional balance, gait symmetry, double stance support, and stride length [97–99].

Exoskeleton type robotic devices are commonly used with body weight support systems with an assist-as-needed control law. The Lokmat [100, 101], shown in Fig. 14.6, is an electromechanical exoskeleton that employs a zero-impedance control mode, or path control [102], which allows patients to freely move their limbs while walking. The concept of virtual tunneling, which guides the patient's motion through a force field, is applied in the lower extremity exoskeleton ALEX [103]. The Lokomat and ALEX both are used with a treadmill, body weight support system, visual feedback, and goal oriented training. However, due to their large size, exoskeletons are not likely candidates for home use.

The robotic platform by Monaco et al. [104, 105] offers an automated lower limb rehabilitation device, named NEUROBike, to patients during the initial acute phase when individuals are not yet able to keep an upright walking posture. The NEUROBike system essentially guides the position and orientation of the individual's feet in the sagittal plane to mimic normal gait. Although still in its developmental stage, this rehabilitation device can potentially offer a simple home-based system, but more study is necessary.

At a relatively lower cost, a simpler, yet effective approach is presented in the commercially available lower and upper limb rehabilitation device named MOTOmed by Reck, shown in Fig. 14.7. The MOTOmed is a lower (or upper) limb cycling device that can be used in a sitting position, in supine position, or

Fig. 14.8 A split-belt treadmill can be used to reduce an asymmetric gait. The downside is that the corrected gait does not efficiently transfer to walking over ground

with Functional Electrical Simulation (FES). It is designed to be used in a home environment on a daily basis. Passive, motor-assisted, or active resistive training make the MOTOmed customized to an individual's rehabilitation needs. Lower limb rehabilitation studies which utilized the MOTOmed five times a week have shown improvement in patient balance, walking distance (or gait), step length, increased muscle tone, and reduction in spasticity [106–108]. Such leg cycling rehabilitation in conjunction with electrical stimulation has also been shown to reduce hypertonia in patients with stroke [108].

Balance control is a concern for individuals with stroke and, for severely impaired individuals, shifting weight so they can take a step is challenging. A recent study examined the effects of robot-assisted balance training in which an external perturbation force field was applied to individuals while leaning only and also when taking a step [109]. The results showed that the stepping group had a larger change in the asymmetry of their gait patterns, which indicates that training needs to occur in a dynamic environment.

Once a hemiparasis patient is able to stand up and walk with appropriate supports, similar corrective forces in the sagittal plane can be applied to the patient's knee joint through Series Elastic Remote Knee Actuator (SERKA) [110] to achieve correct walking movements. SERKA compensates for the patient's lack of strength and endurance during knee flexion by applying corrective torques at key instances during the gait cycle.

While treadmills are not generally categorized as robots from an engineering standpoint, in gait rehabilitation they are classified as robotic devices. Lower-limb rehabilitation commonly includes split-belt treadmills [111, 112], as shown in Fig. 14.8. Such systems enable independent control of the two treads that each leg walks on, forcing one leg to move faster through stance than the other. Healthy participants with typical gait will walk symmetrically on the treadmill when the belts are running at the same speed (i.e., speed ratio is 1:1). When the speed ratio is changed to 2:1, these participants develop an asymmetric gait since their feet are moving at different speeds when in contact with the treadmill. After 10–15 min of walking at a 2:1 ratio, these participants adapt the spatial and temporal relationships between their legs to reestablish a symmetric walking pattern. When the belt speeds are returned to normal (1:1 ratio), the modifications made to gait during split-belt walking are temporarily remembered. The modifications result in an asymmetric gait that is opposite to the asymmetry induced initially by the split-belt treadmill, which is an after-effect similar to that discussed in Sect. 14.3. The same method can be used to correct individuals with asymmetric gaits.

Although the split-belt treadmill can change the interlimb coordination while walking on the treadmill, the effect does not completely transfer to over-ground walking. When after-effects are assessed over ground, the magnitude is diminished to 10 % of the magnitude of treadmill after-effects in control participants [113]. For individuals who have suffered a stroke, the transfer to over-ground walking is better at 30–70 %, but the effect is variable and diminishes rapidly following a single training session [114]. It has also been hypothesized that the limited transfer is due to conflicting sensory experiences between the treadmill environment and the over-ground environment [115]. On a treadmill, the scene is not moving, so there are no visual cues reinforcing the forward motion that would be present when walking over ground. Since walking is highly context dependent [113, 115, 116], these cues indicating a different context may prevent the learned patterns on the treadmill from being expressed during over-ground walking. In other words, if the participant is aware that the training conditions are different from the testing conditions, this may limit the transfer. Also, walking on a treadmill limits one's ability to change velocity whereas, when walking over ground, an individual has complete control over velocity. There are also slight differences in the passive dynamics of walking over ground and walking on a treadmill [117].

One way to counter the context-dependence of walking adaptation is to have participants learn a new walking pattern in the same context in which they typically walk. The Gait Enhancing Mobile Shoe (GEMS) [118, 119] is an alternative to the split-belt treadmill method of rehabilitation that allows one foot to move relative to the ground while walking over ground. It addresses the transference problem and it enables convenient, low cost, and potentially in-home gait rehabilitation for persons with central nervous system damage, such as stroke. The learned motions using the GEMS will generate after-effects resulting in near-symmetric gait, but because learning occurs in a real-world environment with the same dynamic and psychological effects as over-ground walking, the walking pattern transfer is increased. The shoe design and implementation is passive (i.e., has no force producing actuators). The necessary forces are converted from the wearer's own downward and horizontal forces into a backward motion through its Archimedean spiral-shaped wheels [120, 121], as shown in Fig. 14.9. By using the weight of the

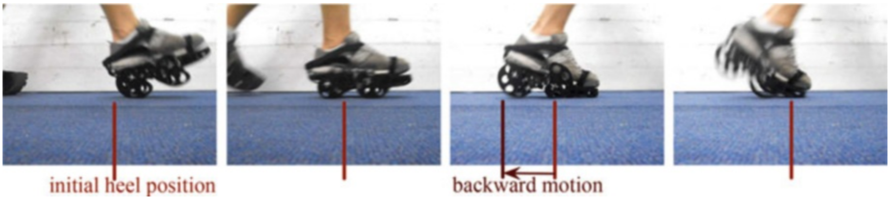

Fig. 14.9 The gait enhancing mobile shoe [119] mimics a split-belt treadmill, but while walking over ground to help transfer the rehabilitation effects to over-ground walking. The motion is generated passively by converting the downward motion of the wearer's weight into a backward motion

wearer to generate the needed motion, the GEMS can be developed at a reasonable size, weight, and cost, which makes it applicable for home-use with adequate safety procedures in place. However, additional testing is needed.

14.6.3 Incorporating Natural Passive Dynamics

In some cases, there are simple solutions to correcting irregular gait. In a study by Gibson-Horn [122], individuals with ataxia wore a 2 lb. mass on their chest. The simple addition of the mass significantly decreased the unstable motions and enabled more steady and efficient walking. In this case, altering the passive dynamics helped correct the individual's gait patterns. Passive dynamics of gait have been theorized to be applicable to rehabilitation for decades and passive dynamic walkers are helping to give insight into human gait.

A passive dynamic walker (PDW) is a device that exhibits a steady and stable gait without any energy inputs except the forces due to gravity [123]. It has been proposed to use a PDW to separate the physical dynamics and the cognitive aspects of walking [124]. The PDW was initially modeled as a rimless wheel [125], was expanded by creating a five-mass system to incorporate knees [126], and then extended so that the leg masses are specified separately, thus allowing physical asymmetries within the model [127]. The gait arising from the PDW model and that of a human have been compared on a treadmill and on over-ground walking with comparable results, but the lack of ankle dorsiflexion causes a discrepancy between the results [117].

When the PDW is asymmetric, the effects of the physical changes that could be added as a means of rehabilitation or assistance can be directly studied without the added complications associated with the cognitive effects. The asymmetric version of the PDW with a heavier weight on one foot shows a similar curvature compared to a human walking with an ankle weight on one leg [128]. The PDW has be used to demonstrate how asymmetric gait can arise in individuals that are physically symmetric [129]. One example application is the design of a transfemoral prosthetic where the knee location is shifted down relative to the intact knee so that the resulting dynamics show symmetric gait [127].

14.6.4 Functional Electrical Simulation (FES) for Hemiparesis

Functional Electrical Simulation (FES) is the stimulation of muscle tissue by electric current delivery. FES has been a rehabilitation method since the mid-twentieth century and was most commonly used for the rehabilitation of drop-foot and control of dorsiflexion of the foot [130]. Studies have indicated that regular use of multichannel FES is a suitable treatment for hemiplegic subjects [131,132], however it is unclear if improvements were maintained after FES was removed. Further, the combination of FES to other techniques such as treadmill walking with body weight support yields a vast improvement in gait pattern. Nevertheless, the regular use of FES combined with over-ground walking is seen to have vastly better enhancement in gait than through over-ground walking alone [133]. FES could potentially be used at home, but the placement of the electrodes is important and may require significant training, and there is high potential for damage if used improperly.

In regards to all of the classic gait rehabilitation techniques, there are not significant outcomes, but they are significantly more effective when used in combination [134]. For home use, an important area of research is to determine how they can most beneficially be combined in a cheap, safe, and easily usable package.

14.7 Future Steps Needed to Bring Rehabilitation Home

A significant amount of research and progress has been made in the past few decades toward improving individuals' quality of life and function after a stroke or other traumatic brain injury. However, there is still a long way to go to restore the motor function more effectively. Below are a summary of the key areas that need to be further enhanced to enable home-based rehabilitation so that extended amounts of training can occur.

- Continue focusing on understanding the plasticity in the brain and optimizing therapy. Some treatments that work in the clinic will be able to be adapted for use at home. A combination of intensive clinic-based therapy and home-based therapies that provide long-term training will likely be most effective.
- There is a need to fundamentally understand how physical therapists physically interact with patients. No studies have examined this interaction. Combining the knowledge of human interaction with the precision of robotics will likely lead to further advances in rehabilitation.
- Design for the home. Economies of scale will only help so much, but the fundamental methods and designs must have use-at-home in mind during the design process. Some of the therapies detailed in this chapter are not well-suited for home use (e.g., Lokomat, MIT Manus) while others are potentially effective when used at home (e.g., Reha-Slide, Tailwind, GEMS, MotoMED), but further testing is needed to determine the efficacy of the home-use devices. There is a severe shortage of studies done on home-based training.

- Safety and monitoring are critical. Devices to be used in the home must be safe and have safe failure modes. Robotic devices with large motors have potential for failure and injury, so designs that incorporate minimal actuation are desired. However, the designs should be able to adequately train individuals with moderate impairment. To facilitate interaction and support from the clinics, the devices should be able to report back to the clinic so that progress or non-use can be followed up to encourage continued improvement.
- The training needs to have a component of motivation, either extrinsically through a game or other form of entertainment, or intrinsically through a clear perception of improvement that will lead to an upward spiral in performance. Typically, in the chronic stages, the progress is not fast enough, so individuals can easily get discouraged. In this stage, providing external motivations will likely to be most effective, but further study is needed on what is most effective.
- The care should be individualized. There is no one method that is highly effective for everyone. Some therapies work for some, but not for others. Particularly as the therapy is moved into one's home, the training needs to be further personalized since the therapist will not be able to change the therapy as frequently.
- When therapy is moved home, the support of caregivers (e.g., family, friends) is even more important. Further training for the primary caregivers needs to be expanded to ensure they can encourage and provide the emotional and physical support needed during the therapy.
- And, most importantly, practice, practice, practice. Physical rehabilitation is a hard and long road that takes effort. In the end, it takes a lot of time and the methods that are developed need to recognize and support the individual through the long road ahead of them. New methods are likely to be discovered that will speed up the therapy, but these points listed above are all going to be necessary as retraining motor function is still going to be time consuming.

References

1. Huang V, Krakauer J (2009) Robotic neurorehabilitation: a computational motor learning perspective. J Neuroeng Rehabil 6(1):5
2. Tyson S, Turner G (2000) Discharge and follow-up for people with stroke: what happens and why. Clin Rehabil 14(4):381–392
3. Gregory P, Edwards L, Faurot K, Williams S, Felix A (2010) Patient preferences for stroke rehabilitation. Top Stroke Rehabil 17(5):394–400
4. Merians AS, Jack D, Boian R, Tremaine M, Burdea GC, Adamovich SV, Recce M, Poizner H (2002) Virtual reality-augmented rehabilitation for patients following stroke. Phys Ther 82(9):898–915
5. Legg L, Langhorne P (2004) Rehabilitation therapy services for stroke patients living at home: systematic review of randomised trials. Lancet 363:352–356
6. Ryan T, Enderby P, Rigby AS (2006) A randomized controlled trial to evaluate intensity of community-based rehabilitation provision following stroke or hip fracture in old age. Clin Rehabil 20(2):123–131

7. Corrigan J (1994) Community integration following traumatic brain injury. NeuroRehabilitation 4(2):109–121
8. Benson DM, Elbaum J (2007) Long-term challenges. In: Elbaum J, Benson DM (eds) Acquired brain injury. Springer, New York, pp 286–292
9. Schweighofer N, Han CE, Wolf SL, Arbib MA, Winstein CJ (2009) A functional threshold for long-term use of hand and arm function can be determined: predictions from a computational model and supporting data from the extremity constraint-induced therapy evaluation (excite) trial. Phys Ther 89(12):1327–1336
10. Fluet M-C, Lambercy O, Gassert R (2011) Upper limb assessment using a virtual peg insertion test. In: Proceedings of the IEEE international conference on rehabilitation robotics, Zurich, pp 192–197
11. Kollen BJ, Lennon S, Lyons B, Wheatley-Smith L, Scheper M, Buurke JH, Halfens J, Geurts AC, Kwakkel G (2009) The effectiveness of the bobath concept in stroke rehabilitation what is the evidence? Stroke 40(4):e89–e97
12. Kwakkel G, Kollen BJ, Krebs HI (2008) Effects of robot-assisted therapy on upper limb recovery after stroke: a systematic review. Neurorehabil Neural Repair 22(2):111–121
13. Marchal-Crespo L, Reinkensmeyer D (2009) Review of control strategies for robotic movement training after neurologic injury. J Neuroeng Rehabil 6(1):20
14. Krebs HI, Hogan N, Aisen ML, Volpe BT (1998) Robot-aided neurorehabilitation. IEEE Trans Rehabil Eng 6:75–87
15. Trafton A (2010) Robotic therapy helps stroke patients regain function. http://web.mit.edu/newsoffice/2010/stroke-therapy-0419.html. Accessed 4 Apr 2013
16. Lloyd-Jones D, Adams RJ, Brown TM, Carnethon M, Dai S, De Simone G, Ferguson TB, Ford E, Furie K, Gillespie C et al (2010) Heart disease and stroke statistics–2010 update a report from the american heart association. Circulation 121(7):e46–e215
17. Association AH et al (2005) Heart disease and stroke statistics–2005 update. American Heart Association, Dallas. This is an informative list of recent stroke statistics on incidence, prevalence, and mortality in the United States, 2004
18. Faul M, Xu L, Wald M, Coronado V (2010) Traumatic brain injury in the united states: emergency department visits, hospitalizations and deaths 2002–2006. Centers for Disease Control and Prevention, National Center for Injury Prevention and Control, Atlanta
19. Selassie AW, Zaloshnja E, Langlois JA, Miller T, Jones P, Steiner C (2008) Incidence of long-term disability following traumatic brain injury hospitalization, united states, 2003. J Head Trauma Rehabil 23(2):123–131
20. Zaloshnja E, Miller T, Langlois JA, Selassie AW (2008) Prevalence of long-term disability from traumatic brain injury in the civilian population of the united states, 2005. J Head Trauma Rehabil 23(6):394–400
21. Corrigan JD, Selassie AW, Orman JAL (2010) The epidemiology of traumatic brain injury. J Head Trauma Rehabil 25(2):72–80
22. Bobath B (1970) Adult hemiplegia: evaluation and treatment. Heinemann Medical Books, London
23. Knott M, Voss D (1968) Proprioceptive neuromuscular facilitation: patterns and techniques, 2nd edn. Harper & Row, New York
24. Oden R (1918) Systematic therapeutic exercises in the management of the paralyses in hemiplegia. JAMA 23:828–833
25. Taub E, Uswatte G, Pidikiti R (1999) Constraint-induced movement therapy: a new family of techniques with broad application to physical rehabilitation–a clinical review. J Rehabil Res 36(3):237–251
26. Wolf SL, Winstein CJ, Miller JP, Taub E, Uswatte G, Morris D, Giuliani C, Light KE, Nichols-Larsen D (2006) Effect of constraint-induced movement therapy on upper extremity function 3 to 9 months after stroke: the EXCITE randomized clinical trial. JAMA 296(17):2095–2104
27. Lacquaniti F, Maioli C (1992) Distributed control of limb position and force. In: Stelmach GE, Requin J (ed) Tutorials in motor behavior II. North-Holland, Amsterdam/New York/Distributors for the U.S. and Canada, Elsevier Science, New York, pp 31–54

28. Karniel A, Meir R, Inbar GF (1999) Exploiting the virtue of redundancy. In: International joint conference on neural networks, Washington, DC
29. Glynn S, Fekieta R, Henning R (2001) Use of force-feedback joysticks to promote teamwork in virtual teleoperation. In: Virtual teleoperation proceedings of the human factors and ergonomics society 45th annual meeting, Minneapolis/St. Paul
30. Shergill SS, Bays PM, Frith CD, Wolpert DM (2003) Two eyes for an eye: the neuroscience of force escalation. Science 301:187
31. Valles N, Reed KB, To know your own strength: overriding natural force attenuation. IEEE Trans Haptics. doi:10.1109/TOH.2013.55
32. Pan P, Lynch KM, Peshkin MA, Colgate JE (2004) Static single-arm force generation with kinematic constraints. In: Proceedings of the IEEE international conference on robotics and automation ICRA ’04, New Orleans, vol 3, pp 2794–2800
33. Reed KB, Peshkin MA, Hartmann MJ, Grabowecky M, Patton J, Vishton PM (2006) Haptically linked dyads: are two motor-control systems better than one? Psychol Sci 17(5):365–366
34. Reed KB, Peshkin MA (2008) Physical collaboration of human-human and human-robot teams. IEEE Trans Haptics 1(2):108–120
35. Krebs H, Ferraro M, Buerger S, Newbery M, Makiyama A, Sandmann M, Lynch D, Volpe B, Hogan N (2004) Rehabilitation robotics: pilot trial of a spatial extension for mit-manus. J Neuroeng Rehabil 1(1):5
36. Timmermans A, Seelen H, Willmann R, Kingma H (2009) Technology-assisted training of arm-hand skills in stroke: concepts on reacquisition of motor control and therapist guidelines for rehabilitation technology design. J Neuroeng Rehabil 6(1). doi:10.1186/1743-0003-6-1
37. Kahn L, Zygman M, Rymer WZ, Reinkensmeyer D (2006) Robot-assisted reaching exercise promotes arm movement recovery in chronic hemiparetic stroke: a randomized controlled pilot study. J Neuroeng Rehabil 3(1):12
38. Liepert J, Uhde I, Gräf S, Leidner O, Weiller C (2001) Motor cortex plasticity during forced-use therapy in stroke patients: a preliminary study. J Neurol 248:315–321
39. Wittenberg GF, Chen R, Ishii K, Bushara KO, Taub E, Gerber LH, Hallett M, Cohen LG (2003) Constraint-induced therapy in stroke: magnetic-stimulation motor maps and cerebral activation. Neurorehabil Neural Repair 17(1):48–57
40. Schmidt RA, Bjork RA (1992) New conceptualizations of practice: common principles in three paradigms suggest new concepts for training. Psychol Sci 3(4):207–217
41. Reed KB (2007) Understanding the haptic interactions of working together. Ph.D. thesis, Northwestern University
42. Patton JL, Stoykov ME, Kovic M, Mussa-Ivaldi FA (2006) Evaluation of robotic training forces that either enhance or reduce error in chronic hemiparetic stroke survivors. Exp Brain Res 168:368–383
43. Smith MA, Ghazizadeh A, Shadmehr R (2006) Interacting adaptive processes with different timescales underlie short-term motor learning. PLoS Biol 4(6):e179
44. Wolpert DM, Diedrichsen J, Flanagan JR (2011) Principles of sensorimotor learning. Nat Rev Neurosci 12(12):739–751
45. Abe M, Schambra H, Wassermann EM, Luckenbaugh D, Schweighofer N, Cohen LG (2011) Reward improves long-term retention of a motor memory through induction of offline memory gains. Curr Biol 21(7):557–562
46. Huang VS, Haith A, Mazzoni P, Krakauer JW (2011) Rethinking motor learning and savings in adaptation paradigms: model-free memory for successful actions combines with internal models. Neuron 70(4):787–801
47. Holden MK, Dyar TA, Dayan-Cimadoro L (2007) Telerehabilitation using a virtual environment improves upper extremity function in patients with stroke. IEEE Trans Neural Syst Rehabil Eng 15(1):36–42
48. Weiss P, Rand D, Katz N, Kizony R (2004) Video capture virtual reality as a flexible and effective rehabilitation tool. J Neuroeng Rehabil 1(1):12

49. Henderson A, Korner-Bitensky N, Levin M (2007) Virtual reality in stroke rehabilitation: a systematic review of its effectiveness for upper limb motor recovery. Top Stroke Rehabil 14(2):52–61
50. Cameirão MS, Bermudez i Badia S, Oller ED, Verschure PF (2008) Using a multi-task adaptive vr system for upper limb rehabilitation in the acute phase of stroke. In: Virtual rehabilitation, Vancouver. IEEE, pp 2–7
51. Broeren J, Sunnerhagen KS, Rydmark M (2007) A kinematic analysis of a haptic handheld stylus in a virtual environment: a study in healthy subjects. J Neuroeng Rehabil 4(1):13
52. Bouzit M, Burdea G, Popescu G, Boian R (2002) The rutgers master II-new design force-feedback glove. IEEE/ASME Trans Mechatron 7(2):256–263
53. Sanchez RJ, Liu J, Rao S, Shah P, Smith R, Rahman T, Cramer SC, Bobrow JE, Reinkensmeyer DJ (2006) Automating arm movement training following severe stroke: functional exercises with quantitative feedback in a gravity-reduced environment. IEEE Trans Neural Syst Rehabil Eng 14:378–389
54. Housman SJ, Scott KM, Reinkensmeyer DJ (2009) A randomized controlled trial of gravity-supported, computer-enhanced arm exercise for individuals with severe hemiparesis. Neurorehabil Neural Repair 23(5):505–514
55. Rotella MF, Guerin K, He X, Okamura AM (2012) Hapi bands: a haptic augmented posture interface. In: 2012 IEEE haptics symposium (HAPTICS), Vancouver. IEEE, pp 163–170
56. Kuchenbecker KJ, Gurari N, Okamura AM (2007) Effects of visual and proprioceptive motion feedback on human control of targeted movement. In: IEEE 10th international conference on rehabilitation robotics (ICORR 2007), Noordwijk. IEEE, pp 513–524
57. Zheng H, Davies R, Zhou H, Hammerton J, Mawson SJ, Ware PM, Black ND, Eccleston C, Hu H, Stone T, Mountain GA, Harris ND (2006) Smart project: application of emerging information and communication technology to homebased rehabilitation for stroke patients. Int J Disabil Human Dev Spec Issue Adv Virtual Real Ther Rehabil 5(3):271–276
58. Reinkensmeyer DJ, Pang CT, Nessler JA, Painter CC (2001) Java therapy: web-based robotic rehabilitation. Integr Assist Technol Inf Age 9:66–71
59. Feng X, Johnson M, Johnson L, Winters J (2005) A suite of computer-assisted techniques for assessing upper-extremity motor impairments. Conf Proc IEEE Eng Med Biol Soc 7:6867–6870
60. Johnson M, Feng X, Johnson L, Winters J (2007) Potential of a suite of robot/computer-assisted motivating systems for personalized, home-based, stroke rehabilitation. J Neuroeng Rehabil 4(1):6
61. Johnson M, Van der Loos H, Burgar C, Shor P, Leifer L (2005) Experimental results using force-feedback cueing in robot-assisted stroke therapy. IEEE Trans Neural Syst Rehabil Eng 13:335–348
62. Johnson M, Ramachandran B, Paranjape R, Kosasih J (2006) Feasibility study of theradrive: a low-cost game-based environment for the delivery of upper arm stroke therapy. Proc IEEE Eng Med Biol Soc 1:695–698
63. Westhoff T, Schmidt S, Gross V, Joppke M, Zidek W, der Giet MV, Dimeo F (2008) The cardiovascular effects of upper-limb aerobic exercise in hypertensive patients. J Hypertens 26:1336–1342
64. Diserens K, Perret N, Chatelain S, Bashir S, Ruegg D, Vuadens P, Vingerhoets F (2007) The effect of repetitive arm cycling on post stroke spasticity and motor control: repetitive arm cycling and spasticity. J Neurol Sci 253(3):18–24
65. Zehr EP, Loadman P, Hundza SR (2012) Neural control of rhythmic arm cycling after stroke. J Neurophysiol 108:891–905
66. Burgar C, Lum P, Shor P, Van der Loos H (2000) Development of robots for rehabilitation therapy: the Palo Alto VA/Stanford experience. J Rehabil Res Dev 37:663–674
67. Wolf SL, LeCraw DE, Barton LA (1989) Comparison of motor copy and targeted biofeedback training techniques for restitution of upper extremity function among patients with neurologic disorders. Phys Ther 69(9):719–735

68. Hesse S, Schulte-Tigges G, Konrad M, Bardeleben A, Werner C (2003) Robot-assisted arm trainer for the passive and active practice of bilateral forearm and wrist movements in hemiparetic subjects. Arch Phys Med Rehabil 84(6):915–920
69. Yang C, Lin K, Chen H, Wu C, Chen C (2012) Pilot comparative study of unilateral and bilateral robotassisted training on upper-extremity performance in patients with stroke. Am J Occup Ther 66(2):198–206
70. Whitall J, Waller S, Silver K, Macko R (2000) Repetitive bilateral arm training with rhythmic auditory cueing improves motor function in chronic hemiparetic stroke. Stroke 31(10):2390–2395
71. Whitall J, Waller S, Sorkin J, Forrester L, Macko R, Hanley D, Goldberg A, Luft A (2011) Bilateral and unilateral arm training improve motor function through differing neuroplastic mechanisms: a single-blinded randomized controlled trial. Neurorehabil Neural Repair 25(2):118–129
72. Hesse S, Werner C, Pohl M, Mehrholz J, Puzich U, Krebs HI (2008) Mechanical arm trainer for the treatment of the severely affected arm after a stroke: a single-blinded randomized trial in two centers. Am J Phys Med Rehabil 87(10):779–788
73. Jordan K, Sampson M, Hijmans J, King M, Hale L (2011) Imable system for upper limb stroke rehabilitation. In: 2011 international conference on virtual rehabilitation (ICVR), Zurich, June 2011, pp 1–2
74. Malabet HG, Robles RA, Reed KB (2010) Symmetric motions for bimanual rehabilitation. In: Proceedings of the IEEE/RSJ international conference on intelligent robots and systems (IROS), Taipei, pp 5133–5138
75. McAmis S, Reed KB (2011) Symmetry modes and stiffnesses for bimanual rehabilitation. In: Proceedings of the IEEE international conference on rehabilitation robotics, Zurich, June 2011, pp 1106–1111
76. McAmis S, Reed KB (2012) Simultaneous perception of forces and motions using bimanual interactions. IEEE Trans Haptics 5(3):220–230
77. McAmis S, Reed KB (2013) Design and analysis of a compliant bimanual rehabilitation device. In: Proceedings of the IEEE international conference on rehabilitation robotics, Seattle, June 2013
78. McAmis S, Reed KB (2013) Effects of compliant coupling on cooperative and bimanual task performance. J Rehabil Robot 1(2):99–108.
79. Brandstater M, de Bruin H, Gowland C, Clark B (1983) Hemiplegic gait: analysis of temporal variables. Arch Phys Med Rehabil 64:583–587
80. Wall J, Turnbull G (1986) Gait asymmetries in residual hemiplegia. Arch Phys Med Rehabil 67:550–553
81. Belda-Lois JM, del Homo M, Bermejo-Bosch I, Moreno JC, Pons J, Farina D, Losa M, Molinari M, Tamburella F, Ramos A, Caria A, Solis-Escalante T, Brunner C, Rea M (2011) Rehabilitation of gait after stroke: a review towards a top-down approach. J Neuroeng Rehabil 8:66
82. Teixeira-Salmela L, Nadeau S, Mcbride I, Olney S (2001) Effects of muscle strengthening and physical conditioning training on temporal kinematic and kinetic variables in gait stroke survivors. J Rehabil Med 33:53–60
83. Teixeira-Salmela L, Olney SJ, Nadeau S, Brouwer B (1999) Muscle strengthening and physical conditioning to reduce impairment and disability in chronic stroke survivors. Arch Phys Med Rehabil 80(10):1211–1218
84. Stern P, McDowell F, Miller J, Robinson M (1970) Effects of facilitation exercise techniques in stroke rehabilitation. Arch Phys Med Rehabil 51:526–31
85. Lennon S (1996) The bobath concept: a critical review of the theoretical assumptions that guide physiotherapy practice in stroke rehabilitation. Phys Ther Rev 1:35–45
86. Perfetti C (2001) L'exercice Thérapeutique Cognitif Pour La Rééducation Du Patient Hémiplégique. Masson

87. Carr JH, Shepherd RB (2003) Stroke rehabilitation: guidelines for exercice and training to optimiza motor skill, 1st edn. Elsevier Health Sciences. Butterworth-Heinemann
88. Hesse S, Bertelt C, Jahnke M, Schaffrin A, Baake P, Malezic M, Mauritz KH (1995) Treadmill training with partial body weight support compared with physiotherapy in nonambulatory hemiparetic patients. Stroke 26:976–81
89. Bates B, Choi J, Duncan P, Glasberg J, Graham G, Katz R, Lamberty K, Reker D, Zorowitz R (2005) Veterans affairs/department of defense clinical practice guideline for the management of adult stroke rehabilitation care. Stroke 36:2049–2056
90. States R, Salem Y, Pappas E (2009) Overground gait training for individuals with chronic stroke: a cochrane systematic review. J Neurol 33:179–86
91. Moseley A, Stark A, Cameron I, Pollock A (2005) Treadmill training and body weight support for walking after stroke. Cochrane Database Syst Rev 19. http://onlinelibrary.wiley.com/doi/10.1002/14651858.CD002840.pub2/abstract
92. Jette D, Latham N, Smout R, Gassaway J, Slavin M, Horn S (2005) Physical therapy interventions for patients with stroke in inpatient rehabilitation facilities. Phys Ther 85:238–248
93. Carrillo-de-la-Pena MT et al (2008) Equivalent is not equal: primary motor cortex (mi) activation during motor imagery and execution of sequential movements. Brain Res 1226(0):134–143
94. Dunsky A, Dickstein R, Marcovitz E, Levy S, Deutsch J (2008) Home-based motor imagery training for gait rehabilitation of people with chronic poststroke hemiparesis. Arch Phys Med Rehab 89:1580–1588
95. Malouin F, Richards C (2010) Mental practice for relearning locomotor skills. Phys Ther 90:240–251
96. Dohring M, Janis J (2008) Automatic synchronization of functional electrical stimulation and robotic assisted treadmill training. IEEE Trans Neural Syst Rehabil Eng 16(3):310–313
97. Barbeau H, Visintin M (2003) Optimal outcomes obtained with body-weight support combined with treadmill training in stroke subjects. Arch Phys Med Rehabil 84:1458–1465
98. Riener R, Lunenburger L, Jezernik S, Anderschitz M, Colombo G, Dietz V (2005) Patient-cooperative strategies for robot-aided treadmill training: first experimental results. IEEE Trans Neural Syst Rehabil Eng 13(3):380–394
99. Bogey R, Hornby G (2007) Gait training strategies utilized in poststroke rehabilitation: are we really making a difference? Top Stroke Rehabil 14:1–8
100. Colombo G (2000) The lokomat: a driven ambulatory orthosis. Med Orthop Technol 6:178–181
101. Swinnen E, Duerinck S, Baeyens J, Meeusen R, Kerckhofs E (2010) Effectiveness of robot-assisted gait training in persons with spinal cord injury: a systematic review. J Rehabil 42:520–526
102. Duschau-Wicke A (2010) Path control: a method for patient-cooperative robot-aided gait rehabilitation. Trans Neural Syst Rehabil Eng 18:38–48
103. Kim S, Banala S, Brackbill E, Agrawal S, Krishnamoorthy V, Scholz J (2010) Robot-assisted modifications of gait in healthy individuals. Exp Brain 202(4):809–824
104. Monaco V, Galardi G, Jung J, Bagnato S, Boccagni C, Micera S (2009) A new robotic platform for gait rehabilitation of bedridden stroke patients. In: IEEE international conference on rehabilitation robotics, ICORR 2009, Kyoto, pp 383–388
105. Monaco V, Jung JH, Macrì G, Bagnato S, Micera S, Carrozza MC, Galardi G (2008) Robotic system for gait rehabilitation of stroke patients during the acute phase. Gerontechnology 7:2
106. Kamps A, Schule K (2005) Cyclic movement training of the lower limb in stroke rehabilitation. Neurol Rehabil 11:1–12
107. Laupheimer M, Hartel S, Schmidt S (2011) Forced exercise effects of motomed®training on parkinson's- typical motor dysfunctions. Neurol Rehabil 17:239–246
108. Diehl W, Schüle K, Kaiser T (2008) Use of an assistive movement training apparatus in the rehabilitation of geriatric patients. NeuroGeriatrie 5(1):3–12

109. Kim SH, Reed KB (2013) Robot-assisted balance training for gait modification. In: Proceedings of the IEEE international conference on rehabilitation robotics, Seattle, June 2013
110. Sulzer J, Gordon K, Hornby TG, Peshkin M, Patton J (2009) Adaptation to knee flexion torque during gait. In: Proceedings of the IEEE international conference on rehabilitation robotics, Kyoto, pp 713–718
111. Reisman D, Wityk R, Silver K, Bastian A (2007) Locomotor adaptation on a split-belt treadmill can improve walking symmetry post-stroke. Brain 130(7):1861–1872
112. Choi JT, Vining EPG, Reisman DS, Bastian AJ (2009) Walking flexibility after hemispherectomy: split-belt treadmill adaptation and feedback control. Brain 132:722–733
113. Reisman DS, Wityk R, Silver K, Bastian AJ (2009) Split-belt treadmill adaptation transfers to overground walking in persons poststroke. Neurorehabil Neural Repair 23:735–744
114. Reisman D, McLean H, Keller J, Danks K, Bastian A (2013) Repeated split-belt treadmill training improves poststroke step length asymmetry. Neurorehabilitation 27:460–468
115. Torres-Oviedo G, Bastian AJ (2010) Seeing is believing: effects of visual contextual cues on learning and transfer of locomotor adaptation. J Neurosci 30(50):17015–17022
116. Bunday KL, Bronstein AM (2009) Locomotor adaptation and aftereffects in patients with reduced somatosensory input due to peripheral neuropathy. J Neurophysiol 102:3119–3128
117. Handžić I, Reed KB (2013) Comparison of the passive dynamics of walking on ground, tied-belt and split-belt treadmills, via the gait enhancing mobile shoe (GEMS). In: Proceedings of the IEEE international conference on rehabilitation robotics, Seattle, June 2013
118. de Groot A, Decker R, Reed KB (2009) Gait enhancing mobile shoe (GEMS) for rehabilitation. In: Proceedings of joint eurohaptics conference and symposium on haptic interfaces for virtual environment and teleoperator systems, Salt Lake City, Mar 2009, pp 190–195
119. Handžić I, Barno E, Vasudevan EV, Reed KB (2011) Design and pilot study of a gait enhancing mobile shoe. J Behav Robot 2(4):193–201
120. Handžić I, Reed KB (2011) Motion controlled gait enhancing mobile shoe for rehabilitation. In: Proceedings of the IEEE international conference on rehabilitation robotics, Zurich, June 2011, pp 583–588
121. Handžić I, Reed K (2014) Kinetic shapes: analysis, verification, and applications. J Mech Des 136(6)
122. Gibson-Horn C (2008) Balance-based torso-weighting in a patient with ataxia and multiple sclerosis: a case report. J Neurol Phys Ther 32(3):139–146
123. McGeer T (1990) Passive dynamic walking. Int J Robot Res 9(2):62–82
124. Honeycutt C, Sushko J, Reed KB (2011) Asymmetric passive dynamic walker. In: Proceedings of the IEEE international conference on rehabilitation robotics, Zurich, June 2011, pp 852–857
125. Margaria R (1976) Biomechanics and energetics of muscular exercise. Clarendon, Oxford
126. Chen VFH (2005) Passive dynamic walking with knees: a point foot model. Master's thesis, Massachusetts Institute of Technology
127. Sushko J, Honeycutt C, Reed KB (2012) Prosthesis design based on an asymmetric passive dynamic walker. In: Proceedings of the IEEE conference on Biorob, Roma, June 2012, pp 1116–1121
128. Handžić I, Reed KB (2013) Validation of a passive dynamic walker model for human gait analysis. In: Proceedings of IEEE engineering in medicine and biology society, Osaka, pp 6945–6948
129. Gregg R, Dhaher Y, Degani A, Lynch K (2012) On the mechanics of functional asymmetry in bipedal walking. IEEE Trans Biomed Eng 59:1310–1318
130. Bogataj U, Gros N, Kljaji M, Malezic M (1995) The rehabilitation of gait in patients with hemiplegia: a comparison between conventional therapy and multichannel functinal electrical stimulation therapy. Phys Ther 75:490–502
131. Stanic U, Acimovi-Janezic R, Gros N, Trnkoczy A, Bajd T, Kljaji M (1978) Multichannel electrical stimulation for correction of hemiplegic gait. Methodology and preliminary results. Scand J Rehabil Med 10:75–92

132. Bogataj U, Gros N, Malezic M, Kelih B, Kljaji M, Acimovi R (1989) Restoration of gait during two to three weeks of therapy with multichannel electrical stimulation. Phys Ther 69:319–327
133. Ng MF, Tong RK, Li LS (2008) A pilot study of randomized clinical controlled trial of gait training in subacute stroke patients with partial body-weight support electromechanical gait trainer and functional electrical stimulation. Stroke 39:154–160
134. Pollock GBA, Pomeroy V, Langhorne P (2007) Physiotherapy treatment approaches for the recovery of postural control and lower limb function following stroke. Cochrane Database Syst Rev 24

Chapter 15
Unilateral and Bilateral Rehabilitation of the Upper Limb Following Stroke via an Exoskeleton

Jacob Rosen, Dejan Milutinović, Levi M. Miller, Matt Simkins, Hyunchul Kim, and Zhi Li

Abstract Recent studies reported positive effects of bilateral arm training on stroke rehabilitations. The development of novel robotic-based therapeutic interventions aims at recovery of the motor control system of the upper limb, in addition to the increase of the understanding of neurological mechanisms underlying the recovery of function post stroke. A dual-arm upper limb exoskeleton EXO-UL7 that is kinematically compatible with the human arm is developed to assist unilateral and bilateral training after stroke. Control algorithms are designed and implemented to improve the synergy of the human arm and the upper limb exoskeleton. Clinical studies on the robot-assisted bilateral rehabilitations show that both the unilateral and bilateral training have a positive effect on the recovery of the paretic arm. Bilateral training outperforms unilateral training by a significant improvement of motion range and movement velocities.

Keywords Unilateral/bilateral stroke rehabilitation • Upper limb exoskeleton • Human arm • Kinematics • Dynamics

---

J. Rosen (✉) • D. Milutinović • M. Simkins • Z. Li
Department of Computer Engineering, University of California, Santa Cruz, CA 95064, USA
e-mail: rosen@ucsc.edu; dejan@soe.ucsc.edu; msimkins@soe.ucsc.edu; zli12@ucsc.edu

L.M. Miller
Carbon Design Group, Seattle, WA, USA
e-mail: levimakaio@gmail.com

H. Kim
Apple Inc., Cupertino, CA, USA
e-mail: hyunchul78@gmail.com

P. Artemiadis (ed.), *Neuro-Robotics: From Brain Machine Interfaces to Rehabilitation Robotics*, Trends in Augmentation of Human Performance 2,
DOI 10.1007/978-94-017-8932-5_15,

15.1 Introduction

Stroke is a leading cause of long-term neurological disability and the top reason for seeking rehabilitative services in the U.S. Challenges in rehabilitation after stroke, especially in the chronic phase are two-fold: the first is the development of systems for intense delivery of targeted rehabilitative interventions based on neural plasticity that will facilitate recovery and the second is to understand neural reorganization that facilitates the recovery of function. Whereas in the acute phase post stroke, medical management focuses on containing and minimizing the extent of the injury, in the chronic phase post stroke, neural plasticity induced by learning/training is the fundamental mechanism for recovery. The development of novel robotic based therapeutic interventions aims at facilitating neural plasticity and inducing sustainable recovery of the motor control system of the upper limb. In addition, studies on the synergy of the human are and wearable robotic system (e.g., an upper limb exoskeleton) improve the understanding of neurological mechanisms which aim to maximize the recovery of function post stroke.

15.1.1 Bilateral Robotic System and Treatment

Research studies suggest that manual bilateral movements in which both arms and hands move simultaneously in a mirror image fashion or work simultaneously while performing a bilateral task have profound effects on the reorganization of the neural system due to inherent brain plasticity. Using such a therapeutic approach for stroke patients is based on the understanding that both brain hemispheres (damaged and undamaged) are going through a natural recovery process, as well as neural reorganization following a learning-based therapy. In spite of significant scientific evidence, translating a mirror image bilateral therapeutic approach into an intense (high dosage) physical rehabilitation treatment regime has been difficult. A therapist administering this regime is challenged to simultaneously control the 16 degrees of freedom (DOF) of both arms (14 DOF) and hands (2 DOF limited to 3-point chuck type grasping).

When considering bilateral symmetric movement training as an option for therapy, there are two aspects to its efficacy. The first aspect relates to neuroscience. Based on experiments relating to bilateral symmetric manual coordination using trans-cranial magnetic stimulation and kinematic modeling, symmetric movement might reduce inhibitions between the left and right hemispheres [1, 2]. In other words, bilateral symmetric movements have been found to increase cross-talk in the corpus callosum. In that vein, multiple studies have demonstrated the effectiveness of mirror therapy. Using mirror therapy, stroke survivors were able to improve function based on the optical illusions of their paretic arm moving normally [3, 4]. Based on such research, it has been proposed that symmetric movement training might exploit such coupling thereby allowing for an increased use of undamaged ipsilateral projections [5]. In this way, symmetric movement training might improve the recovery process after a CVA. With respect to clinical outcomes, the results are somewhat mixed. It is admittedly difficult to detect improvement. For individuals who have chronic motor impairment, improvement after therapy is often subtle. Standard care, unilateral and bilateral movement training have all been shown to result in some improvement. However, distinguishing between training modalities is difficult and the differences are small. To that end, there is virtually no data (such as brain imaging) relating to neurological activity and bilateral therapy. For these reasons, it remains uncertain if bilateral symmetric therapy is truly better than unilateral therapy in the sense that there is more or less cross-talk between the hemispheres. More to the point, there is no conclusive evidence that bilateral symmetric movement training has a neurological basis.

Beyond neurological considerations, there are factors that distinguish the efficacy of bilateral and unilateral movement training. Bilateral movement training was shown to have better results than unilateral movement training in terms of the range of motion (ROM). One explanation for this difference is that the paretic arm was provided robotic assistance, while in the unilateral case, no assistance was provided. Subjects also reported that they preferred assistance [6]. While it is true that a robot can provide assistance for unilateral movement training, the control algorithms and game designs become much more constrained. During movement training, providing assistance that moves the arm through large angles might make the therapy feel unpredictable and might raise safety concerns. However, when the paretic arm is made to move symmetrically with the less affected arm, the subject is in control, and the game play is more predictable and the assistance is more natural. Therefore, bilateral training provides a flexible control paradigm for unstructured assistance.

There are two approaches for bilateral training. One involves full assistance [7] and the other requires partial assistance [6]. For full assistance, the paretic arm is forced into symmetric motion. Using this approach, the subjects may focus entirely on their less affected limb in order to play therapy games or to complete tasks. The subjects might use a minimum of effort to move their paretic arm, and what movements they do make will have little to no effect on the game play or task completion. Bilateral symmetric movement training with partial assistance allows the robot to provide some help for the paretic arm. However, the subjects cannot quite play the game or complete the task with their paretic arm unless they provide some voluntary effort. Subjects also perceived better outcomes for full assistance than partial assistance [6].

Bilateral symmetric movement training does have the potential to aggravate spasticity [6]. The cause for this relates to the speed of motion. It is known that rapid flexion and extension of spastic joints can intensify existing spasticity. This in turn can result in pain, weakness, and reduced coordination. When subjects perform symmetric movements, their less affected arm might move too rapidly. In turn, as the robot attempts to maintain symmetry, the paretic arm might move too quickly thus aggravating spasticity. The largest effects were evident in the hand. Therefore, bilateral symmetric movement is recommended for individuals who have mild spasticity. If robotic training is used with assistance, be it bilateral or unilateral, care is needed not to move the paretic arm too fast.

15.1.2 Robot-Assisted Stroke Rehabilitation

Recently research results have demonstrated that robotic devices can deliver effective rehabilitation therapies to patients suffering from the chronic neuromuscular disorders [8–10]. MIT-MANUS is one of the successful rehabilitation robots which adopted back-drivable hardware and impedance control as a robot control system [11]. ARMin is a 7-DOF upper limb exoskeleton developed in ETH Zurich and the University of Zurich. This robot provides visual, acoustic and haptic interfaces together with cooperative control strategies to facilitate the patient's active participation in the game. The lengths of the upper arm, lower arm, hand and the height of the device are adjustable to accommodate patients of different sizes. The rehabilitation site and robotic system are wheelchair accessible. Pneu-WREX is a 6-DOF exoskeleton robot developed in UC Irvine. This robotic system adopted pneumatic actuators [12]. Although the pneumatic actuator is harder to control due to its non-linear characteristics, it produces relatively large forces with a low on-board weigh [13]. The robot interacts with the virtual-reality game T-WREX based on a Java Therapy 2.0 software system. Arizona State University researchers developed a robotic arm, RUPERT (Robotic Upper Extremity Repetitive Therapy) targeting cost-effective and light-weight stroke patient rehabilitation [14, 15]. The device provides the patient with assistive force to facilitate fluid and natural arm movements essential for the activities of daily living. The controller for the pneumatic muscles can be programmed for each user to improve their arm and hand flexibility, as well as strength by providing a repetitive exercise pattern. In our previous work [16], the seven-DOF exoskeleton robot UL-EXO7 [8, 17, 18] was exploited as a core mechanical system for the long-term clinical trial of the bilateral and unilateral rehabilitation program. The controllers equipped in UL-EXO7 provided the assistive force to help patients make the natural arm posture based on the work in [19, 20]. For the objective and fine-scale rehabilitation assessment, a new assessment metric, an efficiency index, was introduced to tell the therapist how close the patient's arm movements are to the normal subject's arm movements.

15.1.3 Objective and Paper Structure

This chapter describes the EXO-UL7 – an upper limb exoskeleton system and its clinical applications to bilateral stroke rehabilitation. Section 15.2 reviews the kinematic design of the EXO-UL7 with considerations in its compatibility with the kinematics of the human arm. Based on the kinematic modeling of the human arm, the forward and inverse kinematics are derived. The control architectures are addressed, including the control algorithms for admittance control, gravity compensation, inter-arm teleoperation and redundancy resolution. Clinical studies on robot-assisted bilateral rehabilitations are presented in Sect. 15.3, with a comparison of the outcomes of unilateral and bilateral training.

15.2 An Upper Limb Exoskeleton: EXO-UL7

15.2.1 System Overview

The kinematics and dynamics of the human arm during activities of daily living (ADL) have been studied to determine specifications for exoskeleton design (see Fig. 15.1). Articulation of the exoskeleton is achieved by seven single-axis revolute joints which support 99 % of the range of motion required to perform daily activities. Three revolute joints are responsible for shoulder abduction-adduction, flexion-extension and internal-external rotation. A single rotational joint is employed at the elbow, creating elbow flexion-extension. Finally, the lower arm and hand are connected by a three-axis spherical joint resulting in wrist pronation-supination, flexion-extension, and radial-ulnar deviation. As a

Fig. 15.1 The upper limb exoskeleton EXO-UL7 with seven DOFs, supporting 99 % of the range of motion required to preform daily activities

human-machine interface (HMI), four six-axis force/torque sensors (ATI Industrial Automation, model-Mini40) are attached to the upper arm, the lower arm, the hand and the tip of the exoskeleton. The force/torque sensor at the tip of the exoskeleton allows measurements of the interactions between the exoskeleton and the environment [8, 9, 21].

15.2.2 Kinematic Design of the Upper Limb Exoskeleton EXO-UL7

15.2.2.1 Kinematic Modeling of the Human Arm

The upper limb exoskeleton EXO-UL7 is designed to be compatible with the human arm kinematics. The human arm is composed of segments linked by articulations with multiple degrees of freedom. It is a complex structure that is made up of both rigid bone and soft tissue.Although much of the complexity of the soft tissue is difficult to model, the overall arm movement can be represented by a much rigid body model composed of rigid links connected by joints. Three rigid segments, consisting of the upper arm, lower arm and hand, connected by frictionless joints, make up the simplified model of the human arm. The upper arm and torso are rigidly attached by a ball and socket joint. This joint enables shoulder abduction-adduction (abd-add), shoulder flexion-extension (flx-ext) and shoulder internal-external (int-ext) rotation. The upper and lower arm segments are attached by a single rotational joint at the elbow, creating elbow flx-ext. Finally, the lower arm and hand are connected by a 3-axis spherical joint resulting in pronation-supination (pron-sup), wrist flx-ext, and wrist radial-ulnar (rad-uln) deviation. Models of the human arm with seven DOFs have been widely used in various applications, including rendering human arm movements by computer graphics [22, 23], controlling redundant robots [24, 25], kinematic design of the upper limb exoskeletons [18, 26, 27], and biomechanics [28–30]. These models provide a synthesis of proper representation of the human and the exoskeleton arm as redundant mechanisms along with and adequate level of complexity.

The kinematics and dynamics of the human arm during activities of daily living (ADL) were studied in part to determine engineering specifications for the exoskeleton design [8]. Using these specification, two exoskeletons were developed, each with seven DOFs. Each exoskeleton arm is actuated by seven DC brushed motors (Maxon) that transmit the appropriate torque to each joint utilizing a cable-based transmission. The mechanisms are attached to a frame mounted on the wall, which allows both height and distance between the arms to be adjusted. Articulation of the exoskeleton is achieved about seven single axis revolute joints – one for each shoulder abd-add, shoulder flx-ext, shoulder int-ext rotation, elbow flx-ext, forearm pron-sup, wrist flx-ext, and wrist rad-uln deviation. The exoskeleton joints are labeled 1–7 from proximal to distal in the order shown in Fig. 15.2. With seven joint rotations, there is one redundant degree of freedom.

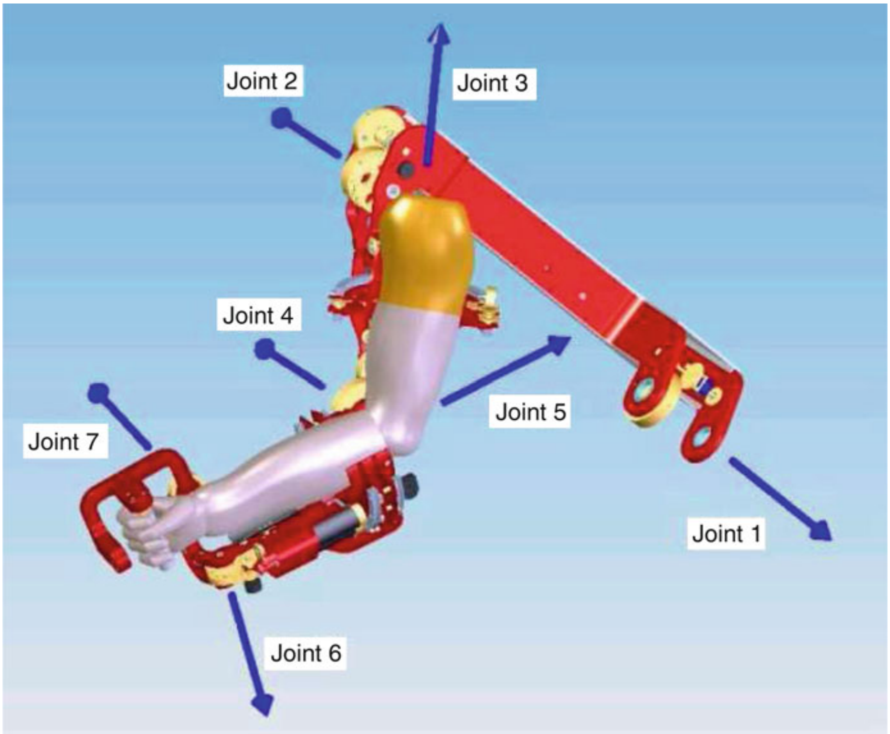

Fig. 15.2 Exoskeleton axes assignment relative to the human arm. Positive rotations about each joint produce the following motions: (*1*) combined flx/adb, (*2*) combined flx/add, (*3*) int rotation, (*4*) elbow flx, (*5*) forearm pron, (*6*) wrist ext, and (*7*) wrist rad dev

The fundamental principle in designing the exoskeleton joints is to align the rotational axis of the exoskeleton with the anatomical rotations axes. If more than one axis is at a particular anatomical joint (e.g. shoulder and wrist), the exoskeleton joints emulate the anatomical joint interaction at the center of the anatomical joint. Consistent with other work, the glenohumeral (G-H) joint is modeled as a spherical joint composed of three intersection axes [31]. The elbow is modeled by a single axis orthogonal to the third shoulder axis, with a joint stop to prevent hyperextension. Exoskeleton pron-sup takes place between the elbow and the wrist as it does. Finally, two intersecting orthogonal axes represent the wrist. The ranges of motion of the exoskeleton joints support 99 % of the ranges of motion required to perform daily activities [8].

Representing the ball and socket joint of the shoulder as three intersecting joins introduces of singularities that are not present in the human arm model. A significant consideration in the exoskeleton design is the placement of singularities [24]. The singularity is a device configuration in which a DOF is lost or compromised as a result of the alignment of two rotational axes. In the development of a three DOF

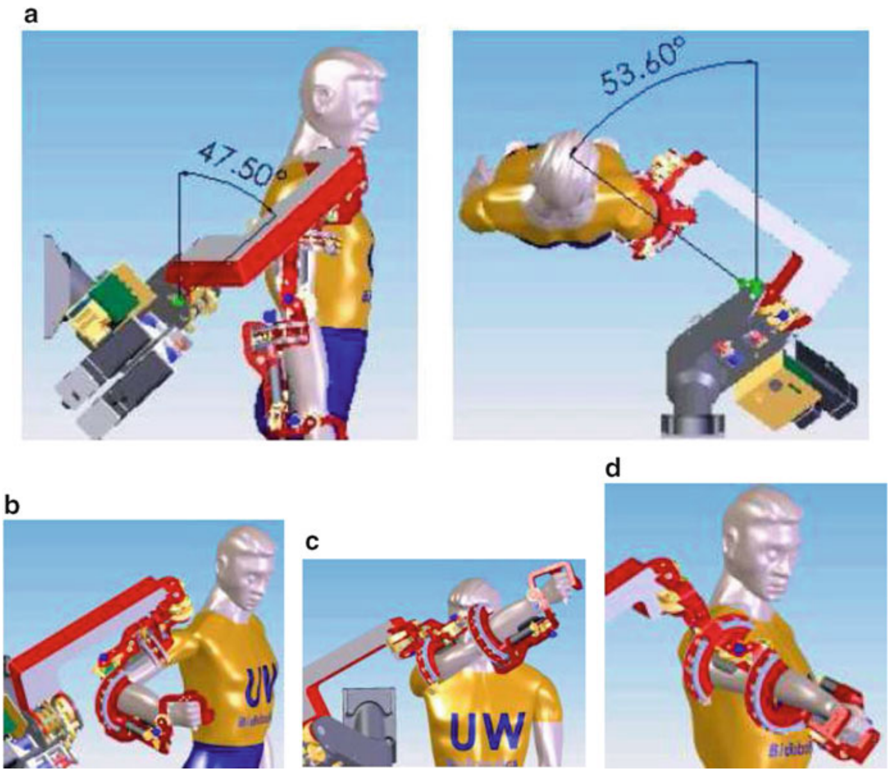

Fig. 15.3 Two singularities exist in the exoskeleton device, one when joints 1 and 3 align and the other when joints 3 and 5 align. (**a**) The orientation of joint 1 places the singularity at the shoulder in an anthropomorphically difficult place to reach. (**b**) Joints 1 and 3 align with simultaneous extension and abduction of the upper arm by 47.5° and 53.6 °. (**c**) Similarly, the same singularity can be reached through flexion and adduction by 132.5° and 53.6°. (**d**) Alignment of joints 3 and 5 naturally occurs only in full elbow extension

spherical joint, the existence or nonexistence of singularities will depend entirely on the desired reachable workspace. Spherical workspace equal to or larger than a hemisphere will always contain singular positions. The challenge is to place the singularity in an unreachable, or near-unreachable location, such as the edge of the workspace. For the exoskeleton arm, singularities occur when joints 1 and 3 or joints 3 and 5 align. To minimize the frequency of this occurrence, the axis of joint 1 is positioned such that singularities with joint 3 take place only at locations that are anthropometrically hard to reach. For the placement shown in Fig. 15.3a, the singularity can be reached through simultaneous extension and abduction of the upper arm by 47.5° and 53.6°, respectively (see Fig. 15.3b). Similarly, the same singularity can be reached through flexion and adduction by 132.5° and 53.6°, respectively (see Fig. 15.3c). The singularity between joints 3

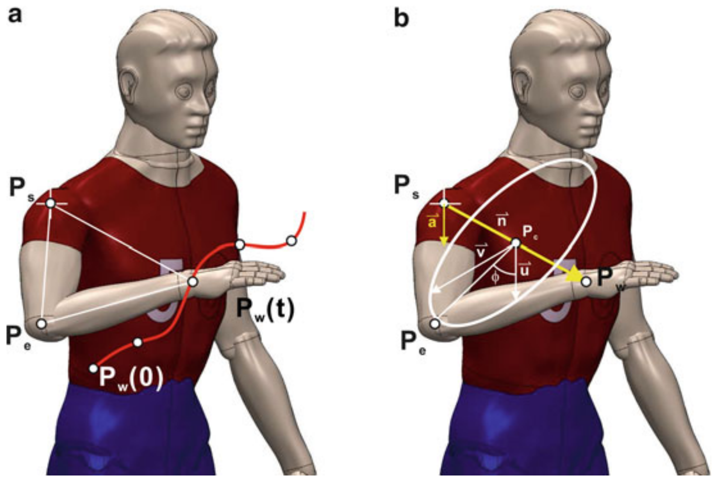

Fig. 15.4 (**a**) Given a fixed wrist position in a 3D workspace, the arm plane formed by the positions of the shoulder (P_s), the elbow (P_e) and the wrist (P_w) can move around an axis that connects the shoulder and the wrist due to the kinematic redundancy. (**b**) The redundant DOF can be represented by a swivel angle ϕ

and 5 naturally occurs only in full elbow extension, i.e., on the edge of the forearm workspace (see Fig. 15.3d). With each of these singularity vectors at or near the edge of the human workspace, the middle and majority of the workspace is free of singularities [8, 9].

15.2.2.2 Representation of the Redundant Degree of Freedom

Given the position (x, y, z) and the orientation (ϕ_x, ϕ_y, and ϕ_z) of a target in a 3-dimensional (3D) workspace, the human arm has a redundant DOF which allows the elbow to move around an axis that goes through the center of the shoulder and the wrist joints. This redundant DOF provides the flexibility in human arm postures when completing the tasks defined in the 3D workspace. When applied to controlling the upper limb exoskeleton, a swivel angle is used to represent the redundant DOF. It specifies how much the elbow position pivots about the axis that goes through the center of shoulder and center of wrist, when the hand has a specific position and orientation.

As shown in Fig. 15.4, the arm plane is formed by the positions of the shoulder, the elbow and the wrist (denoted by P_s, P_e and P_w, respectively). The direction of the axis that the arm plane pivots about (denoted by $\boldsymbol{n}$) is defined as:

$$\mathbf{n} = \frac{P_w - P_s}{||P_w - P_s||} \tag{15.1}$$

Table 15.1 Denavit-Hartenberg (DH) Parameters for upper limb exoskeleton

Robot	$i-1$	i	α_i	a_i	d_i	θ_i
Left arm	0	1	$\pi/2$	0	0	$\theta_1+\pi-32.94°$
	1	2	$\pi/2$	0	0	$\theta_2+\pi/2-28.54°$
	2	3	$\pi/2$	0	0	$\theta_3+\pi-53.6°$
	3	4	$\pi/2$	0	L_1	θ_4
	4	5	$-\pi/2$	0	0	$\theta_5-\pi/2$
	5	6	$-\pi/2$	0	L_2	$\theta_6+\pi/2$
	6	7	$\pi/2$	0	0	$\theta_7+\pi$
Right arm	0	1	$\pi/2$	0	0	$\theta_1-32.94°$
	1	2	$\pi/2$	0	0	$\theta_2-\pi/2-28.54°$
	2	3	$-\pi/2$	0	0	$\theta_3-\pi-53.6°$
	3	4	$-\pi/2$	0	$-L_1$	θ_4
	4	5	$\pi/2$	0	0	$\theta_5+\pi/2$
	5	6	$-\pi/2$	0	$-L_2$	$\theta_6+\pi/2$
	6	7	$\pi/2$	0	0	$\theta_7+\pi$

The plane orthogonal to $\mathbf{n}$ can be determined given the position of P_e. P_c is the intersection point of the orthogonal plane with the vector $P_w - P_s$. $\mathbf{P_e} - \mathbf{P_c}$ is the projection of the upper arm ($\mathbf{P_e} - \mathbf{P_s}$) on the orthogonal plane. $\mathbf{u}$ is the projection of a normalized reference vector $\mathbf{a}$ onto the orthogonal plane, which can be calculated as:

$$\mathbf{u} = \frac{\mathbf{a} - (\mathbf{a} \cdot \mathbf{n})\mathbf{n}}{||\mathbf{a} - (\mathbf{a} \cdot \mathbf{n})\mathbf{n}||} \tag{15.2}$$

The swivel angle ϕ, represents the arm posture, can be defined by the angle between the vector $\mathbf{P_e} - \mathbf{P_c}$ and $\mathbf{u}$. The reference vector $\mathbf{a}$ is suggested to be $[0, 0, -1]^T$ such that the swivel angle $\phi = 0°$ when the elbow is at its lowest possible point [32].

15.2.2.3 The Forward and Inverse Kinematics of the Upper Limb Exoskeleton

This section derives the forward and inverse kinematics of the EXO-UL7 exoskeleton. Table 15.1 shows the Denavit-Hartenberg (DH) parameters of the upper limb exoskeleton, which are derived using the standard method (see [33]). The joint angle variables are θ_i $(i = 1, \cdots, 7)$. L_1 and L_2 are the length of the upper and lower arms, respectively. The forward kinematics derives the transformation matrix ${}^0_7T$, which provides the position and the orientation of the wrist of the exoskeleton with respect to the base frame T_{base}:

Table 15.2 Base rotation of the upper limb exoskeleton

	θ_X (°)	θ_Y (°)	θ_Z (°)
Left arm	132.5	45	90
Right arm	132.5	−45	90

$$
\begin{aligned}
{}^{base}_{7}T &= T_{base} \cdot {}^{0}_{1}T \cdot {}^{1}_{2}T \cdot {}^{2}_{3}T \cdot {}^{3}_{4}T \cdot {}^{4}_{5}T \cdot {}^{5}_{6}T \cdot {}^{6}_{7}T \\
&= \begin{bmatrix} r_{11} & r_{12} & r_{13} & P_{wx} \\ r_{21} & r_{22} & r_{23} & P_{wy} \\ r_{31} & r_{32} & r_{33} & P_{wz} \\ 0 & 0 & 0 & 1 \end{bmatrix}
\end{aligned}
\tag{15.3}
$$

In order to move the singularity out of the range of the daily movements of the human arm, the bases of the two robotic arms of the upper limb exoskeleton are rotated according to Table 15.2. Note that θ_X, θ_Y and θ_Z represent the rotation about the X, Y and Z-axis, respectively. The transformation matrix for the base rotation is described in Eq. (15.4).

$$
T_{base} = Rotx(\theta_X)Rotz(\theta_Y)Rotz(\theta_Z) \tag{15.4}
$$

With the specification of the transformation matrix ${}^{0}_{7}T$, the inverse kinematics of the exoskeleton can be derived for the left and the right arm, respectively. The redundant DOF of the human arm can be constrained by specifying the elbow position ($P_e = [Pe_x, Pe_y, Pe_z]^T$).

Based on the shoulder position P_s, elbow position P_e, and wrist position P_w, θ_4 can be derived as:

$$
W = ||P_w - P_s|| \tag{15.5}
$$

$$
c_4 = \frac{L_1^2 + L_2^2 - W^2}{2L_1L_2} \tag{15.6}
$$

$$
s_4 = \sqrt{1 - c_4^2} \tag{15.7}
$$

$$
\theta_4 = \pi - Atan2(s_4, c_4) \tag{15.8}
$$

The transformation matrix ${}^{3}_{4}T$ and its inverse ${}^{3}_{4}T^{-1}$ can be found based on θ_4.

The transformation matrix without the base rotation, denoted ${}^{base}_{7}T$, can be found by:

$$
{}^{0}_{7}T = T_0^{-1} \cdot {}^{base}_{7}T = \begin{bmatrix} r'_{11} & r'_{12} & r'_{13} & {}^{0}_{7}P_{wx} \\ r'_{21} & r'_{22} & r'_{23} & {}^{0}_{7}P_{wy} \\ r'_{31} & r'_{32} & r'_{33} & {}^{0}_{7}P_{wz} \\ 0 & 0 & 0 & 1 \end{bmatrix} \tag{15.9}
$$

Thus, the wrist position with respect to the rotated base is ${}^{0}_{7}P_w = [{}^{0}_{7}P_{wx}, {}^{0}_{7}P_{wy}, {}^{0}_{7}P_{wz}]^T$.

Similarly, the elbow position with respect to the rotated base, denoted by ${}_7^0P_e = [{}_7^0P_{ex}, {}_7^0P_{ey}, {}_7^0P_{ez}]^T$, is:

$$\begin{bmatrix} {}_7^0P_{ex} \\ {}_7^0P_{ey} \\ {}_7^0P_{ez} \\ 1 \end{bmatrix} = T_0^{-1} \cdot \begin{bmatrix} {}_7^{base}P_{ex} \\ {}_7^{base}P_{ey} \\ {}_7^{base}P_{ez} \\ 1 \end{bmatrix} \tag{15.10}$$

Note that ${}_7^0P_e = {}_4^0P_e$ and

$${}_4^0T = {}_1^0T \cdot {}_2^1T \cdot {}_3^2T \cdot {}_4^3T = \begin{bmatrix} & & & {}_4^0P_{ex} \\ & {}_4^0R & & {}_4^0P_{ey} \\ & & & {}_4^0P_{ez} \\ 0 & 0 & 0 & 1 \end{bmatrix} = \begin{bmatrix} & & & L_1c_1s_2 \\ & {}_4^0R & & L_1c_2 \\ & & & L_1s_1s_2 \\ 0 & 0 & 0 & 1 \end{bmatrix} \tag{15.11}$$

For the both arms,

$$c_2 = \frac{{}_4^0P_{ey}}{L_1} \tag{15.12}$$

For the left arm,

$$s_2 = \sqrt{(1 - c_2^2)} \tag{15.13}$$

For the right arm,

$$s_2 = -\sqrt{(1 - c_2^2)} \tag{15.14}$$

Thus, θ_2 can be resolved as:

$$\theta_2 = Atan2(s_2, c_2) - (\pi/2 - 28.54°) \tag{15.15}$$

To resolve θ_1, for the both arms,

$$c_1 = \frac{{}_4^0P_{ex}}{L_1s_2} \tag{15.16}$$

$$s_1 = \frac{{}_4^0P_{ez}}{L_1s_2} \tag{15.17}$$

Thus, for the left arm,

$$\theta_1 = Atan2(s_1, c_1) - (\pi - 32.94°) \tag{15.18}$$

For the right arm,

$$\theta_1 = Atan2(s_1, c_1) + 32.94^\circ \tag{15.19}$$

The transformation matrices ${}^0_1T$ and ${}^1_2T$ and their inverses ${}^0_1T^{-1}$ and ${}^1_2T^{-1}$ can be found accordingly.

Thus, the wrist position with respect to Frame 2, denoted ${}^2_7P_w = [{}^2_7P_{wx}, {}^2_7P_{wy}, {}^2_7P_{wz}]^T$, can be found:

$$ {}^2_7T = {}^1_2T^{-1} \cdot {}^0_1T^{-1} \cdot {}^0_7T = \begin{bmatrix} & & & {}^2_7P_{wx} \\ & {}^2_7R & & {}^2_7P_{wy} \\ & & & {}^2_7P_{wz} \\ 0 & 0 & 0 & 1 \end{bmatrix} \tag{15.20}$$

For the left arm,

$$ {}^2_7P_w = \begin{bmatrix} -L_2c_3s_4 \\ -L_1 - L_2c_4 \\ -L_2s_3s_4 \end{bmatrix} \tag{15.21}$$

For the right arm,

$$ {}^2_7P_w = \begin{bmatrix} -L_2c_3s_4 \\ -L_1 - L_2c_4 \\ L_2s_3s_4 \end{bmatrix} \tag{15.22}$$

To resolve θ_3, for the both arms,

$$c_3 = \frac{{}^2_7P_{wx}}{-L_2s_4} \tag{15.23}$$

For the left arm,

$$s_3 = \frac{{}^2_7P_{wz}}{L_2s_4} \tag{15.24}$$

$$\theta_3 = Atan2(s_3, c_3) - (\pi - 53.6^\circ) - 2\pi \tag{15.25}$$

For the right arm,

$$s_3 = \frac{{}^2_7P_{wz}}{-L_2s_4} \tag{15.26}$$

$$\theta_3 = Atan2(s_3, c_3) + (\pi + 53.6^\circ) \tag{15.27}$$

The transformation matrix ${}^2_3T$ and its inverse ${}^2_3T^{-1}$ can be found accordingly.

θ_5, θ_6 and θ_7 can be derived from the transformation matrices from Frame 4 to Frame 7 ${}^4_7T$.

$$ {}^4_7T = {}^3_4T^{-1} \cdot {}^2_3T^{-1} \cdot {}^1_2T^{-1} \cdot {}^0_1T^{-1} \cdot {}^0_7T = \begin{bmatrix} {}^4_7r_{11} & {}^4_7r_{12} & {}^4_7r_{13} & {}^4_7P_{wx} \\ {}^4_7r_{21} & {}^4_7r_{22} & {}^4_7r_{23} & {}^4_7P_{wy} \\ {}^4_7r_{31} & {}^4_7r_{32} & {}^4_7r_{33} & {}^4_7P_{wz} \\ 0 & 0 & 0 & 1 \end{bmatrix} \tag{15.28} $$

For the left arm,

$$ \begin{aligned} {}^4_7T &= {}^3_4T^{-1} \cdot {}^2_3T^{-1} \cdot {}^1_2T^{-1} \cdot {}^0_1T^{-1} \cdot {}^0_7T \\ &= \begin{bmatrix} c_5c_6c_7 - s_5s_7 & -c_7s_5 - c_5c_6s_7 & c_5s_6 & 0 \\ -c_7s_6 & s_6s_7 & c_6 & L_2 \\ -c_5s_7 - c_6c_7s_5 & c_5c_7 - c_6s_5s_7 & -s_5s_6 & 0 \\ 0 & 0 & 0 & 1 \end{bmatrix} \end{aligned} \tag{15.29} $$

For the right arm,

$$ \begin{aligned} {}^4_7T &= {}^3_4T^{-1} \cdot {}^2_3T^{-1} \cdot {}^1_2T^{-1} \cdot {}^0_1T^{-1} \cdot {}^0_7T \\ &= \begin{bmatrix} c_5c_6c_7 - s_5s_7 & -c_7s_5 - c_5c_6s_7 & c_5s_6 & 0 \\ c_7s_6 & -s_6s_7 & -c_6 & L_2 \\ c_5s_7 + c_6c_7s_5 & c_5c_7 - c_6s_5s_7 & s_5s_6 & 0 \\ 0 & 0 & 0 & 1 \end{bmatrix} \end{aligned} \tag{15.30} $$

Thus, for the left arm,

$$ c_6 = {}^4_7r_{23} \tag{15.31} $$

$$ s_6 = \sqrt{1 - c_6^2} \tag{15.32} $$

$$ c_5 = \frac{{}^4_7r_{13}}{s_6} \tag{15.33} $$

$$ s_5 = -\frac{{}^4_7r_{33}}{s_6} \tag{15.34} $$

$$ c_7 = -\frac{{}^4_7r_{21}}{s_6} \tag{15.35} $$

$$ s_7 = \frac{{}^4_7r_{22}}{s_6} \tag{15.36} $$

For the right arm,

$$c_6 = -{}^4_7r_{23} \tag{15.37}$$

$$s_6 = \sqrt{1 - c_6^2} \tag{15.38}$$

$$c_5 = -\frac{{}^4_7r_{13}}{s_6} \tag{15.39}$$

$$s_5 = -\frac{{}^4_7r_{33}}{s_6} \tag{15.40}$$

$$c_7 = -\frac{{}^4_7r_{21}}{s_6} \tag{15.41}$$

$$s_7 = -\frac{{}^4_7r_{22}}{s_6} \tag{15.42}$$

For the left arm,

$$\theta_5 = Atan2(s_5, c_5) + \pi/2 \tag{15.43}$$

$$\theta_6 = Atan2(s_6, c_6) - \pi/2 \tag{15.44}$$

$$\theta_7 = Atan2(s_7, c_7) - \pi + 2\pi \tag{15.45}$$

For the right arm,

$$\theta_5 = Atan2(s_5, c_5) - \pi/2 \tag{15.46}$$

$$\theta_6 = Atan2(s_6, c_6) - \pi/2 \tag{15.47}$$

$$\theta_7 = Atan2(s_7, c_7) - \pi + 2\pi \tag{15.48}$$

For reaching movements, the four DOFs in consideration (three DOFs at the shoulder and one DOF at the elbow) can be resolved based on the wrist position P_w and the elbow position P_e: θ_4 is resolved according to Eq. (15.8); θ_1, and θ_2 are resolved according to Eqs. (15.11)–(15.19). With regards to θ_3,

For the left arm,

$$ {}^2_5P_w = \begin{bmatrix} -L_2c_3s_4 \\ -L_1 - L_2c_4 \\ -L_2s_3s_4 \end{bmatrix} \tag{15.49}$$

for the right arm,

$$ {}^2_5P_w = \begin{bmatrix} -L_2c_3s_4 \\ -L_1 - L_2c_4 \\ L_2s_3s_4 \end{bmatrix} \tag{15.50}$$

Therefore, θ_3 can be resolved as Eqs. (15.23)–(15.27).

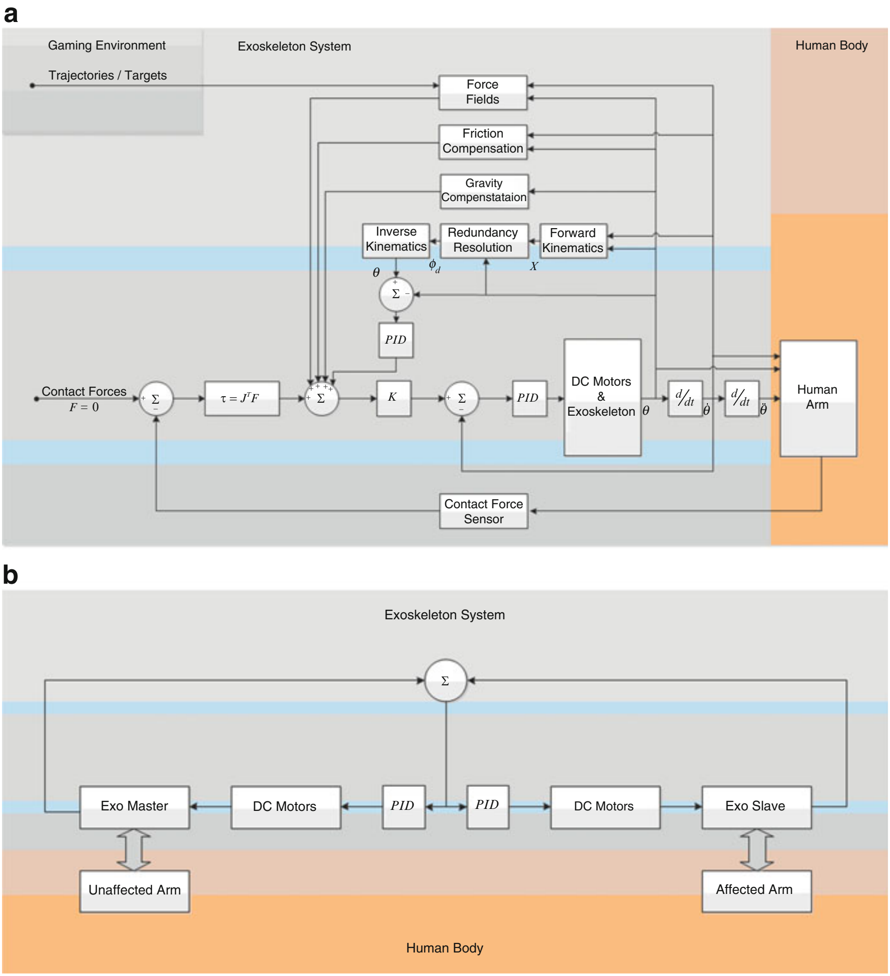

Fig. 15.5 A block Diagram of the exoskeleton control algorithms: (**a**) admittance control scheme – Single arm configuration, (**b**) teleoperation control scheme – dual arm configuration

15.2.3 Control Algorithms

15.2.3.1 Control Architecture of EXO-UL7: Overview

Two unique control algorithms are used to control the exoskeleton system in its unilateral (single arm) and bilateral (dual arm) modes of operation. The control modes guarantee that the system is inherently stable given the bandwidth of the human arm operation as the operators manipulate the system in virtual reality exposing the system to force fields and force feedback (haptic) effects (Fig. 15.5).

15.2.3.2 Admittance Control: Single Arm Exoskeleton

By definition, An admittance is the dynamic mapping from force to velocity. An admittance control scheme utilizes three multi-axis force/torque (F/T) sensors as the primary inputs. These F/T sensors are attached to all the physical interfaces between the operator's arm and the exoskeleton at the upper arm, forearm, and palm. A force applied on the exoskeleton system by the operator commands the exoskeleton arm to move with a velocity that is proportional to the force and along the same direction. As the force increases, the system responds by moving faster. This approach is also known as the "get out of the way" control scheme. As the system moves, the control scheme tries to set the interaction force to zero [34, 35].

15.2.3.3 Teleoperation Control: Dual Arm Exoskeleton

In a teleoperation control scheme, the two arm exoskeleton system is configured as a master and a slave. The exoskeleton arm attached to the human unaffected (healthy) arm is defined as the master and the other exoskeleton arm attached to the affected (disabled) arm is defined as the slave. A local teleoperation scheme is used in which the master arm provides a position commands to the slave arm such that they both move in a mirror image fashion. Any joint angle generated by the unaffected arm is copied to the affected arm. In this mode of operation the unaffected arm controls the movements of the affected arm. The coupling between the arms will be varied. A tight coupling will be induced initially and it will be gradually reduced by 10 % in each treatment such that in the very last treatment, each arm will be completely independent (uncoupled).

15.2.3.4 Assistive Modes and Compensation Elements

The assistive modes are designed to further reduce the energy exchange between the human arm and the exoskeleton and to improve the transparency of human-robot interactions. Several force fields are applied on the patients as part on the training and their application and magnitude will be a function of the specific task.

Gravity Compensation Joint torques are generated in part due to the gravitational loads of the exoskeleton arm and the patient's arm. The gravity compensation algorithm estimates the joint torques for each arm configuration and provides a feed forward command to the actuators which in turn produce joint torques that counter the toque generated by gravity. This compensation will make the weight of the exoskeleton itself transparent to the operator. As such, the operator will feel as if the exoskeleton arm is completely weightless. This compensation mode will be active at all times. Furthermore, an identical algorithm will compensate for the gravitational loads of the patient's own arm such that the operator will not feel the weight of his/her arm. This compensation may vary between full compensation and no compensation. The compensation of the patient's own arm will change during the treatment starting from full compensation during first treatment followed by a reduction of 10 % with each treatment that gradually exposes the patient to the full weight of the arm by the last day of the treatment.

Friction Compensation Friction is a force or a moment that resists the relative motion of the joints. The static/kinetic (coulomb) friction, as well as viscous friction is compensated through the feed forward element of the control algorithm such that the operator does not feel any resistance associated with friction.

Redundancy Resolution The human arm with its seven DOF (excluding scapular motion) is a redundant mechanism meaning that there are infinite arm configurations that can be adopted for the same position and orientation of the hand for grasping an object. Passing a virtual axis through the center of the shoulder joint and the center of the wrist joint allows us to define the position of the elbow joint by an angle defined with respect to this axis. This angle is defined as a swivel angle, which in turn defines in a parametric fashion the redundancy of the arm. Given the anatomical limitations of the shoulder and the wrist joint, the swivel angle has a specific range of angles from which any value to be selected will not change to the position or the orientation of the hand. The motor control system selects a specific swivel angle within the available range, and in that way resolves the arm redundancy. Since the human arm and the exoskeleton system are mechanically coupled, the redundancy resolution imposed by the exoskeleton system has to match the same solution that would have been adopted by an neuromuscular system. The algorithm implemented into the exoskeleton is based on an extensive preliminary study of this problem with both healthy and stroke patients. This algorithm synthesizes three classes of criteria: (1) kinematic criteria, (2) dynamic criteria, and (3) comfort criteria. The weight factors of each one of the three criteria change dynamically and will predict the swivel angle for the next time interval. One should note that the redundancy resolution is only required in the unilateral mode of operation. During the bilateral mode of operation, the swivel angle of the unaffected arm is transmitted to the affected arm, thus the exoskeleton system adopts the motor control redundancy resolution.

15.2.4 Redundancy Resolution

The redundancy resolution is critical in the control of the exoskeleton, in order to achieve the transparency of the interaction between the exoskeleton and its operator. Ideally, the redundancy resolution controls the exoskeleton in the same way that the human motor system controls arm movements. Therefore, the exoskeleton can be used for power augmentation for the healthy human arm movements, as well as for the correction of the abnormal arm movements in stroke rehabilitation.

The problem of controlling redundant degrees of freedom, i.e., redundancy resolution, has been previously considered in the control of robot manipulators. When solving an inverse kinematics or dynamics problem for manipulation tasks, redundant degrees of freedom can be used to achieve secondary goals such as to satisfy certain task constraints or to improve task performances. Task-based redundancy resolutions control the extra DOF by integrating the task-dependent constraints into an augmented Jacobian matrix [36, 37]. Performance-based redundancy resolutions may optimize the manipulability [19, 38–40], energy consumption [41, 42], the smoothness of movement [43–46], task accuracy [47] and control complexity [48].

The EXO-UL7 exoskeleton is designed to assist the operator's arm movements in unexpected tasks and in uncertain environments. It requires a real-time control rather than a pre-planned motion control, and the redundancy resolutions have to be based on local (instead of global) performance optimization. Under the above constraints, we investigate the study of the motor control of the human arm movements and select several control criteria, which are applicable for the control of the exoskeleton. The selected criteria optimize different performances in motion control, including motion efficiency, motion smoothness, energy consumption and etc.

15.2.4.1 Maximizing the Motion Efficiency

H. Kim *et al.* proposed a redundancy resolution that determines the swivel angle by maximizing the motion efficiency [19]. As shown in Fig. 15.6, when the elbow falls on the plane formed by the positions of the shoulder P_s, the wrist P_w and the virtual target P_m, the projection of the longest principle eigen-vector of the manipulability ellipsoid on the direction from the hand to the virtual target P_m is maximized, and so is the motion efficiency towards the virtual target P_m, which is hypothesized to be on the head. Given the role of the head as a cluster of sensing organs and the importance of arm manipulation to deliver food to the mouth, it is hypothesized that the swivel angle is determined by the human motor control system to efficiently retract the hand to the head region.

A good candidate for the position of virtual target is the position of the mouth. This hypothesis is supported by intracortical stimulation experiments that evoked coordinated forelimb movements in conscious primates [49,50]. It has been reported that each stimulation site produced a stereotyped posture in which the arm moved to the same final position regardless of its posture in the initial stimulation. In the most complex example, a monkey formed a frozen pose with its hand in a grasping position in front of its open mouth. This implies that during the arm movement toward an actual target, the virtual target point at the head can be set for the potential retraction of the palm to the virtual target.

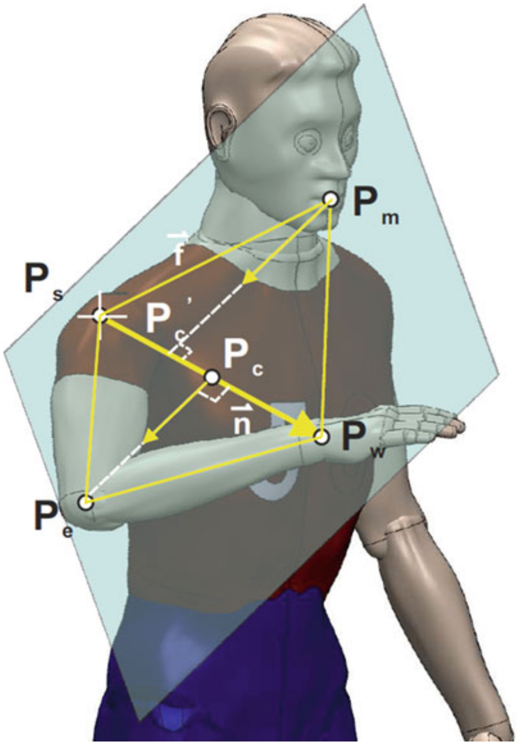

Fig. 15.6 The proposed redundancy resolution intends to maximize the motion efficiency by maximizing the projection of the longest principle eigen-vector of the manipulability ellipsoid on the direction from the hand to the virtual target P_m. The corresponding elbow position falls on the plane formed by P_s, P_w and P_m

15.2.4.2 Minimizing Work in the Joint Space

Minimizing work in the joint space is proposed by T. Kang as a real-time dynamic control criterion, which resolves the inverse kinematics by minimizing the magnitude of total work done by joint torques for each time step [42]. With the dynamic arm model, the joint torques (T) can be extracted given the states of the arm. The calculation of work in the joint space for each time step depends on (1) the joint torques and (2) the difference in joint angles. Therefore, the work in the joint space during the movement interval $[t_k, t_{k+1}]$ can be computed for two different conditions. The dynamic constraint adopted in this chapter is from the original work done by the aerospace medical research laboratory [51]. Here, we briefly include the essential parts of the algorithm for the integrity of the chapter:

if $T_{i,t_k} \cdot T_{i,t_{k+1}} > 0$,

$$W_i = \frac{(T_{i,t_k} + T_{i,t_{k+1}}) \cdot \Delta q_i}{2} \tag{15.51}$$

where T_{i,t_k} and $T_{i,t_{k+1}}$ are the joint torques of the i-th joint at the time t_k and t_{k+1}. $\Delta q_i = (q_{i,t_{k+1}} - q_{i,t_k})$ is the difference of the i-th joint angle during the time interval $[t_k, t_{k+1}]$.

When $T_{i,t_k} \cdot T_{i,t_{k+1}} < 0$,

$$W_i = \frac{(|\Delta q_i| - h_i) \cdot T_{i,t_{k+1}}}{2} - \frac{h_i \cdot T_{i,k}}{2} \tag{15.52}$$

where $h_i = (|T_{i,t_k}| \cdot |\Delta q_i|)/|T_{i,t_{k+1}} - T_{i,t_k}|$ and denotes the difference of the i-th joint angle from q_{i,t_k} to the value corresponding to the zero crossing of joint torque.

To minimize the work done in the joint space at each time step (e.g. $|W|_{t_k,t_{k+1}}$ for the time interval $[t_k, t_{k+1}]$), the swivel angle of the arm for a specified wrist position is optimized by:

$$\begin{aligned} \phi(k+1) &= \underset{\phi'(k+1)}{\arg\min} |W_i|_{t_k,t_{k+1}} \\ &= \underset{\phi'(k+1)}{\arg\min} \sum_{i=1}^{4} |W_i|_{t_k,t_{k+1}} \end{aligned} \tag{15.53}$$

where $|W_i|_{t_k,t_{k+1}}$ denotes the work done by the i-th joint.

15.2.4.3 Minimizing Joint Angle Change

Minimizing joint angle change is a real-time kinematic criterion that impose smooth motion in the joint space. Given the expected positions of the wrist $P_w(k+1)$ and the shoulder $P_s(k+1)$, this criterion explores the possible the swivel angles for the next time step $\phi'(k+1)$ and selects the one which minimizes the norm of the change in the joint angle vector. For daily activities, the change in swivel angle within 0.01 s is supposed to be no larger that 0.5°. Given the current swivel angle $\phi(k)$, we search within the range of $[\phi(k) - 0.5, \phi(k) + 0.5]°$ by the step of $\delta\phi = 0.1°$. The swivel angle for the next time step $\phi(k+1)$ is determined by:

$$\begin{aligned} \phi(k+1) &= \underset{\phi'(k+1)}{\arg\min} |\theta(k) - \theta'(k+1)| \\ &= \underset{\phi'(k+1)}{\arg\min} \sqrt{\sum_{i=1}^{4} (\theta_i(k) - \theta_i'(k+1))^2} \end{aligned} \tag{15.54}$$

In Eq. (15.54), $\theta(k) = [\theta_1(k), \theta_2(k), \theta_3(k), \theta_4(k)]^T$ is the joint angle vector for current time step. $\theta'(k+1)$ is the joint angle vector for the next time step computed from a possible $\phi'(k+1)$ value.

At the kinematic level, alternative control criteria can optimize motion smoothness by minimizing jerk (the square of the first derivative of acceleration) in the joint space and/or task space, to account for the straight paths and bell-shaped speed profiles observed in reaching movements [43, 44, 52]. At the dynamic level, the optimization of smoothness can be achieved by minimizing the change in joint torque [45, 46], which explains the mild curvature in the roughly straight hand-reaching trajectories in the task space. By observing various implementations, we have noticed that minimizing the norm of the change in the joint angle performs better than minimizing the norm of the change in higher order derivatives of the joint angle (e.g., velocity and acceleration). These control strategies are for global motion planning and the computation of the trajectories in the task space and/or the joint space before execution. Since the exoskeleton is designed to move with the operator in unexpected task and uncertain environment, the smoothness of motion is expected to be addressed more locally than globally.

15.2.4.4 Minimizing the Change in Kinetic Energy

Minimizing the change in kinetic energy is based on the following hypothesis: since human movements are well adapted to gravity, unless the dynamics of the human body is significantly affected by additional load, the motor control system may plan the movements at daily-activity speed without compensating much for gravity. With the dynamic model, the kinetic energy (Ke) can be computed given the state of the arm. Similar to Criterion 3, we explore the possible swivel angles for the next time step and find the one that minimizes the change in the kinematic energy.

$$\phi(k+1) = \underset{\phi'(k+1)}{\arg\min} |Ke(k) - Ke'(k+1)| \tag{15.55}$$

For global energy optimization, J.F. Soechting *et l.* minimize the peak value of kinetic energy, which requires the knowledge of the final arm posture [41]. In addition, A. Biess *et al.* integrate the consideration of kinetic energy in the control strategy by looking for a geodesic path in the Riemannian configuration space, which consumes less muscular effort since the sum of all configuration-speed-dependent torques vanishes along the path [53]. For the real-time control of the exoskeleton, we prefer minimizing the change in kinetic energy locally.

15.2.5 Performance Comparison of Different Redundancy Resolutions

To study the performance of different redundancy resolutions, we collect data of the point-to-point reaching movements in a 3D workspace from healthy subjects (see Figs. 15.7 and 15.8). The arm postures predicted by different redundancy resolutions are compared and evaluated with reference to the measured arm postures.

A comparison of the arm posture prediction performance has been conducted between the redundancy resolutions by maximizing motion efficiency (Redundancy Resolution I) and by minimizing work in the joint space (Redundancy Resolution II). The mean (μ) and standard deviation (σ) of the prediction errors are

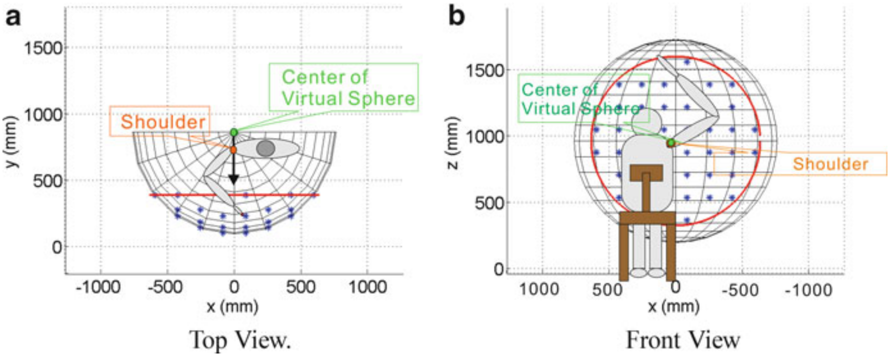

Fig. 15.7 The spherical workspace for the reaching movement experiments: (**a**) the top view and (**b**) the front view. The height of the workspace center is adjustable and is always aligned with the right shoulder of the subject

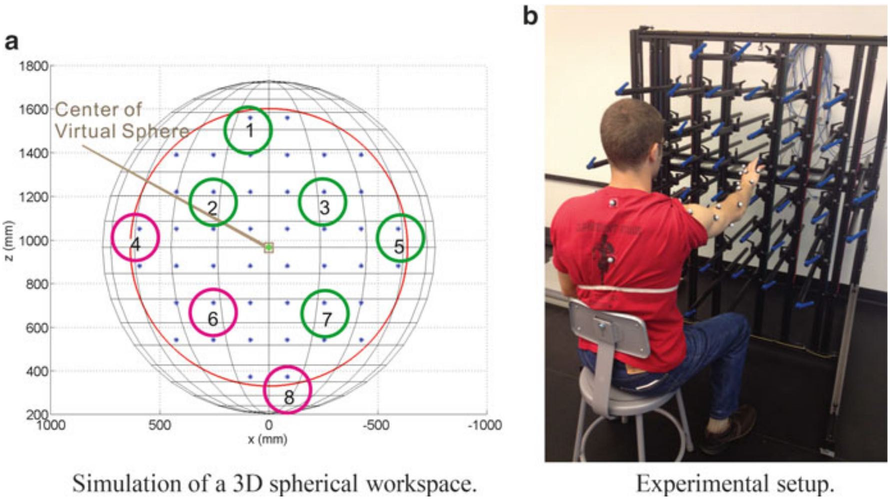

Fig. 15.8 (**a**) Eight targets are selected among all the available targets (denotes as *blue dots*) in the spherical workspace. Considering the motion range of the right arm, Target 1, 2, 3, 5, 7 (in *green circles*) are within the comfortable arm motion range, while Target 4, 6, and 8 (in *magenta circles*) are close to the motion range boundary. (**b**) A subject is performing the instructed reaching movement. The subject is seated in a chair with a straight back support. The right arm is free for reaching movements, while the body of the subject is bounded back to the chair to minimize shoulder displacement. During the experiment, the subject uses index finger to point from one instructed target to another, with his/her wrist kept straight. A motion capture system catches the positions of the passive-reflective markers attached to the torso and the right arm, recording the movements at 100 Hz

computed for each individual valid trail (2,674 out of 2,800 in total), and their distributions are presented in Fig. 15.9. It is shown that the Redundancy Resolution II has higher performance on both the mean and standard deviation of the prediction errors, which results from the fact that Redundancy Resolution II has to start its prediction from the arm posture measured at the beginning of the movement, while Redundancy Resolution I does not need to initialize its prediction with any measured data. One way to improve the performance of Redundancy Resolution I is to estimate the position of the virtual target dynamically based on the recent history of the swivel angle measurements. As shown in Fig. 15.9e,f, the improved performance is slightly higher than that of Redundancy Resolution II [54].

15.3 Clinical Study: Application of EXO-UL7 on Stroke Rehabilitation

15.3.1 Experiment Protocols

15.3.1.1 Apparatus

The system used for this research consisted of the upper limb exoskeleton EXO-UL7, a control computer, and a game computer. The control computer used PID control to provide gravity compensation, as well as bilateral symmetric assistance or unilateral assistance, as needed. In all cases where assistance was provided, the robot only provided partial assistance, helping subjects by giving a helpful push in the desired direction [6, 7, 55].

The games were created using Microsoft Robotic Developer Studio [56]. The game computer was connected to a 50″ flat screen monitor. In addition to generating real time virtual reality [57] game images, the game computer also collected position and force data at 100 Hz.

The games are depicted in Fig. 15.10. The games were played for 10–15 min each. Over the course of the study, each subject played every game multiple times. Therefore, the rehabilitative efficacy of any given game is confounded with the other games [58]. The BSRMT group played each game using both arms and the URMT group played each game using only the paretic arm. For BSRMT, the subject's less-affected arm was the master, and the paretic arm was the slave. As subjects moved their less-affected arm the robot moved the paretic arm in a mirror-image fashion. Aside from gravity compensation, for URMT, the robot only provided partial assistance in the Flower game (see Fig. 15.1a). A more detailed evaluation of these games is provided in [6].

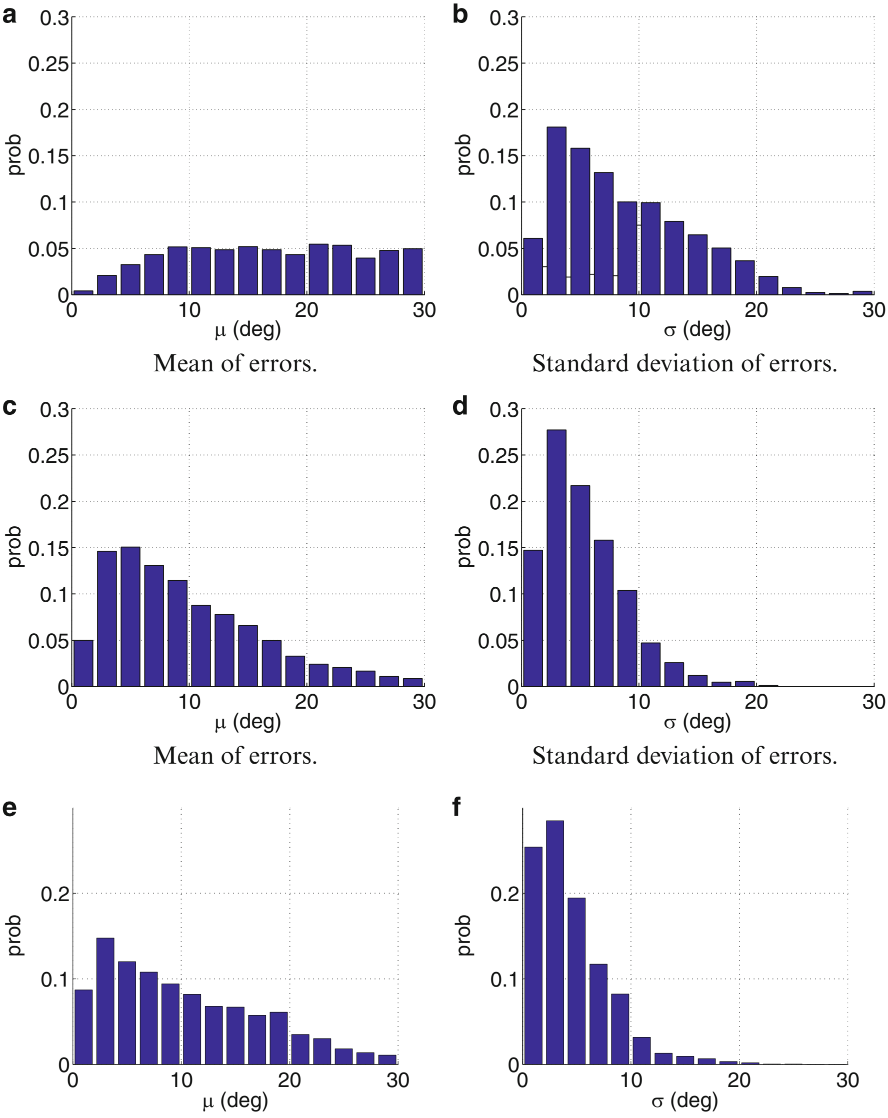

Fig. 15.9 Swivel angle prediction performance of the redundancy resolutions by maximizing the motion efficiency (the Redundancy Resolution I, see (**a**) and (**b**)) and by minimizing the work in joint space (the Redundancy Resolution II, see (**c**) and (**d**)). The performance of Redundancy Resolution I can be improved by dynamic estimation of the position of the virtual target (see (**e**) and (**f**))

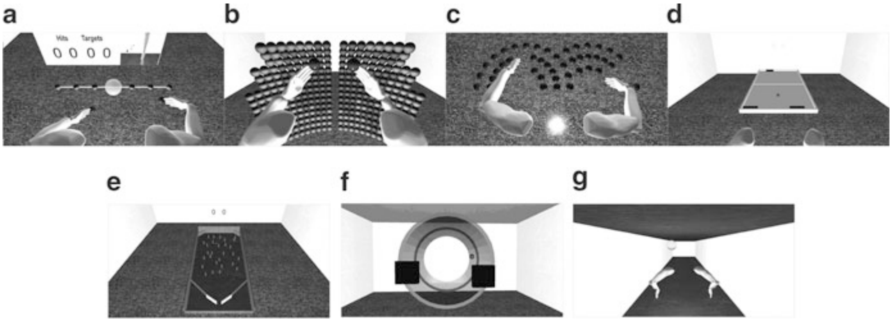

Fig. 15.10 Screen shots from the various games. The avatar arms move in response to the movement of the subject. In the Pinball and Circle games, avatar arms are not visible so that the view of the Pingpong table will not be blocked. (**a**) Flower game. (**b**) Paint game. (**c**) Reach game. (**d**) Pong game. (**e**) Pinball game. (**f**) Circle game. (**g**) Handball game

15.3.1.2 Pilot Study

Ten male and female subjects between 27 and 70 years of age, for more than 6 months post stroke, with a Fugl-Meyer score between 16 and 39 and a score of 19 or greater on the VA Mini Mental Status Exam were recruited for the study. All were screened and consented prior to a random assignment. The subjects were sub-categorized by severity and then randomly assigned to either the unilateral robotic training or to the bilateral robotic training. All subjects were scheduled for 12 training sessions. The visits were scheduled twice a week for 6 weeks. This study was approved by the Committee on Human Research at the University of California-San Francisco (UCSF) and each session was preformed at UCSF under the guidance of a trained therapist.

In the pilot study, subjects sit in front of a screen with a virtual reality game to play. In this game, small target balls are located spherically around the robot. When the target balls with the tip of the virtual arm is touched, the ball color changes (see Fig. 15.11). The ratio of the touched balls to the total number of target balls can be used to assess the mobility improvement of the subjects.

15.3.1.3 Unilateral and Bilateral Robotic Training via the EXO-UL7

The research on the unilateral and bilateral robotic training was approved by the University of California, San Francisco, Committee on Human Research. Interventions consisted of 12, 90-min sessions of robotic assisted training or standard care. An elastic restraint around the torso and thighs helped subjects maintain a neutral sitting position during robotic training. The experimental setup is depicted in Fig. 15.12.

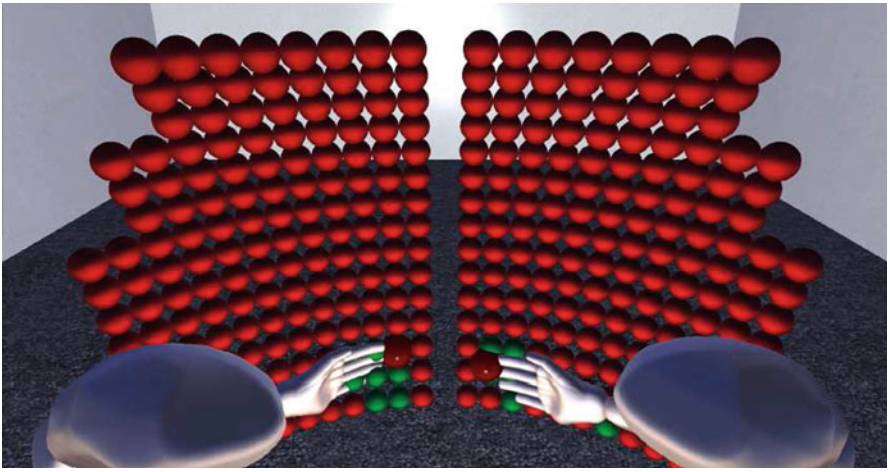

Fig. 15.11 Pilot study: Subjects paint the virtual environment in either a unilateral control or bilateral control architecture

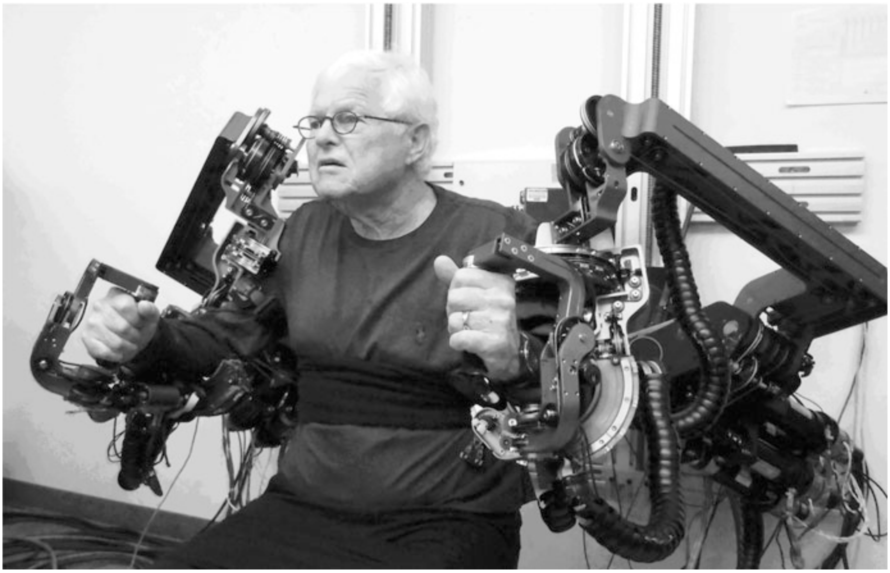

Fig. 15.12 A subject with right-side hemiparetic performing BSRMT

Included were 15 subjects who are more than 6 months post stroke, ranging in ages from 23 to 69 years, with Fugl-Meyer scores between 16 and 39. The subjects were stratified by their Fugl-Meyer score and then randomly assigned to the

BSRMT, URMT or usual care with a physical therapist. With an upper limb Fugl-Meyer score between 16 and 39, each subject had the necessary control of their paretic arm to be able to play the games, while still having the potential for improvement.

Improvement Metrics This work includes just a fraction of clinical measures that were gathered from this study. The measures considered presently include: spasticity, dexterity, hand strength, and shoulder range of motion (ROM). These measures all assess different aspects of motor dysfunction. In that sense, they are independent. The reason for focusing on these measures is because they were explainable using kinematic analysis. For example, it is difficult to relate kinematic analysis to measures such as psychological state or pain scales. Additionally, these metrics all involved data that suggested a significant change in performance as measured before and after the intervention.

Data Analysis Clinical data was analyzed using standard hypothesis testing. Specifically, for each test type, the corresponding subject groups were tested for a significant change in performance as measured before and after the intervention. This includes paired t-tests for parametric measures and 2-Sample Wilcoxon-Mann-Whitney (Wilcoxon) tests for non-parametric data. For both types of tests, p-values were reported. For the Wilcoxon test, p-values were adjusted for ties where applicable. Statistical calculations were performed using Minitab Statistical Software (Minitab Inc., State College, PA, USA). Confidence limits of 95 % ($p < 0.05$) and 90 % ($p < 0.01$) were used to test significance. A confidence limit of 90 % is generally not used for clinical assessments [59,60]. However, 90 % limits are used in other contexts, albeit as a lower limit. Given the comparatively small population of subjects in each training group ($n = 5$), this study is best described as a pilot, or feasibility study. Notwithstanding, only relatively large differences will achieve the 95 % level for sample sizes such as this and it is left to the discretion of the reader how to interpret these levels.

Over the past decades, a large number of metrics have been proposed to assess human movements using robots and/or motion capture [55]. There are two difficulties with such approaches. First, it is often unclear if a change in a given metric is caused by legitimate rehabilitation or if it is related to familiarity with the system. For example, a subject might improve at playing a given game even though there is no actual therapeutic improvement. Second, real-time, multi-joint force and velocity data are generally not available in clinical settings, nor are they standardized. Therefore, measures that are gathered from a given robotic system are difficult to replicate. It is also unlikely that they directly translate to standard clinical measures. For these reasons, this research focused on clinical measures of performance that were collected before and after the intervention. Kinematic data collected from the robot were used to contrast movement training differences between BSRMT and URMT modes, but not as a measure of improvement. For a detailed analysis of subject performance using kinematic data collected from the robot, see [16].

The Data Analysis Section references joints by number. The directions of positive joint rotation are depicted in Fig. 15.2. In words, the axes are defined as follows: Joint 1 is a combination of shoulder flexion and abduction; Joint 2 is a combination of shoulder flexion and adduction; Joint 3 shoulder inner rotation, Joint 4, elbow flexion; Joint 5 is the elbow/wrist supination; Joint 6 is the wrist flexion; and joint 7 is the wrist ulnar deviation.

In an effort to tie the clinical outcomes to training, a metric is needed to quantify overall movement training. A long-standing tenet in the rehabilitation community is that repetition of movement is required for recovery. To quantify overall movement training for a given game during a given trial, seven numbers are calculated, one for each joint. Each of the seven numbers relate to the proportional contribution of movement for a given joint. An eighth number is calculated to capture the overall intensity of movement. With respect to the proportions of movement for each of the seven joints, a row vector is defined as Eq. (15.56):

$$\left| p_1 \;\; p_2 \;\; p_3 \;\; p_4 \;\; p_5 \;\; p_6 \;\; p_7 \right| \tag{15.56}$$

where p1 is the proportion of rotation for joint 1, p2 is the proportion of rotation of joint 2, and so on. Accordingly,

$$\left| \sum_{i=1}^{7} p_i = 1 \right| \tag{15.57}$$

Thus, the sum of the proportions account for 100 % of the total joint rotation for the 7 DOF of the arm. The 8th number being calculated is the "intensity" of the training and is given by I. Thus, the intensity of training for joint j is given by $p_j \dot{I}$.

Equations (15.56) to (15.57) require some measure of movement training intensity. One approach is to calculate the total angular position, velocity, and acceleration for a given joint. As a start, consider the angular position. A change in the angular position is given as $\Delta\Theta$. Summing $\Delta\Theta$ for successive samples in the data set is infeasible because rotations in one direction will be canceled with rotations in the other direction. Therefore, a more suitable calculation for the angular position of the j-th joint is to take the RMS as follows:

$$\mathbf{RMS}_{\Theta_j} = \sqrt{\frac{1}{n} \sum_{i-1}^{n} \Delta\Theta_{i,j}} \tag{15.58}$$

were n is the number of joint measurements, and i is the ith measurement. Angular velocity, ω is given by $\Delta\Theta/\Delta t$. Therefore, the RMS for ω is given by

$$\mathbf{RMS}_{\Theta_{\omega,j}} = \sqrt{\frac{1}{n}\sum_{i-1}^{n}(\frac{\Delta\Theta_{i,j}}{T_s})^2} \qquad (15.59)$$

where T_s is the sample time. In this case, the sampling rate was 100 Hz and $T_s = 0.01$ s. Because T_s is a constant, Eq. (15.58) is essentially the same calculation Eq. (15.59) except that it is scaled by the constant value $1/T_s$. Therefore, calculating the RMS of both angular position and angular velocity is of little value and the discussion that follows considers only angular velocity and acceleration.

In an effort to minimize the effects of noise and finite sampling times, a 5-point numerical differentiation was used to calculate the RMS for angular velocity and acceleration. Thus, the RMS calculation that is used for velocity is

$$\mathbf{RMS}_{\Theta_{\omega,j}} = \sqrt{\frac{1}{n}\sum_{i-1}^{n}(\frac{-\Theta_{i+2,j} + 8\Theta_{i+1,j} - 8\Theta_{i-1,j} + \Theta_{i-2,j}}{12T_s})^2} \qquad (15.60)$$

and for angular acceleration,

$$\mathbf{RMS}_{\Theta_{\omega,j}} = \sqrt{\frac{1}{n}\sum_{i-1}^{n}(\frac{-\Theta_{i+2,j} + 16\Theta_{i+1,j} - 30\Theta_{i,j} + 16\Theta_{i-1,j} - \Theta_{i-2,j}}{12T_s})^2} \qquad (15.61)$$

With the RMS calculations for angular acceleration and velocity in hand, calculating the proportional contributions of each joint according to Eq. (15.56) is obtained by the following equation:

$$\left(\sum_{j=1}^{n} RMS_j\right)^{-1} \left|RMS_1\ RMS_2\ RMS_3\ RMS_4\ RMS_5\ RMS_6\ RMS_7\right| \qquad (15.62)$$

The proportions given in Eq. (15.62) are presented as percentages throughout this chapter. Intensity I is calculated for each game of each trial for both angular acceleration and angular velocity using the average RMS of the 7 joints. The intensity calculation is given as follows:

$$I = \frac{1}{7}\sum_{j=1}^{7} RMS_j \qquad (15.63)$$

Data processing was accomplished using custom MatlabTM scripts (The Mathworks Inc, Natick, MA, USA).

15.3.2 Results

15.3.2.1 Pilot Study

During the clinical trial for the paint game, the travel distance and time-to-finish were recorded. Averaged travel distances show that the bilateral training group traveled 2.2 m/session and unilateral group did 1 m/session. The bilateral group spent 22 s/session and unilateral group spent 12 s/session. The percent improvement defined between the first and last session 12 weeks later showed that the bilateral and unilateral training group had 97 and 2 % improvement, respectively for the travel distance, while both groups showed similar improvement for time-to-finish [16].

15.3.2.2 Clinical Outcomes of the Unilateral and Bilateral Robotic Training

Clinical Measures Non-parametric data are summarizes in Figs. 15.13–15.16 and parametric data are summarized in Figs. 15.17–15.19. For each group the average percent change is calculated for parametric data. For non-parametric data the median change is calculated. Also, a p-value for the corresponding hypothesis test (Wilcoxon or paired-t test) is given below each plot. The bold type indicates significant differences. The strongest changes, $\alpha \leq 0.05$, are distinguished with a dark shade of box plot gray for parametric data. For $0.05 < \alpha \leq 0.10$, the box plots are distinguished with a lighter shade of gray.

There was a statistically significant reduction in finger flexion (see Fig. 15.13b), and elbow flexion/extension spasticity for URMT, see Fig. 15.13c, d, as well as a significant improvement on the Box and Block Test (see Fig. 15.17b). However, there was a significant reduction in grip strength for URMT, as measured with a Jamar hand dynamometer (Lafayette Instrument Company, Lafayette, IN).

There were significant differences for ROM [61] in the shoulder for all three groups, see Fig. 15.18e–g. All ROM measurements were performed with a goniometer. There was a relatively large improvement in shoulder abduction for the BSRMT, see Fig. 15.18e, and the standard care groups. The subjects in the BSRMT group also had significant improvements for shoulder external rotation ROM, see Fig. 15.18g. The URMT group had the least improvement in shoulder ROM. In addition, the BSMRT group had a significant reduction in internal rotation ROM at the shoulder, see Fig. 15.18f.

Movement Training Measures At times subjects would pause their movement training. Causes for such halting could result from a variety of reasons. Examples include: stops for technical corrections for the robot or game, readjustments of straps or restraints, dialog with the subjects, respites, and bathroom breaks. As a specific example, a training interval of approximately 300 s is depicted in Fig. 15.20.

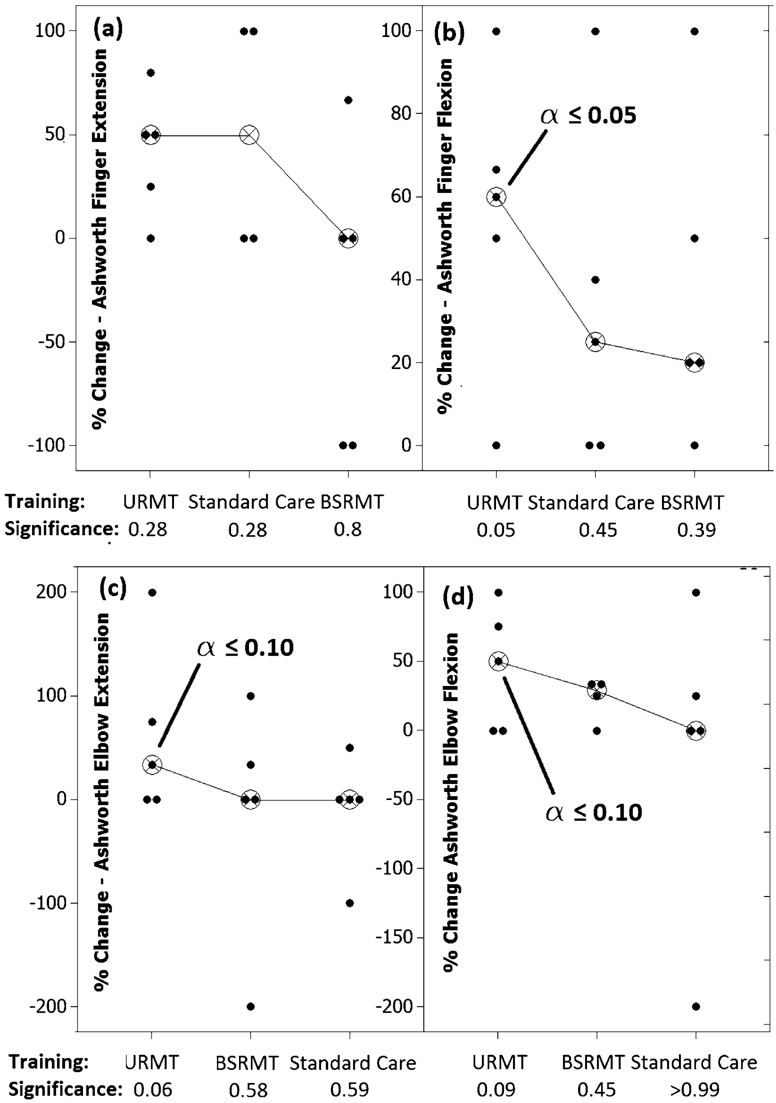

Fig. 15.13 Individual value plots of clinical measures for non-parametric data: **spasticity metrics**. Individual values represent percent improvements as measured before and after the intervention. Also depicted are significant ($p \leq 0.05$), or marginally significant ($p \leq 0.10$) changes as determined by a Wilcoxon test. Connecting lines attach median values. Note, for cases where a decrease in a metric is regarded as an improvement the individual values are given positive, and vice-a-versa

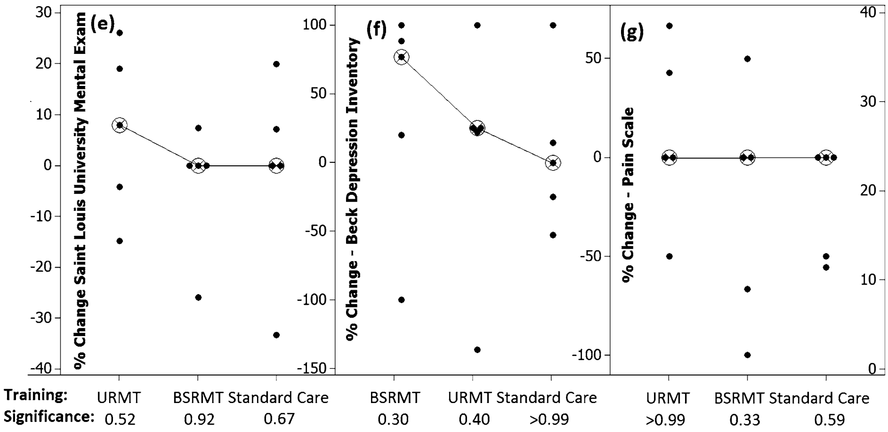

Fig. 15.14 Continue Fig. 15.13. Individual value plots of clinical measures for non-parametric data: **phvchological metrics**

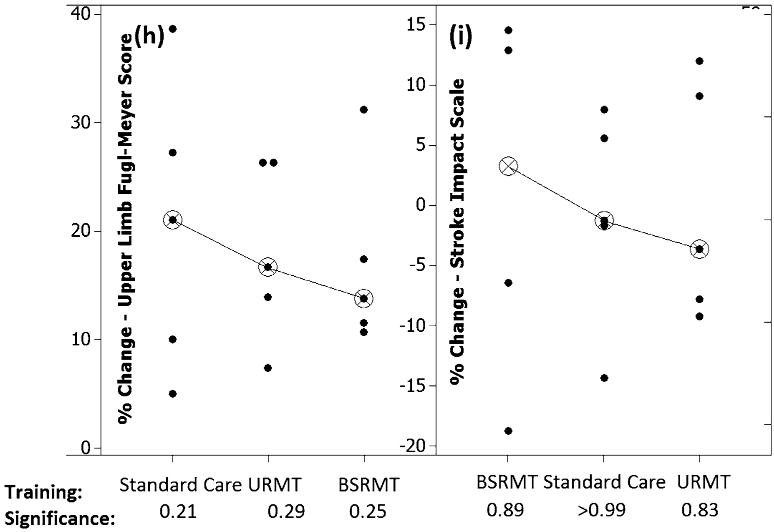

Fig. 15.15 Continue Fig. 15.14. Individual value plots of clinical measures for non-parametric data: **general metrics**

Notice that there are two apparent pauses wherein most of the joints stop moving (flat lines). Pauses such as this will deflate the measures given by Eq. (15.60) and Eq. (15.61). Perhaps the most accurate measure of training intensity Eq. (15.63) and percent contributions Eq. (15.62) would consider only data with the pauses removed. However, such segregation of data is open to interpretation and is fought with uncertainty. For this reason, the following analysis will consider data sets only for the top 50-th percentile of training as measured by intensity. Cases where training is

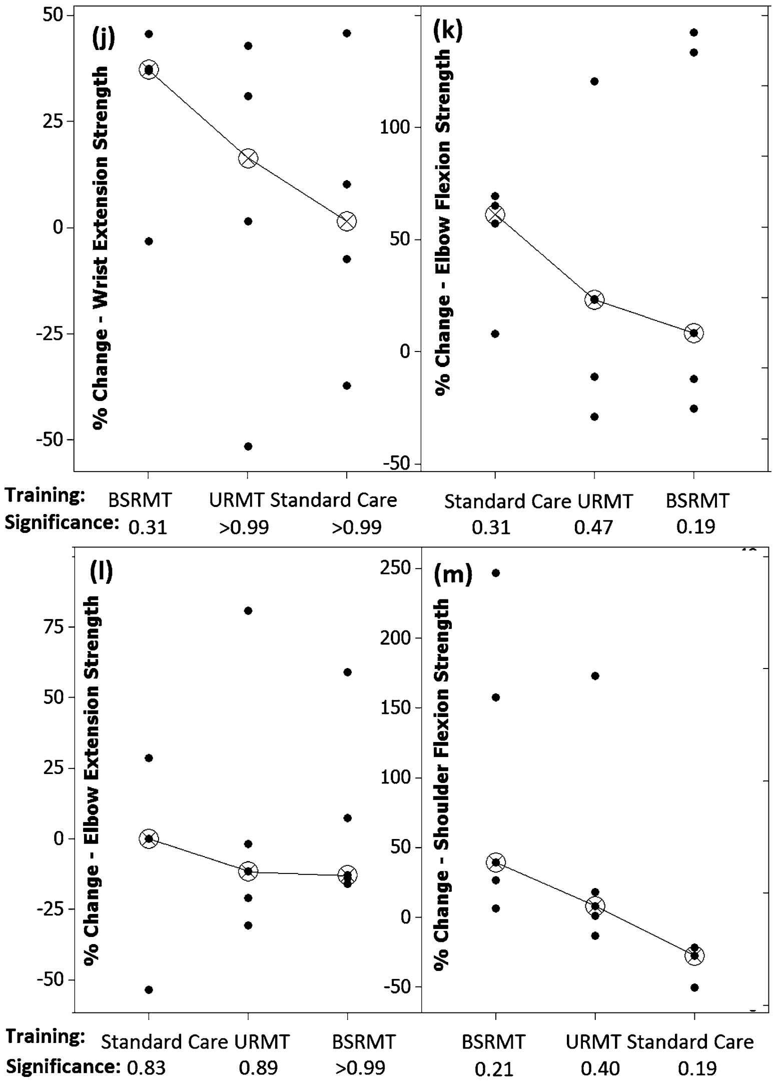

Fig. 15.16 Continue Fig. 15.15. Individual value plots of clinical measures for non-parametric data: **strength metrics**

halted will result in lower intensities. Therefore, by excluding the lower half of the data, it is more assured that data analysis only includes training that was continuous and without interruption.

Figure 15.23 depicts URMT percentage contributions by joint for velocity Eq. (15.60) and acceleration Eq. (15.61). Each element in Eq. (15.62) is summarized statistically as a CI for velocity and acceleration. Notice that angular

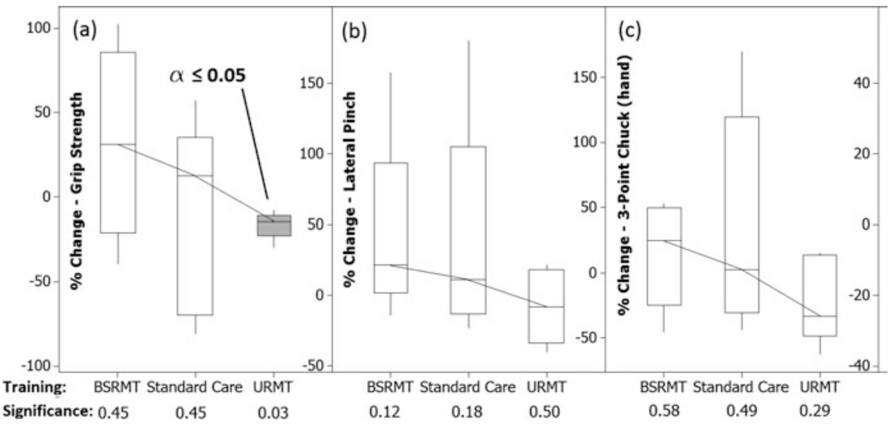

Fig. 15.17 Box plots of clinical measures for parametric data: **hand strength metrics**. Individual values represent percent improvements as measured before and after the intervention. Also depicted are significant ($p \leq 0.05$), or marginally significant ($p \leq 0.10$) changes as determined by a paired t-test. Connecting lines attach mean values

velocity and acceleration track are fairly close for each joint. In general, based on the percent contributions of each joint, and the training intensities, velocity and acceleration tended to co-vary. Putting it in another way, comparison of BSRMT and URMT by velocity was roughly equivalent to using acceleration. Therefore, considering the differences between BSRMT and URMT in terms of velocity and acceleration are of little value. Thus, with the proviso that acceleration would have been an equally valid measure, the remainder of this chapter will consider only velocity RMS values.

Depicted in Fig. 15.21 is a comparison of the affected arm to the control arm for BSRMT. Perhaps not surprisingly, the control arm had similar joint contribution percentages as the affected hemiparetic arm. However, in terms of intensity, the affected was significantly lower than the control arm, $p = 0.017$, see "All joints" in Fig. 15.22.

Bilateral Symmetric Versus Unilateral Training Because the improvement of the affected side is most important, the following comparison between BSRMT and URMT considers only the paretic arms. This comparison is summarized in Fig. 15.23. The most important difference was in terms of intensity. The right most set of CI's in Fig. 15.9 depicts the overall intensity of bilateral versus unilateral training as calculated by Eq. (15.63). A 2-sample t-test indicated that there was a statistically significant difference in intensity between the two training groups ($p - value < 0.001$) with BSRMT having a mean intensity that was 25 % higher than URMT. Additionally, Fig. 15.23 shows that the BSRMT resulted in a higher proportion of movement for Joint 4 (elbow). Thus, the EXO-UL7 imposed significantly higher velocities on the wrist and elbow as it attempted to maintain symmetry between the paretic arm and the faster moving unaffected arm.

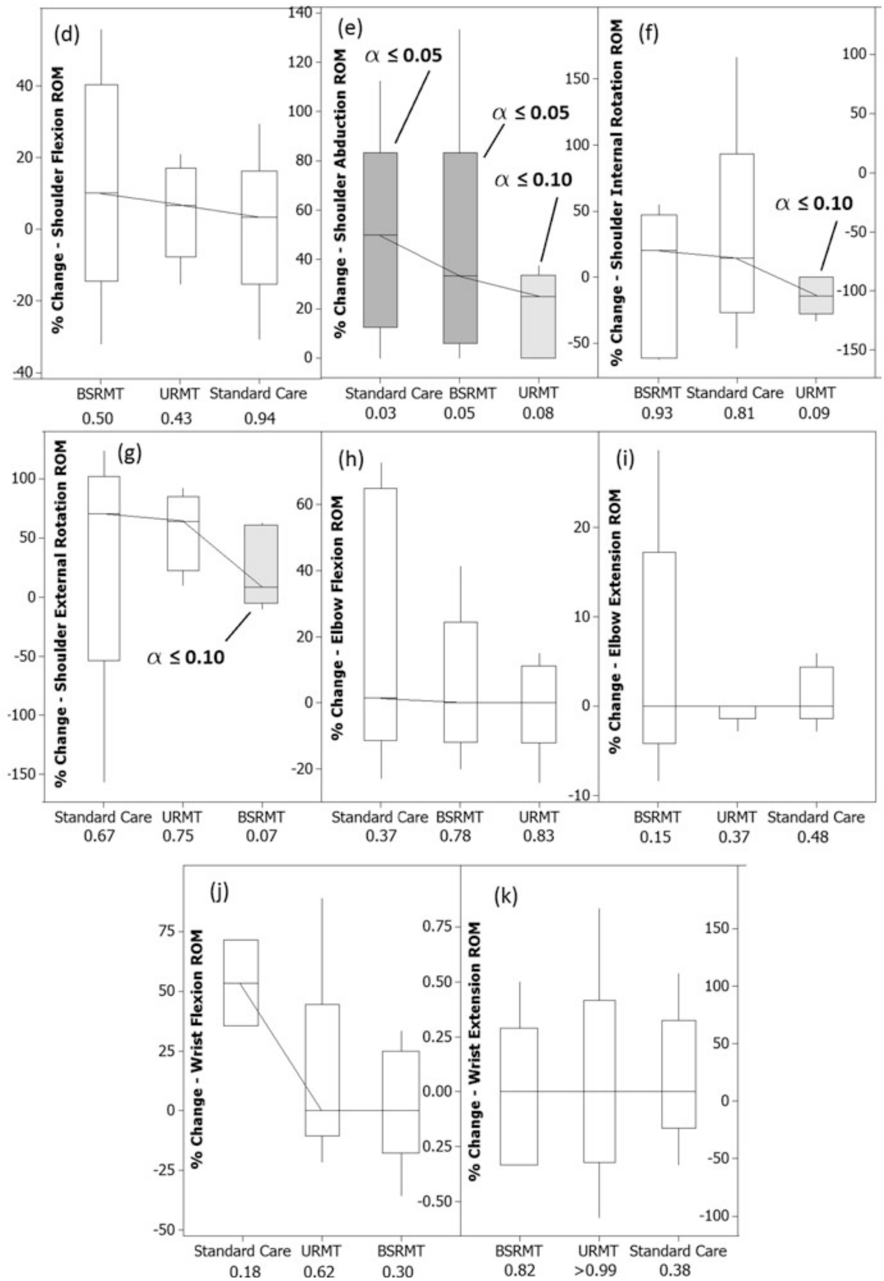

Fig. 15.18 Continue Fig. 15.17. Box plots of clinical measures for parametric data: **range of motion metrics**

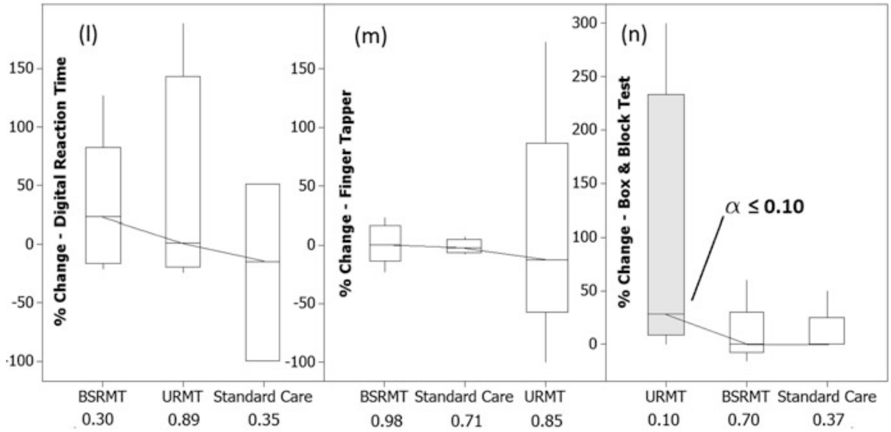

Fig. 15.19 Continue Fig. 15.18. Box plots of clinical measures for parametric data: **dexterity metrics**

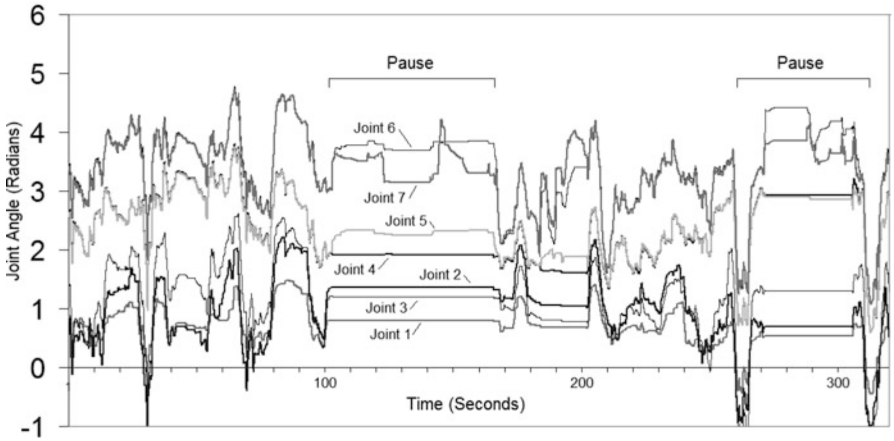

Fig. 15.20 Joint pauses. Bilateral training for subject 5, trial

Fig. 15.21 Joint percentages for velocity and acceleration for all unilateral subjects. *Circles* and *diamonds* indicate average values, whiskers indicate the 95 % CI

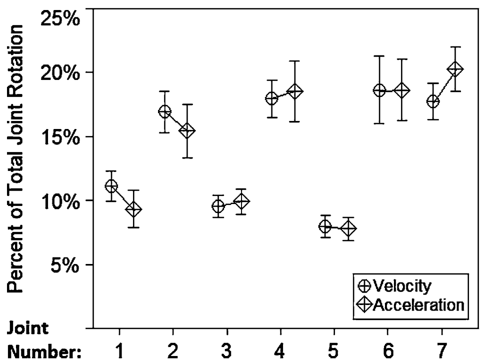

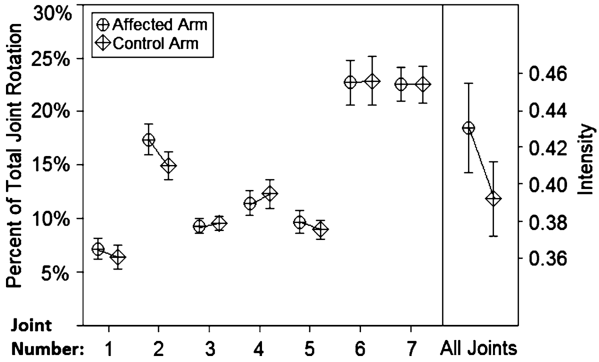

Fig. 15.22 Bilateral percent contributions by joint of the control arm (unimpaired arm), versus the slave (affected) arm given as 95 % CIs with mean values

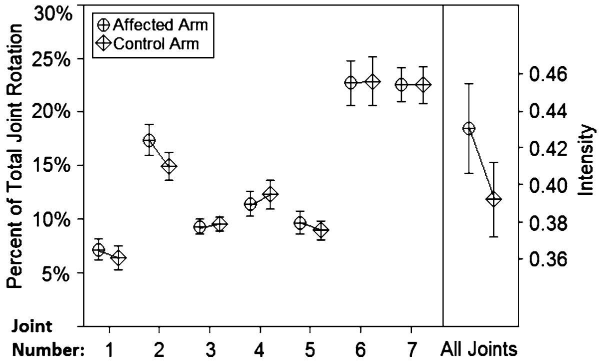

Fig. 15.23 BSRMT versus URMT given as 95 % CIs with mean values

15.4 Discussion

15.4.1 Pilot Study

Patients played the therapy game longer in the bilateral mode with admittance control compared to the unilateral mode and the bilateral group showed more activity for a given therapy session. We can infer that the bilateral with admittance control helped patients spend more time on the therapy compared to the unilateral training group. In physical therapy, it is important to expose the patients to the therapy for as long as possible to maximize the efficiency of the therapy. There is great promise in using assistive methods such as the bilateral with admittance control to improve the therapy results even if it is just by allowing patients to tolerate longer session.

15.4.2 Unilateral vs Bilateral Robotic Training

In this stroke study, there were significant differences in clinical gains following BSRMT versus URMT. The URMT group experienced a greater decrease in tone and the BSRMT group demonstrated greater gains in ROM. Using the approach described in the Data Analysis section, position, velocity, and acceleration were approximately equivalent measures. This approach also allowed for a more detailed comparative analysis of training. With respect to differences between the less affected control arm and the affected arm for BSRMT, the paretic arm did not always move as far, or as fast as the less affected arm. This difference is explainable by the fact that the robot only provided partial assistance. Recall that the EXO-UL7 only provides a helpful push for the paretic arm. Therefore, for USRMT involving partial assistance, the less affected arm will move more vigorously than the affected arm.

For the Box and Block test, there was a significant improvement for URMT subjects. Given that this test involves grasping blocks and transporting them over a barrier [62], improved performance on the Box and Block test was likely related to grasping improvements: reductions in spasticity in the hand and elbow, as well as improved ROM in the shoulder. The changes in grasping strength for URMT are somewhat puzzling. The EXO-UL7 provides no means to explicitly exercise the hand. Instead, subjects simply grasp a handle while performing training. The EXO-UL7 does not measure gripping force in the hand. Therefore, an explanation for reduced grip strength is somewhat speculative. Notwithstanding, a reduction in hand strength has been associated with reduced spasticity [63]. Thus, like the Box and Block test, reductions in hand strength might relate to reduced spasticity.

The analysis of kinematic data showed that BSRMT was associated with higher velocities of movements in the hand and elbow than URMT. Rapid extension of spastic muscles is generally regarded as undesirable. Thus, if reduction in spasticity of the elbow and/or hand is a therapeutic goal, BSRMT should be avoided. If BSRMT is used, precautions are needed to ameliorate the deleterious effects of rapid symmetric movements on the wrist and elbow. One solution could be to adjust the symmetric control algorithm. This adjustment might limit the joint speeds in the paretic elbow and wrist. However, this would lead to asymmetrical rather than symmetrical movements. An alternative approach could involve a control scheme in which speed is limited for the unaffected arm. For example, providing a viscous sensation in the unaffected wrist and elbow would reduce the velocities in both arms and preserve symmetry. Unilateral robotic training has shown promising results in other stroke studies [11,64,65]. With such precautions in place, BSRMT might have had comparably good results with URMT in terms of reduced spasticity in the elbow and wrist.

Given that all three training groups had some improvement in terms of ROM in the shoulder, these results could be interpreted as an indication that ROM in the shoulder was generally more amenable to an intervention. The range of motion was most improved in the shoulder for the BSRMT. It was significantly improved in the standard care groups but results were mixed for the URMT group. It is not clear how improved shoulder ROM for BSRMT is explainable by a greater cross-talk between the hemispheres of the brain. Indeed, BSRMT is unique from other types of robotic assistance in that the movements are self-guided by the patient. In this respect, the movements imposed on the paretic arm are literally a reflection of how, and when a subject chose to move their arm. Self-generated BSRMT did result in more intense training of the paretic arm. Thus, improvement in ROM may have resulted simply from greater intensity, and potentially more natural movements of the paretic shoulder. Lacking more direct measures of neurological activities, we find it exceedingly difficult to make conclusions about the effects of robotic training on hemispheric changes in connectivity with kinematic measures alone.

References

1. Kagerer F, Summers J, Semjen A (2003) Instabilities during antiphase bimanual movements: are ipsilateral pathways involved?. Exp Brain Res 151:489–500
2. Cattaert D, Semjen A, Summers J (1999) Simulating a neural cross-talk model for between-hand interference during bimanual circle drawing. Biol Cybern 81:343–358
3. Yavuzer G, Selles R, Sezer N, Sutbeyaz S, Bussmann J, Koseoglu F, Atay M, Stam H (2008) Mirror therapy improves hand function in subacute stroke: a randomized controlled trial. Biol Cybern 89:393–398
4. Sutbeyaz S, Yavuzer G, Sezer N, Koseoglu B (2007) Mirror therapy enhances lower-extremity motor recovery and motor functioning after stroke: a randomized controlled trial. Arch Phys Med Rehabil 88(5):555–559
5. Cauraugh J, Kim S, Duley A (2005) Coupled bilateral movements and active neuromuscular stimulation: intralimb transfer evidence during bimanual aiming. Neurosci Lett 382(1–2): 39–44
6. Simkins M, Fedulow I, Kim H, Abrams G, Byl N, Rosen J (2012) Robotic rehabilitation game design for chronic stroke. Games Health J 1(6):422–430
7. Lum P, Burgar C, Shor P, Majmundar M, Loos MVD (2002) Robot-assisted movement training compared with conventional therapy techniques for the rehabilitation of upper-limb motor function after stroke. Am Congr Rehabil Med Am Acad Phys Med Rehabil 83:952–959
8. Perry JC, Rosen J, Burns S (2007) Upper-limb powered exoskeleton design. Mechatronics 12(4):408–417
9. Perry JC, Rosen J (2006) Design of a 7 degree-of-freedom upper-limb powered exoskeleton. In: IEEE/RAS-EMBS international conference on biomedical robotics and biomechatronics, Pisa
10. Krebs HI, Ferraro M, Buerger SP, Newbery MJ, Makiyama A, Sandmann M, Lynch D, Volpe BT, Hogan N (2004) Rehabilitation robotics: pilot trial of a spatial extension for mit-manus. J NeuroEng Rehabil 1:5
11. Krebs HI, Hogan N, Aisen ML, Volpe BT (2007) Robot-aided neurorehabilitation: a robot for wrist rehabilitation. IEEE Trans Neural Syst Rehabil Eng 15(3):327–335
12. Reinkensmeyer D, Wolbrecht E, Bobrow J (2007) A computational model of human-robot load sharing during robot-assisted arm movement training after stroke. In: Conf Proc IEEE Eng Med Biol Soc 2007:4019–4023
13. Majumdar S (1995) Pneumatic system: principles and maintenance. Tata McGraw-Hill, New Delhi
14. He J, Koeneman EJ, Schultz RS, Huang H, Wanberg J, Herring DE, Sugar T, Herman R, Koeneman JB (2005) Design of a robotic upper extremity repetitive therapy device. In: ICORR 2005, Chicago
15. He J, Koeneman EJ, Schultz RS, Herring DE, Wanberg J, Huang H, Sugar T, Herman R, Koeneman JB (2005) Rupert: a device for robotic upper extremity repetitive therapy. In: EMBS 2005, Shanghai
16. Kim H, Miller L, Fedulow I, Simkins M, Abrams G, Byl N, Rosen J (2013) Kinematic data analysis for post-stroke patients following bilateral versus unilateral rehabilitation with an upper limb wearable robotic system. IEEE Trans Neural Syst Rehabil Eng 21(2):153–164
17. Perry J, Powell J, Rosen J (2009) Isotropy of an upper limb exoskeleton and the kinematics and dynamics of the human arm. J Appl Bionics Biomech 6(2):175–191

18. Rosen J, Perry J (2007) Upper limb powered exoskeleton. J Humanoid Robot 4(3):1–20
19. Kim H, Miller L, Rosen J (2011) Redundancy resolution of a human arm for controlling a seven dof wearable robotic system. In: EMBC 2011, Boston
20. Kim H, Li Z, Milutinovic D, Rosen J (2012) Resolving the redundancy of a seven dof wearable robotic system based on kinematic and dynamic constraint. In: ICRA 2012, St. Paul
21. Miller LM, Rosen J (2010) Comparison of multi-sensor admittance control in joint space and task space for a seven degree of freedom upper limb exoskeleton. In: Proceedings of the 3rd IEEE RAS & EMBS international conference on biomedical robotics and biomechatronics, Tokyo, pp 26–29
22. Kallmann M (2008) Analytical inverse kinematics with body posture control. Comput Animat Virtual Worlds (CAVW) 19(2):79–91
23. Lee P, Wei S, Zhao J, Badler NI (1990) Strength guided motion. Comput Graph 24:253–262
24. Iossifidis I, Steinhage A (2002) Controlling a redundant robot arm by means of a haptic sensor. In: ROBOTIK 2002, pp 269–274
25. Korein JU (1985) A geometric investigation of reach. MIT, Cambridge
26. Perry J, Rosen J (2006) Design of a 7 degree-of-freedom upper-limb powered exoskeleton. In: Proceedings of the 3rd IEEE RAS & EMBS international conference on biomedical robotics and biomechatronics, Pisa, pp 805–810
27. Tsagarakis N, Caldwell DG (2003) Development and control of a 'Soft-Actuated' exoskeleton for use in physiotherapy and training. Auton Robot 15(1):21–33
28. Wang X (1999) A behavior-based inverse kinematics algorithm to predict arm prehension posture for computer-aided ergonomic evaluation. J Biomech 32(5):453–460
29. Zhang X, Chaffin DB (1999) The effects of speed variation on joint kinematics during multisegment reaching movements. Hum Mov Sci 18:741–757
30. Yang F, Yuan X (2003) An inverse kinematical algorithm for human arm movement with comfort level taken into account. In: Proceedings of 2003 IEEE conference on control applications, Istanbul, Turkey, pp 1296–1300
31. Garner B, Pandy M (1999) Final posture of the upper limb depends on the initial position of the hand during prehension movements. Comput Methods Biomech Biomed Eng 2(2):107–124
32. Badler NI, Tolani D (1996) Real-time inverse kinematics of the human arm. Presence 5(4):393–401
33. Craig J (2003) Introduction to robotics: mechanics and control, 3rd edn. Prentice Hall, Harlow, ch 1
34. Yu W, Rosen J, Li X (2011) Admittance control for an upper limb exoskeleton, 2011 american control conference. In: 2011 American control conference – ACC, San Francisco, pp 1124–1129
35. Kim H, Miller LM, Rosen J (2012) Admittance control of seven-dof upper limb exoskeleton to reduce energy exchange. In: ICRA 2012, Saint Paul, pp 1–4
36. Sciavicco L (1987) A dynamic solution to the inverse kinematic problem for redundant manipulators. In: ICRA 1987, vol 4. Raleigh, NC, USA, pp. 1081–1087
37. Sciavicco L (1988) A solution algorithm to the inverse kinematic problem for redundant manipulators. IEEE Trans Robot Automat 4(4):403–410
38. Asada H, Granito J (1985) Kinematic and static characterization of wrist joints and their optimal design. In: ICRA 1985, St. Louis, pp 244–250
39. Yoshikawa T (1985) Dynamic manipulability of robot manipulators. In: ICRA 1985, St. Louis, pp 1033–1038
40. Yoshikawa T (1990) Foundations of robotics: analysis and control. MIT, Cambridge
41. Soechting J, Buneo C, Herrmann U, Flanders M (1995) Moving effortlessly in three dimensions: does donders' law apply to arm movement? J Neurosci 15(9):6271–6280
42. Kang T, He J, Tillery SIH (2005) Determining natural arm configuration along a reaching trajectory. Exp Brain Res 167:352–361
43. Hogan N (1984) An organizing principle for a class of voluntary movements. J Neurosci 4(2):2745–2754

44. Flash T, Hogan N (1985) The coordination of arm movements: an experimentally confirmed mathematical model. J Neurophysiol 5:1688–1703
45. Uno Y, Kawato M, Suzuki R (1989) Formation and control of optimal trajectory in human multijoint arm movement – minimum torque-change model. Biol Cybern 61:89–101
46. Nakano E, Imamizu H, Osu R, Uno Y, Gomi H, Yoshioka T, Kawato M (1999) Quantitative examinations of internal representations for arm trajectory planning: minimum commanded torque change model. J Neurophysiol 81(5):2140–2155
47. Harris CM, Wolpert DM (1998) Signal-dependent noise determines motor planning. Nature 194:780–784
48. Todorov E, Jordan MI (2002) Optimal feedback control as a theory of motor coordination. Nat Neurosci 5:1226–1235
49. Duma RP, Strick PL (2002) Motor areas in the frontal lobe of the primate. Physiol Behav 77:677–682
50. Graziano MS, Taylor CS, Moore T (2002) Complex movements evoked by micro stimulation of precentral cortex. Neuron 34:841–851
51. Aerospace medical research laboratory (1975) Investigation of inertial properties of human body, Tech rep, Mar 1975
52. Wada Y, Kaneko Y, Nakano E, Osu R, Kawato M (2001) Quantitative examinations for multi joint arm trajectory planningusing a robust calculation algorithm of the minimum commanded torque change trajectory. J Neural Netw 14:381–393
53. Biess A, Liebermann D, Flash T (2007) A computational model for redundant human three-dimensional pointing movements: integration of independent spatial and temporal motor plans simplifies movement dynamics. J Neurosci 27:13 045–064
54. Li Z, Roldan J, Milutinovic D, Rosen J (2013) The rotational axis approach for resolving the kinematic redundancy of the human arm in reaching movements. In: EMBC 2013, Osaka, pp 1–4
55. Secoli R, Milot MH, Rosati G, Reinkensmeyer D (2011) Effect of visual distraction and auditory feedback on patient effort during robot-assisted movement training after stroke. J Neuroeng Rehabil 8:21
56. Microsoft. Microsoft robotic developer studio 2008. (Online). Available: http://www.microsoft.com
57. Krakauer JW (2006) Motor learning: its relevance to stroke recovery and neurorehbilitation. Curr Opin Neurol 19(1):84–90
58. Kato PM (2012) Games for health journal: evaluating efficacy and validating games for health. Curr Opin Neurol 1(1):74–76
59. B U S of Public Health. Random error. (Online). Available: sph.bu.edu/otit/MPH-Modules/EP/EP713-RandomError-print.html
60. Taub E, Uswatte G, Pidikiti R (1999) Constraint-induced movement therapy: a new family of techniques with broad application to physical rehabilitation–a clinical review. J Rehabil Res Dev 36(3):237–251
61. Andrews A, Bohannon R (1989) Decreased shoulder range of motion on paretic side after stroke. Phys Ther 69(9):768–772
62. Mathiowetz V, Volland G, Kashman N, Wever K (1985) Adult norms for the box and block test of manual dexterity. Am J Occup Ther 39(6):386–391
63. O'Dwyer N, Ada L, Neilson P (1996) Spasticity and muscle contracture following stroke. Brain 119(Pt5):1737–1749
64. Prange G, Jannink M, Groothuis-Oudshoorn C, Hermens H, Ijzerman M (2006) Systematic review of the effect of robot-aided therapy on recovery of the hemiparetic arm after stroke. J Rehabil Res Dev 43(2):171–184
65. Norouzi-Gheidari N, Archambault P, Fung J (2012) Effects of robot-assisted therapy on stroke rehabilitation in upper limbs: systematic review and meta-analysis of the literature. J Rehabil Res Dev 49:479–496

Index

P. Artemiadis (ed.), *Neuro-Robotics: From Brain Machine Interfaces to Rehabilitation Robotics*, Trends in Augmentation of Human Performance 2,
DOI 10.1007/978-94-017-8932-5,


YO TIM! WHASSUP?!
CAN YOU HELP ME COLLECT PEOPLE'S FINGERPRINTS??!!
SURE MAN, NO PROBLEM!
WON'T DISAPPOINT YOU
Place Your Finger
DONE!